ALTERNATIVE ANTIGEN PROCESSING AND PRESENTATION IN IMMUNE DISORDERS

EDITED BY: Iñaki Alvarez, Luis C. Anton and Eddie A. James
PUBLISHED IN: Frontiers in Immunology

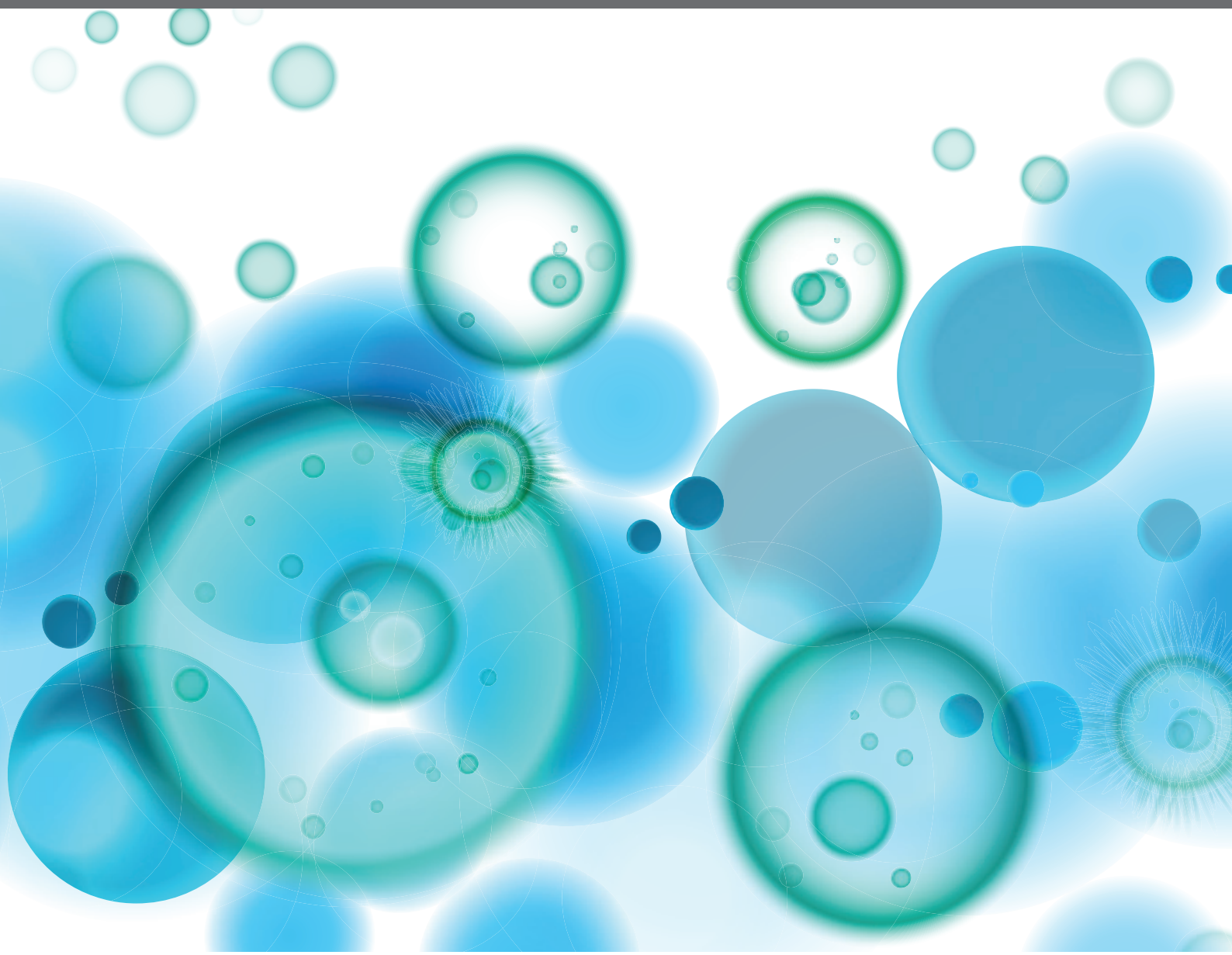

frontiers Research Topics

ISSN 1664-8714
ISBN 978-2-83250-286-0
DOI 10.3389/978-2-83250-286-0

About Frontiers

Frontiers is more than just an open-access publisher of scholarly articles: it is a pioneering approach to the world of academia, radically improving the way scholarly research is managed. The grand vision of Frontiers is a world where all people have an equal opportunity to seek, share and generate knowledge. Frontiers provides immediate and permanent online open access to all its publications, but this alone is not enough to realize our grand goals.

Frontiers Journal Series

The Frontiers Journal Series is a multi-tier and interdisciplinary set of open-access, online journals, promising a paradigm shift from the current review, selection and dissemination processes in academic publishing. All Frontiers journals are driven by researchers for researchers; therefore, they constitute a service to the scholarly community. At the same time, the Frontiers Journal Series operates on a revolutionary invention, the tiered publishing system, initially addressing specific communities of scholars, and gradually climbing up to broader public understanding, thus serving the interests of the lay society, too.

Dedication to Quality

Each Frontiers article is a landmark of the highest quality, thanks to genuinely collaborative interactions between authors and review editors, who include some of the world's best academicians. Research must be certified by peers before entering a stream of knowledge that may eventually reach the public - and shape society; therefore, Frontiers only applies the most rigorous and unbiased reviews.
Frontiers revolutionizes research publishing by freely delivering the most outstanding research, evaluated with no bias from both the academic and social point of view. By applying the most advanced information technologies, Frontiers is catapulting scholarly publishing into a new generation.

What are Frontiers Research Topics?

Frontiers Research Topics are very popular trademarks of the Frontiers Journals Series: they are collections of at least ten articles, all centered on a particular subject. With their unique mix of varied contributions from Original Research to Review Articles, Frontiers Research Topics unify the most influential researchers, the latest key findings and historical advances in a hot research area! Find out more on how to host your own Frontiers Research Topic or contribute to one as an author by contacting the Frontiers Editorial Office: frontiersin.org/about/contact

ALTERNATIVE ANTIGEN PROCESSING AND PRESENTATION IN IMMUNE DISORDERS

Topic Editors:
Iñaki Alvarez, Universitat Autònoma de Barcelona, Spain
Luis C. Anton, Spanish National Research Council (CSIC), Spain
Eddie A. James, Benaroya Research Institute, United States

Citation: Alvarez, I., Anton, L. C., James, E. A., eds. (2022). Alternative Antigen Processing and Presentation in Immune Disorders. Lausanne: Frontiers Media SA. doi: 10.3389/978-2-83250-286-0

Table of Contents

frontiers | Frontiers in Immunology

TYPE Editorial
PUBLISHED 07 September 2022
DOI 10.3389/fimmu.2022.993393

OPEN ACCESS

EDITED AND REVIEWED BY
Florent Ginhoux,
Singapore Immunology Network (A*STAR), Singapore

*CORRESPONDENCE
Iñaki Alvarez
inaki.alvarez@uab.cat
Luis C. Antón
lanton@cbm.csic.es
Eddie A. James
ejames@benaroyaresearch.org

SPECIALTY SECTION
This article was submitted to Antigen Presenting Cell Biology, a section of the journal Frontiers in Immunology

RECEIVED 13 July 2022
ACCEPTED 18 July 2022
PUBLISHED 07 September 2022

CITATION
Alvarez I, Antón LC and James EA (2022) Editorial: alternative antigen processing and presentation in immune disorders.
Front. Immunol. 13:993393.
doi: 10.3389/fimmu.2022.993393

Editorial: alternative antigen processing and presentation in immune disorders

Iñaki Alvarez[1,2*], Luis C. Antón[3*] and Eddie A. James[4*]

[1]Immunology Unit, Department of Cell Biology, Physiology and Immunology, Autonomous University of Barcelona, Bellaterra, Spain, [2]Institute of Biotechnology and Biomedicine, Autonomous University of Barcelona, Bellaterra, Spain, [3]Centro de Biología Molecular Severo Ochoa, CSIC/UAM, C/Nicolás Cabrera, Madrid, Spain, [4]Center for Translational Immunology, Benaroya Research Institute, Seattle, WA, United States

KEYWORDS

antigen (Ag), antigen processing and presentation, MHC class I and class II, alternative processing, immune disorders

Editorial on the Research Topic
Alternative antigen processing and presentation in immune disorders

The key players and processes of the MHC class I and class II pathways were described decades ago and are essential to develop an efficient T cell response. However, they are not confined to canonical pathways only. Indeed, cross-presentation and autophagy are non-canonical processes that allow the presentation of peptides by MHC-I and MHC-II molecules that originate from proteins located in the endocytic or endogenous compartments, respectively. In addition, the structural features of the MHC-peptide interaction were described decades ago. Nevertheless, MHC molecules can bind thousands of different peptides and the complexity of these immunopeptidomes open the door to the study of "non-typical" peptides. Thus, some of them are post-translationally modified peptides, spliced peptides generated by the proteasome, or peptides derived from non-canonical open reading frames. In this special Research Topic issue, we wanted to include an array of manuscripts that provides an extensive view of the alternative processing and presentation by MHC molecules and its involvement in immune disorders. A brief synopsis or each (in topical order) is included below.

Building on their previously reported work, Mansurkhodzhaev et al. investigate the formation of proteasome-generated spliced zwitter peptides originating from self (human) and non-self (viral) antigens. Although such sequences can be envisioned to induce clonal deletion or other tolerance processes and restrain responses against viruses, their analysis suggests that cis-spliced peptides only marginally impinge upon functional anti-viral CD8+ cytotoxic T cell responses.

In his Mini Review Münz highlights basic knowledge about how macroautophagy machinery contributes to antigen processing and presentation, strengthening its noncanonical functions, such as its role in nonconventional phagocytosis and secretion. Therefore, as argued in the manuscript, the multiple tasks played by this

machinery makes it a fascinating object of study and, potentially, a powerful target to modulate antigen presentation in pathological situations.

One of the crucial issues in defining the immunopeptidome is the discrimination of signal from noise, which becomes critical when peptide abundance is limiting. Nanaware et al. addressed this issue aiming at the MHC classs II (MHC-II) immunopeptidome in the mouse thymus. They developed a strategy to discard non-binding peptides and to validate bona fide binders, allowing them to identify distinct structural features of thymus MHC-II ligands compared to those from spleen, pointing to differences in antigen processing in these tissues.

Mei et al. presented original research work focused in the need to use computer-based immunoinformatic analysis to predict T cell targets from different strains of SARS-Cov-2 that may be used in future vaccine design. The authors put emphasis in HLA-A*11:01, the most frequent HLA allele in the Chinese population. They experimentally validated three epitopes from Spike protein.

The role that CD8+ T lymphocytes play in immunosurveillance of cancer cells is highlighted by the evasion mechanisms that they develop that affect MHC-I antigen presentation. This is the topic of the exhaustive Review by Dhatchinamoorthy et al.., where they cover different angles from where this issue can be observed: mechanisms of downregulation of MHC-I expression, mutations affecting MHC-I itself or essential components of the antigen processing pathway, the impact of these immunoevasion mechanisms on cancer cell recognition, as well as potential strategies to restore MHC-I expression.

Carré and Mallone elaborate the physiology and function of beta cells and antigen processing and presentation (APP) pathways. Thus, the authors generated some hypotheses on APPs relevant to beta cells, and directed this analysis to T1D pathogenesis. Finally, the authors raised some gaps regarding the HLA-I immunopeptidomes that need to be filled, as their composition in basal or stress conditions or the differences in the antigenic peptides presented by beta cells or dendritic cells during the T cell priming in draining lymph nodes.

The contribution of neuroinflammatory processes to the development of Parkinson's Disease (PD) has been gaining momentum in recent years. Celastrol, a compound that modulates autophagy and mitophagy, has been proposed to mitigate PD and other neurodegenerative diseases. The work of Ng et al. in this issue explores how this natural product may weaken anti-α-synuclein T cell responses through alterations in the vesicular trafficking of this antigen in dendritic cells. The authors propose that this altered trafficking may preclude its efficient antigen processing, thus thwarting a damaging T cell response.

Ito et al. explore the effects of palladium metal, a well-known allergen, on the surface dynamics of MHC class I protein. Using complementary assays, they demonstrated distinct temporal effects elicited by palladium treatment of murine DC2.4 dendritic cells leading to altered peptide presentation. Inhibition of membrane movement blocked this effect, leading to suppressed Pd-induced T cell-mediated responses.

The impact of sequence defects or variants on the expression and function of MHC molecules provides an important means of understanding the potential impact of natural polymorphisms and acquired mutations. Zhao et al. explore the functional impact of a spontaneous H2-Aa point mutation on MHC II expression and function. They document an atypical type II bare lymphocyte syndrome mediated through a cascade of erroneous mRNA splicing, deletion of eight bases in the mRNA, and a protein frameshift, all leading to a general loss of expression and significantly impaired CD4+ T cell numbers.

In an original research article, Thakur and Luthra-Guptasarma elaborate mechanisms through which some HLA-B27 subtypes are associated with ankylosing spondylitis (AS) and others are not. In their work, they conducted a proteomics-based study to analyze the protein clearance mechanisms in two AS differentially associated alleles (B*27:04, associated, and B*27:09, non-associated). They show that B*27:04 misfolded chains are mainly cleared through activation of the unfolded protein response (UPR), and autophagy. Instead, the B*27:09 misfolded chains are mainly cleared through the endosome-lysosome pathway.

Another topic of great interest is the idea that specific populations of professional antigen presenting cells can play distinct roles in health and disease. Welsh et al. review the often-overlooked role of B cell antigen presentation on the differentiation and longevity of protective memory CD4 T cells. Specifically, they highlight the impact of antigen density and the contributions of MHC Class II accessory molecules (HLA-DM and HLA-DO) to epitope selection and possible impacts on the formation of memory. They propose that low levels of antigen presentation might be to regulate long-term survival of CD4 memory T cells and to prevent cross-reactivity to autoantigens.

In their article, Kang et al. investigate the number and function of Dendritic cells (DCs) in scrub typhus patients. Examining peripheral blood, they observed that plasmacytoid and conventional DCs were numerically deficient and functionally impaired in scrub typhus patients. Alterations in the number and surface phenotype of DCs were absent during disease remission, but phenotypic alterations could be recapitulated through treatment with pro-inflammatory cytokines, suggesting a direct relationship between these alterations and disease severity.

Kawasaki disease (KD) is a severe illness that primarily affects children under the age of five. The condition is characterized by a vasculitis that, if untreated, can cause coronary artery aneurism and adult cardiovascular disease. Intravenous immunoglobulin (IVIG) is an effective treatment for acute KD, but its therapeutic mechanism of action is not completely understood. Wang et al. suggest in their contribution

that IVIG treatment reverts the immature (or tolerant) phenotype of circulating myeloid and plasmacytoid dendritic cells, restoring the numbers of peripheral CD4+ T cells, which circulate at reduced levels prior to the treatment.

We would like to dedicate this ResearchTopic to the memory of two pioneers that the Antigen Presentation field lost in the past few years, Enzo Cerundolo and Nilabh Shastri. Their contributions laid the foundations of a knowledge that pervades many concepts used by the papers published in this ResearchTopic.

Author contributions

EAJ, IA, and LCA each wrote individual sections of the editorial, corresponding to the respective articles that they edited. All three authors organized, revised, and edited the manuscript and agree to its style and content in its final form.

Funding

IA is supported by Grant RTI2018-097414-B-I00 from the Ministerio de Ciencia e Innovación. LCA is supported by Grant PID2019-110407RB-I00 from the Ministerio de Ciencia e Innovación; the Centro de Biología Molecular Severo Ochoa is funded by institutional grants from Fundación Ramón Areces and Banco de Santander. EAJ is supported by NIH/NIDDK grant no U24 DK104162-08 (Niland) NIAID contract no 75N93019C00068 (Kwok), NIAID grant no 2R01DK081166-11 (Haskins), and an award from the Heidner Foundation.

Conflict of interest

The authors declare that the research was conducted in the absence of any commercial or financial relationships that could be construed as a potential conflict of interest.

Publisher's note

frontiers in Immunology

ORIGINAL RESEARCH
published: 24 February 2021
doi: 10.3389/fimmu.2021.614276

Proteasome-Generated *cis*-Spliced Peptides and Their Potential Role in CD8$^+$ T Cell Tolerance

Artem Mansurkhodzhaev[1], *Camila R. R. Barbosa*[2], *Michele Mishto*[2,3*†] *and Juliane Liepe*[1*†]

[1] *Quantitative and Systems Biology, Max-Planck-Institute for Biophysical Chemistry, Göttingen, Germany,* [2] *Centre for Inflammation Biology and Cancer Immunology (CIBCI) and Peter Gorer Department of Immunobiology, King's College London, London, United Kingdom,* [3] *Francis Crick Institute, London, United Kingdom*

OPEN ACCESS

Edited by:
Eddie A. James, Benaroya Research Institute, United States

Reviewed by:
Anthony Wayne Purcell, Monash University, Australia
Dietmar M. W. Zaiss, University of Edinburgh, United Kingdom

***Correspondence:**
Michele Mishto
michele.mishto@kcl.ac.uk
Juliane Liepe
jliepe@mpibpc.mpg.de

† These authors have contributed equally to this work

Specialty section:
This article was submitted to Antigen Presenting Cell Biology, a section of the journal Frontiers in Immunology

Received: *05 October 2020*
Accepted: *28 January 2021*
Published: *24 February 2021*

Citation:
Mansurkhodzhaev A, Barbosa CRR, Mishto M and Liepe J (2021) Proteasome-Generated cis-Spliced Peptides and Their Potential Role in CD8$^+$ T Cell Tolerance. Front. Immunol. 12:614276. doi: 10.3389/fimmu.2021.614276

The human immune system relies on the capability of CD8$^+$ T cells to patrol body cells, spot infected cells and eliminate them. This cytotoxic response is supposed to be limited to infected cells to avoid killing of healthy cells. To enable this, CD8$^+$ T cells have T Cell Receptors (TCRs) which should discriminate between self and non-self through the recognition of antigenic peptides bound to Human Leukocyte Antigen class I (HLA-I) complexes—i.e., HLA-I immunopeptidomes—of patrolled cells. The majority of these antigenic peptides are produced by proteasomes through either peptide hydrolysis or peptide splicing. Proteasome-generated *cis*-spliced peptides derive from a given antigen, are immunogenic and frequently presented by HLA-I complexes. Theoretically, they also have a very large sequence variability, which might impinge upon our model of self/non-self discrimination and central and peripheral CD8$^+$ T cell tolerance. Indeed, a large variety of *cis*-spliced epitopes might enlarge the pool of viral-human *zwitter* epitopes, i.e., peptides that may be generated with the exact same sequence from both self (human) and non-self (viral) antigens. Antigenic viral-human *zwitter* peptides may be recognized by CD8$^+$ thymocytes and T cells, induce clonal deletion or other tolerance processes, thereby restraining CD8$^+$ T cell response against viruses. To test this hypothesis, we computed *in silico* the theoretical frequency of *zwitter* non-spliced and *cis*-spliced epitope candidates derived from human proteome (self) and from the proteomes of a large pool of viruses (non-self). We considered their binding affinity to the representative HLA-A*02:01 complex, self-antigen expression in Medullary Thymic Epithelial cells (mTECs) and the relative frequency of non-spliced and *cis*-spliced peptides in HLA-I immunopeptidomes. Based on the present knowledge of proteasome-catalyzed peptide splicing and neglecting CD8$^+$ TCR degeneracy, our study suggests that, despite their frequency, the portion of the *cis*-spliced peptides we investigated could only marginally impinge upon the variety of functional CD8$^+$ cytotoxic T cells (CTLs) involved in anti-viral response.

Keywords: bioinformatics, antigen presentation, MHC-I, peptide splicing, negative selection, T-cell repertoire, T-cell tolerance

INTRODUCTION

$CD8^+$ T cells are the ultimate response against viral infections. Their TCRαβ selectively recognizes viral epitope-HLA-I complexes, triggering a cytotoxic attack against infected cells in order to kill the infected cells and destroy any internal viruses. To enable this crucial immunological process, $CD8^+$ TCRαβs should ideally recognize any viral (non-self) antigen to enable a robust response against viruses, and not recognize any self-antigens to avoid an autoimmune reaction resulting from cytotoxic responses directed against non-infected parenchymal cells presenting only self-antigenic peptides at their cell surface. CD8+ T cells are able to recognize a wide variety of possible non-self-antigens due to the large variety of TCRαβ variants generated during $CD8^+$ T Cell maturation in the thymic cortex. Here, double negative thymocytes undergo somatic rearrangement of VDJ gene segments, causing variation in the structure and thereby binding affinities of TCRαβs expressed by different thymocytes. Through subsequent sequential positive and negative selection, only thymocytes possessing TCRαβs that do not recognize self-peptide-HLA-I complexes survive, transform into naïve $CD8^+$ T cells and migrate to periphery (1). A key step of the negative selection is the recognition, by $CD8^+$ TCRαβ T cell clones, of self-antigenic peptide-HLA-I complexes, which are presented by professional antigen presenting cells (APCs) in the thymic medulla. These APCs, such as mTECs and thymic Dendritic cells (DCs), express transcription factors that promote the expression of a very large variety of self-antigens, thereby promoting the identification of potentially autoreactive $CD8^+$ TCRαβ T cell clones and their elimination (2). Nonetheless, thymic deletion of self-reactive $CD8^+$ T cells is not perfect and many potentially autoreactive $CD8^+$ T cells are present in periphery (3–6). There, they can be controlled by peripheral tolerance mechanisms such as quiescence, ignorance, anergy, and tolerance-induced cell death (5). If some of the self-epitopes recognized by potentially autoreactive $CD8^+$ T cells are identical to non-self-epitopes which could be generated from viral antigens, we would expect an impaired $CD8^+$ T cell response against viruses, since these potentially autoreactive $CD8^+$ T cell clones would have been eliminated in the thymus or pruned in periphery.

We recently named these troubling peptides, *zwitter* epitopes (7). *Zwitter* is the German word for "hybrid," "hermaphrodites," originating from *zwi-*, meaning "duplex." For example, in chemistry, a zwitterion is an ion which possesses both positively- and negatively-charged groups.

If $CD8^+$ T cells specific for *zwitter* epitopes were eliminated in the thymus, they could not recognize the virus-derived *zwitter* epitope during an infection, which could create "holes" in the T cell repertoire. Likewise, if the inefficient stimulation of naïve $CD8^+$ T cells or the excessive and persistent stimulation of $CD8^+$ effector T cells mediated by self-derived *zwitter* epitopes induced anergy, exhaustion or peripheral deletional tolerance, these $CD8^+$ T cells would be eliminated and therefore unable to recognize the virus-derived *zwitter* epitopes and to tackle a second infection.

For example, a non-synonymous mutation in a Hepatitis C Virus (HCV), which did not affect peptide-HLA-A*02:01 binding affinity, hampered the immune response against HCV. Since this phenomenon seemed to derive from the lack of $CD8^+$ T cells with TCRαβ recognizing the mutated peptide, Wölfl et al. (8) hypothesized that HCV exploited a "hole" in the T cell repertoire. Similarly, in mouse models of vaccinia infection, ∼ one-half of the vaccinia-derived epitope candidates predicted to bind Major Histocompatibility Complexes class I (MHC-I) molecules and ∼ 20% of the vaccinia-derived epitope candidates identified in MHC-I immunopeptidomes by mass spectrometry (MS) did not trigger a detectable CTL response in vaccinia-immunized mice (9, 10).

Previous studies have investigated whether *zwitter* epitopes could contribute to these "holes" in the T cell repertoire by computing the overlaps between self and non-self-antigens in terms of canonical non-spliced peptide sequences (11–16). Calis et al. (17) computed that just 0.15% of all theoretical 9 amino acid long (9mer) canonical peptides derived from hundreds of viral strains completely overlap with 9mer peptide sequences present in the human proteome. Likely, this ∼0.15% frequency of virus-human *zwitter* non-spliced epitopes is not sufficient to justify the hypothesized size of "holes" in the $CD8^+$ TCRαβ T cell repertoire. Calis et al. (17) suggested that these "holes" could arise from the degeneracy of $CD8^+$ TCRαβ specificity, as this could lead to cross-recognition of multiple antigenic peptides, thereby increasing the immunological overlap between self and non-self-antigens. However, the immunological relevance of $CD8^+$ TCRαβ cross-reactivity is still a matter of debate (18–20), and even largely overlapping viral epitopes can induce an independent and non-cross-reactive T cell response (21).

Alternatively, we can consider what APCs present rather than how $CD8^+$ TCRαβs recognizes epitope-HLA-I complexes on APCs. For instance, the research in this field has so far only considered canonical "non-spliced" peptides and neglected non-canonical spliced peptides bound to HLA-I complexes. Both spliced and non-spliced peptides presented to $CD8^+$ T cells are mainly produced by proteasomes. These proteases can cleave antigens and release non-spliced peptides as well as ligate non-contiguous peptide fragments, thereby producing spliced peptides (22). Proteasome-catalyzed peptide splicing (PCPS) can occur by combining non-contiguous peptide fragments of the same molecule—*cis*-PCPS—or of two distinct proteins—*trans*-PCPS (**Figure 1A**). *Cis*-spliced peptides are produced and presented by various cells (22). They can target $CD8^+$ T cell responses against otherwise neglected bacterial antigens *in vivo* in a mouse model of *Listeria monocytogenes* infection (23). They can also activate $CD8^+$ T cells specific for *Listeria monocytogenes* or HIV through cross-recognition *in vivo* (24, 25). They can be neoepitopes and present recurrent driver mutations such as KRAS G12V at the cell surface of cancer cell lines (26). While, *cis*-spliced epitopes derived from melanoma-associated antigens are recognized by $CD8^+$ T cells in peripheral blood of melanoma patients (27, 28). A melanoma patient with metastasis was cured through adoptive T cell therapy using an autologous tumor-infiltrating lymphocyte clone, which was proved, in a later study,

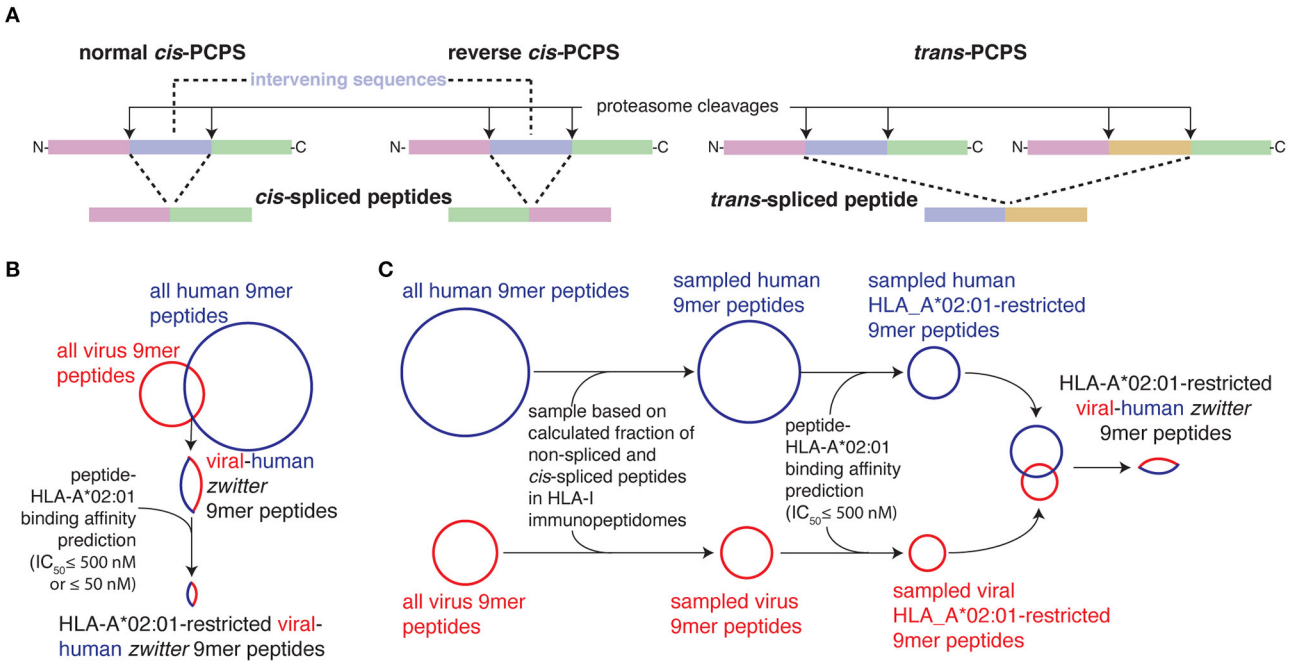

FIGURE 1 | Proteasome-generated spliced peptides and *in silico* pipelines. **(A)** Proteasome-generated spliced peptides can be formed by: (i). *cis*-PCPS, when the two splice-reactants, i.e., the non-contiguous peptide fragments ligated by proteasomes, derive from the same polypeptide molecule; the ligation can occur in normal order, i.e., following the orientation from N- to C-terminus of the parental protein (normal *cis*-PCPS), or in the reverse order (reverse *cis*-PCPS); (ii). *trans*-PCPS, when the two splice-reactants originate from two distinct protein molecules or two distinct proteins. **(B,C)** *In silico* pipelines to estimate the frequency of *zwitter* epitope candidates predicted to bind HLA-A*02:01 complexes not accounting **(B)** or accounting **(C)** for non-spliced and *cis*-spliced peptide frequency in HLA-I immunopeptidomes.

to be specific for a *cis*-spliced epitope rather than any non-spliced peptides derived from the melanoma-associated antigen (29, 30).

Cis-spliced peptide identification is quite challenging. Estimation of their frequency in HLA-I immunopeptidomes varies from 1 to 34%, depending on the method used for their identification (31). While, although *trans*-spliced peptides have been identified in *in vitro* (26, 32–34), *in cellulo* (35) and in HLA-I immunopeptidomes (36), their immunological relevance still needs to be investigated (7).

Nevertheless, since the theoretical size of the human *cis*-spliced peptide database is extremely vast, they could make up a significant portion of the viral-human *zwitter* epitope pool and, thereby, play a role in $CD8^+$ T cell tolerance. To test this hypothesis, we here computed the frequency of *zwitter cis*-spliced and non-spiced epitope candidates through comparison of human and viral proteomes. We accounted for these *zwitter* candidates' binding affinity to the most predominant HLA-I allele in Caucasian population, HLA-A*02:01, their estimated expression in human mTECs and their frequency in HLA-I immunopeptidomes, to accommodate these factors' potential impact on *zwitter* candidates' involvement in central tolerance.

MATERIALS AND METHODS

Statistical Analysis

Significant difference between groups was computed by applying the Kolmogorov-Smirnov test. A $p < 0.05$ was considered statistically significant. The effect size of 9mer non-*zwitter* vs. *zwitter* peptides in binding HLA-A*02:01 complexes was computed via odds ratio and significance was tested using Fisher exact test, or alternatively chi square test if the sample size was too large for Fisher exact test to test significance of association. Test for association between virus length and number of *zwitter* peptides was based on Pearson's product moment correlation coefficient. Statistical values are reported in **Supplementary Table 1**.

In this study, we defined viral-human *zwitter* non-spiced peptides as all those non-spliced peptides from viral proteomes that completely overlapped with human non-spliced peptides. Viral-human *zwitter cis*-spliced peptides, on the contrary, included the following categories of peptides that completely overlapped between each other: viral *cis*-spliced with human non-spliced peptides, viral *cis*-spliced with human *cis*-spliced peptides, and viral non-spliced with human *cis*-spliced peptides.

Peptide-HLA-A*02:01 Binding Affinity Prediction

Binding of non-spliced and *cis*-spliced 9mers to HLA-A*02:01 molecules was predicted using Stabilized Matrix Method (SMM) (37). This predictor showed good performance in the prediction of the binding affinity to a hundred *cis*-spliced peptides in a previous study (38). The standalone version of prediction tool was downloaded from the IEDB Analysis Resource (39). As

cut-off for peptide-HLA-A*02:01 binding affinity we set an $IC_{50} \leq 500$ nM.

In order to assess whether *zwitter* 9mer peptides were more likely to be HLA-A*02:01 binders than non-*zwitter* 9mer peptides on a per virus basis, we separately counted the number of non-*zwitter* and *zwitter* 9mer peptides predicted to be either non-binders or binders. Based on this contingency table the odds ratios for each virus were computed.

Estimation of Viral-Human *zwitter* Peptides

Viral proteomes were obtained via ViralZone and the Human proteome referred to Swiss-Prot Version 2016 excluding protein isoforms (40, 41). Only viruses with human trophism were included in any downstream analysis presented here ($n = 109$; **Supplementary Table 2**). The Human proteome database contained 20,191 protein entries with a total of 11,323,862 amino acid residues.

We focused our study on 9mer peptides since they represent the majority of non-spliced and *cis*-spliced peptides in HLA-I immunopeptidomes (36, 38, 42). Furthermore, we focused our study on HLA-A*02:01 variant since it is likely the most studied HLA-I variant and is the predominant HLA-I allele in Caucasian population.

We defined viral-human *zwitter* 9mer peptides as any 9mer peptide that had a sequence that could be obtained by either peptide hydrolysis or *cis*-peptide splicing both from self-proteins and from viral proteins.

For viral and human proteomes, we first computed all possible 9mer sequences of non-spliced peptides by cutting proteins into fragments of length nine amino acids; normal and reverse *cis*-spliced peptide sequences were computed by combining splice-reactants of any length such that the resulting *cis*-spliced peptide sequence had a length of nine amino acids and by imposing a maximal intervening sequence length ≤25 amino acids (**Figure 1A**), as previously described (42). Afterwards, an alignment was performed between all resulting virus and human derived peptides. We considered two peptides as identical, i.e., as viral-human *zwitter* peptides, if all of their nine amino acid residues were exactly matching. The relative frequency of viral-human *zwitter* peptides (*Fv*) was calculated as:

$$F_v = 100\,\frac{z_v}{p_v},$$

where z_v is the number of all viral-human *zwitter* peptides of a given virus v; and p_v is the number of all possible unique 9mer peptides derived from virus v. The number of viral-human zwitter peptides, z, can be computed for the comparison of non-spliced peptides only ($z_{v,i}$), of *cis*-spliced peptides only ($z_{v,j}$), of non-spliced viral peptides compared to *cis*-spliced human peptides ($z_{v,k}$), and of *cis*-spliced viral peptides compared to non-spliced human peptides ($z_{v,l}$). In our analysis, we depicted either the relative frequency of viral-human non-spliced *zwitter* peptides ($F_{v,i}$), viral-human *cis*-spliced *zwitter* peptides ($F_{v,cis}$) or of all (non-spliced and *cis*-spliced) viral-human *zwitter* peptides ($F_{v,all}$). The latter was obtained via:

$$F_{v,all} = 100\frac{\{z_{v,i},z_{v,j},z_{v,k},z_{v,l}\}}{\{p_{v,\mathrm{all}}\}},$$

Where {} denotes the unique set of peptide sequences and $p_{v,all}$ are all unique non-spliced and *cis*-spliced peptides derived from virus v.

The above-described analysis was done based on all theoretical possible non-spliced and *cis*-spliced peptides. Next, we repeated the estimation of viral-human zwitter peptide frequency by restricting the analysis to human- and virus-derived non-spliced and *cis*-spliced peptides that efficiently bind to the HLA-A*02:01 molecule, i.e., to peptides that have a predicted $IC_{50} \leq 500$ nM, resulting in:

$$B_v = 100\frac{z_b}{b_v},$$

where B_v is the frequency of viral-human *zwitter* peptide restricted to HLA-A*02:01, $z_{v,b}$ is the number of all viral-human *zwitter* peptides of a given virus v that bind HLA-A*02:01 and b_v is the number of all possible unique 9mer epitope candidates derived from virus v that are predicted to bind HLA-A*02:01 with an $IC_{50} \leq 500$ nM.

Estimation of Viral-Human *zwitter* Epitope Candidates Considering the Potential Antigen Repertoire of Human mTECs

To determine the potential antigen repertoire of human mTECs, we analyzed two transcriptome databases: (i) microarray gene expression values of human mTECs (43), and (ii) single-cell RNA sequencing of TECs in human embryos (44). Although mRNA expression does not perfectly mimic HLA-I immunopeptidomes (45), it was shown to be one of the strongest factors correlated with HLA-I immunopeptidomes (46).

In (43), the material was derived from patients that underwent corrective cardiac surgery. Here, we calculated average gene expression values (reported as $\log_2$ transformed fluorescence intensities) across technical replicates of each mTEC subset obtained with differing versions of microarrays provided in the dataset, and took the maximum average value.

In (44), the material was derived from healthy human fetuses as a result of medically interrupted pregnancy at weeks 8, 9, and 10. We used the subset of data that ostensibly corresponded to TECs with progenitor property of mTECs (based on the expression of the mTEC markers CLDN4 and JAG1).

We performed log-normalization of gene expression values of individual cells—reported as copy number of transcripts per individual gene—number of distinct unique molecular identifiers (*UMI*)—to mitigate the relationship between sequencing depth and gene expression. We then took an average normalized gene expression value between individual cells (47, 48):

$$x_i = \log\left(\frac{100000 * UMI_{ij}}{\sum_i UMI_{ij}} + 1\right),$$

where x_i is the log-normalized expression of gene i, UMI_{ij} is the expression value of gene i in cell j prior to normalization expressed as UMI counts, and UMI_j is the sum of UMI counts per cell j.

Afterward, we defined a crude model for antigen presentation based on the gene expression values. We assumed that the chance of an antigen being presented in mTECs' HLA-I immunopeptidomes was directly correlated with the gene expression of that antigen. The limitation of this assumption is discussed above.

We first scaled and normalized the gene expression values of the processed data obtaining weights for each antigen (w_i):

$$w_i = \frac{(E_i - \min(E))/(\max(E) - \min(E))}{\sum_{i=1}^{n}(E_i - \min(E))/(\max(E) - \min(E))},$$

where E_i is the expression value of gene i prior to normalization, and $min(E)$ and $max(E)$ are the minimum and maximum gene expression values in the dataset, respectively. We next sampled from the pre-computed pool of viral-human *zwitter* peptides a subset of peptides based on the weights (w_i) of the human antigen (i), which the respective *zwitter* peptide was derived from. The sampling size was set at 100% of the total number of *zwitter* peptides to reflect the odds of presentation of each given peptide. Sampling was performed with replacement based on the calculated probabilities 60 times. Finally, the frequency of viral-human *zwitter* peptides considering potential antigen repertoire of mTECs compared to all viral 9mer peptides (M_v) was computed as:

$$M_v = 100\,\frac{z_{m,v}}{p_v},$$

where $z_{m,v}$ is the number of sampled viral-human *zwitter* peptides with weights w_i and p_v is the number of all possible 9mer peptides of virus v. Similarly, when we considered both predicted peptide-HLA-A*02:01 binding affinity and potential antigen repertoire of mTECs, the viral-human *zwitter* peptide frequency (MB_v) was computed as:

$$MB_v = 100\,\frac{z_{mb,v}}{b_v},$$

where $z_{mb,v}$ is the number of sampled viral-human *zwitter* peptides restricted to HLA-A*02:01 binding with weights w_i, and b_v is the number of all possible 9mer peptides restricted to HLA-A*02:01 binding of virus v.

Estimation of the Frequency of Viral-Human *zwitter* Epitope Candidates Weighing up PCPS Frequency

Not all 9mer non-spliced and *cis*-spliced peptides that could derive from the human proteome are in reality produced by proteasomes and presented through HLA-I antigen processing and presentation (APP) pathway (22). Therefore, we implemented this factor in our *in silico* analysis of *zwitter* peptides. We aimed to determine the fractions of non-spliced (f_{non}) and *cis*-spliced peptides (f_{cis}) produced and presented in HLA-I immunopeptidomes relative to all theoretically possible sequences:

$$f_{non} = \frac{n_{non}}{N_{non}},$$
$$f_{cis} = \frac{n_{cis}}{N_{cis}},$$

where n_{non} and n_{cis} is the number of presented non-spliced and *cis*-spliced peptides, respectively, and N_{non} and N_{cis} is the number of all theoretically possible non-spliced and *cis*-spliced peptides, respectively, derived from a given antigen.

An estimate of f_{non} can be directly obtained from *in vitro* digestions of synthetic polypeptides with purified proteasomes. For this dataset, we used the peptide product database derived from 4 h digestions of 47 synthetic polypeptides with purified 20S standard proteasomes (34). This large database contains 2,429 unique non-spliced and 2,379 unique *cis*-spliced peptide products, which passed several quality control steps (34). We calculated the fraction of all produced 9mer non-spliced peptides (included in Specht's database) relative to all theoretically possible 9mer non-spliced peptides for each synthetic polypeptide substrate in the database. Then, we took the median value between all polypeptides as estimation of the fraction of non-spliced 9mer peptides generated by proteasomes. These calculations resulted in $f_{non} \sim 0.27$, i.e., ∼27% of all possible non-spliced 9mer peptides are generated *in vitro* by proteasomes and detected through MS. Therefore, in the following analysis, we randomly sampled 27% of all theoretical 9mer non-spliced peptides to recompute the number of viral-human *zwitter* peptides in absence of reliable proteasome peptide hydrolysis and peptide *cis*-splicing predictors.

We could have used the same strategy to compute the fraction of *cis*-spliced peptides produced by proteasomes compared to all theoretical *cis*-spliced peptide products. However, *cis*-spliced peptides have been proved to be produced in significantly lower amount than non-spliced peptides (26, 33, 34). Bearing this in mind, we speculated that a large number of *cis*-spliced peptides produced by proteasomes *in vitro* could not pass all APP steps and become antigenic as compared to non-spliced peptides.

On the contrary, HLA-I immunopeptidomes should be more informative in such a matter, since the APP pathway should already have filtered out many *cis*-spliced peptides generated in low amount. Therefore, we used the information available about *cis*-spliced peptide frequency in HLA-I immunopeptidomes measured through MS and combined with the information of non-spliced peptide frequency in *in vitro* digestions (f_{non}). Indeed, the estimation of f_{cis} based on *cis*-spliced peptide product frequency *in vitro* digestions as measured through MS could have resulted in an overestimation of f_{cis}. Therefore, we defined the relative frequencies of *cis*-spliced peptides in HLA-I immunopeptidomes (f) as measured by MS as:

$$f = \frac{100\,n_{cis}}{n_{cis}+n_{non}},$$

where $n_{cis}$is the number of *cis*-spliced peptides detected in HLA-I immunopeptidomes and $n_{non}$is the number of non-spliced

peptides detected in HLA-I immunopeptidomes. Since f was estimated to be in the range of 1–34% (31). For a given estimate of f we could then compute the number of *cis*-spliced peptides presented in HLA-I immunopeptidomes (n_{cis}) as:

$$n_{cis} = \frac{f\ N_{non} f_{non}}{100 - f}.$$

Furthermore, we could compute the total number of all theoretical *cis*-spliced peptides (N_{cis}) as:

$$N_{cis} = \boldsymbol{\gamma} N_{non},$$

where γ was estimate to have a value of 398 for proteins of length 500 amino acids or longer (42). This resulted in:

$$f_{cis} = \frac{f f_{non}}{\boldsymbol{\gamma}(100 - f)}.$$

We used a range of potential frequencies of observed *cis* spliced peptides relative to the whole HLA-I immunopeptidome f (1–35%) to determine a range of f_{cis}. Based on f_{cis} and f_{non}, we randomly sampled non-spliced and *cis* spliced peptides 600 times from all viral and human proteomes without replacement. For each of the 600 samples for each f_{cis}, we counted the number of all sampled HLA-A*02:01-restricted *zwitter* peptides.

HIV-Derived HLA-A*02:01-Restricted Non-immunogenic 9mer Peptides

As proof of principle, we selected a pool of HIV-derived HLA-A*02:01-restricted 9mer peptides, which were previously suggested to be non-immunogenic. This pool included non-spliced epitope candidates derived from HIV, which:

(i) were investigated by Perez et al. (49) through IFN-γ ELIspot assay in HIV- infected donor peripheral blood mononuclear cells (PBMCs) pulsed/non-pulsed with synthetic epitope candidates. We considered as non-immunogenic those peptides that did not induce immune response after peptide stimulation.

(ii) were included in a database by Ogishi and Yotsuyanagi (50). This database collected outcomes of various T cell activation assays on HLA-I-restricted non-spliced peptide sequences (8–11 mer peptides). In this database, we selected HIV-derived HLA-A*02:01-restricted 9mer peptides, which were confirmed as non-immunogenic among all studies considered in the database.

(iii) were included in the EPIMHC database (51), which collected datasets of T cell response against epitope candidates. In this database, non-immunogenic peptides were selected by applying the following parameters: Allele, HLA A0201; Length, 9mer; MHC source, Human; Peptide source organism, HIV1; Peptide Binding Level, all; T-cell activity, all; Immunogenicity level, all; Processing, all.

The pool of peptide candidates derived from these three databases were then analyzed for peptide-HLA-I bind affinity prediction—as described above—and only peptides with predicted peptide-HLA-A*02:01 $IC_{50} \leq 500$ nM were selected (**Table 1**).

Modeling of Protein 3D Structures

For visualization purpose, the structures of Gag-Pol polyprotein of the HIV strain MVP5180 and of the human Major Vault protein (MVP) were predicted and visualized through the fully automated protein structure homology-modeling server, accessible via Expasy web server (52).

Data Availability

A summary of the files accessible via repository is reported in the following Mendeley dataset: http://dx.doi.org/10.17632/hw686hytfs.1.

The mTEC's RNA sequencing data published by Pinto et al. (43) are available at Gene Expression Omnibus (GEO) under identifier GSE49625.

The single-cell RNA sequencing of TECs in human embryos published by Zeng et al. (44) are available at Gene Expression Omnibus (GEO) under identifier GSE133341.

RESULTS

Estimation of the Upper Bond Frequency of Viral-Human *zwitter* Epitope Candidates

By applying the *in silico* pipeline described in **Figure 1B** and focusing on 9mer peptides, which represent the majority of non-spliced and *cis*-spliced peptides in HLA-I immunopeptidomes (28, 36, 38, 42), we identified 2,340 and 9,350,135 theoretical viral-human *zwitter* non-spliced and *cis*-spliced 9mer peptides, respectively (**Supplementary Table 3**). On average per virus, these represent 0.06 and 2.93% of the pool of virus non-spliced and *cis* spliced 9mer peptides, respectively (**Figure 2A**). We then predicted their binding affinity to the most predominant HLA-I allele in Caucasian population, i.e., HLA-A*02:01, and filtered out all peptides with predicted $IC_{50} > 500$ nM. This step removed ∼96% of the peptides (on average, only ∼5% of peptides per virus are left; see **Supplementary Figure 1A**). This left 87 and 504,209 viral-human *zwitter* non-spliced and *cis*-spliced 9mer epitope candidates in total, which correspond, on average per virus, to 0.05 and 3.84% of the pool of HLA-A*02:01-restricted viral non-spliced and *cis*-spliced 9mer peptides, respectively (**Figure 2B**). This frequency did not account for antigen processing via the APP pathway and assumed that each and every non-spliced and *cis*-spliced peptide that could be produced by proteasomes was indeed produced. Therefore, it represents the upper bond of viral-human *zwitter* 9mer epitope candidates. Interestingly, viral-human *zwitter* peptides were more often predicted to bind HLA-A*02:01 with an $IC_{50} \leq 500$ nM than non-*zwitter* peptides (**Supplementary Figure 1B**).

When we loosen up the IC_{50} cut-off, the number of viral-human *zwitter* non-spliced and *cis*-spliced 9mer epitope candidates would increase (**Figure 2C**). To further investigate the theoretical frequency of viral-human *zwitter* non-spliced and *cis*-spliced 9mer epitope candidates among the potentially immunodominant epitopes, we focused on a more stringent IC_{50} cut-off of 50 nM. For instance, Platteel et al. (23) reported a correlation between the immunogenicity of *cis*-spliced epitope candidates, their predicted binding affinity to H2-K^b ($IC_{50} \leq 2$ nM) and the measured *cis*-spliced peptide-H2-K^b

TABLE 1 | List of HIV-derived HLA-A*02:01-restricted 9mer peptides not immunogenic and their *zwitter* peptide pair.

Peptide	IC_{50} (nM)	Rank	References	*cis*-spliced, 25 int. seq.	Any *cis*-spliced
WLWYIKIFI	24.1	0.5	(51)		
MLQLTVWGI	34.8	0.6	(49)		
LTFGWCFEL	43.5	0.8	(49)		
SITNWLWYI	44.9	0.8	(49)		
LLNATAIAV	50.7	0.9	(51)		Q9P273|TEN3_HUMAN. 1504-1506/1405-1410
QLAEVVQKV	50.5	0.9	(49)	Q14764|MVP_HUMAN.786-790/762-765	Q9NRD9|DUOX1_HUMAN. 895-900/687-689
ALQDSGLEV	56.3	1.1	(49)		Q13263|TIF1B_HUMAN. 655-658/601-605
ALQDSGSEV	90.5	1.5	(49)		sp|Q8IZJ1|UNC5B_HUMAN. 458-462/31-34
LLQYWSQEL	87.9	1.5	(51)		
IVGAETFYV	93.9	1.6	(51)		
QMHEDVISL	93.9	1.6	(49)		
QLQARILAV	109.4	1.8	(51)		Q9P2M7|CING_HUMAN. 1138-1143/660-662
HLEGKIILV	150.6	2.3	(49)		
RMYSPISIL	162.9	2.3	(51)		Q9P225|DYH2_HUMAN. 1840-1843/3935-3939
HLEGKVILV	177.4	2.5	(51)		Q8N2C7|UNC80_HUMAN. 264-267/2799-2803
EMMTACQGV	210.4	2.9	(49)		
TLQEQIAWM	259.4	3.3	(49)		
FLQSRPEPT	371.6	4.1	(51)		
MTNNPPIPV	427.6	4.4	(50)		
QLTEVVQKI	424.7	4.4	(49)		

*List of 9mer non-spliced peptides derived from various strains of HIV and predicted to bind HLA-A*02:01 complex with an $IC_{50} \leq 500$ nM. These peptides also failed to trigger a specific $CD8^+$ T cell response in HIV-infected donors (see Materials & Methods). The related papers are cited. The corresponding prediction of the peptide-HLA-A*02:01 binding affinity is reported as IC_{50} and rank, and it was computed by applying SMM algorithm. The potential human origin of the same sequences through peptide splicing by allowing either only cis-spliced peptides with intervening sequence ≤ 25 amino acid residues (cis-spliced 25, int. seq.) or any cis-spliced peptides is described through the UniprotKB's protein code and their location within the antigen.*

complex stability in a mouse model of *Listeria monocytogenes* infection. While, Assarsson et al. (9) showed that all vaccinia immunodominant HLA-A*02:01-restricted non-spliced epitopes analyzed in their study on a transgenic mouse model had a measured peptide-HLA-A*02:01 $IC_{50} \leq 50$ nM. With this latter IC_{50} cut-off, 11 non-spliced and 87,154 *cis*-spliced peptides were left among the viral-human *zwitter* epitope candidates, which correspond, on average per virus, to 0.06 and 4.19% of the pool of HLA-A*02:01-restricted (predicted $IC_{50} \leq 50$ nM) viral non-spliced and *cis*-spliced 9mer peptides, respectively (**Figure 2D**).

Example of T Cell Tolerance Against Viral-Human *zwitter* Epitope Candidate

As proof of principle, we selected a pool of HIV-derived HLA-A*02:01-restricted 9mer peptides, which were demonstrated to be non-immunogenic in previous studies (see Materials and Methods). Among them, we selected non-spliced peptides that were predicted to bind HLA-A*02:01 complex with $IC_{50} \leq 500$ nM and, upon testing for $CD8^+$ T cell response in HIV patients, were non-immunogenic (**Table 1**). We investigated whether any of them may also have been a viral-human *zwitter* 9mer epitope candidate. We considered both *cis*-spliced peptides with intervening sequence shorter than 26 amino acid residues, as in the rest of the study, as well as any theoretical *cis*-spliced peptide computed from the human proteasome. Out of twenty peptides with these characteristics, we identified the peptide QLAEVVQKV, which may derive from the Gag-Pol polyprotein of the HIV strain MVP5180 ($Gag\text{-}Pol_{955-963}$). This epitope candidate has a predicted $IC_{50} = 50$ nM for HLA-A*02:01 (**Table 1**). Despite the good binding affinity, this epitope candidate did not trigger a PBMC response in HIV patients, according to Perez et al. (49). In their cohort of 31 HIV patients, 10 were HLA-A*02:01$^+$ and none of them recognized the epitope candidate upon peptide stimulation. No other studies showed a recognition of this epitope candidate by $CD8^+$ T cells, to our knowledge. According to our computation, the same peptide sequence may also derive from the Major Vault protein as a *cis*-spliced peptide—i.e., $MVP_{786-790/762-765}$ [QLAE][VVQKV]—with intervening sequence smaller than 26 amino acid residues (**Figure 2E**). MVP's gene mRNA was identified in mTECs by both Pinto et al. (43) and Zeng et al. (44), thereby suggesting its expression in mTECs and, in theory, the potential presentation of the $MVP_{786-790/762-765}$ *cis*-spliced epitope candidate to thymocytes. That might lead to negative selection of $CD8^+$ T cell clones recognizing the peptide QLAEVVQKV, which might explain the absence of immunogenicity of the $Gag\text{-}Pol_{955-963}$ [QLAEVVQKV] in HLA-A*02:01$^+$ HIV patients.

If we expanded our research to any *cis*-spliced epitope candidate, regardless of the intervening sequence length, we identified six other *cis*-spliced epitope candidates with a sequence present in **Table 1**. Therefore, we should bear in mind that the pool of viral-human *zwitter* 9mer *cis*-spliced epitope candidates,

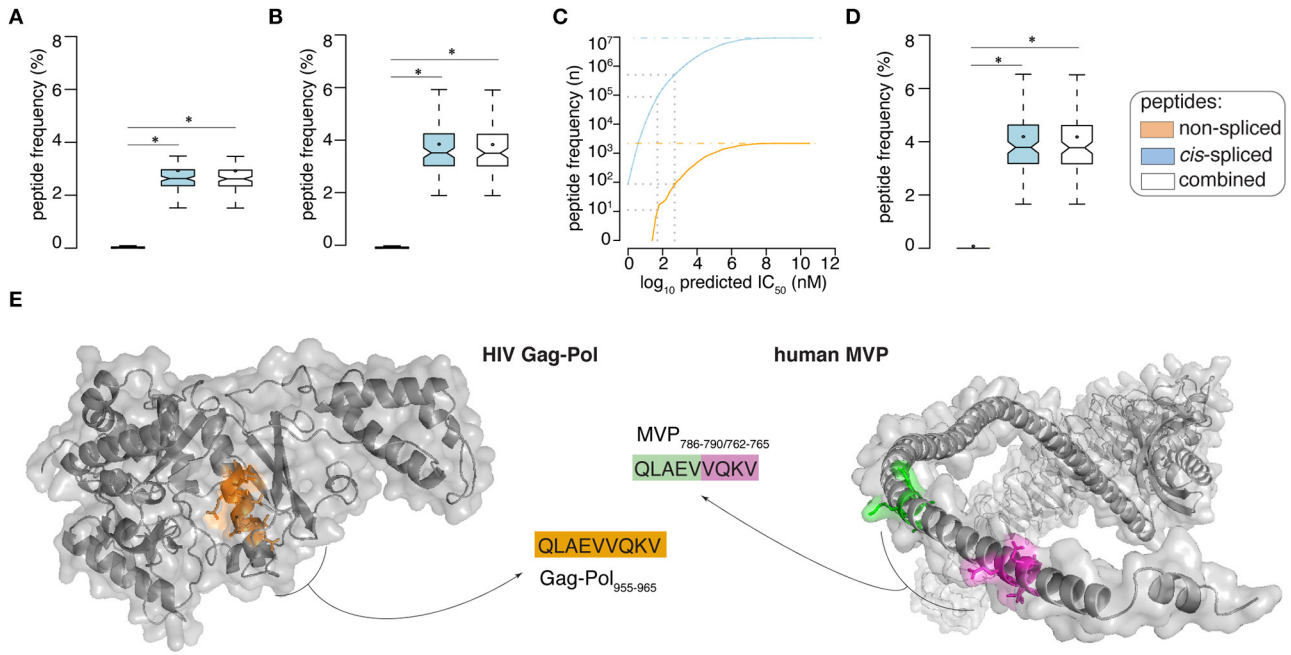

FIGURE 2 | Viral-human *zwitter* epitope candidate frequency and examples. **(A,B)** Frequency of viral-human 9-mer **(A)** *zwitter* peptides and **(B)** HLA-A02:01-restricted (predicted $IC_{50} \leq 500$ nM) *zwitter* epitope candidates, compared to their cognate viral peptide database and considering the whole human proteome database. **(C)** Number of viral-human *zwitter* non-spliced and *cis*-spliced epitope candidates depending on the peptide-HLA-A02:01predicted IC_{50}. Gray dot lines mark the predicted IC_{50} of 500 nM and 50 nM. The blue and orange dot lines depict the number of viral-human *zwitter cis*-spliced and non-spliced peptide without peptide-HLA-A02:01predicted IC_{50} cut-off. **(D)** Frequency of HLA-A02:01-restricted (predicted $IC_{50} \leq 50$ nM) viral-human *zwitter* 9mer epitope candidates, compared to their cognate viral peptide database and considering the whole human proteome database. **(E)** Example of HIV-human zwitter epitope candidate QLAEVVQKV, which may be derived from HIV Gag-Pol as non-spliced peptide ($Gag\text{-}Pol_{955-963}$), and from the human MVP as *cis*-spliced peptide ($MVP_{786-790/762-765}$). Both peptides are depicted in the cognate antigens. Color code corresponds to **Figure 1A**. In **(A,B,D)** Box plots depict the median and 25–75 percentiles of peptides per virus. Bars represent 5–95 percentiles. Dots represent the mean. Significant difference between groups is labeled with * (see **Supplementary Table 1**).

which had an intervening sequence length smaller than 26 amino acid residues, represented only part of the whole theoretical *cis*-spliced peptides.

Estimation of Viral-Human *zwitter* Epitope Candidate Frequency Weighing Up mTEC Transcriptome

Viral-human *zwitter* non-spliced and *cis*-spliced 9mer epitopes may impinge upon the functional $CD8^+$ T cell repertoire through both central and peripheral tolerance. Herein, we focused solely on the negative selection step of the central tolerance. We hypothesized that TCRαβ T cell clones that recognize self-derived *zwitter* epitopes bound to HLA-I complexes of mTECs and other professional APCs with high avidity are tolerized.

In tolerance, the amount of antigen presented at the cell surface is relevant to the fate of T cell clones (5). Although gene expression does not mirror the HLA-I immunopeptidomes, it appears, to some extent, to be a predictor of antigen presentation (46). Bearing this in mind, we repeated our analysis by weighing up the probability of an antigen to be represented in mTEC's HLA-I immunopeptidome, based on transcriptome data from either microarray analysis of human mTECs (43) or single-cell RNA sequencing of TECs in human embryos (44).

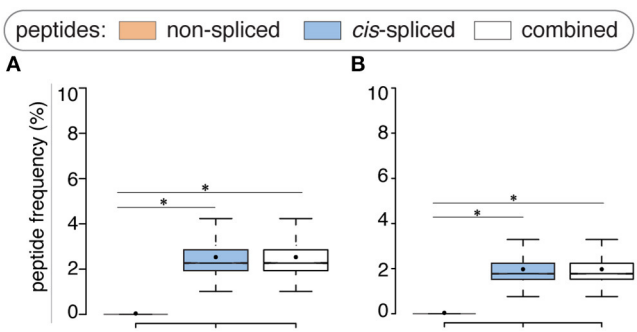

FIGURE 3 | Viral-human *zwitter* epitope candidates considering mTEC's transcriptome. **(A)** Frequency of HLA-A02:01-restricted viral-human *zwitter* 9mer epitope candidates compared to their cognate viral peptide databases considering the human mTEC transcriptome computed either **(A)** from (43) or **(B)** from (44). Box plots depict the median and 25–75 percentiles. Bars represent 5–95 percentiles. Dots represent the mean. Significant difference between groups is labeled with * (see **Supplementary Table 1**).

To this end, we transformed gene expression values of mTECs into probabilities of antigens being represented in HLA-I immunopeptidomes through a crude model for antigen

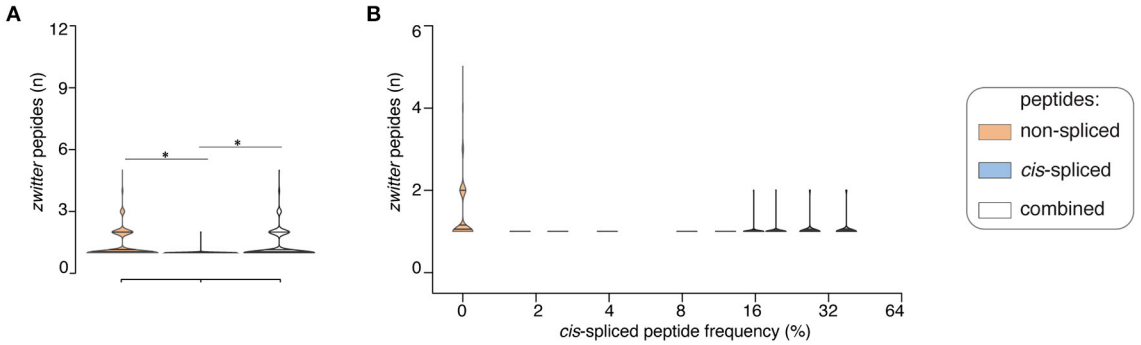

FIGURE 4 | Viral-human *zwitter* epitope candidates considering *cis*-spliced peptide frequency in HLA-I immunopeptidomes. **(A)** Distribution of the number of viral-human 9mer HLA-A02:01-restricted (non-spliced, *cis*-spliced and combined) *zwitter* epitope candidates per virus across all 600 random samples presented as violin plots (rotated densities). Significant difference between groups is labeled with * (see **Supplementary Table 1**). This analysis was carried out by hypothesizing that *cis*-spliced peptides represent ∼15% of peptides in HLA-I immunopeptidomes and by using the whole human proteome as database. The distribution of the number of viral-human *zwitter cis*-spliced epitope candidates has been displayed among viruses that had at least one *zwitter* peptide. **(B)** Number of HLA-A*02:01-restricted viral-human *zwitter* non-spliced and *cis*-spliced 9mer epitope candidates per virus per sampling iteration, depending on a broad range of theoretical *cis*-spliced peptide frequencies in HLA-I immunopeptidomes. Here, viral proteomes are compared to the whole human proteome database. The number of viral-human *zwitter* non-spliced and *cis*-spliced 9mer epitope candidates per virus per iteration has been computed among viruses that had at least one *zwitter* peptide.

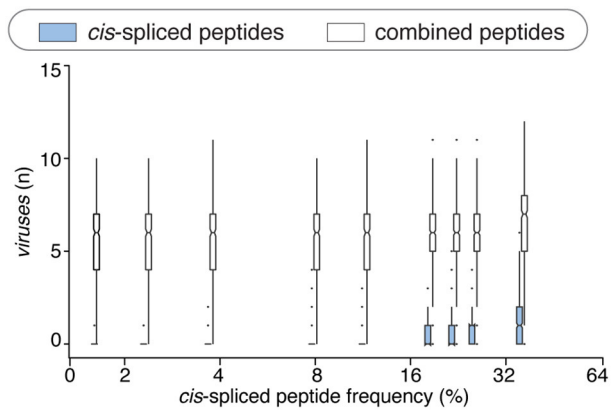

FIGURE 5 | Viruses that have *zwittter* epitope candidates depending on *cis*-spliced peptide frequency in HLA-I immunopeptidomes. Average number of viruses that contain at least one HLA-A02:01-restricted viral-human *zwitter* 9mer peptide per iteration, depending on a broad range of theoretical *cis*-spliced peptide frequencies in HLA-I immunopeptidomes. Viral proteomes are compared to the whole human proteome database. The boxplots of the combined peptides have been slightly shifted on the x axis for representation purpose.

presentation based on the gene expression values (see Material and Methods). Furthermore, in our analysis, the probability of an antigen to be represented in mTEC's HLA-I immunopeptidomes was weighted by the number of *zwitter* non-spliced and *cis* spliced 9mer peptides predicted to bind HLA-A*02:01 (with $IC_{50} \leq 500$ nM) and theoretically derived from that antigen (see Material and Methods). Indeed, the chance of an antigen being presented in HLA-I immunopeptidomes also depends on the number of HLA-I-binding peptides that could be derived from that given antigen. Since we introduced a probability score in our analysis, we had to sample the viral-human *zwitter* non-spliced and *cis*-spliced 9mer epitope candidate pool, thereby estimating the average frequency rather than the absolute frequency of these peptides, which has been shown so far.

Compared to the whole human proteome, incorporation of potential antigen repertoire based on mTEC transcriptome resulted in a decreased average number of both *zwitter* non-spliced and *cis*-spliced epitope candidates. On average per virus, 0.04% and 2.53% of the pool of HLA-A*02:01-restricted virus non-spliced and *cis*-spliced 9mer epitope candidates, respectively, were *zwitter* peptides using Pinto's RNA sequencing database (**Figure 3A**). Similar results were obtained using Zeng's RNA sequencing database (**Figure 3B**).

Estimation of Viral-Human *zwitter* Epitope Candidate Frequency Weighing Up *cis*-PCPS Frequency

The computation done so far did not take into account the frequency of peptides produced by proteasomes through peptide hydrolysis and peptide *cis*-splicing and presented at the cell surface. Despite not being physiological, one of the most detailed approaches to determine what proteasomes can produce via peptide hydrolysis and peptide splicing is, in our experience, the measurement through MS of non-spliced and *cis*-spliced peptides produced *in vitro* by purified 20S proteasomes during the degradation of synthetic polypeptides recapitulating antigenic sequence. Correspondence between *in vitro* experiments carried out with purified 20S proteasomes and *in cellulo* and *in vivo* experiments has been demonstrated in various studies investigating both viral and tumor epitopes (23, 24, 26, 27, 30, 53–62). The analysis of *in vitro* digestions of synthetic polypeptides by 20S proteasomes showed that, although these proteases can cleave—and likely ligate—any amino acid, they have substrate sequence preferences (34). It also showed that *cis*-spliced peptides are produced, on average, in significantly smaller amount than

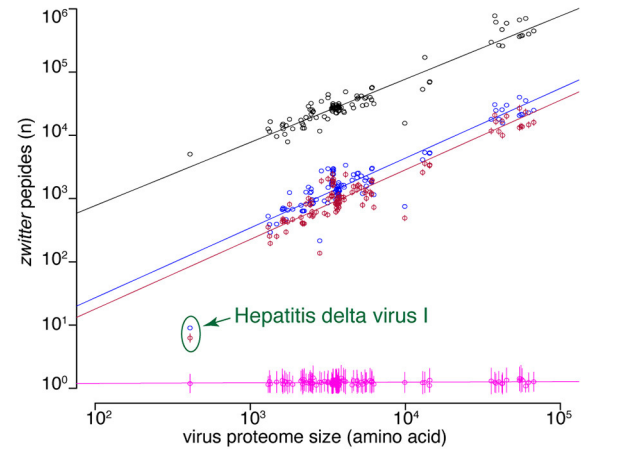

FIGURE 6 | Viral-human *zwitter* epitope candidate frequency depends on virus length and sequence motifs. Number of viral-human *zwitter* combined (i.e., non-spliced + *cis* spliced peptides) 9mer peptides per virus, depending on the number of amino acid residues in its proteome. For the groups labeled in pink, we considered a *cis*-spliced peptide frequency of ∼15%, as in **Figure 3A**. Viral-human *zwitter* 9mer peptides and HLA-A*02:01-restricted viral-human *zwitter* 9mer epitope candidates are represented with a dot each virus. HLA-A*02:01-restricted viral-human *zwitter* 9mer epitope candidates either using mTEC's RNA-based proteome database (43) or considering the theoretical *cis*-spliced peptide frequency in HLA-I immunopeptidomes are represented with a dot (mean) and bars (SD) of sampling iterations. Regression lines are shown. The Hepatitis delta virus I has an underrepresented number of HLA-A*02:01-restricted viral-human *zwitter* 9mer epitope candidates, which are here labeled.

non-spliced peptides by proteasomes (26, 32, 33). Therefore, not all non-spliced peptides, and even less *cis*-spliced peptides, are likely generated by proteasomes in sufficient amount to be detected *in vitro* by MS as well as to survive all steps of HLA-I APP pathway.

We weighed up the impact of this phenomenon in our computational analysis by gathering information from two experimental dataset sources measured by MS: a large database of non-spliced and spliced peptides produced *in vitro* by purified proteasomes (34) and HLA-I immunopeptidome elutions.

Through the analysis of *in vitro* digestion database (34), we estimated that ∼27% of all theoretical non-spliced 9mer peptides that could be produced by proteasomes are in fact generated in a detectable amount. This figure is much smaller for *cis*-spliced peptides.

The frequency of *cis*-spliced peptides in HLA-I immunopeptidomes is still a controversial topic, with their frequency in HLA-I immunopeptidomes being estimated in a range from 1 to 34%, depending on the method used for their identification (31).

Using these two sets of information, we determined the relative frequency of non-spliced and *cis* spliced peptides generated by proteasomes and presented in HLA-I immunopeptidomes compared to all theoretical non-spliced and *cis*-spliced peptide products; we then implemented it into our model to better estimate viral-human *zwitter* peptide frequency. Based on this new analysis, we randomly selected non-spliced and *cis*-spliced peptides from our viral and human proteome databases, repeated sampling 600 times to reach statistical power and then repeated our entire analysis for each sample (**Figure 1C**).

If we assumed a ∼15% *cis*-spliced peptide frequency in HLA-I immunopeptidomes, over all randomly sampled peptide pools, we identified, on average, a total of 7 HLA-A*02:01-restricted viral-human *zwitter* non-spliced 9mer epitope candidates. They correspond to 0.079% of the pool of HLA-A*02:01-restricted virus non-spliced 9mer peptides. This figure strongly varied from virus to virus. On average of sampling, 6 viruses had at least one HLA-A*02:01-restricted viral-human *zwitter* non-spliced 9mer peptide. No more than 5 epitope candidates per virus were estimated in this analysis (**Figure 4A**). In the same analysis, we identified, on average, a total of 0.3 HLA-A*02:01-restricted viral-human *zwitter cis*-spliced 9mer epitope candidates. They correspond to 0.0008% of the pool of HLA-A*02:01-restricted virus *cis*-spliced 9mer peptides, which is a frequency dramatically smaller than the 3.84% computed without accounting for *cis*-spliced peptide frequency in HLA-I immunopeptidomes (see **Figure 2B**). On average of sampling, only 1 virus had an HLA-A*02:01-restricted viral-human *zwitter cis*-spliced 9mer epitope candidate and no more than 2 epitope candidates per virus were estimated (**Figure 4A**).

Since *cis*-spliced peptide frequencies in HLA-I immunopeptidomes is so controversial, we repeated the non-spliced and *cis*-spliced peptides' sampling and downstream analysis considering a broad range of frequencies of *cis*-spliced peptides in HLA-I immunopeptidomes. As shown in **Figure 4B**, the overall picture did not change much. The average number of HLA-A*02:01-restricted viral-human *zwitter* non-spliced epitope candidates was estimated to be always largely higher than *cis*-spliced epitope candidates. Only few outliers of *cis*-spliced epitope candidates were identified when we assumed very large frequencies of *cis*-spliced peptide in HLA-I immunopeptidomes.

This phenomenon was reflected also in terms of number of viruses that, on average of sampling, had one or more HLA-A*02:01-restricted viral-human *zwitter* epitope candidates. The average number of viruses with one or more HLA-A*02:01-restricted viral-human *zwitter* epitope candidates was only increased by including cis-spliced epitope candidates if we assumed a frequency of *cis*-spliced peptides in HLA-I immunopeptidomes larger than 30% (**Figure 5**).

There are various factors that can impinge upon the number of viral-human *zwitter* epitope candidates that could be derived from a given virus. One of them is the number of amino acid residues present in viral proteomes. The direct correlation between viral-human *zwitter* epitope candidates and the size of virus proteome databases was however stronger if we did not consider the frequencies of *cis*-spliced peptide in HLA-I immunopeptidomes (**Figure 5**, **Supplementary Table 1**). Another factor can be the sequence motifs of viral proteome, which may not favor the presentation of viral-human *zwitter* epitope candidates through a specific HLA-I allele. For example, this is the case of the Hepatitis delta virus I, which has an

underrepresentation of viral-human *zwitter* epitope candidates among those that are predicted to bind HLA-A*02:01 molecules as compared to the total number of its theoretical viral-human *zwitter* peptides (**Figure 6**).

DISCUSSION

Despite proteasome-generated spliced epitopes being known about for more than a decade (61, 63), the potential implications of their presentation by HLA-I complexes only started to concern the scientific community in recent years when we and others showed that spliced peptides represented a sizeable portion of HLA-I immunopeptidomes (28, 36, 38, 42). One of these concerns was the hypothetical impact of spliced peptides on central and peripheral tolerance and on the repertoire of $CD8^+$ T cells recognizing viruses. Indeed, the theoretical substantial sequence variability of *cis*-spliced peptides may strongly increase the number of viral-human *zwitter* epitope candidates, thereby reducing the ability of the $CD8^+$ T cell repertoire able to recognize viruses (7, 64). Here we showed *in silico* evidence that *cis*-spliced peptides might not play such an unsettling role in the central and peripheral tolerance of the $CD8^+$ T cell repertoire. The main reason is that *cis*-spliced peptides produced and presented through APP pathway represent just a tiny fraction of all theoretical *cis*-spliced peptide sequences, as suggested by biochemical and immunopeptidomics studies. According to our preliminary estimations, *zwitter cis*-spliced epitopes would only significantly impinge upon the virus-specific repertoire of $CD8^+$ T cells if we assumed a very large frequency of these unconventional peptides in HLA-I immunopeptidomes. Although, our analysis was restricted to *cis*-spliced epitope candidates with intervening sequence shorter than 26 amino acid residues, which may represent only part of HLA-I spliced immunopeptidomes (36).

Additionally, we should bear in mind that our analysis did not consider two potentially important factors: $CD8^+$ TCR specificity degeneracy and driving forces that can restrict the variety of non-spliced and *cis*-spliced peptides produced by proteasomes.

The former has already been investigated in a seminal work of Calis et al. (17), who focused on non-spliced epitope candidates. Some examples of TCR cross-recognition of pathogen-derived *cis*-spliced and non-spliced epitopes have been already reported (24, 25). However, we think that we would need data on a larger pool of TCRs before accounting for this factor in our model. To note, this aspect would be even more relevant if we wanted to extend this investigation to $CD4^+$ T cell repertoire, bearing in mind that $CD4^+$ TCR degeneracy is more pronounced than in $CD8^+$ T cells, and *trans*-spliced peptides are under the spotlight in type 1 Diabetes (65–68).

The latter factor is the impact that substrate sequences have on both peptide hydrolysis and splicing. Proteasomes can cleave and likely splice after any amino acid, as confirmed by a large database of non-spliced and spliced peptides produced *in vitro* by these enzymes (34). However, peptide sequence motifs seem to impinge upon proteasome dynamics (69) as well as the variety and quantity of non-spliced and *cis*-spliced peptides that they generate (26, 33, 34, 70–72). This factor may reduce the variety of non-spliced and *cis*-spliced peptides that are finally presented through HLA-I complexes to $CD8^+$ T cells, and thus alter the frequency of viral-human *zwitter* epitope candidates.

Finally, in future studies we might also consider the impact that proteasome isoforms might have on the frequency of *zwitter* epitope candidates. Indeed, standard proteasomes, immunoproteasomes and thymoproteasomes seem to have, at least from a quantitative perspective, different dynamics and substrate sequence preferences for both peptide hydrolysis and splicing (27, 33, 55, 56, 59, 69, 70, 73–75). This can impinge upon the proteome and antigenic landscape of both professional APCs and infected cells (28, 76), and ultimately upon central and peripheral tolerance of $CD8^+$ T cells potentially specific for viral-human *zwitter* epitopes.

DATA AVAILABILITY STATEMENT

The datasets presented in this study can be found in online repositories. The names of the repository/repositories and accession number(s) can be found below: A summary of the files accessible via repository is reported in the following Mendeley dataset: http://dx.doi.org/10.17632/hw686hytfs.1. The mTEC's RNA sequencing data published by Pinto et al. (43) are available at Gene Expression Omnibus (GEO) under identifier GSE49625. The single-cell RNA sequencing of TECs in human embryos published by Zeng et al. (44) are available at Gene Expression Omnibus (GEO) under identifier GSE133341.

AUTHOR CONTRIBUTIONS

JL conceived the project. AM implemented the *in silico* pipelines and carried out the data analysis and figure preparation, which were supervised by JL and MM. CRRB identified the epitope candidates reported in **Table 1**. MM critically revised the immunological implication of the study and the project development. MM, JL, AM, and CRRB wrote the manuscript. All authors contributed to the article and approved the submitted version.

FUNDING

This study was in part supported by: (i) MPI-BPC collaboration agreement 2018, Cancer Research UK [C67500; A29686] and National Institute for Health Research (NIHR) Biomedical Research Center based at Guy's and St Thomas' NHS Foundation Trust and King's College London and/or the NIHR Clinical Research Facility to MM. AM was supported by the International Max-Planck Research School (IMPRS) for Genome Sciences.

ACKNOWLEDGMENTS

We thank A.C. Graham (KCL) for proofreading the manuscript.

SUPPLEMENTARY MATERIAL

The Supplementary Material for this article can be found online at: https://www.frontiersin.org/articles/10.3389/fimmu.2021.614276/full#supplementary-material

REFERENCES

1. Huseby E, White J, Crawford F, Vass T, Becker D, Pinilla C, et al. How the T cell repertoire becomes peptide and MHC specific. *Cell*. (2005) 122:247–69. doi: 10.1016/j.cell.2005.05.013
2. Klein L, Kyewski B, Allen PM, Hogquist KA. Positive and negative selection of the T cell repertoire: what thymocytes see (and don't see). *Nat Rev Immunol.* (2014) 14:377–91. doi: 10.1038/nri3667
3. Bouneaud C, Kourilsky P, Bousso P. Impact of negative selection on the T cell repertoire reactive to a self-peptide: a large fraction of T cell clones escapes clonal deletion. *Immunity*. (2000) 13:829–40. doi: 10.1016/S1074-7613(00)00080-7
4. Culina S, Lalanne AI, Afonso G, Cerosaletti K, Pinto S, Sebastiani G, et al. Islet-reactive CD8(+) T cell frequencies in the pancreas, but not in blood, distinguish type 1 diabetic patients from healthy donors. *Sci Immunol.* (2018) 3:eaao4013. doi: 10.1126/sciimmunol.aao4013
5. ElTanbouly MA, Noelle RJ. Rethinking peripheral T cell tolerance: checkpoints across a T cell's journey. *Nat Rev Immunol.* (2020). doi: 10.1038/s41577-020-00454-2. [Epub ahead of print].
6. Yu W, Jiang N, Ebert PJ, Kidd BA, Muller S, Lund PJ, et al. Clonal deletion prunes but does not eliminate self-specific alphabeta CD8(+) T Lymphocytes. *Immunity*. (2015) 42:929–41. doi: 10.1016/j.immuni.2015.05.001
7. Liepe J, Ovaa H, Mishto M. Why do proteases mess up with antigen presentation by re-shuffling antigen sequences? *Curr Opin Immunol.* (2018) 52:81–6. doi: 10.1016/j.coi.2018.04.016
8. Wolfl M, Rutebemberwa A, Mosbruger T, Mao Q, Li HM, Netski D, et al. Hepatitis C virus immune escape via exploitation of a hole in the T cell repertoire. *J Immunol.* (2008) 181:6435–46. doi: 10.4049/jimmunol.181.9.6435
9. Assarsson E, Sidney J, Oseroff C, Pasquetto V, Bui HH, Frahm N, et al. A quantitative analysis of the variables affecting the repertoire of T cell specificities recognized after vaccinia virus infection. *J Immunol.* (2007) 178:7890–901. doi: 10.4049/jimmunol.178.12.7890
10. Croft NP, Smith SA, Pickering J, Sidney J, Peters B, Faridi P, et al. Most viral peptides displayed by class I MHC on infected cells are immunogenic. *Proc Natl Acad Sci USA*. (2019) 116:3112–7. doi: 10.1073/pnas.1815239116
11. Kanduc D, Stufano A, Lucchese G, Kusalik A. Massive peptide sharing between viral and human proteomes. *Peptides*. (2008) 29:1755–66. doi: 10.1016/j.peptides.2008.05.022
12. Kusalik A, Bickis M, Lewis C, Li Y, Lucchese G, Marincola FM, et al. Widespread and ample peptide overlapping between HCV and Homo sapiens proteomes, Peptides, United States. *Peptides*. (2007) 28:1260–7. doi: 10.1016/j.peptides.2007.04.001
13. Ricco R, Kanduc D. Hepatitis B virus and Homo sapiens proteome-wide analysis: a profusion of viral peptide overlaps in neuron-specific human proteins. *Biologics*. (2010) 4:75–81. doi: 10.2147/BTT.S8890
14. Trost B, Kusalik A, Lucchese G, Kanduc D. Bacterial peptides are intensively present throughout the human proteome. *Self Nonself*. (2010) 1:71–4. doi: 10.4161/self.1.1.9588
15. Trost B, Lucchese G, Stufano A, Bickis M, Kusalik A, Kanduc D. No human protein is exempt from bacterial motifs, not even one. *Self Nonself.* (2010) 1:328–34. doi: 10.4161/self.1.4.13315
16. S. Frankild, de Boer RJ, Lund O, Nielsen M, Kesmir C. Amino acid similarity accounts for T cell cross-reactivity and for "holes" in the T cell repertoire. *PLoS ONE*. (2008) 3:e1831. doi: 10.1371/journal.pone.0001831
17. Calis JJ, de Boer RJ, Kesmir C. Degenerate T-cell recognition of peptides on MHC molecules creates large holes in the T-cell repertoire. *PLoS Comput Biol.* (2012) 8:e1002412. doi: 10.1371/journal.pcbi.1002412
18. Ishizuka J, Grebe K, Shenderov E, Peters B, Chen Q, Peng Y, et al. Quantitating T cell cross-reactivity for unrelated peptide antigens. *J Immunol.* (2009) 183:4337–45. doi: 10.4049/jimmunol.0901607
19. Rossjohn J, Gras S, Miles JJ, Turner SJ, Godfrey DI, McCluskey J. T cell antigen receptor recognition of antigen-presenting molecules. *Annu Rev Immunol.* (2015) 33:169–200. doi: 10.1146/annurev-immunol-032414-112334
20. Whalley T, Dolton G, Brown PE, Wall A, Wooldridge L, van den Berg H, et al. GPU-accelerated discovery of pathogen-derived molecular mimics of a T-cell insulin epitope. *Front Immunol.* (2020) 11:296. doi: 10.3389/fimmu.2020.00296
21. Assmus LM, Guan J, Wu T, Farenc C, Sng XYX, Zareie P, et al. Overlapping peptides elicit distinct CD8(+) T cell responses following influenza a virus infection. *J Immunol.* (2020) 205:1731–42. doi: 10.4049/jimmunol.2000689
22. Mishto M, Liepe J. Post-translational peptide splicing and T cell responses. *Trends Immunol.* (2017) 38:904–15. doi: 10.1016/j.it.2017.07.011
23. Platteel ACM, Liepe J, Textoris-Taube K, Keller C, Henklein P, Schalkwijk HH, et al. Multi-level strategy for identifying proteasome-catalyzed spliced epitopes targeted by CD8+ T cells during bacterial infection. *Cell Rep.* (2017) 20:1242–53. doi: 10.1016/j.celrep.2017.07.026
24. Platteel AC, Mishto M, Textoris-Taube K, Keller C, Liepe J, Busch DH, et al. CD8(+) T cells of Listeria monocytogenes-infected mice recognize both linear and spliced proteasome products. *Eur J Immunol.* (2016) 46:1109–18. doi: 10.1002/eji.201545989
25. Paes W, Leonov G, Partridge T, Chikata T, Murakoshi H, Frangou A, et al. Contribution of proteasome-catalyzed peptide cis-splicing to viral targeting by CD8(+) T cells in HIV-1 infection. *Proc Natl Acad Sci USA*. (2019) 116:24748–59. doi: 10.1073/pnas.1911622116
26. Mishto M, Mansurkhodzhaev A, Ying G, Bitra A, Cordfunke RA, Henze S, et al. An in silico-in vitro pipeline identifying an HLA-A(*)02:01(+) KRAS G12V(+) spliced epitope candidate for a broad tumor-immune response in cancer patients. *Front Immunol.* (2019) 10:2572. doi: 10.3389/fimmu.2019.02572
27. Ebstein F, Textoris-Taube K, Keller C, Golnik R, Vigneron N, Van den Eynde BJ, et al. Proteasomes generate spliced epitopes by two different mechanisms and as efficiently as non-spliced epitopes. *Sci Rep.* (2016) 6:24032. doi: 10.1038/srep24032
28. Faridi P, Woods K, Ostrouska S, Deceneux C, Aranha R, Duscharla D, et al. Spliced peptides and cytokine-driven changes in the immunopeptidome of melanoma. *Cancer Immunol Res.* (2020) 8:1322–34. doi: 10.1158/2326-6066.CIR-19-0894
29. Robbins PF, el-Gamil M, Kawakami Y, Stevens E, Yannelli JR, Rosenberg SA. Recognition of tyrosinase by tumor-infiltrating lymphocytes from a patient responding to immunotherapy. *Cancer Res.* (1994) 54:3124–6.
30. Dalet A, Robbins PF, Stroobant V, Vigneron N, Li YF, El-Gamil M, et al. An antigenic peptide produced by reverse splicing and double asparagine deamidation. *Proc Natl Acad Sci USA*. (2011) 108:E323–31. doi: 10.1073/pnas.1101892108
31. Mishto M. What we see, what we do not see and what we do not want to see in HLA class I Immunopeptidomes. *Proteomics*. (2020). doi: 10.1002/pmic.202000112. [Epub ahead of print].
32. Berkers CR, de Jong A, Schuurman KG, Linnemann C, Meiring HD, Janssen L, et al. Definition of proteasomal peptide splicing rules for high-efficiency spliced peptide presentation by MHC class i molecules. *J Immunol.* (2015) 195:4085–95. doi: 10.4049/jimmunol.1402455
33. Mishto M, Goede A, Taube KT, Keller C, Janek K, Henklein P, et al. Driving forces of proteasome-catalyzed peptide splicing in yeast and humans. *Mol Cell Proteomics*. (2012) 11:1008–23. doi: 10.1074/mcp.M112.020164
34. Specht G, Roetschke HP, Mansurkhodzhaev A, Henklein P, Textoris-Taube K, Urlaub H, et al. Large database for the analysis and prediction of spliced and non-spliced peptide generation by proteasomes. *Sci Data*. (2020) 7:146. doi: 10.1038/s41597-020-0487-6
35. Dalet A, Vigneron N, Stroobant V, Hanada K, Van den Eynde BJ. Splicing of distant Peptide fragments occurs in the proteasome by transpeptidation and produces the spliced antigenic peptide derived from fibroblast growth factor-5. *J Immunol.* (2010) 184:3016–24. doi: 10.4049/jimmunol.0901277
36. Faridi P, Li C, Ramarathinam SH, Vivian JP, Illing PT, Mifsud NA, et al. A subset of HLA-I peptides are not genomically templated: evidence for cis- and trans-spliced peptide ligands. *Sci Immunol.* (2018) 3:eaar3947. doi: 10.1126/sciimmunol.aar3947
37. Peters B, Sette A. Generating quantitative models describing the sequence specificity of biological processes with the stabilized matrix method. *BMC Bioinformatics*. (2005) 6:132. doi: 10.1186/1471-2105-6-132

38. Liepe J, Marino F, Sidney J, Jeko A, Bunting DE, Sette A, et al. A large fraction of HLA class I ligands are proteasome-generated spliced peptides. *Science.* (2016) 354:354–358. doi: 10.1126/science.aaf4384
39. Peters B, Tong W, Sidney J, Sette A, Weng, Z. Examining the independent binding assumption for binding of peptide epitopes to MHC-I molecules. *Bioinformatics.* (2003) 2003:1765–72. doi: 10.1093/bioinformatics/btg247
40. Hulo C, Castro E, Masson P, Bougueleret L., Bairoch A, Xenarios I, et al. ViralZone: a knowledge resource to understand virus diversity. *Nucleic Acids Res.* (2011) 39:D576–82. doi: 10.1093/nar/gkq901
41. Bairoch A, Apweiler R. The SWISS-PROT protein sequence data bank and its supplement TrEMBL in 1999. *Nucleic Acids Res.* (1999) 27:49–54. doi: 10.1093/nar/27.1.49
42. Liepe J, Sidney J, Lorenz FKM, Sette A, Mishto M. Mapping the MHC class I-spliced immunopeptidome of cancer cells. *Cancer Immunol Res.* (2019) 7:62–76. doi: 10.1158/2326-6066.CIR-18-0424
43. Pinto S, Michel C, Schmidt-Glenewinkel H, Harder N, Rohr K, Wild S, et al. Overlapping gene coexpression patterns in human medullary thymic epithelial cells generate self-antigen diversity. *Proc Natl Acad Sci USA.* (2013) 110:E3497–505. doi: 10.1073/pnas.1308311110
44. Zeng Y, Liu C, Gong Y, Bai Z, Hou S, He J, et al. Single-cell RNA sequencing resolves spatiotemporal development of pre-thymic lymphoid progenitors and thymus organogenesis in human embryos. *Immunity.* (2019) 51:930–48 e6. doi: 10.1016/j.immuni.2019.09.008
45. Weinzierl AO, Lemmel C, Schoor O, Muller M, Kruger T, Wernet D, et al. Distorted relation between mRNA copy number and corresponding major histocompatibility complex ligand density on the cell surface. *Mol Cell Proteomics.* (2007) 6:102–13. doi: 10.1074/mcp.M600310-MCP200
46. Pearson H, Daouda T, Granados DP, Durette C, Bonneil E, Courcelles M, et al. MHC class I-associated peptides derive from selective regions of the human genome. *J Clin Invest.* (2016) 126:4690–701. doi: 10.1172/JCI88590
47. Satija R, Farrell JA, Gennert D, Schier AF, Regev A. Spatial reconstruction of single-cell gene expression data. *Nat Biotechnol.* (2015) 33:495–502. doi: 10.1038/nbt.3192
48. Stuart T, Butler A, Hoffman P, Hafemeister C, Papalexi E, Mauck W. Comprehensive integration of single-cell data. *Cell.* (2019) 177:1888–902. doi: 10.1016/j.cell.2019.05.031
49. Perez CL, Larsen MV, Gustafsson R, Norstrom MM, Atlas A, Nixon DF, et al. Broadly immunogenic HLA class I supertype-restricted elite CTL epitopes recognized in a diverse population infected with different HIV-1 subtypes. *J Immunol.* (2008) 180:5092–100. doi: 10.4049/jimmunol.180.7.5092
50. Ogishi M, Yotsuyanagi H. Quantitative prediction of the landscape of T cell epitope immunogenicity in sequence space. *Front Immunol.* (2019) 10:827. doi: 10.3389/fimmu.2019.00827
51. Molero-Abraham M, Lafuente EM, Reche P. Customized predictions of peptide-MHC binding and T-cell epitopes using EPIMHC. *Methods Mol Biol.* (2014) 1184:319–32. doi: 10.1007/978-1-4939-1115-8_18
52. Waterhouse A, Bertoni M, Bienert S, Studer G, Tauriello G, Gumienny R, et al. SWISS-MODEL: homology modelling of protein structures and complexes. *Nucleic Acids Res.* (2018) 46:W296–303. doi: 10.1093/nar/gky427
53. Chapiro J, Claverol S, Piette F, Ma W, Stroobant V, Guillaume B, et al. Destructive cleavage of antigenic peptides either by the immunoproteasome or by the standard proteasome results in differential antigen presentation. *J Immunol.* (2006) 176:1053–61. doi: 10.4049/jimmunol.176.2.1053
54. Deol P, Zaiss DM, Monaco JJ, Sijts AJ. Rates of processing determine the immunogenicity of immunoproteasome-generated epitopes. *J Immunol.* (2007) 178:7557–62. doi: 10.4049/jimmunol.178.12.7557
55. Guillaume B, Chapiro J, Stroobant V, Colau D, Van Holle B, Parvizi G, et al. Two abundant proteasome subtypes that uniquely process some antigens presented by HLA class I molecules. *Proc Natl Acad Sci USA.* (2010) 107:18599–604. doi: 10.1073/pnas.1009778107
56. Guillaume B, Stroobant V, Bousquet-Dubouch MP, Colau D, Chapiro J, Parmentier N, et al. Dalet, and B.J. *Van den Eynde, Analysis of the processing of seven human tumor antigens by intermediate proteasomes. J Immunol.* (2012) 189:3538–47. doi: 10.4049/jimmunol.1103213
57. Tenzer S, Wee E, Burgevin A, Stewart-Jones G, Friis L, Lamberth K, et al. Antigen processing influences HIV-specific cytotoxic T lymphocyte immunodominance. *Nat Immunol.* (2009) 10:636–46. doi: 10.1038/ni.1728
58. Zanker D, Waithman J, Yewdell JW, Chen W. Mixed proteasomes function to increase viral peptide diversity and broaden antiviral CD8+ T cell responses. *J Immunol.* (2013) 191:52–9. doi: 10.4049/jimmunol.1300802
59. Dalet A, Stroobant V, Vigneron N, Van den Eynde BJ. Differences in the production of spliced antigenic peptides by the standard proteasome and the immunoproteasome. *Eur J Immunol.* (2011) 41:39–46. doi: 10.1002/eji.201040750
60. Michaux A, Larrieu P, Stroobant V, Fonteneau JF, Jotereau F, Van den Eynde BJ, et al. A spliced antigenic peptide comprising a single spliced amino acid is produced in the proteasome by reverse splicing of a longer peptide fragment followed by trimming. *J Immunol.* (2014) 192:1962–71. doi: 10.4049/jimmunol.1302032
61. Vigneron N, Stroobant V, Chapiro J, Ooms A, Degiovanni G, Morel S, et al. An antigenic peptide produced by peptide splicing in the proteasome. *Science.* (2004) 304:587–90. doi: 10.1126/science.1095522
62. Warren EH, Vigneron NJ, Gavin MA, Coulie PG, Stroobant V, Dalet A, et al. An antigen produced by splicing of noncontiguous peptides in the reverse order. *Science.* (2006) 313:1444–7. doi: 10.1126/science.1130660
63. Hanada K, Yewdell JW, Yang JC. Immune recognition of a human renal cancer antigen through post-translational protein splicing. *Nature.* (2004) 427:252–6. doi: 10.1038/nature02240
64. Grignolio A, Mishto M, Faria AM, Garagnani P, Franceschi C, Tieri P. Towards a liquid self: how time, geography, and life experiences reshape the biological identity. *Front Immunol.* (2014) 5:153. doi: 10.3389/fimmu.2014.00153
65. Arribas-Layton D, Guyer P, Delong T, Dang M, Chow IT, Speake C, et al. Hybrid insulin peptides are recognized by human T cells in the context of DRB1*04:01. *Diabetes.* (2020) 69:1492–502. doi: 10.2337/db19-0620
66. Babon JA, DeNicola ME, Blodgett DM, Crevecoeur I, Buttrick TS, Maehr R, et al. Analysis of self-antigen specificity of islet-infiltrating T cells from human donors with type 1 diabetes. *Nat Med.* (2016) 22:1482–7. doi: 10.1038/nm.4203
67. Wang Y, Sosinowski T, Novikov A, Crawford F, White J, Jin N, et al. How C-terminal additions to insulin B-chain fragments create superagonists for T cells in mouse and human type 1 diabetes. *Sci Immunol.* (2019) 4:eaav7517. doi: 10.1126/sciimmunol.aav7517
68. Delong T, Wiles TA, Baker RL, Bradley B, Barbour G, Reisdorph R, et al. Pathogenic CD4 T cells in type 1 diabetes recognize epitopes formed by peptide fusion. *Science.* (2016) 351:711–4. doi: 10.1126/science.aad2791
69. Liepe J, Holzhutter HG, Bellavista E, Kloetzel PM, Stumpf MP, Mishto M. Quantitative time-resolved analysis reveals intricate, differential regulation of standard- and immuno-proteasomes. *Elife.* (2015) 4:e07545. doi: 10.7554/eLife.07545
70. Mishto M, Liepe J, Textoris-Taube K, Keller C, Henklein P, Weberruss M, et al. Proteasome isoforms exhibit only quantitative differences in cleavage and epitope generation. *Eur J Immunol.* (2014) 44:3508–21. doi: 10.1002/eji.201444902
71. Textoris-Taube K, Keller C, Liepe J, Henklein P, Sidney J, Sette A, et al. The T210M substitution in the HLA-a*02:01 gp100 epitope strongly affects overall proteasomal cleavage site usage and antigen processing. *J Biol Chem.* (2015) 290:30417–28. doi: 10.1074/jbc.M115.695189
72. Toes RE, Nussbaum AK, Degermann S, Schirle M, Emmerich NP, Kraft M, et al. Discrete cleavage motifs of constitutive and immunoproteasomes revealed by quantitative analysis of cleavage products. *J Exp Med.* (2001) 194:1–12. doi: 10.1084/jem.194.1.1
73. Dianzani C, Vecchio D, Clemente N, Chiocchetti A, Martinelli Boneschi F, Galimberti D, et al. Untangling extracellular proteasome-osteopontin circuit dynamics in multiple sclerosis. *Cells.* (2019) 8:262. doi: 10.3390/cells8030262

74. Kuckelkorn U, Stubler S, Textoris-Taube K, Kilian C, Niewienda A, Henklein P, et al. Proteolytic dynamics of human 20S thymoproteasome. *J Biol Chem.* (2019) 294:7740–54. doi: 10.1074/jbc.RA118.007347
75. Fabre B, Lambour T, Garrigues L, Amalric F, Vigneron N, Menneteau T, et al. Deciphering preferential interactions within supramolecular protein complexes: the proteasome case. *Mol Syst Biol.* (2015) 11:771. doi: 10.15252/msb.20145497
76. Apavaloaei A, Brochu S, Dong M, Rouette A, Hardy MP, Villafano G, et al. PSMB11 orchestrates the development of CD4 and CD8 thymocytes via regulation of gene expression in cortical thymic epithelial cells. *J Immunol.* (2019) 202:966–78. doi: 10.4049/jimmunol.1801288

Conflict of Interest: The authors declare that the research was conducted in the absence of any commercial or financial relationships that could be construed as a potential conflict of interest.

frontiers in Immunology

MINI REVIEW
published: 25 February 2021
doi: 10.3389/fimmu.2021.628429

The Macroautophagy Machinery in MHC Restricted Antigen Presentation

*Christian Münz**

Viral Immunobiology, Institute of Experimental Immunology, University of Zürich, Zürich, Switzerland

Autophagy-related (ATG) gene products regulate macroautophagy, LC3-associated phagocytosis (LAP) and LC3-dependent extracellular vesicle loading and secretion (LDELS). These processes also influence antigen processing for presentation on major histocompatibility complex (MHC) molecules to T cells. Here, I summarize how these different pathways use the macroautophagy machinery, contribute to MHC class I and II restricted antigen presentation and influence autoimmunity, tumor immunology and immune control of infectious diseases. Targeting these different pathways should allow the regulation of intracellular and extracellular antigen presentation to T cells to modulate protective and pathological immune responses.

Keywords: cytotoxic CD8$^+$ T cells, helper CD4$^+$ T cells, cross-presentation, LC3-associated phagocytosis, exocytosis

OPEN ACCESS

Edited by:
Luis C. Anton, Consejo Superior de Investigaciones Científicas (CSIC), Spain

Reviewed by:
Ludger Klein, Ludwig Maximilian University of Munich, Germany
Heung Kyu Lee, Korea Advanced Institute of Science and Technology, South Korea
Payel Sil, National Institute of Environmental Health Sciences (NIEHS), United States

***Correspondence:**
Christian Münz
christian.muenz@uzh.ch

Specialty section:
This article was submitted to Antigen Presenting Cell Biology, a section of the journal Frontiers in Immunology

Received: *11 November 2020*
Accepted: *18 January 2021*
Published: *25 February 2021*

Citation:
Münz C (2021) The Macroautophagy Machinery in MHC Restricted Antigen Presentation. Front. Immunol. 12:628429. doi: 10.3389/fimmu.2021.628429

THE MACROAUTOPHAGY MACHINERY

Yoshinori Ohsumi described in a landmark paper in 1993 15 genes that are required in yeast to survive starvation (1). These formed the core of the more than 40 autophagy-related proteins that regulate macroautophagy, one of at least three pathways by which cytoplasmic constituents are imported into lysosomes for degradation (2). This machinery consists of a protein kinase complex, a lipid kinase complex, enzymes that couple ubiquitin-like molecules to membranes and recruit substrates to them, as well as a fusion machinery that delivers the result of the first three complexes, a double-membrane surrounded autophagosome, to lysosomes for the degradation of the cargo and the inner membrane of autophagosomes (**Figure 1**). Many of the molecular components of this machinery are abbreviated as ATG (autophagy-related) proteins. The protein kinase complex of ATG1/ULK1 gets inhibited by mammalian target of rapamycin complex 1 (mTORC1) and activated by AMP kinase (AMPK) *via* differential phosphorylation. This allows eukaryotic cells to initiate macroautophagy upon nutrient deprivation. The ATG1/ULK1 complex then phosphorylates itself and components of all stages of autophagosome maturation and degradation (3). However, one of its main targets is the VPS34 phosphatidylinositol 3 (PI3) kinase complex containing ATG6/Beclin-1. This complex generates the phospholipid PI3P that recruits the ATG8/LC3B lipidation machinery to membranes *via* WIPI proteins, predominantly WIPI2. The ATG8/LC3B lipidation machinery consists of the E1-like enzyme ATG7. The E2-like enzymes ATG3 and 10, and the E3-like enzyme ATG5-ATG12-ATG16L1 that finally couples the six mammalian ATG8 orthologues LC3A, LC3B, LC3C, GABARAP, GABARAP-L1, and GABARAP-L2 primarily to phosphatidylethanolamine (PE) in the forming autophagosome that is called isolation membrane or phagophore. Attached to the phagophore membrane these ATG8 orthologues assist in membrane fusion during phagophore extension by ATG9 containing vesicles and ATG2 mediated lipid transfer

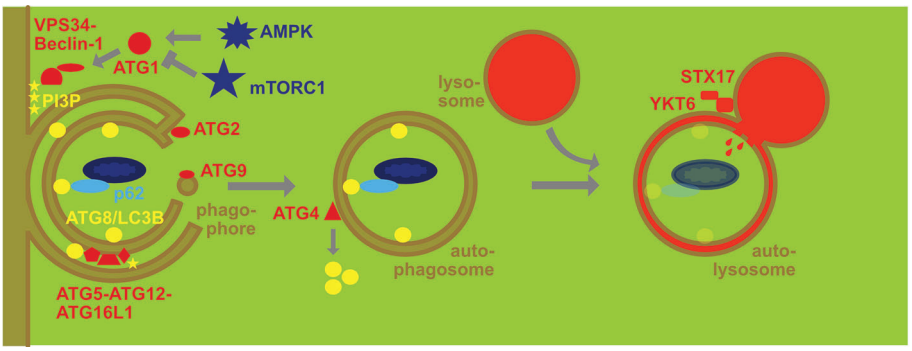

FIGURE 1 | Molecular machinery of macroautophagy. The protein kinase ATG1/ULK1 is activated by AMP kinase (AMPK) and inhibited by mammalian target of rapamycin complex 1 (mTORC1). It then activates the lipid kinase complex containing VPS34 and Beclin-1 to generate phosphatidylinositol-3-phosphate (PI3P) that then recruits the ATG8/LC3B lipidation complex ATG5-ATG12-ATG16L1 that couples ATG8/LC3B to phosphatidylethanolamine at the inner and outer membrane of the phagophore. Membranes are donated to the phagophore *via* ATG2 associated channels and ATG9 carrying vesicles. Once this double membrane closes around cargo that is recruited by macroautophagy receptors like p62 *via* binding to ATG8/LC3 to form an autophagosome ATG4 recycles ATG8/LC3B from the outer membrane. The autophagosome fuses then with late endosomes and lysosomes in a syntaxin 17 (STX17) and YKT6 dependent fashion for degradation of the cargo and the inner autophagosome membrane with coupled ATG8/LC3B.

(4–6). Prior to their lipidation the ATG8 orthologues need to be processed by the ATG4 proteases (ATG4A-D in higher eukaryotes) that also remove them from the outer membrane upon autophagosomes completion (7). The ATG8 orthologues also serve as anchors to recruit macroautophagy cargo to phagophores. Proteins with LC3-interacting regions (LIRs) bind to ATG8 orthologues and then the phagophore grows around the respective cargo, including damaged mitochondria, chloroplasts, ribosomes, proteasomes, endoplasmic reticulum, protein aggregates, damaged endosomes, bacteria, and some viral capsids. These LIR containing autophagy receptors, like sequestosome 1/p62 or NBR1 that cross-link for example ubiquitinated cytoplasmic constituents with LC3B (8). After removal of most lipidated ATG8 orthologues from the outer membrane of the completed autophagosome, residual autophagy receptor binding at this site supports autophagosome transport along microtubules and recruitment of the fusion machinery with lysosomes or late endosomes (9, 10). Finally, the soluble N-ethylmaleimide-sensitive-factor attachment receptors (SNAREs) syntaxin 17 and YKT6 are required for autophagosome fusion with lysosomes (11, 12). In the resulting autolysosome macroautophagy substrates and the inner autophagosomal membrane are degraded by lysosomal hydrolases. Therefore, macroautophagic flux is coupled to lysosomal activity and transcriptionally linked to transcription factor EB (TFEB) the master transcription factor of lysosomal biogenesis (13). The resulting molecular building blocks of lysosomal degradation, including amino acids, nucleic acids, sugars, and phospholipids are then recycled for energy generation and synthesis of new macromolecules to survive periods of starvation. Once such a catabolic machinery is in place it can be used for a multitude of other cellular processes, including degradation of pathogens, regulation of intercellular communication like inflammation and immune cell activation. In this review I will focus on its role in antigen presentation on major histocompatibility complex (MHC) molecules to T cells which utilizes proteolytic product display on MHC molecules at the cell surface.

MACROAUTOPHAGY IN MHC CLASS II RESTRICTED ANTIGEN PRESENTATION

The two classes of classical MHC molecules monitor different proteolytic machineries in cells by sampling a subset of these that they then transport to the cell surface for T cell stimulation (14–16). Pathogen-derived or otherwise foreign peptides can then be recognized by the T cell repertoire that has been tolerized against self-peptides. MHC class I molecules present primarily products of proteasomal degradation that are then imported *via* the transporter associated with antigen presentation (TAP) into the endoplasmic reticulum and loaded in the MHC-I peptide-loading complex (17). After transport to the cell surface MHC class I molecules and their presented mostly nonameric peptides are then screened by cytotoxic $CD8^+$ T cells. In contrast MHC class II molecules are loaded with usually longer peptides but a nonameric core sequence in MHC class II containing compartments (MIICs) which are late endosomes with lysosomal proteolytic capacity. MHC class II molecules are transported to MIICs as complexes with the invariant chain (Ii) that is then degraded and peptides loaded with the assistance of HLA-DM (H2-M in mice) onto MHC class II molecules (18). MHC class II molecules with their bound peptide ligands then migrate to the cell surface for surveillance by helper $CD4^+$ T cells.

MHC class II restricted antigen presentation monitors therefore lysosomal proteolysis which degrades both endocytosed proteins and macroautophagy substrates (**Figure 2**). Indeed 20-30% of MHC class II ligands originate from cytosolic and nuclear sources, including the three ATG8 orthologues LC3B, GABARAP and GABARP-L2 (19, 20). MHC class II presentation of cytoplasmic constituents after macroautophagy was indeed

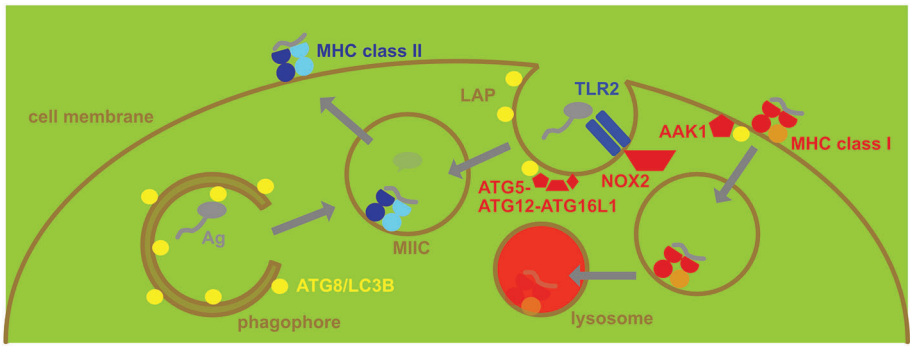

FIGURE 2 | Regulation of MHC presentation by the macroautophagy machinery. MHC class II gets loaded with peptides in MHC class II containing vesicles (MIICs). They receive antigens (Ag) from intracellular sources *via* macroautophagy and from extracellular sources *via* phagocytosis, including LC3-associated phagocytosis (LAP). LAP recruits ATG8/LC3B to the phagosomal membrane after for example TLR2 engagement and is dependent on NADPH oxidase 2 (NOX2). The ATG8/LC3B lipidation complex of ATG5-ATG12-ATG16L1 conjugates ATG8/LC3B to the cytosolic side of phagosomes that then deliver the endocytosed antigen to MIICs. In contrast MHC class I restricted antigen presentation is restricted by the macroautophagy machinery, supporting MHC class I internalization and lysosomal degradation. Adaptor associated kinase 1 (AAK1) is recruited to MHC class I molecules for the respective internalization.

initially demonstrated for three pathogen derived antigens, namely the nuclear antigen 1 of the Epstein Barr virus, bacterial neomycin phosphotransferase II (NeoR) and Ag85B of Mycobacterium tuberculosis (21–24). Processing of antigens for MHC class II presentation by macroautophagy can also be demonstrated by targeting them to phagophores *via* N-terminal conjugation to LC3B (25). This increases intracellular antigen presentation on MHC class II, but not MHC class I molecules. Furthermore, LC3B can be found in MIICs (25, 26). Enhanced presentation of antigens on MHC class II molecules after macroautophagy targeting has now been demonstrated for viral and tumor proteins (25, 27–30). The above listed studies demonstrate that macroautophagy contributes to antigen processing for MHC class II presentation in a variety of cell types, including B cells (19, 21, 22), epithelial cells (25), melanocytes (29) and myeloid antigen presenting cells (24, 28, 30). Therefore, MHC class II molecules can sample cytoplasmic antigens of pathogens for presentation *via* macroautophagy.

Possibly even more important, however, is the role of this pathway for $CD4^+$ T cell tolerance induction. This tolerance induction requires in part MHC class II presentation by epithelial cells without significant phagocytic activity, such as thymic epithelial cells (TECs) (31). Medullary TECs (mTECs) express tissue-restricted self-antigens (TRAs) under the influence of the autoimmune regulator (AIRE). The intracellular expression of these TRAs leads to negative selection of autoimmune $CD4^+$ T cell clones in the thymus to ensure tolerance of the T cell repertoire against self. It was shown that macroautophagy deficient thymi were not able to sufficiently perform this negative selection, resulting in colitis and multi-organ inflammation in mice (32). Moreover, this primarily affected antigens that are endogenously expressed at low levels and cannot be efficiently transferred to neighboring cells for uptake, as is the case for most TRA expression in mTECs (33). As for the pathogen derived antigens, targeting of these to phagophores *via* N-terminal conjugation to LC3B led to improved negative selection of $CD4^+$ T cells. These findings suggest that efficient negative selection by TRAs in the thymus requires macroautophagy. Furthermore, regulatory $CD4^+$ T cell stability in the periphery seems also to benefit from macroautophagy in dendritic cells (DCs) (34). However, this might not only depend on its role in endogenous self-antigen presentation on MHC class II molecules, but rather on a role of ATGs in co-stimulatory molecule expression. Nevertheless, macroautophagy can process cytoplasmic proteins for MHC class II presentation to $CD4^+$ T cells and this seems particularly important for self-antigens that are expressed at low levels by cells with limited phagocytic potential in order to induce tolerance against these.

LC3 ASSOCIATED PHAGOCYTOSIS IN MHC CLASS II RESTRICTED ANTIGEN PRESENTATION

In addition it was, however, already noted in the first study that abolished ATG5 expression in DCs to study the influence of the macroautophagy machinery on MHC restricted antigen presentation and T cell responses *in vivo* that also extracellular antigen presentation to $CD4^+$ T cells benefits from ATGs (35). Indeed, apart from the ATG1/ULK1 protein kinase complex the other components of the macroautophagy machinery also regulate phagocytosis. This was coined LC3-associated phagocytosis (LAP) (**Figure 2**), and the respective LC3B conjugation to the cytosolic side of phagosomes is primarily observed after co-engagement of pathogen associated molecular pattern receptors, such as toll-like receptor (TLR) 2, during uptake of extracellular material (36–40). During LAP, PI3P is deposited in a VPS34 dependent manner at the cytosolic side of phagosomes (41). This might be required to assemble efficiently NADPH oxidase (NOX2) at these phagosomes (42) and NOX2 mediated reactive oxygen species (ROS) production is required

for LAP (37, 41, 43). The exact role of this ROS production is unclear to date, but the recruitment of the ATG8/LC3B lipidation seems to neither depend on ROS not PI3P at phagosomes (44). Instead it depends on the WD40 domain of ATG16L1 that is not required for macroautophagy (44, 45). The ATG16L1 dependent conjugation of LC3B to the cytosolic side of phagosomes is then removed prior to fusion with lysosomes as was observed by live cell imaging (36, 37). Dependent on the cell type LAP leads to accelerated fusion with lysosomes, delayed phagosome maturation or redirection of phagocytosed cargo to TLR containing endosomes (36, 37, 46). This probably depends on the recruitment of different vesicular transport factors to LAP phagosomes in different cellular backgrounds.

Nevertheless, in both human and mouse phagocytes LAP supports MHC class II presentation of endocytosed antigens (37, 39, 44, 47, 48). Since yeast cell wall components efficiently engage TLR2 Zymosan and Candida albicans spores or extracts were often used in these assays, and MHC class II presentation to Candida specific Th17 cells was monitored (37, 39). Phagocytosed Candida antigen presentation on MHC class II molecules to Th17 cells requires ATG5, ATG16L1 and more specifically the WD40 domain of ATG16L1 (37, 39, 44). Bacterial outer membrane vesicles (OMVs) might also be processed *via* this LAP for regulatory $CD4^+$ T cell stimulation (49). In addition to TLR mediated LAP induction it was also described that B cell stimulation activates ATG1/ULK1 independent use of the macroautophagy machinery (50). Accordingly, B cell receptor (BCR) mediated antigen uptake was found to use the ATG8/LC3B lipidation machinery (51, 52). This allows BCR bound antigens to be delivered to TLR containing endosomes and to MIICs for antigen processing towards MHC class II presentation. Finally, myelin autoantigen presentation by DCs in the central nervous system (CNS) also depends on ATG5 and NOX2 as hallmarks of LAP, even so the receptor that mediates LC3B recruitment to phagocytosed oligodendrocyte derived apoptotic blebs has not been identified yet (47, 48). However, in mouse macrophages the phosphatidylserine binding scavenger receptor TIM4 was found to be involved in the clearance of apoptotic bodies by LAP (38). Thus, LAP supports autoimmune $CD4^+$ T cell stimulation in the CNS for experimental autoimmune encephalomyelitis (EAE) development.

Therefore, ATG proteins support both intracellular and extracellular antigen presentation on MHC class II molecules to $CD4^+$ T cells *via* macroautophagy and LAP, respectively.

REGULATION OF MHC CLASS I RESTRICTED ANTIGEN PRESENTATION BY THE MACROAUTOPHAGY MACHINERY

In contrast to the support of MHC class II restricted antigen presentation by the macroautophagy machinery, loss of ATGs leads to up-regulation of MHC class I restricted presentation of intracellular antigens (53–57). This affects both classical MHC class I molecules and the non-classical MHC class I molecule CD1D that restricts glycolipid presentation to NKT cells. In these studies it was found that the stimulation of anti-viral, anti-tumor and alloreactive $CD8^+$ T cell responses as well as anti-bacterial NKT cell immunity is enhanced in the absence of ATG3, ATG5, ATG7 or ATG16L1 (53–56). Higher classical and non-classical MHC class I expression on the surface of DCs and pancreatic carcinoma cells is at least in part responsible for this increased stimulation (54–56). This elevated surface expression of MHC class I molecules seems to be due to MHC class I targeting for lysosomal degradation by ATG proteins (**Figure 2**). In DCs this seems to be due to increased internalization and then degradation with the support of the macroautophagy machinery (54, 56). The identification of the adaptor associated kinase 1 (AAK1) and the adaptor complex AP2 point towards ATG proteins supporting clathrin mediated endocytosis (54, 56). This is reminiscent of the internalization of the amyloid precursor protein (APP) in Alzheimer's disease that was reported to require LC3 mediated recruitment of AP2 for efficient clathrin mediated turn-over (58, 59). In contrast in pancreatic carcinoma cells an NBR1 dependency of MHC class I degradation was observed and the authors suggested that macroautophagy of ER might redirect MHC class I molecules to lysosomes and therefore diminish surface expression for $CD8^+$ T cell stimulation (55). In both instances, deficiencies in the macroautophagy machinery, however, increase anti-viral (influenza and lymphocytic choriomeningitis virus) and anti-tumor $CD8^+$ T cell responses *via* increased surface expression of MHC class I molecules. Lysosomal degradation of MHC class I molecules by the macroautophagy machinery seems to be also induced by ORF8 of the severe acute respiratory syndrome coronavirus 2 (SARS-CoV-2) (60). Moreover, autophagy inhibition can also redirect intracellular antigen degradation to proteasomes leading to increased MHC class I antigen presentation (57). Therefore, multiple pathways might account for increased MHC class I presentation of intracellular antigens by both somatic cells, such as tumor cells, and antigen presenting cells upon inhibition of the macroautophagy machinery.

With respect to extracellular antigen processing for MHC class I presentation, so called cross-presentation, the contribution of the macroautophagy machinery is not entirely clear yet. So far only soluble proteins have been described to benefit from the macroautophagy machinery in cross-presenting classical type 1 DCs and B cells (61, 62). However, long-term storage of antigen by DCs for cross-presentation was rather compromised by the macroautophagy machinery (63). Another function for antigen cross-presentation on MHC class I molecules was described for the macroautophagy machinery in antigen donor cells like virus-infected stromal or tumor cells (64, 65). In these studies, exocytosis of antigen containing vesicles that get efficiently cross-presented for $CD8^+$ T cell stimulation by DCs seemed to benefit from the macroautophagy machinery. The packaging of antigens into the respective vesicles was improved by inhibiting both proteasomal and lysosomal degradation in the antigen donor cells (66–70). The respective pathway that utilizes the ATG8/LC3B lipidation machinery for cross-presentable vesicle export could be overlapping or identical to LC3-dependent extracellular vesicle loading and secretion (LDELS) (71–76). Potentially more

than one exocytosis pathway seems to benefit from the macroautophagy machinery and neutral sphingomyelinase 2 (nSMase2) or Golgi reassembly stacking proteins (GRASPs) have been reported to be involved in this ATG supported exocytosis. Thus, extracellular antigen processing for MHC class I presentation seems to benefit from a functional macroautophagy machinery in both antigen donor cells and for short-term cross-presentation of certain antigen formulations also in antigen presenting cells, while the autophagic machinery limits MHC class I surface expression for intracellular antigen presentation.

CONCLUSIONS AND FUTURE PERSPECTIVES

Lysosomal and proteasomal protein degradation are the two main proteolytic machineries of cells and their products sampled by MHC class II and I molecules for $CD4^+$ and $CD8^+$ T cell stimulation, respectively. Accordingly, macroautophagy as a component of lysosomal degradation, targeting cytoplasmic constituents, supports MHC class II restricted antigen presentation to helper $CD4^+$ T cells. Recent years have, however, demonstrated that the same molecular machinery that supports macroautophagy also regulates endocytosis and exocytosis. While the role of ATG proteins in endocytosis seems to promote MHC class II presentation of phagocytosed antigens *via* LAP and inhibit MHC class I presentation of intracellular antigens through lysosomal degradation of MHC class I plus peptide complexes, exocytosis might package antigens optimally for processing onto MHC class I molecules during cross-presentation. Since not all modules of the macroautophagy machinery are used in all these pathways, regulation of specific ATG proteins in antigen donor or presenting cells might be used to influence MHC class I or II presentation in the tumor microenvironment or during viral infections. However, which manipulation might be beneficial in which setting needs to be determined on a case by case basis, considering, in addition to the role of the macroautophagy machinery for MHC restricted antigen presentation, also its anti-inflammatory role in myeloid cells and its pro-survival role in lymphocytes as well as in virus infected and tumor cells.

AUTHOR CONTRIBUTIONS

The author confirms being the sole contributor of this work and has approved it for publication.

FUNDING

My research is supported by Cancer Research Switzerland (KFS-4091-02-2017 and KFS-4962-02-2020), KFSP-Precision^{MS} and HMZ ImmunoTargET of the University of Zurich, the Cancer Research Center Zurich, the Vontobel Foundation, the Baugarten Foundation, the Sobek Foundation, the Swiss Vaccine Research Institute, Roche, Novartis and the Swiss National Science Foundation (310030B_182827, 310030L_197952/1, and CRSII5_180323).

REFERENCES

1. Tsukada M, Ohsumi Y. Isolation and characterization of autophagy-defective mutants of Saccharomyces cerevisiae. *FEBS Lett* (1993) 333:169–74. doi: 10.1016/0014-5793(93)80398-E
2. Mizushima N, Yoshimori T, Ohsumi Y. The Role of Atg Proteins in Autophagosome Formation. *Annu Rev Cell Dev Biol* (2011) 27:107–32. doi: 10.1146/annurev-cellbio-092910-154005
3. Hu Z, Raucci S, Jaquenoud M, Hatakeyama R, Stumpe M, Rohr R, et al. Multilayered Control of Protein Turnover by TORC1 and Atg1. *Cell Rep* (2019) 28:3486–96.e6. doi: 10.1016/j.celrep.2019.08.069
4. Nakatogawa H, Ichimura Y, Ohsumi Y. Atg8, a ubiquitin-like protein required for autophagosome formation, mediates membrane tethering and hemifusion. *Cell* (2007) 130:165–78. doi: 10.1016/j.cell.2007.05.021
5. Osawa T, Kotani T, Kawaoka T, Hirata E, Suzuki K, Nakatogawa H, et al. Atg2 mediates direct lipid transfer between membranes for autophagosome formation. *Nat Struct Mol Biol* (2019) 26:281–8. doi: 10.1038/s41594-019-0203-4
6. Matoba K, Kotani T, Tsutsumi A, Tsuji T, Mori T, Noshiro D, et al. Atg9 is a lipid scramblase that mediates autophagosomal membrane expansion. *Nat Struct Mol Biol* (2020) 27:1185–93. doi: 10.1038/s41594-020-00538-6
7. Maruyama T, Noda NN. Autophagy-regulating protease Atg4: structure, function, regulation and inhibition. *J Antibiot (Tokyo)* (2017) 71:72–8. doi: 10.1038/ja.2017.104
8. Rogov V, Dotsch V, Johansen T, Kirkin V. Interactions between autophagy receptors and ubiquitin-like proteins form the molecular basis for selective autophagy. *Mol Cell* (2014) 53:167–78. doi: 10.1016/j.molcel.2013.12.014
9. Verlhac P, Gregoire IP, Azocar O, Petkova DS, Baguet J, Viret C, et al. Autophagy receptor NDP52 regulates pathogen-containing autophagosome maturation. *Cell Host Microbe* (2015) 17:515–25. doi: 10.1016/j.chom.2015.02.008
10. McEwan DG, Popovic D, Gubas A, Terawaki S, Suzuki H, Stadel D, et al. PLEKHM1 Regulates Autophagosome-Lysosome Fusion through HOPS Complex and LC3/GABARAP Proteins. *Mol Cell* (2015) 57:39–54. doi: 10.1016/j.molcel.2014.11.006
11. Itakura E, Kishi-Itakura C, Mizushima N. The hairpin-type tail-anchored SNARE syntaxin 17 targets to autophagosomes for fusion with endosomes/lysosomes. *Cell* (2012) 151:1256–69. doi: 10.1016/j.cell.2012.11.001
12. Matsui T, Jiang P, Nakano S, Sakamaki Y, Yamamoto H, Mizushima N. Autophagosomal YKT6 is required for fusion with lysosomes independently of syntaxin 17. *J Cell Biol* (2018) 217:2633–45. doi: 10.1083/jcb.201712058
13. Settembre C, Di Malta C, Polito VA, Garcia Arencibia M, Vetrini F, Erdin S, et al. TFEB links autophagy to lysosomal biogenesis. *Science* (2011) 332:1429–33. doi: 10.1126/science.1204592
14. Trombetta ES, Mellman I. Cell biology of antigen processing in vitro and in vivo. *Annu Rev Immunol* (2005) 23:975–1028. doi: 10.1146/annurev.immunol.22.012703.104538
15. Dersh D, Holly J, Yewdell JW. A few good peptides: MHC class I-based cancer immunosurveillance and immunoevasion. *Nat Rev Immunol* (2020) 20:644. doi: 10.1038/s41577-020-0390-6
16. Moore TV, Nishimura MI. Improved MHC II epitope prediction - a step towards personalized medicine. *Nat Rev Clin Oncol* (2020) 17:71–2. doi: 10.1038/s41571-019-0315-0
17. Blees A, Januliene D, Hofmann T, Koller N, Schmidt C, Trowitzsch S, et al. Structure of the human MHC-I peptide-loading complex. *Nature* (2017) 551:525–8. doi: 10.1038/nature24627
18. Pos W, Sethi DK, Call MJ, Schulze MS, Anders AK, Pyrdol J, et al. Crystal structure of the HLA-DM-HLA-DR1 complex defines mechanisms for rapid peptide selection. *Cell* (2012) 151:1557–68. doi: 10.1016/j.cell.2012.11.025

19. Dengjel J, Schoor O, Fischer R, Reich M, Kraus M, Muller M, et al. Autophagy promotes MHC class II presentation of peptides from intracellular source proteins. *Proc Natl Acad Sci USA* (2005) 102:7922–7. doi: 10.1073/pnas.0501190102
20. Suri A, Walters JJ, Rohrs HW, Gross ML, Unanue ER. First Signature of Islet {beta}-Cell-Derived Naturally Processed Peptides Selected by Diabetogenic Class II MHC Molecules. *J Immunol* (2008) 180:3849–56. doi: 10.4049/jimmunol.180.6.3849
21. Paludan C, Schmid D, Landthaler M, Vockerodt M, Kube D, Tuschl T, et al. Endogenous MHC class II processing of a viral nuclear antigen after autophagy. *Science* (2005) 307:593–6. doi: 10.1126/science.1104904
22. Leung CS, Haigh TA, Mackay LK, Rickinson AB, Taylor GS. Nuclear location of an endogenously expressed antigen, EBNA1, restricts access to macroautophagy and the range of CD4 epitope display. *Proc Natl Acad Sci U S A* (2010) 107:2165–70. doi: 10.1073/pnas.0909448107
23. Nimmerjahn F, Milosevic S, Behrends U, Jaffee EM, Pardoll DM, Bornkamm GW, et al. Major histocompatibility complex class II-restricted presentation of a cytosolic antigen by autophagy. *Eur J Immunol* (2003) 33:1250–9. doi: 10.1002/eji.200323730
24. Jagannath C, Lindsey DR, Dhandayuthapani S, Xu Y, Hunter RLJr, Eissa NT. Autophagy enhances the efficacy of BCG vaccine by increasing peptide presentation in mouse dendritic cells. *Nat Med* (2009) 15:267–76. doi: 10.1038/nm.1928
25. Schmid D, Pypaert M, Münz C. MHC class II antigen loading compartments continuously receive input from autophagosomes. *Immunity* (2007) 26:79–92. doi: 10.1016/j.immuni.2006.10.018
26. Kasai M, Tanida I, Ueno T, Kominami E, Seki S, Ikeda T, et al. Autophagic compartments gain access to the MHC class II compartments in thymic epithelium. *J Immunol* (2009) 183:7278–85. doi: 10.4049/jimmunol.0804087
27. Comber JD, Robinson TM, Siciliano NA, Snook AE, Eisenlohr LC. Functional Macroautophagy Induction by Influenza A Virus Without a Contribution to MHC-Class II Restricted Presentation. *J Virol* (2011) 85:6453–63. doi: 10.1128/JVI.02122-10
28. Jin Y, Sun C, Feng L, Li P, Xiao L, Ren Y, et al. Regulation of SIV antigen-specific $CD4^+$ T cellular immunity via autophagosome-mediated MHC II molecule-targeting antigen presentation in mice. *PloS One* (2014) 9:e93143. doi: 10.1371/journal.pone.0093143
29. Fonteneau JF, Brilot F, Münz C, Gannage M. The Tumor Antigen NY-ESO-1 Mediates Direct Recognition of Melanoma Cells by $CD4^+$ T Cells after Intercellular Antigen Transfer. *J Immunol* (2016) 196:64–71. doi: 10.4049/jimmunol.1402664
30. Coulon PG, Richetta C, Rouers A, Blanchet FP, Urrutia A, Guerbois M, et al. HIV-Infected Dendritic Cells Present Endogenous MHC Class II-Restricted Antigens to HIV-Specific $CD4^+$ T Cells. *J Immunol* (2016) 197:517–32. doi: 10.4049/jimmunol.1600286
31. Kyewski B, Klein L. A central role for central tolerance. *Annu Rev Immunol* (2006) 24:571–606. doi: 10.1146/annurev.immunol.23.021704.115601
32. Nedjic J, Aichinger M, Emmerich J, Mizushima N, Klein L. Autophagy in thymic epithelium shapes the T-cell repertoire and is essential for tolerance. *Nature* (2008) 455:396–400. doi: 10.1038/nature07208
33. Aichinger M, Wu C, Nedjic J, Klein L. Macroautophagy substrates are loaded onto MHC class II of medullary thymic epithelial cells for central tolerance. *J Exp Med* (2013) 210:287–300. doi: 10.1084/jem.20122149
34. Niven J, Madelon N, Page N, Caruso A, Harle G, Lemeille S, et al. Macroautophagy in Dendritic Cells Controls the Homeostasis and Stability of Regulatory T Cells. *Cell Rep* (2019) 28:21–9.e6. doi: 10.1016/j.celrep.2019.05.110
35. Lee HK, Mattei LM, Steinberg BE, Alberts P, Lee YH, Chervonsky A, et al. In vivo requirement for Atg5 in antigen presentation by dendritic cells. *Immunity* (2010) 32:227–39. doi: 10.1016/j.immuni.2009.12.006
36. Sanjuan MA, Dillon CP, Tait SW, Moshiach S, Dorsey F, Connell S, et al. Toll-like receptor signalling in macrophages links the autophagy pathway to phagocytosis. *Nature* (2007) 450:1253–7. doi: 10.1038/nature06421
37. Romao S, Gasser N, Becker AC, Guhl B, Bagajic M, Vanoaica LD, et al. Essential autophagy proteins stabilize pathogen containing phagosomes for prolonged MHC class II antigen processing. *J Cell Biol* (2013) 203:757–66. doi: 10.1083/jcb.201308173
38. Martinez J, Almendinger J, Oberst A, Ness R, Dillon CP, Fitzgerald P, et al. Microtubule-associated protein 1 light chain 3 alpha (LC3)-associated phagocytosis is required for the efficient clearance of dead cells. *Proc Natl Acad Sci USA* (2011) 108:17396–401. doi: 10.1073/pnas.1113421108
39. Ma J, Becker C, Lowell CA, Underhill DM. Dectin-1-triggered Recruitment of Light Chain 3 Protein to Phagosomes Facilitates Major Histocompatibility Complex Class II Presentation of Fungal-derived Antigens. *J Biol Chem* (2012) 287:34149–56. doi: 10.1074/jbc.M112.382812
40. Florey O, Kim SE, Sandoval CP, Haynes CM, Overholtzer M. Autophagy machinery mediates macroendocytic processing and entotic cell death by targeting single membranes. *Nat Cell Biol* (2011) 13:1335–43. doi: 10.1038/ncb2363
41. Martinez J, Malireddi RK, Lu Q, Cunha LD, Pelletier S, Gingras S, et al. Molecular characterization of LC3-associated phagocytosis reveals distinct roles for Rubicon, NOX2 and autophagy proteins. *Nat Cell Biol* (2015) 17:893–906. doi: 10.1038/ncb3192
42. Ellson C, Davidson K, Anderson K, Stephens LR, Hawkins PT. PtdIns3P binding to the PX domain of p40phox is a physiological signal in NADPH oxidase activation. *EMBO J* (2006) 25:4468–78. doi: 10.1038/sj.emboj.7601346
43. Huang J, Canadien V, Lam GY, Steinberg BE, Dinauer MC, Magalhaes MA, et al. Activation of antibacterial autophagy by NADPH oxidases. *Proc Natl Acad Sci U S A* (2009) 106:6226–31. doi: 10.1073/pnas.0811045106
44. Fletcher K, Ulferts R, Jacquin E, Veith T, Gammoh N, Arasteh JM, et al. The WD40 domain of ATG16L1 is required for its non-canonical role in lipidation of LC3 at single membranes. *EMBO J* (2018) 37:e97840. doi: 10.15252/embj.201797840
45. Rai S, Arasteh M, Jefferson M, Pearson T, Wang Y, Zhang W, et al. The ATG5-binding and coiled coil domains of ATG16L1 maintain autophagy and tissue homeostasis in mice independently of the WD domain required for LC3-associated phagocytosis. *Autophagy* (2019) 15:599–612. doi: 10.1080/15548627.2018.1534507
46. Henault J, Martinez J, Riggs JM, Tian J, Mehta P, Clarke L, et al. Noncanonical autophagy is required for type I interferon secretion in response to DNA-immune complexes. *Immunity* (2012) 37:986–97. doi: 10.1016/j.immuni.2012.09.014
47. Keller CW, Sina C, Kotur MB, Ramelli G, Mundt S, Quast I, et al. ATG-dependent phagocytosis in dendritic cells drives myelin-specific $CD4^+$ T cell pathogenicity during CNS inflammation. *Proc Natl Acad Sci USA* (2017) 114:E11228–37. doi: 10.1073/pnas.1713664114
48. Keller CW, Kotur MB, Mundt S, Dokalis N, Ligeon LA, Shah AM, et al. CYBB/NOX2 in conventional DCs controls T cell encephalitogenicity during neuroinflammation. *Autophagy* (2020). doi: 10.1080/15548627.2020.1756678
49. Chu H, Khosravi A, Kusumawardhani IP, Kwon AH, Vasconcelos AC, Cunha LD, et al. Gene-microbiota interactions contribute to the pathogenesis of inflammatory bowel disease. *Science* (2016) 352:1116–20. doi: 10.1126/science.aad9948
50. Martinez-Martin N, Maldonado P, Gasparrini F, Frederico B, Aggarwal S, Gaya M, et al. A switch from canonical to noncanonical autophagy shapes B cell responses. *Science* (2017) 355:641–7. doi: 10.1126/science.aal3908
51. Arbogast F, Arnold J, Hammann P, Kuhn L, Chicher J, Murera D, et al. ATG5 is required for B cell polarization and presentation of particulate antigens. *Autophagy* (2019) 15:280–94. doi: 10.1080/15548627.2018.1516327
52. Chaturvedi A, Dorward D, Pierce SK. The B cell receptor governs the subcellular location of Toll-like receptor 9 leading to hyperresponses to DNA-containing antigens. *Immunity* (2008) 28:799–809. doi: 10.1016/j.immuni.2008.03.019
53. Hubbard-Lucey VM, Shono Y, Maurer K, West ML, Singer NV, Ziegler CGK, et al. Autophagy Gene Atg16l1 Prevents Lethal T Cell Alloreactivity Mediated by Dendritic Cells. *Immunity* (2014) 41:579–91. doi: 10.1016/j.immuni.2014.09.011
54. Loi M, Muller A, Steinbach K, Niven J, Barreira da Silva R, Paul P, et al. Macroautophagy Proteins Control MHC Class I Levels on Dendritic Cells and Shape Anti-viral $CD8^+$ T Cell Responses. *Cell Rep* (2016) 15:1076–87. doi: 10.1016/j.celrep.2016.04.002
55. Yamamoto K, Venida A, Yano J, Biancur DE, Kakiuchi M, Gupta S, et al. Autophagy promotes immune evasion of pancreatic cancer by degrading MHC-I. *Nature* (2020) 581:100–5. doi: 10.1038/s41586-020-2229-5
56. Keller CW, Loi M, Ewert S, Quast I, Theiler R, Gannage M, et al. The autophagy machinery restrains iNKT cell activation through CD1D1 internalization. *Autophagy* (2017) 13:1025–36. doi: 10.1080/15548627.2017.1297907

57. Wenger T, Terawaki S, Camosseto V, Abdelrassoul R, Mies A, Catalan N, et al. Autophagy inhibition promotes defective neosynthesized proteins storage in ALIS, and induces redirection toward proteasome processing and MHCI-restricted presentation. *Autophagy* (2012) 8:350–63. doi: 10.4161/auto.18806
58. Tian Y, Bustos V, Flajolet M, Greengard P. A small-molecule enhancer of autophagy decreases levels of Abeta and APP-CTF via Atg5-dependent autophagy pathway. *FASEB J* (2011) 25:1934–42. doi: 10.1096/fj.10-175158
59. Tian Y, Chang JC, Fan EY, Flajolet M, Greengard P. Adaptor complex AP2/PICALM, through interaction with LC3, targets Alzheimer's APP-CTF for terminal degradation via autophagy. *Proc Natl Acad Sci USA* (2013) 110:17071–6. doi: 10.1073/pnas.1315110110
60. Zhang Y, Zhang J, Chen Y, Luo B, Yuan Y, Huang F, et al. The ORF8 Protein of SARS-CoV-2 Mediates Immune Evasion through Potently Downregulating MHC-I. *bioRxiv* (2020). doi: 10.1101/2020.05.24.111823
61. Mintern JD, Macri C, Chin WJ, Panozza SE, Segura E, Patterson NL, et al. Differential use of autophagy by primary dendritic cells specialized in cross-presentation. *Autophagy* (2015) 11:906–17. doi: 10.1080/15548627.2015.1045178
62. Dasari V, Rehan S, Tey SK, Smyth MJ, Smith C, Khanna R. Autophagy and proteasome interconnect to coordinate cross-presentation through MHC class I pathway in B cells. *Immunol Cell Biol* (2016) 94:964–74. doi: 10.1038/icb.2016.59
63. Ho NI, Camps MGM, Verdoes M, Münz C, Ossendorp F. Autophagy regulates long-term cross-presentation by murine dendritic cells. *Eur J Immunol* (2020). doi: 10.1002/eji.202048961
64. Uhl M, Kepp O, Jusforgues-Saklani H, Vicencio JM, Kroemer G, Albert ML. Autophagy within the antigen donor cell facilitates efficient antigen cross-priming of virus-specific $CD8^+$ T cells. *Cell Death Differ* (2009) 16:991–1005. doi: 10.1038/cdd.2009.8
65. Li Y, Wang LX, Yang G, Hao F, Urba WJ, Hu HM. Efficient cross-presentation depends on autophagy in tumor cells. *Cancer Res* (2008) 68:6889–95. doi: 10.1158/0008-5472.CAN-08-0161
66. Li Y, Hahn T, Garrison K, Cui ZH, Thorburn A, Thorburn J, et al. The vitamin E analogue alpha-TEA stimulates tumor autophagy and enhances antigen cross-presentation. *Cancer Res* (2012) 72:3535–45. doi: 10.1158/0008-5472.CAN-11-3103
67. Li Y, Wang LX, Pang P, Cui Z, Aung S, Haley D, et al. Tumor-derived autophagosome vaccine: mechanism of cross-presentation and therapeutic efficacy. *Clin Cancer Res* (2011) 17:7047–57. doi: 10.1158/1078-0432.CCR-11-0951
68. Fan J, Wu Y, Jiang M, Wang L, Yin D, Zhang Y, et al. IFN-DC Loaded with Autophagosomes containing Virus Antigen is Highly Efficient in Inducing Virus-Specific Human T Cells. *Int J Med Sci* (2019) 16:741–50. doi: 10.7150/ijms.31830
69. Ye W, Xing Y, Paustian C, van de Ven R, Moudgil T, Hilton TL, et al. Cross-presentation of viral antigens in dribbles leads to efficient activation of virus-specific human memory T cells. *J Transl Med* (2014) 12:100. doi: 10.1186/1479-5876-12-100
70. Yi Y, Zhou Z, Shu S, Fang Y, Twitty C, Hilton TL, et al. Autophagy-assisted antigen cross-presentation: Autophagosome as the argo of shared tumor-specific antigens and DAMPs. *Oncoimmunology* (2012) 1:976–8. doi: 10.4161/onci.20059
71. Leidal AM, Huang HH, Marsh T, Solvik T, Zhang D, Ye J, et al. The LC3-conjugation machinery specifies the loading of RNA-binding proteins into extracellular vesicles. *Nat Cell Biol* (2020) 22:187–99. doi: 10.1038/s41556-019-0450-y
72. Duran JM, Anjard C, Stefan C, Loomis WF, Malhotra V. Unconventional secretion of Acb1 is mediated by autophagosomes. *J Cell Biol* (2010) 188:527–36. doi: 10.1083/jcb.200911154
73. Manjithaya R, Anjard C, Loomis WF, Subramani S. Unconventional secretion of Pichia pastoris Acb1 is dependent on GRASP protein, peroxisomal functions, and autophagosome formation. *J Cell Biol* (2010) 188:537–46. doi: 10.1083/jcb.200911149
74. Dupont N, Jiang S, Pilli M, Ornatowski W, Bhattacharya D, Deretic V. Autophagy-based unconventional secretory pathway for extracellular delivery of IL-1beta. *EMBO J* (2011) 30:4701–11. doi: 10.1038/emboj.2011.398
75. Kimura T, Jia J, Kumar S, Choi SW, Gu Y, Mudd M, et al. Dedicated SNAREs and specialized TRIM cargo receptors mediate secretory autophagy. *EMBO J* (2017) 36:42–60. doi: 10.15252/embj.201695081
76. Zhang M, Kenny S, Ge L, Xu K, Schekman R. Translocation of interleukin-1beta into a vesicle intermediate in autophagy-mediated secretion. *Elife* (2015) 4:e11205. doi: 10.7554/eLife.11205

Conflict of Interest: The author declares that the research was conducted in the absence of any commercial or financial relationships that could be construed as a potential conflict of interest.

frontiers in Immunology

REVIEW
published: 09 March 2021
doi: 10.3389/fimmu.2021.636568

Cancer Immune Evasion Through Loss of MHC Class I Antigen Presentation

*Karthik Dhatchinamoorthy, Jeff D. Colbert and Kenneth L. Rock**

Department of Pathology, UMass Medical School, Worcester, MA, United States

Major histocompatibility class I (MHC I) molecules bind peptides derived from a cell's expressed genes and then transport and display this antigenic information on the cell surface. This allows CD8 T cells to identify pathological cells that are synthesizing abnormal proteins, such as cancers that are expressing mutated proteins. In order for many cancers to arise and progress, they need to evolve mechanisms to avoid elimination by CD8 T cells. MHC I molecules are not essential for cell survival and therefore one mechanism by which cancers can evade immune control is by losing MHC I antigen presentation machinery (APM). Not only will this impair the ability of natural immune responses to control cancers, but also frustrate immunotherapies that work by re-invigorating anti-tumor CD8 T cells, such as checkpoint blockade. Here we review the evidence that loss of MHC I antigen presentation is a frequent occurrence in many cancers. We discuss new insights into some common underlying mechanisms through which some cancers inactivate the MHC I pathway and consider some possible strategies to overcome this limitation in ways that could restore immune control of tumors and improve immunotherapy.

Keywords: antigen presentation, cancer immune evasion, MHC I antigen presentation, interferon, TAP1, Tapasin, epigenetic regulation

OPEN ACCESS

Edited by:
Luis C. Anton, Consejo Superior de Investigaciones Científicas (CSIC), Spain

Reviewed by:
Barbara Seliger, Martin Luther University of Halle-Wittenberg, Germany
David A. Scheinberg, Memorial Sloan Kettering Cancer Center, United States

****Correspondence:***
Kenneth L. Rock
Kenneth.Rock@umassmed.edu

Specialty section:
This article was submitted to Antigen Presenting Cell Biology, a section of the journal Frontiers in Immunology

Received: *01 December 2020*
Accepted: *05 February 2021*
Published: *09 March 2021*

Citation:
Dhatchinamoorthy K, Colbert JD and Rock KL (2021) Cancer Immune Evasion Through Loss of MHC Class I Antigen Presentation. Front. Immunol. 12:636568. doi: 10.3389/fimmu.2021.636568

INTRODUCTION

Highly immunodeficient mice, which completely lack adaptive immunity, develop high rates of spontaneous and carcinogen-induced cancers (1, 2). Similarly, immunodeficient humans suffer from higher rates of malignancy (3–5). Therefore, the immune system is capable of recognizing and eliminating many cancers before they become clinically evident. Moreover, cancers that are infiltrated with activated T cells often have better prognosis, indicating that the immune system can exert some control on cancers, even after they have become clinically evident (6–15). Further evidence that the immune system has the potential to control and/or eliminate cancers has come from the success of immunotherapies, such as checkpoint blockade. In checkpoint blockade immunotherapy, patients are treated with antibodies that block negative regulatory molecules, such as PD-1/PD-L1 or CTLA4, which normally restrain T cell responses. This kind of therapy can reinvigorate a patient's anti-tumor T cell responses, which then can cause tumors to shrink and even lead to cures in some patients (16, 17). While all these observations show that the immune system has the capacity to fight cancer, the unfortunate fact is that once the majority of cancers have become clinically evident, untreated they almost always continue to progress and a majority fail to respond and/or be eliminated by checkpoint blockade immunotherapy. Therefore, understanding how cancers evade immune control is important for understanding tumor pathogenesis and for devising ways to improve immunotherapy.

While there are several immune effector mechanisms that can damage tumors, the most important ones are carried out by CD8 T cells. This has been shown [e.g., in experiments where tumor rejection was inhibited in mice that were depleted of CD8 T cells (18, 19)]. Similar principles are thought to apply in humans as shown [e.g., by the observations that the presence of activated CD8 T cells in cancers are associated with improved survival (20) and adoptive immunotherapy with T cells engineered to express TCRs from tumor-reactive CD8 T cells can lead to cancer regression (21)]. Tumor-reactive CD8 T cells identify cancers by recognizing peptide-MHC I complexes that are generated through the MHC I antigen presentation pathway (**Figure 1** and below). Upon recognizing a cancer, CD8 T cells go on to kill these cells *via* perforin or FAS-dependent pathways and also can injure tumors by inciting inflammation. Such mechanisms are important in controlling cancer as shown [e.g., by the finding that higher frequencies of cancers develop in perforin-null or FAS-deficient mice (22, 23) compared to their wild type counterparts and potentially also in perforin-deficient humans (24)].

In order to progress, cancers need to circumvent immune control. This was nicely illustrated by a study of carcinogen-induced cancers that arose in immunodeficient vs. immunosufficient mice. Cancers from immunodeficient mice grew when transplanted into other immunodeficient mice. However, these same cancers were generally rejected in wild type mice, showing that they were inherently immunogenic (1). In contrast, tumors that arose in wild type mice would often grow when transplanted into other wild type mice (1). These findings indicated that tumors that arose in the presence of the intact immune system in wild type mice evolved in ways that allowed them to evade immune elimination (2). This evolution of cancers under selection pressure from CD8 T cells has been referred to as "immunoediting" (2, 25).

Cancers are often genetically unstable and can lose expression of non-essential molecules through gene loss or epigenetic silencing. MHC I molecules and most of the other molecules of the MHC I antigen presentation pathway are not essential for cell viability or growth (see below). Consequently, cancers can down-regulate or lose MHC I antigen presentation, and thereby become less stimulatory or even invisible to CD8 T cells, without impairing their ability to grow and metastasize. In this article we will review the incidence, underlying mechanism, and therapeutic implications of loss of MHC I in cancers. Except where noted, this review primarily focuses on human cancers, because of their clinical importance. It should be noted that cancers can also evade immune elimination by expressing "non-classical" MHC class Ib molecules, HLA-E and HLA-G (26–28). However, since this immune evasion mechanism is not due to a loss of antigen presentation by "classical" MHC class Ia molecules, but rather through engagement of inhibitory receptors on T lymphocytes and other immune cells (26–28), this subject is not covered in this review, except as it relates to how MHC I low cancers may evade NK cell recognition. Similarly, MHC II molecules can play a role in cancer immunity, however, since MHC I and MHC II antigen presentation are separate and non-intersecting pathways, this review does not cover the MHC II pathway in cancer.

THE MHC CLASS I PATHWAY OF ANTIGEN PRESENTATION

To understand some of the mechanisms by which many cancers evade immune surveillance, it is necessary to first understand the MHC I pathway of antigen presentation (**Figure 1**). This pathway is the mechanism that allows CD8 T cells to identify cells producing "foreign" proteins, such as ones from viruses in infected cells or mutant genes in cancers. In this pathway, MHC I-presented peptides are generated as part of the normal catabolism of cellular proteins. All endogenously synthesized proteins are continuously degraded into oligopeptides by the ubiquitin-proteasome pathway (29). This catabolic pathway is responsible for making the initial cleavages, and particularly the proper C-terminal cut, needed for the generation of a majority of MHC I-presented peptides (29–32).

There are several forms of proteasomes, known as proteasomes, immunoproteasomes and thymoproteasomes (33). Immunoproteasomes are formed when three alternate versions of proteasome active site subunits are expressed in cells and preferentially incorporate into newly assembling proteasomes in place of the standard active site subunits. Since these alternate active sites have different catalytic properties, immunoproteasomes generate many different (as well as some of the same) peptides as proteasomes and it seems that the ones produced by immunoproteasomes are often better for presentation on MHC I molecules (34, 35). Cells and animals that genetically lack the three immunoproteasome subunits are viable (35).

A fraction of the peptides produced by proteasomes and immunoproteasomes are transferred into the lumen of the endoplasmic reticulum (ER) by a peptide transporter called TAP (36). TAP can transport most, but not all, peptides that are between 9 and 13 residues in length (37–39). TAP is composed of two different subunits (TAP1 and TAP2) and both are needed for transporting peptides (40–43). Upon transport into the lumen of the ER, peptides are in the vicinity of newly assembling MHC I molecules.

The heavy and light [ß2-microglobulin (ß2M)] chains of MHC I molecules are co-translationally transported into the ER where they fold into the MHC I heterodimer. Before binding these complexes are inherently unstable and are stabilized through interactions with chaperones such as calreticulin within a multi-protein complex, called the peptide-loading complex (44, 45). Other components of this complex include the peptide transporter TAP, the oxidoreductase ERP57 and the peptide "editor" Tapasin. Tapasin helps retain peptide-empty MHC I molecules in the ER and also promotes their loading with high affinity peptides (46, 47). There is another peptide-editor called TAPBPR, which is not part of the peptide-loading complex, that also promotes peptide-loading of MHC I molecules (48). Cells and animals that lack Tapasin, ERP57, or TAP are viable (49, 50).

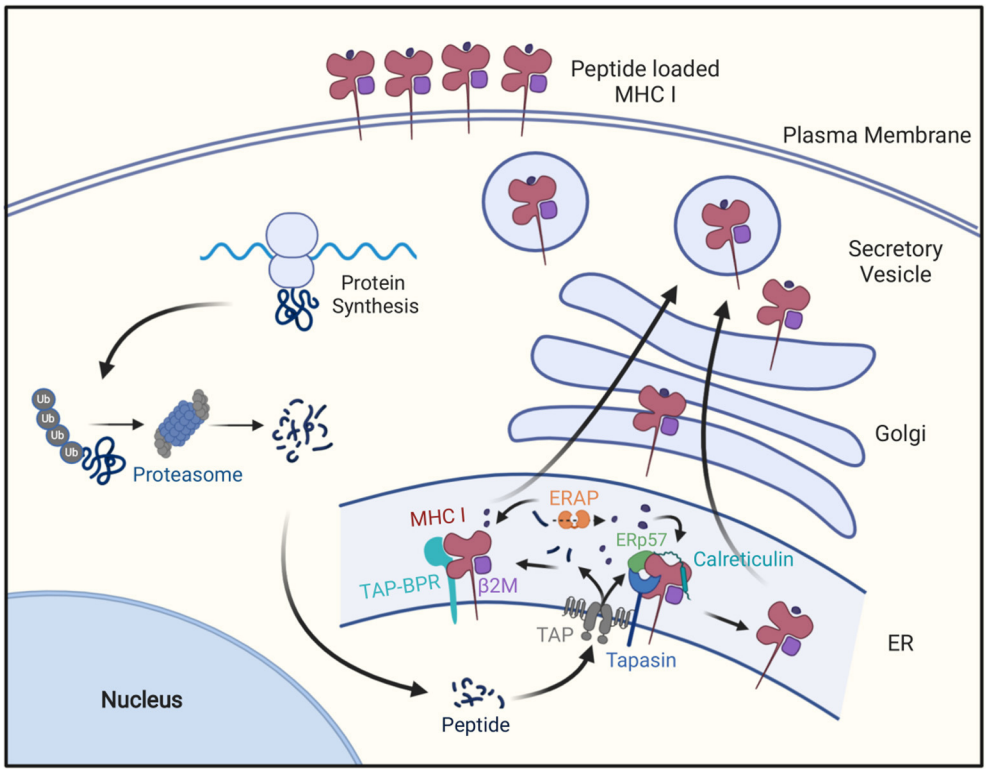

FIGURE 1 | The MHC class I antigen presentation pathway. Cellular proteins are hydrolyzed by the ubiquitin-proteosome pathway into oligopeptides, which are subsequently transported into endoplasmic reticulum through the TAP transporter. In the ER these peptides may be further trimmed by ERAP1 and then peptides of the right length and sequence bind to MHC I molecules with the help of Tapasin in a peptide-loading complex containing Tapasin, TAP, calreticulim, and ERP57, or the with the help of TAPBPR. After MHCI molecules bind peptide, they are transported to the cell surface for display to $CD8^+$ T cells.

The empty MHC I molecule contains a groove that binds peptides (51, 52). Peptides are bound *via* molecular interactions typically with two of their side chains, some of their main chain atoms and their free N- and C-termini (47). Because the interactions with the peptide's two ends contributes substantially to the affinity with which peptides are bound, most MHC I-bound peptides are of a uniform length, which depending on the particular MHC I molecule is typically 8, 9, or 10 residues (53). Proteasomes and immunoproteasomes make some peptides in this size range, but also many more that are too short or too long for stable binding to MHC I molecules (54). However, the long peptides can be trimmed to the proper size for presentation. Much of the trimming of long peptides occurs in the endoplasmic reticulum by an aminopeptidase called ERAP1 (ERAAP) (55, 56) and in humans also a second related peptidase called ERAP2 (57). ERAP1 is specialized in trimming long peptides to the optimal length for binding MHC I molecules, as it slows or stops trimming most peptide substrates when they are 8–9 residues in length (55). Long peptides can also be trimmed by aminopeptidases in the cytosol and the resulting shorter peptides can be transported by TAP into the ER (58). Similar to TAP and MHC I mentioned above, cells and animals that lack ERAP1 are also viable (59–62).

The peptides produced by these various mechanisms that have the right length and sequences can then bind to the empty MHC I molecules in the ER, often assisted by the peptide-editors Tapasin and TAPBPR. Upon binding peptides MHC I complexes are both stabilized and released from the ER, whereupon they follow the default exocytic pathway to the plasma membrane for display to CD8 T cells. In cells that have defects in making, transporting or MHC I-loading of peptides, most of their MHC I molecules are retained in ER and ultimately degraded, resulting in a paucity of MHC I molecules on the cell surface (29, 32, 63). As will be discussed further below, such defects underlie the MHC I low phenotype in many cancers.

REGULATION OF THE MHC I PATHWAY OF ANTIGEN PRESENTATION

Regulation of MHC I antigen presentation is also relevant to tumor immune evasion. The expression of most components of the MHC I antigen presentation pathway, including MHC I heavy chains, ß2M, immunoproteasome subunits, TAP, Tapasin and ERAP1, are coordinately regulated. This is because these antigen presentation components all have similar gene control elements in their promoters/enhancers (64, 65) (**Figure 2**). These elements include sequences that bind the transcription factors NLRC5-enhanceosome, NF-κB, and IRF1/IRF2 (66). Gene silencing or editing experiments have shown that the NLRC5, IRF1, and IRF2 transcription factors are essential for

basal and/or interferon (IFN)-induced MHC I expression, but not for cell viability or growth (67–70). Since these are non-essential genes (71, 72), their expression can be lost in cancer cells, as will be discussed below.

Many cells of hematopoietic origin, such as dendritic cells and lymphocytes, constitutively express relatively high amounts of all of the MHC I antigen presentation components and consequently without any stimulation have high levels of MHC I molecules on their cell surface (73, 74). In contrast, under basal conditions, most other cells have lower expression of these components and have less MHC I on the cell surface (74). However, in all cells, the expression of MHC I pathway components and surface MHC I levels are increased upon stimulation with interferons, especially type 2 IFN (IFNγ) (75). In such responses, IFNs upregulate expression of IRF1, STAT1, and NLRC5 (76), which then binds to the promoters of the antigen presenting gene and drives their expression (**Figure 3**). IFNs are induced in response to infections and T cell responses, this upregulated expression is thought to enhance detection of pathological cells. That this mechanism is important in cancers is suggested from studies that have documented an increased incidence of cancer in mice that have defects in the IFN pathway (77, 78), and that in humans IFNγ-signaling signatures in cancers correlate with response to immunotherapy (79).

CANCERS ANTIGENS AND THEIR VISIBILITY TO THE IMMUNE SYSTEM

Through the mechanisms describe above, all cells display on their surface peptides from a majority of the proteins that they are making. This process allows CD8 T cells to identify and eliminate cells that are synthesizing "foreign" or other immunogenic proteins. Foreign (non-self) sequences in cancer may come from endogenous genes harboring mutations, which are often referred to as neoantigens, or in some cases from viral sequences in cancers (e.g., human papilloma viral proteins in human cervical carcinomas) (80).

Mutational burdens vary substantially among cancers. Tumors with higher mutational burdens are theoretically more immunogenic, and there is some evidence to support this concept. Melanomas and non-small cell lung carcinoma (NSCLC) often have high mutational burdens (81) and are considered more immunogenic tumors. There is also a correlation between the number of mutations in cancers and their responses to checkpoint blockade or adoptive T cell immunotherapy (82–84). This has been interpreted to suggest that cancers, which display many immunogenic peptides, will be much more likely to be attacked by CD8 T cells that have been reinvigorated by immunotherapy. In addition to mutated peptides, there are other kinds of immunogenic tumor antigens. For example, anti-cancer CD8 T cells can recognize de-repressed oncofetal antigens, cancer germline antigens, and even normal (non-mutated) cellular antigens, such as tyrosinase in melanomas and melanocytes (85, 86). In this latter case, the responding T cells are autoreactive ones that have escaped normal tolerance mechanisms and are present in the T cell repertoire. However, cancers that lack any immunogenic antigens are ones that can't be controlled by CD8 T cells.

Cancers that are initially immunogenic can lose visibility to CD8 T cells in two general ways. If the immunogenic antigens are non-essential for cell survival, and this is probably true for a majority of tumor antigens, then genetically unstable cancer cells can lose expression of the cancer antigens (87–90). After this occurs, CD8 T cells will be ineffective in controlling the cancer because despite the tumors having plenty of MHC I molecules, the cancer cells have lost all antigenic peptides that CD8 T cells can recognize. This route of immune evasion will be less likely in cancers that express many immunogenic cancer antigens because it would require simultaneous loss of expression of many independent gene products. This may be another reason as to why tumors with high mutational burdens are more susceptible to T cell immunotherapy. The other general way that cancers can lose visibility to CD8 T cells is by down regulating the MHC I antigen presentation pathway. The evidence that this occurs, and its underlying mechanisms and clinical importance are considered in the following sections.

CANCERS OFTEN LOSE EXPRESSION OF MHC I MOLECULES

A large number of many different types of human cancers have been reported to lose expression of MHC I molecules to varying degrees (**Figure 4**). An MHC-low phenotype has been observed in many of the most frequent human cancers including NSCLC, breast, prostate, colorectal, head and neck squamous cell carcinoma (HNSC), hepatocellular carcinoma, and melanoma. The number of cases that have lost MHC I expression varies for different types of these cancers and between different studies, and ranges from 0 to 93% (**Figure 4**). Cancers may not be homogeneous and can have variable expression of MHC I among its cells and/or in different regions. In addition, expression may change over time as a cancer progresses and may differ between the primary site and metastases (91–94).

The vast majority of these studies have analyzed MHC I expression in primary patient samples by immunohistochemistry (IHC) using antibodies specific for monomorphic determinants on the heavy chains of classical MHC I molecules (HLA-A, HLA-B, and HLA-C) or for ß2M. Therefore, many cancers have downregulated MHC I antigen presentation broadly. Loss of expression of a single MHC I molecule has also been reported (95, 96). Many studies have reported cancers that are MHC I negative, however because of the limits of sensitivity of IHC, it is possible that some of these cases may still express some MHC I molecules.

As described above, because peptide empty MHC I molecules are unstable without chaperone-binding and retained in the ER, defects almost anywhere in the MHC I pathway (e.g., loss of MHC I heavy chain, ß2-microglobulin, immunoproteasome subunits, TAP, Tapasin, and ERAP1) results in a loss of MHC I molecules from the cell surface. In mouse and human cells, genetic deletion of TAP reduces MHC I levels by 30–70% for most MHC I alleles (40, 97). Similarly, loss of Tapasin decreases MHC I expression

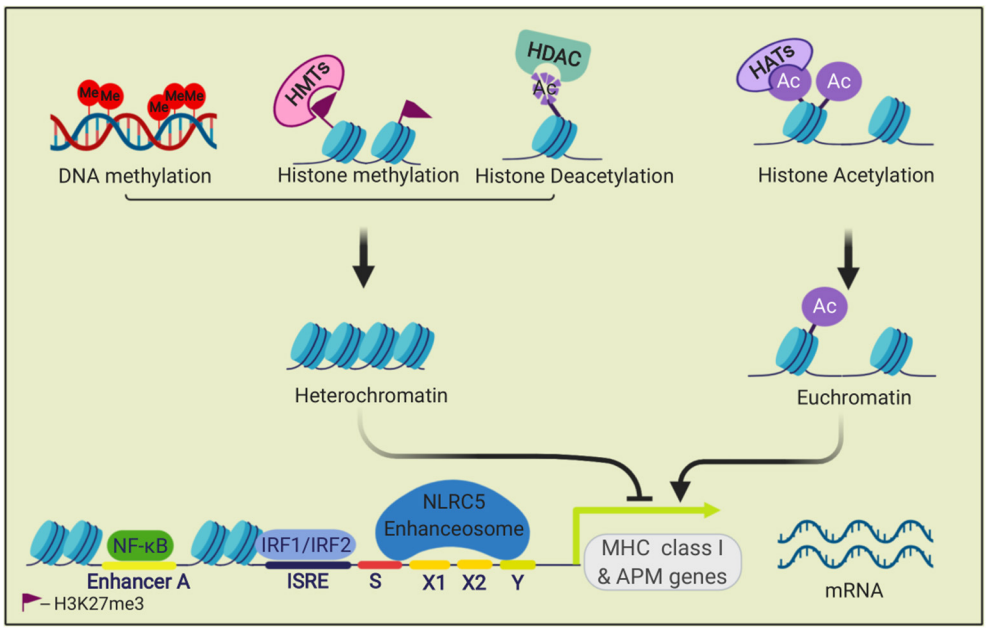

FIGURE 2 | Transcriptional regulation of MHC class I genes. The transcription factors NF-κB, IRF1, and IRF2, and the NLRC5 enhanceosome bind to promoter and enhancer elements in the 5' upstream sequences of MHC I APM genes and drive their transcription. This process is regulated by epigenetic modifications. Methylation of histone (H3K27me3) by histone methyltransferases (HMTs) and DNA methylation repress transcription. Histone acetyltransferases (HATs) acetylate histones, which can open the chromatin for transcription. Histone deacetylases (HDACs) can remove histone acetylation marks and silence transcription.

by as much as 90% and deletion of immunoproteasome subunits reduces MHC I levels by ∼50% (35, 98). MHC I levels are reduced in ERAP1 KO cells by 20–70% (59, 99, 100).

The expression of these antigen presentation pathway components in cancers has been studied (101) but much less extensively than for MHC I and ß2M. Of these components, TAP has been studied most extensively. Loss of TAP expression, ranging from 10 to 80.4%, has been documented in colorectal, renal cell cervical cancers, and melanomas (102–110) (**Figure 5**). There are more limited studies that have documented loss of expression of Tapasin (111–114), Immunoproteasomes (113, 115), and ERAP1 (116–119) (**Figure 5**). Individual cancers can lose expression of multiple of these antigen presenting components (see section on transcriptional regulation below) and the net effect of these multiple loses on MHC I expression should be compounded.

CLINICAL IMPORTANCE OF LOSS OF MHC I EXPRESSION IN CANCERS

As discussed above, the loss of MHC I antigen presentation will make cancers less visible to the immune system and this is predicted to impair control of such tumors by CD8 T cells. There are three lines of evidence that support this concept in human cancer patients. First, in some cancers the presence of tumor-infiltrating lymphocytes (TIL), which is often an indication of a host immune response, is positively correlated with MHC I molecule expression on tumor cells. For example, MHC I-low cancers (e.g., breast cancer) contain fewer TIL than their MHC I-high counterparts (10, 11, 120, 121). Since TILs are a positive prognostic feature in many cancers (7–10, 12, 13, 15, 122), the correlation of TIL with MHC I expression is consistent with a role of antigen presentation in immune control of cancers.

A second line of evidence for the clinical significance of MHC I-loss, comes from studies that have correlated MHC I expression with prognosis. In many cancers, including melanoma, glioblastoma, colorectal, bladder, uterine, cervical, head/neck, breast and other cancers, loss of MHC I is associated with worse clinical outcomes (14, 110, 111, 122–140). Since loss of the MHC I antigen presentation pathway does not alter intrinsic cell growth or viability, this correlation is also consistent with a role for antigen presentation in immune control of cancers (128).

The third line of evidence for the clinical importance of MHC I-loss comes from studies of immunotherapy. In several studies, loss of MHC I expression has been correlated with resistance to checkpoint blockade (124, 141–147) and adoptive immunotherapy (148, 149). Moreover, during immunotherapy it was observed that MHC I high metastases were the ones that regressed while MHC low metastases progressed (150). Similarly, defects in IFN-response pathways, which regulate MHC I levels, as described above, are also correlated with resistance to checkpoint immunotherapy (79, 122, 151–153).

These three lines of evidence point to the likely importance of MHC I-loss to clinical outcomes. However, there is a "chicken and egg issue" that should be considered. Since activated CD8 T cells and CD4 Th1 cells produce IFNγ, which can upregulate the MHC I pathway, this raises the question of which of

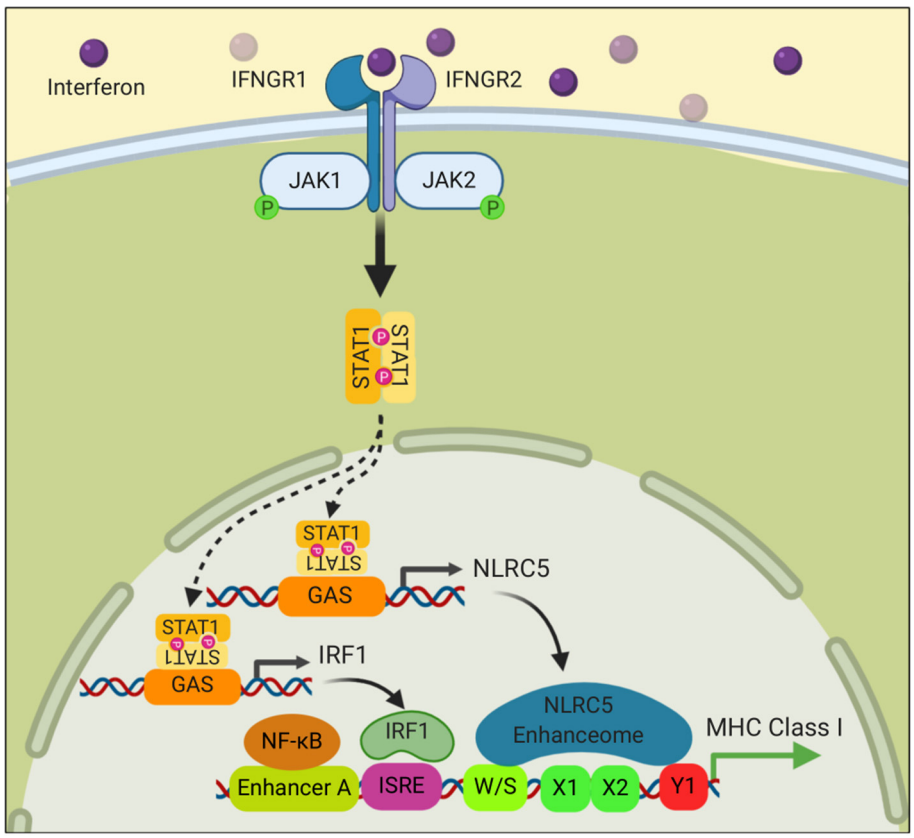

FIGURE 3 | Interferon signaling stimulates the transcription of MHC class I genes. Binding of Interferon to its receptor stimulates phosphorylation of the Janus kinases, JAK1 and JAK2, which in turn phosphorylate STAT1. Phosphorylated STAT1 translocates into the nucleus where it binds to promoter elements of NLRC5 and IRF1 and drives their transcription. NLRC5 and IRF1 then stimulate MHC I gene transcription as described in **Figure 2**.

the events came first: High MHC I or the T cell immune response. Similarly, if higher MHC I levels are a consequence of a preexisting T cell responses, then the presence of the responsive T cells could also be the reason that these cases are more responsive to checkpoint blockade immunotherapy. In other words, high MHC I could be an effect rather than a cause of TIL infiltration and the consequent improved clinical responses. While there is undoubtably interplay between MHC I stimulating T cells and T cells stimulating MHC I antigen presentation, the fact is that MHC I is needed to initiate this process (154). Therefore, loss of MHC I antigen presentation is likely causally related to clinical outcomes. In support of this concept, in an experimental human xenograft model, wherein the preexisting T cell repertoire is identical and the only variable is whether a tumor is MHC I high vs. low, loss of MHC I antigen presentation results in resistance to checkpoint blockade (141).

If MHC I expression is a key factor needed for immune control of cancers, as is expected from the underlying science and suggested by the above clinical data, then it is important to understand the underlying mechanisms for MHC I loss. This is of obvious importance for understanding pathogenesis and also for evaluating whether there are ways to potentially restore MHC I expression to improve therapy.

LOSS OF MHC I EXPRESSION IN CANCERS THROUGH MUTATION OR DELETION OF STRUCTURAL GENES

Many cancers are genetically unstable and can lose gene expression through deletions or mutation of chromosomal sequences (**Figure 7**). Many of the MHC I antigen presenting components (e.g., MHC I heavy chains, TAP, Tapasin, immunoproteasome subunits) are encoded in the MHC on Chromosome 6. Cells that sustain homozygous deletion of large regions of the MHC region are viable and proliferate (155–157) and therefore such chromosomal deletions are permissive in cancers, as are inactivating mutations in the antigen presenting components.

Loss of both copies of MHC I heavy chain genes or of ß2M will eliminate essentially all MHC I expression, and such loss does occur in cancers (96, 141, 158, 159). Loss of one copy of MHC I heavy chain or ß2M genes (loss of heterozygosity) also has been documented in many cancers (95, 143, 158, 160–165). In a survey of 59 cancer types, loss of MHC I heterozygosity was observed to occur in 17% of cancers (166). That this might be a consequence of immunoediting was suggested by the observation that this loss occurred more frequently in cancers with higher mutational burdens and therefore ones that were expressing potentially more

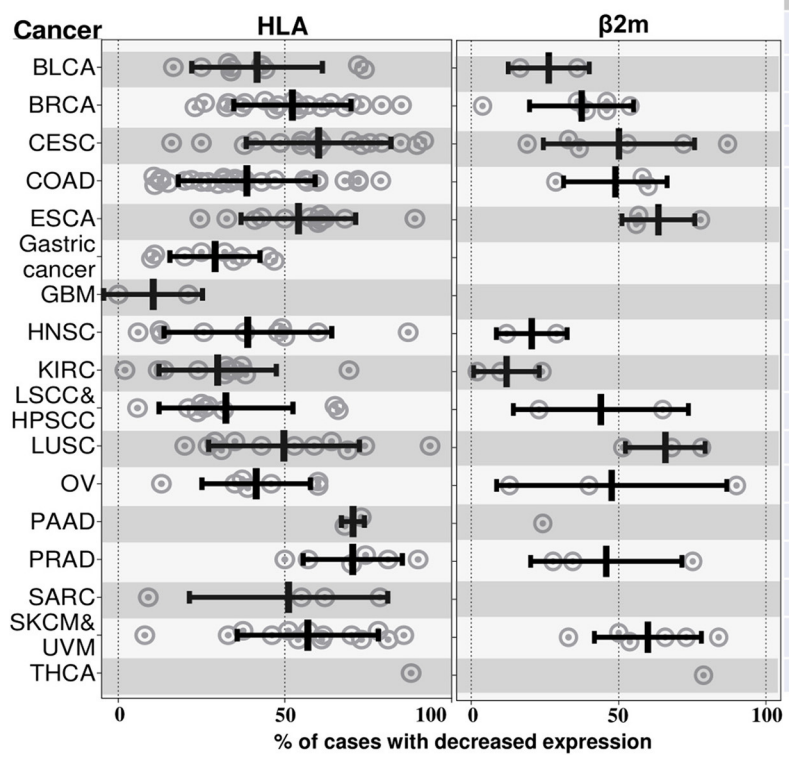

Cancer	# of studies		# of patient samples		Reference
	HLA	β2m	HLA	β2m	
BLCA	10	2	480	33	[171,297-305]
BRCA	20	5	3019	795	[297,306-323]
CESC	18	6	1393	382	[102,109,113,116,118, 286,314,324-333]
COAD	28	3	7028	349	[105,112,122,297,314,334-356]
ESCA	12	3	945	370	[110,114,115,119,137-139, 181,357-360]
Gastric cancer	9	n/a	1004	n/a	[174,338,357,361-366]
GBM	2	n/a	47	n/a	[367,368]
HNSC	10	2	549	75	[125,135,164,173,369-374]
KIRC	11	3	795	275	[104,297,311,375-379]
LSCC& HPSCC	9	2	515	99	[14,338,339,380-385]
LUSC	13	3	1371	291	[106,297,314,386-392]
OV	7	3	1190	538	[393-400]
PAAD	2	1	122	37	[401,402]
PRAD	6	3	795	553	[314,403-408,419]
SARC	4	n/a	160	n/a	[409-412]
SKCM& UVM	14	6	1174	211	[132,133,314,339,402,413-418]
THCA	1	1	33	33	[120]

FIGURE 4 | HLA and β2M are frequently downregulated in many different cancers. This graph illustrates the findings from a number of studies that have measured MHC I expression in various cancers by immunohistochemistry. Cancers are annotated by their TCGA abbreviations (see abbreviation list). Each dot represents the percent of cases with loss of MHC I expression in an individual study. The mean % reductions and standard deviations for all of the studies combined are shown by the black bars. The data to the right of the graph shows the number of studies and number of patients samples used to quantify the MHC class I. The studies that were included are shown in the references; this is not an exhaustive list of all such analyses. BLCA, Bladder urothelial carcinoma; BRCA, Breast invasive carcinoma; CESC, Cervical squamous cell carcinoma and endocervical adenocarcinoma; COAD, Colon adenocarcinoma; ESCA, Esophageal carcinoma; GBM, Glioblastoma multiforme; HNSC, Head and neck squamous cell carcinoma; KIRC, Kidney renal clear cell carcinoma; LSCC, Lung squamous cell carcinoma; HPSCC, Hypopharyngeal squamous cell carcinoma; LUSC, Lung squamous cell carcinoma; OV, Ovarian serous cystadenocarcinoma; PAAD, Pancreatic adenocarcinoma; PRAD, Prostate adenocarcinoma; SARC, Sarcoma; SKCM, Skin cutaneous melanoma; UVM, Uveal melanoma; THCA, Thyroid carcinoma; IFN, Interferon; LIHC, Liver hepatocellular carcinoma; NSCLC, Nonsmall cell lung carcinoma.

immunogenic neoantigens (166). Because MHC I heavy chain genes are co-dominantly expressed from both chromosomes, loss of one copy of an MHC I heavy chain gene reduces MHC I expression by about 50% (35). In cells with MHC I loss of heterozygosity, a single inactivating mutation in a remaining MHC I gene will lead to a null phenotype and such mutations do occur in the coding regions of individual MHC I heavy chain genes (143, 167). Over time MHC I expression can decrease in patients, with e.g., primary lesions being MHC I positive but metastasis losing such expression, presumably the result of immunoediting (93, 168).

Mutations and deletions also occur in all of the other components of the MHC I antigen presentation and IFN pathways as shown in sequencing data of many human cancers (**Figure 6**) (171). Much of this data has not been analyzed to tell whether and how often these genetic alterations have led to a loss of function, nor how many of the various cancers are free of any mutation in an MHC I pathway component. However, there are a number of reports of inactivating mutations and deletions of several of these components (95).

LOSS OF THE MHC I ANTIGEN PRESENTATION PATHWAY IN CANCERS THROUGH TRANSCRIPTIONAL REGULATION

In many cancers with MHC I pathway defects, there is an underlying loss of transcription of MHC I pathway genes (172, 173). In an individual cancer, this process can affect the expression of multiple MHC I pathway genes at the same time, including MHC I heavy chains, ß2M, TAP, Tapasin, ERAP1, and immunoproteasome subunits (105, 173–176). The underlying mechanisms for such loss of MHC I pathway gene expression have been elucidated for some cancers.

One mechanism that affects transcription of MHC I pathway genes in cancers is a loss of key transcription factors. The NLRC5 transcription factor is reduced in multiple cancers including prostate, lung, uterine, melanoma, and thyroid cancers and this is correlated with a reduction in the expression of its target genes, including MHC I, ß2M, TAP, and immunoproteasome subunits

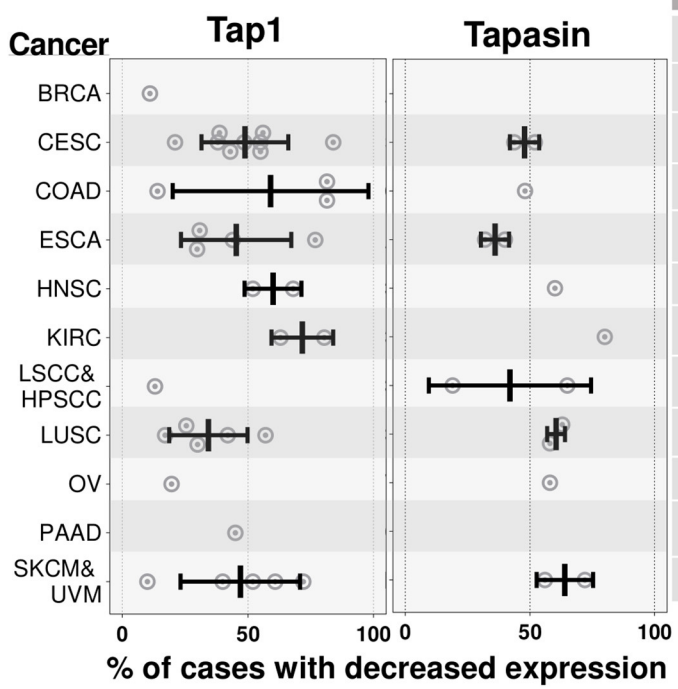

# of studies		# of patients sample		Reference
Tap1	Tapasin	Tap1	Tapasin	
1	n/a	11	n/a	[318]
9	2	586	127	[102,109,113,116,118, 324,326,327,330,333]
3	1	753	198	[105,112,343]
4	2	375	80	[110,114,115,119,359]
2	1	50	25	[135,173]
2	1	184	51	[104,379]
1	2	63	99	[14,377]
5	2	233	61	[106,297,391]
1	1	51	150	[396,400]
1	n/a	37	n/a	[401]
4	1	244	41	[132,133,413,418]

FIGURE 5 | Tap1 and Tapasin are downregulated in many cancer types. Similar to **Figure 4**, except summarizing results from studies quantifying loss of Tap1 (one of the chains of the TAP transporter) and Tapasin, instead of MHC I. There are fewer studies of the expression of these proteins in cancers relative to the studies of MHC I expression in cancers. n/a-data is not available. Cancer abbreviation are as in **Figure 4**.

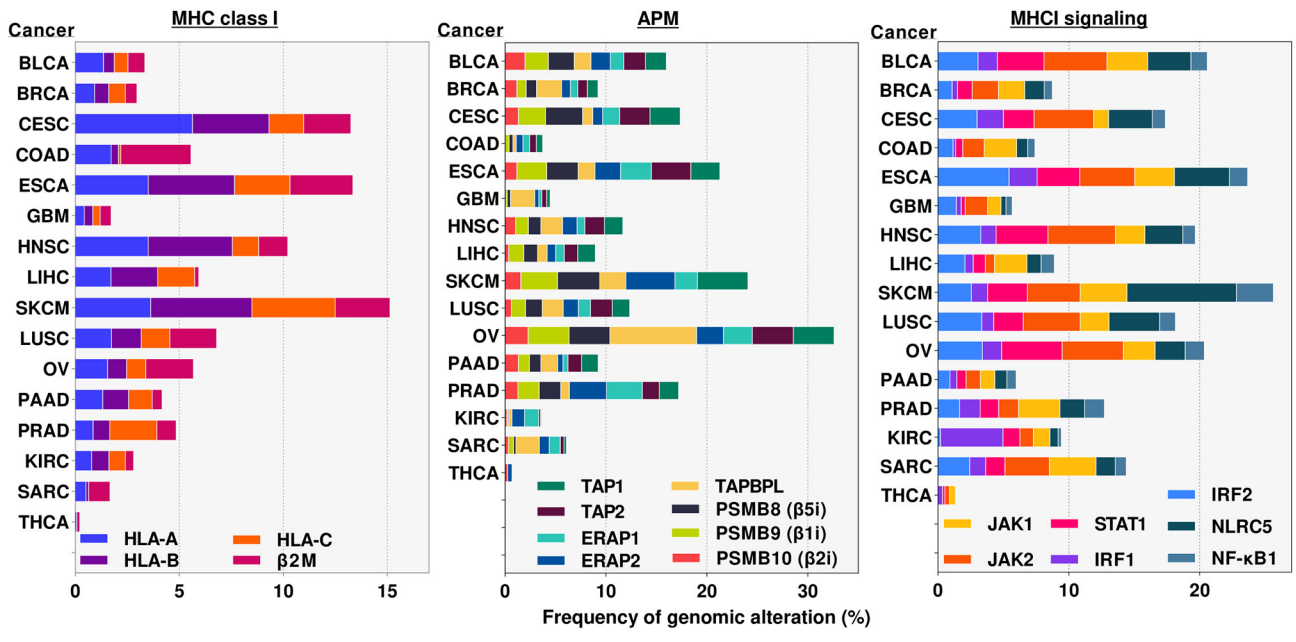

FIGURE 6 | Frequency of alterations in genomic sequences of MHC class I pathway genes in various cancers. Genomic alterations include any mutation, deletion and/or amplification occurring in either intron or exon regions of the indicated genes. Results were obtained from cBioportal.org (169, 170). analyses of publicly available TCGA data sets for the indicated genes and cancers. APM, Antigen Presentation Machinery. Cancer abbreviation are as in **Figure 4**.

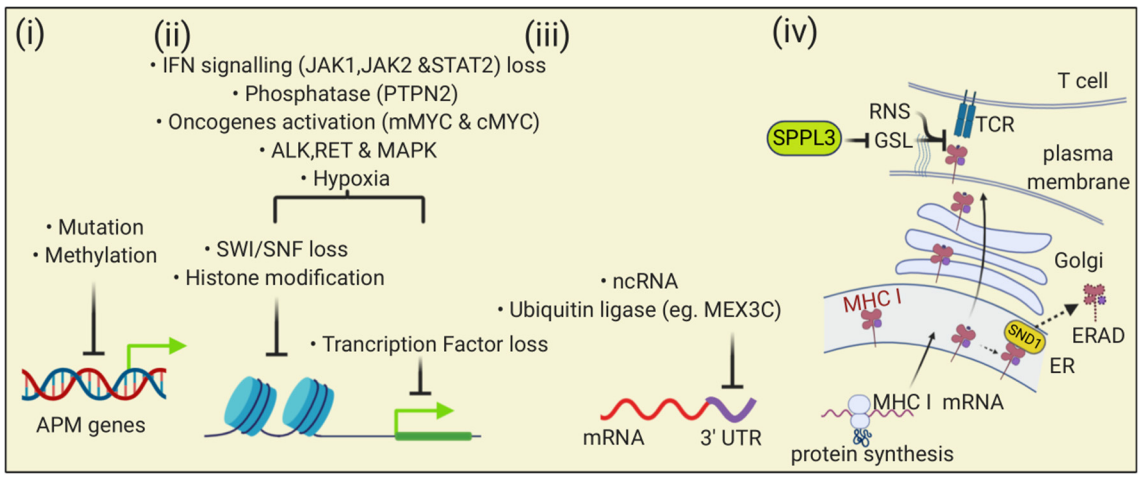

FIGURE 7 | The MHC I antigen presentation pathway is down-regulated by multiple mechanisms in cancers. (i) At the level of DNA, mutation and methylation of nucleotides can reduce expression of APM genes; (ii) Transcription of APM can be reduced by changes in chromatin that impair gene accessibility or through loss of transcription factors. Multiple mechanisms can affect these processes including altered signaling pathways, oncogene activity, and the tumor microenvironment; (iii) At the level of transcription, binding of ncRNA or proteins to the 3′ UTR of APM mRNAs can reduce transcription; (iv) At the level of protein, Staphylococcal nuclease and tudor domain containing 1 (SND1) can bind to MHC I in the ER and trigger endoplasmic reticulum-associated degradation (ERAD). At the cell surface, loss of SPPL3 increases glycosphingolipids (GSL) that then sterically inhibit MHC I and TCR interactions. Reactive nitrogen species can nitrosylate peptide-MHC I complexes in ways that impair TCR interactions.

(123) The loss of NLRC5 could arise from loss or mutation of the gene (**Figure 6**), or methylation of its promoter or associated histones (123, 177, 178). Loss of nuclear IRF1 in melanomas is associated with resistance to checkpoint blockade (179). Loss of expression of NF-κB and IRF1 in neuroblastomas results in a loss of MHC I expression (180). Loss of IRF2 caused a downregulation of many components of the MHC I antigen presentation pathway (MHC I heavy chains, immunoproteasomes, TAP, TAPBPR, and ERAP1) as well as an increase in CD274 (PDL-1) (69). Many human cancers (e.g., breast, NSCLC, prostate, colorectal, and uterine) downregulate IRF2 expression, which results in an immune evasion phenotype with MHC I low and PD-L1 high expression (69).

The expression of antigen presentation pathway genes can be downregulated through epigenetic silencing (**Figures 2**, **7**). One such mechanism that has been observed in several cancer types is hypermethylation of the promoters or enhancers of these genes. This modification has been documented in the regulatory elements of MHC I (176, 181–183), TAP (128), Tapasin (184), IFNR pathway components (185–187). This DNA modification silences gene expression by recruiting repressive factors, such as methyl-CpG binding domain protein 1 (MBD1) and methyl-CpG binding protein 2 (MeCP2) and interfering with transcription. As cancer cells divide, these methylated sequences are passed onto daughter cells, thereby perpetuating the gene silencing. Treatment with agents that cause DNA demethylation has restored MHC I expression in some cancers, demonstrating the importance of this silencing mechanism (182, 188). Cancer neoantigen genes can also be subjected to DNA hypermethylation (189).

Another epigenetic silencing mechanism involves histone modifications, which are also heritable to daughter cells. Histone acetylation can alter chromatin in ways that increase DNA accessibility and thereby allowing entry and binding of transcription factors. Histone deacetylase (HDAC) inhibitors, which lead to increased acetylation levels, have restored expression of MHC I molecules and other antigen presentation components in some cancers, suggesting that histone deacetylation silences expression of MHC I pathway genes (190–194). Trimethylation of histones (e.g., H3K27me3) can also downregulate genes by affecting the state of heterochromatin. In some MHC I low cancers, H3K27me3 repressive marks are associated with the promoters of NLRC5, MHC I heavy chain genes, β2M, immunoproteasomes and TAP, and loss of this repressive modification results in an increase in MHC I pathway expression (177, 195).

The polycomb repressive complex 2 (PRC2) was found to be a repressor of MHC I expression in some cancer cells, such as neuroblastomas and small cell lung carcinomas (177). PRC2 silences the basal expression of NLRC2, MHC I, immunoproteasomes, and TAP and also inhibits IFNγ-induced MHC I upregulation (177). A subunit of the PRC2 complex binds and activates the lysine methyltransferase EZH2. Consistent with this mode of action, the repression caused by PRC2 was associated with increased H2K27me3 histone repressive marks associated with MHC I pathway genes, which when reversed, increased transcription factor binding and MHC I expression. Consistent with these results, deletion of EZH2 in leukemia cells increased MHC I expression (196) and activating mutations of EZH2 caused a loss of MHC I expression in these cancers (197).

SWI/SNF factors affect gene expression by regulating chromatin accessibility. The Polybromo-associated BAF (PBAF) SWI/SNF complexes were found to be a positive regulator of MHC I expression (198). The expression of PBAF in cancers is correlated with better prognosis and responsiveness to checkpoint blockade. Interestingly for PBAF, it particularly

affects promoter accessibility of IRF2 and interferon-stimulated response elements (ISREs) (198).

LOSS OF THE MHC I ANTIGEN PRESENTATION PATHWAY IN CANCERS THROUGH POST-TRANSCRIPTIONAL/PRE-TRANSLATIONAL REGULATION

The expression of proteins can be regulated through post-transcriptional mechanisms (**Figure 7**) and one of these mechanisms is mediated by non-coding RNAs (ncRNA) (199). One class of ncRNAs are small (22 bp average length) microRNAs (miRNA). These sequences can bind to the 3′ untranslated regions (UTR) of mRNAs and inhibit their translation through repression or by targeting them for degradation.

There are a number of examples of miRNAs that regulate the expression of components of the MHC I antigen presentation pathway and can contribute to a loss of antigen presentation in cancers (66, 200). In some cancers, there is increased expression miRNAs and it has been shown that overexpression of these miRNAs leads to a reduction in MHC I pathway components. For example, in esophageal cancer, miR-148a-3p was found to bind to untranslated regions (UTR) of MHC I transcripts and miR-125a-5p bound to UTRs of TAP2 transcripts. Moreover, the overexpression of these miRNAs reduced the expression of these antigen presentation components (201). In melanomas, miR-26b-5p and miR-21-3P bind the UTR of TAP1 transcripts and downregulate TAP1 expression (202). In colorectal cancers, miR-27a expression is increased and causes reduced MHC I expression by suppressing expression of calreticulin (203). Mir-502-5P in gastric cancer and miR-23a in hepatocellular cancer were found to reduce IRF1 expression (204, 205). Thus, miRNAs, which can be highly expressed in cancers, can negatively regulate many of the components of the MHC I antigen presentation pathway. Investigations in this subject area have been relatively limited and therefore it is likely that many more examples of miRNA-mediated inhibition of MHC I antigen presentation in cancers are yet to be discovered.

Another class of ncRNAs are long (>200 bp) non-coding RNAs (lncRNA). These sequences can regulate gene expression in many ways, including epigenetically, transcriptionally and post-transcriptionally (199, 206). One interesting example of a lncRNA that regulates MHC I antigen presentation post-transcriptionally is LINK-A. In a breast cancer model, LINK-A inhibited antigen presentation by indirectly stimulating an E3 ubiquitin ligase which led to the degradation of the peptide-loading complex (207). Again, it is highly likely that additional lncRNAs will be found to negatively regulate components of the MHC I antigen presentation pathway.

ncRNAs can also be positive regulators of MHC I. For example, in head and neck squamous cell carcinomas, expression of the lncRNA, lnc02195, increases MHC I expression and is associated with a better prognosis (208). In nasopharyngeal carcinomas miR9 expression increases expression of MHC I molecules and TAP1 (209). Whether down-regulation of these ncRNAs in cancers is an important mechanism for immune evasion remains to be determined.

The UTR regions of mRNAs can be regulated not only by ncRNAs, but also by proteins binding to these sequences. An RNA-binding E3 ubiquitin ligase, MEX-3C, binds to the 3′ UTR of the transcript for MHC class I molecule HLA-A2 leading to its degradation (210); whether this mechanism is operative in and important to cancer immune evasion has not yet been examined.

LOSS OF THE MHC I ANTIGEN PRESENTATION PATHWAY IN CANCERS THROUGH POST-TRANSLATIONAL MECHANISMS

There are post-translational mechanisms that can impair MHC I antigen presentation in cancers (**Figure 7**). One such post-translational mechanism is analogous to immune evasion mechanisms employed by some viral pathogens. Some viruses encode immune evasion molecules that cause MHC I complexes to be dislocated from the ER into the cytoplasm, where they are degraded through a process referred to as endoplasmic reticulum-associated degradation (ERAD). It turns out that the oncoprotein Staphylococcal nuclease and tudor domain containing 1 (SND1), which is highly expressed in a number of cancers (e.g., Prostate and Melanoma), binds MHC I molecules and causes them to undergo ERAD. Deletion of SND1 in some cancer cell lines increases MHC I expression (211).

Another interesting mechanism that inhibits MHC I antigen presentation is a change in glycolipids on the plasma membrane that occurs in cancer cells that lose the signal peptide peptidase-like 3 (SPPL3) protease (212). SPPL3 cleaves and inactivates a glycosyltransferases B3GNT5, and loss of B3GNT5 reduces levels of negatively charged glycosphingolipids (GSL). Loss of SPPL3 results in an increase in these GSLs, which then associate with MHC I molecules in ways that appear to sterically inhibit their interaction with T cells. This process occurs in gliomas (and potentially some other cancers) and impairs T cell responses to these cells.

Yet another interesting post-translational mechanism that interferes with MHC I antigen presentation is modification of amino acid residues in the peptide-binding groove of MHC I molecules that alters peptide binding; this mechanism is described in more detail in the next section.

LOSS OF THE MHC I ANTIGEN PRESENTATION PATHWAY IN CANCERS DUE TO SIGNALING MECHANISMS AND EXTRINSIC STIMULI FROM THE TUMOR MICROENVIRONMENT

Alterations in signaling pathways can lead to MHC I downregulation in cancers (**Figure 7**). MAPKs, which are activated in some cancers, are negative regulators of MHC I

(213, 214). Inhibiting or silencing of MAPKs increased levels of IRF1 and STAT1 (215) as well as MHC I expression (214). MAPK inhibitors increased mRNA expression of MHC I, TAP, and ß2M (214). Similarly, inhibition of the ALK and RET kinases, which are upstream activators of MAPK, also increase MHC I expression and interestingly also results in the presentation of a different repertoire of peptides (216). Another example is that signaling though the EGFR oncogene HER2/neu is associated with a loss of transcripts for immunoproteasome subunits and TAP, resulting in a loss of MHC I surface expression and antigen presentation (217, 218). Yet another example is that n-MYC and c-MYC overexpression caused loss of MHC I expression, potentially by affecting NF-κB (219–221).

IFNs that are present in the tumor microenvironment [e.g., IFNγ produced by activated T cells or type I interferons produced by a variety of cells, bind to interferon receptors (IFNR) on tumor cells]. Signaling through the IFNRs (**Figure 2**) leads to an increase in expression of many components of the MHC I antigen presentation pathway (e.g., MHC I, TAP, Tapasin, immunoproteasomes, and ERAP1). Components of the IFN pathway can also be lost (**Figure 7**) and this prevents IFN-induced upregulation of the MHC I pathway of antigen presentation. Such loss can also reduce basal levels of MHC I molecule expression (222, 223). IFN receptors signal through Janus kinases (Jak1 and Jak2) and STAT (STAT 1 and STAT2) proteins (224) (**Figure 3**). LOH and/or mutations in Jaks, and STATs are observed in cancers (143, 171). Loss of function mutations in Jak kinases with consequent loss of responsiveness to INFγ were found in Melanomas that became resistant to checkpoint blockade, pointing to the likely clinical significance of the inactivation of the IFN pathway (147, 151, 225). Loss of function in a receptor (APLNR) that interacts with Jak1, reduces IFNγ-stimulated Jak1 and STAT signaling and MHC I upregulation. Mutations in this receptor are found in melanoma patients that are resistant to checkpoint blockade and similarly such resistance is conferred upon knock out of this receptor from mouse melanoma cells (142). Loss of the tyrosine protein phosphatase Ptpn2 that represses IFNγ signaling by dephosphorylating both JAK1 and STAT1. Deletion of Ptpn2 in mouse tumors increases MHC I antigen presentation and improve immunotherapy (226); whether increased Ptpn2 activity in human tumors causes a loss of MHC I antigen presentation is not known. Finally, TGF-ß, which can be present in the tumor microenvironment, can cause a down-regulation of MHC I molecules in some cancers (e.g., ovarian, prostate, and ocular melanoma) (227–229).

Other events in the tumor microenvironment can lead to impaired MHC I antigen presentation in cancers (**Figure 7**). Tumor microenvironments can be hypoxic and hypoxia can impair MHC I antigen presentation in cancers, in part by inhibition of STAT1 (230). Tumor-infiltrating myeloid cells produce reactive nitrogen species in the tumor microenvironment, and this can impair MHC I antigen presentation in cancers. In this situation, the reactive nitrogen species cause nitrosylation of residues in the MHC I peptide binding site, which can inhibit the binding of peptides (231). In tumor-bearing mice, myeloid suppressor cells cause defective IFN responses in host cells (responses in tumors were not examined) likely due to a STAT1 defect potentially caused by nitrosylation (232).

GENE DISRUPTIONS THAT AFFECT MHC I ANTIGEN PRESENTATION: EVIDENCE FROM FORWARD GENETIC SCREENS IN CANCERS

Recently, a number of forward genetic screens have been performed in cancer cells subjected to selection for decreased or increased MHC I expression and have identified a large number of new gene candidates that are potentially involved in MHC class I antigen presentation (69, 142, 167, 174, 177, 226, 233–235). In fact, several of the genes described above (IRF2, PBAF, PRC2, and SPPL3) were discovered in such screens. It is important to note that many of the gene candidates that are initially identified may be artifacts. Therefore, all candidates require further validation and analyses to determine whether they are affecting the MHC I antigen presentation pathway and involved in cancer immune evasion.

A recent CRISPR-cas9 screen in B cell lymphoma cell lines did repeat gene disruptions for individual candidates and were able to reproduce a loss or increase in MHC I expression upon disruption of ∼200 genes (196). Among these genes were ones that are thought to be involved in endocytosis and vesicular trafficking, ubiquitin conjugation, ER quality control, as well as other processes. Further work is needed on these and candidates from other screens to determine whether they are involved in cancer immune evasion. However, interestingly, 30 of these genes showed correlations with CD8 T cell infiltration in multiple cancers; 10 negative-regulatory genes were correlated with less tumor infiltrating CD8 T cells and 20 positive-regulatory were correlated with more infiltrating CD8 T cells. The field can look forward to much more information on the role of these genes and other validated ones in MHC I antigen presentation and cancer immune evasion.

POTENTIAL FOR RESTORING MHC I EXPRESSION IN CANCERS

The fact that the loss of MHC I antigen presentation is common in cancers and allows these cells to evade immune surveillance, raises the question of whether the MHC I pathway defects could be reversed so as to reestablish immune control and responses to immunotherapy. For cancers with deletions or inactivating mutations in structural antigen presenting genes, this would require gene replacement or editing in most cases. *In vitro*, this has been successfully accomplished by transfection of MHC I pathway genes into cancer cell lines. Similarly, gene therapy with a ß2M-adeno-viral vector has been successful in restoring MHC I expression *in vivo* in a murine model (236–238). However, for gene transfer or editing to be a viable therapy, it will likely require that all cancer cells (in the primary site and metastasis) to be transduced and "repaired," because otherwise MHC I-low clones would continue to grow. Achieving this level of gene expression

or repair is probably not feasible with current gene therapy technology. An exception for overcoming the loss of structural genes is the situation where the function of the lost gene can be replaced by inducing another functionally redundant gene. One example of this is where MHC I expression in cancer cells was lost by deletion of the IRF2 transcription factor, but then restored by inducing IRF1 with IFN-stimulation (69). In this case IRF1 and IRF2 are both activating transcription factors that bind to the same promotor element (239).

In situations where the MHC I pathway structural genes are intact but their expression is downregulated, there is the potential to restore gene expression. In some MHC I low cancers, treatment with IFNs has increased MHC I levels (120, 240, 241). The mechanism as to how IFN is restoring MHC I expression has not been investigated in detail, except in one study, IFN was shown to cause increased histone acetylation, DNA demethylation of the promoters of TAP and immunoproteasome genes, and increased transcription of these and other antigen presenting genes (241). In addition, it is possible that IFN is also increasing MHC I levels in MHC I-low cancers through induction of IRF1, which then drives more transcription of the MHC I pathway genes (69), but this has not generally been examined. There are recombinant type I and II IFNs that work *in vivo* and are FDA-approved for other indications. In a small phase 2 trial in which two patients had MHC I negative melanomas, systemic IFNγ-administration induced MHC I expression (240). IFNγ has been shown to improve outcomes of checkpoint blockade in one clinical trial in melanoma (242), however whether and how much this had to do with MHC I expression is unknown.

For cancers that have lost MHC I expression due to epigenetic silencing mechanisms, there may be the potential to restore MHC I expression by reversing the repressive epigenetic marks. There are several examples where MHC I low cancer cell lines have been treated with drugs that inhibit DNA methyltransferases, the enzymes that are responsible for methylating DNA (181, 182, 243, 244), and thereby reverse gene silencing, presumably through demethylation of promoters. Such treatment has increased MHC I expression in several MHC I low cancers cell lines (181, 182, 188, 245). Where examined, this class of epigenetic modifying drugs was found to restore MHC I expression by upregulating expression of many IFN-responsive gene (246) including MHC I antigen presentation pathway genes in cell lines (95, 241, 245). These findings raised the possibility that this class of agents could augment T cell-based immunotherapy. Consistent with this idea, this class of agents has been shown to augment or give additive effects with checkpoint inhibitors in preclinical mouse models (182, 247, 248). There are several DNA methyltransferase inhibitors that are approved by the FDA for cancer treatment, although the exact basis for their efficacy (i.e., what are the key pathways that are affected to give the anti-cancer effects, isn't known). These drugs have been shown to increase expression of IFN and MHC I antigen presentation pathway genes in cancers *in vivo* (182, 245) and in limited clinical trials have improved responses to checkpoint blockade immunotherapy (249) and a tumor vaccine (250). Currently there are further ongoing trials of these agents in combination with immunotherapy (251). Inhibitors of the EZH2 methyltransferase, which as described above is a negative regulator of MHC I antigen presentation, can restore MHC I levels in lymphomas (196, 197).

Similarly, a number of MHC I low cancer cell lines have been treated with histone deacetylase (HDAC) inhibitors, which by increasing histone acetylation can restore promoter activity. HDAC inhibitors have also increased MHC I expression and MHC I pathway components in cancer cell lines (182, 190, 192, 193, 243, 252, 253). There are FDA-approved HDAC and DNA methyltransferase inhibitors that are used to treat cancers. Where studied *in vivo*, methyltransferase inhibitors increased expression of MHC I and MHC I pathway components in multiple types of cancers in patients (182, 245) and a xenograft model (192). In preclinical models, HDAC inhibitors and anti-PDL1 antibody (186, 193, 254–257) or with T cell therapy (258) gave additive effects. Combinations of HDAC inhibitors and checkpoint blockade have and continue to be tested in clinical trials (194, 259–261).

Based on the data just discussed, it is clear that epigenetic modifying agents can increase the MHC I antigen presentation pathway in some MHC I low cancers and that these drugs can improve responses to immunotherapy, however whether these two observations are causally related is not yet established. This is because epigenetic modifying drugs effect the promoter landscapes in potentially all cells. Therefore, these agents can affect not only the tumor, but also cells within the tumor microenvironment and immune system. Moreover, the drugs can affect the expression of many genes within these cells. In most studies, which of the key gene regulatory events that are responsible for therapeutic effects of these drugs is not known. Interestingly, in one animal study the therapeutic effect of an HDAC inhibitor was lost in immunodeficient mice (191), providing evidence that the drug was acting to improve immune control a cancer; however, whether this effect is *via* the restoration of the MHC I pathway or some other immune mechanism is not known.

The broad effects of the epigenetic modifying agents lead to multiple and sometimes opposing effects. For example, global DNA hypomethylation may increase MHC I expression, but also upregulate immunosuppressive mechanisms such as suppressive cytokines and checkpoint inhibitors (262, 263). Such complexity might be overcome, and outcomes improved if there were ways to more selectively modify epigenetic marks of particular genes. At present, drugs that inhibit individual HDAC enzymes are available, and perhaps even more selective agents will be developed. New gene editing approaches using modified Cas9 fusion proteins (e.g., Cas9-p300 acetyltransferase, Cas9-methyltransferases can Cas9-demethylases) have the ability to alter epigenetic marks and/or transcriptionally activate or repress expression of specific genes (264, 265). Whether such approaches could somehow be used *in vivo* to efficiently edit all cancer cells remains to be seen.

MicroRNAs that reduce MHC I antigen presentation are a potential therapeutic target. MiRNAs can be blocked in cells by treatment with complementary anti-sense RNAs (antimirRs/antagomiRs) and overexpression of miRNAs can be achieved using miRNA duplexes (miRNA mimetics) (199, 266).

These approaches require chemical modifications to stabilize RNA oligonucleotides and methods to deliver these compounds into cells (e.g., lipid nanoparticles). Such agents have been used successfully in preclinical models and have and/or are being tested in phase 1 and 2 clinical trials, but not yet for affecting MHC I antigen presentation. LncRNAs can be targeted for degradation with anti-sense oligonucleotides.

Inhibitors of enzymes that lead to a loss of MHC I antigen presentation also have the potential to restore antigen presentation in some cancers. Inhibitors of ALK, RET, and MAPK kinases can reverse the downregulation of the MHC I antigen presentation caused by these enzymes (213, 214, 216). There are FDA approved inhibitors of glycosyltransferases, and these agents were shown to reverse the suppression of MHC I stimulatory activity caused by the increase in negatively charged glycosphingolipids from loss of SPPL3 (212). Inhibitors of thymidylate synthetase were found to increase MHC I levels in lymphoma cells in a targeted small molecule screen, *via* an as yet unknown mechanism (196).

Finally, in cells that have lost some MHC I antigen presentation pathway components, such as TAP (40, 267) and ERAP1 (60, 100), novel peptides peptides [aka "T cell epitopes associated with impaired **peptide** processing (**TEIPP)**] are presented that are not displayed in wild type cells and can be immunogenic. There is limited data that immunization with such sequences can elicit anti-tumor responses (268, 269). Therefore, an alternate approach to restoring the loss of MHC I antigen presentation components could be to exploit the presentation of unique antigen peptides that are displayed on such cancer cells (269).

The elucidation of the many mechanisms that lead to a loss of MHC I antigen presentation and the identification of tractable therapeutic targets to reverse this loss, brings the hope of restoring immune control and improving T cell-based immunotherapy. Given the differences between different cancer types, the heterogeneity within a single type of cancer, and the many different mechanisms that can disable the MHC class I pathway, it seems likely that such approaches will require precision medicine, where the cause of immune evasion in an individual patient is identified and then the appropriate therapy selected. The advances in identifying the underlying mechanisms that cripple MHC I antigen presentation are necessary steps in attempting to achieve this goal.

RECOGNITION AND CONTROL OF MHC I LOW CANCERS BY NK CELLS

Cancers that have lost MHC I expression through the mechanisms discussed above, can avoid control and elimination by CD8 T lymphocytes. This is analogous to the situation where some viruses encode immune evasion molecules that inhibit MHC I antigen presentation and thereby allow virally infected cells to avoid being killed by CD8 T cells and help establish chronic infections. In these situations, there is a second line of defense that can kill these abnormal cells and this immune function is provided by natural killer (NK) cells. NK cells identify these cells in part by sensing the presence or absence of MHC I molecules.

NK cells are a lineage of lymphocyte that is distinct from B and T cells. These cells have similar effector functions (cytotoxicity and cytokine production), as CD8 T cells. However, NK cells are innate lymphoid cells (ILC) and the receptors they use to recognize their target cells are fundamentally different from the ones used by T (and B) lymphocytes. Instead of employing a mechanism that recombines gene segments to generate clonally unique and diverse receptors, NK cells use non-rearranging germ-line encoded receptors of several different types (270). Some of these NK receptors are activating ones and others provide inhibitory signals.

Human NK cells express several killer inhibitory receptors (KIR) that upon engagement of their ligands, impart inhibitory signals through ITIM motifs in the receptors' intracytoplasmic domains. HLA-A and HLA-B are ligands for KIR3D receptors and HLA-C is recognized by KIR2D receptors. In addition, NK cells express other types of inhibitory receptors that recognize MHC I molecules, including CD94-NKG2A, which recognizes HLA-E, and LILRB1, which recognizes all MHC I molecules. Moreover, NK cells express other inhibitory receptors that are not involved in MHC I recognition (270). Because of their inhibitory receptors that recognize MHC I molecules, NK cells ignore normal MHC I-sufficient cells but are disinhibited when they encounter abnormal-MHC I low cells. This loss of inhibition is a necessary but not a sufficient event to trigger the NK cell's effector mechanisms.

Activation of NK cells requires engagement of activating receptors, which in humans include NKG2D, NKp20, NKp44, and NKp46 (270). These receptors associate with and signal through ITAM-containing proteins (270). Other stimulatory receptors expressed by NK include 2B4 (CD244) and DNAM1 (CD226) (270).

The ligands of some of the activating receptors are ones whose expression is induced on cancers, virally infected and stressed cells. The best characterized examples are the MHC class I polypeptide–related sequence A and B (MICA and MICB) molecules, which are the ligands of the activating NKG2D receptor. MIC A and MIC B are structurally similar to HLA class heavy chains but are not associated with ß2M and do not bind peptides. Because of these properties, MICA's and MICB's expression is not affected by defects in the MHC I antigen presentation pathway and therefore can be expressed in MHC I negative cancer cells. The activation of NK cells depends on the balance of stimulatory and inhibitor signals they receive. Cancers or virally infected cells that both express activating ligands and lack inhibitory ligands can be killed by NK cells.

Mice that lack functional NKs cell due to antibody treatment or genetic knock outs develop a higher frequency of some cancers (271, 272). Similarly, humans that have NK cell defects have increases in some cancers, particularly ones that may be induced by viruses (273). A caveat in many of these studies is that the mouse models and NK deficient humans may have defects beyond just a loss of NK cells (273). Nevertheless, the data in aggregate suggest that NK cells play a role in immune surveillance. Whether the protection against carcinogenesis

afforded by NK cells is primarily against MHC I low cancers is not clear (274).

NK cells may still exert some control after cancers have arisen. Depletion of NK cells in mouse models promotes the growth and metastasis of transplanted tumors (271, 275, 276). Moreover, adoptive transfer of NK cells into tumor-bearing mice can lead to tumor rejection. In humans, the level of cytolytic activity of circulating NK cells correlates with the risk of cancer (277) and infiltration of NK cells in some cancers is associated with a better prognosis (278, 279). Similarly, adoptive transfer of NK cells into human cancer patients has shown therapeutic effects in some patients, demonstrating that similar principles likely apply in humans (280). Such studies have led to considerable interest in exploiting NK cells for tumor therapy and there are many efforts underway to do so [e.g., developing CAR-NK cell therapy and antibodies that recruit activated NK cells to cancers (270, 281, 282)].

Despite NK cells being a potential second line of defense against tumors that have lost MHC I, once such tumors become clinically evident, they almost always progress. In fact, as noted above, loss of MHC I is often a negative prognostic indicator. Moreover, there is no evidence that MHC I negative cancers are infiltrated with more NK cells than MHC I sufficient cancers (283). Therefore, for many MHC I low cancers, either they were never targets of NK cells or such tumors have evolved ways to evade control by NK cells.

In fact, there are many mechanisms through which cancers can evade NK cells. For example, HLA A, B&C low cancers can express the non-classical MHC I molecules HLA-G and HLA-E, which can inhibit NK cells by engaging their inhibitory receptors (284–288). In addition, NK cells may not penetrate into solid tumors or once within the cancer can become anergic or exhausted, including in MHC I low tumors (289–291). Furthermore, tumors can shed their MIC molecules, thereby removing an activation signal and creating a soluble ligand that can block the NK cell's cognate receptor (292, 293). Moreover, cancers can also create an immunosuppressive environment [e.g., producing TGFß, which can lead to inhibition of NK cells (294)]. A fuller consideration of these mechanisms is beyond the scope of this article and readers are referred to recent reviews (270, 295, 296).

FUTURE DIRECTIONS

While there is abundant evidence that loss of MHC I antigen presentation is a frequent event in cancers that results in immune evasion, we still have much to learn. As reviewed above, new mechanisms for MHC I downregulation have recently been discovered and there will be more to be uncovered. Forward genetic screens are identifying new components that contribute to the MHC I pathway and it will be of importance to investigate how they contribute to MHC I phenotypes in cancers. Even among the known mechanisms for loss of antigen presentation, a majority of the analyses have been performed in limited cancer types and a more comprehensive understanding across more types of cancer is needed. Moreover, many of the underlying mechanisms for MHC I pathway loss need to be elucidated at higher resolution (e.g., causes and specific targets of epigenetic modifications).

Given the importance of MHC I antigen presentation for the immune control and immunotherapy of cancers, there is a need to develop therapeutic approaches to restore the MHC I pathway in cancers and this should be feasible in at least some cancers. This might itself be an immunotherapy by allowing a restoration of immune control. It might also provide adjunct therapy that could improve the percentage of patients that respond to immunotherapies and potentially extend the efficacy of immunotherapies to cancers that have been largely resistant to such therapy. The various mechanisms that cause MHC I pathway-loss might also serve as biomarkers to help identify patients that have the potential to respond, or not, to immunotherapy and/or have the potential for the loss of MHC I to be reversed. The hope for such biomarkers is that they could make immunotherapy more personalized (e.g., sparing those patients who won't respond to such therapy from the risks and enormous expense of the treatment).

CONCLUSIONS

A sizable percentage of many different types of cancers lose MHC I antigen presentation partially or completely. This is almost certainly the result of immunoediting where MHC I low variants emerge under selection pressure imposed by CD8 T cells. The result of this process is that CD8 T cells can no longer "see" these MHC I-deficient variants and are therefore unable to control or eliminate them. This process reflects the fact that the MHC I pathway is non-essential for viability and growth and therefore when lost does not compromise cancer progression. Where examined, this escape of immune control is generally associated with worse prognoses and resistance to immunotherapy. There are many mechanisms that underlie the loss of MHC I antigen presentation. Some mechanisms involve mutations and deletions of structural genes of one or more component(s) of the antigen presentation pathway; others effect transcription of pathway genes *via* loss of transcription factors or epigenetic silencing of gene regulatory elements; and yet others can affect the stability of mRNAs for MHC I pathway components or the molecules themselves, or signaling pathways that regulate MHC I expression. Some of these alterations are unique to an individual cancer and others are common in multiple patients and cancer types. It will be important to further understand the multiple mechanisms for loss of the MHC I pathway that are operative in all cancer types and their clinical significance. The hope is that in the future, characterizing MHC I pathway lesions in individual patient samples would lead to actionable information about what therapies will or will not be likely to work and prognosis. Moreover, some of the mechanisms that cause the loss of the MHC I pathway in cancers are reversible and may be amenable to the development of therapeutic interventions that could make T cell-based immunotherapies more efficacious in more patients and in more kinds of cancer.

AUTHOR CONTRIBUTIONS

The text was written by KR, KD, and JC. Figures were made by KD and JC. All authors contributed to the article and approved the submitted version.

FUNDING

This work was supported by grants R01CA247624, R01AI114495, and R01 AI145932 to KR.

REFERENCES

1. Shankaran V, Ikeda H, Bruce AT, White JM, Swanson PE, Old LJ, et al. IFNgamma and lymphocytes prevent primary tumour development and shape tumour immunogenicity. *Nature*. (2001) 410:1107–11. doi: 10.1038/35074122
2. Koebel CM, Vermi W, Swann JB, Zerafa N, Rodig SJ, Old LJ, et al. Adaptive immunity maintains occult cancer in an equilibrium state. *Nature*. (2007) 450:903–7. doi: 10.1038/nature06309
3. Mayor PC, Eng KH, Singel KL, Abrams SI, Odunsi K, Moysich KB, et al. Cancer in primary immunodeficiency diseases: cancer incidence in the United States Immune Deficiency Network Registry. *J Allergy Clin Immunol*. (2018) 141:1028–35. doi: 10.1016/j.jaci.2017.05.024
4. Vajdic CM, van Leeuwen MT. Cancer incidence and risk factors after solid organ transplantation. *Int J Cancer*. (2009) 125:1747–54. doi: 10.1002/ijc.24439
5. Mortaz E, Tabarsi P, Mansouri D, Khosravi A, Garssen J, Velayati A, et al. Cancers related to immunodeficiencies: update and perspectives. *Front Immunol*. (2016) 7:365. doi: 10.3389/fimmu.2016.00365
6. Zhang L, Conejo-Garcia JR, Katsaros D, Gimotty PA, Massobrio M, Regnani G, et al. Intratumoral T cells, recurrence, and survival in epithelial ovarian cancer. *N Engl J Med*. (2003) 348:203–13. doi: 10.1056/NEJMoa020177
7. Sato E, Olson SH, Ahn J, Bundy B, Nishikawa H, Qian F, et al. Intraepithelial CD8+ tumor-infiltrating lymphocytes and a high CD8+/regulatory T cell ratio are associated with favorable prognosis in ovarian cancer. *Proc Natl Acad Sci USA*. (2005) 102:18538–43. doi: 10.1073/pnas.0509182102
8. Galon J, Costes A, Sanchez-Cabo F, Kirilovsky A, Mlecnik B, Lagorce-Pages C, et al. Type, density, and location of immune cells within human colorectal tumors predict clinical outcome. *Science*. (2006) 313:1960–4. doi: 10.1126/science.1129139
9. Pages F, Kirilovsky A, Mlecnik B, Asslaber M, Tosolini M, Bindea G, et al. I*n situ* cytotoxic and memory T cells predict outcome in patients with early-stage colorectal cancer. *J Clin Oncol*. (2009) 27:5944–51. doi: 10.1200/JCO.2008.19.6147
10. Rusakiewicz S, Semeraro M, Sarabi M, Desbois M, Locher C, Mendez R, et al. Immune infiltrates are prognostic factors in localized gastrointestinal stromal tumors. *Cancer Res*. (2013) 73:3499–510. doi: 10.1158/0008-5472.CAN-13-0371
11. Ryschich E, Notzel T, Hinz U, Autschbach F, Ferguson J, Simon I, et al. Control of T-cell-mediated immune response by HLA class I in human pancreatic carcinoma. *Clin Cancer Res*. (2005) 11:498–504.
12. Sharma P, Shen Y, Wen S, Yamada S, Jungbluth AA, Gnjatic S, et al. CD8 tumor-infiltrating lymphocytes are predictive of survival in muscle-invasive urothelial carcinoma. *Proc Natl Acad Sci USA*. (2007) 104:3967–72. doi: 10.1073/pnas.0611618104
13. Matsumoto H, Thike AA, Li H, Yeong J, Koo SL, Dent RA, et al. Increased CD4 and CD8-positive T cell infiltrate signifies good prognosis in a subset of triple-negative breast cancer. *Breast Cancer Res Treat*. (2016) 156:237–47. doi: 10.1007/s10549-016-3743-x
14. Ogino T, Shigyo H, Ishii H, Katayama A, Miyokawa N, Harabuchi Y, et al. HLA class I antigen down-regulation in primary laryngeal squamous cell carcinoma lesions as a poor prognostic marker. *Cancer Res*. (2006) 66:9281–9. doi: 10.1158/0008-5472.CAN-06-0488
15. Fridman WH, Pages F, Sautes-Fridman C, Galon J. The immune contexture in human tumours: impact on clinical outcome. *Nat Rev Cancer*. (2012) 12:298–306. doi: 10.1038/nrc3245
16. Sharma P, Hu-Lieskovan S, Wargo JA, Ribas A. Primary, adaptive, and acquired resistance to cancer immunotherapy. *Cell*. (2017) 168:707–23. doi: 10.1016/j.cell.2017.01.017
17. Patel SA, Minn AJ. Combination cancer therapy with immune checkpoint blockade: mechanisms and strategies. *Immunity*. (2018) 48:417–33. doi: 10.1016/j.immuni.2018.03.007
18. Boesen M, Svane IM, Engel AM, Rygaard J, Thomsen AR, Werdelin O. CD8+ T cells are crucial for the ability of congenic normal mice to reject highly immunogenic sarcomas induced in nude mice with 3-methylcholanthrene. *Clin Exp Immunol*. (2000) 121:210–5. doi: 10.1046/j.1365-2249.2000.01292.x
19. Walsh SR, Simovic B, Chen L, Bastin D, Nguyen A, Stephenson K, et al. Endogenous T cells prevent tumor immune escape following adoptive T cell therapy. *J Clin Invest*. (2019) 129:5400–10. doi: 10.1172/JCI126199
20. Pages F, Berger A, Camus M, Sanchez-Cabo F, Costes A, Molidor R, et al. Effector memory T cells, early metastasis, and survival in colorectal cancer. *N Engl J Med*. (2005) 353:2654–66. doi: 10.1056/NEJMoa051424
21. Morgan RA, Dudley ME, Wunderlich JR, Hughes MS, Yang JC, Sherry RM, et al. Cancer regression in patients after transfer of genetically engineered lymphocytes. *Science*. (2006) 314:126–9. doi: 10.1126/science.1129003
22. van den Broek ME, Kagi D, Ossendorp F, Toes R, Vamvakas S, Lutz WK, et al. Decreased tumor surveillance in perforin-deficient mice. *J Exp Med*. (1996) 184:1781–90. doi: 10.1084/jem.184.5.1781
23. Brennan AJ, Chia J, Trapani JA, Voskoboinik I. Perforin deficiency and susceptibility to cancer. *Cell Death Differ*. (2010) 17:607–15. doi: 10.1038/cdd.2009.212
24. Voskoboinik I, Trapani JA. Perforinopathy: a spectrum of human immune disease caused by defective perforin delivery or function. *Front Immunol*. (2013) 4: 441. doi: 10.3389/fimmu.2013.00441
25. Schreiber RD, Old LJ, Smyth MJ. Cancer immunoediting: integrating immunity's roles in cancer suppression and promotion. *Science*. (2011) 331:1565–70. doi: 10.1126/science.1203486
26. Rizzo R, Fainardi E, Rouas-Freiss N, Morandi F. The role of HLA-class Ib molecules in immune-related diseases, tumors, and infections. *J Immunol Res.* (2017) 2017:2309574. doi: 10.1155/2017/2309574
27. da Silva IL, Montero-Montero L, Ferreira E, Quintanilla M. New insights into the role of Qa-2 and HLA-G non-classical MHC-I complexes in malignancy. *Front Immunol*. (2018) 9:2894. doi: 10.3389/fimmu.2018.02894
28. Bukur J, Jasinski S, Seliger B. The role of classical and non-classical HLA class I antigens in human tumors. *Semin Cancer Biol*. (2012) 22:350–8. doi: 10.1016/j.semcancer.2012.03.003
29. Rock KL, Gramm C, Rothstein L, Clark K, Stein R, Dick L, et al. Inhibitors of the proteasome block the degradation of most cell proteins and the generation of peptides presented on MHC class I molecules. *Cell*. (1994) 78:761–71. doi: 10.1016/S0092-8674(94)90462-6
30. Michalek MT, Grant EP, Gramm C, Goldberg AL, Rock KL. A role for the ubiquitin-dependent proteolytic pathway in MHC class I-restricted antigen presentation. *Nature*. (1993) 363:552–4. doi: 10.1038/363552a0
31. Shen L, Rock KL. Cellular protein is the source of cross-priming antigen i*n vivo*. *Proc Natl Acad Sci USA*. (2004) 101:3035–40. doi: 10.1073/pnas.0308345101
32. Wei J, Zanker D, Di Carluccio AR, Smelkinson MG, Takeda K, Seedhom MO, et al. Varied role of ubiquitylation in generating MHC class I peptide ligands. *J Immunol*. (2017) 198:3835–45. doi: 10.4049/jimmunol.1602122
33. Murata S, Takahama Y, Kasahara M, Tanaka K. The immunoproteasome and thymoproteasome: functions, evolution and human disease. *Nat Immunol*. (2018) 19:923–31. doi: 10.1038/s41590-018-0186-z
34. Rock KL, Goldberg AL. Degradation of cell proteins and the generation of MHC class I-presented peptides. *Annu Rev Immunol*. (1999) 17:739–79. doi: 10.1146/annurev.immunol.17.1.739
35. Kincaid EZ, Che JW, York I, Escobar H, Reyes-Vargas E, Delgado JC, et al. Mice completely lacking immunoproteasomes show major changes

in antigen presentation. *Nat Immunol*. (2011) 13:129–35. doi: 10.1038/ni.2203
36. Eggensperger S, Tampe R. The transporter associated with antigen processing: a key player in adaptive immunity. *Biol Chem*. (2015) 396:1059–72. doi: 10.1515/hsz-2014-0320
37. Roelse J, Gromme M, Momburg F, Hammerling G, Neefjes J. Trimming of TAP-translocated peptides in the endoplasmic reticulum and in the cytosol during recycling. *J Exp Med*. (1994) 180:1591–7. doi: 10.1084/jem.180.5.1591
38. Momburg F, Roelse J, Hammerling GJ, Neefjes JJ. Peptide size selection by the major histocompatibility complex-encoded peptide transporter. *J Exp Med*. (1994) 179:1613–23. doi: 10.1084/jem.179.5.1613
39. Schumacher TN, Kantesaria DV, Heemels MT, Ashton-Rickardt PG, Shepherd JC, Fruh K, et al. Peptide length and sequence specificity of the mouse TAP1/TAP2 translocator. *J Exp Med*. (1994) 179:533–40. doi: 10.1084/jem.179.2.533
40. Van Kaer L, Ashton-Rickardt PG, Ploegh HL, Tonegawa S. TAP1 mutant mice are deficient in antigen presentation, surface class I molecules, and CD4-8+ T cells. *Cell*. (1992) 71:1205–14. doi: 10.1016/S0092-8674(05)80068-6
41. Sandberg JK, Chambers BJ, Van Kaer L, Karre K, Ljunggren HG. TAP1-deficient mice select a CD8+ T cell repertoire that displays both diversity and peptide specificity. *Eur J Immunol*. (1996) 26:288–93. doi: 10.1002/eji.1830260203
42. Gadola SD, Moins-Teisserenc HT, Trowsdale J, Gross WL, Cerundolo V. TAP deficiency syndrome. *Clin Exp Immunol*. (2000) 121:173–8. doi: 10.1046/j.1365-2249.2000.01264.x
43. Hanalioglu D, Ayvaz DC, Ozgur TT, van der Burg M, Sanal O, Tezcan I. A novel mutation in TAP1 gene leading to MHC class I deficiency: report of two cases and review of the literature. *Clin Immunol*. (2017) 178:74–8. doi: 10.1016/j.clim.2017.01.011
44. Cresswell P, Bangia N, Dick T, Diedrich G. The nature of the MHC class I peptide loading complex. *Immunol Rev*. (1999) 172:21–8. doi: 10.1111/j.1600-065X.1999.tb01353.x
45. Blees A, Januliene D, Hofmann T, Koller N, Schmidt C, Trowitzsch S, et al. Structure of the human MHC-I peptide-loading complex. *Nature*. (2017) 551:525–8. doi: 10.1038/nature24627
46. Schoenhals GJ, Krishna RM, Grandea AG 3rd, Spies T, Peterson PA, Yang Y, et al. Retention of empty MHC class I molecules by tapasin is essential to reconstitute antigen presentation in invertebrate cells. *EMBO J*. (1999) 18:743–53. doi: 10.1093/emboj/18.3.743
47. Hafstrand I, Sayitoglu EC, Apavaloaei A, Josey BJ, Sun R, Han X, et al. Successive crystal structure snapshots suggest the basis for MHC class I peptide loading and editing by tapasin. *Proc Natl Acad Sci USA*. (2019) 116:5055–60. doi: 10.1073/pnas.1807656116
48. Boyle LH, Hermann C, Boname JM, Porter KM, Patel PA, Burr ML, et al. Tapasin-related protein TAPBPR is an additional component of the MHC class I presentation pathway. *Proc Natl Acad Sci USA*. (2013) 110:3465–70. doi: 10.1073/pnas.1222342110
49. Grandea AG 3rd, Golovina TN, Hamilton SE, Sriram V, Spies T, Brutkiewicz RR, et al. Impaired assembly yet normal trafficking of MHC class I molecules in Tapasin mutant mice. *Immunity*. (2000) 13:213–22. doi: 10.1016/S1074-7613(00)00021-2
50. Coe H, Jung J, Groenendyk J, Prins D, Michalak M. ERp57 modulates STAT3 signaling from the lumen of the endoplasmic reticulum. *J Biol Chem*. (2010) 285:6725–38. doi: 10.1074/jbc.M109.054015
51. Bjorkman PJ, Saper MA, Samraoui B, Bennett WS, Strominger JL, Wiley DC. Structure of the human class I histocompatibility antigen, HLA-A2. *Nature*. (1987) 329:506–12. doi: 10.1038/329506a0
52. Bjorkman PJ, Parham P. Structure, function, and diversity of class I major histocompatibility complex molecules. *Annu Rev Biochem*. (1990) 59:253–88. doi: 10.1146/annurev.bi.59.070190.001345
53. Rammensee HG, Falk K, Rotzschke O. Peptides naturally presented by MHC class I molecules. *Annu Rev Immunol*. (1993) 11:213–44. doi: 10.1146/annurev.iy.11.040193.001241
54. Cascio P, Hilton C, Kisselev AF, Rock KL, Goldberg AL. 26S proteasomes and immunoproteasomes produce mainly N-extended versions of an antigenic peptide. *EMBO J*. (2001) 20:2357–66. doi: 10.1093/emboj/20.10.2357
55. York IA, Chang SC, Saric T, Keys JA, Favreau JM, Goldberg AL, et al. The ER aminopeptidase ERAP1 enhances or limits antigen presentation by trimming epitopes to 8–9 residues. *Nat Immunol*. (2002) 3:1177–84. doi: 10.1038/ni860
56. Serwold T, Gonzalez F, Kim J, Jacob R, Shastri N. ERAAP customizes peptides for MHC class I molecules in the endoplasmic reticulum. *Nature*. (2002) 419:480–3. doi: 10.1038/nature01074
57. Evnouchidou I, Weimershaus M, Saveanu L, van Endert P. ERAP1-ERAP2 dimerization increases peptide-trimming efficiency. *J Immunol*. (2014) 193:901–8. doi: 10.4049/jimmunol.1302855
58. Hearn A, York IA, Bishop C, Rock KL. Characterizing the specificity and cooperation of aminopeptidases in the cytosol and endoplasmic reticulum during MHC class I antigen presentation. *J Immunol*. (2010) 184:4725–32. doi: 10.4049/jimmunol.0903125
59. York IA, Brehm MA, Zendzian S, Towne CF, Rock KL. Endoplasmic reticulum aminopeptidase. (2006) 1 (ERAP1) trims MHC class I-presented peptides *in vivo* and plays an important role in immunodominance. *Proc Natl Acad Sci USA* 103:9202–7. doi: 10.1073/pnas.0603095103
60. Nagarajan NA, de Verteuil DA, Sriranganadane D, Yahyaoui W, Thibault P, Perreault C, et al. ERAAP shapes the peptidome associated with classical and nonclassical MHC class I molecules. *J Immunol*. (2016) 197:1035–43. doi: 10.4049/jimmunol.1500654
61. Kanaseki T, Blanchard N, Hammer GE, Gonzalez F, Shastri N. ERAAP synergizes with MHC class I molecules to make the final cut in the antigenic peptide precursors in the endoplasmic reticulum. *Immunity*. (2006) 25:795–806. doi: 10.1016/j.immuni.2006.09.012
62. Kanaseki T, Lind KC, Escobar H, Nagarajan N, Reyes-Vargas E, Rudd B, et al. ERAAP and tapasin independently edit the amino and carboxyl termini of MHC class I peptides. *J Immunol*. (2013) 191:1547–55. doi: 10.4049/jimmunol.1301043
63. Townsend A, Ohlen C, Bastin J, Ljunggren HG, Foster L, Karre K. Association of class I major histocompatibility heavy and light chains induced by viral peptides. *Nature*. (1989) 340:443–8. doi: 10.1038/340443a0
64. van den Elsen PJ, Holling TM, Kuipers HF, van der Stoep N. Transcriptional regulation of antigen presentation. *Curr Opin Immunol*. (2004) 16:67–75. doi: 10.1016/j.coi.2003.11.015
65. Kelly A, Trowsdale J. Genetics of antigen processing and presentation. *Immunogenetics*. (2019) 71:161–70. doi: 10.1007/s00251-018-1082-2
66. Jongsma MLM, Guarda G, Spaapen RM. The regulatory network behind MHC class I expression. *Mol Immunol*. (2019) 113:16–21. doi: 10.1016/j.molimm.2017.12.005
67. Meissner TB, Li A, Biswas A, Lee KH, Liu YJ, Bayir E, et al. NLR family member NLRC5 is a transcriptional regulator of MHC class I genes. *Proc Natl Acad Sci USA*. (2010) 107:13794–9. doi: 10.1073/pnas.1008684107
68. Hobart M, Ramassar V, Goes N, Urmson J, Halloran PF. IFN regulatory factor-1 plays a central role in the regulation of the expression of class I and II MHC genes *in vivo*. *J Immunol*. (1997) 158:4260–9
69. Kriegsman BA, Vangala P, Chen BJ, Meraner P, Brass AL, Garber M, et al. Frequent loss of IRF2 in cancers leads to immune evasion through decreased MHC class I antigen presentation and increased PD-L1 expression. *J Immunol*. (2019) 203:1999–2010. doi: 10.4049/jimmunol.1900475
70. Chang CH, Hammer J, Loh JE, Fodor WL, Flavell RA. The activation of major histocompatibility complex class I genes by interferon regulatory factor-1 (IRF-1). *Immunogenetics*. (1992) 35:378–84. doi: 10.1007/BF00179793
71. Biswas A, Meissner TB, Kawai T, Kobayashi KS. Cutting edge: impaired MHC class I expression in mice deficient for Nlrc5/class I transactivator. *J Immunol*. (2012) 189:516–20. doi: 10.4049/jimmunol.1200064
72. Matsuyama T, Kimura T, Kitagawa M, Pfeffer K, Kawakami T, Watanabe N, et al. Targeted disruption of IRF-1 or IRF-2 results in abnormal type I IFN gene induction and aberrant lymphocyte development. *Cell*. (1993) 75:83–97. doi: 10.1016/S0092-8674(05)80086-8
73. Uhlen M, Karlsson MJ, Zhong W, Tebani A, Pou C, Mikes J, et al. A genome-wide transcriptomic analysis of protein-coding genes in human blood cells. *Science*. (2019) 366:aax9198. doi: 10.1126/science.aax9198
74. Boegel S, Lower M, Bukur T, Sorn P, Castle JC, Sahin U. HLA and proteasome expression body map. *BMC Med Genom*. (2018) 11:36. doi: 10.1186/s12920-018-0354-x

75. Zhou F. Molecular mechanisms of IFN-gamma to up-regulate MHC class I antigen processing and presentation. *Int Rev Immunol*. (2009) 28:239–60. doi: 10.1080/08830180902978120
76. Der SD, Zhou A, Williams BR, Silverman RH. Identification of genes differentially regulated by interferon alpha, beta, or gamma using oligonucleotide arrays. *Proc Natl Acad Sci USA*. (1998) 95:15623–8. doi: 10.1073/pnas.95.26.15623
77. Kaplan DH, Shankaran V, Dighe AS, Stockert E, Aguet M, Old LJ, et al. Demonstration of an interferon gamma-dependent tumor surveillance system in immunocompetent mice. *Proc Natl Acad Sci USA*. (1998) 95:7556–61. doi: 10.1073/pnas.95.13.7556
78. Reyal F, Guyader C, Decraene C, Lucchesi C, Auger N, Assayag F, et al. Molecular profiling of patient-derived breast cancer xenografts. *Breast Cancer Res*. (2012) 14:R11. doi: 10.1186/bcr3095
79. Grasso CS, Tsoi J, Onyshchenko M, Abril-Rodriguez G, Ross-Macdonald P, Wind-Rotolo M, et al. Conserved interferon-gamma signaling drives clinical response to immune checkpoint blockade therapy in melanoma. *Cancer Cell*. (2020) 38:500–15 e3. doi: 10.1016/j.ccell.2020.08.005
80. Schumacher TN, Scheper W, Kvistborg P. Cancer neoantigens. *Annu Rev Immunol*. (2019) 37:173–200. doi: 10.1146/annurev-immunol-042617-053402
81. Galuppini F, Dal Pozzo CA, Deckert J, Loupakis F, Fassan M, Baffa R. Tumor mutation burden: from comprehensive mutational screening to the clinic. *Cancer Cell Int*. (2019) 19:209. doi: 10.1186/s12935-019-0929-4
82. Yarchoan M, Johnson BA 3rd, Lutz ER, Laheru DA, Jaffee EM. Targeting neoantigens to augment antitumour immunity. *Nat Rev Cancer*. (2017) 17:209–22. doi: 10.1038/nrc.2016.154
83. Maleki Vareki S. High and low mutational burden tumors versus immunologically hot and cold tumors and response to immune checkpoint inhibitors. *J Immunother Cancer*. (2018) 6:157. doi: 10.1186/s40425-018-0479-7
84. Yarchoan M, Hopkins A, Jaffee EM. Tumor mutational burden and response rate to PD-1 inhibition. *N Engl J Med*. (2017) 377:2500–1. doi: 10.1056/NEJMc1713444
85. Ilyas S, Yang JC. Landscape of tumor antigens in T cell immunotherapy. *J Immunol*. (2015) 195:5117–22. doi: 10.4049/jimmunol.1501657
86. Disis ML, Bernhard H, Jaffee EM. Use of tumour-responsive T cells as cancer treatment. *Lancet*. (2009) 373:673–83. doi: 10.1016/S0140-6736(09)60404-9
87. Xiong D, Wang Y, You M. Tumor intrinsic immunity related proteins may be novel tumor suppressors in some types of cancer. *Sci Rep*. (2019) 9:10918. doi: 10.1038/s41598-019-47382-3
88. Safonov A, Jiang T, Bianchini G, Gyorffy B, Karn T, Hatzis C, et al. Immune gene expression is associated with genomic aberrations in breast cancer. *Cancer Res*. (2017) 77:3317–24. doi: 10.1158/0008-5472.CAN-16-3478
89. Kim R, Emi M, Tanabe K. Cancer immunoediting from immune surveillance to immune escape. *Immunology*. (2007) 121:1–14. doi: 10.1111/j.1365-2567.2007.02587.x
90. Teng MW, Swann JB, Koebel CM, Schreiber RD, Smyth MJ. Immune-mediated dormancy: an equilibrium with cancer. *J Leukoc Biol*. (2008) 84:988–93. doi: 10.1189/jlb.1107774
91. Schrors B, Lubcke S, Lennerz V, Fatho M, Bicker A, Wolfel C, et al. HLA class I loss in metachronous metastases prevents continuous T cell recognition of mutated neoantigens in a human melanoma model. *Oncotarget*. (2017) 8:28312–27. doi: 10.18632/oncotarget.16048
92. Romero I, Garrido C, Algarra I, Chamorro V, Collado A, Garrido F, et al. MHC intratumoral heterogeneity may predict cancer progression and response to immunotherapy. *Front Immunol*. (2018) 9:102. doi: 10.3389/fimmu.2018.00102
93. del Campo AB, Kyte JA, Carretero J, Zinchencko S, Mendez R, Gonzalez-Aseguinolaza G, et al. Immune escape of cancer cells with beta2-microglobulin loss over the course of metastatic melanoma. *Int J Cancer*. (2014) 134:102–13. doi: 10.1002/ijc.28338
94. Erdogdu IH. MHC class 1 and PDL-1 status of primary tumor and lymph node metastatic tumor tissue in gastric cancers. *Gastroenterol Res Pract*. (2019) 2019:4785098. doi: 10.1155/2019/4785098
95. Chang CC, Pirozzi G, Wen SH, Chung IH, Chiu BL, Errico S, et al. Multiple structural and epigenetic defects in the human leukocyte antigen class I antigen presentation pathway in a recurrent metastatic melanoma following immunotherapy. *J Biol Chem*. (2015) 290:26562–75. doi: 10.1074/jbc.M115.676130
96. Maeurer MJ, Gollin SM, Storkus WJ, Swaney W, Karbach J, Martin D, et al. Tumor escape from immune recognition: loss of HLA-A2 melanoma cell surface expression is associated with a complex rearrangement of the short arm of chromosome 6. *Clin Cancer Res*. (1996) 2:641–52.
97. Wei ML, Cresswell P. HLA-A2 molecules in an antigen-processing mutant cell contain signal sequence-derived peptides. *Nature*. (1992) 356:443–6. doi: 10.1038/356443a0
98. Williams AP, Peh CA, Purcell AW, McCluskey J, Elliott T. Optimization of the MHC class I peptide cargo is dependent on tapasin. *Immunity*. (2002) 16:509–20. doi: 10.1016/S1074-7613(02)00304-7
99. Yan J, Parekh VV, Mendez-Fernandez Y, Olivares-Villagomez D, Dragovic S, Hill T, et al. *In vivo* role of ER-associated peptidase activity in tailoring peptides for presentation by MHC class Ia and class Ib molecules. *J Exp Med*. (2006) 203:647–59. doi: 10.1084/jem.20052271
100. Hammer GE, Gonzalez F, James E, Nolla H, Shastri N. In the absence of aminopeptidase ERAAP, MHC class I molecules present many unstable and highly immunogenic peptides. *Nat Immunol*. (2007) 8:101–8. doi: 10.1038/ni1409
101. Cai L, Michelakos T, Yamada T, Fan S, Wang X, Schwab JH, et al. Defective HLA class I antigen processing machinery in cancer. *Cancer Immunol Immunother*. (2018) 67:999–1009. doi: 10.1007/s00262-018-2131-2
102. Cromme FV, Airey J, Heemels MT, Ploegh HL, Keating PJ, Stern PL, et al. Loss of transporter protein, encoded by the TAP-1 gene, is highly correlated with loss of HLA expression in cervical carcinomas. *J Exp Med*. (1994) 179:335–40. doi: 10.1084/jem.179.1.335
103. Seliger B, Hohne A, Knuth A, Bernhard H, Ehring B, Tampe R, et al. Reduced membrane major histocompatibility complex class I density and stability in a subset of human renal cell carcinomas with low TAP and LMP expression. *Clin Cancer Res*. (1996) 2:1427–33.
104. Seliger B, Atkins D, Bock M, Ritz U, Ferrone S, Huber C, et al. Characterization of human lymphocyte antigen class I antigen-processing machinery defects in renal cell carcinoma lesions with special emphasis on transporter-associated with antigen-processing down-regulation. *Clin Cancer Res*. (2003) 9:1721–7.
105. Kaklamanis L, Townsend A, Doussis-Anagnostopoulou IA, Mortensen N, Harris AL, Gatter KC. Loss of major histocompatibility complex-encoded transporter associated with antigen presentation (TAP) in colorectal cancer. *Am J Pathol*. (1994) 145:505–9.
106. Lou Y, Vitalis TZ, Basha G, Cai B, Chen SS, Choi KB, et al. Restoration of the expression of transporters associated with antigen processing in lung carcinoma increases tumor-specific immune responses and survival. *Cancer Res*. (2005) 65:7926–33. doi: 10.1158/0008-5472.CAN-04-3977
107. Bernal M, Garcia-Alcalde F, Concha A, Cano C, Blanco A, Garrido F, et al. Genome-wide differential genetic profiling characterizes colorectal cancers with genetic instability and specific routes to HLA class I loss and immune escape. *Cancer Immunol Immunother*. (2012) 61:803–16. doi: 10.1007/s00262-011-1147-7
108. Bernal M, Ruiz-Cabello F, Concha A, Paschen A, Garrido F. Implication of the beta2-microglobulin gene in the generation of tumor escape phenotypes. *Cancer Immunol Immunother*. (2012) 61:1359–71. doi: 10.1007/s00262-012-1321-6
109. Keating PJ, Cromme FV, Duggan-Keen M, Snijders PJ, Walboomers JM, Hunter RD, et al. Frequency of down-regulation of individual HLA-A and -B alleles in cervical carcinomas in relation to TAP-1 expression. *Br J Cancer*. (1995) 72:405–11. doi: 10.1038/bjc.1995.346
110. Tanaka K, Tsuchikawa T, Miyamoto M, Maki T, Ichinokawa M, Kubota KC, et al. Down-regulation of Human Leukocyte Antigen class I heavy chain in tumors is associated with a poor prognosis in advanced esophageal cancer patients. *Int J Oncol*. (2012) 40:965–74. doi: 10.3892/ijo.2011.1274
111. Shionoya Y, Kanaseki T, Miyamoto S, Tokita S, Hongo A, Kikuchi Y, et al. Loss of tapasin in human lung and colon cancer cells and escape from tumor-associated antigen-specific CTL recognition. *Oncoimmunology*. (2017) 6:e1274476. doi: 10.1080/2162402X.2016.1274476
112. Sokol L, Koelzer VH, Rau TT, Karamitopoulou E, Zlobec I, Lugli A. Loss of tapasin correlates with diminished CD8(+) T-cell

immunity and prognosis in colorectal cancer. *J Transl Med*. (2015) 13:279. doi: 10.1186/s12967-015-0647-1
113. Hasim A, Abudula M, Aimiduo R, Ma JQ, Jiao Z, Akula G, et al. Post-transcriptional and epigenetic regulation of antigen processing machinery (APM) components and HLA-I in cervical cancers from Uighur women. *PLoS ONE*. (2012) 7:e44952. doi: 10.1371/journal.pone.0044952
114. Sheyhidin I, Hasim A, Zheng F, Ma H. Epigenetic changes within the promoter regions of antigen processing machinery family genes in Kazakh primary esophageal squamous cell carcinoma. *Asian Pac J Cancer Prev*. (2014) 15:10299–306. doi: 10.7314/APJCP.2014.15.23.10299
115. Liu Q, Hao C, Su P, Shi J. Down-regulation of HLA class I antigen-processing machinery components in esophageal squamous cell carcinomas: association with disease progression. *Scand J Gastroenterol*. (2009) 44:960–9. doi: 10.1080/00365520902998679
116. Mehta AM, Jordanova ES, Kenter GG, Ferrone S, Fleuren GJ. Association of antigen processing machinery and HLA class I defects with clinicopathological outcome in cervical carcinoma. *Cancer Immunol Immunother*. (2008) 57:197–206. doi: 10.1007/s00262-007-0362-8
117. Stratikos E, Stamogiannos A, Zervoudi E, Fruci D. A role for naturally occurring alleles of endoplasmic reticulum aminopeptidases in tumor immunity and cancer pre-disposition. *Front Oncol*. (2014) 4:363. doi: 10.3389/fonc.2014.00363
118. Lee D, Das Gupta J, Gaughan C, Steffen I, Tang N, Luk KC, et al. In-depth investigation of archival and prospectively collected samples reveals no evidence for XMRV infection in prostate cancer. *PLoS ONE*. (2012) 7:e44954. doi: 10.1371/journal.pone.0044954
119. Ayshamgul H, Ma H, Ilyar S, Zhang LW, Abulizi A. Association of defective HLA-I expression with antigen processing machinery and their association with clinicopathological characteristics in Kazak patients with esophageal cancer. *Chin Med J*. (2011) 124:341–6. doi: 10.3760/cma.j.issn.0366-6999.2011.03.004
120. Angell TE, Lechner MG, Jang JK, LoPresti JS, Epstein AL. MHC class I loss is a frequent mechanism of immune escape in papillary thyroid cancer that is reversed by interferon and selumetinib treatment *in vitro*. *Clin Cancer Res*. (2014) 20:6034–44. doi: 10.1158/1078-0432.CCR-14-0879
121. Jang M, Yew PY, Hasegawa K, Ikeda Y, Fujiwara K, Fleming GF, et al. Characterization of T cell repertoire of blood, tumor, and ascites in ovarian cancer patients using next generation sequencing. *Oncoimmunology*. (2015) 4:e1030561. doi: 10.1080/2162402X.2015.1030561
122. Simpson JA, Al-Attar A, Watson NF, Scholefield JH, Ilyas M, Durrant LG. Intratumoral T cell infiltration, MHC class I and STAT1 as biomarkers of good prognosis in colorectal cancer. *Gut*. (2010) 59:926–33. doi: 10.1136/gut.2009.194472
123. Yoshihama S, Roszik J, Downs I, Meissner TB, Vijayan S, Chapuy B, et al. NLRC5/MHC class I transactivator is a target for immune evasion in cancer. *Proc Natl Acad Sci USA*. (2016) 113:5999–6004. doi: 10.1073/pnas.1602069113
124. Ito S, Okano S, Morita M, Saeki H, Tsutsumi S, Tsukihara H, et al. Expression of PD-L1 and HLA class I in esophageal squamous cell carcinoma: prognostic factors for patient outcome. *Ann Surg Oncol*. (2016) 23:508–15. doi: 10.1245/s10434-016-5376-z
125. Yoo SH, Keam B, Ock CY, Kim S, Han B, Kim JW, et al. Prognostic value of the association between MHC class I downregulation and PD-L1 upregulation in head and neck squamous cell carcinoma patients. *Sci Rep*. (2019) 9:7680. doi: 10.1038/s41598-019-44206-2
126. Rodig SJ, Gusenleitner D, Jackson DG, Gjini E, Giobbie-Hurder A, Jin C, et al. MHC proteins confer differential sensitivity to CTLA-4 and PD-1 blockade in untreated metastatic melanoma. *Sci Transl Med*. (2018) 10. doi: 10.1126/scitranslmed.aar3342
127. Pedersen MH, Hood BL, Beck HC, Conrads TP, Ditzel HJ, Leth-Larsen R. Downregulation of antigen presentation-associated pathway proteins is linked to poor outcome in triple-negative breast cancer patient tumors. *Oncoimmunology*. (2017) 6:e1305531. doi: 10.1080/2162402X.2017.1305531
128. Ling A, Lofgren-Burstrom A, Larsson P, Li X, Wikberg ML, Oberg A, et al. TAP1 down-regulation elicits immune escape and poor prognosis in colorectal cancer. *Oncoimmunology*. (2017) 6:e1356143. doi: 10.1080/2162402X.2017.1356143
129. Basile MS, Mazzon E, Russo A, Mammana S, Longo A, Bonfiglio V, et al. Differential modulation and prognostic values of immune-escape genes in uveal melanoma. *PLoS ONE*. (2019) 14:e0210276. doi: 10.1371/journal.pone.0210276
130. Thuring C, Follin E, Geironson L, Freyhult E, Junghans V, Harndahl M, et al. HLA class I is most tightly linked to levels of tapasin compared with other antigen-processing proteins in glioblastoma. *Br J Cancer*. (2015) 113:952–62. doi: 10.1038/bjc.2015.297
131. Marincola FM, Jaffee EM, Hicklin DJ, Ferrone S. Escape of human solid tumors from T-cell recognition: molecular mechanisms and functional significance. *Adv Immunol*. (2000) 74:181–273. doi: 10.1016/S0065-2776(08)60911-6
132. Kageshita T, Hirai S, Ono T, Hicklin DJ, Ferrone S. Down-regulation of HLA class I antigen-processing molecules in malignant melanoma: association with disease progression. *Am J Pathol*. (1999) 154:745–54. doi: 10.1016/S0002-9440(10)65321-7
133. Kamarashev J, Ferrone S, Seifert B, Boni R, Nestle FO, Burg G, et al. TAP1 down-regulation in primary melanoma lesions: an independent marker of poor prognosis. *Int J Cancer*. (2001) 95:23–83. doi: 10.1002/1097-0215(20010120)95:1<23::AID-IJC1004>3.0.CO;2-4
134. Ogino T, Bandoh N, Hayashi T, Miyokawa N, Harabuchi Y, Ferrone S. Association of tapasin and HLA class I antigen down-regulation in primary maxillary sinus squamous cell carcinoma lesions with reduced survival of patients. *Clin Cancer Res*. (2003) 9:4043–51.
135. Bandoh N, Ogino T, Katayama A, Takahara M, Katada A, Hayashi T, et al. HLA class I antigen and transporter associated with antigen processing downregulation in metastatic lesions of head and neck squamous cell carcinoma as a marker of poor prognosis. *Oncol Rep*. (2010) 23:933–9. doi: 10.3892/or_00000717
136. Hosch SB, Meyer AJ, Schneider C, Stoecklein N, Prenzel KL, Pantel K, et al. Expression and prognostic significance of HLA class I, ICAM-1, and tumor-infiltrating lymphocytes in esophageal cancer. *J Gastrointest Surg*. (1997) 1:316–23. doi: 10.1016/S1091-255X(97)80051-0
137. Hosch SB, Izbicki JR, Pichlmeier U, Stoecklein N, Niendorf A, Knoefel WT, et al. Expression and prognostic significance of immunoregulatory molecules in esophageal cancer. *Int J Cancer*. (1997) 74:582–73. doi: 10.1002/(SICI)1097-0215(19971219)74:6<582::AID-IJC4>3.0.CO;2-Q
138. Mizukami Y, Kono K, Maruyama T, Watanabe M, Kawaguchi Y, Kamimura K, et al. Downregulation of HLA Class I molecules in the tumour is associated with a poor prognosis in patients with oesophageal squamous cell carcinoma. *Br J Cancer*. (2008) 99:1462–7. doi: 10.1038/sj.bjc.6604715
139. Zhang X, Lin A, Zhang JG, Bao WG, Xu DP, Ruan YY, et al. Alteration of HLA-F and HLA I antigen expression in the tumor is associated with survival in patients with esophageal squamous cell carcinoma. *Int J Cancer*. (2013) 132:82–9. doi: 10.1002/ijc.27621
140. Zhao J, Guo C, Xiong F, Yu J, Ge J, Wang H, et al. Single cell RNA-seq reveals the landscape of tumor and infiltrating immune cells in nasopharyngeal carcinoma. *Cancer Lett*. (2020) 477:131–43. doi: 10.1016/j.canlet.2020.02.010
141. Gettinger S, Choi J, Hastings K, Truini A, Datar I, Sowell R, et al. Impaired HLA class I antigen processing and presentation as a mechanism of acquired resistance to immune checkpoint inhibitors in lung cancer. *Cancer Discov*. (2017) 7:1420–35. doi: 10.1158/2159-8290.CD-17-0593
142. Patel SJ, Sanjana NE, Kishton RJ, Eidizadeh A, Vodnala SK, Cam M, et al. Identification of essential genes for cancer immunotherapy. *Nature*. (2017) 548:537–42. doi: 10.1038/nature23477
143. Sade-Feldman M, Jiao YJ, Chen JH, Rooney MS, Barzily-Rokni M, Eliane JP, et al. Resistance to checkpoint blockade therapy through inactivation of antigen presentation. *Nat Commun*. (2017) 8:1136. doi: 10.1038/s41467-017-01062-w
144. Paulson KG, Voillet V, McAfee MS, Hunter DS, Wagener FD, Perdicchio M, et al. Acquired cancer resistance to combination immunotherapy from transcriptional loss of class I HLA. *Nat Commun*. (2018) 9:3868. doi: 10.1038/s41467-018-06300-3
145. Chowell D, Morris LGT, Grigg CM, Weber JK, Samstein RM, Makarov V, et al. Patient HLA class I genotype influences cancer response to checkpoint blockade immunotherapy. *Science*. (2018) 359:582–7. doi: 10.1126/science.aao4572

146. Lee JH, Shklovskaya E, Lim SY, Carlino MS, Menzies AM, Stewart A, et al. Transcriptional downregulation of MHC class I and melanoma de- differentiation in resistance to PD-1 inhibition. *Nat Commun*. (2020) 11:1897. doi: 10.1038/s41467-020-15726-7
147. Zaretsky JM, Garcia-Diaz A, Shin DS, Escuin-Ordinas H, Hugo W, Hu-Lieskovan S, et al. Mutations associated with acquired resistance to PD-1 blockade in melanoma. *N Engl J Med*. (2016) 375:819–29. doi: 10.1056/NEJMoa1604958
148. Lauss M, Donia M, Harbst K, Andersen R, Mitra S, Rosengren F, et al. Mutational and putative neoantigen load predict clinical benefit of adoptive T cell therapy in melanoma. *Nat Commun*. (2017) 8:1738. doi: 10.1038/s41467-017-01460-0
149. Khong HT, Wang QJ, Rosenberg SA. Identification of multiple antigens recognized by tumor-infiltrating lymphocytes from a single patient: tumor escape by antigen loss and loss of MHC expression. *J Immunother*. (2004) 27:184–90. doi: 10.1097/00002371-200405000-00002
150. Carretero R, Romero JM, Ruiz-Cabello F, Maleno I, Rodriguez F, Camacho FM, et al. Analysis of HLA class I expression in progressing and regressing metastatic melanoma lesions after immunotherapy. *Immunogenetics*. (2008) 60:439–47. doi: 10.1007/s00251-008-0303-5
151. Gao J, Shi LZ, Zhao H, Chen J, Xiong L, He Q, et al. Loss of IFN-gamma Pathway genes in tumor cells as a mechanism of resistance to anti-CTLA-4 therapy. *Cell*. (2016) 167:397–404 e9. doi: 10.1016/j.cell.2016.08.069
152. Burrack AL, Spartz EJ, Raynor JF, Wang I, Olson M, Stromnes IM. Combination PD-1 and PD-L1 blockade promotes durable neoantigen-specific T cell-mediated immunity in pancreatic ductal adenocarcinoma. *Cell Rep*. (2019) 28:2140–55 e6. doi: 10.1016/j.celrep.2019.07.059
153. Chew GL, Campbell AE, De Neef E, Sutliff NA, Shadle SC, Tapscott SJ, et al. DUX4 suppresses MHC class I to promote cancer immune evasion and resistance to checkpoint blockade. *Dev Cell*. (2019) 50:658–71 e7. doi: 10.1016/j.devcel.2019.06.011
154. Buferne M, Chasson L, Grange M, Mas A, Arnoux F, Bertuzzi M, et al. IFNgamma producing CD8(+) T cells modified to resist major immune checkpoints induce regression of MHC class I-deficient melanomas. *Oncoimmunology*. (2015) 4:e974959. doi: 10.4161/2162402X.2014.974959
155. Kavathas P, Bach FH, DeMars R. Gamma ray-induced loss of expression of HLA and glyoxalase I alleles in lymphoblastoid cells. *Proc Natl Acad Sci USA*. (1980) 77:4251–5. doi: 10.1073/pnas.77.7.4251
156. Erlich H, Lee JS, Petersen JW, Bugawan T, DeMars R. Molecular analysis of HLA class I and class II antigen loss mutants reveals a homozygous deletion of the DR, DQ, and part of the DP region: implications for class II gene order. *Hum Immunol*. (1986) 16:205–19. doi: 10.1016/0198-8859(86)90049-2
157. Shimizu Y, Geraghty DE, Koller BH, Orr HT, DeMars R. Transfer and expression of three cloned human non-HLA-A,B,C class I major histocompatibility complex genes in mutant lymphoblastoid cells. *Proc Natl Acad Sci USA*. (1988) 85:227–31. doi: 10.1073/pnas.85.1.227
158. McGranahan N, Rosenthal R, Hiley CT, Rowan AJ, Watkins TBK, Wilson GA, et al. Allele-specific HLA loss and immune escape in lung cancer evolution. *Cell*. (2017) 171:1259–71 e11. doi: 10.1016/j.cell.2017.10.001
159. Benitez R, Godelaine D, Lopez-Nevot MA, Brasseur F, Jimenez P, Marchand M, et al. Mutations of the beta2-microglobulin gene result in a lack of HLA class I molecules on melanoma cells of two patients immunized with MAGE peptides. *Tissue Antigens*. (1998) 52:520–9. doi: 10.1111/j.1399-0039.1998.tb03082.x
160. Maleno I, Aptsiauri N, Cabrera T, Gallego A, Paschen A, Lopez-Nevot MA, et al. Frequent loss of heterozygosity in the beta2-microglobulin region of chromosome. (2011) 15 in primary human tumors. *Immunogenetics*. 63:65–71. doi: 10.1007/s00251-010-0494-4
161. Maleno I, Cabrera CM, Cabrera T, Paco L, Lopez-Nevot MA, Collado A, et al. Distribution of HLA class I altered phenotypes in colorectal carcinomas: high frequency of HLA haplotype loss associated with loss of heterozygosity in chromosome region 6p21. *Immunogenetics*. (2004) 56:244–53. doi: 10.1007/s00251-004-0692-z
162. Maleno I, Lopez-Nevot MA, Cabrera T, Salinero J, Garrido F. Multiple mechanisms generate HLA class I altered phenotypes in laryngeal carcinomas: high frequency of HLA haplotype loss associated with loss of heterozygosity in chromosome region 6p21. *Cancer Immunol Immunother*. (2002) 51:389–96. doi: 10.1007/s00262-002-0296-0
163. Maleno I, Romero JM, Cabrera T, Paco L, Aptsiauri N, Cozar JM, et al. LOH at 6p21.3 region and HLA class I altered phenotypes in bladder carcinomas. *Immunogenetics*. (2006) 58:503–10. doi: 10.1007/s00251-006-0111-8
164. Feenstra M, Veltkamp M, van Kuik J, Wiertsema S, Slootweg P, van den Tweel J, et al. HLA class I expression and chromosomal deletions at 6p and 15q in head and neck squamous cell carcinomas. *Tissue Antigens*. (1999) 54:235–45. doi: 10.1034/j.1399-0039.1999.540304.x
165. Seliger B, Ritz U, Abele R, Bock M, Tampe R, Sutter G, et al. Immune escape of melanoma: first evidence of structural alterations in two distinct components of the MHC class I antigen processing pathway. *Cancer Res*. (2001) 61:8647–50.
166. Montesion M, Murugesan K, Jin DX, Sharaf R, Sanchez N, Guria A, et al. Somatic HLA class I loss is a widespread mechanism of immune evasion which refines the use of tumor mutational burden as a biomarker of checkpoint inhibitor response. *Cancer Discov*. (2020) 11:282–92. doi: 10.1158/2159-8290.CD-20-0672
167. Chang CC, Campoli M, Restifo NP, Wang X, Ferrone S. Immune selection of hot-spot beta. (2005) 2-microglobulin gene mutations, HLA-A2 allospecificity loss, and antigen-processing machinery component down-regulation in melanoma cells derived from recurrent metastases following immunotherapy. *J Immunol* 174:1462–71. doi: 10.4049/jimmunol.174.3.1462
168. Garrido F, Aptsiauri N. Cancer immune escape: MHC expression in primary tumours versus metastases. *Immunology*. (2019) 158:255–66. doi: 10.1111/imm.13114
169. Carretero R, Cabrera T, Gil H, Saenz-Lopez P, Maleno I, Aptsiauri N, et al. Bacillus Calmette-Guerin immunotherapy of bladder cancer induces selection of human leukocyte antigen class I-deficient tumor cells. *Int J Cancer*. (2011) 129:839–46. doi: 10.1002/ijc.25733
170. Cabrera T, Pedrajas G, Cozar JM, Garrido A, Vicente J, Tallada M, et al. HLA class I expression in bladder carcinomas. *Tissue Antigens*. (2003) 62:324–7. doi: 10.1034/j.1399-0039.2003.00104.x
171. Shen T, Chen Z, Zhao ZJ, Wu J. Genetic defects of the IRF1-mediated major histocompatibility complex class I antigen presentation pathway occur prevalently in the JAK2 gene in non-small cell lung cancer. *Oncotarget*. (2017) 8:60975–86. doi: 10.18632/oncotarget.17689
172. Georgopoulos NT, Proffitt JL, Blair GE. Transcriptional regulation of the major histocompatibility complex (MHC) class I heavy chain, TAP1 and LMP2 genes by the human papillomavirus (HPV) type 6b, 16 and 18 E7 oncoproteins. *Oncogene*. (2000) 19:4930–5. doi: 10.1038/sj.onc.1203860
173. Romero JM, Jimenez P, Cabrera T, Cozar JM, Pedrinaci S, Tallada M, et al. Coordinated downregulation of the antigen presentation machinery and HLA class I/beta2-microglobulin complex is responsible for HLA-ABC loss in bladder cancer. *Int J Cancer*. (2005) 113:605–10. doi: 10.1002/ijc.20499
174. Restifo NP, Esquivel F, Kawakami Y, Yewdell JW, Mule JJ, Rosenberg SA, et al. Identification of human cancers deficient in antigen processing. *J Exp Med*. (1993) 177:265–72. doi: 10.1084/jem.177.2.265
175. Meissner M, Reichert TE, Kunkel M, Gooding W, Whiteside TL, Ferrone S, et al. Defects in the human leukocyte antigen class I antigen processing machinery in head and neck squamous cell carcinoma: association with clinical outcome. *Clin Cancer Res*. (2005) 11:2552–60. doi: 10.1158/1078-0432.CCR-04-2146
176. Ye Q, Shen Y, Wang X, Yang J, Miao F, Shen C, et al. Hypermethylation of HLA class I gene is associated with HLA class I down-regulation in human gastric cancer. *Tissue Antigens*. (2010) 75:30–9. doi: 10.1111/j.1399-0039.2009.01390.x
177. Burr ML, Sparbier CE, Chan KL, Chan YC, Kersbergen A, Lam EYN, et al. An evolutionarily conserved function of polycomb silences the MHC class I antigen presentation pathway and enables immune evasion in cancer. *Cancer Cell*. (2019) 36:385–401 e8. doi: 10.1016/j.ccell.2019.08.008
178. Ozcan M, Janikovits J, von Knebel Doeberitz M, Kloor M. Complex pattern of immune evasion in MSI colorectal cancer. *Oncoimmunology*. (2018) 7:e1445453. doi: 10.1080/2162402X.2018.1445453
179. Smithy JW, Moore LM, Pelekanou V, Rehman J, Gaule P, Wong PF, et al. Nuclear IRF-1 expression as a mechanism to assess "Capability" to express PD-L1 and response to PD-1 therapy in metastatic melanoma. *J Immunother Cancer*. (2017) 5:25. doi: 10.1186/s40425-017-0229-2

180. Lorenzi S, Forloni M, Cifaldi L, Antonucci C, Citti A, Boldrini R, et al. IRF1 and NF-kB restore MHC class I-restricted tumor antigen processing and presentation to cytotoxic T cells in aggressive neuroblastoma. *PLoS ONE*. (2012) 7:e46928. doi: 10.1371/journal.pone.0046928
181. Serrano A, Tanzarella S, Lionello I, Mendez R, Traversari C, Ruiz-Cabello F, et al. Rexpression of HLA class I antigens and restoration of antigen-specific CTL response in melanoma cells following 5-aza-2'-deoxycytidine treatment. *Int J Cancer*. (2001) 94:243–51. doi: 10.1002/ijc.1452
182. Luo N, Nixon MJ, Gonzalez-Ericsson PI, Sanchez V, Opalenik SR, Li H, et al. DNA methyltransferase inhibition upregulates MHC-I to potentiate cytotoxic T lymphocyte responses in breast cancer. *Nat Commun*. (2018) 9:248. doi: 10.1038/s41467-017-02630-w
183. Nie Y, Yang G, Song Y, Zhao X, So C, Liao J, et al. DNA hypermethylation is a mechanism for loss of expression of the HLA class I genes in human esophageal squamous cell carcinomas. *Carcinogenesis*. (2001) 22:1615–23. doi: 10.1093/carcin/22.10.1615
184. Jiang Q, Pan HY, Ye DX, Zhang P, Zhong LP, Zhang ZY. Downregulation of tapasin expression in primary human oral squamous cell carcinoma: association with clinical outcome. *Tumour Biol*. (2010) 31:451–9. doi: 10.1007/s13277-010-0054-4
185. Chiappinelli KB, Strissel PL, Desrichard A, Li H, Henke C, Akman B, et al. Inhibiting DNA methylation causes an interferon response in cancer *via* dsRNA including endogenous retroviruses. *Cell*. (2015) 162:974–86. doi: 10.1016/j.cell.2015.07.011
186. Stone ML, Chiappinelli KB, Li H, Murphy LM, Travers ME, Topper MJ, et al. Epigenetic therapy activates type I interferon signaling in murine ovarian cancer to reduce immunosuppression and tumor burden. *Proc Natl Acad Sci USA*. (2017) 114: E10981–90. doi: 10.1073/pnas.1712514114
187. Kim JY, Choi JK, Jung H. Genome-wide methylation patterns predict clinical benefit of immunotherapy in lung cancer. *Clin Epigenetics*. (2020) 12:119. doi: 10.1186/s13148-020-00907-4
188. Fonsatti E, Nicolay HJ, Sigalotti L, Calabro L, Pezzani L, Colizzi F, et al. Functional up-regulation of human leukocyte antigen class I antigens expression by 5-aza-2'-deoxycytidine in cutaneous melanoma: immunotherapeutic implications. *Clin Cancer Res*. (2007) 13:3333–8. doi: 10.1158/1078-0432.CCR-06-3091
189. Rosenthal R, Cadieux EL, Salgado R, Bakir MA, Moore DA, Hiley CT, et al. Neoantigen-directed immune escape in lung cancer evolution. *Nature*. (2019) 567:479–85. doi: 10.1038/s41586-019-1032-7
190. Magner WJ, Kazim AL, Stewart C, Romano MA, Catalano G, Grande C, et al. Activation of MHC class I, II, and CD40 gene expression by histone deacetylase inhibitors. *J Immunol*. (2000) 165:7017–24. doi: 10.4049/jimmunol.165.12.7017
191. Setiadi AF, Omilusik K, David MD, Seipp RP, Hartikainen J, Gopaul R, et al. Epigenetic enhancement of antigen processing and presentation promotes immune recognition of tumors. *Cancer Res*. (2008) 68:9601–7. doi: 10.1158/0008-5472.CAN-07-5270
192. Ritter C, Fan K, Paschen A, Reker Hardrup S, Ferrone S, Nghiem P, et al. Epigenetic priming restores the HLA class-I antigen processing machinery expression in Merkel cell carcinoma. *Sci Rep*. (2017) 7:2290. doi: 10.1038/s41598-017-02608-0
193. Briere D, Sudhakar N, Woods DM, Hallin J, Engstrom LD, Aranda R, et al. The class I/IV HDAC inhibitor mocetinostat increases tumor antigen presentation, decreases immune suppressive cell types and augments checkpoint inhibitor therapy. *Cancer Immunol Immunother*. (2018) 67:381–92. doi: 10.1007/s00262-017-2091-y
194. Ugurel S, Spassova I, Wohlfarth J, Drusio C, Cherouny A, Melior A, et al. MHC class-I downregulation in PD-1/PD-L1 inhibitor refractory Merkel cell carcinoma and its potential reversal by histone deacetylase inhibition: a case series. *Cancer Immunol Immunother*. (2019) 68:983–90. doi: 10.1007/s00262-019-02341-9
195. Zhou L, Mudianto T, Ma X, Riley R, Uppaluri R. Targeting EZH2 enhances antigen presentation, antitumor immunity, and circumvents anti-PD-1 resistance in head and neck cancer. *Clin Cancer Res*. (2020) 26:290–300. doi: 10.1158/1078-0432.CCR-19-1351
196. Almeida L, Dhillon-LaBrooy A, Castro CN, Adossa N, Carriche GM, Guderian M, et al. Ribosome-targeting antibiotics impair T cell effector function and ameliorate autoimmunity by blocking mitochondrial protein synthesis. *Immunity*. (2020) 54:68–83.e6. doi: 10.1101/832956
197. Ennishi D, Takata K, Beguelin W, Duns G, Mottok A, Farinha P, et al. Molecular and genetic characterization of MHC deficiency identifies EZH2 as therapeutic target for enhancing immune recognition. *Cancer Discov*. (2019) 9:546–63. doi: 10.1158/2159-8290.CD-18-1090
198. Pan D, Kobayashi A, Jiang P, Ferrari de Andrade L, Tay RE, Luoma AM, et al. A major chromatin regulator determines resistance of tumor cells to T cell-mediated killing. *Science*. (2018) 359:770–5. doi: 10.1126/science.aao1710
199. Slack FJ, Chinnaiyan AM. The role of non-coding RNAs in oncology. *Cell*. (2019) 179:1033–55. doi: 10.1016/j.cell.2019.10.017
200. Liu L, Wang Q, Qiu Z, Kang Y, Liu J, Ning S, et al. Non-coding RNAs: the shot callers in tumor immune escape. *Signal Transduct Target Ther*. (2020) 5:102. doi: 10.1038/s41392-020-0194-y
201. Mari L, Hoefnagel SJM, Zito D, van de Meent M, van Endert P, Calpe S, et al. microRNA 125a regulates MHC-I expression on esophageal adenocarcinoma cells, associated with suppression of antitumor immune response and poor outcomes of patients. *Gastroenterology*. (2018) 155:784–98. doi: 10.1053/j.gastro.2018.06.030
202. Lazaridou MF, Massa C, Handke D, Mueller A, Friedrich M, Subbarayan K, et al. Identification of microRNAs targeting the transporter associated with antigen processing TAP1 in Melanoma. *J Clin Med*. (2020) 9:92690. doi: 10.3390/jcm9092690
203. Colangelo T, Polcaro G, Ziccardi P, Pucci B, Muccillo L, Galgani M, et al. Proteomic screening identifies calreticulin as a miR-27a direct target repressing MHC class I cell surface exposure in colorectal cancer. *Cell Death Dis*. (2016) 7:e2120. doi: 10.1038/cddis.2016.28
204. Yan Y, Liang Z, Du Q, Yang M, Geller DA. MicroRNA-23a downregulates the expression of interferon regulatory factor-1 in hepatocellular carcinoma cells. *Oncol Rep*. (2016) 36:633–40. doi: 10.3892/or.2016.4864
205. Wang B, Yang H, Shen L, Wang J, Pu W, Chen Z, et al. Rs56288038 (C/G) in 3′UTR of IRF-1 regulated by MiR-502-5p promotes gastric cancer development. *Cell Physiol Biochem*. (2016) 40:391–9. doi: 10.1159/000452554
206. Yao RW, Wang Y, Chen LL. Cellular functions of long noncoding RNAs. *Nat Cell Biol*. (2019) 21:542–51. doi: 10.1038/s41556-019-0311-8
207. Hu Q, Ye Y, Chan LC, Li Y, Liang K, Lin A, et al. Oncogenic lncRNA downregulates cancer cell antigen presentation and intrinsic tumor suppression. *Nat Immunol*. (2019) 20:835–51. doi: 10.1038/s41590-019-0400-7
208. Li H, Xiong HG, Xiao Y, Yang QC, Yang SC, Tang HC, et al. Long non-coding RNA LINC02195 as a regulator of MHC I molecules and favorable prognostic marker for head and neck squamous cell carcinoma. *Front Oncol*. (2020) 10:615. doi: 10.3389/fonc.2020.00615
209. Gao F, Zhao ZL, Zhao WT, Fan QR, Wang SC, Li J, et al. miR-9 modulates the expression of interferon-regulated genes and MHC class I molecules in human nasopharyngeal carcinoma cells. *Biochem Biophys Res Commun*. (2013) 431:610–6. doi: 10.1016/j.bbrc.2012.12.097
210. Cano F, Bye H, Duncan LM, Buchet-Poyau K, Billaud M, Wills MR, et al. The RNA-binding E3 ubiquitin ligase MEX-3C links ubiquitination with MHC-I mRNA degradation. *EMBO J*. (2012) 31:3596–606. doi: 10.1038/emboj.2012.218
211. Wang Y, Wang X, Cui X, Zhuo Y, Li H, Ha C, et al. Oncoprotein SND1 hijacks nascent MHC-I heavy chain to ER-associated degradation, leading to impaired CD8(+) T cell response in tumor. *Sci Adv*. (2020) 6:aba5412. doi: 10.1126/sciadv.aba5412
212. Jongsma MLM, de Waard AA, Raaben M, Zhang T, Cabukusta B, Platzer R, et al. The SPPL3-defined glycosphingolipid repertoire orchestrates HLA class I-mediated immune responses. *Immunity*. (2020) 54:132–50.e9. doi: 10.1016/j.immuni.2021.01.016
213. Mimura K, Shiraishi K, Mueller A, Izawa S, Kua LF, So J, et al. The MAPK pathway is a predominant regulator of HLA-A expression in esophageal and gastric cancer. *J Immunol*. (2013) 191:6261–72. doi: 10.4049/jimmunol.1301597
214. Brea EJ, Oh CY, Manchado E, Budhu S, Gejman RS, Mo G, et al. Kinase regulation of human MHC class I molecule expression on cancer cells. *Cancer Immunol Res*. (2016) 4:936–47. doi: 10.1158/2326-6066.CIR-16-0177

215. Lulli D, Carbone ML, Pastore S. The MEK inhibitors trametinib and cobimetinib induce a type I interferon response in human keratinocytes. *Int J Mol Sci*. (2017) 18:102227. doi: 10.3390/ijms18102227
216. Oh CY, Klatt MG, Bourne C, Dao T, Dacek MM, Brea EJ, et al. ALK and RET inhibitors promote HLA class I antigen presentation and unmask new antigens within the tumor immunopeptidome. *Cancer Immunol Res*. (2019) 7:1984–97. doi: 10.1158/2326-6066.CIR-19-0056
217. Mimura K, Ando T, Poschke I, Mougiakakos D, Johansson CC, Ichikawa J, et al. T cell recognition of HLA-A2 restricted tumor antigens is impaired by the oncogene HER2. *Int J Cancer*. (2011) 128:390–401. doi: 10.1002/ijc.25613
218. Maruyama T, Mimura K, Sato E, Watanabe M, Mizukami Y, Kawaguchi Y, et al. Inverse correlation of HER2 with MHC class I expression on oesophageal squamous cell carcinoma. *Br J Cancer*. (2010) 103:552–9. doi: 10.1038/sj.bjc.6605772
219. Bernards R, Dessain SK, Weinberg RA. N-myc amplification causes down-modulation of MHC class I antigen expression in neuroblastoma. *Cell*. (1986) 47:667–74. doi: 10.1016/0092-8674(86)90509-X
220. Versteeg R, Noordermeer IA, Kruse-Wolters M, Ruiter DJ, Schrier PI. c-myc down-regulates class I HLA expression in human melanomas. *EMBO J*. (1988) 7:1023–9. doi: 10.1002/j.1460-2075.1988.tb02909.x
221. van 't Veer LJ, Beijersbergen RL, Bernards R. N-myc suppresses major histocompatibility complex class I gene expression through down-regulation of the p50 subunit of NF-kappa B. *EMBO J*. (1993) 12:195–200. doi: 10.1002/j.1460-2075.1993.tb05645.x
222. Goes N, Sims T, Urmson J, Vincent D, Ramassar V, Halloran PF. Disturbed MHC regulation in the IFN-gamma knockout mouse. Evidence for three states of MHC expression with distinct roles for IFN-gamma. *J Immunol*. (1995) 155:4559–66.
223. Lee CK, Gimeno R, Levy DE. Differential regulation of constitutive major histocompatibility complex class I expression in T and B lymphocytes. *J Exp Med*. (1999) 190:1451–64. doi: 10.1084/jem.190.10.1451
224. Majoros A, Platanitis E, Kernbauer-Holzl E, Rosebrock F, Muller M, Decker T. Canonical and non-canonical aspects of JAK-STAT signaling: lessons from interferons for cytokine responses. *Front Immunol*. (2017) 8:29. doi: 10.3389/fimmu.2017.00029
225. Sucker A, Zhao F, Pieper N, Heeke C, Maltaner R, Stadtler N, et al. Acquired IFNgamma resistance impairs anti-tumor immunity and gives rise to T-cell-resistant melanoma lesions. *Nat Commun*. (2017) 8:15440. doi: 10.1038/ncomms15440
226. Manguso RT, Pope HW, Zimmer MD, Brown FD, Yates KB, Miller BC, et al. *In vivo* CRISPR screening identifies Ptpn2 as a cancer immunotherapy target. *Nature*. (2017) 547:413–8. doi: 10.1038/nature23270
227. Marijt KA, Sluijter M, Blijleven L, Tolmeijer SH, Scheeren FA, van der Burg SH, et al. Metabolic stress in cancer cells induces immune escape through a PI3K-dependent blockade of IFNgamma receptor signaling. *J Immunother Cancer*. (2019) 7:152. doi: 10.1186/s40425-019-0627-8
228. Lu T, Ramakrishnan R, Altiok S, Youn JI, Cheng P, Celis E, et al. Tumor-infiltrating myeloid cells induce tumor cell resistance to cytotoxic T cells in mice. *J Clin Invest*. (2011) 121:4015–29. doi: 10.1172/JCI45862
229. Mundy-Bosse BL, Lesinski GB, Jaime-Ramirez AC, Benninger K, Khan M, Kuppusamy P, et al. Myeloid-derived suppressor cell inhibition of the IFN response in tumor-bearing mice. *Cancer Res*. (2011) 71:5101–10. doi: 10.1158/0008-5472.CAN-10-2670
230. Dong MB, Wang G, Chow RD, Ye L, Zhu L, Dai X, et al. Systematic immunotherapy target discovery using genome-scale *in vivo* CRISPR screens in CD8 T cells. *Cell*. (2019) 178:1189–204 e23. doi: 10.1016/j.cell.2019.07.044
231. Cruz FM, Colbert JD, Merino E, Kriegsman BA, Rock KL. The biology and underlying mechanisms of cross-presentation of exogenous antigens on MHC-I molecules. *Annu Rev Immunol*. (2017) 35:149–76. doi: 10.1146/annurev-immunol-041015-055254
232. Dersh D, Phelan JD, Gumina ME, Wang B, Arbuckle JH, Holly J, et al. Genome-wide screens identify lineage- and tumor-specific genes modulating MHC-I- and MHC-II-restricted immunosurveillance of human lymphomas. *Immunity*. (2020) 54:116–31.e10. doi: 10.2139/ssrn.3584739
233. del Campo AB, Aptsiauri N, Mendez R, Zinchenko S, Vales A, Paschen A, et al. Efficient recovery of HLA class I expression in human tumor cells after beta2-microglobulin gene transfer using adenoviral vector: implications for cancer immunotherapy. *Scand J Immunol*. (2009) 70:125–35. doi: 10.1111/j.1365-3083.2009.02276.x
234. del Campo AB, Carretero J, Aptsiauri N, Garrido F. Targeting HLA class I expression to increase tumor immunogenicity. *Tissue Antigens*. (2012) 79:147–54. doi: 10.1111/j.1399-0039.2011.01831.x
235. Del Campo AB, Carretero J, Munoz JA, Zinchenko S, Ruiz-Cabello F, Gonzalez-Aseguinolaza G, et al. Adenovirus expressing beta2-microglobulin recovers HLA class I expression and antitumor immunity by increasing T-cell recognition. *Cancer Gene Ther*. (2014) 21:317–32. doi: 10.1038/cgt.2014.32
236. Oshima S, Nakamura T, Namiki S, Okada E, Tsuchiya K, Okamoto R, et al. Interferon regulatory factor. (2004) 1 (IRF-1) and IRF-2 distinctively up-regulate gene expression and production of interleukin-7 in human intestinal epithelial cells. *Mol Cell Biol* 24:6298–310. doi: 10.1128/MCB.24.14.6298-6310.2004
237. Propper DJ, Chao D, Braybrooke JP, Bahl P, Thavasu P, Balkwill F, et al. Low-dose IFN-gamma induces tumor MHC expression in metastatic malignant melanoma. *Clin Cancer Res*. (2003) 9:84–92.
238. Vlkova V, Stepanek I, Hruskova V, Senigl F, Mayerova V, Sramek M, et al. Epigenetic regulations in the IFNgamma signalling pathway: IFNgamma-mediated MHC class I upregulation on tumour cells is associated with DNA demethylation of antigen-presenting machinery genes. *Oncotarget*. (2014) 5:6923–35. doi: 10.18632/oncotarget.2222
239. Davar D, Wang H, Chauvin JM, Pagliano O, Fourcade JJ, Ka M, et al. Phase Ib/II study of pembrolizumab and pegylated-interferon alfa-2b in advanced melanoma. *J Clin Oncol*. (2018) 36:JCO1800632. doi: 10.1200/JCO.18.00632
240. Mora-Garcia Mde L, Duenas-Gonzalez A, Hernandez-Montes J, De la Cruz-Hernandez E, Perez-Cardenas E, Weiss-Steider B, et al. Up-regulation of HLA class-I antigen expression and antigen-specific CTL response in cervical cancer cells by the demethylating agent hydralazine and the histone deacetylase inhibitor valproic acid. *J Transl Med*. (2006) 4:55. doi: 10.1186/1479-5876-4-55
241. van den Elsen PJ, Holling TM, van der Stoep N, Boss JM. DNA methylation and expression of major histocompatibility complex class I and class II transactivator genes in human developmental tumor cells and in T cell malignancies. *Clin Immunol*. (2003) 109:46–52. doi: 10.1016/S1521-6616(03)00200-6
242. Li H, Chiappinelli KB, Guzzetta AA, Easwaran H, Yen RW, Vatapalli R, et al. Immune regulation by low doses of the DNA methyltransferase inhibitor 5-azacitidine in common human epithelial cancers. *Oncotarget*. (2014) 5:587–98. doi: 10.18632/oncotarget.1782
243. Chiossone L, Dumas PY, Vienne M, Vivier E. Natural killer cells and other innate lymphoid cells in cancer. *Nat Rev Immunol*. (2018) 18:671–88. doi: 10.1038/s41577-018-0061-z
244. Covre A, Coral S, Nicolay H, Parisi G, Fazio C, Colizzi F, et al. Antitumor activity of epigenetic immunomodulation combined with CTLA-4 blockade in syngeneic mouse models. *Oncoimmunology*. (2015) 4:e1019978. doi: 10.1080/2162402X.2015.1019978
245. Wang L, Amoozgar Z, Huang J, Saleh MH, Xing D, Orsulic S, et al. Decitabine enhances lymphocyte migration and function and synergizes with CTLA-4 blockade in a murine ovarian cancer model. *Cancer Immunol Res*. (2015) 3:1030–41. doi: 10.1158/2326-6066.CIR-15-0073
246. Daver N, Garcia-Manero G, Basu S, Boddu PC, Alfayez M, Cortes JE, et al. Efficacy, safety, and biomarkers of response to azacitidine and nivolumab in relapsed/refractory acute myeloid leukemia: a nonrandomized, open-label, phase II study. *Cancer Discov*. (2019) 9:370–83. doi: 10.1158/2159-8290.CD-18-0774
247. Odunsi K, Matsuzaki J, James SR, Mhawech-Fauceglia P, Tsuji T, Miller A, et al. Epigenetic potentiation of NY-ESO-1 vaccine therapy in human ovarian cancer. *Cancer Immunol Res*. (2014) 2:37–49. doi: 10.1158/2326-6066.CIR-13-0126
248. Emran AA, Chatterjee A, Rodger EJ, Tiffen JC, Gallagher SJ, Eccles MR, et al. Targeting DNA methylation and EZH2 activity to overcome melanoma resistance to immunotherapy. *Trends Immunol*. (2019) 40:328–44. doi: 10.1016/j.it.2019.02.004
249. Khan AN, Gregorie CJ, Tomasi TB. Histone deacetylase inhibitors induce TAP, LMP, Tapasin genes and MHC class I antigen

presentation by melanoma cells. *Cancer Immunol Immunother*. (2008) 57:647–54. doi: 10.1007/s00262-007-0402-4
250. Sun T, Li Y, Yang W, Wu H, Li X, Huang Y, et al. Histone deacetylase inhibition up-regulates MHC class I to facilitate cytotoxic T lymphocyte-mediated tumor cell killing in glioma cells. *J Cancer*. (2019) 10:5638–45. doi: 10.7150/jca.34471
251. Terranova-Barberio M, Thomas S, Ali N, Pawlowska N, Park J, Krings G, et al. HDAC inhibition potentiates immunotherapy in triple negative breast cancer. *Oncotarget*. (2017) 8:114156–72. doi: 10.18632/oncotarget.23169
252. Woods DM, Sodre AL, Villagra A, Sarnaik A, Sotomayor EM, Weber J. HDAC inhibition upregulates PD-1 ligands in melanoma and augments immunotherapy with PD-1 blockade. *Cancer Immunol Res*. (2015) 3:1375–85. doi: 10.1158/2326-6066.CIR-15-0077-T
253. Knox T, Sahakian E, Banik D, Hadley M, Palmer E, Noonepalle S, et al. Selective HDAC6 inhibitors improve anti-PD-1 immune checkpoint blockade therapy by decreasing the anti-inflammatory phenotype of macrophages and down-regulation of immunosuppressive proteins in tumor cells. *Sci Rep*. (2019) 9:6136. doi: 10.1038/s41598-019-42237-3
254. Khan AN, Magner WJ, Tomasi TB. An epigenetic vaccine model active in the prevention and treatment of melanoma. *J Transl Med*. (2007) 5:64. doi: 10.1186/1479-5876-5-64
255. Vo DD, Prins RM, Begley JL, Donahue TR, Morris LF, Bruhn KW, et al. Enhanced antitumor activity induced by adoptive T-cell transfer and adjunctive use of the histone deacetylase inhibitor LAQ824. *Cancer Res*. (2009) 69:8693–9. doi: 10.1158/0008-5472.CAN-09-1456
256. Banik D, Moufarrij S, Villagra A. Immunoepigenetics combination therapies: an overview of the role of HDACs in cancer immunotherapy. *Int J Mol Sci*. (2019) 20:92241. doi: 10.3390/ijms20092241
257. Gray JE, Saltos A, Tanvetyanon T, Haura EB, Creelan B, Antonia SJ, et al. Phase I/Ib study of pembrolizumab plus vorinostat in advanced/metastatic non-small cell lung cancer. *Clin Cancer Res*. (2019) 25:6623–32. doi: 10.1158/1078-0432.CCR-19-1305
258. Wang X, Waschke BC, Woolaver RA, Chen Z, Zhang G, Piscopio AD, et al. Histone deacetylase inhibition sensitizes PD1 blockade-resistant B-cell lymphomas. *Cancer Immunol Res*. (2019) 7:1318–31. doi: 10.1158/2326-6066.CIR-18-0875
259. Elashi AA, Sasidharan Nair V, Taha RZ, Shaath H, Elkord E. DNA methylation of immune checkpoints in the peripheral blood of breast and colorectal cancer patients. *Oncoimmunology*. (2019) 8:e1542918. doi: 10.1080/2162402X.2018.1542918
260. Sasidharan Nair V, El Salhat H, Taha RZ, John A, Ali BR, Elkord E. DNA methylation and repressive H3K9 and H3K27 trimethylation in the promoter regions of PD-1, CTLA-4, TIM-3, LAG-3, TIGIT, and PD-L1 genes in human primary breast cancer. *Clin Epigenetics*. (2018) 10:78. doi: 10.1186/s13148-018-0512-1
261. Hilton IB, D'Ippolito AM, Vockley CM, Thakore PI, Crawford GE, Reddy TE, et al. Epigenome editing by a CRISPR-Cas9-based acetyltransferase activates genes from promoters and enhancers. *Nat Biotechnol*. (2015) 33:510–7. doi: 10.1038/nbt.3199
262. Haldeman JM, Conway AE, Arlotto ME, Slentz DH, Muoio DM, Becker TC, et al. Creation of versatile cloning platforms for transgene expression and dCas9-based epigenome editing. *Nucleic Acids Res*. (2019) 47:e23. doi: 10.1093/nar/gky1286
263. Rupaimoole R, Slack FJ. MicroRNA therapeutics: towards a new era for the management of cancer and other diseases. *Nat Rev Drug Discov*. (2017) 16:203–22. doi: 10.1038/nrd.2016.246
264. El Hage F, Durgeau A, Mami-Chouaib F. TAP expression level in tumor cells defines the nature and processing of MHC class I peptides for recognition by tumor-specific cytotoxic T lymphocytes. *Ann N Y Acad Sci*. (2013) 1283:75–80. doi: 10.1111/j.1749-6632.2012.06777.x
265. Durgeau A, Virk Y, Gros G, Voilin E, Corgnac S, Djenidi F, et al. Human preprocalcitonin self-antigen generates TAP-dependent and -independent epitopes triggering optimised T-cell responses toward immune-escaped tumours. *Nat Commun*. (2018) 9:5097. doi: 10.1038/s41467-018-07603-1
266. Marijt KA, Van Der Burg SH, van Hall T. TEIPP peptides: exploration of unTAPped cancer antigens. *Oncoimmunology*. (2019) 8:1599639. doi: 10.1080/2162402X.2019.1599639
267. Miller JS, Lanier LL. Natural killer cells in cancer immunotherapy. *Ann Rev Cancer Biol*. (2019) 3:77–103. doi: 10.1146/annurev-cancerbio-030518-055653
268. Kim S, Iizuka K, Aguila HL, Weissman IL, Yokoyama WM. *In vivo* natural killer cell activities revealed by natural killer cell-deficient mice. *Proc Natl Acad Sci USA*. (2000) 97:2731–6. doi: 10.1073/pnas.050588297
269. Smyth MJ, Swann J, Cretney E, Zerafa N, Yokoyama WM, Hayakawa Y. NKG2D function protects the host from tumor initiation. *J Exp Med*. (2005) 202:583–8. doi: 10.1084/jem.20050994
270. Moon WY, Powis SJ. Does natural killer cell deficiency (NKD) increase the risk of cancer? NKD may increase the risk of some virus induced cancer. *Front Immunol*. (2019) 10:1703. doi: 10.3389/fimmu.2019.01703
271. Marcus A, Gowen BG, Thompson TW, Iannello A, Ardolino M, Deng W, et al. Recognition of tumors by the innate immune system and natural killer cells. *Adv Immunol*. (2014) 122:91–128. doi: 10.1016/B978-0-12-800267-4.00003-1
272. Wu J, Lanier LL. Natural killer cells and cancer. *Adv Cancer Res*. (2003) 90:127–56. doi: 10.1016/S0065-230X(03)90004-2
273. Hayakawa Y, Smyth MJ. Innate immune recognition and suppression of tumors. *Adv Cancer Res*. (2006) 95:293–322. doi: 10.1016/S0065-230X(06)95008-8
274. Imai K, Matsuyama S, Miyake S, Suga K, Nakachi K. Natural cytotoxic activity of peripheral-blood lymphocytes and cancer incidence: an 11-year follow-up study of a general population. *Lancet*. (2000) 356:1795–9. doi: 10.1016/S0140-6736(00)03231-1
275. Coca S, Perez-Piqueras J, Martinez D, Colmenarejo A, Saez MA, Vallejo C, et al. The prognostic significance of intratumoral natural killer cells in patients with colorectal carcinoma. *Cancer*. (1997) 79:2320–83. doi: 10.1002/(SICI)1097-0142(19970615)79:12<2320::AID-CNCR5>3.0.CO;2-P
276. Ishigami S, Natsugoe S, Tokuda K, Nakajo A, Che X, Iwashige H, et al. Prognostic value of intratumoral natural killer cells in gastric carcinoma. *Cancer*. (2000) 88:577–833. doi: 10.1002/(SICI)1097-0142(20000201)88:3<577::AID-CNCR13>3.0.CO;2-V
277. Hsu KC, Keever-Taylor CA, Wilton A, Pinto C, Heller G, Arkun K, et al. Improved outcome in HLA-identical sibling hematopoietic stem-cell transplantation for acute myelogenous leukemia predicted by KIR and HLA genotypes. *Blood*. (2005) 105:4878–84. doi: 10.1182/blood-2004-12-4825
278. Xie G, Dong H, Liang Y, Ham JD, Rizwan R, Chen J. CAR-NK cells: a promising cellular immunotherapy for cancer. *EBioMedicine*. (2020) 59:102975. doi: 10.1016/j.ebiom.2020.102975
279. Liu E, Marin D, Banerjee P, Macapinlac HA, Thompson P, Basar R, et al. Use of CAR-transduced natural killer cells in CD19-positive lymphoid tumors. *N Engl J Med*. (2020) 382:545–53. doi: 10.1056/NEJMoa1910607
280. Garrido F, Aptsiauri N, Doorduijn EM, Garcia Lora AM, van Hall T. The urgent need to recover MHC class I in cancers for effective immunotherapy. *Curr Opin Immunol*. (2016) 39:44–51. doi: 10.1016/j.coi.2015.12.007
281. de Kruijf EM, Sajet A, van Nes JG, Natanov R, Putter H, Smit VT, et al. HLA-E and HLA-G expression in classical HLA class I-negative tumors is of prognostic value for clinical outcome of early breast cancer patients. *J Immunol*. (2010) 185:7452–9. doi: 10.4049/jimmunol.1002629
282. Urosevic M, Dummer R. Human leukocyte antigen-G and cancer immunoediting. *Cancer Res*. (2008) 68:627–30. doi: 10.1158/0008-5472.CAN-07-2704
283. Lin A, Yan WH. Heterogeneity of HLA-G expression in cancers: facing the challenges. *Front Immunol*. (2018) 9:2164. doi: 10.3389/fimmu.2018.02164
284. Wagner SN, Rebmann V, Willers CP, Grosse-Wilde H, Goos M. Expression analysis of classic and non-classic HLA molecules before interferon alfa-2b treatment of melanoma. *Lancet*. (2000) 356:220–1. doi: 10.1016/S0140-6736(00)02486-7
285. Rodriguez JA, Galeano L, Palacios DM, Gomez C, Serrano ML, Bravo MM, et al. Altered HLA class I and HLA-G expression is associated with IL-10 expression in patients with cervical cancer. *Pathobiology*. (2012) 79:72–83. doi: 10.1159/000334089

286. Ardolino M, Azimi CS, Iannello A, Trevino TN, Horan L, Zhang L, et al. Cytokine therapy reverses NK cell anergy in MHC-deficient tumors. *J Clin Invest*. (2014) 124:4781–94. doi: 10.1172/JCI74337
287. Bi J, Tian Z. NK cell exhaustion. *Front Immunol*. (2017) 8:760. doi: 10.3389/fimmu.2017.00760
288. Platonova S, Cherfils-Vicini J, Damotte D, Crozet L, Vieillard V, Validire P, et al. Profound coordinated alterations of intratumoral NK cell phenotype and function in lung carcinoma. *Cancer Res*. (2011) 71:5412–22. doi: 10.1158/0008-5472.CAN-10-4179
289. Groh V, Wu J, Yee C, Spies T. Tumour-derived soluble MIC ligands impair expression of NKG2D and T-cell activation. *Nature*. (2002) 419:734–8. doi: 10.1038/nature01112
290. Salih HR, Rammensee HG, Steinle A. Cutting edge: down-regulation of MICA on human tumors by proteolytic shedding. *J Immunol*. (2002) 169:4098–102. doi: 10.4049/jimmunol.169.8.4098
291. Castriconi R, Cantoni C, Della Chiesa M, Vitale M, Marcenaro E, Conte R, et al. Transforming growth factor beta 1 inhibits expression of NKp30 and NKG2D receptors: consequences for the NK-mediated killing of dendritic cells. *Proc Natl Acad Sci USA*. (2003) 100:4120–5. doi: 10.1073/pnas.0730640100
292. Souza-Fonseca-Guimaraes F, Cursons J, Huntington ND. The emergence of natural killer cells as a major target in cancer immunotherapy. *Trends Immunol*. (2019) 40:142–58. doi: 10.1016/j.it.2018.12.003
293. Wu Y, Li J, Jabbarzadeh Kaboli P, Shen J, Wu X, Zhao Y, et al. Natural killer cells as a double-edged sword in cancer immunotherapy: a comprehensive review from cytokine therapy to adoptive cell immunotherapy. *Pharmacol Res*. (2020) 155:104691. doi: 10.1016/j.phrs.2020.104691
294. Cerami E, Gao J, Dogrusoz U, Gross BE, Sumer SO, Aksoy BA, et al. The cBio cancer genomics portal: an open platform for exploring multidimensional cancer genomics data. *Cancer Discov*. (2012) 2:401–4. doi: 10.1158/2159-8290.CD-12-0095
295. Gao J, Aksoy BA, Dogrusoz U, Dresdner G, Gross B, Sumer SO, et al. Integrative analysis of complex cancer genomics and clinical profiles using the cBioPortal. *Sci Signal*. (2013) 6:pl1. doi: 10.1126/scisignal.2004088
296. Torigoe T, Asanuma H, Nakazawa E, Tamura Y, Hirohashi Y, Yamamoto E, et al. Establishment of a monoclonal anti-pan HLA class I antibody suitable for immunostaining of formalin-fixed tissue: unusually high frequency of down-regulation in breast cancer tissues. *Pathol Int*. (2012) 62:303–8. doi: 10.1111/j.1440-1827.2012.02789.x
297. Mariya T, Hirohashi Y, Torigoe T, Asano T, Kuroda T, Yasuda K, et al. Prognostic impact of human leukocyte antigen class I expression and association of platinum resistance with immunologic profiles in epithelial ovarian cancer. *Cancer Immunol Res*. (2014) 2:1220–9. doi: 10.1158/2326-6066.CIR-14-0101
298. Rolland P, Deen S, Scott I, Durrant L, Spendlove I. Human leukocyte antigen class I antigen expression is an independent prognostic factor in ovarian cancer. *Clin Cancer Res*. (2007) 13:3591–6. doi: 10.1158/1078-0432.CCR-06-2087
299. Krishnakumar S, Abhyankar D, Sundaram AL, Pushparaj V, Shanmugam MP, Biswas J. Major histocompatibility antigens and antigen-processing molecules in uveal melanoma. *Clin Cancer Res*. (2003) 9:4159–64.
300. Lee HW, Min SK, Ju YS, Sung J, Lim MS, Yang DH, et al. Prognostic significance of HLA class I expressing in gastric carcinoma defined by monoclonal anti-pan HLA class I antibody, EMR8-5. *J Gastrointest Surg*. (2011) 15:1336–43. doi: 10.1007/s11605-011-1545-3
301. Krishnakumar S, Lakshmi S, Abhyankar D, Biswas J. Expression of HLA class I, beta(2)-microglobulin and HLA class II antigens in primary orbital melanoma. *Orbit*. (2003) 22:257–63. doi: 10.1076/orbi.22.4.257.17242
302. Saenz-Lopez P, Gouttefangeas C, Hennenlotter J, Concha A, Maleno I, Ruiz-Cabello F, et al. Higher HLA class I expression in renal cell carcinoma than in autologous normal tissue. *Tissue Antigens*. (2010) 75:110–8. doi: 10.1111/j.1399-0039.2009.01409.x
303. Morabito A, Dozin B, Salvi S, Pasciucco G, Balbi G, Laurent S, et al. Analysis and clinical relevance of human leukocyte antigen class I, heavy chain, and beta2-microglobulin downregulation in breast cancer. *Hum Immunol*. (2009) 70:492–5. doi: 10.1016/j.humimm.2009.04.029
304. Sanders H, McCue P, Graham SD Jr. ABO(H) antigens and beta-2 microglobulin in transitional cell carcinoma. Predictors of response to intravesical bacillus Calmette-Guerin. *Cancer*. (1991) 67:3024–83. doi: 10.1002/1097-0142(19910615)67:12<3024::AID-CNCR2820671216>3.0.CO;2-Q
305. Urosevic M, Kurrer MO, Kamarashev J, Mueller B, Weder W, Burg G, et al. Human leukocyte antigen G up-regulation in lung cancer associates with high-grade histology, human leukocyte antigen class I loss and interleukin-10 production. *Am J Pathol*. (2001) 159:817–24. doi: 10.1016/S0002-9440(10)61756-7
306. Koopman LA, Mulder A, Corver WE, Anholts JD, Giphart MJ, Claas FH, et al. HLA class I phenotype and genotype alterations in cervical carcinomas and derivative cell lines. *Tissue Antigens*. (1998) 51:623–36. doi: 10.1111/j.1399-0039.1998.tb03005.x
307. Vitale M, Rezzani R, Rodella L, Zauli G, Grigolato P, Cadei M, et al. HLA class I antigen and transporter associated with antigen processing (TAP1 and TAP2) down-regulation in high-grade primary breast carcinoma lesions. *Cancer Res*. (1998) 58:737–42.
308. Gudmundsdottir I, Gunnlaugur Jonasson J, Sigurdsson H, Olafsdottir K, Tryggvadottir L, Ogmundsdottir HM. Altered expression of HLA class I antigens in breast cancer: association with prognosis. *Int J Cancer*. (2000) 89:500–53. doi: 10.1002/1097-0215(20001120)89:6<500::AID-IJC6>3.0.CO;2-#
309. Atkins D, Breuckmann A, Schmahl GE, Binner P, Ferrone S, Krummenauer F, et al. MHC class I antigen processing pathway defects, ras mutations and disease stage in colorectal carcinoma. *Int J Cancer*. (2004) 109:265–73. doi: 10.1002/ijc.11681
310. Seliger B, Stoehr R, Handke D, Mueller A, Ferrone S, Wullich B, et al. Association of HLA class I antigen abnormalities with disease progression and early recurrence in prostate cancer. *Cancer Immunol Immunother*. (2010) 59:529–40. doi: 10.1007/s00262-009-0769-5
311. Iwayama Y, Tsuruma T, Mizuguchi T, Furuhata T, Toyota N, Matsumura M, et al. Prognostic value of HLA class I expression in patients with colorectal cancer. *World J Surg Oncol*. (2015) 13:36. doi: 10.1186/s12957-015-0456-2
312. Esteban F, Concha A, Delgado M, Perez-Ayala M, Ruiz-Cabello F, Garrido F. Lack of MHC class I antigens and tumour aggressiveness of the squamous cell carcinoma of the larynx. *Br J Cancer*. (1990) 62:1047–51. doi: 10.1038/bjc.1990.437
313. Sandel MH, Speetjens FM, Menon AG, Albertsson PA, Basse PH, Hokland M, et al. Natural killer cells infiltrating colorectal cancer and MHC class I expression. *Mol Immunol*. (2005) 42:541–6. doi: 10.1016/j.molimm.2004.07.039
314. Levin I, Klein T, Kuperman O, Segal S, Shapira J, Gal R, et al. The expression of HLA class I antigen in prostate cancer in relation to tumor differentiation and patient survival. *Cancer Detect Prev*. (1994) 18:443–5.
315. Tsuda H, Hirohashi S, Higuchi K, Shimosato Y. Beta-2-microglobulin expression in relation to amplification of oncogenes and prognosis in breast carcinoma. *Histopathology*. (1990) 16:500–2. doi: 10.1111/j.1365-2559.1990.tb01552.x
316. Kitamura H, Torigoe T, Honma I, Asanuma H, Nakazawa E, Shimozawa K, et al. Expression and antigenicity of survivin, an inhibitor of apoptosis family member, in bladder cancer: implications for specific immunotherapy. *Urology*. (2006) 67:955–9. doi: 10.1016/j.urology.2005.11.052
317. Na HY, Park Y, Nam SK, Lee KS, Oh HK, Kim DW, et al. Expression of human leukocyte antigen class I and beta2-microglobulin in colorectal cancer and its prognostic impact. *Cancer Sci*. (2021) 112:91–100. doi: 10.1111/cas.14723
318. Ferris RL, Hunt JL, Ferrone S. Human leukocyte antigen (HLA) class I defects in head and neck cancer: molecular mechanisms and clinical significance. *Immunol Res*. (2005) 33:113–33. doi: 10.1385/IR:33:2:113
319. Grandis JR, Falkner DM, Melhem MF, Gooding WE, Drenning SD, Morel PA. Human leukocyte antigen class I allelic and haplotype loss in squamous cell carcinoma of the head and neck: clinical and immunogenetic consequences. *Clin Cancer Res*. (2000) 6:2794–802.
320. Mattijssen V, De Mulder PH, Schalkwijk L, Manni JJ, Van 't Hof-Grootenboer B, Ruiter DJ. HLA antigen expression in routinely processed head and neck squamous cell carcinoma primary lesions of different sites. *Int J Cancer Suppl*. (1991) 6:95–100. doi: 10.1002/ijc.2910470719

321. Kabawat SE, Bast RC Jr, Welch WR, Knapp RC, Bhan AK. Expression of major histocompatibility antigens and nature of inflammatory cellular infiltrate in ovarian neoplasms. *Int J Cancer*. (1983) 32:547–54. doi: 10.1002/ijc.2910320505
322. Hilders CG, Houbiers JG, Krul EJ, Fleuren GJ. The expression of histocompatibility-related leukocyte antigens in the pathway to cervical carcinoma. *Am J Clin Pathol*. (1994) 101:5–12. doi: 10.1093/ajcp/101.1.5
323. Yuan J, Liu S, Yu Q, Lin Y, Bi Y, Wang Y, et al. Down-regulation of human leukocyte antigen class I (HLA-I) is associated with poor prognosis in patients with clear cell renal cell carcinoma. *Acta Histochem*. (2013) 115:470–4. doi: 10.1016/j.acthis.2012.11.002
324. Kaklamanis L, Leek R, Koukourakis M, Gatter KC, Harris AL. Loss of transporter in antigen processing 1 transport protein and major histocompatibility complex class I molecules in metastatic versus primary breast cancer. *Cancer Res*. (1995) 55:5191–4.
325. Shen YQ, Zhang JQ, Miao FQ, Zhang JM, Jiang Q, Chen H, et al. Relationship between the downregulation of HLA class I antigen and clinicopathological significance in gastric cancer. *World J Gastroenterol*. (2005) 11:3628–31. doi: 10.3748/wjg.v11.i23.3628
326. Cordon-Cardo C, Fuks Z, Drobnjak M, Moreno C, Eisenbach L, Feldman M. Expression of HLA-A,B,C antigens on primary and metastatic tumor cell populations of human carcinomas. *Cancer Res*. (1991) 51:6372–80.
327. Yang Y, Zhang J, Miao F, Wei J, Shen C, Shen Y, et al. Loss of heterozygosity at 6p21 underlying [corrected] HLA class I downregulation in Chinese primary esophageal squamous cell carcinomas. *Tissue Antigens*. (2008) 72:105–14. doi: 10.1111/j.1399-0039.2008.01078.x
328. Vermeulen CF, Jordanova ES, ter Haar NT, Kolkman-Uljee SM, de Miranda NF, Ferrone S, et al. Expression and genetic analysis of transporter associated with antigen processing in cervical carcinoma. *Gynecol Oncol*. (2007) 105:593–9. doi: 10.1016/j.ygyno.2007.02.016
329. Ishigami S, Arigami T, Uenosono Y, Matsumoto M, Okumura H, Uchikado Y, et al. Cancerous HLA class I expression and regulatory T cell infiltration in gastric cancer. *Cancer Immunol Immunother*. (2012) 61:1663–9. doi: 10.1007/s00262-012-1225-5
330. Kaklamanis L, Gatter KC, Hill AB, Mortensen N, Harris AL, Krausa P, et al. Loss of HLA class-I alleles, heavy chains and beta. (1992) 2-microglobulin in colorectal cancer. *Int J Cancer* 51:379–85. doi: 10.1002/ijc.2910510308
331. Hanak L, Slaby O, Lauerova L, Kren L, Nenutil R, Michalek J. Expression pattern of HLA class I antigens in renal cell carcinoma and primary cell line cultures: methodological implications for immunotherapy. *Med Sci Monit*. (2009) 15:CR638–43.
332. Kloth JN, Gorter A, Fleuren GJ, Oosting J, Uljee S, ter Haar N, et al. Elevated expression of SerpinA1 and SerpinA3 in HLA-positive cervical carcinoma. *J Pathol*. (2008) 215:222–30. doi: 10.1002/path.2347
333. Redondo M, Concha A, Oldiviela R, Cueto A, Gonzalez A, Garrido F, et al. Expression of HLA class I and II antigens in bronchogenic carcinomas: its relationship to cellular DNA content and clinical-pathological parameters. *Cancer Res*. (1991) 51:4948–54.
334. Ishigami S, Natsugoe S, Nakajo A, Arigami T, Kitazono M, Okumura H, et al. HLA-class I expression in gastric cancer. *J Surg Oncol*. (2020) 97:605–8. doi: 10.1002/jso.21029
335. Klein B, Klein T, Nyska A, Shapira J, Figer A, Schwartz A, et al. Expression of HLA class I and class II in gastric carcinoma in relation to pathologic stage. *Tumour Biol*. (1991) 12:68–74. doi: 10.1159/000217690
336. Tsuchikawa T, Ikeda H, Cho Y, Miyamoto M, Shichinohe T, Hirano S, et al. Association of CD8+ T cell infiltration in oesophageal carcinoma lesions with human leucocyte antigen (HLA) class I antigen expression and survival. *Clin Exp Immunol*. (2011) 164:50–6. doi: 10.1111/j.1365-2249.2010.04311.x
337. Kaneko K, Ishigami S, Kijima Y, Funasako Y, Hirata M, Okumura H, et al. Clinical implication of HLA class I expression in breast cancer. *BMC Cancer*. (2011) 11:454. doi: 10.1186/1471-2407-11-454
338. Dierssen JW, de Miranda NF, Mulder A, van Puijenbroek M, Verduyn W, Claas FH, et al. High-resolution analysis of HLA class I alterations in colorectal cancer. *BMC Cancer*. (2006) 6:233. doi: 10.1186/1471-2407-6-233
339. Wintzer HO, Benzing M, von Kleist S. Lacking prognostic significance of beta 2-microglobulin, MHC class I and class II antigen expression in breast carcinomas. *Br J Cancer*. (1990) 62:289–95. doi: 10.1038/bjc.1990.280
340. Redondo M, Garcia J, Villar E, Rodrigo I, Perea-Milla E, Serrano A, et al. Major histocompatibility complex status in breast carcinogenesis and relationship to apoptosis. *Hum Pathol*. (2003) 34:1283–9. doi: 10.1016/j.humpath.2003.06.001
341. Maiorana A, Cesinaro AM, Fano RA, Collina G. Expression of MHC class I and class II antigens in primary breast carcinomas and synchronous nodal metastases. *Clin Exp Metastasis*. (1995) 13:43–8. doi: 10.1007/BF00144017
342. Lopez-Nevot MA, Esteban F, Ferron A, Gutierrez J, Oliva MR, Romero C, et al. HLA class I gene expression on human primary tumours and autologous metastases: demonstration of selective losses of HLA antigens on colorectal, gastric and laryngeal carcinomas. *Br J Cancer*. (1989) 59:221–6. doi: 10.1038/bjc.1989.45
343. Baba T, Shiota H, Kuroda K, Shigematsu Y, Ichiki Y, Uramoto H, et al. Clinical significance of human leukocyte antigen loss and melanoma-associated antigen 4 expression in smokers of non-small cell lung cancer patients. *Int J Clin Oncol*. (2013) 18:997–1004. doi: 10.1007/s10147-012-0491-8
344. Ueda Y, Ishikawa K, Shiraishi N, Yokoyama S, Kitano S. Clinical significance of HLA class I heavy chain expression in patients with gastric cancer. *J Surg Oncol*. (2008) 97:451–5. doi: 10.1002/jso.20985
345. Saito T, Tanaka R, Yoshida S, Washiyama K, Kumanishi T. Immunohistochemical analysis of tumor-infiltrating lymphocytes and major histocompatibility antigens in human gliomas and metastatic brain tumors. *Surg Neurol*. (1988) 29:435–42. doi: 10.1016/0090-3019(88)90137-1
346. Mink SR, Hodge A, Agus DB, Jain A, Gross ME. Beta-2-microglobulin expression correlates with high-grade prostate cancer and specific defects in androgen signaling. *Prostate*. (2010) 70:1201–10. doi: 10.1002/pros.21155
347. Zeestraten EC, Van Hoesel AQ, Speetjens FM, Menon AG, Putter H, van de Velde CJ, et al. FoxP3- and CD8-positive infiltrating immune cells together determine clinical outcome in colorectal cancer. *Cancer Microenviron*. (2013) 6:31–9. doi: 10.1007/s12307-011-0071-x
348. Reimers MS, Bastiaannet E, Langley RE, van Eijk R, van Vlierberghe RL, Lemmens VE, et al. Expression of HLA class I antigen, aspirin use, and survival after a diagnosis of colon cancer. *JAMA Intern Med*. (2014) 174:732–9. doi: 10.1001/jamainternmed.2014.511
349. Ferron A, Perez-Ayala M, Concha A, Cabrera T, Redondo M, Oliva MR, et al. MHC class I and II antigens on gastric carcinomas and autologous mucosa. *J Immunogenet*. (1989) 16:413–23. doi: 10.1111/j.1744-313X.1989.tb00489.x
350. Zeestraten EC, Reimers MS, Saadatmand S, Goossens-Beumer IJ, Dekker JW, Liefers GJ, et al. Combined analysis of HLA class I, HLA-E and HLA-G predicts prognosis in colon cancer patients. *Br J Cancer*. (2014) 110:459–68. doi: 10.1038/bjc.2013.696
351. Redondo M, Ruiz-Cabello F, Concha A, Cabrera T, Perez-Ayala M, Oliva MR, Garrido F. Altered HLA class I expression in non-small cell lung cancer is independent of c-myc activation. *Cancer Res*. (1991) 51:2463–8.
352. Ruiter DJ, Bergman W, Welvaart K, Scheffer E, van Vloten WA, Russo C, et al. Immunohistochemical analysis of malignant melanomas and nevocellular nevi with monoclonal antibodies to distinct monomorphic determinants of HLA antigens. *Cancer Res*. (1984) 44:3930–5.
353. Vitale M, Pelusi G, Taroni B, Gobbi G, Micheloni C, Rezzani R, et al. HLA class I antigen down-regulation in primary ovary carcinoma lesions: association with disease stage. *Clin Cancer Res*. (2005) 11:67–72.
354. Menon AG, Morreau H, Tollenaar RA, Alphenaar E, Van Puijenbroek M, Putter H, et al. Down-regulation of HLA-A expression correlates with a better prognosis in colorectal cancer patients. *Lab Invest*. (2002) 82:1725–33. doi: 10.1097/01.LAB.0000043124.75633.ED
355. Ichinokawa K, Nakanishi Y, Hida Y, Tsuchikawa T, Kato T, Itoh T, et al. Downregulated expression of human leukocyte antigen class I heavy chain is associated with poor prognosis in non-small-cell lung cancer. *Oncol Lett*. (2019) 18:117–26. doi: 10.3892/ol.2019.10293
356. Kasajima A, Sers C, Sasano H, Johrens K, Stenzinger A, Noske A, et al. Down-regulation of the antigen processing machinery is linked to a loss of inflammatory response in colorectal cancer. *Hum Pathol*. (2010) 41:1758–69. doi: 10.1016/j.humpath.2010.05.014
357. Ericsson C, Seregard S, Bartolazzi A, Levitskaya E, Ferrone S, Kiessling R, et al. Association of HLA class I and class II antigen expression and mortality in uveal melanoma. *Invest Ophthalmol Vis Sci*. (2001) 42:2153–6.

358. Kooi S, Zhang HZ, Patenia R, Edwards CL, Platsoucas CD, Freedman RS. HLA class I expression on human ovarian carcinoma cells correlates with T-cell infiltration *in vivo* and T-cell expansion *in vitro* in low concentrations of recombinant interleukin-2. *Cell Immunol*. (1996) 174:116–28. doi: 10.1006/cimm.1996.0301
359. Shehata M, Mukherjee A, Deen S, Al-Attar A, Durrant LG, Chan S. Human leukocyte antigen class I expression is an independent prognostic factor in advanced ovarian cancer resistant to first-line platinum chemotherapy. *Br J Cancer*. (2009) 101:1321–8. doi: 10.1038/sj.bjc.6605315
360. Yabe H, Tsukahara T, Kawaguchi S, Wada T, Torigoe T, Sato N, et al. Prognostic significance of HLA class I expression in Ewing's sarcoma family of tumors. *J Surg Oncol*. (2011) 103:380–5. doi: 10.1002/jso.21829
361. Nouri AM, Smith ME, Crosby D, Oliver RT. Selective and non-selective loss of immunoregulatory molecules (HLA-A,B,C antigens and LFA-3) in transitional cell carcinoma. *Br J Cancer*. (1990) 62:603–6. doi: 10.1038/bjc.1990.338
362. Kikuchi E, Yamazaki K, Torigoe T, Cho Y, Miyamoto M, Oizumi S, et al. HLA class I antigen expression is associated with a favorable prognosis in early stage non-small cell lung cancer. *Cancer Sci*. (2007) 98:1424–30. doi: 10.1111/j.1349-7006.2007.00558.x
363. Koelzer VH, Dawson H, Andersson E, Karamitopoulou E, Masucci GV, Lugli A, et al. Active immunosurveillance in the tumor microenvironment of colorectal cancer is associated with low frequency tumor budding and improved outcome. *Transl Res*. (2015) 166:207–17. doi: 10.1016/j.trsl.2015.02.008
364. Haimiti A, Hailiman Y, Gulina A, Du J, Hao Z, Rong XL, et al. Reduced expression of members of the mhc-i antigen processing machinery in ethnic Uighur women with cervical cancer in the Xinjiang region of China. *Curr Oncol*. (2014) 21:e67–74. doi: 10.3747/co.21.1595
365. Dierssen JW, de Miranda NF, Ferrone S, van Puijenbroek M, Cornelisse CJ, Fleuren GJ, et al. HNPCC versus sporadic microsatellite-unstable colon cancers follow different routes toward loss of HLA class I expression. *BMC Cancer*. (2007) 7:33. doi: 10.1186/1471-2407-7-33
366. Houck JR, Sexton FM, Zajdel G. HLA class I and class II antigen expression on squamous cell carcinoma of the head and neck. *Arch Otolaryngol Head Neck Surg*. (1990) 116:1181–5. doi: 10.1001/archotol.1990.01870100075016
367. Cabrera T, Angustias Fernandez M, Sierra A, Garrido A, Herruzo A, Escobedo A, et al. High frequency of altered HLA class I phenotypes in invasive breast carcinomas. *Hum Immunol*. (1996) 50:127–34. doi: 10.1016/0198-8859(96)00145-0
368. Carretero FJ, Del Campo AB, Flores-Martin JF, Mendez R, Garcia-Lopez C, Cozar JM, et al. Frequent HLA class I alterations in human prostate cancer: molecular mechanisms and clinical relevance. *Cancer Immunol Immunother*. (2016) 65:47–59. doi: 10.1007/s00262-015-1774-5
369. Vermeulen CF, Jordanova ES, Zomerdijk-Nooijen YA, ter Haar NT, Peters AA, Fleuren GJ. Frequent HLA class I loss is an early event in cervical carcinogenesis. *Hum Immunol*. (2005) 66:1167–73. doi: 10.1016/j.humimm.2005.10.011
370. Levin I, Klein T, Goldstein J, Kuperman O, Kanetti J, Klein B. Expression of class I histocompatibility antigens in transitional cell carcinoma of the urinary bladder in relation to survival. *Cancer*. (1991) 68:2591–43. doi: 10.1002/1097-0142(19911215)68:12<2591::AID-CNCR2820681212>3.0.CO;2-L
371. Miyagi K, Ingram M, Techy GB, Jacques DB, Freshwater DB, Sheldon H. Immunohistochemical detection and correlation between MHC antigen and cell-mediated immune system in recurrent glioma by APAAP method. *Neurol Med Chir*. (1990) 30:649–55. doi: 10.2176/nmc.30.649
372. Krishnakumar S, Abhyankar D, Lakshmi SA, Pushparaj V, Shanmugam MP, Biswas J. HLA expression in choroidal melanomas: correlation with clinicopathological features. *Curr Eye Res*. (2004) 28:409–16. doi: 10.1080/02713680490503741
373. Liu S, Qi L, Yu Q, Song Y, Han W, Zu X, et al. Survivin and HLA-I expression predicts survival of patients with clear cell renal cell carcinoma. *Tumour Biol*. (2014) 35:8281–8. doi: 10.1007/s13277-014-2058-y
374. Toquet C, Jarry A, Bou-Hanna C, Bach K, Denis MG, Mosnier JF, et al. Altered Calreticulin expression in human colon cancer: maintenance of Calreticulin expression is associated with mucinous differentiation. *Oncol Rep*. (2007) 17:1101–7. doi: 10.3892/or.17.5.1101
375. Garrido MA, Rodriguez T, Zinchenko S, Maleno I, Ruiz-Cabello F, Concha A, et al. HLA class I alterations in breast carcinoma are associated with a high frequency of the loss of heterozygosity at chromosomes 6 and 15. *Immunogenetics*. (2018) 70:647–59. doi: 10.1007/s00251-018-1074-2
376. Speetjens FM, de Bruin EC, Morreau H, Zeestraten EC, Putter H, van Krieken JH, et al. Clinical impact of HLA class I expression in rectal cancer. *Cancer Immunol Immunother*. (2008) 57:601–9. doi: 10.1007/s00262-007-0396-y
377. Ramnath N, Tan D, Li Q, Hylander BL, Bogner P, Ryes L, et al. Is downregulation of MHC class I antigen expression in human non-small cell lung cancer associated with prolonged survival? *Cancer Immunol Immunother*. (2006) 55:891–9. doi: 10.1007/s00262-005-0085-7
378. Tao J, Li Y, Liu YQ, Li L, Liu J, Shen X, et al. Expression of transporters associated with antigen processing and human leucocyte antigen class I in malignant melanoma and its association with prognostic factors. *Br J Dermatol*. (2008) 158:88–94. doi: 10.1111/j.1365-2133.2007.08294.x
379. Tsukahara T, Kawaguchi S, Torigoe T, Asanuma H, Nakazawa E, Shimozawa K, et al. Prognostic significance of HLA class I expression in osteosarcoma defined by anti-pan HLA class I monoclonal antibody, EMR8-5. *Cancer Sci*. (2006) 97:1374–80. doi: 10.1111/j.1349-7006.2006.00317.x
380. Kostine M, Cleven AH, de Miranda NF, Italiano A, Cleton-Jansen AM, Bovee JV. Analysis of PD-L1, T-cell infiltrate and HLA expression in chondrosarcoma indicates potential for response to immunotherapy specifically in the dedifferentiated subtype. *Mod Pathol*. (2016) 29:1028–37. doi: 10.1038/modpathol.2016.108
381. Cabrera CM, Jimenez P, Cabrera T, Esparza C, Ruiz-Cabello F, Garrido F. Total loss of MHC class I in colorectal tumors can be explained by two molecular pathways: beta2-microglobulin inactivation in MSI-positive tumors and LMP7/TAP2 downregulation in MSI-negative tumors. *Tissue Antigens*. (2003) 61:211–9. doi: 10.1034/j.1399-0039.2003.00020.x
382. Watson NF, Ramage JM, Madjd Z, Spendlove I, Ellis IO, Scholefield JH, et al. Immunosurveillance is active in colorectal cancer as downregulation but not complete loss of MHC class I expression correlates with a poor prognosis. *Int J Cancer*. (2006) 118:6–10. doi: 10.1002/ijc.21303
383. Reimers MS, Engels CC, Putter H, Morreau H, Liefers GJ, van de Velde CJ, et al. Prognostic value of HLA class I, HLA-E, HLA-G and Tregs in rectal cancer: a retrospective cohort study. *BMC Cancer*. (2014) 14:486. doi: 10.1186/1471-2407-14-486
384. Zhao X, Sun Q, Tian H, Cong B, Jiang X, Peng C. Loss of heterozygosity at 6p21 and HLA class I expression in esophageal squamous cell carcinomas in China. *Asian Pac J Cancer Prev*. (2011) 12:2741–5.
385. Han LY, Fletcher MS, Urbauer DL, Mueller P, Landen CN, Kamat AA, et al. HLA class I antigen processing machinery component expression and intratumoral T-Cell infiltrate as independent prognostic markers in ovarian carcinoma. *Clin Cancer Res*. (2008) 14:3372–9. doi: 10.1158/1078-0432.CCR-07-4433
386. Ogino T, Moriai S, Ishida Y, Ishii H, Katayama A, Miyokawa N, et al. Association of immunoescape mechanisms with Epstein-Barr virus infection in nasopharyngeal carcinoma. *Int J Cancer*. (2007) 120:2401–10. doi: 10.1002/ijc.22334
387. Kloor M, Becker C, Benner A, Woerner SM, Gebert J, Ferrone S, et al. Immunoselective pressure and human leukocyte antigen class I antigen machinery defects in microsatellite unstable colorectal cancers. *Cancer Res*. (2005) 65:6418–24. doi: 10.1158/0008-5472.CAN-05-0044
388. Atkins D, Ferrone S, Schmahl GE, Storkel S, Seliger B. Down-regulation of HLA class I antigen processing molecules: an immune escape mechanism of renal cell carcinoma? *J Urol*. (2004) 171:885–9. doi: 10.1097/01.ju.0000094807.95420.fe
389. Vora AR, Rodgers S, Parker AJ, Start R, Rees RC, Murray AK. An immunohistochemical study of altered immunomodulatory molecule expression in head and neck squamous cell carcinoma. *Br J Cancer*. (1997) 76:836–44. doi: 10.1038/bjc.1997.472

390. Zhang H, Melamed J, Wei P, Cox K, Frankel W, Bahnson RR, et al. Concordant down-regulation of proto-oncogene PML and major histocompatibility antigen HLA class I expression in high-grade prostate cancer. *Cancer Immun*. (2003) 3:2. doi: 10.1111/j.1399-0039.2007.00892.x
391. de Miranda NF, Nielsen M, Pereira D, van Puijenbroek M, Vasen HF, Hes FJ, et al. MUTYH-associated polyposis carcinomas frequently lose HLA class I expression—a common event amongst DNA-repair-deficient colorectal cancers. *J Pathol*. (2009) 219:69–76. doi: 10.1002/path.2569
392. Kitamura H, Torigoe T, Asanuma H, Honma I, Sato N, Tsukamoto T. Down-regulation of HLA class I antigens in prostate cancer tissues and up-regulation by histone deacetylase inhibition. *J Urol*. (2007) 178:692–6. doi: 10.1016/j.juro.2007.03.109
393. Saio M, Teicher M, Campbell G, Feiner H, Delgado Y, Frey AB. Immunocytochemical demonstration of down regulation of HLA class-I molecule expression in human metastatic breast carcinoma. *Clin Exp Metastasis*. (2004) 21:243–9. doi: 10.1023/B:CLIN.0000037707.07428.ff
394. Sato H, Suzuki Y, Ide M, Katoh T, Noda SE, Ando K, et al. HLA class I expression and its alteration by preoperative hyperthermo-chemoradiotherapy in patients with rectal cancer. *PLoS ONE*. (2014) 9:e108122. doi: 10.1371/journal.pone.0108122
395. de Boer MA, Jordanova ES, van Poelgeest MI, van den Akker BE, van der Burg SH, Kenter GG, et al. Circulating human papillomavirus type. (2007) 16 specific T-cells are associated with HLA Class I expression on tumor cells, but not related to the amount of viral oncogene transcripts. *Int J Cancer* 121:2711–5. doi: 10.1002/ijc.23035
396. Momburg F, Degener T, Bacchus E, Moldenhauer G, Hammerling GJ, Moller P. Loss of HLA-A,B,C and *de novo* expression of HLA-D in colorectal cancer. *Int J Cancer*. (1986) 37:179–84. doi: 10.1002/ijc.2910370203
397. Cabrera T, Salinero J, Fernandez MA, Garrido A, Esquivias J, Garrido F. High frequency of altered HLA class I phenotypes in laryngeal carcinomas. *Hum Immunol*. (2000) 61:499–506. doi: 10.1016/S0198-8859(00)00097-5
398. de Kruijf EM, van Nes JG, Sajet A, Tummers QR, Putter H, Osanto S, et al. The predictive value of HLA class I tumor cell expression and presence of intratumoral Tregs for chemotherapy in patients with early breast cancer. *Clin Cancer Res*. (2010) 16:1272–80. doi: 10.1158/1078-0432.CCR-09-1844
399. van Duinen SG, Ruiter DJ, Broecker EB, van der Velde EA, Sorg C, Welvaart K, et al. Level of HLA antigens in locoregional metastases and clinical course of the disease in patients with melanoma. *Cancer Res*. (1988) 48:1019–25.
400. Hanagiri T, Shigematsu Y, Shinohara S, Takenaka M, Oka S, Chikaishi Y, et al. Clinical significance of expression of cancer/testis antigen and down-regulation of HLA class-I in patients with stage I non-small cell lung cancer. *Anticancer Res*. (2013) 33:2123–8.
401. Li K, Du H, Lian X, Yang S, Chai D, Wang C, et al. Characterization of beta2-microglobulin expression in different types of breast cancer. *BMC Cancer*. (2014) 14:750. doi: 10.1186/1471-2407-14-750
402. Cromme FV, van Bommel PF, Walboomers JM, Gallee MP, Stern PL, Kenemans P, et al. Differences in MHC and TAP-1 expression in cervical cancer lymph node metastases as compared with the primary tumours. *Br J Cancer*. (1994) 69:1176–81. doi: 10.1038/bjc.1994.231
403. van Driel WJ, Tjiong MY, Hilders CG, Trimbos BJ, Fleuren GJ. Association of allele-specific HLA expression and histopathologic progression of cervical carcinoma. *Gynecol Oncol*. (1996) 62:33–41. doi: 10.1006/gyno.1996.0186
404. Pandha H, Rigg A, John J, Lemoine N. Loss of expression of antigen-presenting molecules in human pancreatic cancer and pancreatic cancer cell lines. *Clin Exp Immunol*. (2007) 148:127–35. doi: 10.1111/j.1365-2249.2006.03289.x
405. Koene G, Mulder A, van der Ven K, Eijsink C, Franke M, Slootweg P, et al. Human monoclonal antibodies as a tool for the detection of HLA class I allele-specific expression loss in head-and-neck squamous cell carcinoma and corresponding lymph node metastases. *Hum Immunol*. (2006) 67:692–9. doi: 10.1016/j.humimm.2006.06.001
406. Homma I, Kitamura H, Torigoe T, Tanaka T, Sato E, Hirohashi Y, et al. Human leukocyte antigen class I down-regulation in muscle-invasive bladder cancer: its association with clinical characteristics and survival after cystectomy. *Cancer Sci*. (2009) 100:2331–4. doi: 10.1111/j.1349-7006.2009.01329.x
407. Korkolopoulou P, Kaklamanis L, Pezzella F, Harris AL, Gatter KC. Loss of antigen-presenting molecules (MHC class I and TAP-1) in lung cancer. *Br J Cancer*. (1996) 73:148–53. doi: 10.1038/bjc.1996.28
408. Lu QL, Abel P, Mitchell S, Foster C, Lalani EN. Decreased HLA-A expression in prostate cancer is associated with normal allele dosage in the majority of cases. *J Pathol*. (2000) 190:169–763. doi: 10.1002/(SICI)1096-9896(200002)190:2169::AID-PATH517>3.0.CO;2-#
409. Tomita Y, Matsumoto Y, Nishiyama T, Fujiwara M. Reduction of major histocompatibility complex class I antigens on invasive and high-grade transitional cell carcinoma. *J Pathol*. (1990) 162:157–64. doi: 10.1002/path.1711620209
410. Connor ME, Stern PL. Loss of MHC class-I expression in cervical carcinomas. *Int J Cancer*. (1990) 46:1029–34. doi: 10.1002/ijc.2910460614
411. Leffers N, Lambeck AJ, de Graeff P, Bijlsma AY, Daemen T, van der Zee AG, et al. Survival of ovarian cancer patients overexpressing the tumour antigen p53 is diminished in case of MHC class I down-regulation. *Gynecol Oncol*. (2008) 110:365–73. doi: 10.1016/j.ygyno.2008.04.043
412. Jimenez P, Canton J, Concha A, Cabrera T, Fernandez M, Real LM, et al. Microsatellite instability analysis in tumors with different mechanisms for total loss of HLA expression. *Cancer Immunol Immunother*. (2000) 48:684–90. doi: 10.1007/s002620050017
413. Nada OH, Ahmed NS, Abou Gabal HH. Prognostic significance of HLA EMR8-5 immunohistochemically analyzed expression in osteosarcoma. *Diagn Pathol*. (2014) 9:72. doi: 10.1186/1746-1596-9-72
414. Madjd Z, Spendlove I, Pinder SE, Ellis IO, Durrant LG. Total loss of MHC class I is an independent indicator of good prognosis in breast cancer. *Int J Cancer*. (2005) 117:248–55. doi: 10.1002/ijc.21163
415. Esteban F, Concha A, Huelin C, Perez-Ayala M, Pedrinaci S, Ruiz-Cabello F, et al. Histocompatibility antigens in primary and metastatic squamous cell carcinoma of the larynx. *Int J Cancer*. (1989) 43:436–42. doi: 10.1002/ijc.2910430316
416. Pistillo MP, Nicolo G, Salvi S, Capanni P, Perdelli L, Pasciucco G, et al. Biochemical analysis of HLA class I subunits expression in breast cancer tissues. *Hum Immunol*. (2000) 61:397–407. doi: 10.1016/S0198-8859(99)00179-2

Conflict of Interest: The authors declare that the research was conducted in the absence of any commercial or financial relationships that could be construed as a potential conflict of interest.

GLOSSARY

APM, Antigen presentation machinery; ß2M, Beta2 microglobulin; CTLA-4, Cytotoxic T-lymphocyte-associated protein; ER, Endoplasmic reticulum; ERAD, Endoplasmic-reticulum-associated protein degradation; ERAP1, Endoplasmic reticulum aminopeptidase 1; EZH2, Enhancer of zeste 2 polycomb repressive complex 2; GSL, Glycosphingolipid; HDAC, Histone deacyetylase; HLA, Human leukocyte antigen; ILC, Innate lymphoid cells; JAK, Janus kinase; KIR, Killer inhibitory receptor; lnkRNA, Long noncoding RNA; NK, Natural killer; NLRC5, NLR Family CARD domain Containing 5; MHC, Major histocompatibility complex; miRNA, microRNA; PD1/PD-L1, Programmed cell death protein 1/ Programmed death-ligand 1; TAP, Transporter of antigen presentation; TIL, Tumor infiltrating lymphocytes; UTR, Untranslated region.

frontiers in Immunology

MINI REVIEW
published: 29 March 2021
doi: 10.3389/fimmu.2021.639682

Making Insulin and Staying Out of Autoimmune Trouble: The Beta-Cell Conundrum

Alexia Carré[1*] *and Roberto Mallone*[1,2*]

[1] Université de Paris, Institut Cochin, CNRS, INSERM, Paris, France, [2] Assistance Publique Hôpitaux de Paris, Service de Diabétologie et Immunologie Clinique, Cochin Hospital, Paris, France

Autoimmune type 1 diabetes (T1D) results from the intricate crosstalk of various immune cell types. CD8+ T cells dominate the pro-inflammatory milieu of islet infiltration (insulitis), and are considered as key effectors of beta-cell destruction, through the recognition of MHC Class I-peptide complexes. The pathways generating MHC Class I-restricted antigens in beta cells are poorly documented. Given their specialized insulin secretory function, the associated granule processing and degradation pathways, basal endoplasmic reticulum stress and susceptibility to additional stressors, alternative antigen processing and presentation (APP) pathways are likely to play a significant role in the generation of the beta-cell immunopeptidome. As direct evidence is missing, we here intersect the specificities of beta-cell function and the literature about APP in other cellular models to generate some hypotheses on APPs relevant to beta cells. We further elaborate on the potential role of these pathways in T1D pathogenesis, based on the current knowledge of antigens presented by beta cells. A better understanding of these pathways may pinpoint novel mechanisms amenable to therapeutic targeting to modulate the immunogenicity of beta cells.

Keywords: antigen presentation, antigen processing, autophagy, crinophagy, insulin granule, MHC class I, neo-epitopes, signal peptide

OPEN ACCESS

Edited by:
Iñaki Alvarez, Universitat Autònoma de Barcelona, Spain

Reviewed by:
Howard Davidson, University of Colorado Anschutz Medical Campus, United States
Bruce Verchere, University of British Columbia, Canada

***Correspondence:**
Alexia Carré
alexia.carre@inserm.fr
Roberto Mallone
roberto.mallone@inserm.fr

Specialty section:
This article was submitted to Antigen Presenting Cell Biology, a section of the journal Frontiers in Immunology

Received: *09 December 2020*
Accepted: *12 March 2021*
Published: *29 March 2021*

Citation:
Carré A and Mallone R (2021) Making Insulin and Staying Out of Autoimmune Trouble: The Beta-Cell Conundrum. Front. Immunol. 12:639682. doi: 10.3389/fimmu.2021.639682

INTRODUCTION

Type 1 diabetes (T1D) is an autoimmune disease characterized by the destruction of insulin-producing beta cells. It stems from a complex interplay of innate and adaptive immune cells. CD8+ T cells dominate the immune infiltration of islets and play a prominent role as final effectors of beta-cell loss (1). There is also growing evidence supporting the idea that beta-cell dysfunction is another key driver of T1D pathogenesis (2). The heterogeneity of pancreas histopathology between T1D donors and even across islets from the same pancreas, both in terms of immune infiltrates and residual beta cells, have led to the definition of age-related endotypes (3), in which the component of beta-cell dysfunction may be dominant in adult-onset cases (4, 5). Effector CD8+ T cells recognize MHC Class I (MHC-I)-peptide complexes at the surface of beta cells. The conventional MHC-I antigen processing and presentation (APP) machinery is a multi-step process (**Figure 1A**) where *i)* cytosolic proteins of microbial or self-origin are degraded into peptides in a proteasome-mediated manner; *ii)* the resulting peptides are transported into the endoplasmic reticulum (ER) *via* the

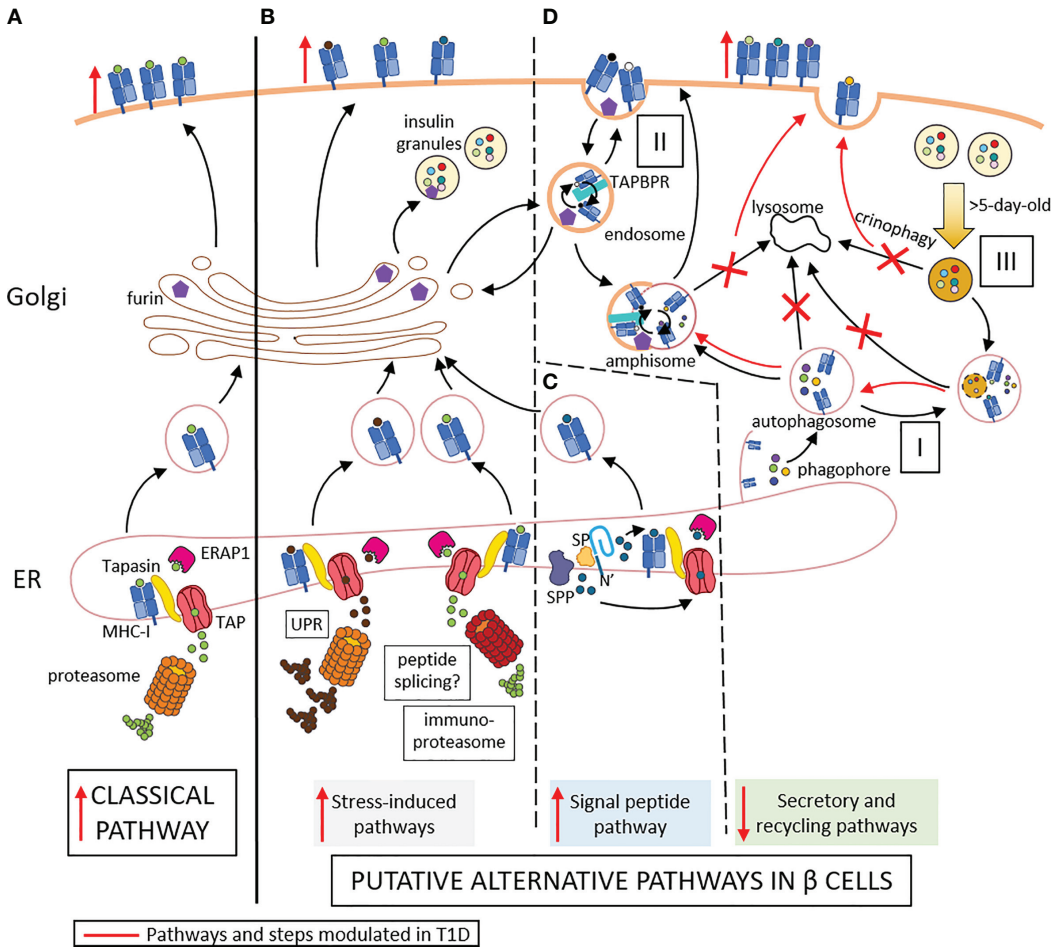

FIGURE 1 | Conventional **(A)** and putative alternative APP pathways **(B–D)** in beta cells. **(A)** In conventional APP pathways, misfolded proteins are degraded by the proteasome into peptides that are transported through TAP into the ER lumen. Here, they are further trimmed by ERAP1 and loaded onto MHC-I molecules that are associated to TAP *via* tapasin. The peptide-MHC-I complexes are exported to the Golgi and then to the cell surface. **(B)** Under inflammatory conditions, ER stress induces the UPR, which increases protein degradation and antigen presentation. The immuno-proteasome is also induced, further increasing APP and possibly resulting in alternative peptide splicing events and neo-epitopes generated. **(C)** Signal peptides are docked within the ER membrane. While the protein translation continues, the signal peptide is cleaved by the signal peptidase (SP) and further trimmed by the signal peptide peptidase (SPP). The N-terminal cleavage products of the signal peptide are released in the cytosol and can re-enter the ER through TAP for antigen presentation. The C-terminal cleavage products remaining in the ER can be loaded onto MHC-I molecules in a TAP- and proteasome-independent manner. **(D)** I. Cellular components are engulfed by nascent phagophore at the ER membrane, thus forming autophagosome, likely containing MHC-I molecules. II. Endocytosis of cell surface component forms endosomes, which can contain both MHC-I molecules and TAPBR promoting peptide exchange within endosomes. These vesicles can be directed to the Golgi apparatus, where peptides (free or released from MHC-I) can be trimmed by Golgi enzymes such as furins prior to loading onto MHC-I molecules. Autophagosomes, if not directly fused to lysosomes for degradation of their content, can fuse with endosome to form amphisomes, thus opening another peptide exchange pathway. These vesicles can subsequently be directed to lysosomes for degradation. III. Old insulin granules can be degraded by crinophagy. T1D induces changes (in red) characterized by enhanced ER stress **(B)**, increased insulin production and signal peptide processing **(C)**, and altered vesicle trafficking **(D)**, thus enhancing surface exposure of MHC-I complexes. Red marks indicate changes occuring in T1D: vertical arrows represent the increase or decrease of a step or pathway; bended arrows represent favored events; crosses represent blocked events. Some cellular components were modified from Servier Medical Art (smart.servier.com).

transporter associated with antigen processing (TAP). Here, *iii)* they are further trimmed by ER aminopeptidase (ERAP)1 prior to *iv)* loading on nascently-formed MHC-I molecules that are associated to TAP through tapasin; *v)* the stable peptide-MHC-I complexes are finally translocated to the Golgi complex and to the cell surface (6). This review addresses the specificities of the direct alternative MHC-I APP (aAPP) machinery within beta cells and its potential role in T1D pathogenesis (**Figures 1B–D**). It therefore focuses on the CD8+ T-cell responses that are triggered by MHC-I APP, notwithstanding the role of other cell types, and particularly of MHC-I and MHC-II APP by professional antigen-presenting cells (APCs) for the priming of naïve T cells. Since the beta-cell APP pathways are poorly if at all documented, we here provide a hypothesis-generating review that bridges the separate bodies of knowledge available for MHC-I APP and beta-cell biology.

SECRETING INSULIN: THE ACHILLES' HEEL OF BETA CELLS?

Like other endocrine cells, beta cells are hormone-secreting cells organized in glands that are highly vascularized, allowing the secretion of their products directly into the bloodstream. These features may influence the APP pathways used by these cells (2). Indeed, beta cells are equipped to sense changes in blood glucose levels and to respond by releasing appropriate amounts of insulin. For this purpose, they need to constantly adapt their secretory response to changes in metabolic and nutritional state. This adaptation is critical compared to that of other tissues because beta cells are long-lived and virtually non-proliferating, hence they can only modulate their function but not their cell numbers. Beta cells accommodate these metabolic variations by intensifying the synthesis of insulin and its precursor proinsulin. Under these intense bio-synthetic rates, misfolded proteins are more likely to accumulate within the ER, activating the unfolded protein response (UPR) (7). The UPR is a natural adaptive response that maintains cellular homeostasis by fulfilling three main tasks: to decrease the protein translation rate, to enhance the synthesis of protein-folding chaperones, and to increase the degradation of misfolded proteins into peptides through the proteasome (7). While part of the free cytosolic peptides generated by this process is further hydrolyzed to single amino acids, another portion is transported to the ER *via* TAP for the loading onto MHC-I molecules, thus shaping the catalog of MHC-I-bound peptides (immunopeptidome) presented at the beta-cell surface (**Figure 1B**). Beta cells rely on a well-balanced UPR to ensure their function and survival (8). Thus, beta cells are constantly functioning on the edge between physiological and pathological UPR and are exquisitely sensitive to additional stressors that can flip this delicate balance and lead to a compensatory maladaptive UPR further increasing ER stress prior to apoptosis (9, 10). Metabolic overload can act as an accelerator but is unlikely to drive this UPR transition on its own, as such overload is more common in type 2 diabetes and yet does not usually trigger islet autoimmunity. The environmental factors at play are likely multiple, but their identity and interaction with a susceptible genetic background remain ill-defined, with the possible exception of enteroviral infections (11). Considering the link between the UPR and APP through increased proteasomal degradation of misfolded proteins, the shift from physiological to pathological UPR may modulate the immunopeptidome and the beta-cell visibility to the immune system.

Under physiological conditions, the beta cells maintain consistent intracellular stores of insulin granules to allow their rapid exocytosis when the glycemia rises. While insulin granules are found by thousands in individual beta cells (12), not all are secreted. Indeed, the remarkable functional plasticity of beta cells includes recycling pathways to dispose of old (>5 days) or excess secretory granules. Commonly, insulin granules are degraded through macro-autophagy, by which they are engulfed by autophagosomes prior to degradation in lysosomes. Another endocrine-specific recycling pathway is a specialized macro-autophagy process named crinophagy, by which insulin granules fuse directly with lysosomes, thus generating so-called crinosomes (**Figure 1D**). While the role of these different types of autophagy has been extensively studied in type 2 diabetes, investigations in T1D are scanty. One recent study (13) reported defective macro-autophagy and diminished crinophagy in the beta cells of non-obese diabetic (NOD) mice compared to non-diabetic NOD littermates and non-obese resistant (NOR) mice. These conclusions were confirmed in T1D pancreas specimens and were based on the lack of co-localization of the lysosomal marker Lamp1 with either the granule marker proinsulin or the autophagosome marker LC3, thus suggesting a defect in the late stage of autophagy, when granules/autophagosomes fuse with lysosomes. An alternative explanation is that this reduced crinophagy may simply reflect a limited accumulation of old granules due to a compensatory higher insulin exocytosis rate in remaining beta cells. Interestingly, this study also reported a parallel increase of autophagosomes in insulin-positive cells of pancreata from autoantibody-positive non-diabetic donors in comparison to both control and T1D donors, whose autophagosome content was instead similar. As autophagy helps to prevent oxidative damage and promote cell survival, we can hypothesize that the beta-cell stress imposed by the inflammatory milieu of insulitis triggers an increase in their autophagy rate (14), prior to, and likely independently of, overt hyperglycemia. Interestingly, lysosomal autophagy can also degrade mitochondria (15). This process, known as mitophagy, is also part of stress responses (16), and is regulated by CLEC16A, whose genetic locus encodes variants associated with T1D risk (17). Pancreatic CLEC16A knockout mice harbor a defect in both mitochondrial and granule turnover (16), pointing to an intersection between the mitophagy and crinophagy pathway. It is thus possible that the altered granule disposal observed in stressed beta cells may also reflect overloading of this pathway by mitochondrial substrates. Its modulation by the *CLEC16A* genetic background may exacerbate the effect of stress on aAPPs. This feature also emphasizes the current view of lysosomes as dynamic structures that interact with different intracellular organelles and are continuously consumed and re-formed rather than just being end-stage degradation hubs (15).

Given this notion of impaired autophagy in T1D (13), what is the fate of the autophagosomes and insulin granules that are not degraded by lysosomes? In non-professional APCs, surface peptide-loaded MHC-I molecules seem to be recycled by clathrin-independent mechanisms, forming endosomes (18, 19). Whether and how these endosomes are degraded by lysosomes or targeted toward an early or late recycling pathway is unclear. Nonetheless, peptide exchange for MHC-I loading is likely to occur within the endosome. The TAP binding protein related (TAPBPR) chaperone is currently held as the main candidate for this role (20), and its preference for a slightly acidic to neutral pH is in the range of that found in endosomes. Another possibility is the encounter between endosomes and autophagosomes prior to recycling (21), forming so-called amphisomes (**Figure 1D**). Hence, the autophagosomes that are not degraded by lysosomes may be more likely to fuse with

endosomes and gain access to the cell surface. Considering that the autophagosome membrane is thought to derive from the ER and can thus harbor MHC-I molecules amenable to peptide loading (22), this process may provide an aAPP pathway. Similarly, insulin granules that are not degraded by lysosomes could indirectly participate in APP through engulfment by autophagosomes. Collectively, these data suggest that alternative autophagy-derived pathways for MHC-I loading could be operational in beta cells and participate in the recycling processes needed for disposing of insulin granules. While these pathways are active in resting beta cells, they may be further enriched in T1D as autophagy is impaired, possibly providing novel disease-enhanced pathways.

Besides insulin, secretory granules contain other proteins that we reported to dominate the beta-cell-specific immunopeptidome targeted by islet autoimmunity. First, a large fraction of MHC-I-bound peptides recovered from a human beta-cell line and primary islets originate from these granule proteins (23), which is not unexpected given the abundance and fast turnover of these proteins in beta cells (24). Second and most important however, these granule-derived peptides were also prominent targets recognized by circulating CD8+ T cells (23, 25). More recently, we found that H2-Kd-restricted peptides derived from the murine orthologues of some of these proteins, namely secretogranin-5, urocortin-3 and proconvertase-2, are also recognized by islet-infiltrating CD8 + T cells in prediabetic NOD mice (25). Moreover, CD8+ T cells recognizing these peptides were diabetogenic upon in-vivo transfer into NOD/*scid* recipients (25). Besides their localization in granules, it is noteworthy that these novel antigens (together with chromogranin A and others) (26) share several other features with insulin. First, they are all soluble proteins that are released along with insulin during granule exocytosis, a feature that could endow beta cells with a unique capability of sensitizing T cells at distance following APP of these proteins by extra-pancreatic APCs (2, 27). Second, they are all produced as precursors (pro-proteins) and subsequently undergo intermediate processing, first in the ER to cleave the signal peptide (see below), and then in immature granules through proconvertases, carboxypeptidase E (CPE) and furins that lead to their bioactive products (**Figure 2**). Intriguingly, reduced levels of proconvertases and CPE along with impaired proconvertase activity and proinsulin processing in beta cells has been repeatedly reported for T1D, even before clinical onset (4, 28–32). These enzymatic defects could lead to increase protein misfolding, which might feed the proteasomal recycling pathway and further fuel the APP machinery. It is also possible that granule protein byproducts may accumulate in the ER, the Golgi or the cytosol and thus become accessible for processing by other enzymes and for loading onto MHC-I molecules, either directly, through retrograde transport to the ER, or indirectly, *via* TAP. Of further note, proconvertases themselves as well as (pro) cathepsins are also synthesized as inactive precursors and subsequently activated, often through auto-enzymatic reactions. We can thus speculate that ER stress and impaired proconvertase activity may also negatively impact these processes since their earliest steps of ER export and self-activation.

An unsolved conundrum is how the T-cell targeting of granule antigens that are mostly shared with other endocrine cells such as alpha cells leads to an autoimmune response that is exquisitely beta-cell-specific. This question is even more

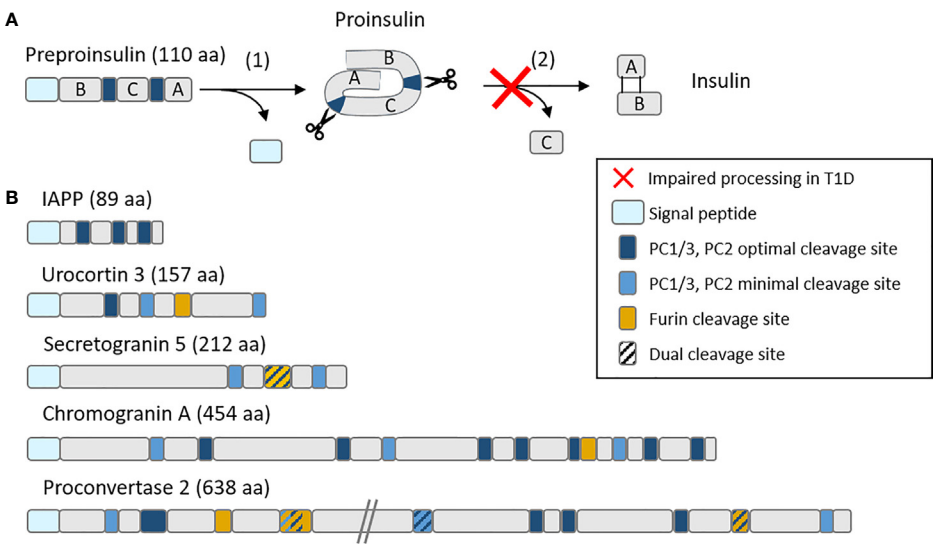

FIGURE 2 | Schematic representation of **(A)** the insulin maturation process and **(B)** mapping of proconvertase cleavage sites within insulin granule proteins. **(A)** Insulin is translated as a preprohormone comprising a signal peptide (light blue), followed by the B chain, C peptide and A chain. The first processing step (1) consists in the cleavage of the signal peptide, followed by (2) the cleavage by proconvertases of the C peptide and formation of disulfide bonds between the A and B chain. In T1D, this second step is often impaired, leading to proinsulin accumulation. **(B)** PC1/3 and PC2 optimal (RR, KR) and minimal (KK, RK) cleavage sites along with furin cleavage sites (R-X-X-R) (where X is any amino acid) are mapped on major insulin granules proteins. aa, amino acids.

important in light of recent reports suggesting that MHC–I upregulation is more prominent in alpha cells, even before clinical T1D (33). Protective factors at play in alpha cells may include their lower biosynthetic rate, the narrower dynamic range of their secretory response (34), their lower susceptibility to ER stress-induced apoptosis (35), and their higher expression of non-classical, inhibitory MHC-I molecules, i.e. human leukocyte antigen (HLA)-E (36). Moreover, autophagy seems less important for the maintenance of alpha-cell metabolism (37) than it is for beta cells (38), possibly making autophagy-related APP pathways less active.

NEO-EPITOPE GENERATION IN BETA CELLS

The large stores of insulin granules and the functional adaptability to metabolic changes of beta cells point to a remarkably active translation machinery, which enhances the odds of neo-epitope generation. Neo-epitopes are unconventional peptides such as post-translational modified sequences, defective ribosomal products (DRiPs), alternative mRNA splicing products and proteasomal peptide splicing products (i.e. resulting from the fusion of two non-adjacent regions of a protein). We reported that some of these products contribute to the MHC-I peptidome of beta cells (23, 25, 26). Very little is however known about how such peptides are generated and whether the required pathways are active in beta cells and/or professional APCs. In spite of their tissue specificity, the overall quantitative contribution of neo-epitopes to the beta-cell immunopeptidome appears to be minor, as only a limited number of MHC-I-restricted neo-epitopes has been reported to date (26). A possible scenario is that these neo-epitopes might be symptomatic of early beta-cell dysfunction, e.g. altered granule bio-synthesis/disposal, and become visible to T cells *via* the uptake of granules or of their exocytosed content by APCs (2). The combination of generation mechanisms favored by early beta-cell dysfunction and of recognition mechanisms favored by T cells that have escaped thymic deletion may endow them with a crucial role in the onset of islet autoimmunity.

Another aspect is the central role that the constitutive proteasome, and its inflammation-induced counterpart, the immunoproteasome, play in the generation of some of these neo-epitopes (39). It is noteworthy that in-vitro exposure of beta cells to interferon (IFN)-γ induces the expression of the immunoproteasome (40) which is known to enhance proteolysis, whereas immunoproteasome-deficient cells accumulate reactive oxygen species (ROS) (41). The immunoproteasome deficiency has also been investigated by in-vivo knockout in mice (42), which led to a CD8+ T-cell-mediated multi-organ autoimmunity comprising insulitis and CD8+ T cells reactive to an IGRP beta-cell peptide with low affinity H-2Kb binding. The authors hypothesized that the constitutive proteasome alone could fail at generating enough high-affinity MHC-I binders. This possibility is supported by other studies highlighting that the immunoproteasome uses the same cleavage sites as the constitutive proteasome, hence impacting the relative quantity rather than the quality of the peptides produced (39, 43, 44). Defective immunoproteasome activity and the resulting decrease in peptide output could thus allow weak-binding immunogenic peptides usually outcompeted by stronger binders to be processed and presented. Conversely, the inflammatory insulitis microenvironment of T1D may induce the well-known MHC-I upregulation (45), but also immunoproteasome expression, thus further enriching the immunopeptidome and favoring strong MHC binders. The higher binding affinity of these peptides may synergize with MHC-I upregulation to increase their availability for T-cell recognition. This increase in beta-cell visibility to T cells may provide one explanation to our recent observation that beta-cell-reactive CD8+ T cells circulate at similar frequencies in T1D and healthy donors (23, 46). This observation suggests that the difference between the 'benign' autoimmunity of healthy donors and the progressive autoimmunity of T1D patients may lie not only in their T-cell repertoire, but also in their beta-cell vulnerability (2).

PATHWAYS FOR SIGNAL PEPTIDE EPITOPES

Insulin is a protein hormone that is initially synthesized as a preprohormone. Preproinsulin is linearly composed of a signal peptide, as most secretory and membrane proteins, a B chain, a C peptide and an A chain (**Figure 2A**). Once the signal peptide is translated, it binds the signal recognition particle that docks to its receptor within the ER membrane and thus allows the direct translocation of newly synthesized insulin into the ER (**Figure 1C**). As the translation continues, the signal peptide is cleaved by signal peptidase (SP) and undergoes intramembrane proteolysis by the signal peptide peptidase (SPP) (47) while the nascent proinsulin is released in the ER. Proinsulin is further cleaved by endopeptidases that remove the C peptide, and folded by chaperones that favor the formation of two disulfide bonds between the B and the A chain, leading to mature insulin stored into granules until its exocytosis. The biosynthesis and secretion of insulin are two distinct and thoroughly regulated processes. Secretion is triggered by a higher glucose concentration (48, 49), meaning that insulin biosynthesis is continually active even at normal glucose concentrations and that most regulation occurs at the secretion stage. This feature has two consequences for APP. First, high numbers of free signal peptides are continually cleaved and released in the cytosol and ER. Second, this high bio-synthetic rate leads to a high number of misfolded insulin molecules, estimated to represent up to 20% of insulin production in normal, unstressed, beta cells (7).

The fate of post-cleavage signal peptides is poorly described. The most studied instance is that of non-classical HLA-E molecules, which present signal-peptide sequences derived from classical HLA-A, -B and -C molecules (50). Surface

peptide-loaded HLA-E complexes serve as a marker of proper MHC-I expression and prevent NK-cell activation and killing (51). Even though the presentation of HLA signal sequences by HLA-E is altered when TAP or tapasin are inhibited or knocked-out (52, 53), most reports suggest that the MHC-I presentation of signal peptides is a TAP- and proteasome-independent process (47, 54, 55). The presentation of signal-peptide-derived sequences is also increasingly recognized for classical MHC-I molecules, as described for tumor epitopes (56) and beta-cell peptides (23). We identified several HLA-A2-restricted sequences presented by beta cells and originating from the signal peptide of insulin granule proteins such as insulin, urocortin-3 (UCN3), islet amyloid polypeptide (IAPP) and proconvertase 2 (PCKS2), although the latter was not recognized by CD8+ T cells (23). Interestingly, preproinsulin epitopes restricted for HLA-A2 (23) and other MHC-I variants (57) map to the short (24 aa) signal peptide region. Focused investigations have therefore been conducted to characterize the generation of preproinsulin signal peptides for MHC-I presentation (57, 58). Using K562 cells transfected with a single MHC-I allele and insulin gene, different signal peptide products were found bound to each variant tested, and the fate of insulin signal peptide sequences was dependent on their ER intramembrane location. Indeed, after SPP cleavage within the ER membrane, N-terminal peptides are more likely to be released in the cytosol (**Figure 1C**). These cytosolic free peptides can follow the conventional APP route and be translocated to the ER through TAP transport and subsequently loaded on nascent MHC-I molecules after ERAP1 trimming. On the opposite, upon SPP cleavage, C-terminal peptides are directly released in the ER lumen and loaded on MHC-I molecules, in a TAP- and proteasome-independent manner (57, 58). It is unknown how a peptide can be loaded into MHC-I molecules without TAP and whether ERAP1 trimming is always required, as is the case for a $PPI_{15\text{-}24}$ peptide (59). TAPBPR is the chaperone that likely replaces TAP, as tapasin and TAPBPR are mutually exclusive in their binding to MHC-I (55). One of the enzymes suspected to assist peptide trimming in the trans-Golgi network (TGN) is furin. Furin is a proconvertase that is known to traffic from the TGN to the cell surface *via* the vesicular pathway, where it can cleave peptides and proteins (60). Besides being involved in the maturation of secreted proteins such as those of the granule, furin has been shown to process antigens and direct them to the secretory route for MHC-I presentation in a TAP-independent manner (61). Similarly to another proconvertase from the same protein family (PC7) that has been shown to rescue unstable HLA-B51 complexes (62), furin could be crucial in post-ER stabilization of peptide-MHC-I binding. Indeed, resident TGN enzymes like furin could ensure an allele-dependent stability of these complexes against the destabilizing effect of the slightly acidic pH of the TGN. The mono-allelic HLA-I-expressing cells used in these studies may however introduce some bias and might not be representative of (multi-allelic) human beta cells. Consistent with their functional pH range, furin could also be involved in peptide exchanges occurring in the endosomes.

Collectively, the considerable translation rate of insulin and other granule proteins may provide a major source of aAPP pathways already within resting beta cells, through the release of high amounts of signal peptides and further protein processing.

CONCLUDING REMARKS AND FUTURE DIRECTIONS

Beta cells are very active cells with a specialized secretory activity. On one hand, this activity requires unique recycling pathways to maintain homeostasis. On the other, it is a burden that makes beta cells more vulnerable to additional ER stress. These properties may enhance the contribution of MHC-I aAPP pathways in beta cells. Although direct evidence is missing, data from other cellular models make this possibility plausible and invite further investigations. Gaps in knowledge that need to be filled include: 1) the relative contribution of each APP pathway to the beta-cell immunopeptidome under basal and stressed conditions; 2) how these pathways are modulated in the pro-inflammatory environment of insulitis; and 3) whether the same antigenic peptides are generated by professional APCs, a required step to prime naïve T cells in draining lymph nodes before their homing to the pancreas.

AUTHOR CONTRIBUTIONS

AC and RM wrote the manuscript. All authors contributed to the article and approved the submitted version.

FUNDING

Work in our Laboratory is supported by The Leona M. and Harry B. Helmsley Charitable Trust (1901–03689), JDRF (2-SRA-2016-164-Q-R), the *Agence Nationale de la Recherche* (ANR-19-CE15-0014-01), the *Fondation pour la Recherche Medicale* (EQU20193007831), and the Innovative Medicines Initiative 2 Joint Undertaking under grant agreements 115797 and 945268 (INNODIA and INNODIA HARVEST), which receive support from the EU Horizon 2020 program, the European Federation of Pharmaceutical Industries and Associations, JDRF, and The Leona M. & Harry B. Helmsley Charitable Trust.

ACKNOWLEDGMENTS

We thank Dr Loredana Saveanu (Université de Paris, Centre de Recherche sur l'Inflammation, INSERM U1149, CNRS ERL8252) for her critical reviewing of the manuscript and expert advice.

REFERENCES

1. Pugliese A. Autoreactive T cells in type 1 diabetes. *J Clin Invest* (2017) 127:2881–91. doi: 10.1172/JCI94549
2. Mallone R, Eizirik DL. Presumption of innocence for beta cells: why are they vulnerable autoimmune targets in type 1 diabetes? *Diabetologia* (2020) 63:1999–2006. doi: 10.1007/s00125-020-05176-7
3. Battaglia M, Ahmed S, Anderson MS, Atkinson MA, Becker D, Bingley PJ, et al. Introducing the Endotype Concept to Address the Challenge of Disease Heterogeneity in Type 1 Diabetes. *Diabetes Care* (2020) 43:5–12. doi: 10.2337/dc19-0880
4. Leete P, Oram RA, McDonald TJ, Shields BM, Ziller CTIGI study team, et al. Studies of insulin and proinsulin in pancreas and serum support the existence of aetiopathological endotypes of type 1 diabetes associated with age at diagnosis. *Diabetologia* (2020) 63:1258–67. doi: 10.1007/s00125-020-05115-6
5. Carré A, Richardson SJ, Larger E, Mallone R. Presumption of guilt for T cells in type 1 diabetes: lead culprits or partners in crime depending on age of onset? *Diabetologia* (2021) 64:15–25. doi: 10.1007/s00125-020-05298-y
6. Blum JS, Wearsch PA, Cresswell P. Pathways of Antigen Processing. *Annu Rev Immunol* (2013) 31:443–73. doi: 10.1146/annurev-immunol-032712-095910
7. Sun J, Cui J, He Q, Chen Z, Arvan P, Liu M. Proinsulin misfolding and endoplasmic reticulum stress during the development and progression of diabetes. *Mol Aspects Med* (2015) 42:105–18. doi: 10.1016/j.mam.2015.01.001
8. Engin F, Yermalovich A, Nguyen T, Ngyuen T, Hummasti S, Fu W, et al. Restoration of the unfolded protein response in pancreatic β cells protects mice against type 1 diabetes. *Sci Transl Med* (2013) 5:211ra156. doi: 10.1126/scitranslmed.3006534
9. Eizirik DL, Pasquali L, Cnop M. Pancreatic β-cells in type 1 and type 2 diabetes mellitus: different pathways to failure. *Nat Rev Endocrinol* (2020) 16:349–62. doi: 10.1038/s41574-020-0355-7
10. Eizirik DL, Miani M, Cardozo AK. Signalling danger: endoplasmic reticulum stress and the unfolded protein response in pancreatic islet inflammation. *Diabetologia* (2013) 56:234–41. doi: 10.1007/s00125-012-2762-3
11. Craig ME, Kim KW, Isaacs SR, Penno MA, Hamilton-Williams EE, Couper JJ, et al. Early-life factors contributing to type 1 diabetes. *Diabetologia* (2019) 62:1823–34. doi: 10.1007/s00125-019-4942-x
12. Dean PM. Ultrastructural morphometry of the pancreatic beta-cell. *Diabetologia* (1973) 9:115–9. doi: 10.1007/BF01230690
13. Muralidharan C, Conteh AM, Marasco MR, Crowder JJ, Kuipers J, de Boer P, et al. Pancreatic beta cell autophagy is impaired in type 1 diabetes. *Diabetologia* (2021) 64:865–77. doi: 10.1007/s00125-021-05387-6
14. Marasco MR, Conteh AM, Reissaus CA, Cupit JE, Appleman EM, Mirmira RG, et al. Interleukin-6 Reduces β-Cell Oxidative Stress by Linking Autophagy With the Antioxidant Response. *Diabetes* (2018) 67:1576–88. doi: 10.2337/db17-1280
15. Trivedi PC, Bartlett JJ, Pulinilkunnil T. Lysosomal Biology and Function: Modern View of Cellular Debris Bin. *Cells* (2020) 9:1131. doi: 10.3390/cells9051131
16. Soleimanpour SA, Gupta A, Bakay M, Ferrari AM, Groff DN, Fadista J, et al. The Diabetes Susceptibility Gene Clec16a Regulates Mitophagy. *Cell* (2014) 157:1577–90. doi: 10.1016/j.cell.2014.05.016
17. Hakonarson H, Grant SFA, Bradfield JP, Marchand L, Kim CE, Glessner JT, et al. A genome-wide association study identifies KIAA0350 as a type 1 diabetes gene. *Nature* (2007) 448:591–4. doi: 10.1038/nature06010
18. Grant BD, Donaldson JG. Pathways and mechanisms of endocytic recycling. *Nat Rev Mol Cell Biol* (2009) 10:597–608. doi: 10.1038/nrm2755
19. Montealegre S, van Endert PM. Endocytic Recycling of MHC Class I Molecules in Non-professional Antigen Presenting and Dendritic Cells. *Front Immunol* (2019) 9:3098:3098. doi: 10.3389/fimmu.2018.03098
20. Ilca FT, Neerincx A, Hermann C, Marcu A, Stevanović S, Deane JE, et al. TAPBPR mediates peptide dissociation from MHC class I using a leucine lever. *eLife* (2018) 7:e40126. doi: 10.7554/eLife.40126
21. Jahreiss L, Menzies FM, Rubinsztein DC. The Itinerary of Autophagosomes: From Peripheral Formation to Kiss-and-Run Fusion with Lysosomes. *Traffic* (2008) 9:574–87. doi: 10.1111/j.1600-0854.2008.00701.x
22. Yorimitsu T, Klionsky DJ. Eating the endoplasmic reticulum: quality control by autophagy. *Trends Cell Biol* (2007) 17:279–85. doi: 10.1016/j.tcb.2007.04.005
23. Gonzalez-Duque S, Azoury ME, Colli ML, Afonso G, Turatsinze J-V, Nigi L, et al. Conventional and Neo-Antigenic Peptides Presented by β Cells Are Targeted by Circulating Naïve CD8+ T Cells in Type 1 Diabetic and Healthy Donors. *Cell Metab* (2018) 28:946–60. doi: 10.1016/j.cmet.2018.07.007
24. Bassani-Sternberg M, Pletscher-Frankild S, Jensen LJ, Mann M. Mass spectrometry of human leukocyte antigen class I peptidomes reveals strong effects of protein abundance and turnover on antigen presentation. *Mol Cell Proteomics* (2015) 14:658–73. doi: 10.1074/mcp.M114.042812
25. Azoury ME, Tarayrah M, Afonso G, Pais A, Colli ML, Maillard C, et al. Peptides Derived From Insulin Granule Proteins are Targeted by CD8+ T Cells Across MHC Class I Restrictions in Humans and NOD Mice. *Diabetes* (2020) 69:2678–90. doi: 10.2337/db20-0013
26. James EA, Mallone R, Kent SC, DiLorenzo TP. T-Cell Epitopes and Neo-epitopes in Type 1 Diabetes: A Comprehensive Update and Reappraisal. *Diabetes* (2020) 69:1311–35. doi: 10.2337/dbi19-0022
27. Wan X, Zinselmeyer BH, Zakharov PN, Vomund AN, Taniguchi R, Santambrogio L, et al. Pancreatic islets communicate with lymphoid tissues via exocytosis of insulin peptides. *Nature* (2018) 560:107–11. doi: 10.1038/s41586-018-0341-6
28. Sims EK, Chaudhry Z, Watkins R, Syed F, Blum J, Ouyang F, et al. Elevations in the Fasting Serum Proinsulin–to–C-Peptide Ratio Precede the Onset of Type 1 Diabetes. *Diabetes Care* (2016) 39:1519–26. doi: 10.2337/dc15-2849
29. Rodriguez-Calvo T, Zapardiel-Gonzalo J, Amirian N, Castillo E, Lajevardi Y, Krogvold L, et al. Increase in Pancreatic Proinsulin and Preservation of β-Cell Mass in Autoantibody-Positive Donors Prior to Type 1 Diabetes Onset. *Diabetes* (2017) 66:1334–45. doi: 10.2337/db16-1343
30. Wasserfall C, Nick HS, Campbell-Thompson M, Beachy D, Haataja L, Kusmartseva I, et al. Persistence of Pancreatic Insulin mRNA Expression and Proinsulin Protein in Type 1 Diabetes Pancreata. *Cell Metab* (2017) 26:568–75. doi: 10.1016/j.cmet.2017.08.013
31. Sims EK, Bahnson HT, Nyalwidhe J, Haataja L, Davis AK, Speake C, et al. Proinsulin Secretion Is a Persistent Feature of Type 1 Diabetes. *Diabetes Care* (2019) 42:258–64. doi: 10.2337/dc17-2625
32. Sims EK, Syed F, Nyalwidhe J, Bahnson HT, Haataja L, Speake C, et al. Abnormalities in proinsulin processing in islets from individuals with longstanding T1D. *Transl Res* (2019) 213:90–9. doi: 10.1016/j.trsl.2019.08.001
33. Benkahla MA, Sabouri S, Kiosses WB, Rajendran S, Quesada-Masachs E, von Herrath M. HLA class I hyper-expression unmasks beta cells but not alpha cells to the immune system in pre-diabetes. *J Autoimmun* (2020) 119:102628. doi: 10.1016/j.jaut.2021.102628
34. Vieira E, Salehi A, Gylfe E. Glucose inhibits glucagon secretion by a direct effect on mouse pancreatic alpha cells. *Diabetologia* (2007) 50:370–9. doi: 10.1007/s00125-006-0511-1
35. Marroqui L, Masini M, Merino B, Grieco FA, Millard I, Dubois C, et al. Pancreatic α Cells are Resistant to Metabolic Stress-induced Apoptosis in Type 2 Diabetes. *EBioMedicine* (2015) 2:378–85. doi: 10.1016/j.ebiom.2015.03.012
36. Wyatt RC, Lanzoni G, Russell MA, Gerling I, Richardson SJ. What the HLA-I! —Classical and Non-classical HLA Class I and Their Potential Roles in Type 1 Diabetes. *Curr Diabetes Rep* (2019) 19:159. doi: 10.1007/s11892-019-1245-z
37. Himuro M, Miyatsuka T, Suzuki L, Miura M, Katahira T, Goto H, et al. Cellular Autophagy in α Cells Plays a Role in the Maintenance of Islet Architecture. *J Endocr Soc* (2019) 3:1979–92. doi: 10.1210/js.2019-00075
38. Sheng Q, Xiao X, Prasadan K, Chen C, Ming Y, Fusco J, et al. Autophagy protects pancreatic beta cell mass and function in the setting of a high-fat and high-glucose diet. *Sci Rep* (2017) 7:16348. doi: 10.1038/s41598-017-16485-0
39. Dalet A, Stroobant V, Vigneron N, Van den Eynde BJ. Differences in the production of spliced antigenic peptides by the standard proteasome and the immunoproteasome. *Eur J Immunol* (2011) 41:39–46. doi: 10.1002/eji.201040750
40. Lundh M, Bugliani M, Dahlby T, Chou DH-C, Wagner B, Ghiasi SM, et al. The immunoproteasome is induced by cytokines and regulates apoptosis in human islets. *J Endocrinol* (2017) 233:369–79. doi: 10.1530/JOE-17-0110
41. Seifert U, Bialy LP, Ebstein F, Bech-Otschir D, Voigt A, Schröter F, et al. Immunoproteasomes Preserve Protein Homeostasis upon Interferon-Induced Oxidative Stress. *Cell* (2010) 142:613–24. doi: 10.1016/j.cell.2010.07.036
42. Zaiss DMW, Bekker CPJ, Gröne A, Lie BA, Sijts AJAM. Proteasome immunosubunits protect against the development of CD8 T-cell-mediated

autoimmune diseases. *J Immunol* (2011) 187:2302–9. doi: 10.4049/jimmunol.1101003
43. Mishto M, Liepe J, Textoris-Taube K, Keller C, Henklein P, Weberruß M, et al. Proteasome isoforms exhibit only quantitative differences in cleavage and epitope generation. *Eur J Immunol* (2014) 44:3508–21. doi: 10.1002/eji.201444902
44. Winter MB, La Greca F, Arastu-Kapur S, Caiazza F, Cimermancic P, Buchholz TJ, et al. Immunoproteasome functions explained by divergence in cleavage specificity and regulation. *eLife* (2017) 6:e27364. doi: 10.7554/eLife.27364
45. Marroqui L, Dos Santos RS, Op de Beeck A, Coomans de Brachène A, Marselli L, Marchetti P, et al. Interferon-α mediates human beta cell HLA class I overexpression, endoplasmic reticulum stress and apoptosis, three hallmarks of early human type 1 diabetes. *Diabetologia* (2017) 60:656–67. doi: 10.1007/s00125-016-4201-3
46. Culina S, Lalanne AI, Afonso G, Cerosaletti K, Pinto S, Sebastiani G, et al. Islet-reactive CD8+ T cell frequencies in the pancreas, but not in blood, distinguish type 1 diabetic patients from healthy donors. *Sci Immunol* (2018) 3:eaao4013. doi: 10.1126/sciimmunol.aao4013
47. Martoglio B, Dobberstein B. Signal sequences: more than just greasy peptides. *Trends Cell Biol* (1998) 8:410–5. doi: 10.1016/S0962-8924(98)01360-9
48. Alarcón C, Lincoln B, Rhodes CJ. The biosynthesis of the subtilisin-related proprotein convertase PC3, but no that of the PC2 convertase, is regulated by glucose in parallel to proinsulin biosynthesis in rat pancreatic islets. *J Biol Chem* (1993) 268:4276–80. doi: 10.1016/S0021-9258(18)53606-1
49. Schuit FC, In't Veld PA, Pipeleers DG. Glucose stimulates proinsulin biosynthesis by a dose-dependent recruitment of pancreatic beta cells. *Proc Natl Acad Sci USA* (1988) 85:3865–9. doi: 10.1073/pnas.85.11.3865
50. Braud V, Jones EY, McMichael A. The human major histocompatibility complex class Ib molecule HLA-E binds signal sequence-derived peptides with primary anchor residues at positions 2 and 9. *Eur J Immunol* (1997) 27:1164–9. doi: 10.1002/eji.1830270517
51. Braud VM, Allan DSJ, O'Callaghan CA, Söderström K, D'Andrea A, Ogg GS, et al. HLA-E binds to natural killer cell receptors CD94/NKG2A, B and C. *Nature* (1998) 391:795–9. doi: 10.1038/35869
52. Lampen MH, Hassan C, Sluijter M, Geluk A, Dijkman K, Tjon JM, et al. Alternative peptide repertoire of HLA-E reveals a binding motif that is strikingly similar to HLA-A2. *Mol Immunol* (2013) 53:126–31. doi: 10.1016/j.molimm.2012.07.009
53. Celik AA, Kraemer T, Huyton T, Blasczyk R, Bade-Döding C. The diversity of the HLA-E-restricted peptide repertoire explains the immunological impact of the Arg107Gly mismatch. *Immunogenetics* (2016) 68:29–41. doi: 10.1007/s00251-015-0880-z
54. Wei ML, Cresswell P. HLA-A2 molecules in an antigen-processing mutant cell contain signal sequence-derived peptides. *Nature* (1992) 356:443–6. doi: 10.1038/356443a0
55. Oliveira CC, van Hall T. Alternative Antigen Processing for MHC Class I: Multiple Roads Lead to Rome. *Front Immunol* (2015) 6:298:298. doi: 10.3389/fimmu.2015.00298
56. Hage FE, Stroobant V, Vergnon I, Baurain J-F, Echchakir H, Lazar V, et al. Preprocalcitonin signal peptide generates a cytotoxic T lymphocyte-defined tumor epitope processed by a proteasome-independent pathway. *Proc Natl Acad Sci USA* (2008) 105:10119–24. doi: 10.1073/pnas.0802753105
57. Kronenberg-Versteeg D, Eichmann M, Russell MA, de Ru A, Hehn B, Yusuf N, et al. Molecular Pathways for Immune Recognition of Preproinsulin Signal Peptide in Type 1 Diabetes. *Diabetes* (2018) 67:687–96. doi: 10.2337/db17-0021
58. Skowera A, Ellis RJ, Varela-Calviño R, Arif S, Huang GC, Van-Krinks C, et al. CTLs are targeted to kill beta cells in patients with type 1 diabetes through recognition of a glucose-regulated preproinsulin epitope. *J Clin Invest* (2008) 118:3390–402. doi: 10.1172/JCI35449
59. Thomaidou S, Kracht MJL, van der Slik A, Laban S, de Koning EJ, Carlotti F, et al. β-Cell Stress Shapes CTL Immune Recognition of Preproinsulin Signal Peptide by Posttranscriptional Regulation of Endoplasmic Reticulum Aminopeptidase 1. *Diabetes* (2020) 69:670–80. doi: 10.2337/db19-0984
60. Thomas G. Furin At The Cutting Edge: From Protein Traffic To Embryogenesis And Disease. *Nat Rev Mol Cell Biol* (2002) 3:753–66. doi: 10.1038/nrm934
61. Medina F, Ramos M, Iborra S, de León P, Rodríguez-Castro M, Del Val M. Furin-processed antigens targeted to the secretory route elicit functional TAP1-/-CD8+ T lymphocytes in vivo. *J Immunol* (2009) 183:4639–47. doi: 10.4049/jimmunol.0901356
62. Leonhardt RM, Fiegl D, Rufer E, Karger A, Bettin B, Knittler MR. Post-Endoplasmic Reticulum Rescue of Unstable MHC Class I Requires Proprotein Convertase PC7. *J Immunol* (2010) 184:2985–98. doi: 10.4049/jimmunol.0900308

Conflict of Interest: The authors declare that the research was conducted in the absence of any commercial or financial relationships that could be construed as a potential conflict of interest.

frontiers in Immunology

ORIGINAL RESEARCH
published: 29 April 2021
doi: 10.3389/fimmu.2021.658601

Distinguishing Signal From Noise in Immunopeptidome Studies of Limiting-Abundance Biological Samples: Peptides Presented by I-A^b in C57BL/6 Mouse Thymus

*Padma P. Nanaware[1], Mollie M. Jurewicz[1], Cristina C. Clement[2], Liying Lu[1], Laura Santambrogio[2] and Lawrence J. Stern[1,3]**

[1] Department of Pathology, University of Massachusetts Medical School, Worcester, MA, United States, [2] Department of Radiation Oncology, Weill Cornell Medicine, New York, NY, United States, [3] Department of Biochemistry and Molecular Pharmacology, University of Massachusetts Medical School, Worcester, MA, United States

OPEN ACCESS

Edited by:
Luis C. Anton,
Consejo Superior de Investigaciones Científicas (CSIC), Spain

Reviewed by:
Christian Freund,
Freie Universität Berlin, Germany
Joshua E. Elias,
Stanford University, United States
Nathan Croft,
Monash University, Australia

***Correspondence:**
Lawrence J. Stern
lawrence.stern@umassmed.edu

Specialty section:
This article was submitted to Antigen Presenting Cell Biology, a section of the journal Frontiers in Immunology

Received: 26 January 2021
Accepted: 09 April 2021
Published: 29 April 2021

Citation:
Nanaware PP, Jurewicz MM, Clement CC, Lu L, Santambrogio L and Stern LJ (2021) Distinguishing Signal From Noise in Immunopeptidome Studies of Limiting-Abundance Biological Samples: Peptides Presented by I-A^b in C57BL/6 Mouse Thymus. Front. Immunol. 12:658601. doi: 10.3389/fimmu.2021.658601

Antigen presentation by MHC-II proteins in the thymus is central to selection of CD4 T cells, but analysis of the full repertoire of presented peptides responsible for positive and negative selection is complicated by the low abundance of antigen presenting cells. A key challenge in analysis of limiting abundance immunopeptidomes by mass spectrometry is distinguishing true MHC-binding peptides from co-eluting non-specifically bound peptides present in the mixture eluted from immunoaffinity-purified MHC molecules. Herein we tested several approaches to minimize the impact of non-specific background peptides, including analyzing eluates from isotype-control antibody-conjugated beads, considering only peptides present in nested sets, and using predicted binding motif analysis to identify core epitopes. We evaluated these methods using well-understood human cell line samples, and then applied them to analysis of the I-A^b presented immunopeptidome of the thymus of C57BL/6 mice, comparing this to the more easily characterized splenic B cell and dendritic cell populations. We identified a total of 3473 unique peptides eluted from the various tissues, using a data dependent acquisition strategy with a false-discovery rate of <1%. The immunopeptidomes presented in thymus as compared to splenic B cells and DCs identified shared and tissue-specific epitopes. A broader length distribution was observed for peptides presented in the thymus as compared to splenic B cells or DCs. Detailed analysis of 61 differentially presented peptides indicated a wider distribution of I-A^b binding affinities in thymus as compared to splenic B cells. These results suggest different constraints on antigen processing and presentation pathways in central versus peripheral tissues.

Keywords: antigen presentation, MHC protein, peptide processing, mass spectrometry, thymic selection

INTRODUCTION

MHC-II antigen presentation pathways have been explored mostly in professional antigen-presenting cells (APC) such as B cells and dendritic cells, because of their important role in generating and regulating immune responses. That work has been aided by robust MHC-II expression in these cells. However, MHC-II is expressed by other cells types including epithelial cells in several tissues. Of these, thymic epithelial cells are of particular interest because of their role in T cell selection (1, 2). AIRE expression by medullary thymic medullary epithelial cells provides a regulated mechanism for stochastic expression of genes usually expressed in a tissue-specific fashion and is required for efficient T cell negative selection (3, 4). In addition to thymic epithelial cells, migratory DC and B cells also are known to bring tissue-specific proteins and processed peptides into the thymus for negative selection (5–7). Pioneering differential peptidome analysis by Marrack et al., showed that the major peptides presented by MHC-II in the thymus also were associated with MHC-II in the spleen (8). This was somewhat surprising given the idea that efficient T cell negative selection against all possible self-antigens depends on antigen presentation in the thymus of peptides derived from tissue-specific gene products, many of which would not be expected to be expressed in the spleen. However, due to experimental sensitivity constraints at that time, few peptides overall (<20) were identified, and many low-abundance peptides likely evaded detection. Subsequent work on peptides presented by MHC-II in human thymus reported substantially more peptides (~120) (9, 10), with experimental validation of thymic presentation of several AIRE-dependent transcripts (10). Self-peptides broadly expressed in most tissues also were well-represented in the thymic MHC-II peptidomes, as expected from earlier work on murine MHC-I and CD8 T cells showing that expression of such peptides was required for positive selection of developing thymocytes (11, 12). Challenges in analyzing thymic immunopeptidomes include presence of large numbers of non-MHC expressing cells in same tissue, and relatively low expression levels on cells that do express MHC-II. Much of the technology development for immunopeptidome analysis has grown out of analysis of cell lines and highly enriched samples, and strategies for dealing with analysis of limiting abundance biological samples are being developed (13–17).

Here, we evaluated ways to address these issues in a comparative analysis of the MHC-II peptidomes expressed in thymus and spleen of C57BL/6 mice. This strain of mice expresses only a single MHC-II molecule, I-A^b, simplifying assignment of eluted peptides to MHC molecules, and is a mainstay of antigen presentation and T cell selection studies. Previous studies of these mice reported analysis and quantitation of ~150 peptides eluted from splenic B cells and dendritic cells (DC) (18), and more recently over 2700 peptides from unfractionated splenocytes (15), but to our knowledge no study utilizing modern immunopeptidome techniques to characterize the C57BL/6 thymic peptidome has been reported. The thymus consists of over 95% thymocytes, which do not express MHC-II, together with the much smaller MHC-II expressing populations that include cortical and medullary thymic epithelial cells (cTECs and mTECs) (19), resident and migratory DC, B cells, macrophages, and a variety of endothelial cells, neural crest-derived pericytes and mesenchymal cells (20–24). Although one of the human thymus studies fractionated this population into DC and non-DC populations using CD11c-bead enrichment (9), because of the small size of mouse thymi and substantial losses that we encountered during fractionation in preliminary studies, we analyzed the various cell types in the thymus all together. We did fractionate the spleen into B cells and DC, as in a previous mouse spleen study (18). We included both natural abundance and FLT3L induced splenic DC populations; provision of FLT3L *in vivo* is common way to expand murine DC populations, analogous to human G-CSF induction therapy (25, 26). Finally, we included both resting splenic DC as well as splenic DC matured by systemic LPS administration, for comparison with antigens presented by DC in the thymus where DC in various activation states are believed to contribute to thymic selection (3, 27).

We explored several methods to mitigate the effects of the low abundance of MHC-II-expressing cells in the thymus, including characterization of peptides captured by non-specific immunoaffinity and control resins, enrichment of membrane and vesicular compartments prior to isolation, and consideration of MHC-II length preferences and antigen presentation pathways leading to nested sets of peptides sharing a core epitope. These methods proved crucial to obtaining reliable information on thymic peptidomes. We found that the thymic I-A^b-presented peptidome was characterized by a broader distribution of lengths and binding affinities than the splenic B cell peptidome or splenic DC peptidomes, suggestive of possible differences in antigen processing pathways.

MATERIALS AND METHODS

Isolation of Splenic B Cells From C57BL/6 Mice

Spleens were isolated from C57BL/6 mice and were dissociated into single-cell suspensions by treatment with collagenase type II enzyme (Sigma-C6885), in order to facilitate separation from extracellular matrix and other unwanted tissue-derived material that might mask the ionization of low abundant peptides, and to promote detergent solubilization. Splenic B cells were evaluated for I-A^b expression by gating on the $B220^+$ $CD43^-$ $CD11b^-$ population. The cells were blocked with 50 μg/ml anti-mouse CD16/CD32 (2.4G2, BioXCell, West Lebanon, NH) prior to staining. Cells were acquired on an LSR II flow cytometer (Becton Dickinson) and analyzed using FlowJo version 9.8.5 software (Tree Star, Ashland, OR). To isolate mature B cells from the splenocyte population, $CD43^-$ and $CD11b^-$ expressing cells were depleted using biotinylated anti-mouse CD43 and CD11b (BioLegend) in conjunction with the EasySep Mouse Streptavidin RapidSpheres Isolation Kit (Stem Cell Technologies, Cambridge, MA) according to the manufacturer's instructions. Purity post-isolation was determined by FACS to be >90% for each sample, with an average purity of 94 ± 2.6%.

Splenic B cells were isolated from 9 mice for each replicate sample.

Isolation of Dendritic Cells From C57BL/6 Mice

Splenic DC were isolated from C57BL/6 mice either untreated or after *in vivo* expansion of DC using Flt3L (**Table 1**). For Flt3L treatment, C57BL/6 mice were injected subcutaneously with 40 x 10^6 B16-FLt3L-producing melanoma cells and humanely sacrificed 12-14 days later. (Clement et al., 2016a). For LPS treatment, mice were injected intraperitoneally with 0.5mg/kg and humanely sacrificed 6 hours later. Spleens were isolated and dissociated into single-cell suspensions, and DC populations were enriched by negative selection using magnetic beads, or by 30% bovine albumin solution density-gradient centrifugation (Sigma-Aldrich). As determined by flow cytometry, after enrichment the preparation routinely contains 70 to 80% $CD11c^+$ DCs with intermediate MHC-II levels, and includes both the $CD8\alpha^+$ and $CD8\alpha^-$ populations (13). Splenic DCs were isolated from 1-6 mice for each replicate sample of Flt3L-treated mice, or from 20 untreated mice.

Isolation of Thymus Cells

Thymi were isolated from C57BL/6 mice were dissociated into single-cell suspensions using collagenase type II enzyme (Sigma-C6885). Total thymic cell populations from 3 mice were used for each of the four replicate samples. For three of these samples, splenic B cells were prepared from the same sets of mice, and processed in parallel with the thymic samples, although to increase cell numbers the B cell samples also included spleens from additional mice (see **Table 1**).

Culture and Isolation of Human B Cells

The human EBV (Epstein Barr virus) transformed B lymphoblastoid cell line LG-2 (28), which is homozygous DRA1*01:01, DRB1*01:01, was cultured in RPMI medium with 10% fetal calf serum. Cells were pelleted at 400 × g and washed in PBS for 2 times before analysis.

ELISA Assays for I-A^b and HLA-DR1

MHC levels samples of the initial cell lysates prior to immunoaffinity purification were measured by ELISA assay to estimate the total MHC present, and the flow-through portions from the various immunoaffinity steps were measured to evaluate stepwise recoveries (**Supplementary Table S1**). For determination of I-A^b, the monoclonal antibody 17/227 of 200ng/well, diluted in bicarbonate/carbonate buffer pH 9.0 was used to coat the wells of high binding 96 well plates (Immulon 4 HBX-ND541225). The plates were incubated at 4°C for O/N or at 37°C for 2hrs. The wells were blocked using 3% BSA in 1X PBS for 1hr at 37°C. The recombinantly purified I-A^b-peptide complex was used as standards protein to calculate the amounts of I-A^b in each preparation. The standards ranging from 2ug-1ng were used. The monoclonal anti-murine MHCII antibody (M5/114) was used as the primary antibody for the detection. HRP-conjugated goat anti-rat IgG (KPL:14-16-12) was used as the secondary antibody followed by the ABTS substrate solution (Roche-11 684 302 001) for the colorimetric detection. Incubations were done at 1hr at 37°C and the washes between every incubation was performed using 1X PBST buffer (1X PBS, 0.05% triton X-100) three times. The dilutions of protein and antibody was done in dilution buffer 0.3% BSA, 0.1% Triton-X100 in 1X PBS. The HLA-DR1 ELISA assay was performed essentially as described (29). The procedure is similar to that for I-A^b, except that mouse anti-HLA-DR monoclonal antibody LB3.1 (30), polyclonal anti-HLA-DR1, and HRP-conjugated goat anti-rabbit IgG (Life technologies) were used as capture, primary, and secondary antibodies, respectively.

TABLE 1 | I-A^b preparations Summary of the I-A^b peptides eluted from four biological replicates of thymus, three biological replicates of splenic B cells, four different preparations of splenic DCs, and four different amounts of human LG2 cells.

Preparation	Number of mice used for tissue preparation	Number of cells used for I-A^b isolation	Amount of I-A^b isolated (μg)	Total number of peptide sequences identified	Number of peptides: ≥3 peptides/core
Splenic B #1	9	200 million	22	909	404
Splenic B #2	9	100 million	10.5	507	316
Splenic B #3	9	100 million	8.5	510	300
Thymus #1	3	200 million	14	622	256
Thymus #2	3	100 million	3.5	391	125
Thymus #3	3	100 million	7	481	187
Thymus #4	3	100 million	4	418	160
DC #1 (Flt3L)	1	140 million	11	570	280
DC #2 (Flt3L+LPS)	1	70 million	11.2	532	295
DC #3 (untreated)	20	247 million	8	833	425
DC #4 (Flt3L)	6	244 million	17.5	1180	618
LG2 cells	–	10 million	9.4	1422	752
LG2 cells	–	1 million	1.1	643	296
LG2 cells	–	100 thousand	0.107	179	37
LG2 cells	–	50 thousand	0.062	85	3

Preparation of Affinity Resins

M5/114 antibody was coupled to CNBr-activated sepharose 4B beads. M5/114 antibody was purified using hybridoma and dialyzed using 0.1M $NaHCO_3$. The concentration of the antibody used for the coupling was ~1-10mg/ml. We used 5mg of antibody for coupling to 1 ml of the CNBr-activated sepharose 4B beads. The beads were washed rapidly with coupling buffer-0.1M $NaHCO_3$, 0.5M NaCl pH 8.5. The beads were then mixed with the antibody slowly on the rotor at RT for 1 h. The beads were then thoroughly washed with the coupling buffer and blocked the remaining active groups on beads by incubating the antibody conjugated beads with blocking buffer (0.1M glycine in coupling buffer, pH 8.5) for 2 h at RT. The beads are then washed with alternating cycles of coupling buffer and the acetate buffer (0.1M sodium acetate, 0.5M NaCl, pH 4.0). A isotype control antibody (IgG2b) resin was prepared similarly. LB3.1 and isotype control antibody was coupled to recombinant Staphyloccal Protein A agarose-based resin (IPA300S, Repligen, Cambridge MA) using dimethyl pimelimidate coupling essentially as described (28). The antibody-conjugated beads were stored in 1X PBS buffer containing 0.02% sodium azide until the further usage.

Isolation of MHC-Peptide Complexes

For isolation of I-A^b and HLA-DR1 peptide complexes we used a sequential immunoaffinity chromatography protocol previously developed for biochemical studies, optimized for sample yield and purity, and used in many immunopeptidome characterizations (28). The procedure employs pre-columns with unconjugated beads as well as beads conjugated with isotype control antibody. These are intended to remove peptides, proteins, and other contaminants that can bind to the agarose substrate, protein A capture ligand if present, or immobilized antibodies outside of their combining site, for example Fc receptors abundant on B cells and DC. In preliminary experiments we eluted peptides from these columns separately and found distinct sets of non-specifically-bound peptides, so we included both types of pre-columns, although in most experiments peptides eluted from these columns were pooled. Four independent samples of thymus, three independent samples of splenic B cells and dendritic cells from four different preparations were analyzed for I-A^b peptidomes. In other experiments samples containing various numbers of LG2 cells were analyzed for HLA-DR1 peptidomes. Cell pellets were resuspended in 50 mM Tris-HCl, 150 mM NaCl, pH 8.0, containing protease inhibitor cocktail (Sigma-P2714) and 5% β-octylglucoside, freeze-thawed for 5-6 times. The lysate was spun at 4000×g for 5 min at 4°C to remove the cellular debris. The supernatant was collected and further spun using ultracentrifuge at 100,000 × g for 1 h at 4°C. In some experiments, total cell membranes were solubilized instead of whole cell pellet. Cells were suspended in ice-cold hypotonic buffer (10 mM Tris-HCl, pH 8.0, containing protease inhibitors). Repeated (4–5) freeze-thaw cycles were used for cell disruptions and in between the cycles the cells were homogenized using dounce homogenizer with 10 strokes each cycle. Cellular debris was removed by centrifuging the lysate at 4000 × g for 5 min at 4°C. The supernatant was collected and further centrifuged at 100,000 × g for 1 h at 4°C to pellet the membrane fraction. The membrane pellet was solubilized in ice-cold 50 mM Tris-HCl, 150 mM NaCl, pH 8.0, containing protease inhibitors and 5% β-octylglucoside, and then mixed slowly overnight on shaker at 4°C. Supernatant containing the solubilized membrane was recovered by centrifuging the lysate at 100,000 × g for 1 h at 4°C. The supernatant was used for the isolation of the MHCII-peptide complexes using an immunoaffinity column of M5/114 monoclonal antibody immobilized onto CNBr activated Sepharose CL-4B using following steps. The lysates were then allowed to mix with the CNBr activated Sepharose beads only, followed by isotype control antibody conjugated beads slowly on shaker for 1 h at 4°C to prevent nonspecific binding of proteins to beads. This equilibrated lysate was incubated with M5/114 conjugated beads and allowed to mix slowly for 2 h on shaker at 4°C. The column was washed by passing several buffers in succession as follows: (1) 50 mM Tris-HCl, 150 mM NaCl, pH 8.0, containing protease inhibitors and 5% β-octylglucoside (5 times the bead volume); (2) 50 mM Tris-HCl, 150 mM NaCl, pH 8.0, containing protease inhibitors and 1% β-octylglucoside (10 times the bead volume); (3) 50 mM Tris-HCl, 150 mM NaCl, pH 8.0, containing protease inhibitors (30 times the bead volume); (4) 50 mM Tris-HCl, 300 mM NaCl, pH 8.0, containing protease inhibitors (10 times the bead volume); (5) 1X PBS (30 times the bead volume); and (6) HPLC water (100 times the bead volume). Recovery of MHC-peptide complexes at various steps in the procedure was assessed by ELISA assay as described above (**Supplemental Table S1**). MHC proteins were released from the resin and HLA-DR1/I-A^b peptides eluted using 2% TFA (The Nest Group, USA). Eluted peptide mixtures were then separated from MHC proteins, residual detergent, and cellular material by binding to a Vydac C4 macrospin column and eluting with 30% acetonitrile containing 0.1% (v/v) TFA. Solvent was removed by Speed-Vac and the dried peptide extracts were stored at -80° C or used immediately.

Analysis of Peptides Eluted From I-A^b or HLA-DR1

Peptide extracts were reconstituted in 25 µl 5% acetonitrile containing 0.1% (v/v) trifluoroacetic acid and separated on a nano-ACQUITY (Waters Corporation, Milford, MA) UPLC with technical triplicate injections. In brief, a 3.0 µl injection was loaded in 5% acetonitrile containing 0.1% formic acid at 4.0 µl/min for 4.0 min onto a 100 µm I.D. fused-silica precolumn packed with 2 cm of 5 µm (200Å) Magic C18AQ (Bruker-Michrom, Auburn, CA) and eluted using a gradient at 300 nL/min onto a 75 µm I.D. analytical column packed with 25 cm of 3 µm (100Å) Magic C18AQ particles to a gravity-pulled tip. The solvents were A) water (0.1% formic acid); and B) acetonitrile (0.1% formic acid). A linear gradient was developed from 5% solvent A to 35% solvent B in 90 min. Ions were introduced by positive electrospray ionization *via* liquid junction into a Q Exactive hybrid mass spectrometer (Thermo Fisher Scientific). Mass spectra were acquired over m/z 300–1750

at 70,000 resolution (m/z-200), and data-dependent acquisition (DDA) selected the top 10 most abundant precursor ions in each scan for tandem mass spectrometry by HCD fragmentation using an isolation width of 1.6 Da, collision energy of 27, and a resolution of 17,500.

Peptide Identification

Raw data files were peak processed with Proteome Discoverer (version 2.1, Thermo Fisher Scientific) prior to database searching with Mascot Server (version 2.5, Matrix Science, Boston, MA) against the combined database of UniProt_Mouse which was downloaded on 10/7/16 with 57,984 entries. Search parameters included "no enzyme" specificity to detect peptides generated by cleavage after any residue. The variable modifications of oxidized methionine and pyroglutamic acid for N-terminal glutamine were considered. The mass tolerances were 10 ppm for the precursor and 0.05Da for the fragments. Search results were then loaded into the Scaffold Viewer (Proteome Software, Inc., Portland, OR) for peptide/protein validation and label-free quantitation. Scaffold assigns probabilities using PeptideProphet or the LDFR algorithm for peptide identification and the ProteinProphet algorithm for protein identification, allowing the peptide and protein identification to be scored on the level of probability. An FDR of 1% was adjusted for reliable identification of peptides.

Label-Free Quantitation

Label-free relative quantitation of all peptides eluted from thymic cells and splenic B cells was performed using precursor intensity analysis in Scaffold, Scaffold Q&/Q&S. Scaffold uses the precursor intensity information from the Thermo Proteome Discoverer. The software normalizes total precursor intensity values across the samples and calculates fold change or log2 normalized intensity across the samples while considering different statistical parameters like t test, ANOVA and coefficient of variance. The log2 normalized intensity values were converted to intensities for subsequent analyses. Triplicate technical replicates were run for each sample and the single average value was used to represent the three technical replicates. For analysis of core epitope intensities, the intensity values for all peptides sharing the same core epitope were summed within each technical replicate. The core epitopes were predicted using the NetMHCIIpan algorithm. The technical replicates were averaged for core epitopes as described above for peptides.

Gibbs Clustering

GibbsCluster-2.0 (31) was used to align the eluted peptide sequences and analyze the motifs, which were displayed with Seq2Logo 2.0 (32). We allowed the software to include cluster sizes of 1-5 with a motif length of 9 amino acids and clustering sequence weighting. Default values were used for other parameters: number of seeds =1, penalty factor for inter-cluster similarity =0.8, small cluster weight = 5, no outlier removal, iterations per temperature step =10, Monte Carlo temperature =1.5, intervals for indel, single peptide and phase-shift moves = 10, 20, and 100, respectively, and Uniprot amino acid frequencies were used. For each sample, we selected the cluster that included the largest number of peptides analyzed. In most cases a single cluster included most of the sequences, but for the total thymus sample (**Figure 2D**) two clusters were required. A preference for hydrophobic residue at P1 was used to align the motifs at the P1 position. The fraction of sequences that contributed to each cluster is shown in the figures.

Expression and Purification of I-A^b-3R Complex for Binding Affinity Measurements

The soluble I-A^b-3R, a mouse MHC-II protein contains α and β subunit. The peptide 3R (FEAFMARAKAAV) was engineered at its C-terminus on the beta subunit and expressed from a baculovirus plasmid p3288 I-A^b-BirA. The I-A^b-3R protein complex is about 62kDa molecular weight. The I-A^b-3R was expressed in Hi5 cells in a shake flask to a density of 2 million cells/ml in a mixture of 70% EX-CELL 405 serum free medium for insect cells (Sigma, cat. #14405C) and 30% complete graces medium (Thermo Fisher Scientific, cat. #11605-094) in presence of antimycotic. The cells were further infected using I-A^b-3R virus and incubated for 5 days in a 27°C at 100 rpm. Post-incubation, the supernatant was collected and filtered through a 0.45μm filter. Protease inhibitors (0.02% NaN3, 0.7μg/ml pepstatin, 1μg/ml leupeptin and 0.25mM PMSF) were added to supernatant and purified using M5/114 antibody conjugated Sepharose CL-4B column. The eluted purified protein was further purified using Superdex 200 gel filtration column.

Peptide Synthesis and Labeling

The CLIP peptide Ac-VSKMRMATPLLMQ were synthesized (21st Century Biochemicals, Marlboro, MA) and labeled with Alexa Fluor 488 tetrafluorophenyl ester (Invitrogen, Eugene, OR) through primary amine of lysine. For this purpose, the peptide (2 mg) was dissolved in 400 μl of sodium bicarbonate (150 mM pH 9.8) and mixed with Alexa488-tetrafluorophenyl ester (1mg) (Molecular Probes). After one-hour incubation at room temperature, labeled peptide was purified by reverse HPLC (Agilent) using a C18 column (Jupiter 300A 00G-4053-E0) and a gradient of acetonitrile in 0.02% trifluoracetic acid.

I-A^b-CLIP Peptide Exchange Assay

A fluorescence polarization (FP) assay was used to measure the IC50 of using N-terminally-acetylated CLIP peptide labeled with Alexa Fluor 488 tetrafluorophenyl ester (Invitrogen, Carlsbad, CA) *via* the primary amine at K3 as probe peptide as previously described (34). The binding reactions were carried in buffer conditions of 100 mM sodium citrate, 50 mM sodium chloride, 0.1% octyl β-D-glucopyranoside, 5 mM ethylenediaminetetraacetic acid, 0.1% sodium azide, 0.2 mM iodoacetic acid, 1 mM dithiothreitol). The I-A^b-3R complex has a thrombin linker to cleave off the 3R peptide from I-A^b protein. Thrombin is added during all the reactions at a concentration of 1U/ug and inactivated after 3hrs of reaction using 0.1mM phenylmethanesulfonyl fluoride. The I-A^b-3R concentration used was selected by titrating I-A^b-3R

against fixed labeled peptide concentration (25 nM) and choosing the concentration of I-A^b-3R that showed ~50% maximum binding. For calculating IC50 values, 100 nM I-A^b-3R was incubated with 25 nM Alexa488-labeled CLIP probe peptide, in combination with a serial dilution of test peptides, beginning at 100 μM followed by 5-fold dilutions in presence of 0.5μM HLA-DM. The reaction mixture was incubated at 37°C. The capacity of each test peptide to compete for binding of probe peptide was measured by FP after 72 h at 37°C. The assay was read using a Victor X5 Multilabel plate reader (PerkinElmer, Shelton, CT). FP values were converted to fraction bound by calculating [(FP_sample - FP_free)/(FP_no_comp - FP_free)], where FP_sample represents the FP value in the presence of test peptide; FP_free represents the value for free Alexa488-conjugated CLIP peptide; and FP_no_comp represents values in the absence of competitor peptide. We plotted fraction bound versus concentration of test peptide and fit the curve to the equation y = 1/(1 +[pep]/IC50), where [pep] is the concentration of test peptide, y is the fraction of probe peptide bound at that concentration of test peptide, and IC_{50} is the 50% inhibitory concentration of the test peptide.

Source Protein Tissue Location/Gene Ontogeny Analysis

Source proteins for peptides eluted from thymus, splenic B cells and splenic DCs were analyzed for tissue sources. The proteins having 2 or more peptides were analyzed using Uniprot Consortium (35). The fraction of the total is plotted for each tissue type.

Statistics

Specific t-tests were used for different analyses, which are indicated in the figure legends of each plot. Prism (version 7.03, GraphPad, San Diego, CA) was used for statistical analysis and graphing data.

RESULTS

Isolation of I-A^b From Total Thymus, Splenic B Cells and Splenic Dendritic Cells

For immunopeptidome analysis, spleen and thymus were isolated from C57BL/6 mice and dissociated into single cell suspensions before detergent lysis, I-A^b isolation, peptide elution, and mass spectrometry. Spleen samples were fractionated into splenic B and splenic DC preparations, but whole thymus preparations were used as noted above. Triplicate preparations of splenic B, quadruplet preparations of thymus, and a total of four different preparations of splenic DC were analyzed. Splenic DC preparations included samples from normal mice, mice harboring a Flt3L secreting tumor to promote production of DC, and Flt3L treated mice injected with lipopolysaccharide to induce DC maturation. Thymii were pooled from 3 mice for each preparation, and spleens were pooled from 9 mice for each B cell preparation or from 1-20 mice for each DC preparation depending on treatment. Typical preparations contained ~10 micrograms of I-A^b (range 3.5-22) (**Table 1**).

Characterization of Eluted Peptides by Mass Spectrometry

We used a standardized protocol to isolate the I-A^b-presented peptides from the different tissues and cell types (see Materials and Methods and **Figure 1A**). Whole-cell detergent lysates of single-cell suspensions were prepared, non-solubilized material was removed by ultracentrifugation, and the clarified supernatants were used for isolation of I-A^b followed by peptide elution. We used a three-step sequential immunoaffinity procedure (28), in which the samples were incubated first with control Sepharose-CL-4B beads, then with CNBR-activated Sepharose-4B beads coupled with an isotype control antibody, and finally with CNBR-activated Sepharose-4B beads coupled with the I-A^b-specific antibody M5/114 (**Figure 1A**). After a series of stringent washes, I-A^b-peptide complexes were eluted using trifluoroacetic acid solution to denature the MHC-II protein. Released peptides were separated from I-A^b and desalted using a reverse-phase C4 column. Eluted peptides were analyzed using a standard LC/MS/MS data-dependent acquisition and analysis pipeline (see Materials and Methods and **Figure 1B**). Three biological replicates of each sample were analyzed. For each biological replicate the eluted peptide sample was split into thirds, which were injected separately as technical replicates. The peptide ion fragmentation spectra were associated with peptide sequences using Mascot Server and the UniProt_Mouse sequence database and were filtered to a 1% false-discovery rate based on the Protein Prophet algorithm. Peptide sequences identified in bead-only and the isotype control eluates were removed from the I-A^b-specific eluates. These control-elution peptides included both high and low abundance species, and were not always observed reproducibly in biological replicates, and so peptide sequences appearing in any of the control elutions for any of the samples were removed from each of the specific elution datasets. The filtered sets of peptide sequences were further analyzed to identify predicted MHC-II core epitopes, binding motifs, and length distributions.

Peptides Eluted From Immunoaffinity-Purified I-A^b Preparations From Thymus, Splenic B Cells, and Splenic Dendritic Cells of C57BL/6 Mouse

Overall, we identified 1316 peptide sequences in the thymus eluates, 1383 peptides in the splenic B cell eluates, and 2439 peptides in the splenic DC eluates (**Figures 2A–C** and **Supplementary Table S2**). The thymus and splenic B cell peptides represented four and three biological replicate samples respectively. The splenic DC peptides represented four samples including conventional and Flt3-ligand induced populations from resting mice and those treated with LPS to induce DC maturation, likely accounting for the greater variety of DC sequences identified. The median peptide lengths for the three samples were similar, 15 amino acid residues (aa) for the thymic peptides, splenic B and splenic DC peptides. However,

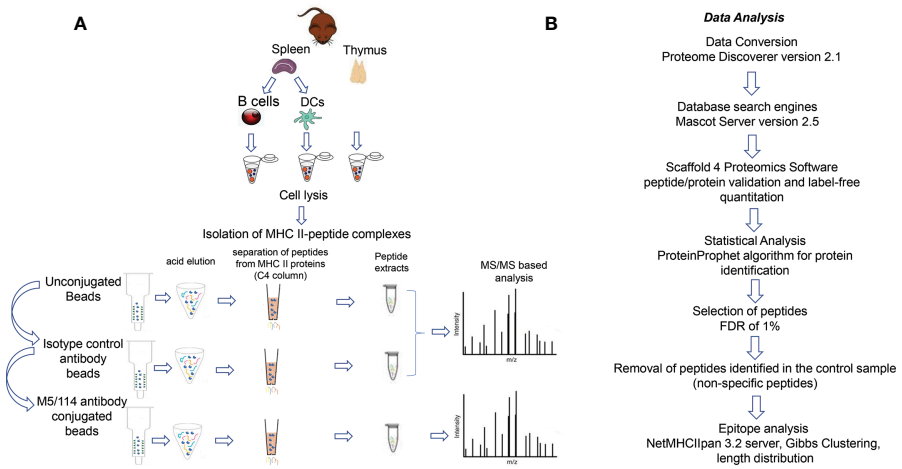

FIGURE 1 | Workflow **(A)** Schematic representation of I-A^b peptide elution workflow from thymus, splenic B cells and splenic DCs. **(B)** Strategy for peptide identification and I-A^b-peptidome characterization.

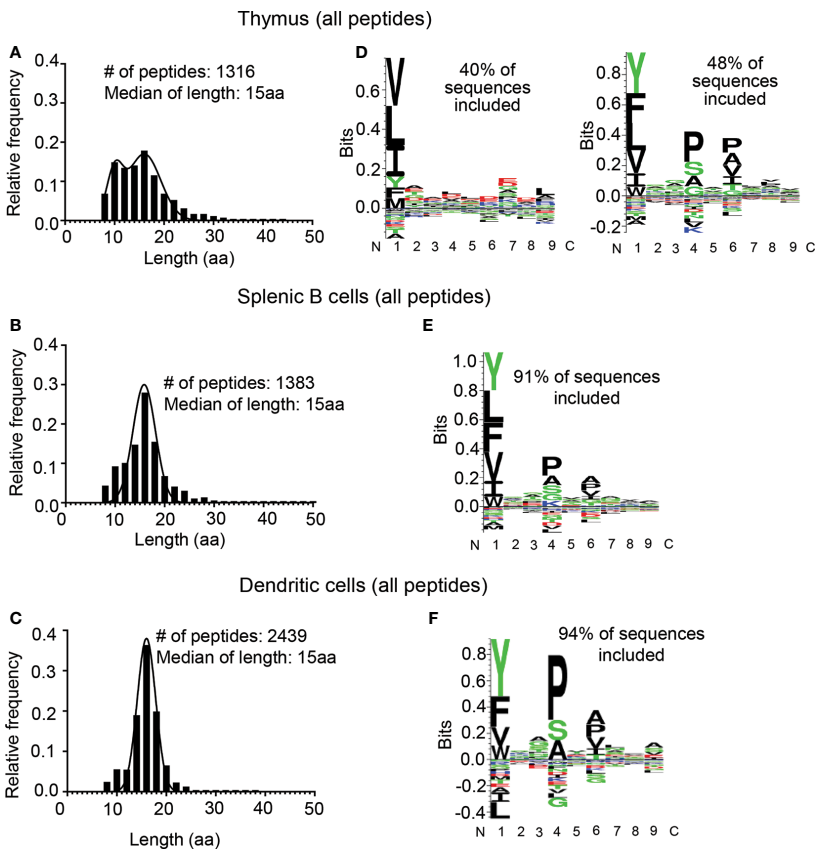

FIGURE 2 | Length distribution and motif analysis for all eluted peptides from thymus, splenic B cells, and splenic DCs. **(A–C)** Length distribution; **(D–F)** motif analysis. **(A, D)** Eluted peptides from thymus; **(B, E)** from splenic B cells; and **(C, F)** from splenic dendritic cells (DCs). Motifs determined using the GibbsCluster 2.0 algorithm (33) and displayed using Seq2Logo (32); note different vertical scales. The fraction of total sequences represented by the GibbsCluster motif is shown. For the thymus sample two clusters were required to include the majority of the peptides.

the distribution of peptides lengths was different, with the thymic peptide distribution showing two peaks, one centered at ~16 aa and another at ~10aa (**Figure 2A**), whereas the B cell and DC samples showed monomodal distributions centered around the median length of ~15aa (**Figures 2B, C**), as observed previously for naturally processed MHC-II-bound peptides from several sources (10, 15, 17). The consensus sequence motifs as identified by an unsupervised Gibbs sampling alignment/clustering algorithm (33) also differed for the thymic peptides as compared to the other sets. The splenic B and DC samples showed the expected pattern of preferences at the P1, P4, and P6 positions with a large hydrophobic residue at P1 and small residues at P4 and P6 (**Figures 2E, F**), as previously observed for other high-density I-A^b peptidomes from spleen, lymph nodes, and pancreas (15, 17). By contrast the thymic sample showed two clusters, one with an unexpected preference for leucine at the P1 and to a lesser extend at the P9 positions, and another that corresponded to the known I-A^b motif as observed in the other samples (**Figure 2D**). Although the unusual length distribution observed for the thymic peptides was suggestive of possible differences in thymus and spleen antigen processing, the cluster of sequences representing ~40% of the sample that lacked a clear I-A^b binding motif suggested that some of the peptides identified in this sample might not represent actual I-A^b binders.

Non-Specific Peptides

To help identify characteristics of non-I-A^b-binding peptides that might be present in the immunoaffinity-purified preparations, we analyzed the length distribution and sequences characteristics for the non-specific peptides eluted from the beads-only and isotype-antibody columns of the thymus sample preparation. The length distribution for these non-specific peptides were centered around a median of ~10 aa (**Supplementary Figure S1A** and **Supplementary Table S6**). A similar length distribution and motif analysis profile was observed for the peptides eluted from the beads only column from a variety of different mouse cell types investigated in our laboratory (**Supplementary Figure S1B**). We suspected that the peptides eluted from thymus I-A^b preparations might include peptides similar to the non-specific peptides eluted from the control columns, and that this might help to explain the bimodal length distribution observed for the thymus samples. Indeed, computational fractionation of the total thymus eluted peptides into pools for each length showed that the shorter peptides (8-12 aa) had non-I-A^b-like preferences (**Supplementary Figure S2**) as also observed for one of the clusters in the full thymus sample (**Figure 2D**). Longer peptides (14-18aa) had the expected the expected I-A^b motif (**Supplementary Figure S2**). However, we did not want to apply an arbitrary length cutoff to the eluted peptide datasets, because we observed that the I-A^b-specific peptide distributions from spleen included peptides shorter than 12 aa (**Figures 2B, C**), as previously reported for other published I-A^b immunopeptidomes, because the non-specific peptide length distributions had tails extending well beyond 12 aa (**Supplementary Figure S1A, B**), and because MHC-II antigen processing pathways in the thymus are poorly characterized and we wanted to investigate the possibility of an altered length distribution in that tissue.

In order to try to eliminate the contribution of apparently non-specific peptides in the thymus samples, we evaluated two strategies used in previous immunopeptidome characterizations. First, we tested whether isolating I-A^b from total cellular membrane preparations instead of whole cell lysates would provide enriched samples with lower levels of background peptides. However, the length distribution of all the peptides eluted from the membrane fraction of the thymus showed the same two peaks, one at ~10 aa and another at ~16aa, as for the thymus whole cell preparation (**Supplementary Figure S3A**). Also, the distribution of peptides eluted from the beads-only column of the membrane preparation looked similar to the beads-only eluted peptides of the whole cell preparation (**Supplementary Figure S3B**). These results indicated that a membrane fractionation strategy as used previously (13, 36, 37) was not helpful in removing the non-specific peptides. Second, we tested whether restricting the analysis to peptides identified reproducibly in every sample would help to remove non-specific peptides, with the idea that the non-specific peptides might be present sporadically as a result of low-frequency random binding or sampling events. However, considering only peptides present in all four biological replicate samples, and at least two technical replicates in each sample, did not provide cleaner thymic peptidome datasets (**Supplementary Figure S4**). Although both strategies removed many peptides from the datasets, the considerably trimmed datasets still retained many apparently non-specific peptides, and we sought other ways to identify bona-fide MHC-II binders in eluates from low-abundance samples.

Limiting Sample Amounts Results in Increasing Proportion of Non-Specific Peptides and Masks the Presence of MHC Binders in the Sample

To systematically evaluate the effect of low-abundance sample amounts on the proportion of non-specific peptides detected in immunopeptidome workflows, we switched to the well-characterized human B-lymphoblastoid cell line LG2. These cells provide several advantages for validating methods to distinguish true MHC binders from non-specific peptides. LG2 cells have been used previously in many MHC-I and MHC-II immunopeptidome studies (29, 37–39), and large libraries of validated peptides are available. For example, in a recent study of the effect of HLA-DO on the MHC-II immunopeptidome we characterized >6000 DR1-bound peptides from this cell line (37). As in previous studies, in that work we used a large sample size of 100 million cells per preparation. LG2 cells are homozygous across the entire MHC, removing ambiguities often associated with HLA assignment common to studies of natural abundance MHC proteins in human cells. Finally, the peptide binding motif for HLA-DR1, the protein investigated here, is highly accurate in predicting experimental binding affinities (40), and can be used as an additional criterion to distinguish true binders from false positives. Here, we wanted to examine the effect of reduced

sample sizes on non-specific peptide identification, and so we characterized the DR1 immunopeptidomes from LG2 samples of 10 million, 1 million, 100 thousand and 50 thousand cells (**Figure 3**). The length distributions of peptides eluted from 10 million, 1 million cells were centered around ~16 aa, with no peak around ~10 aa (**Figures 3A, B**). For the 100 thousand cells sample the median length was just slightly reduced to 15 aa, with a minor peak in the length distribution at 10 aa, indicating a small but appreciable level of non-specific peptides were present in these samples (**Figure 3C**). By contrast, the length distribution for the peptides eluted from 50 thousand cells showed very few peptides ~16 aa and a large number of shorter peptides, with an overall median length of ~ 11 aa, indicating that this sample was dominated by non-specific peptides (**Figure 3D**). Peptide binding preferences for DR1 are very well characterized (41) and we could confidently assign predicted peptide binding affinities to all of the eluted peptides using the NetMHCIIpan3.2 algorithm (with prediction performance of 0.83 as assessed by area under the receiver-operator curve analysis (42)). For the 10 million cell sample, >90% of the eluted peptides are predicted to bind with submicromolar affinity (**Figure 3E**, black symbols). As the number of cells analyzed is lowered, the fraction of peptides with predicted affinity <1000 nM decreases (**Figures 3F–H**). The peptides with low predicted affinity (**Figures 3E–H**, gray symbols) were dominated by short peptides with length ~9-11, similar to the non-specific peptides in the mouse samples, whereas the peptides predicted to bind more tightly with submicromolar predicted affinity had a length distribution centered around 16 aa (**Figures 3E–H**, black symbols), as expected for true DR1 binders (37). Thus, the amount of MHCII present in a sample can determine the fraction of non-specific peptides versus true MHC II binders in the pool of eluted peptides. As such, we used these datasets to investigate ways to parse out the specific binders present in low-abundance samples.

Identifying True MHC-II Binders in Low Abundance Samples by Clustering Overlapping Peptides Into Core Epitopes

Naturally-processed MHCII-bound peptides typically are found as nested sets with varying lengths centered around a core epitope, as a consequence of the MHC-II epitope generation pathway in which MHC-bound precursors are trimmed by endosomal endoproteases, leaving peptides with frayed ends that overhang the ~13aa-long MHC-II peptide binding site (43). We investigated whether this characteristic would be useful to help distinguish MHCII-bound from non-specific peptides present in the LG2 eluates, since non-specific peptides would not be expected to be present as nested sets surrounding a core epitope. We grouped eluted peptides with different lengths but having the same binding core (as predicted by NetMHCIIpan) into core epitopes. The fraction of peptides with only one peptide per core epitope increased from <16% for the 10 million cell sample (223 of 1422 total) to >75% for the 50,000 cell sample (64 of 85 total) (**Figures 4A, B**). The length distribution of peptides having only one peptide per core epitope included many shorter peptides, particularly in the 100,000 and 50,000 cell samples (**Figure 4B**). By contrast, the length distribution of the peptides having 2 or more peptides per core epitope was centered around ~16 aa for 10 million, 1 million and 100,000 cells, although the 50,000 cells sample still had many short peptides (**Figure 4C**). For peptides having 3 or more peptides per core epitope, essentially all the peptides had the expected length distribution, although for the 50,000 cells sample these peptides comprised only 1 nested set with three peptides (**Figure 4D**).

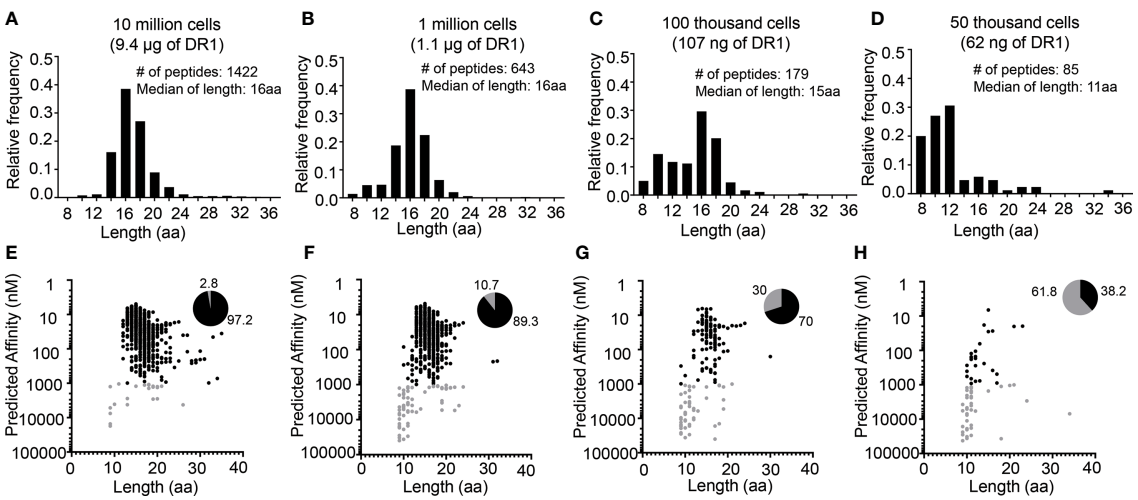

FIGURE 3 | Distribution of length and predicted binding affinities for peptides eluted from different numbers of human LG2 cells. Length distribution of **(A)** 10 million, **(B)** 1 million, **(C)** 100 thousand and **(D)** 50 thousand cells. Predicted affinity versus the length distribution for the peptides eluted from **(E)** 10 million, **(F)** 1 million, **(G)** 100 thousand and **(H)** 50 thousand cells. Black dots represent peptides with high predicted I-A^b binding affinity (IC_{50} <1µM), gray dots represent peptides low predicted I-A^b binding affinity (IC_{50} ≥1µM). Pie charts indicate the fraction of eluted peptides in each sample with predicted high and low binding affinities.

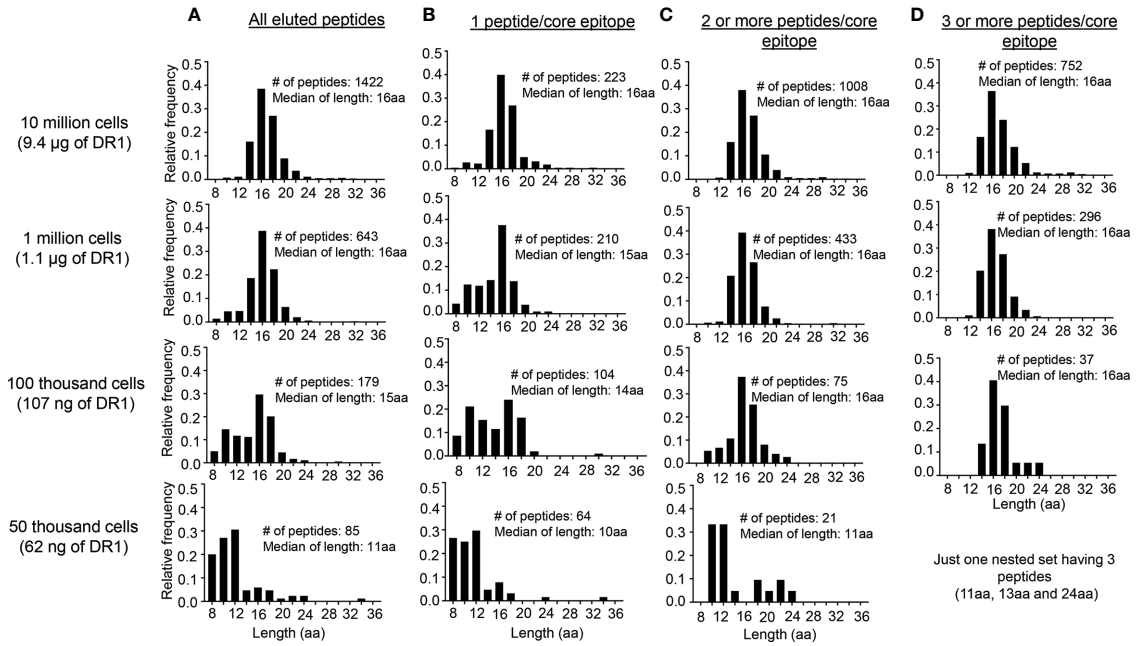

FIGURE 4 | Length distribution of peptides eluted from LG2 cells with different numbers of sequences per core epitope. **(A)** All of the peptides eluted from 10 million, 1 million, 100 thousand and 50 thousand cells. NetMHCIIpan 3.2 was used for predicting the 9-residue binding frame from all peptides eluted from different numbers of LG2 cells. All peptides having identical predicted binding frames were considered as a single core epitope. **(B)** Length distribution for peptides having 1 peptide/core epitope from different numbers of LG2 cells. **(C)** Length distribution for peptides having 2 or more peptides/core epitope and **(D)** Length distribution for peptides having 3 or more peptides/core epitope. The number of peptides and median of length distribution for each set has been indicated.

Thymic I-A^b Epitopes Have Broader Length Distribution as Compared to Splenic B Cells and DC

Having validated the strategy of clustering peptides into core epitopes using the human LG2 cell line, we switch back to analysis of the peptidomes eluted from thymus, splenic B cells and splenic DCs (**Figure 5** and **Supplementary Table S3**). Similarly to the LG2 studies described above, the fraction of peptides present with only one peptide per core epitope decreased with increasing amounts of I-A^b in the sample, whereas the reverse trend was observed for peptides present at two or more per core (**Supplementary Figure S5**). Considering only the peptides present as 3 or more peptides per core epitope, the number of shorter peptides was considerably reduced in each sample as compared to the total peptidomes (**Figures 5A–C**, cf. **Figures 2A–C**), and all of the samples had length distributions centered around 16 aa (**Figure 5G**). Again, considering only peptides present at 3 or more peptides per core epitope, sequence motifs for the splenic B cell and DC peptidomes showed the strong concentration of hydrophobic amino acid residues at the P1 and small residues at the P4 and P6 positions (**Figures 5E, F**). The thymic peptidome sequence motif had similar preferences at P1, but the P4 and P6 preferences were more muted (**Figure 5D**). We used the 3+ peptides per core epitope datasets to begin to investigate differences in antigen processing and presentation pathways between thymus and spleen. Despite the similar median lengths, the shape of the peptide length distribution was much broader for the thymic peptidome as compared to splenic B cell and DC peptidomes (**Figures 5G, H**). There appears to be a significantly longer component with median length 28 residues present specifically in the thymus, but even excluding that component the width of the main peak centered around 16 aa is broader for the thymus than for the splenic samples.

Differences Between I-A^b-Presented Peptidome of Thymus, Splenic B Cells, and Splenic DCs

To explore differences between the immunopeptidomes of thymus, splenic B cells and DCs, we performed an overlap analysis to identify core epitopes shared or uniquely presented in the various cell types. We use the same parsed datasets as in **Figure 5**, only considering peptides present as 3 or more peptides per core epitope, but for the overlap analysis we analyzed core epitopes rather than the individual peptides. The pairwise between-sample overlap was 25% for comparisons of splenic B and DC samples, but only 17% and 5% for comparison of the thymic samples with either splenic B or DC respectively (**Figure 6A**). The lowest overlap was found for the thymus and splenic DC samples, despite the larger number of peptides present in DC samples (**Table 1**). By contrast, the within-sample core epitope overlap between biological replicates was much larger, varying from an average of ~44% for the DC samples to ~81% for the splenic B cells (**Figure 6A**). Thus, the smaller overlaps seen between

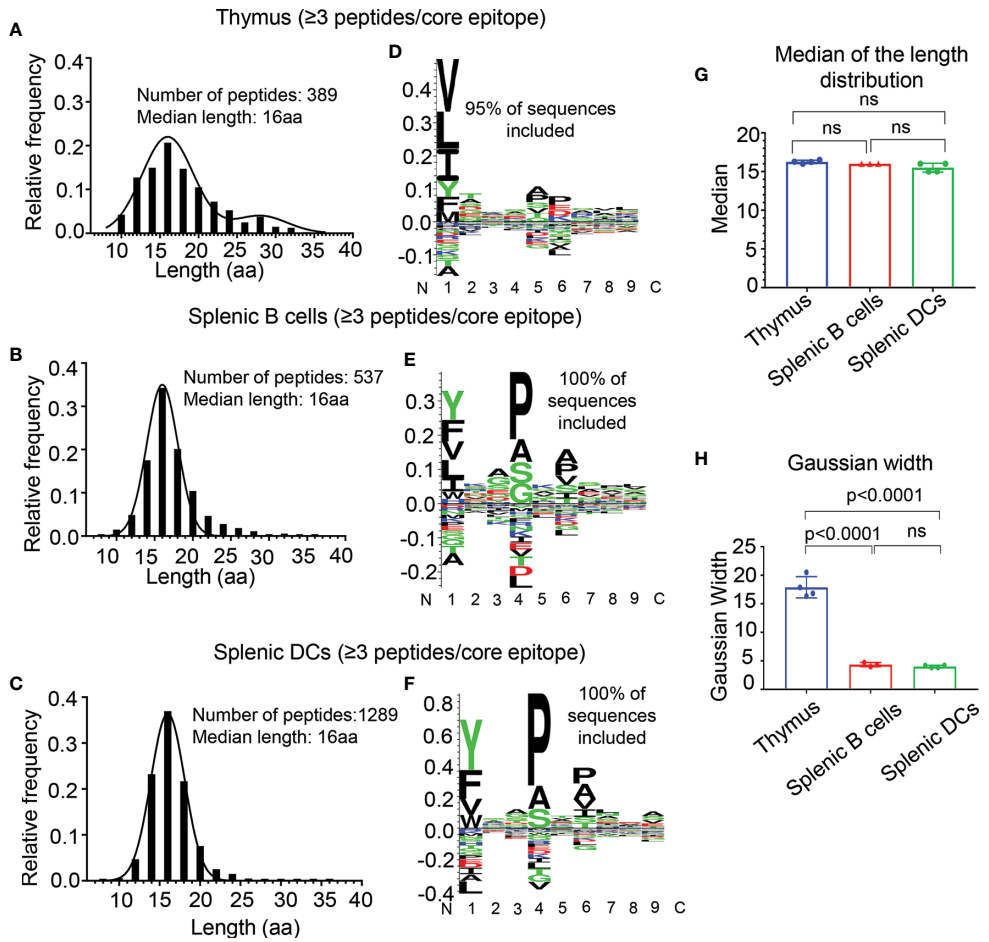

FIGURE 5 | Length distribution **(A–C)** and motif analysis **(D–F)** for peptides present in nested sets of at least three peptides per core epitope, eluted from thymus, splenic B cells, and splenic DCs. **(A, D)** Eluted peptides from thymus; **(B, E)** from splenic B cells; and **(C, F)** from splenic dendritic cells (DCs). **(G)** Median of the length distribution for thymus, splenic B cells and DCs is ~16 aa for each biological replicate. **(H)** Gaussian width analysis for each the distribution of peptide lengths in each biological replicate, showing that the thymic peptides having broader length distribution as compared to splenic B cells and DCs. Motifs determined as in **Figure 2**. Mean ± SD are plotted, and p-values are calculated using unpaired t-test. The non-significant differences are denoted as ns.

thymus and splenic B cells, or between thymus and splenic DC, likely reflect substantial differences in these immmunopeptidomes. These differences between immunopeptidomes from the various cell types also are apparent also in Venn diagrams showing the distribution of core epitopes with 3+ peptides among the different samples (**Figure 6B**, **Supplementary Table S4**), and the distribution of all core epitopes (**Figure 6C** and **Supplementary Table S4**).

To see if the somewhat less distinct sequence motif observed for the thymic peptidome as compared to the splenic B cell and DC peptidomes was accompanied by reduced MHC-peptide binding affinity, we evaluated I-A^b binding activity. For this purpose, we compared thymic and splenic B cell peptidomes, because for these datasets the thymus and spleen preparation came from the same mice and were processed and analyzed in parallel. To minimize the effects of sample-to-sample variation we considered only core epitopes present in most of the biological replicates from thymus (at least 3 of the four samples) or all of the biological replicates of splenic B cells (three samples). As in the previous analysis, we considered only core epitopes present in three or more peptides, to minimize any possible effect of non-specific peptides. For each core epitope we synthesized the most abundant peptide sequence carrying that core, and measured the relative binding affinity using purified recombinant I-A^b and an *in vitro* fluorescent peptide competition binding assay (34), reporting the results as IC_{50} values (**Figure 6D**). We compared core epitopes presented preferentially in thymus (**Figure 6D**, blue symbols) with those presented preferentially in splenic B cells (red symbols), including those found exclusively (filled symbols) or in at least 2-fold greater abundance (open symbols) in each sample type. The thymic epitopes were characterized by lower binding affinity (average IC_{50} = 37 μM) as compared to the splenic B cell epitopes (1.7 μM), and spanned a wider range of affinities despite being represented by fewer epitopes (**Figure 6D** and **Supplementary Table S5**). Since examining just the outlier core epitopes uniquely present only in thymus or splenic B might exaggerate

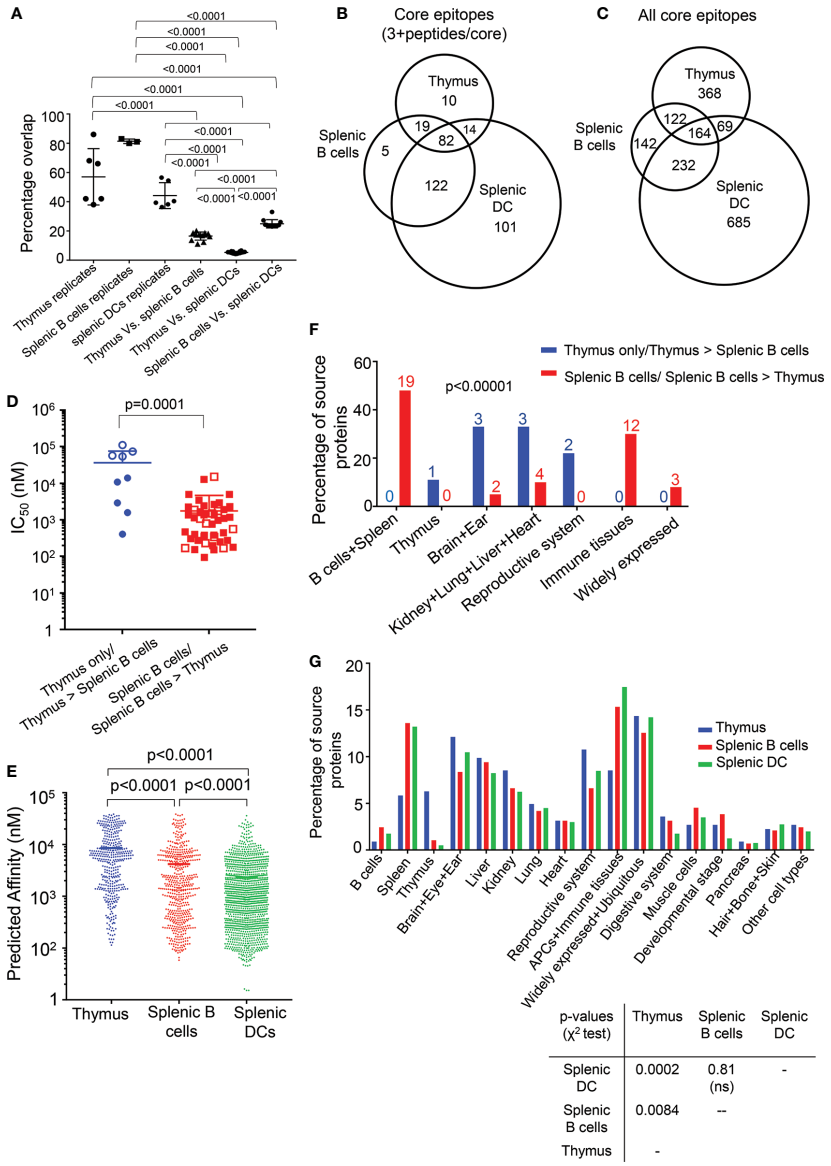

p-values (χ^2 test)	Thymus	Splenic B cells	Splenic DC
Splenic DC	0.0002	0.81 (ns)	-
Splenic B cells	0.0084	--	
Thymus	-		

FIGURE 6 | Overlap, affinity, and tissue distribution analysis for peptides eluted from thymus, splenic B cells, and splenic DC. **(A)** The percentage overlap of core epitopes between replicates of thymus, splenic B cells and DCs is shown, along with the percentage overlap between the different cell types. The p values shown represent differences in the percentage overlap for within-sample and between-sample values, and for differences between thymus and splenic B and DCs. The mean ± SD are plotted, and the p values are calculated using unpaired t test. **(B)** Venn diagram showing the overlap between the core epitopes of thymus, splenic B cells and DCs, for epitopes represented by at least three nested peptides. **(C)** As **(B)**, but for all core epitopes. **(D)** The experimental I-A^b binding affinity was determined for the most abundant peptide from each differentially presented core epitope having at least three peptides per core. Filled blue circles show epitopes present in at least three of the four biological replicates of thymus and absent from all replicates of splenic B cells, open blue circles show epitopes present in at least three of the four biological replicates of thymus and present with at least 2-fold higher amounts in thymus as compared to splenic B cells, filled red squares show epitopes present in all three biological replicates of splenic B cells and absent from all replicates of thymus, and open red squares show epitopes present in all three biological replicates of splenic B cells and present with at least 2-fold higher amounts in in splenic B cells as compared to thymus. The peptides present only in the splenic B cells or in higher abundance in splenic B cells have higher affinity as compared to the peptides present only in thymus or in higher abundance in thymus. Binding affinities are reported as IC_{50} values. The p values were calculated using Mann-Whitney test. **(E)** Predicted affinity for peptides present in nested sets of at least three peptides per core epitope, eluted from thymus, splenic B cells and splenic DCs. The predicted affinity for the peptides eluted from the DCs are of higher than the splenic B cells and the peptides eluted from the splenic B cells have higher predicted affinity as compared to the thymic peptides. The p values were calculated using Mann-Whitney test. **(F)** The tissue sources for the proteins of the peptides from panel **(D)** differentially present in thymus (blue) or splenic B cells (red) were identified using the Uniprot database. The immunopeptidome from the brain specific proteins, reproductive system proteins, heart, ear, lung and kidney are found to be enriched in thymus. The p values were calculated using Fisher's exact test. **(G)** Tissue sources for all the source proteins eluted from the thymus, splenic B cells and splenic DCs samples and that have ≥ 2 peptides/source protein were analyzed using the Uniprot database. The p-values between each set are indicated and were calculated using chi-square test.

differences between the samples, and to examine the generality of these results in the full immunopeptidome datasets, we used a computational approach, predicting IC_{50} values for all the peptides eluted from thymus, splenic B cells, or splenic DC, using the NetMHCIIpan 3.2 algorithm. The average predicted binding affinities of all the peptides eluted from the three different cell types were significantly different, with the DC peptides having the highest average predicted affinity (**Figure 6E**). As for the experimental determination in **Figure 6D**, the full set of thymic peptides had predicted affinity lower than the splenic B cells peptides.

Finally, we compared the tissue distribution of source proteins for core epitopes eluted from the various cell types. First, we compared the closely matched thymic and B cell samples, identifying the typical physiological location or tissue expression of the source proteins for each of the differentially presented core epitopes as in **Figure 6D**. Both B cell and thymic epitopes derived from a wide range of tissue sources. The representation of thymic peptides was significantly greater than B cell peptides for source proteins from several tissues, including brain, ear, and reproductive system, but less in other tissues (**Figure 6F**). This pattern was apparent, although to a lesser degree, for the full set of source proteins (represented by at least two eluted peptides) from all tissue sources (**Figure 6G**).

DISCUSSION

To explore possible differences in MHCII antigen processing and presentation pathways between thymus and spleen, we characterized the I-A^b-presented peptidomes from these tissues in C57BL/6 mice. We evaluated several strategies to reduce the contribution of non-specific peptides that appeared to dominate the thymus sample, using a well-characterized human B-lymphoblastoid cell line as a test system. Limiting the analysis only to peptides present in nested sets surrounding a core epitope essentially eliminated the contribution of non-specific peptides in the peptidomes. Even with the consequent reduction in the number of peptides identified, we nonetheless identified >400 peptides from mouse thymus present in nested sets of at least three peptides. This represents a substantial improvement over previous description of mouse and human thymic immunopeptidomes (8–10). We observed substantial differences in peptide length distribution and binding affinity for the thymic as compared to splenic peptidomes, suggestive of differences in the stringency of antigen processing and editing in these tissues.

In initial studies we observed many apparently non-specific peptides present in the thymic samples. We found that removal of peptides identified in control elutions from isotype and bead-only experiments was useful in reducing this background, however many remained, as indicated by peptide length distributions and sequence motifs inconsistent with known I-A^b features. The same behavior was observed for test human cell line samples when assayed at very low abundance, where we could unambiguously identify non-specifically-bound peptides. Why didn't the isotype-control approach to background subtraction, routinely applied in flow cytometry and cell biology applications, work in this case? We suspect that a contributing factor is the stochastic nature of data-dependent acquisition pipelines, wherein selection of peptide ions for fragmentation and sequence determination is directed at identification of a greater number of species rather than greater reproducibility between samples, with the result that low abundance species are difficult to reproducibly detect across samples. Using different strategies for identification of non-specifically bound peptides, including length cutoffs, predicted MHC binding affinity, and absence from nested sets, we identified non-specific peptides with characteristics similar to those eluted from the control affinity beads, although the particular sequences identified were different. A previous approach employing the PLAtEAU algorithm (44) used sequence overlaps rather than shared MHC-binding cores to identified peptides in nested sets; that approach likely would also reduce any contribution from non-specifically bound peptides as we observe here. For our purposes in this study, consideration of peptides present only in nested sets provided a convenient approach to reduction of the contribution of these non-specifically bound peptides. However, this approach is likely to remove some specifically bound peptides, particularly those present at low abundances, and may not be appropriate for other immunopeptidome study designs or goals. We note that this approach would not be appropriate for most class I MHC proteins, which typically do not bind nested sets of peptides because of constraints in the MHC-I peptide binding site with binding sites for both peptide N- and C- termini. Strategies employed in other studies should help to mitigate this issue, including imposition of a length-cutoff, predicted affinity cutoff, or consideration of peptides present only in most or all biological or technical replicates (44), with the choice of strategy guided by the goals of the study and the relative enrichment of specific versus non-specific species.

The problem of identification of non-specific peptides present in an eluted peptide sample is distinct from that addressed by measures to control the false discovery rate, which seek to reduce the frequency of incorrect identification of peptide sequences in the database matching algorithm. Here, the issue is one of biochemical specificity; the peptides appear to be identified correctly and are present in the samples but are not specifically bound by the MHC protein of interest. Possible sources for such peptides include co-purifying peptide-binding proteins such as heat-shock proteins, scavenger receptors, or potentially even MHC-I proteins, as well as exogenously or endogenously processed peptides that bind directly to the immunoaffinity resin. All protein purification procedures have a finite purification ratio and entail some degree of sample loss. In attempting to increase recovery of the desired MHC-bound peptides while minimizing undesired non-specific peptides, a balance must be struck between sensitivity and specificity. Additional optimization of our isolation strategy might improve its performance, particularly for low-abundance samples. However, non-specific peptides likely will be present

to some extent in all immunopeptidome samples, particularly those for which the MHC-peptide content is low, but how to address these non-specifically isolated co-purifying peptides seems not to have been addressed specifically in the literature. Strategies employed in other studies should help to mitigate this issue, including imposition of a length-cutoff, predicted affinity cutoff, or consideration of peptides present only in most or all biological or technical replicates, with the choice of strategy guided by the goals of the study and the relative enrichment of specific versus non-specific species.

Despite considerable overlap between the thymic and splenic peptidomes, almost 2/3 of the confidently identified MHC-II core epitopes from thymus, i.e. those present in at least three nested peptides, were not found in the splenic B cell or DC elutes. Among the thymus-specific peptides were many deriving from source proteins expressed from tissue-specific genes, including those typically expressed in brain, skin, eyes, etc. In previous studies of human thymus, a few such peptides presented by MHC-I or MHC-II proteins were identified and associated with Aire-dependent transcription in medullary thymic epithelial cells (mTEC) (10, 45). Whether thymus-specific peptides that we identified are Aire-dependent transcripts expressed in mTEC or represent true tissue-specific proteins brought into thymus by migratory DC, B cells, or other antigen presenting cells requires further work, possibly including fractionating the various cells types present in thymus before elution, as previously reported for murine thymus CD11c+ DC in a study of MHC-I peptidomes (9). In addition to differences in source protein distribution, we observed substantial differences in length distribution and I-A^b binding affinity for the I-A^b-binding peptides eluted from thymus compared to splenic DC and B cells. The thymic immunopeptidome had a broader distribution of lengths than the splenic peptidomes, possibly indicative of less aggressive trimming by cellular proteases, and a broader distribution of I-A^b affinity. The affinity differences might indicate that thymic peptides have undergone less efficient editing by DM, a non-classical MHC protein known to select for tightly-bound MHCII-peptide complexes (46, 47). Thymic epithelial cells express abundant DO, another non-classical MHC protein that inhibits DM (48) and its expression increases presentation of low affinity peptides (37). The less aggressive processing and less efficient editing characteristics of antigen presentation in the thymus might help to preserve many delicate, rare, or low-affinity epitopes for presentation to developing thymocytes during selection in the thymus.

One limitation of our study is that absolute quantitation approaches, such as internal standard doping with known amounts of stable-isotope-labeled eluted-peptide variants (37) were not performed, so that comparisons of the abundances of different peptides are not available. Another limitation is our reliance on datasets obtained by data-dependent acquisition workflows, which are optimized for identifying as many peptides as possible. If larger spectral libraries were available, a data-independent (DIA) approach, as recently applied to low-abundance human blood MHC-II peptidomes (49), could allow for better control of sample-to-sample differences. As in other studies of limited-abundance biological samples (10, 49, 50), our conclusions are constrained by the small size of the available immunopeptidomes. Finally, tagging approaches that allow for more efficient MHC purification might reduce the impact of non-specific peptides (51).

In summary, our initial efforts to characterize the peptides presented by I-A^b in the thymus of C57BL/6 mice using conventional immunopeptidome sample processing and analysis pipelines were complicated by the presence of a substantial fraction of non-specifically bound, co-purifying peptides, apparently the result of the low levels of I-A^b present in this tissue. We used a well-characterized human cell line, for which HLA-DR-binding peptides could easily be identified, to test several strategies to reduce the contribution of background peptides. By considering only peptides present in nested sets surrounding a core epitope, we distinguished binders from background peptides, in low abundance human and mouse thymus samples. Comparison of the mouse thymus immunopeptidome with those of mouse splenic B cells or DC suggested that antigen presentation pathways in the thymus are characterized by less aggressive processing and less stringent editing than those in the spleen.

DATA AVAILABILITY STATEMENT

The datasets presented in this study can be found in MassIVE data repository (http://massive.ucsd.edu) developed by Center for Computational Mass Spectrometry (University of California, San Diego) with the project accession MSV000087031.

ETHICS STATEMENT

The animal study was reviewed and approved by University of Massachusetts Medical School Institutional Animal Care and Use Committee.

AUTHOR CONTRIBUTIONS

PN and LJS designed the research. PN isolated peptidomes, performed binding studies, and analyzed mass spectrometry data. MJ isolated thymus, splenic B cells, and dendritic cells. CC isolated dendritic cells. LL assisted in recombinant protein purification. PN, LS, and LJS analyzed the data and wrote the paper. All authors contributed to the article and approved the submitted version.

FUNDING

This work was supported by NIH grant R01AI137198 (LS and LJS).

ACKNOWLEDGMENTS

We thank Sharlene Hubbard for assistance with mouse husbandry, and the efforts of the UMass Medical School Mass Spectrometry Facility.

SUPPLEMENTARY MATERIAL

The Supplementary Material for this article can be found online at: https://www.frontiersin.org/articles/10.3389/fimmu.2021.658601/full#supplementary-material

REFERENCES

1. Abramson J, Anderson G. Thymic Epithelial Cells. *Annu Rev Immunol* (2017) 35:85–118. doi: 10.1146/annurev-immunol-051116-052320
2. Starr TK, Jameson SC, Hogquist KA. Positive and Negative Selection of T Cells. *Annu Rev Immunol* (2003) 21:139–76. doi: 10.1146/annurev.immunol.21.120601.141107
3. Abramson J, Giraud M, Benoist C, Mathis D. Aire's Partners in the Molecular Control of Immunological Tolerance. *Cell* (2010) 140:123–35. doi: 10.1016/j.cell.2009.12.030
4. Derbinski J, Schulte A, Kyewski B, Klein L. Promiscuous Gene Expression in Medullary Thymic Epithelial Cells Mirrors the Peripheral Self. *Nat Immunol* (2001) 2:1032–9. doi: 10.1038/ni723
5. Hadeiba H, Lahl K, Edalati A, Oderup C, Habtezion A, Pachynski R, et al. Plasmacytoid Dendritic Cells Transport Peripheral Antigens to the Thymus to Promote Central Tolerance. *Immunity* (2012) 36:438–50. doi: 10.1016/j.immuni.2012.01.017
6. Goldschneider I, Cone RE. A Central Role for Peripheral Dendritic Cells in the Induction of Acquired Thymic Tolerance. *Trends Immunol* (2003) 24:77–81. doi: 10.1016/S1471-4906(02)00038-8
7. Kleindienst P, Chretien I, Winkler T, Brocker T. Functional Comparison of Thymic B Cells and Dendritic Cells In Vivo. *Blood* (2000) 95:2610–6. doi: 10.1182/blood.V95.8.2610.008k11_2610_2616
8. Marrack P, Ignatowicz L, Kappler JW, Boymel J, Freed JH. Comparison of Peptides Bound to Spleen and Thymus Class II. *J Exp Med* (1993) 178:2173–83. doi: 10.1084/jem.178.6.2173
9. Adamopoulou E, Tenzer S, Hillen N, Klug P, Rota IA, Tietz S, et al. Exploring the MHC-peptide Matrix of Central Tolerance in the Human Thymus. *Nat Commun* (2013) 4:2039. doi: 10.1038/ncomms3039
10. Collado JA, Alvarez I, Ciudad MT, Espinosa G, Canals F, Pujol-Borrell R, et al. Composition of the HLA-DR-associated Human Thymus Peptidome. *Eur J Immunol* (2013) 43:2273–82. doi: 10.1002/eji.201243280
11. Santori FR, Kieper WC, Brown SM, Lu Y, Neubert TA, Johnson KL, et al. Rare, Structurally Homologous Self-Peptides Promote Thymocyte Positive Selection. *Immunity* (2002) 17:131–42. doi: 10.1016/S1074-7613(02)00361-8
12. Hogquist KA, Tomlinson AJ, Kieper WC, McGargill MA, Hart MC, Naylor S, et al. Identification of a Naturally Occurring Ligand for Thymic Positive Selection. *Immunity* (1997) 6:389–99. doi: 10.1016/S1074-7613(00)80282-4
13. Clement CC, Becerra A, Yin L, Zolla V, Huang L, Merlin S, et al. The Dendritic Cell Major Histocompatibility Complex Ii (Mhc II) Peptidome Derives From a Variety of Processing Pathways and Includes Peptides With a Broad Spectrum of HLA-DM Sensitivity. *J Biol Chem* (2016) 291:5576–95. doi: 10.1074/jbc.M115.655738
14. Schuster H, Shao W, Weiss T, Pedrioli PGA, Roth P, Weller M, et al. A Tissue-Based Draft Map of the Murine MHC Class I Immunopeptidome. *Sci Data* (2018) 5:180157. doi: 10.1038/sdata.2018.157
15. Fugmann T, Sofron A, Ritz D, Bootz F, Neri D. The MHC Class II Immunopeptidome of Lymph Nodes in Health and in Chemically Induced Colitis. *J Immunol* (2017) 198:1357–64. doi: 10.4049/jimmunol.1601157
16. Fortier MH, Caron E, Hardy MP, Voisin G, Lemieux S, Perreault C, et al. The MHC class I peptide repertoire is molded by the transcriptome. *J Exp Med* (2008) 205(3):595–610. doi: 10.1084/jem.20071985
17. Wan X, Vomund AN, Peterson OJ, Chervonsky AV, Lichti CF, Unanue ER. The MHC-II Peptidome of Pancreatic Islets Identifies Key Features of Autoimmune Peptides. *Nat Immunol* (2020) 21:455–63. doi: 10.1038/s41590-020-0623-7
18. Bozzacco L, Yu H, Zebroski HA, Dengjel J, Deng H, Mojsov S, et al. Mass Spectrometry Analysis and Quantitation of Peptides Presented on the MHC II Molecules of Mouse Spleen Dendritic Cells. *J Proteome Res* (2011) 10:5016–30. doi: 10.1021/pr200503g
19. Xing Y, Hogquist KA. Isolation, Identification, and Purification of Murine Thymic Epithelial Cells. *J Vis Exp* (2014) 90:e51780. doi: 10.3791/51780
20. Rezzani R, Bonomini F, Rodella LF. Histochemical and Molecular Overview of the Thymus as Site for T-cells Development. *Prog Histochem Cytochem* (2008) 43:73–120. doi: 10.1016/j.proghi.2008.03.001
21. Rodewald HR. Thymus Organogenesis. *Annu Rev Immunol* (2008) 26:355–88. doi: 10.1146/annurev.immunol.26.021607.090408
22. Itoi M, Tsukamoto N, Yoshida H, Amagai T. Mesenchymal Cells are Required for Functional Development of Thymic Epithelial Cells. *Int Immunol* (2007) 19:953–64. doi: 10.1093/intimm/dxm060
23. Petrie HT, Zuniga-Pflucker JC. Zoned Out: Functional Mapping of Stromal Signaling Microenvironments in the Thymus. *Annu Rev Immunol* (2007) 25:649–79. doi: 10.1146/annurev.immunol.23.021704.115715
24. Anderson G, Jenkinson EJ, Moore NC, Owen JJ. MHC Class II-positive Epithelium and Mesenchyme Cells are Both Required for T-cell Development in the Thymus. *Nature* (1993) 362:70–3. doi: 10.1038/362070a0
25. Waskow C, Liu K, Darrasse-Jeze G, Guermonprez P, Ginhoux F, Merad M, et al. The Receptor Tyrosine Kinase Flt3 is Required for Dendritic Cell Development in Peripheral Lymphoid Tissues. *Nat Immunol* (2008) 9:676–83. doi: 10.1038/ni.1615
26. Maraskovsky E, Brasel K, Teepe M, Roux ER, Lyman SD, Shortman K, et al. Dramatic Increase in the Numbers of Functionally Mature Dendritic Cells in Flt3 Ligand-Treated Mice: Multiple Dendritic Cell Subpopulations Identified. *J Exp Med* (1996) 184:1953–62. doi: 10.1084/jem.184.5.1953
27. Ardouin L, Luche H, Chelbi R, Carpentier S, Shawket A, Montanana Sanchis F, et al. Broad and Largely Concordant Molecular Changes Characterize Tolerogenic and Immunogenic Dendritic Cell Maturation in Thymus and Periphery. *Immunity* (2016) 45:305–18. doi: 10.1016/j.immuni.2016.07.019
28. Gorga JC, Horejsi V, Johnson DR, Raghupathy R, Strominger JL. Purification and Characterization of Class II Histocompatibility Antigens From a Homozygous Human B Cell Line. *J Biol Chem* (1987) 262:16087–94. doi: 10.1016/S0021-9258(18)47699-5
29. Chicz RM, Urban RG, Lane WS, Gorga JC, Stern LJ, Vignali DA, et al. Predominant Naturally Processed Peptides Bound to HLA-DR1 are Derived From MHC-related Molecules and are Heterogeneous in Size. *Nature* (1992) 358:764–8. doi: 10.1038/358764a0
30. Gorga JC, Knudsen PJ, Foran JA, Strominger JL, Burakoff SJ. Immunochemically Purified DR Antigens in Liposomes Stimulate Xenogeneic Cytolytic T Cells in Secondary In Vitro Cultures. *Cell Immunol* (1986) 103:160–73. doi: 10.1016/0008-8749(86)90077-8
31. Andreatta M, Alvarez B, Nielsen M. GibbsCluster: Unsupervised Clustering and Alignment of Peptide Sequences. *Nucleic Acids Res* (2017) 45:W458–63. doi: 10.1093/nar/gkx248
32. Thomsen MC, Nielsen M. Seq2Logo: A Method for Construction and Visualization of Amino Acid Binding Motifs and Sequence Profiles Including Sequence Weighting, Pseudo Counts and Two-Sided Representation of Amino Acid Enrichment and Depletion. *Nucleic Acids Res* (2012) 40:W281–7. doi: 10.1093/nar/gks469
33. Andreatta M, Lund O, Nielsen M. Simultaneous Alignment and Clustering of Peptide Data Using a Gibbs Sampling Approach. *Bioinformatics* (2013) 29:8–14. doi: 10.1093/bioinformatics/bts621
34. Yin L, Stern LJ. Measurement of Peptide Binding to MHC Class II Molecules by Fluorescence Polarization. *Curr Protoc Immunol* (2014) 106:5101–51012. doi: 10.1002/0471142735.im0510s106
35. UniProt C. UniProt: A Worldwide Hub of Protein Knowledge. *Nucleic Acids Res* (2019) 47:D506–15. doi: 10.1093/nar/gky1049
36. Becerra-Artiles A, Cruz J, Leszyk JD, Sidney J, Sette A, Shaffer SA, et al. Naturally Processed HLA-DR3-restricted Hhv-6B Peptides are Recognized Broadly With Polyfunctional and Cytotoxic CD4 T-Cell Responses. *Eur J Immunol* (2019) 49:1167–85. doi: 10.1002/eji.201948126

37. Nanaware PP, Jurewicz MM, Leszyk JD, Shaffer SA, Stern LJ. Hla-do Modulates the Diversity of the MHC-II Self-Peptidome. *Mol Cell Proteomics* (2019) 18:490–503. doi: 10.1074/mcp.RA118.000956
38. Urban RG, Chicz RM, Lane WS, Strominger JL, Rehm A, Kenter MJ, et al. A Subset of HLA-B27 Molecules Contains Peptides Much Longer Than Nonamers. *Proc Natl Acad Sci USA* (1994) 91:1534–8. doi: 10.1073/pnas.91.4.1534
39. Jardetzky TS, Lane WS, Robinson RA, Madden DR, Wiley DC. Identification of Self Peptides Bound to Purified HLA-B27. *Nature* (1991) 353:326–9. doi: 10.1038/353326a0
40. Jensen KK, Andreatta M, Marcatili P, Buus S, Greenbaum JA, Yan Z, et al. Improved Methods for Predicting Peptide Binding Affinity to MHC Class II Molecules. *Immunology* (2018) 154:394–406. doi: 10.1111/imm.12889
41. Wang P, Sidney J, Dow C, Mothe B, Sette A, Peters B. A Systematic Assessment of MHC Class II Peptide Binding Predictions and Evaluation of a Consensus Approach. *PLoS Comput Biol* (2008) 4:e1000048. doi: 10.1371/journal.pcbi.1000048
42. Buus S, Lauemoller SL, Worning P, Kesmir C, Frimurer T, Corbet S, et al. Sensitive Quantitative Predictions of peptide-MHC Binding by a 'Query by Committee' Artificial Neural Network Approach. *Tissue Antigens* (2003) 62:378–84. doi: 10.1034/j.1399-0039.2003.00112.x
43. Stern LJ, Wiley DC. Antigenic Peptide Binding by Class I and Class II Histocompatibility Proteins. *Structure* (1994) 2:245–51. doi: 10.1016/S0969-2126(00)00026-5
44. Alvaro-Benito M, Morrison E, Abualrous ET, Kuropka B, Freund C. Quantification of HLA-DM-Dependent Major Histocompatibility Complex of Class Ii Immunopeptidomes by the Peptide Landscape Antigenic Epitope Alignment Utility. *Front Immunol* (2018) 9:872. doi: 10.3389/fimmu.2018.00872
45. Alvarez I, Collado JA, Colobran R, Carrascal M, Ciudad MT, Canals F, et al. Central T Cell Tolerance: Identification of Tissue-Restricted Autoantigens in the Thymus HLA-DR Peptidome. *J Autoimmun* (2015) 60:12–9. doi: 10.1016/j.jaut.2015.03.004
46. Alvaro-Benito M, Freund C. Revisiting Nonclassical HLA II Functions in Antigen Presentation: Peptide Editing and its Modulation. *HLA* (2020) 96:415–29. doi: 10.1111/tan.14007
47. Mellins ED, Stern LJ, HLA-DM and HLA-DO. Key Regulators of MHC-II Processing and Presentation. *Curr Opin Immunol* (2014) 26:115–22. doi: 10.1016/j.coi.2013.11.005
48. Guce AI, Mortimer SE, Yoon T, Painter CA, Jiang W, Mellins ED, et al. Hla-DO Acts as a Substrate Mimic to Inhibit HLA-DM by a Competitive Mechanism. *Nat Struct Mol Biol* (2013) 20:90–8. doi: 10.1038/nsmb.2460
49. Ritz D, Sani E, Debiec H, Ronco P, Neri D, Fugmann T. Membranal and Blood-Soluble Hla Class Ii Peptidome Analyses Using Data-Dependent and Independent Acquisition. *Proteomics* (2018) 18:e1700246. doi: 10.1002/pmic.201700246
50. Heyder T, Kohler M, Tarasova NK, Haag S, Rutishauser D, Rivera NV, et al. Approach for Identifying Human Leukocyte Antigen (Hla)-Dr Bound Peptides From Scarce Clinical Samples. *Mol Cell Proteomics* (2016) 15:3017–29. doi: 10.1074/mcp.M116.060764
51. Abelin JG, Harjanto D, Malloy M, Suri P, Colson T, Goulding SP, et al. Defining HLA-II Ligand Processing and Binding Rules with Mass Spectrometry Enhances Cancer Epitope Prediction. *Immunity* (2019) 51 (4):766–79.e17. doi: 10.1016/j.immuni.2019.08.012

Conflict of Interest: The authors declare that the research was conducted in the absence of any commercial or financial relationships that could be construed as a potential conflict of interest.

frontiers in Immunology

REVIEW
published: 10 June 2021
doi: 10.3389/fimmu.2021.677036

How Does B Cell Antigen Presentation Affect Memory CD4 T Cell Differentiation and Longevity?

Robin A. Welsh[1†], *Nianbin Song*[2†] *and Scheherazade Sadegh-Nasseri*[1,3*]

[1] Graduate Program in Immunology, Johns Hopkins School of Medicine, Baltimore, MD, United States, [2] Department of Biology, Krieger School of Arts & Sciences, Johns Hopkins University, Baltimore, MD, United States, [3] Department of Pathology, Johns Hopkins School of Medicine, Baltimore, MD, United States

Dendritic cells are the antigen presenting cells that process antigens effectively and prime the immune system, a characteristic that have gained them the spotlights in recent years. B cell antigen presentation, although less prominent, deserves equal attention. B cells select antigen experienced CD4 T cells to become memory and initiate an orchestrated genetic program that maintains memory CD4 T cells for life of the individual. Over years of research, we have demonstrated that low levels of antigens captured by B cells during the resolution of an infection render antigen experienced CD4 T cells into a quiescent/resting state. Our studies suggest that in the absence of antigen, the resting state associated with low-energy utilization and proliferation can help memory CD4 T cells to survive nearly throughout the lifetime of mice. In this review we would discuss the primary findings from our lab as well as others that highlight our understanding of B cell antigen presentation and the contributions of the MHC Class II accessory molecules to this outcome. We propose that the quiescence induced by the low levels of antigen presentation might be a mechanism necessary to regulate long-term survival of CD4 memory T cells and to prevent cross-reactivity to autoantigens, hence autoimmunity.

Keywords: memory, CD4 lymphocyte, gene regulation, longevity, B cell Ag presentation, new CD4 memory markers, resting memory CD4+ T-cells

OPEN ACCESS

Edited by:
Eddie A. James, Benaroya Research Institute, United States

Reviewed by:
Bénédicte Manoury, Institut National de la Santé et de la Recherche Médicale (INSERM), France
Reinhard Obst, Ludwig Maximilian University of Munich, Germany

***Correspondence:**
Scheherazade Sadegh-Nasseri
ssadegh@jhmi.edu

[†]*These authors have contributed equally to this work*

Specialty section:
This article was submitted to Antigen Presenting Cell Biology, a section of the journal Frontiers in Immunology

Received: *07 March 2021*
Accepted: *18 May 2021*
Published: *10 June 2021*

Citation:
Welsh RA, Song N and Sadegh-Nasseri S (2021) How Does B Cell Antigen Presentation Affect Memory CD4 T Cell Differentiation and Longevity? Front. Immunol. 12:677036. doi: 10.3389/fimmu.2021.677036

DENDRITIC CELLS AS ANTIGEN PRESENTING CELLS TO INITIATE A PRIMARY RESPONSE

Initiation of an adaptive immune response begins with naïve T cells being activated by antigens presented on dendritic cells (DCs), a highly specialized professional antigen presenting cell (APC) (1, 2). As a frontline defender, DCs are key APCs bridging the gap between innate and adaptive immunity. Located primarily in peripheral tissues, immature DCs are well known for their ability to recognize and capture invading pathogens mainly through phagocytosis and micropinocytosis. Uptake of antigen (Ag) is closely followed by upregulation of MHC Class I, Class II and co-stimulatory molecules on the surface of DCs, as they lose the ability to perform macropinocytosis (3, 4). Mature DCs then migrate to draining lymph nodes where they present pathogen-derived epitopes to naïve CD4 and CD8 T cells (5). One unique characteristic of DCs is their ability to uptake Ag *via* phagocytosis and cross-present it on MHC Class I molecules.

This makes DCs a perfect primary antigen presenter for initiation of an immune response (2). Moreover, it has also been noted that activation of immature DCs by various Toll-like receptor ligands (TLR3 and TLR9) transiently increases antigen specific micropinocytosis (6), which likely increases the ability of DCs to capture Ag within an inflammatory context. To date, research into what contributions DCs make to memory development has been limited and mainly focuses on memory CD8 T cells development (7–11). Use of Batf3 knock-out (KO) mice, which lack CD8a DCs responsible for cross-presentation, found no impact on primary CD4 T cell responses but drastically impaired CD8 responses (12). Likewise, work using *Toxoplasma gondii* showed a crucial role for CD4 T cells in protecting Batf3 KO mice from succumbing to *T. gondii* infection (13). Yet none of these studies using DC KO mice investigated a role for DCs in memory CD4 T cell development. Data from Dalai et al., however suggests that loss of DCs does not likely impact the formation of memory CD4 T cells as removal of CD11c+ DCs did not affect the development of quiescent memory CD4 T cells (14).

B CELLS AS APCS IN SECONDARY RESPONSES

B cells are another major professional APCs, which unlike DCs, take up antigens specifically by B cell receptor (BCR) (1). Upon interaction with a cognate Ag, the BCR-Ag complex would be internalized and shuttled to the specialized MHC class II enriched compartments (MIIC) for processing and presentation to the Ag-specific CD4 T cells (15). These CD4 T-B interactions provide essential activation signals to B cells for affinity maturation and differentiation into memory B, or antibody-secreting plasma B cells (16). The memory B cells generated from this T-B interaction have been found to also be important for CD4 T cell memory responses (17).

HOW B CELLS AND DCS IMPACT MEMORY T CELL DEVELOPMENT

It is generally accepted that memory T cells differentiate after exposure to Ag followed by multiple rounds of proliferation (18–20). While characterization of memory T cells has been explored intensely, the onset of differentiation of Ag-experienced T cells into memory, and how APCs influence this process is less appreciated. Especially that in rare publications, it has been proposed that CD8 memory T cells may be generated upon asymmetric cell division, which precludes the need for interaction with antigen presenting cells (14, 21, 22). On another line of studies, CD8 memory T cell development and homeostasis has been reported to be mediated by IL-15Rα expressed by DCs and Macrophages (23, 24). It is also found that long-lasting CD8 memory can be achieved in the absence of CD4 T cells or B cells (25).

For CD4 Memory T development, however, TCR-pMHC interaction appears to drive CD4 Memory T development (14, 26–30). In this regard, Williams et al. found that lower levels of LCMV antigen density led to high functional avidity CD4 T memory differentiation, while higher levels of LCMV antigen density promoted both high avidity and low avidity CD4 T cells expansion (28). However, the authors did not explore whether DCs or B cells were the APCs to drive such differentiation. Studies addressing contributions of B cells to activation of naïve CD4 T cells has been inconclusive (31). Conversely, several investigations have reported that B cells play a critical role in regulating CD4 memory T development and differentiation (14, 17, 26, 30, 32–37). It is noteworthy that among these studies, both Chowdhury (17) and Misumi (35) found that absence of antigen specific B cells either from SCID mice without B cells or treatment of anti-CD20 mAb did not impact the priming of CD4 T cells in viral infection but impaired the development and effector function of memory CD4 T cells. By virtue of having antigen specific B Cell Receptors, B cells can recognize and internalize specific antigens, process, and present them to cognate CD4 T cells (15). As such, B cell antigen presentation adds a new and exciting dimension to our current knowledge.

The first clear demonstration that B cells play a role in memory CD4 T cell generation/differentiation came from Bradley and colleagues who reported B cell knockout mice did not develop memory CD4 T cells (32). Further studies have shown that loss of B cells adversely affects development of Tuberculosis (TB)-specific CD4 memory precursor effector cells (MPECs) in TB vaccinated B cell deficient mice (36). Because of the ability of B cells to produce antibodies that bind to Ag, it has been postulated that contribution of B cells to CD4 memory T cell development might be linked to Ag-Ab complexes. However, when this issue was specifically addressed by Whitmire et al., T cell responses to lymphocytic choriomeningitis virus (LCMV) infection, the team found that in contrast to B cell-deficient mice, membrane Ig expressing Tg mice retained functional Th cell memory, indicating that B cells selectively preserve CD4 T cell memory independently of immune complex formation (33).

To directly test if B cells were important for the development of CD4 T cell memory, Dalai et al. tested the specific interactions of various APCs with Ag experienced CD4 T cells (14). Using an *ex vivo* anergy assay, the group showed that only B cells, but not DCs, induced a resting state in Ag experienced CD4 T cells. Further *in vivo* characterization using an adoptive cell transfer assay further confirmed the *ex vivo* observations. Previous findings had demonstrated that sub-optimal levels of agonist peptides had induced a resting state in T cells *in vitro*, and *in vivo* (34, 38–44). Thus, the above observations that B cells, but not DCs, pulsed with low doses of Ag induced resting memory CD4 T cells confirmed prior findings that B cells are indispensable for memory CD4 T cell development/differentiation. In agreement with the above findings, B cell deficient mice did not develop quiescent CD4 memory T cells. However, when B cells were transferred to the B cell deficient mice, hyporesponsive CD4 memory T cells were developed. Importantly, B2 (B220+CD43+)

follicular B cells, which have diverse BCR were identified as the cells that rendered CD4 memory T cells hyporesponsive (14). These finding were later supported by Keck et al, who found that B cells were required for both optimal expansion and T-bet expression in response to weak TCR stimulation and optimal generation of CD4 T memory (30).

CONTRIBUTION OF AG DENSITY PRESENTED BY FOLLICULAR B CELLS TO CD4 MEMORY T CELL INDUCTION/DIFFERENTIATION

Building upon those initial findings, Dalai et al. tested the effects of B cell presentation of peptide-MHC (pMHC) density on the induction of quiescent memory CD4 T cells. They used a clever strategy by recovering B cells from mice at various timepoints post immunization and transferring them into recipient mice harboring CD4 T memory precursor cells at 4-day intervals (26). This staggered timeframe allowed Dalai et al. to correlate the amount of pMHC presented by the B cells to the time post immunization; earlier time points displayed more pMHC, and later time points fewer pMHC. Interestingly, the group found that only B cells harvested between day 16-20 post OVA immunization induced resting hyporesponsive CD4 memory T cells. These findings supported the idea that CD4 memory T cells are signaled to a resting state by the presentation of a subthreshold numbers of pMHC. These conclusions were further expanded to HEL-specific B cells (45) HEL-specific B cells when used for induction of quiescence/resting state of Ag experienced T cells were more efficient in capturing the Ag and induced quiescence in Ag experienced CD4 T cells at much later time points, i.e., 41-48 days *vs* 16-20 days post immunization by non-specific B cells. In those experiments B cells immunized with protein antigens were transferred to mice that carried primed T cells at 4-day intervals. The rationale was to find out when during an immune response B cell presentation of pMHC reaches to the levels necessary for the induction of quiescence naturally, *in vivo*. It was quite gratifying to see that HEL-specific B cells had captured far more antigen so that the required densities of pMHC for inducing quiescence had reached 20 plus days later than the polyclonal B cells (26). Altogether, Dalai et al. established that: (1) B cells are the APCs responsible for rendering CD4 memory T cells the quiescent, and (2) low levels of pMHC presentation are the main driving force that signal CD4 T cells to enter a resting state (26).

More recently, we have explored how this state of anergy impacts both the longevity and function of CD4 T memory cells. Song et al. investigated gene expression dynamics in CD4 T memory cells at different stages post immunization representing activated, early memory, late memory, and long-term memory stages (46). OVA-specific DO11.10 T cells were adoptively transferred into naïve mice before infecting them with Vaccinia-OVA virus, followed by harvesting the $CD44^{hi}DO11.1^{pos}$ T cells at different time points post immunization and subjecting their mRNA for gene expression analyses. Through this approach, the group was able to illustrate the gene expression dynamics occurring during CD4 T memory development up to almost 1 year. In agreement with findings of others (47–51), authors found that the OVA-specific CD4 memory T cells adopted a resting phenotype. Furthermore, the memory phenotype associated with multiple genetic programs regulating cellular proliferation, DNA repair, prevention of apoptosis, glucose, and lipid metabolism (**Figure 1**). Specifically, most genes regulating cellular proliferation and DNA repair response were found to be associated with p53 pathways, which highlights the importance of limiting cell proliferation and promoting DNA repair in long-lived CD4 Memory T cells. Also, of note was that like CD8 Memory T cells, genes regulating lipid metabolism were upregulated indicating that long-lived CD4 Memory T cells may also rely on lipid metabolism. However, unlike CD8 memory, the genes regulating lipid metabolism in CD4 T memory were found to be centered on regulating cellular cholesterol and ceramide levels, which could be related to the T cell signaling and prevention of apoptosis. Altogether, these programs play important roles in CD4 Memory T development and maintenance.

The above genetic studies also revealed upregulated levels of CD99, CCR10 and Itga3 as potentially new surface markers for long-lived CD4 memory T cells. Importantly, the high expression levels of these new CD4 memory markers at the protein level were confirmed to hold true across different animal models and antigens. For example, CD99hi resting human CD4 T cells from flu vaccinated donors had much better proliferation responses than the CD99lo CD4 subsets to *in vitro* challenges, indicating that the gene expression programs found in murine CD4 memory T cells could also be applicable to human CD4 memory T cells. Overall speaking, this work indicated not only that the resting state of CD4 memory T cells was mediated by multiple genes and could be part of the reason for CD4 memory longevity, but also the surprising findings that the murine CD4 memory differentiation is regulated by genetic programs that evolve upwards of 6 months to fully appear.

CONTRIBUTION OF CLASS II ACCESSORY MOLECULES IN CD4 MEMORY FORMATION

The finding that proper development of CD4 T memory cells relies on quantitative differences in presentation of immunodominant epitopes by B cells, brings the focus to the potential roles that accessory molecules in antigen processing play in the selection of epitopes for binding to MHC Class II. It is demonstrated that as the main Class II peptide-editor, HLA-DM (human DM; murine H2-M) contributes to the selection of immunodominant epitopes by generating higher quantities of those epitopes (52–55). HLA-DO (human DO; murine H2-O), is a second accessory molecule, which requires DM for its expression; DO is mainly expressed in thymic epithelium and B cells (54–56). Both DM and DO contribute to T cell immunity in a significant way, because lymphocytes usually respond to a small portion of the potential determinants on a protein antigen,

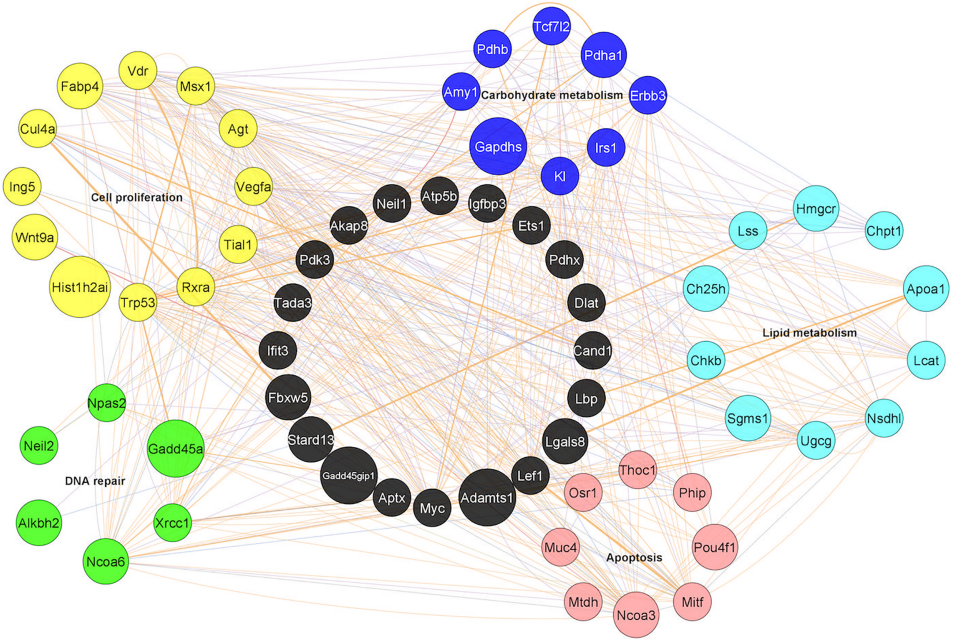

FIGURE 1 | Gene networks in long-lived CD4 memory T cells. Five different gene programs were identified as dynamically regulated during memory CD4 T cell differentiation. The genes shown were from the long-lived memory CD4 cells 10.5 months post immunization as compared to naïve controls and are marked in different colors: Yellow: cell proliferation; Green: DNA repair; Red: Apoptosis; Light blue: Lipid metabolism; Dark blue: Carbohydrate metabolism; Black: Not identified in the five gene programs but served as connecting genes. Each line represents an interaction/co-expression of genes as identified by literature report.

defined as '*immunodominant*' (57). Immunodominant epitopes are the essential targets of the immune response against infectious diseases, cancer, autoimmune diseases, and allergy. Hence, deserve the attention devoted to the understanding of epitope selection and immunodominance. To better understand how each accessory molecule impacts immunodominant epitope selection, we must discuss each molecule individually.

Mechanism of DM in Finding the Immunodominant Determinants During Antigen Processing

It has been well established that the MHC II groove is flexible and requires a bound peptide to maintain its shape. Without a peptide, the MHC II groove would close and becomes inefficient in binding peptides (58–60). Thus, newly synthesized MHC II molecules bind to a domain of the Class II invariant chain (CLIP) that serves two functions; a) protects the groove from binding to peptide in the ER (61), and b) acts as a place-keeper, while another domain of Ii guides the complex to the specialized vesicular compartments filled with pathogen-derived antigenic peptides, MIIC. Within MIIC, DM is necessary to first dissociate CLIP to form a peptide-receptive conformation that can quickly scan unfolded exogenous proteins to find its suitable determinant (62). DM does this job by effectively dissociating any peptide sequences that do not fill in the pockets of the MHC II groove. Only when a sequence of antigenic determinant that would fit in the MHC II groove leading to formation of a compact folded conformation, the complex becomes resistant to DM-mediated dissociation (*DM-resistant*). Next, the proteases would trim the MHC II bound determinant. The proteases also cut the antigenic determinants that do not fit the groove, hence are susceptible to DM-mediated dissociation (*DM-sensitive*) and are dislodged by DM (63–71). The solution of the crystal structure of the DM/DR complex (72) using DR1/peptide complexes that enforced an open DR1 groove, revealed that DM would bind the P1 pocket of HLA-DR molecules tightly if empty, and would remain bound until a P1 filling peptide would bind the groove and induce closing of the groove, and displacing DM (72–74). The above findings were complemented by the measured thermodynamics of peptide binding to DR1, indicating that a greater entropic penalty, versus a smaller penalty, was associated with structural rigidity rather than with the flexibility of the pMHC complexes (75). These findings suggested that an overall dynamic MHC II conformation in addition to P1 pocket occupancy, determines susceptibility to DM-mediated peptide exchange and provides a molecular mechanism for DM to efficiently target poorly fitting pMHC II complexes and editing them for more stable ones. Hence, in addition to the removal of CLIP, DM helps in shaping epitope selection and immunodominance by producing a higher abundance of those determinants (62).

Different Models on How DO Fine-Tunes Antigenic Epitope Selection

DO also contributes to the selection of immunodominant epitopes, although understanding the contributions of DO to

epitope selection has proven to be highly challenging (54–56, 76). In brief, our knowledge about DO can be distilled into two working hypotheses: (1) DO binds to DM to inhibit its activity, mainly removal of the CLIP peptide and, (2) DO differentially affects presentation of structurally diverse peptides and acts as a second accessory molecule working together with DM in fine tuning MHC II repertoire selection. Data in support of the former hypothesis mainly comes from studying over-expression of DO genes in cell lines, or dendritic cells (77, 78); Welsh, 2019 #13} and the recent mutagenesis and structural studies of DM/DO interactions (79, 80). The 3D structure of DM/DO showed that DO binds to DM at the same interface with which DM interacts with DR1 (74). Studies supporting the latter hypothesis came from biochemical (81) and biophysical studies demonstrating that DO only affected *association* kinetics of certain peptides to DR but, had no effect on the *dissociation* kinetics of any tested peptide/DR1 complexes (76, 82). The effects of DO on association kinetics directly correlated with peptide sensitivity to *DM-mediated dissociation*. DO reduced binding of peptides that formed *DM-sensitive* complexes with DR and enhanced the binding of peptides that formed *DM-resistant* complexes. In a nutshell, it was clearly shown that; i) DO works directly on DR1, and not by regulating the effect of DM, ii) DO can only bind the *peptide-receptive* MHC Class II, and iii) that this *peptide-receptive* conformation is generated by DM. Hence, authors proposed that DM and DO cooperate for a more effective epitope selection. Thus, in one model, DO would reduce presentation of *immunodominant epitopes*, whereas in the other, DO would increase the abundance of immunodominant epitopes.

Speculations for Future Research

The question of the potential contributions of DO and DM to memory CD4 T cell development is of most interest and is discussed below. A few characteristics of DO hint to its possible link to CD4 memory differentiation. First, DO is mainly expressed in B cells (81, 83, 84) and it enhances the presentation of immunodominant epitopes (56, 76). Next, it has been documented that successful entry of B cells into the germinal center (GC) requires high expression levels of pMHC (85–89). B cells enter GC and interact with CD4 T cells in search of proper signaling for affinity maturation. It is conceivable that CD4 T cells also receive signals from GC B cells for their own differentiation into resting memory T cells. One might say if high levels of pMHC equip B cells for entry into GC, how could B cells signal T cells to differentiate into resting memory, as this process requires suboptimal densities of pMHC presentation. An answer worth considering is that once B cells enter GC, their expression levels of DO and DM decreases, leading to a reduced level of pMHC II expression (90–92). As such, those GC B cells can interact with Ag-specific CD4 T cells in the Light Zone (LZ), selecting them to become memory precursor cells. In support of this argument, in an elegant study, Kim et al. have documented that memory CD4 T cells bear high affinity TCR for pMHC II (27), hence memory CD4 T cells are selected based on TCR affinity. One may predict that alterations in this controlled entry into the GC reaction could lead to faulty CD4 T cell memory development and possibly the development of increased autoreactivity.

Since biology tends to repeat itself, it would be interesting to compare the effects of pMHC numbers on APCs and their effects on CD8 memory T cell development. While as far as we know no studies has made such data available, in an exciting new study authors reported that in the absence of B cells CD8 T Cell memory formation was compromised, while CD8 effector function was enhanced. One might speculate that since CD4 T cells are essential for CD8 memory T cell development (93), perhaps their contributions to CD8 memory is mediated indirectly *via* CD4 memory T cells.

Future experimental evidence is needed to clarify the proposed relationship of these MHC II accessory molecules to the development and maintenance of CD4 memory T cells, and hopefully this review would prompt new research on the qualitative and quantitative antigen presentation on CD8 memory T cell development.

AUTHOR CONTRIBUTIONS

All authors listed have made a substantial, direct, and intellectual contribution to the work and approved it for publication.

FUNDING

Supported by grants from NIAID, R01AI063764, R21AI101987, and R01AI120634, to SS-N.

REFERENCES

1. Murphy K, Weaver C. *Janeway's Immunobiology*. New York & London: Garland Science (2016).
2. Itano AA, McSorley SJ, Reinhardt RL, Ehst BD, Ingulli E, Rudensky AY, et al. Distinct Dendritic Cell Populations Sequentially Present Antigen to CD4 T Cells and Stimulate Different Aspects of Cell-Mediated Immunity. *Immunity* (2003) 19:47–57. doi: 10.1016/S1074-7613(03)00175-4
3. Sallusto F, Cella M, Danieli C, Lanzavecchia A. Dendritic Cells Use Macropinocytosis and the Mannose Receptor to Concentrate Macromolecules in the Major Histocompatibility Complex Class II Compartment: Downregulation by Cytokines and Bacterial Products. *J Exp Med* (1995) 182:389–400. doi: 10.1084/jem.182.2.389
4. Lutz MB, Schuler G. Immature, Semi-Mature and Fully Mature Dendritic Cells: Which Signals Induce Tolerance or Immunity? *Trends Immunol* (2002) 23:445–9. doi: 10.1016/S1471-4906(02)02281-0
5. Chudnovskiy A, Pasqual G, Victora GD. Studying Interactions Between Dendritic Cells and T Cells In Vivo. *Curr Opin Immunol* (2019) 58:24–30. doi: 10.1016/j.coi.2019.02.002
6. West MA, Wallin RP, Matthews SP, Svensson HG, Zaru R, Ljunggren HG, et al. Enhanced Dendritic Cell Antigen Capture *Via* Toll-Like Receptor-Induced Actin Remodeling. *Science* (2004) 305:1153–7. doi: 10.1126/science.1099153
7. Zammit DJ, Lefrancois L. Dendritic Cell-T Cell Interactions in the Generation and Maintenance of CD8 T Cell Memory. *Microbes Infect* (2006) 8:1108–15. doi: 10.1016/j.micinf.2005.12.002

8. Zammit DJ, Cauley LS, Pham QM, Lefrancois L. Dendritic Cells Maximize the Memory CD8 T Cell Response to Infection. *Immunity* (2005) 22:561–70. doi: 10.1016/j.immuni.2005.03.005
9. Enamorado M, Khouili SC, Iborra S, Sancho D. Genealogy, Dendritic Cell Priming, and Differentiation of Tissue-Resident Memory Cd8(+) T Cells. *Front Immunol* (2018) 9:1751. doi: 10.3389/fimmu.2018.01751
10. Yu B, Zhang K, Milner JJ, Toma C, Chen R, Scott-Browne JP, et al. Epigenetic Landscapes Reveal Transcription Factors That Regulate CD8(+) T Cell Differentiation. *Nat Immunol* (2017) 18:573–82. doi: 10.1038/ni.3706
11. Johnnidis JB, Muroyama Y, Ngiow SF, Chen Z, Manne S, Cai Z, et al. Inhibitory Signaling Sustains a Distinct Early Memory CD8(+) T Cell Precursor That Is Resistant to DNA Damage. *Sci Immunol* (2021) 6:1–16. doi: 10.1126/sciimmunol.abe3702
12. Hildner K, Edelson BT, Purtha WE, Diamond M, Matsushita H, Kohyama M, et al. Batf3 Deficiency Reveals a Critical Role for CD8alpha+ Dendritic Cells in Cytotoxic T Cell Immunity. *Science* (2008) 322:1097–100. doi: 10.1126/science.1164206
13. Tussiwand R, Behnke MS, Kretzer NM, Grajales-Reyes GE, Murphy TL, Schreiber RD, et al. An Important Role for CD4(+) T Cells in Adaptive Immunity to Toxoplasma Gondii in Mice Lacking the Transcription Factor Batf3. *mSphere* (2020) 5:1–11. doi: 10.1128/mSphere.00634-20
14. Dalai SK, Mirshahidi S, Morrot A, Zavala F, Sadegh-Nasseri S. Anergy in Memory CD4+ T Cells is Induced by B Cells. *J Immunol* (2008) 181:3221–31. doi: 10.4049/jimmunol.181.5.3221
15. Adler LN, Jiang W, Bhamidipati K, Millican M, Macaubas C, Hung SC, et al. The Other Function: Class Ii-Restricted Antigen Presentation by B Cells. *Front Immunol* (2017) 8:319. doi: 10.3389/fimmu.2017.00319
16. Tarlinton D. B Cells Still Front and Centre in Immunology. *Nat Rev Immunol* (2019) 19:85–6. doi: 10.1038/s41577-018-0107-2
17. Chowdhury MG, Maeda K, Yasutomo K, Maekawa Y, Furukawa A, Azuma M, et al. Antigen-Specific B Cells Are Required for the Secondary Response of T Cells But Not for Their Priming. *Eur J Immunol* (1996) 26:1628–33. doi: 10.1002/eji.1830260733
18. Moulton VR, Farber DL. Committed to Memory: Lineage Choices for Activated T Cells. *Trends Immunol* (2006) 27:261–7. doi: 10.1016/j.it.2006.04.006
19. van Stipdonk MJ, Lemmens EE, Schoenberger SP. Naive CTLs Require a Single Brief Period of Antigenic Stimulation for Clonal Expansion and Differentiation. *Nat Immunol* (2001) 2:423–9. doi: 10.1038/87730
20. Hataye J, Moon JJ, Khoruts A, Reilly C, Jenkins MK. Naive and Memory CD4 + T Cell Survival Controlled by Clonal Abundance. *Science* (2006) 312:114–6. doi: 10.1126/science.1124228
21. Chang JT, Palanivel VR, Kinjyo I, Schambach F, Intlekofer AM, Banerjee A, et al. Asymmetric T Lymphocyte Division in the Initiation of Adaptive Immune Responses. *Science* (2007) 315:1687–91. doi: 10.1126/science.1139393
22. Pollizzi KN, Sun IH, Patel CH, Lo YC, Oh MH, Waickman AT, et al. Asymmetric Inheritance of mTORC1 Kinase Activity During Division Dictates CD8(+) T Cell Differentiation. *Nat Immunol* (2016) 17:704–11. doi: 10.1038/ni.3438
23. Stonier SW, Ma LJ, Castillo EF, Schluns KS. Dendritic Cells Drive Memory CD8 T-Cell Homeostasis *Via* IL-15 Transpresentation. *Blood* (2008) 112:4546–54. doi: 10.1182/blood-2008-05-156307
24. Mortier E, Advincula R, Kim L, Chmura S, Barrera J, Reizis B, et al. Macrophage- and Dendritic-Cell-Derived Interleukin-15 Receptor Alpha Supports Homeostasis of Distinct CD8+ T Cell Subsets. *Immunity* (2009) 31:811–22. doi: 10.1016/j.immuni.2009.09.017
25. Di Rosa F, Matzinger P. Long-Lasting CD8 T Cell Memory in the Absence of CD4 T Cells or B Cells. *J Exp Med* (1996) 183:2153-63.
26. Dalai SK, Khoruzhenko S, Drake CG, Jie CC, Sadegh-Nasseri S. Resolution o Infection Promotes a State of Dormancy and Long Survival of CD4 Memory T Cells. *Immunol Cell Biol* (2011) 89(8):870–81. doi: 10.1038/icb.2011.2
27. Kim C, Wilson T, Fischer KF, Williams MA. Sustained Interactions Between T Cell Receptors and Antigens Promote the Differentiation of CD4(+) Memory T Cells. *Immunity* (2013) 39:508–20. doi: 10.1016/j.immuni.2013.08.033
28. Williams MA, Ravkov EV, Bevan MJ. Rapid Culling of the CD4+ T Cell Repertoire in the Transition From Effector to Memory. *Immunity* (2008) 28:533–45. doi: 10.1016/j.immuni.2008.02.014
29. Rees W, Bender J, Teague TK, Kedl RM, Crawford F, Marrack P, et al. An Inverse Relationship Between T Cell Receptor Affinity and Antigen Dose During CD4(+) T Cell Responses In Vivo and *In Vitro*. *Proc Natl Acad Sci USA* (1999) 96:9781–6. doi: 10.1073/pnas.96.17.9781
30. Keck S, Schmaler M, Ganter S, Wyss L, Oberle S, Huseby ES, et al. Antigen Affinity and Antigen Dose Exert Distinct Influences on CD4 T-Cell Differentiation. *Proc Natl Acad Sci USA* (2014) 111:14852–7. doi: 10.1073/pnas.1403271111
31. Chen X, Jensen PE. MHC Class II Antigen Presentation and Immunological Abnormalities Due to Deficiency of MHC Class II and its Associated Genes. *Exp Mol Pathol* (2008) 85:40–4. doi: 10.1016/j.yexmp.2008.03.011
32. Linton PJ, Harbertson J, Bradley LM. A Critical Role for B Cells in the Development of Memory CD4 Cells. *J Immunol* (2000) 165:5558–65. doi: 10.4049/jimmunol.165.10.5558
33. Whitmire JK, Asano MS, Kaech SM, Sarkar S, Hannum LG, Shlomchik MJ, et al. Requirement of B Cells for Generating CD4+ T Cell Memory. *J Immunol* (2009) 182:1868–76. doi: 10.4049/jimmunol.0802501
34. Sadegh-Nasseri S, Dalai SK, Korb Ferris LC, Mirshahidi S. Suboptimal Engagement of the T-cell Receptor by a Variety of peptide-MHC Ligands Triggers T-cell Anergy. *Immunology* (2010) 129:1–7. doi: 10.1111/j.1365-2567.2009.03206.x
35. Misumi I, Whitmire JK. B Cell Depletion Curtails CD4+ T Cell Memory and Reduces Protection Against Disseminating Virus Infection. *J Immunol* (2014) 192:1597–608. doi: 10.4049/jimmunol.1302661
36. Dubois Cauwelaert N, Baldwin SL, Orr MT, Desbien AL, Gage E, Hofmeyer KA, et al. Antigen Presentation by B Cells Guides Programing of Memory CD4(+) T-Cell Responses to a TLR4-agonist Containing Vaccine in Mice. *Eur J Immunol* (2016) 46:2719–29. doi: 10.1002/eji.201646399
37. Pepper M, Jenkins MK. Origins of CD4(+) Effector and Central Memory T Cells. *Nat Immunol* (2011) 12:467–71. doi: 10.1038/ni.2038
38. Korb LC, Mirshahidi S, Ramyar K, Sadighi Akha AA, Sadegh-Nasseri S. Induction of T Cell Anergy by Low Numbers of Agonist Ligands. *J Immunol* (1999) 162:6401–9.
39. Ryan KR, Evavold BD. Persistence of Peptide-Induced CD4+ T Cell Anergy In Vitro. *J Exp Med* (1998) 187:89–96. doi: 10.1084/jem.187.1.89
40. Mirshahidi S, Ferris LC, Sadegh-Nasseri S. The Magnitude of TCR Engagement is a Critical Predictor of T Cell Anergy or Activation. *J Immunol* (2004) 172:5346–55. doi: 10.4049/jimmunol.172.9.5346
41. Ryan KR, McNeil LK, Dao C, Jensen PE, Evavold BD. Modification of Peptide Interaction With MHC Creates TCR Partial Agonists. *Cell Immunol* (2004) 227:70–8. doi: 10.1016/j.cellimm.2004.01.003
42. Ford ML, Evavold BD. Regulation of Polyclonal T Cell Responses by an MHC Anchor-Substituted Variant of Myelin Oligodendrocyte Glycoprotein 35-55. *J Immunol* (2003) 171:1247–54. doi: 10.4049/jimmunol.171.3.1247
43. Robertson JM, Evavold BD. Cutting Edge: Dueling TCRs: Peptide Antagonism of CD4+ T Cells With Dual Antigen Specificities. *J Immunol* (1999) 163:1750–4.
44. Mirshahidi S, Huang CT, Sadegh-Nasseri S. Anergy in Peripheral Memory CD4(+) T Cells Induced by Low Avidity Engagement of T Cell Receptor. *J Exp Med* (2001) 194:719–31. doi: 10.1084/jem.194.6.719
45. Garside P, Ingulli E, Merica RR, Johnson JG, Noelle RJ, Jenkins MK. Visualization of Specific B and T Lymphocyte Interactions in the Lymph Node. *Science* (1998) 281:96–9. doi: 10.1126/science.281.5373.96
46. Song N, Sengupta S, Khoruzhenko S, Welsh RA, Kim A, Kumar MR, et al. Multiple Genetic Programs Contribute to CD4 T Cell Memory Differentiation and Longevity by Maintaining T Cell Quiescence. *Cell Immunol* (2020) 357:104210. doi: 10.1016/j.cellimm.2020.104210
47. Tokoyoda K, Zehentmeier S, Hegazy AN, Albrecht I, Grun JR, Lohning M, et al. Professional Memory CD4+ T Lymphocytes Preferentially Reside and Rest in the Bone Marrow. *Immunity* (2009) 30:721–30. doi: 10.1016/j.immuni.2009.03.015
48. Prlic M, Bevan MJ. Immunology: A Metabolic Switch to Memory. *Nature* (2009) 460:41–2. doi: 10.1038/460041a
49. Pearce EL, Walsh MC, Cejas PJ, Harms GM, Shen H, Wang LS, et al. Enhancing CD8 T-Cell Memory by Modulating Fatty Acid Metabolism. *Nature* (2009) 460:103–7. doi: 10.1038/nature08097
50. Araki K, Turner AP, Shaffer VO, Gangappa S, Keller SA, Bachmann MF, et al. mTOR Regulates Memory CD8 T-Cell Differentiation. *Nature* (2009) 460:108–12. doi: 10.1038/nature08155

51. Waickman AT, Powell JD. mTOR, Metabolism, and the Regulation of T-cell Differentiation and Function. *Immunol Rev* (2012) 249:43–58. doi: 10.1111/j.1600-065X.2012.01152.x
52. Kim A, Sadegh-Nasseri S. Determinants of Immunodominance for CD4 T Cells. *Curr Opin Immunol* (2015) 34:9–15. doi: 10.1016/j.coi.2014.12.005
53. Kim C, Jay DC, Williams MA. Dynamic Functional Modulation of CD4+ T Cell Recall Responses is Dependent on the Inflammatory Environment of the Secondary Stimulus. *PLoS Pathog* (2014) 10:e1004137. doi: 10.1371/journal.ppat.1004137
54. Welsh RA, Song N, Foss CA, Boronina T, Cole RN, Sadegh-Nasseri S. Lack of the MHC Class II Chaperone H2-O Causes Susceptibility to Autoimmune Diseases. *PLoS Biol* (2020) 18:e3000590. doi: 10.1371/journal.pbio.3000590
55. Welsh R, Song N, Sadegh-Nasseri S. What to do With HLA-DO/H-2O Two Decades Later? *Immunogenetics* (2019) 71:189–96. doi: 10.1007/s00251-018-01097-3
56. Welsh RA, Sadegh-Nasseri S. The Love and Hate Relationship of HLA-DM/DO in the Selection of Immunodominant Epitopes. *Curr Opin Immunol* (2020) 64:117–23. doi: 10.1016/j.coi.2020.05.007
57. Sercarz EE, Lehmann PV, Ametani A, Benichou G, Miller A, Moudgil K. Dominance and Crypticity of T Cell Antigenic Determinants. *Annu Rev Immunol* (1993) 11:729–66. doi: 10.1146/annurev.iy.11.040193.003501
58. Natarajan SK, Assadi M, Sadegh-Nasseri S. Stable Peptide Binding to MHC Class II Molecule is Rapid and is Determined by a Receptive Conformation Shaped by Prior Association With Low Affinity Peptides. *J Immunol* (1999) 162:4030–6.
59. Sadegh-Nasseri S, Stern LJ, Wiley DC, Germain RN. MHC Class II Function Preserved by Low-Affinity Peptide Interactions Preceding Stable Binding. *Nature* (1994) 370:647–50. doi: 10.1038/370647a0
60. Rabinowitz JD, Vrljic M, Kasson PM, Liang MN, Busch R, Boniface JJ, et al. Formation of a Highly Peptide-Receptive State of Class II Mhc. *Immunity* (1998) 9:699–709. doi: 10.1016/S1074-7613(00)80667-6
61. Roche PA, Cresswell P. Invariant Chain Association With HLA-DR Molecules Inhibits Immunogenic Peptide Binding. *Nature* (1990) 345:615–8. doi: 10.1038/345615a0
62. Kim A, Hartman IZ, Poore B, Boronina T, Cole RN, Song N, et al. Divergent Paths for the Selection of Immunodominant Epitopes From Distinct Antigenic Sources. *Nat Commun* (2014) 5:5369. doi: 10.1038/ncomms6369
63. Chou CL, Sadegh-Nasseri S. Hla-DM Recognizes the Flexible Conformation of Major Histocompatibility Complex Class II. *J Exp Med* (2000) 192:1697–706. doi: 10.1084/jem.192.12.1697
64. Zarutskie JA, Busch R, Zavala-Ruiz Z, Rushe M, Mellins ED, Stern LJ. The Kinetic Basis of Peptide Exchange Catalysis by HLA-DM. *Proc Natl Acad Sci USA* (2001) 98:12450–5. doi: 10.1073/pnas.211439398
65. Belmares MP, Busch R, Mellins ED, McConnell HM. Formation of Two Peptide/MHC II Isomers is Catalyzed Differentially by HLA-DM. *Biochemistry* (2003) 42:838–47. doi: 10.1021/bi020466p
66. Pashine A, Busch R, Belmares MP, Munning JN, Doebele RC, Buckingham M, et al. Interaction of HLA-DR With an Acidic Face of HLA-DM Disrupts Sequence-Dependent Interactions With Peptides. *Immunity* (2003) 19:183–92. doi: 10.1016/S1074-7613(03)00200-0
67. Stratikos E, Wiley DC, Stern LJ. Enhanced Catalytic Action of HLA-DM on the Exchange of Peptides Lacking Backbone Hydrogen Bonds Between Their N-terminal Region and the MHC Class II Alpha-Chain. *J Immunol* (2004) 172:1109–17. doi: 10.4049/jimmunol.172.2.1109
68. Nicholson MJ, Moradi B, Seth NP, Xing X, Cuny GD, Stein RL, et al. Small Molecules That Enhance the Catalytic Efficiency of HLA-DM. *J Immunol* (2006) 176:4208–20. doi: 10.4049/jimmunol.176.7.4208
69. Chou CL, Mirshahidi S, Su KW, Kim A, Narayan K, Khoruzhenko S, et al. Short Peptide Sequences Mimic HLA-DM Functions. *Mol Immunol* (2008) 45:1935–43. doi: 10.1016/j.molimm.2007.10.033
70. Narayan K, Su KW, Chou CL, Khoruzhenko S, Sadegh-Nasseri S. Hla-DM Mediates Peptide Exchange by Interacting Transiently and Repeatedly With HLA-DR1. *Mol Immunol* (2009) 46:3157–62. doi: 10.1016/j.molimm.2009.07.001
71. Zhou Z, Callaway KA, Weber DA, Jensen PE. Cutting Edge: HLA-DM Functions Through a Mechanism That Does Not Require Specific Conserved Hydrogen Bonds in Class II MHC-Peptide Complexes. *J Immunol* (2009) 183:4187–91. doi: 10.4049/jimmunol.0901663
72. Anders AK, Call MJ, Schulze MS, Fowler KD, Schubert DA, Seth NP, et al. Hla-DM Captures Partially Empty HLA-DR Molecules for Catalyzed Removal of Peptide. *Nat Immunol* (2011) 12:54–61. doi: 10.1038/ni.1967
73. Painter CA, Negroni MP, Kellersberger KA, Zavala-Ruiz Z, Evans JE, Stern LJ. Conformational Lability in the Class II MHC 310 Helix and Adjacent Extended Strand Dictate HLA-DM Susceptibility and Peptide Exchange. *Proc Natl Acad Sci U S A* (2011) 108:19329–34. doi: 10.1073/pnas.1108074108
74. Pos W, Sethi DK, Call MJ, Schulze MS, Anders AK, Pyrdol J, et al. Crystal Structure of the HLA-DM-HLA-DR1 Complex Defines Mechanisms for Rapid Peptide Selection. *Cell* (2012) 151:1557–68. doi: 10.1016/j.cell.2012.11.025
75. Ferrante A, Templeton M, Hoffman M, Castellini MJ. The Thermodynamic Mechanism of Peptide-MHC Class II Complex Formation is a Determinant of Susceptibility to HLA-DM. *J Immunol* (2015) 195:1251–61. doi: 10.4049/jimmunol.1402367
76. Poluektov YO, Kim A, Hartman IZ, Sadegh-Nasseri S. Hla-DO as the Optimizer of Epitope Selection for MHC Class II Antigen Presentation. *PLoS One* (2013) 8:e71228. doi: 10.1371/journal.pone.0071228
77. Denzin LK, Cresswell P. Sibling Rivalry: Competition Between MHC Class II Family Members Inhibits Immunity. *Nat Struct Mol Biol* (2013) 20:7–10. doi: 10.1038/nsmb.2484
78. Nanaware PP, Jurewicz MM, Leszyk J, Shaffer SA, Stern LJ. Hla-DO Modulates the Diversity of the MHC-II Self-Peptidome. *Mol Cell Proteomics* (2018) 18(3):490–503 doi: 10.1074/mcp.RA118.000956
79. Yoon T, Macmillan H, Mortimer SE, Jiang W, Rinderknecht CH, Stern LJ, et al. Mapping the HLA-DO/HLA-DM Complex by FRET and Mutagenesis. *Proc Natl Acad Sci USA* (2012) 109:11276–81. doi: 10.1073/pnas.1113966109
80. Guce AI, Mortimer SE, Yoon T, Painter CA, Jiang W, Mellins ED, et al. Hla-DO Acts as a Substrate Mimic to Inhibit HLA-DM by a Competitive Mechanism. *Nat Struct Mol Biol* (2013) 20:90–8. doi: 10.1038/nsmb.2460
81. Kropshofer H, Vogt AB, Thery C, Armandola EA, Li BC, Moldenhauer G, et al. A Role for HLA-DO as a Co-Chaperone of HLA-DM in Peptide Loading of MHC Class II Molecules. *EMBO J* (1998) 17:2971–81. doi: 10.1093/emboj/17.11.2971
82. Poluektov YO, Kim A, Sadegh-Nasseri S. Hla-DO and Its Role in MHC Class II Antigen Presentation. *Front Immunol* (2013) 4:260. doi: 10.3389/fimmu.2013.00260
83. Liljedahl M, Winqvist O, Surh CD, Wong P, Ngo K, Teyton L, et al. Altered Antigen Presentation in Mice Lacking H2-O. *Immunity* (1998) 8:233–43. doi: 10.1016/S1074-7613(00)80475-6
84. Roucard C, Thomas C, Pasquier MA, Trowsdale J, Sotto JJ, Neefjes J, et al. In Vivo and *In Vitro* Modulation of HLA-DM and HLA-DO is Induced by B Lymphocyte Activation. *J Immunol* (2001) 167:6849–58. doi: 10.4049/jimmunol.167.12.6849
85. Yeh CH, Nojima T, Kuraoka M, Kelsoe G. Germinal Center Entry Not Selection of B Cells is Controlled by peptide-MHCII Complex Density. *Nat Commun* (2018) 9:928. doi: 10.1038/s41467-018-03382-x
86. Mesin L, Schiepers A, Ersching J, Barbulescu A, Cavazzoni CB, Angelini A, et al. Restricted Clonality and Limited Germinal Center Reentry Characterize Memory B Cell Reactivation by Boosting. *Cell* (2020) 180:92–106.e11. doi: 10.1016/j.cell.2019.11.032
87. Bannard O, McGowan SJ, Ersching J, Ishido S, Victora GD, Shin JS, et al. Ubiquitin-Mediated Fluctuations in MHC Class II Facilitate Efficient Germinal Center B Cell Responses. *J Exp Med* (2016) 213:993–1009. doi: 10.1084/jem.20151682
88. Shulman Z, Gitlin AD, Weinstein JS, Lainez B, Esplugues E, Flavell RA, et al. Dynamic Signaling by T Follicular Helper Cells During Germinal Center B Cell Selection. *Science* (2014) 345:1058–62. doi: 10.1126/science.1257861
89. Finney J, Kelsoe G. Ideal Vaccines: Balancing B Cell Recruitment and Differentiation. *Immunity* (2020) 53:473–5. doi: 10.1016/j.immuni.2020.08.008
90. Chalouni C, Banchereau J, Vogt AB, Pascual V, Davoust J. Human Germinal Center B Cells Differ From Naive and Memory B Cells by Their Aggregated MHC Class II-Rich Compartments Lacking HLA-do. *Int Immunol* (2003) 15:457–66. doi: 10.1093/intimm/dxg037
91. Glazier KS, Hake SB, Tobin HM, Chadburn A, Schattner EJ, Denzin LK. Germinal Center B Cells Regulate Their Capability to Present Antigen by

Modulation of HLA-DO. *J Exp Med* (2002) 195:1063–9. doi: 10.1084/jem.20012059
92. Chen X, Laur O, Kambayashi T, Li S, Bray RA, Weber DA, et al. Regulated Expression of Human Histocompatibility Leukocyte Antigen (HLA)-DO During Antigen-Dependent and Antigen-Independent Phases of B Cell Development. *J Exp Med* (2002) 195:1053–62. doi: 10.1084/jem.20012066
93. Janssen EM, Lemmens EE, Wolfe T, Christen U, von Herrath MG, Schoenberger SP. Cd4+ T Cells Are Required for Secondary Expansion and Memory in CD8+ T Lymphocytes. *Nature* (2003) 421:852–6. doi: 10.1038/nature01441

Conflict of Interest: The authors declare that the research was conducted in the absence of any commercial or financial relationships that could be construed as a potential conflict of interest.

frontiers in Immunology

ORIGINAL RESEARCH
published: 01 July 2021
doi: 10.3389/fimmu.2021.700755

Circulating Plasmacytoid and Conventional Dendritic Cells Are Numerically and Functionally Deficient in Patients With Scrub Typhus

Seung-Ji Kang[1†], Ki-Jeong Park[2†], Hye-Mi Jin[2†], Young-Nan Cho[2], Tae Hoon Oh[1], Seong Eun Kim[1], Uh Jin Kim[1], Kyung-Hwa Park[1], Sook-In Jung[1], Tae-Ok Kim[3], Hyo Shin Kim[4], Young-Goun Jo[4], Jae Kyun Ju[4], Seung-Jung Kee[5] and Yong-Wook Park[2*]*

[1] Department of Infectious Diseases, Chonnam National University Medical School and Hospital, Gwangju, South Korea,
[2] Department of Rheumatology, Chonnam National University Medical School and Hospital, Gwangju, South Korea,
[3] Department of Pulmonology, Chonnam National University Medical School and Hospital, Gwangju, South Korea,
[4] Department of Surgery, Chonnam National University Medical School and Hospital, Gwangju, South Korea,
[5] Department of Laboratory Medicine, Chonnam National University Medical School and Hospital, Gwangju, South Korea

Background: Dendritic cells (DCs) are specialized antigen-presenting cells known to bridge innate and adaptive immune reactions. However, the relationship between circulating DCs and *Orientia tsutsugamushi* infection is unclear. Therefore, this study aimed to examine the level and function of plasmacytoid DCs (pDCs) and conventional DCs (cDCs), two subsets of circulating DCs, in scrub typhus patients.

Methods: The study included 35 scrub typhus patients and 35 healthy controls (HCs). pDC and cDC levels, CD86 and CD274 expression, and cytokine levels were measured using flow cytometry.

Results: Circulating pDC and cDC levels were found to be significantly reduced in scrub typhus patients, which were correlated with disease severity. The patients displayed increased percentages of $CD86^+$ pDCs, $CD274^+$ pDCs, and $CD274^+$ cDCs in the peripheral blood. The alterations in the levels and surface phenotypes of pDCs and cDCs were recovered in the remission state. In addition, the production of interferon (IFN)-α and tumor necrosis factor (TNF)-α by circulating pDCs, and interleukin (IL)-12 and TNF-α by circulating cDCs was reduced in scrub typhus patients. Interestingly, our *in vitro* experiments showed that the percentages of $CD86^+$ pDCs, $CD274^+$ pDCs, and $CD274^+$ cDCs were increased in cultures treated with cytokines including IFN-γ, IL-12, and TNF-α.

Conclusions: This study demonstrates that circulating pDCs and cDCs are numerically deficient and functionally impaired in scrub typhus patients. In addition, alterations in the

OPEN ACCESS

Edited by:
Eddie A. James, Benaroya Research Institute, United States

Reviewed by:
Vincent C. Lombardi, University of Nevada, United States
Jonas J. W. Kuiper, University Medical Center Utrecht, Netherlands

***Correspondence:**
Seung-Jung Kee
sjkee@jnu.ac.kr
Yong-Wook Park
parkyw@jnu.ac.kr

[†]These authors have contributed equally to this work and share first authorship

Specialty section:
This article was submitted to Antigen Presenting Cell Biology, a section of the journal Frontiers in Immunology

Received: *26 April 2021*
Accepted: *21 June 2021*
Published: *01 July 2021*

Citation:
Kang S-J, Park K-J, Jin H-M, Cho Y-N, Oh TH, Kim SE, Kim UJ, Park K-H, Jung S-I, Kim T-O, Kim HS, Jo Y-G, Ju JK, Kee S-J and Park Y-W (2021) Circulating Plasmacytoid and Conventional Dendritic Cells Are Numerically and Functionally Deficient in Patients With Scrub Typhus. Front. Immunol. 12:700755. doi: 10.3389/fimmu.2021.700755

expression levels of surface phenotypes of pDCs and cDCs could be affected by pro-inflammatory cytokines.

Keywords: cytokine, Orientia tsutsugamushi, plasmacytoid dendritic cells, scrub typhus, conventional dendritic cells.

INTRODUCTION

Orientia tsutsugamushi is an obligate intracellular bacterium that causes scrub typhus, a febrile illness widespread across the world (1). The disease initially exhibits typical eschar, rash, and if not managed sufficiently, fatal conditions including acute kidney injury, liver failure, meningoencephalitis, and multiple organ failure can develop (2, 3). Approximately a million patients are diagnosed each year in a broad area from the Asian-Pacific region, the so-called "Tsutsugamushi Triangle", to Africa, Europe, and South America (1). Furthermore, it is spreading from rural to urban areas, which raises considerable concern in endemic countries (4).

Though the exact pathophysiology remains unclear, *O. tsutsugamushi* induces a range of dysregulated immune responses (5). The pathogen invades endothelial cells (ECs), monocytes, and dendritic cells (DCs), which are activated to secrete various cytokines and chemokines, provoking Th1 and Th2 dysregulation and the functional impairment of T lymphocytes (6–9). Recent investigations on unconventional immune cells such as mucosal-associated invariant T (MAIT) cells, natural killer (NK) cells, and natural killer T (NKT) cells suggest variations in frequency and function along with clinical relevance to the disease (10–12). Among these antigen-presenting cells (APCs), DCs are the most potent, central, and professional component that initiates and orchestrates immune reactions at the interface between innate and adaptive immunity (13). Currently, DCs can be classified into different subsets of conventional DCs (cDCs, formerly myeloid DC), plasmacytoid DCs (pDCs), monocyte-derived DCs (moDCs), and Langerhans cells based on their surface phenotype and functions (13–15). Of these different DCs, cDCs and pDCs are two main subsets of naturally occurring DCs that circulate in the peripheral blood. pDCs release type I interferon (IFN) against viruses, produce pro-inflammatory cytokines, and express major histocompatibility class (MHC) class II antigens and co-stimulatory molecules that activate numerous immune cells, including NK cells and NKT cells (16). cDCs are potent and specialized activators of T cells (13).

Several studies have described the relevance of DCs to scrub typhus. In one murine model, *O. tsutsugamushi* evaded autophagy and effectively invaded bone marrow-derived DCs, which showed impaired maturation and migration into lymphatic tissues (17). Another research study using human moDCs, a distinct DC population that matures during inflammation, reported that the pathogen replicated in moDCs, provoked the maturation of the cells, and triggered the secretion of cytokines, consequently stimulating $CD4^+$ T cells (18). However, a study on the levels and functions of pDCs and cDCs in scrub typhus has yet to be conducted. Therefore, this study aimed to examine the levels and functions of pDCs and cDCs in scrub typhus, evaluate their clinical relevance, and investigate their roles under inflammatory conditions.

MATERIALS AND METHODS

Study Subjects

The study cohort was comprised of 35 patients with scrub typhus (20 women and 15 men; mean age ± SD, 65.6 ± 15.4 years) and 35 healthy controls (HCs; 25 women and 10 men; mean age ± SD, 37.1 ± 7.5 years). The diagnosis of scrub typhus was performed by detecting *O. tsutsugamushi* antibodies in the patient's serum using a passive hemagglutination assay kit (Genedia Tsutsu PHA II Test Kit; GreenCross SangA, Yongin, Korea). A positive result was defined as a titer of ≥ 1:80 in a single serum sample or at least a 4-fold rise in antibody titer at a follow-up examination, as described previously (10–12, 19). According to the number of dysfunctional organs, scrub typhus was graded into severe (≥ 2 organ dysfunctions), moderate (one organ dysfunction), and mild disease (no organ dysfunction) as previously described (20). The definition of organ dysfunction was: (1) renal dysfunction, creatinine ≥ 2.5 mg/dL; (2) hepatic dysfunction, total bilirubin ≥ 2.5 mg/dL; (3) pulmonary dysfunction, bilateral pulmonary infiltration on chest X-rays with moderate to severe hypoxia (PaO_2/FiO_2 < 300 mmHg or PaO_2 < 60 mmHg or SpO_2 < 90%); (4) cardiovascular dysfunction, systolic blood pressure < 80 mmHg despite fluid resuscitation; and (5) central nervous system dysfunction, significantly altered sensorium with a Glasgow Coma Scale (GCS) score of eight out of 15. All HCs were recruited in the same area (Jeollanam-do, South Korea) as the patients resided. HCs had no severe comorbidity such as malignancy, chronic liver, pulmonary, renal diseases, autoimmune disease, or fever within 72 hours prior to enrollment.

Monoclonal Antibodies and Flow Cytometry

The following monoclonal antibodies (mAbs) and reagents were used in this study: fluorescein isothiocyanate (FITC)-conjugated Lineage Cocktail 1(CD3, CD14, CD16, CD19, CD20, CD56), phycoerythrin (PE)-conjugated anti-CD123, anti-CD86, and anti-CD274; allophycocyanin (APC)-conjugated anti-CD11c, anti-CD86, and anti-CD274; BV421-conjugated anti-HLA-DR; Alexa Fluor 647-conjugated anti-IFN-α; PE-conjugated anti-

interleukin-12 (anti-IL-12), PE-Cy7-conjugated anti-tumor necrosis factor-α (anti-TNF-α) mAb, and PE-conjugated mouse IgG isotype control (all from Becton Dickinson, San Diego, CA, USA). The cells were stained with combinations of the appropriate mAbs for 20 minutes at 4°C. The stained cells were analyzed on a Navios flow cytometer using Kaluza software (version 1.5a; Beckman Coulter, Brea, CA, USA).

Isolation of Peripheral Blood Mononuclear Cells (PBMCs) and Identification of pDCs and cDCs

Peripheral venous blood samples were collected in heparin-containing tubes, and PBMCs were isolated by density-gradient centrifugation using Ficoll-Paque Plus solution (Amersham Biosciences, Uppsala, Sweden). pDCs and cDCs were identified phenotypically as $Lin1^-HLA\text{-}DR^+CD123^+$ cells and $Lin1^-HLA\text{-}DR^{++}CD11c^+$ cells by flow cytometry, as previously described (21).

Intracellular Cytokine Staining

Freshly isolated PBMCs (1×10^6/well) were incubated in 1 mL of complete media, consisting of RPMI 1640, 2 mM $_L$-glutamine, 100 units/mL of penicillin, and 100 μg/mL of streptomycin, and supplemented with 10% fetal bovine serum (FBS) for 2 hours in the presence of 10 μg/mL CpG (ODN2336; InvivoGen, San Diego, CA, USA) or 10 μg/mL non-CpG ODN control (InvivoGen) to stimulate pDCs and in the presence of 10 ng/mL IFN-γ (PeproTech, London, UK) and 2 μg/mL lipopolysaccharide (LPS; Sigma-Aldrich, St. Louis, MO, USA) to stimulate cDCs. For intracellular cytokine staining, 1 μL of brefeldin A (GolgiPlug; BD Biosciences, San Diego, CA, USA) was added for each 1 mL of cell culture. After incubation for an additional 4 hours, the cells were stained with FITC-conjugated Lineage Cocktail 1, PE-conjugated anti-CD123, APC-conjugated anti-CD11c, and BV421-conjugated anti-HLA-DR mAbs for 20 minutes at 4°C, fixed in 4% paraformaldehyde for 15 minutes at room temperature, and permeabilized with Perm/Wash solution (BD Biosciences) for 10 minutes. The cells were then stained with Alexa Fluor 647-conjugated anti-IFN-α, PE-conjugated anti-IL-12, and PE-Cy7-conjugated anti-TNF-α mAbs for 30 minutes at 4°C and analyzed by flow cytometry.

Statistical Analysis

All comparisons of percentages, absolute numbers, cytokine levels, and expression levels of CD86 and CD274 in pDCs and cDCs were performed by analysis of covariance after adjusting for age and sex using the Bonferroni correction for multiple comparisons (ANCOVA). The Wilcoxon matched-pairs signed-rank test was used to compare changes in the cell numbers and expression of pDC and cDC phenotypes according to disease activity. To compare changes in surface phenotypes of pDCs and cDCs treated by pro-inflammatory cytokines, Kruskal-Wallis analysis with Dunn's *post hoc* test was used for multiple comparisons. *P*-values of less than 0.05 were considered statistically significant. Statistical analysis was performed and graphs were generated using SPSS version 26.0 software (SPSS, Chicago, IL, USA) and GraphPad Prism version 5.03 software (GraphPad Software, San Diego, CA, USA), respectively.

RESULTS

Subject Characteristics

The clinical and laboratory characteristics of 35 patients with scrub typhus are summarized in **Table 1**. According to disease severity based on the number of organs with dysfunction in these patients, 16 (45.7%), 12 (34.3%), and 7 (20.0%) had mild, moderate, and severe disease, respectively. Longitudinal monitoring was performed for 20 patients from the active state (before antibiotic therapy) to the remitted state (defined as resolution of all presenting symptoms after antibiotic therapy). Nine of those patients were available for measuring cell levels and surface phenotypes of circulating pDCs and cDCs.

TABLE 1 | Clinical and laboratory characteristics of 35 patients with scrub typhus.

Variables	Scrub typhus
Age, years, mean ± SD	65.6 ± 15.4
Male/female, n	15/20
Clinical variables, n (%)	
Fever	31 (88.6)
Rash	24 (68.6)
Eschar	28 (80.0)
Confusion	5 (14.3)
Severity of disease, n (%)	
Mild disease	16 (45.7)
Moderate disease	12 (34.3)
Severe disease	7 (20.0)
Organ dysfunction, n (%)	
Renal dysfunction	2 (5.71)
Hepatic dysfunction	4 (11.4)
CNS dysfunction	4 (11.4)
Respiratory dysfunction	14 (40.0)
Circulatory dysfunction	7 (20.0)
Comorbid conditions, n (%)	
Diabetes mellitus	8 (22.9)
Cardiovascular disease	3 (8.57)
Chronic kidney disease	1 (2.86)
Chronic hepatic disease	1 (2.86)
Chronic lung disease	0 (0.00)
Malignancy	2 (5.71)
Laboratory variables, mean ± SD	
Leukocyte count, cells/μL	7760 ± 3416
Lymphocyte count, cells/μL	2109 ± 1169
Hemoglobin level, g/dL	11.7 ± 1.7
Neutrophil count, cells/μL	5008 ± 3198
Platelet count, $\times 10^3$ cells/μL	173 ± 99
Total bilirubin level, mg/dL	0.9 ± 0.6
Total protein level, g/dL	6.0 ± 0.7
Albumin level, g/dL	2.9 ± 0.6
AST level, U/L	159 ± 178
ALT level, U/L	122 ± 200
Alkaline phosphatase level, U/L	192 ± 137
LDH level, U/L	908 ± 276
CRP level, mg/dL	10.4 ± 8.4
Time at hospital visit[a], days, mean ± SD	6.1 ± 3.3

ALT, alanine aminotransferase; AST, aspartate aminotransferase; CNS, central nervous system; CRP, C-reactive protein; LDH, lactate dehydrogenase; n, number; SD, standard deviation.
[a]*Time from symptom onset to antibiotic therapy.*

Reduced Numbers of pDCs and cDCs in Scrub Typhus Patients

The percentage and absolute numbers of pDCs and cDCs in the peripheral blood samples of 35 scrub typhus patients and 35 HCs were determined by flow cytometry. pDCs and cDCs were defined as $Lin1^-HLA\text{-}DR^+CD123^+$ cells and $Lin1^-HLA\text{-}DR^{++}CD11c^+$ cells, respectively (**Figures 1A, D**). The percentage of circulating pDCs and cDCs were significantly lower in the patients than in the HCs (for pDCs, median 0.01% *versus* 0.17%, $P < 0.0001$; for cDCs, median 0.01% *versus* 0.12%, $P = 0.001$; **Figures 1B, E**). The absolute numbers of pDCs and cDCs were calculated by multiplying the pDC and cDC fractions in the mononuclear cells gate (using a flow cytometer) by absolute PBMC count (per milliliter of peripheral blood) determined using a standard hemocytometer. Scrub typhus patients had significantly lower absolute numbers of pDCs and cDCs than the HCs (for pDCs, median 267 cells/mL *versus* 3744 cells/mL, $P = 0.007$; for cDCs, median 259 cells/mL *versus* 3170 cells/mL, $P < 0.0001$; **Figures 1C, F**).

Relationship Between pDC and cDC Levels and Clinical Parameters in Scrub Typhus Patients

To evaluate the clinical relevance of pDC and cDC levels in 35 patients with scrub typhus, we investigated the correlation between pDC and cDC percentages in the peripheral blood and clinical parameters by Spearman's rank correlation analysis. The correlation results revealed that both circulating pDC and cDC percentages were significantly correlated with albumin levels ($P = 0.003$ and $P = 0.019$, respectively) and disease severity ($P = 0.038$ and $P = 0.034$, respectively). However, our experiments showed no significant correlation between circulating pDC and cDC percentages and leukocyte count, lymphocyte count, hemoglobin level, neutrophil count, platelet count, total bilirubin level, total protein level, aspartate aminotransferase level, alanine aminotransferase level, alkaline phosphatase level, lactate dehydrogenase level, or C-reactive protein level (**Table 2**).

Activity of pDCs and cDCs in Scrub Typhus Patients

DCs can either induce or regulate immune reactions using specific molecules (14). Among those molecules, CD86 is known as a co-stimulatory marker that activates T cells, whereas CD274 is a co-inhibitory marker that restricts T cell function (14, 22). To examine the activity of both pDCs and cDCs, the expression levels of CD86 and CD274 molecules by each DC subset were compared between 22 scrub typhus patients and 16 HCs by flow cytometry. The percentages of both $CD86^+$ and $CD274^+$ pDCs were significantly higher in scrub typhus patients compared to the HCs (for $CD86^+$ pDCs, median 39.9% *versus* 11.3%, $P = 0.031$; and for $CD274^+$ pDCs, 13.6% *versus* 0.2%, $P = 0.001$; **Figures 2A, B**). The percentages of $CD274^+$ cDCs were significantly higher in scrub typhus patients than in the HCs (median 17.0% *versus* 2.9%, $P = 0.006$; **Figure 2D**).

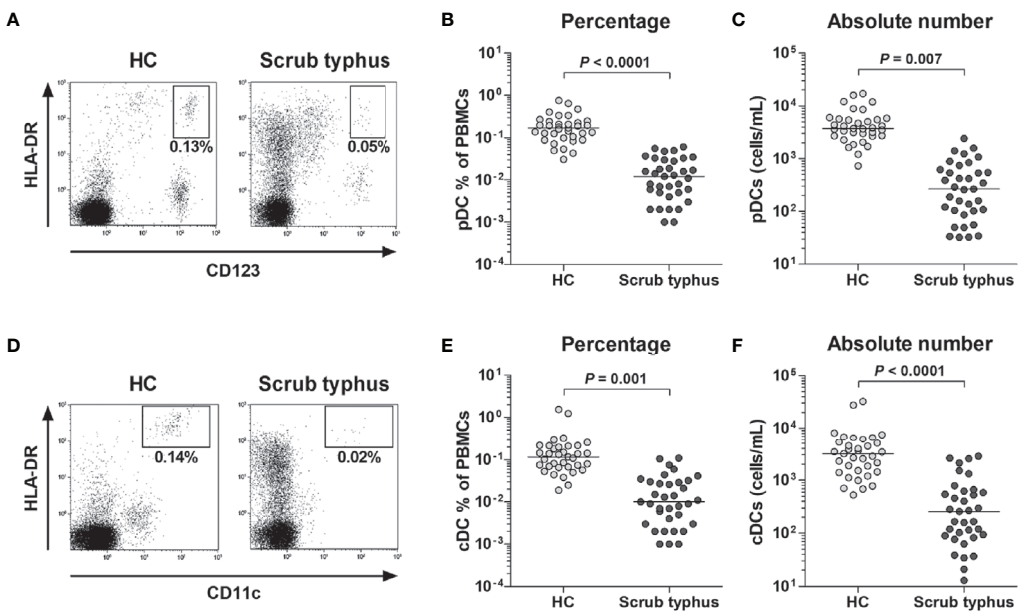

FIGURE 1 | Decreased numbers of circulating pDCs and cDCs in peripheral blood samples of scrub typhus patients. Freshly isolated PBMCs from 35 HCs and 35 scrub typhus patients were stained with APC-conjugated anti-CD11c, BV421-conjugated anti-HLA-DR, FITC-conjugated Lineage Cocktail 1, and PE-conjugated anti-CD123 mAbs and then analyzed by flow cytometry. The percentages of pDCs and cDCs were calculated using a large gate including lymphocytes and monocytes. **(A, D)** Representative percentages of pDCs and cDCs determined by flow cytometry. **(B, E)** Percentages of pDCs and cDCs in PBMCs. **(C, F)** Absolute numbers of pDCs and cDCs (per milliliter of blood). The symbols represent individual subjects and the horizontal lines are median values. *P* values were calculated by ANCOVA test.

TABLE 2 | Spearman's correlation coefficients for the percentages of pDCs and cDCs with respect to clinical and laboratory parameters in 35 patients with scrub typhus.

Variable	pDCs		cDCs	
	ρ	*P* value	ρ	*P* value
Age (years)	-0.215	0.215	-0.152	0.383
Leukocyte count (cells/μL)	0.030	0.863	-0.013	0.942
Lymphocyte count (cells/μL)	0.087	0.621	-0.045	0.796
Hemoglobin level (g/dL)	0.255	0.140	-0.038	0.827
Neutrophil count (cells/μL)	0.028	0.871	-0.044	0.802
Platelet count ($\times10^3$ cells/μL)	-0.106	0.545	-0.017	0.922
Total bilirubin level (mg/dL)	-0.136	0.459	-0.085	0.643
Total protein level (g/dL)	0.303	0.098	0.097	0.604
Albumin level (g/dL)	0.509	0.003*	0.411	0.019*
AST level (U/L)	-0.258	0.147	-0.087	0.632
ALT level (U/L)	0.089	0.623	0.280	0.114
Alkaline phosphatase level (U/L)	-0.146	0.418	-0.098	0.586
LDH level (U/L)	0.026	0.900	0.028	0.895
CRP level (mg/dL)	0.115	0.511	-0.171	0.326
Severity	-0.358	0.038*	-0.364	0.034*

ALT, alanine aminotransferase; AST, aspartate aminotransferase; CRP, C-reactive protein; LDH, lactate dehydrogenase; cDCs, conventional dendritic cells; pDCs, plasmacytoid dendritic cells; ρ, correlation coefficient.
**Indicates statistical significance.*

However, no significant difference was observed in $CD86^+$ cDC percentages between the patients and HCs (**Figure 2C**).

Impaired Cytokine Production in pDCs and cDCs From Scrub Typhus Patients

We next measured the levels of representative cytokines secreted by pDCs and cDCs from scrub typhus patients. The PBMCs from 15 scrub typhus patients and 15 HCs were incubated for 2 hours in the presence of CpG (for pDCs stimulation) or IFN-γ and LPS (for cDCs stimulation) and the expression levels of IFN-α, IL-12, and TNF-α in the pDC and cDC populations were examined at the single-cell level by intracellular flow cytometry (**Figures 3A, C**). The percentages of IFN-α^+ and TNF-α^+ pDCs were found to be significantly lower in scrub typhus patients than in HCs (for IFN-α^+ cells, median 1.0% *versus* 23.2%, $P = 0.001$; for TNF-α^+ cells, median 2.8% *versus* 22.0%, $P = 0.005$; **Figure 3B**). In addition, the percentages of IL-12^+ and TNF-α^+ cDCs were found to be significantly lower in scrub typhus patients compared to HCs (for IL-12^+ cells, median 9.3% *versus* 28.8%, $P = 0.003$; for TNF-α^+ cells, median 24.7% *versus* 49.0%, $P = 0.019$; **Figure 3D**).

Changes in Levels and Surface Phenotypes of Circulating pDCs and cDCs According to Disease Activity

Based on our observation that the percentage of pDCs and cDCs was reduced during the active state of scrub typhus but the expression of CD86 and CD274 on pDCs and CD274 on cDCs was increased, we investigated whether changes in the proportion and surface phenotypes of pDCs and cDCs were related to disease activity. We found that the percentage of both pDCs and cDCs was greater when the disease was in remission than when it was active (for pDCs, median 0.13% *versus* 0.01%, $P < 0.0001$; for cDCs, median 0.12% *versus* 0.01%, $P = 0.0002$; **Figures 4A, D**). In the surface phenotypes, the percentages of CD86-expressing pDCs, and CD274-expressing pDCs and cDCs were lower in the remission state than in the active state (for $CD86^+$ pDCs, median 44.3% *versus* 50.0%, $P = 0.02$; for $CD274^+$ pDCs, median 8.4% *versus* 25.0%, $P = 0.0024$; for $CD274^+$ cDCs, median 6.1% *versus* 20.0%, $P = 0.004$; **Figures 4B, C, F**). Conversely, the percentage of CD86-expressing cDCs was higher in the remission state compared to the active state (median 98.5% *versus* 88.4%, $P = 0.014$; **Figure 4E**).

Effect of Stimulation With Pro-Inflammatory Cytokine Cocktail on the Activation of pDCs and cDCs

To determine whether pDCs and cDCs could be activated by pro-inflammatory cytokines, PBMCs from six HCs were incubated for 24 hours in the presence or absence of cytokine inhibitors (i.e., blocking antibodies against a cocktail of IFN-γ, IL-12, and TNF-α) and then stimulated with a cytokine cocktail consisting of IFN-γ, IL-12, and TNF-α for 16 hours. Kruskal-Wallis analysis showed signficant differences among baseline, cytokine-treated, and blocking antibody-treated groups for the expression of CD86 ($P = 0.0135$) or CD274 ($P = 0.0023$) in pDCs and CD274 ($P = 0.0227$) in cDCs, except for the expression of CD86 ($P = 0.1443$) in cDCs. In addition, Dunn's *post hoc* test was used for correction for multiple comparisons to analyze the differences between baseline and cytokine-treated groups or between cytokine-treated and blocking antibody-treated groups. The percentages of $CD86^+$ pDCs were found to be significantly higher in cytokine-treated cultures compared to cytokine-untreated cultures (median 10.4% *versus* 2.3%, $P = 0.0067$), and then normalized to the untreated levels after treatment with blocking antibodies (median 10.4% *versus* 2.2, $P = 0.0198$; **Figure 5A**). The percentages of $CD274^+$ pDCs significantly increased in cytokine-treated cultures compared to cytokine-untreated cultures (median 11.8% *versus* 0.8%, $P = 0.0045$), and then normalized to the untreated levels after treatment with blocking antibodies (median 11.8% *versus* 0.01%, $P = 0.0015$; **Figure 5B**). The percentages of $CD274^+$ cDCs significantly increased in cytokine-treated cultures compared to cytokine-untreated cultures (median 32.8% *versus* 6.7%, $P = 0.0326$), and then normalized to the untreated levels after treatment with blocking antibodies (median 32.8% *versus* 3.2%, $P = 0.0102$; **Figure 5D**). However, the percentage of $CD86^+$ cDCs remained unchanged regardless of cytokine stimulation or cytokine blocking (**Figure 5C**).

DISCUSSION

To the best of our knowledge, this was the first study to examine the levels and functions of pDCs and cDCs and assess the clinical relevance in scrub typhus patients. The patients exhibited decreased percentages and absolute numbers of circulating pDCs and cDCs, which was correlated with disease severity, and they had increased percentages of $CD86^+$ pDCs, $CD274^+$ pDCs, and $CD274^+$ cDCs in the peripheral blood. These

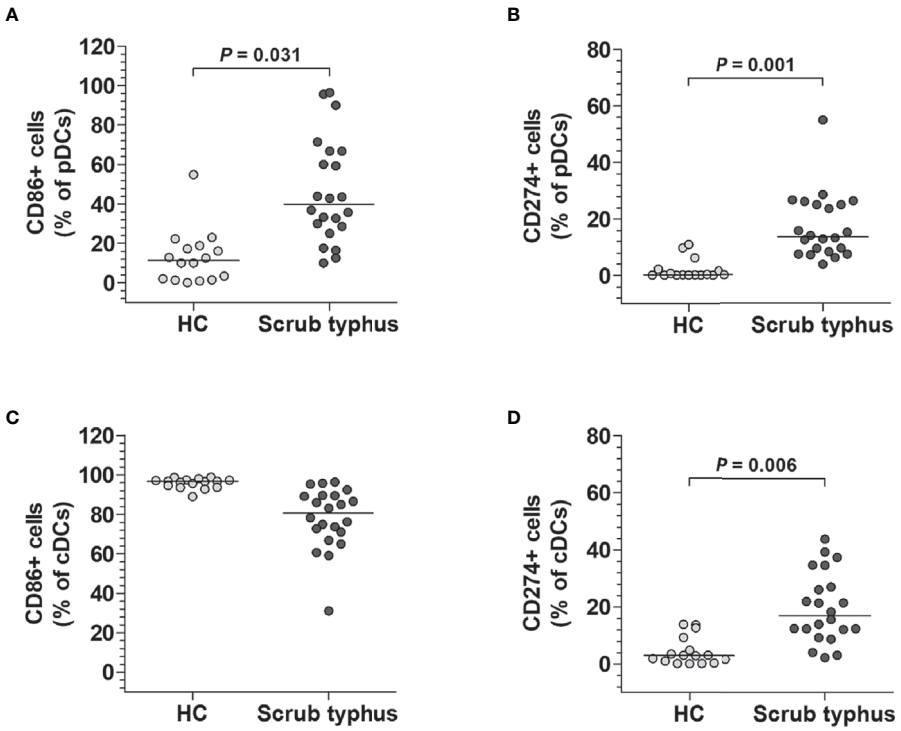

FIGURE 2 | Phenotypes of circulating pDCs and cDCs in scrub typhus patients. Freshly isolated PBMCs were stained with APC-conjugated anti-CD11c, anti-CD86, and anti-CD274; BV421-conjugated anti-HLA-DR; FITC-conjugated Lineage Cocktail 1; and PE-conjugated anti-CD86, anti-CD123, and anti-CD274 mAbs and then analyzed by flow cytometry. **(A, C)**, Percentages of CD86-expressing pDCs and cDCs. **(B, D)**, Percentages of CD274-expressing pDCs and cDCs. The data were obtained from 16 HCs and 22 scrub typhus patients. The symbols represent individual subjects and the horizontal lines are median values. *P* values were calculated by ANCOVA test.

alterations in the levels and surface phenotypes of pDCs and cDCs were recovered in the remission state. In addition, the production of IFN-α and TNF-α by circulating pDCs, and IL-12 and TNF-α by circulating cDCs was reduced in scrub typhus patients. Interestingly, our *in vitro* experiments showed that the activation of pDCs and cDCs may be affected by pro-inflammatory cytokines.

In this study, scrub typhus patients displayed dramatic drops in circulating pDC and cDC levels, and this trend reflected disease severity. Consistent with the present study, septic shock patients displayed reductions in both pDCs and cDCs, which were associated with the development of intensive care unit infection or fatal outcomes (23, 24). A model that used *Citrobacter rodentium*-treated pDC-depleted mice showed increased systemic inflammation, and polymicrobial sepsis-induced cDC-depleted mice demonstrated increased mortality, indicating that pDCs and cDCs play protective roles in bacterial infections (25, 26). Collectively, these results suggest that the depletion of both pDCs and cDCs is a feature of infection-induced immune dysregulation, leading to the propagation and aggravation of systemic inflammation in scrub typhus infection.

Our data revealed enhanced co-stimulatory and co-inhibitory marker expression in both pDCs and cDCs. The expression of a co-stimulatory marker, indicated by CD86, was increased on pDCs during scrub typhus infection, which reflected their T-cell co-stimulatory function, consistent with previous studies on human immunodeficiency virus (HIV) and hepatitis C virus (HCV) infections (27, 28). *In vitro* experiments reported that *O. tsutsugamushi*-infected murine bone marrow-derived DCs or human moDCs exhibited increased CD86 expression (17, 18). Of note, the $CD86^+$ cDCs were sustained at high levels regardless of the infection status, indicating that the T-cell priming function of cDCs was not solely dependent upon the scrub typhus infection. In contrast, the expression of a co-inhibitory marker, indicated by CD274, was higher in both pDCs and cDCs of scrub typhus patients than in those of HCs, in agreement with several studies on HIV and HCV infections (27, 28). Together, our findings suggest that both pDCs and cDCs expressed co-stimulatory and co-inhibitory molecules during scrub typhus infection, which could subsequently modulate the various immune reactions.

IFN-α, TNF-α, and IL-12 are well-known critical cytokines for controlling the intracellular growth of *O. tsutsugamushi* (5, 9, 29, 30). In the present study, the production of IFN-α and TNF-α by pDCs upon CpG stimulation was found to be diminished in scrub typhus patients. In addition, following IFN-γ/LPS stimulation, cDCs exhibited the reduced production of IL-12 and TNF-α in scrub typhus patients. Consistent with our study, the production of these cytokines by pDCs and cDCs was decreased after stimulation with TLR 7/8 ligands in HIV

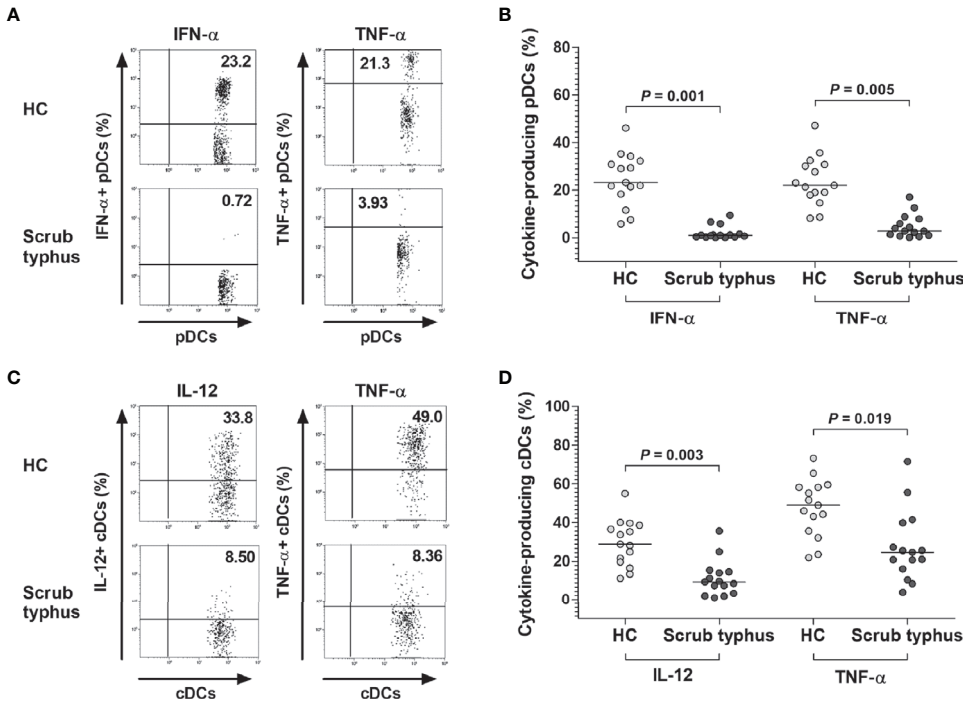

FIGURE 3 | Decreased expression of IFN-α, IL-12, and TNF-α in pDCs and cDCs of scrub typhus patients. Freshly isolated PBMCs (1×10^6/well) were incubated for 2 hours in the presence of CpG or the non-CpG ODN control for pDC stimulation, and in the presence of IFN-γ and LPS for cDC stimulation. **(A, C)** Representative IFN-α-, IL-12-, and TNF-α-expressing pDCs or cDCs as determined by flow cytometry. The data in **(B, D)** were obtained from 15 HCs and 15 patients with scrub typhus. The symbols represent individual subjects and the horizontal lines are median values. *P* values were calculated by ANCOVA test.

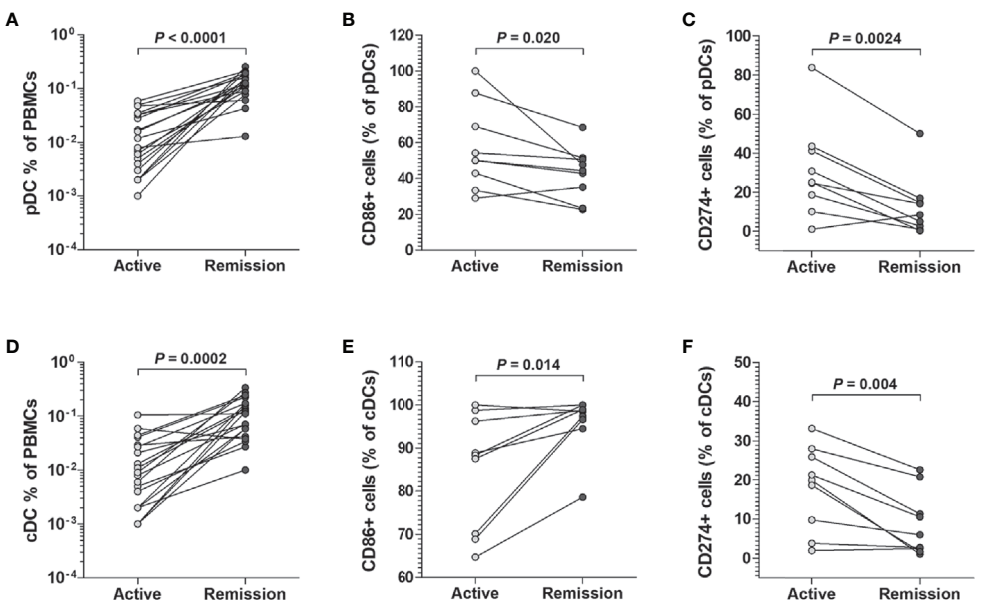

FIGURE 4 | Changes in cell percentages and surface phenotypes of circulating pDCs and cDCs from scrub typhus patients. The percentages of pDCs **(A)** and cDCs **(D)** in the peripheral blood of 20 scrub typhus patients during active and remission states were determined by flow cytometry. The percentages of CD86-expressing **(B, E)**, and CD274-expressing **(C, F)** pDCs and cDCs were determined by flow cytometry. The data in **(B C, E, F)** were obtained from nine patients with scrub typhus. The symbols represent individual subjects. *P* values were calculated by Wilcoxon matched-pairs signed-rank test.

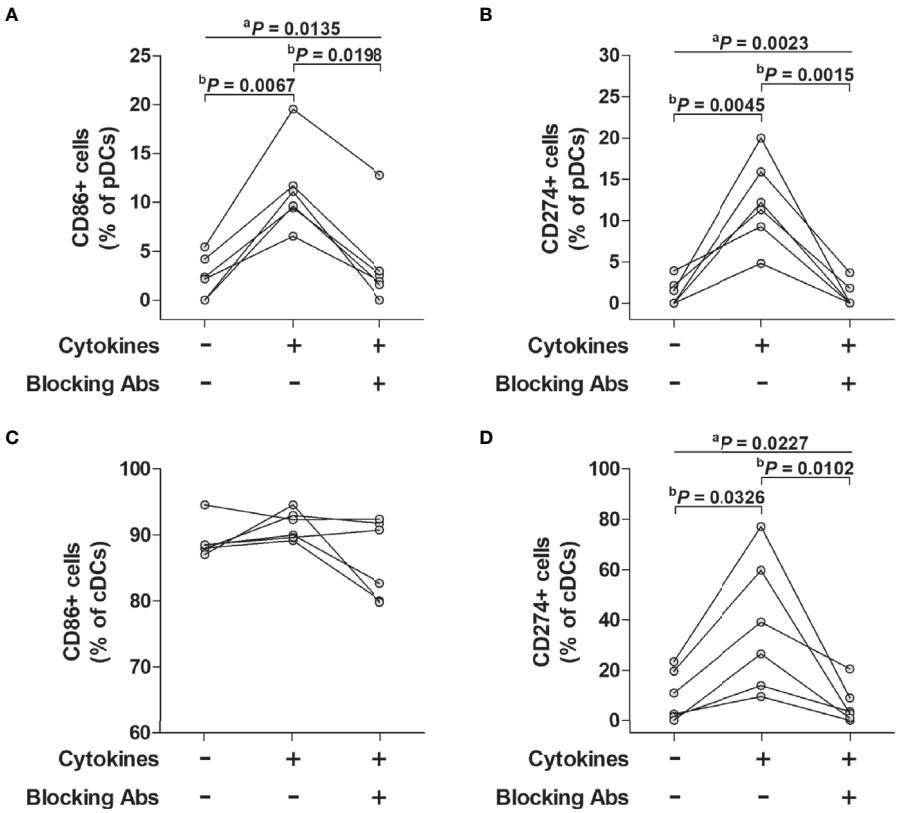

FIGURE 5 | Effect of a pro-inflammatory cytokine cocktail and its blocking antibody on surface phenotypes of pDCs and cDCs. Freshly isolated PBMCs were incubated for 24 hours in the presence or absence of cytokine inhibitors (i.e., blocking antibodies against a cocktail of IFN-α, IL-12, and TNF-α and then stimulated with the cytokine cocktail for 16 hours. The stimulated cells were stained with APC-conjugated anti-CD11c, anti-CD86, and anti-CD274; BV421-conjugated anti-HLA-DR; FITC-conjugated Lineage Cocktail 1; PE-conjugated anti-CD86, anti-CD123, and anti-CD274 mAbs and then analyzed by flow cytometry. **(A, C)** Percentage of CD86-expressing pDCs and cDCs. **(B, D)** Percentage of CD274-expressing pDCs and cDCs. The data were obtained from six HCs. ^{a}P values among three groups were calculated by Kruskal-Wallis test. ^{b}P values between two groups were calculated by Dunn's *post hoc* test.

infection (27, 31). In contrast, Chu et al. reported increased IL-12 and TNF-α secretion from *O. tsutsugamushi*-infected human moDCs (18). Interestingly, the TNF-α expression in monocytes varied from study to study according to the strains and dose of *O. tsutsugamushi*, the nature of the infected cell line or tissue, and animal or human models. For example, low-dose *O. tsutsugamushi* infection was found to induce the inhibition of a pro-inflammatory pathway as well as the up-regulation of an anti-inflammatory pathway, promoting bacterial replication, whereas high-dose infection reversed this response, enhancing bacterial clearance (5). One possible explanation for the decreased pDC and cDC cytokine function in scrub typhus patients is the delayed or impaired maturation of pDC and cDC during *O. tsutsugamushi* infection, suppressing immune function. Another explanation is the hypo-responsiveness of preactivated human DCs to *in vitro* restimulation.

Our data revealed that the proportion of circulating pDCs and cDCs were significantly correlated with disease severity in scrub typhus patients. Consistent with our data, previous studies showed that only blood cDC levels but not pDC levels were inversely correlated with the severity of dengue virus infection and severe fever with thrombocytopenia syndrome (32, 33). Compared to viral infections, however, little is known about the correlation between disease severity and the numbers of circulating pDCs or cDCs in other bacterial infections. Our novel observation revealed that the numerical depletion of both pDCs and cDCs was recovered during the remission state of the infection, with changes in co-stimulatory and co-inhibitory surface marker expression. The recovery of pDC and cDC numbers strongly supports our data reflecting the inversed correlation between those cell numbers and disease severity. Moreover, the recovery of circulating pDC numbers was accompanied by a decreased expression of CD86 and CD274, suggesting that the antigen presentation or tolerogenic function of pDCs might be limited during the acute phase of the infection. This phenomenon was also firmly supported by our data demonstrating that pDC numbers were positively correlated with albumin levels, known as a negative acute phase reactant marker. Similar to pDCs, the expression of CD274 on cDCs was also decreased in the remission state, but the expression of CD86 was increased. Unlike pDCs, the difference in the CD86 expression pattern in cDCs might be due to the constitutionally

high expression of CD86 in cDCs. Taken together, our findings indicate that DC activation and depletion reflects the severity of scrub typhus infection.

We hypothesized that a pro-inflammatory cytokine-rich environment could affect the expression of co-stimulatory and co-inhibitory markers in pDCs and cDCs during a scrub typhus infection. Our previous study reported the increased levels of cytokines such as IFN-γ, IL-12, and TNF-α in the early stage of a scrub typhus infection (11). After reproducing the pro-inflammatory milieu using a cytokine cocktail including IFN-γ, IL-12, and TNF-α, we observed the dynamics of CD86 and CD274 expression patterns in pDCs and cDCs, which was similar to our data in scrub typhus patients. These results suggest that the altered features of pDCs and cDCs might be secondary to the pro-inflammatory environment in the acute stage of the infection.

CpG-containing oligonucleotides (CpG ODNs) act on Toll-like receptor 9 (TLR9) that is expressed on B cells and pDCs to stimulate the innate immune system. Three types of stimulatory CpG ODNs have been identified: CpG-A, CpG-B, and CpG-C, which differ in their immune stimulatory activities. CpG-As are known to induce high production of type I IFN in pDCs but are not recognized in human B cells (34). Krug et al. have reported that CpG-A induced monocyte-derived DC-like phenotypes in PBMCs within 3 days but not such changes in purified monocytes (35). In the present study, however, CpG ODN 2336, a prototype of CpG-A, was used for culturing PBMCs for 2 hours, which was too short to induce significant changes in monocytes among PBMCs. Nonetheless, there are concerns that the cytokines that these cells produce may impact our DCs so in reality. It would have been optimal to sort the DCs prior to treatment.

There are some limitations in the present study. Based on recent advances through the emergence of powerful single-cell RNA sequencing and deep phenotyping technologies, originally three key DC subsets (cDC1, cDC2, and pDC) in peripheral blood have been expanded to six putative subsets (cDC1, cDC2-A, cDC2-B, $CD16^+$ DC, Axl^+ DC, and pDC) (36). In the present study, the antibody panels used for classification of circulating DCs comprised Lineage cocktail 1, CD123, HLA-DR, and CD11c, limiting our ability to distinguish among cDC subtypes or between pDCs and Axl^+ DCs. CD11c positivity has been known as the marker selecting cDCs. Circulating $Lin^-HLA\text{-}DR^{high}CD11c^+$ cells were defined as cDCs. By selecting CD11c, we may have excluded a subset of cDCs which are $CD11c^{low}$ and are typically about 10% of total cDCs. This subset was mostly presumed to be cDC1, according to human blood and tissue dendritic cell phenotypes described by Rhodes et al. (36). Furthermore, $CD16^+$ DC reported newly by Villani et al. also expressed CD11c (37). Some lineage marker panels included only CD3, CD19 and CD56, whereas ours additionally included CD14 and CD16. Thus, both classical ($CD14^{++}CD16^-$) and non-classical ($CD14^+CD16^{++}$) monocytes as well as T cells, B cells, and NK cells were negatively selected by our lineage panel. It is presumed that all monocyte subsets as well as $CD16^+$ DCs might have been excluded from $CD11c^+$ cDCs in the present study. Moreover, a number of computational flow cytometry tools such as FlowSOM, tSNE, oneSENSE, and ISOMAP have been developed to scale and represent high dimensional data of multiparametric flow cytometry (38). This approach could provide unbiased mapping and discovery of new cell phenotypes different from ones here identified using sequential manual gating. Further studies are warranted to answer this issue using unbiased gating strategy.

There are two methods for enumeration of absolute numbers of circulating DCs: dual-platform and single-platform. The dual-platform method is to calculate absolute numbers of circulating DCs by multiplying the percent amount of DCs in the mononuclear cells gate (using a flow cytometer) by absolute PBMC count determined using a standard hemocytometer. However, calculating absolute counts based on isolated PBMCs is not reliable, because PBMC isolations vary significantly from batch to batch. In contrast, the single-platform method, which is more accurate and easier than the former, is to enumerate absolute numbers of circulating DCs directly in a true count tube containing flow differential beads using a flow cytometer without hemocytometer. Unfortunately, the dual-platform method was used in the present study. The strategy used for quantification of absolute numbers is also to measure a fraction per volume (a relative metric).

In conclusion, this study firstly demonstrated that circulating pDCs and cDCs were numerically deficient and functionally impaired in scrub typhus patients. In addition, reduced cDC and pDC numbers reflected disease severity. We reported the novel finding that alterations in the expression levels of surface phenotypes of pDCs and cDCs could be affected by pro-inflammatory cytokines. These findings provide important insight into the dynamics of DC responses, which could present useful clues for future immunotherapy or vaccine development.

DATA AVAILABILITY STATEMENT

The original contributions presented in the study are included in the article/supplementary material. Further inquiries can be directed to the corresponding authors.

ETHICS STATEMENT

The study protocol was approved by the Institutional Review Board of Chonnam National University Hospital. Written informed consent was obtained from all participants in accordance with the Declaration of Helsinki.

AUTHOR CONTRIBUTIONS

S-JiK, K-JP, H-MJ, Y-NC, TO, SK, UK, K-HP, S-IJ, T-OK, HK, Y-GJ, JJ, S-JuK, and Y-WP designed this study, collected clinical information, analyzed raw data, performed statistical analysis, and contributed to writing of the paper. S-JiK, K-JP, H-MJ, and

Y-NC performed experiments. All authors contributed to the article and approved the submitted version.

FUNDING

This work was supported by the National Research Foundation of Korea (2019R1A2C1003238, 2019R1I1A1A01040762), the Korea Health Technology R&D Project through the Korea Health Industry Development Institute funded by the Ministry of Health & Welfare, Republic of Korea (HI20C0079) and the Chonnam National University Hospital Biomedical Research Institute (CRI18042-21).

ACKNOWLEDGMENTS

We thank all subjects who participated in this study. We would like to especially thank Ms. Hyun-Ju Jung, Jiwon Jeon, Sehyeon Ji, and Ah Young Kim for their support in facilitating patient recruitment at Chonnam National University Hospital, Gwangju, Republic of Korea.

REFERENCES

1. Xu G, Walker DH, Jupiter D, Melby PC, Arcari CM. A Review of the Global Epidemiology of Scrub Typhus. *PloS Negl Trop Dis* (2017) 11(11):e0006062. doi: 10.1371/journal.pntd.0006062
2. Taylor AJ, Paris DH, Newton PN. A Systematic Review of Mortality From Untreated Scrub Typhus (Orientia Tsutsugamushi). *PloS Negl Trop Dis* (2015) 9(8):e0003971. doi: 10.1371/journal.pntd.0003971
3. Huang MH, Juan YH, Chen YT. Prolonged Coma in a Scrub Typhus Patient. *Int J Infect Dis* (2018) 77:5–7. doi: 10.1016/j.ijid.2018.09.015
4. Park SW, Ha NY, Ryu B, Bang JH, Song H, Kim Y, et al. Urbanization of Scrub Typhus Disease in South Korea. *PloS Negl Trop Dis* (2015) 9(5): e0003814. doi: 10.1371/journal.pntd.0003814
5. Diaz FE, Abarca K, Kalergis AM. An Update on Host-Pathogen Interplay and Modulation of Immune Responses During Orientia Tsutsugamushi Infection. *Clin Microbiol Rev* (2018) 31(2):e00076–17. doi: 10.1128/CMR.00076-17
6. Moron CG, Popov VL, Feng HM, Wear D, Walker DH. Identification of the Target Cells of Orientia Tsutsugamushi in Human Cases of Scrub Typhus. *Mod Pathol* (2001) 14(8):752–9. doi: 10.1038/modpathol.3880385
7. Paris DH, Phetsouvanh R, Tanganuchitcharnchai A, Jones M, Jenjaroen K, Vongsouvath M, et al. Orientia Tsutsugamushi in Human Scrub Typhus Eschars Shows Tropism for Dendritic Cells and Monocytes Rather Than Endothelium. *PloS Negl Trop Dis* (2012) 6(1):e1466. doi: 10.1371/journal.pntd.0001466
8. Soong L. Dysregulated Th1 Immune and Vascular Responses in Scrub Typhus Pathogenesis. *J Immunol* (2018) 200(4):1233–40. doi: 10.4049/jimmunol.1701219
9. Min CK, Kim HI, Ha NY, Kim Y, Kwon EK, Yen NTH, et al. A Type I Interferon and IL-10 Induced by Orientia Tsutsugamushi Infection Suppresses Antigen-Specific T Cells and Their Memory Responses. *Front Immunol* (2018) 9:2022. doi: 10.3389/fimmu.2018.02022
10. Kang SJ, Jin HM, Won EJ, Cho YN, Jung HJ, Kwon YS, et al. Activation, Impaired Tumor Necrosis Factor-Alpha Production, and Deficiency of Circulating Mucosal-Associated Invariant T Cells in Patients With Scrub Typhus. *PloS Negl Trop Dis* (2016) 10(7):e0004832. doi: 10.1371/journal.pntd.0004832
11. Kang SJ, Jin HM, Cho YN, Kim SE, Kim UJ, Park KH, et al. Increased Level and Interferon-Gamma Production of Circulating Natural Killer Cells in Patients With Scrub Typhus. *PloS Negl Trop Dis* (2017) 11(7):e0005815. doi: 10.1371/journal.pntd.0005815
12. Kang SJ, Jin HM, Cho YN, Oh TH, Kim SE, Kim UJ, et al. Dysfunction of Circulating Natural Killer T Cells in Patients With Scrub Typhus. *J Infect Dis* (2018) 218(11):1813–21. doi: 10.1093/infdis/jiy402
13. Balan S, Saxena M, Bhardwaj N. Dendritic Cell Subsets and Locations. *Int Rev Cell Mol Biol* (2019) 348:1–68. doi: 10.1016/bs.ircmb.2019.07.004
14. Wculek SK, Cueto FJ, Mujal AM, Melero I, Krummel MF, Sancho D. Dendritic Cells in Cancer Immunology and Immunotherapy. *Nat Rev Immunol* (2020) 20(1):7–24. doi: 10.1038/s41577-019-0210-z
15. Bakdash G, Schreurs I, Schreibelt G, Tel J. Crosstalk Between Dendritic Cell Subsets and Implications for Dendritic Cell-Based Anticancer Immunotherapy. *Expert Rev Clin Immunol* (2014) 10(7):915–26. doi: 10.1586/1744666X.2014.912561
16. Swiecki M, Colonna M. The Multifaceted Biology of Plasmacytoid Dendritic Cells. *Nat Rev Immunol* (2015) 15(8):471–85. doi: 10.1038/nri3865
17. Choi JH, Cheong TC, Ha NY, Ko Y, Cho CH, Jeon JH, et al. Orientia Tsutsugamushi Subverts Dendritic Cell Functions by Escaping From Autophagy and Impairing Their Migration. *PloS Negl Trop Dis* (2013) 7(1): e1981. doi: 10.1371/journal.pntd.0001981
18. Chu H, Park SM, Cheon IS, Park MY, Shim BS, Gil BC, et al. Orientia Tsutsugamushi Infection Induces CD4+ T Cell Activation Via Human Dendritic Cell Activity. *J Microbiol Biotechnol* (2013) 23(8):1159–66. doi: 10.4014/jmb.1303.03019
19. Kim IS, Seong SY, Woo SG, Choi MS, Kang JS, Chang WH. Rapid Diagnosis of Scrub Typhus by a Passive Hemagglutination Assay Using Recombinant 56-Kilodalton Polypeptides. *J Clin Microbiol* (1993) 31(8):2057–60. doi: 10.1128/JCM.31.8.2057-2060.1993
20. Astrup E, Janardhanan J, Otterdal K, Ueland T, Prakash JA, Lekva T, et al. Cytokine Network in Scrub Typhus: High Levels of Interleukin-8 Are Associated With Disease Severity and Mortality. *PloS Negl Trop Dis* (2014) 8(2):e2648. doi: 10.1371/journal.pntd.0002648
21. Pacanowski J, Kahi S, Baillet M, Lebon P, Deveau C, Goujard C, et al. Reduced Blood CD123+ (Lymphoid) and CD11c+ (Myeloid) Dendritic Cell Numbers in Primary HIV-1 Infection. *Blood* (2001) 98(10):3016–21. doi: 10.1182/blood.v98.10.3016
22. Marin E, Cuturi MC, Moreau A. Tolerogenic Dendritic Cells in Solid Organ Transplantation: Where Do We Stand? *Front Immunol* (2018) 9:274. doi: 10.3389/fimmu.2018.00274
23. Grimaldi D, Louis S, Pene F, Sirgo G, Rousseau C, Claessens YE, et al. Profound and Persistent Decrease of Circulating Dendritic Cells Is Associated With ICU-Acquired Infection in Patients With Septic Shock. *Intensive Care Med* (2011) 37(9):1438–46. doi: 10.1007/s00134-011-2306-1
24. Guisset O, Dilhuydy MS, Thiebaut R, Lefevre J, Camou F, Sarrat A, et al. Decrease in Circulating Dendritic Cells Predicts Fatal Outcome in Septic Shock. *Intensive Care Med* (2007) 33(1):148–52. doi: 10.1007/s00134-006-0436-7
25. Rahman T, Brown AS, Hartland EL, van Driel IR, Fung KY. Plasmacytoid Dendritic Cells Provide Protection Against Bacterial-Induced Colitis. *Front Immunol* (2019) 10:608. doi: 10.3389/fimmu.2019.00608
26. Scumpia PO, McAuliffe PF, O'Malley KA, Ungaro R, Uchida T, Matsumoto T, et al. CD11c+ Dendritic Cells Are Required for Survival in Murine Polymicrobial Sepsis. *J Immunol* (2005) 175(5):3282–6. doi: 10.4049/jimmunol.175.5.3282
27. Cavaleiro R, Baptista AP, Soares RS, Tendeiro R, Foxall RB, Gomes P, et al. Major Depletion of Plasmacytoid Dendritic Cells in HIV-2 Infection, an Attenuated Form of HIV Disease. *PloS Pathog* (2009) 5(11):e1000667. doi: 10.1371/journal.ppat.1000667
28. Shen T, Chen X, Chen Y, Xu Q, Lu F, Liu S. Increased PD-L1 Expression and PD-L1/CD86 Ratio on Dendritic Cells Were Associated With Impaired Dendritic Cells Function in HCV Infection. *J Med Virol* (2010) 82(7):1152–9. doi: 10.1002/jmv.21809
29. Geng P, Jerrells TR. The Role of Tumor Necrosis Factor in Host Defense Against Scrub Typhus Rickettsiae. I. Inhibition of Growth of Rickettsia Tsutsugamushi, Karp Strain, in Cultured Murine Embryonic Cells and Macrophages by Recombinant Tumor Necrosis Factor-Alpha. *Microbiol Immunol* (1994) 38(9):703–11. doi: 10.1111/j.1348-0421.1994.tb01845.x
30. Jerrells TR, Geng P. The Role of Tumor Necrosis Factor in Host Defense Against Scrub Typhus Rickettsiae. II. Differential Induction of Tumor Necrosis Factor-

Alpha Production by Rickettsia Tsutsugamushi and Rickettsia Conorii. *Microbiol Immunol* (1994) 38(9):713–9. doi: 10.1111/j.1348-0421.1994.tb01846.x
31. Huang J, Yang Y, Al-Mozaini M, Burke PS, Beamon J, Carrington MF, et al. Dendritic Cell Dysfunction During Primary HIV-1 Infection. *J Infect Dis* (2011) 204(10):1557–62. doi: 10.1093/infdis/jir616
32. Lertjuthaporn S, Khowawisetsut L, Keawvichit R, Polsrila K, Chuansumrit A, Chokephaibulkit K, et al. Identification of Changes in Dendritic Cell Subsets That Correlate With Disease Severity in Dengue Infection. *PloS One* (2018) 13 (7):e0200564. doi: 10.1371/journal.pone.0200564
33. Zhang W, Li M, Xiong S, Wang H, Xiong Y, Li M, et al. Decreased Myeloid Dendritic Cells Indicate a Poor Prognosis in Patients With Severe Fever With Thrombocytopenia Syndrome. *Int J Infect Dis* (2017) 54:113–20. doi: 10.1016/j.ijid.2016.11.418
34. Hartmann G, Battiany J, Poeck H, Wagner M, Kerkmann M, Lubenow N, et al. Rational Design of New CpG Oligonucleotides That Combine B Cell Activation With High IFN-Alpha Induction in Plasmacytoid Dendritic Cells. *Eur J Immunol* (2003) 33(6):1633–41. doi: 10.1002/eji.200323813
35. Krug A, Rothenfusser S, Selinger S, Bock C, Kerkmann M, Battiany J, et al. CpG-A Oligonucleotides Induce a Monocyte-Derived Dendritic Cell-Like Phenotype That Preferentially Activates CD8 T Cells. *J Immunol* (2003) 170 (7):3468–77. doi: 10.4049/jimmunol.170.7.3468
36. Rhodes JW, Tong O, Harman AN, Turville SG. Human Dendritic Cell Subsets, Ontogeny, and Impact on HIV Infection. *Front Immunol* (2019) 10:1088. doi: 10.3389/fimmu.2019.01088
37. Villani AC, Satija R, Reynolds G, Sarkizova S, Shekhar K, Fletcher J, et al. Single-Cell RNA-Seq Reveals New Types of Human Blood Dendritic Cells, Monocytes, and Progenitors. *Science* (2017) 356(6335):eaah4573. doi: 10.1126/science.aah4573
38. Collin M, Bigley V. Human Dendritic Cell Subsets: An Update. *Immunology* (2018) 154(1):3–20. doi: 10.1111/imm.12888

Conflict of Interest: The authors declare that the research was conducted in the absence of any commercial or financial relationships that could be construed as a potential conflict of interest.

frontiers in Immunology

ORIGINAL RESEARCH
published: 23 December 2021
doi: 10.3389/fimmu.2021.736936

Palladium-Induced Temporal Internalization of MHC Class I Contributes to T Cell-Mediated Antigenicity

Koyu Ito[1]*, *Takayuki Kanaseki*[2], *Serina Tokita*[2,3], *Toshihiko Torigoe*[2], *Noriyasu Hirasawa*[4] *and Kouetsu Ogasawara*[1]*

[1] Department of Immunobiology, Institute of Development Aging and Cancer, Tohoku University, Sendai, Japan, [2] Department of Pathology, Sapporo Medical University School of Medicine, Sapporo, Japan, [3] Academic Center, Sapporo Dohto Hospital, Sapporo, Japan, [4] Laboratory of Pharmacotherapy of Life-Style Related Diseases, Graduate School of Pharmaceutical Sciences, Tohoku University, Sendai, Japan

OPEN ACCESS

Edited by:
Eddie A. James,
Benaroya Research Institute,
United States

Reviewed by:
Naoki Sato,
Tohoku University, Japan
Claudia Kitzmueller,
Medical University of Vienna, Austria
Shaodong Dai,
University of Colorado Anschutz Medical Campus, United States
Sidonia Barbara Guiomar Eckle,
Peter Doherty Institute for Infection and Immunity, Australia

***Correspondence:**
Koyu Ito
koyu.ito.c6@tohoku.ac.jp
Kouetsu Ogasawara
immunobiology@grp.tohoku.ac.jp

Specialty section:
This article was submitted to Antigen Presenting Cell Biology, a section of the journal Frontiers in Immunology

Received: 06 July 2021
Accepted: 08 December 2021
Published: 23 December 2021

Citation:
Ito K, Kanaseki T, Tokita S, Torigoe T, Hirasawa N and Ogasawara K (2021) Palladium-Induced Temporal Internalization of MHC Class I Contributes to T Cell-Mediated Antigenicity. Front. Immunol. 12:736936. doi: 10.3389/fimmu.2021.736936

Palladium (Pd) is a widely used metal and extremely important biomaterial for the reconstruction of occlusions during dental restorations. However, metallic biomaterials can cause serious allergic reactions, such as Pd-related oral mucositis seen in dentistry. Metal allergy is categorized as a type IV allergy and we demonstrated that CD8 T cells play an important role in Pd allergy previously. As TCR of CD8 T cells recognizes MHC class I/peptide complex, the antigen specificity to this complex seems to be generated during Pd allergy. However, it remains unknown if Pd affects the MHC class I/peptide complex. In this study, we investigated the behavior of the MHC class I/peptide complex in response to Pd treatment. We found that $PdCl_2$ treatment altered peptide presentation on MHC class I and that co-culture with Pd-treated DC2.4 cells induced activation of Pd-responsive TCR-expressing T cell line. Furthermore, $PdCl_2$ treatment induced temporal MHC class I internalization and inhibition of membrane movement suppressed Pd-induced T cell-mediated antigenicity. These data suggest that Pd-induced MHC class I internalization is critical for generation of antigenicity through a mechanism including differential peptide loading on MHC class I, which results in Pd allergy.

Keywords: metal allergy, palladium, MHC class I internalization, alternative peptide presentation, dental biomaterials

INTRODUCTION

Biomaterials contribute widely to the development of human therapeutics (1–3). Metals, in particular, are broadly useful in many fields due to their hardness, strength, durability, and workability. Palladium (Pd) is commonly used, including in dentistry as an extremely important metallic biomaterial for the reconstruction of occlusions. However, metallic biomaterials can cause allergy, and in dentistry Pd-related oral mucositis is a serious problem. In addition, the allergic response can also result in skin conditions, such as palmoplantar pustulosis (4, 5).

Metal allergy is categorized as a type IV allergy, which is mediated by T cells (6). An inherent conflict exists in T cell-mediated immune responses between the induction of tolerance and the activation of appropriate immune responses (7). Classically, T cell-mediated allergic reactions against foreign substances have been considered a process to eliminate exogeneous antigens phagocytosed and presented by antigen-presenting cells (APCs) (8). However, recent reports of the two major types of T cell-mediated delayed type hypersensitivity, metal allergy and drug hypersensitivity, suggest that antigenicity is acquired through various mechanisms, and the target of the resulting allergic reaction is not always exogeneous antigens phagocytosed by APCs (9–11). Classical understanding of metal or drug hypersensitivity was based on the concept that exogenous substances form haptenated antigens with self-proteins (10, 11). In this concept, haptenated antigens phagocytosed by APCs are cross-presented by MHC class I after undergoing processing (12). In other words, the peptide loading onto the MHC class I is derived from haptenated antigens. However, this hapten theory does not address all mechanisms of antigen induction for metals and drugs. Some metals, like beryllium, cobalt and nickel, can bind directly to MHC molecules and some drugs, such as abacavir, cause adverse effects related to the HLA haplotype of an individual (6, 9, 13–17). These direct associations between MHC molecules and metals/drugs result in altered antigenicity through conformational changes or peptide exchange, which in turn enable escape from tolerance and induction of antigen-specific T cell-immune responses.

Although it has been reported that both CD4 and CD8 T cells are responsible for the induction of Pd allergy (18–21), our previous study showed that repeated adoptive transfer of lymph node cells from Pd-treated mice skews the CD4/CD8 T cell-balance toward CD8 T cells. Thus, this suggests CD8 T cells play a more important role in Pd allergy than do CD4 T cells (22). Moreover, the TCR repertoires of CD8 T cells from Pd-treated mice were significantly biased, suggesting that the activation of CD8 T cells is antigen specific (21). Considering that TCR of CD8 T cells recognizes MHC class I in complex with peptide, the antigen specificity of CD8 T cells seems to be generated through events related to this complex. However, the detailed mechanisms underlying the generation of antigenicity in Pd allergy are not well understood. To this end, we investigated the behavior of the MHC class I/peptide complex in response to Pd treatment.

MATERIALS AND METHODS

Ethics Statement

Mice were maintained under specific pathogen-free conditions, and all procedures were performed according to the protocols approved by the Institutional Committee for Use and Care of Laboratory Animals of Tohoku University, which was granted by Tohoku University Ethics Review Board (2019AcA-003). For collection of tissue samples, mice were sacrificed by cervical dislocation, and all efforts were made to minimize suffering.

Mice

C57BL/6 mice (6 to 8-week-old females) were purchased from CLEA Japan. OT-I mice were purchased from Jackson Laboratories.

Induction of Palladium Allergy

Palladium allergy was induced as described previously (23). In brief, mice were injected twice into both sides of the groin with 250 µl PBS containing 10 mM $PdCl_2$ and 10 µg/ml LPS at an interval of seven days. Seven days after the 2nd injection, mice were challenged by intradermal injection of 25 µl of 10 mM $PdCl_2$ in PBS into both the left and right footpads.

Generation of Pd-Responsive T Cells

Pd-responsive T cells were generated as described in a previous report (24). In brief, Pd allergy was induced in mice as described above. Twenty-four hours after challenge, inguinal and popliteal lymph nodes (LN) were collected. LN cells were cultured in the presence of 20 µM $PdCl_2$ for 5 days. After washing, these cells were further co-cultured with irradiated (20 Gy) splenocytes in the presence of 20 µM $PdCl_2$ and 100 U/ml recombinant IL-2 (Wako) for 5 days. Finally, LN cells were cultured in the presence of 100 U/ml IL-2 alone for 3 days. TCR repertoire analysis was performed as described previously (21).

Cell Lines

The murine dendritic cell line DC2.4 (H-2K^b, H-2D^b) was purchased from Merck Millipore. Human CD8-expressing TG40 cells were a kind gifted from Dr. Kishi (Toyama University).

Antibodies for Flow Cytometric Analysis

All antibodies used in flow cytometric analysis were purchased from Biolegend: FITC-conjugated anti-H-2K^{b}D^b antibody (clone 28-8-6), FITC-conjugated anti-H-2K^b antibody (clone AF6-88.5), APC-conjugated anti-H-2D^b antibody (clone KH95), APC-conjugated anti-CD8α antibody (clone 53-6.7), APC-conjugated antibody for H-2K^b bound to SIINFEKL (clone 25D1.16), FITC-conjugated anti-CD69 antibody (clone H1.2F3) and APC-conjugated anti-TCRβ antibody (clone H57-597).

Flow Cytometric Analysis

DC2.4 (2 x 10^5 cells) were cultured with 200 µM $PdCl_2$ in AIM-V medium (Gibco) at 37°C for 0 15, 30, 60, and 120 min. Cells were then washed with FACS buffer (0.5% BSA, 0.5 mM EDTA, 0.09% NaN_3/PBS) and stained with FITC-anti H-2K^{b}D^b antibody at 4°C for 20 min. All analyses were performed on FACS Canto II (BD Biosciences) with FlowJo software (TOMY digital biology). In some experiments, prior to staining cells were fixed and permeabilized with BD Fix/Perm Buffer according to the manufacturers' instruction.

Analysis of Antigen Recognition by $PdCl_2$-Treated Cells

Mice were treated intravenously with 1 mg OVA protein (SIGMA) 50 µg $OVA_{257-264}$ (SIINFEKL) (Iwaki Bioservice). Twelve hours after injection, mice were administrated intraperitoneally with 300 µl of 10 mM $PdCl_2$. Twelve hours

after $PdCl_2$ treatment, spleens were collected and lysed with ACK lysis buffer (155 mM NH_4Cl, 10 mM $KHCO_3$, 1 mM EDTA), and then washed. Splenocytes were irradiated (20 Gy) for use as antigen presenting cells. For preparation of responder cells, splenocytes was obtained from OT-I mice. These cells were labeled with 5 μM CFSE (Dojindo). Antigen-presenting cells and responder cells were then co-cultured for 48 hours. CFSE dilution in CD8α+ cells were evaluated by flow cytometric analysis to assess proliferation in response to OVA antigen recognition.

Peptide Alteration Assay by 25D1.16

DC2.4 cells were pulsed with 5 ng/ml $OVA_{257-264}$ (SIINFEKL) (Iwaki Bioservice) in 10% fetal bovine serum (FBS)/RPMI for 1 hour at 26°C and washed with PBS. Then cells were treated with 200 μM $PdCl_2$ for 2 hours at 26°C. In some experiments, cells were washed and recovered in 10% FBS/RPMI for 1 hour. Finally, cells were stained with antibodies against H-$2K^b$ or 25D1.16.

Western Blot Analysis

DC2.4 cells were treated with 25 U/ml recombinant mouse IFN-γ (Peprotech) for 48 hours. Cells were then treated with 100 μM $PdCl_2$ for 30 min followed by lysis with RIPA buffer (50 mM Tris-HCl (pH 7.4), 150 mM NaCl, 1% Triton X-100, 1% Sodium deoxycholate, 0.1% SDS) supplemented with protease inhibitor cocktail cOmplete™ (Roche) and kept on ice for 30 min. Lysates were centrifugated for 30 min at 4°C. Proteins in supernatant were quantified by MicroBCA protein assay kit (ThermoFicher Scientific). Supernatants were then used for SDS-PAGE, electrotransferred onto polyvinylidene difluoride membranes (Millipore), and membranes probed with the indicated primary antibodies for MHC class I, H-$2K^b$ and H-$2D^b$ (Abcam), followed by HRP-conjugated secondary antibodies. Membranes were then washed, and bands visualized with the enhanced chemiluminescence detection system (ECL) by Chemilumi One L (Nacalai Tesque). Band Intensity was quantified using Image J software.

Confocal Microscopy

DC2.4 cells were treated with 1 μg/ml SIINFEKL for 1 hour at 37°C and then cells were cultured in the presence or absence of $PdCl_2$ for 30 min. Cells were fixed with 1% paraformaldehyde/PBS for 10 min at 4°C, and then permeabilized with 0.1% Triton X100 for 10 min at room temperature. Cells were stained with antibody 25D1.16 prior to analysis with a TCS SP8 microscope (Leica).

MHC Ligandome Analysis Using Mass Spectrometry

DC2.4 cells were treated with and 10 ng/ml LPS with or without 50 μM $PdCl_2$ (depicted as (+) or (-) $PdCl_2$ in the figures, respectively) for 18 hours at 37°C. Cells were then washed with PBS and harvested using a cell scraper. Approximately 2 $x10^9$ cells were used in the analysis. MHC ligands were isolated and sequenced using mass spectrometry as previously described (25). Briefly, peptide-MHC complexes in samples were captured by affinity chromatography using monoclonal antibodies (Y-3 for K^b and 28-14-8S for D^b). The MHC ligands were eluted, desalted, and injected into LC-MS/MS (Easy-nLC 1000 system and Q Exactive Plus, Thermo). In mass spectrometry, data were acquired with a data-dependent top 10 method. Survey scan spectra were acquired at a resolution of 70,000 at 200 m/z with an AGC target value of 3e6 ions and a maximum IT of 100 ms, ranging from 350 to 2,000 m/z with charge states between 1+ and 4+. MS/MS resolution was 17,500 at 200 m/z with an AGC target value of 1e5 ions and a maximum IT of 120 ms. MS/MS data were searched against the Swiss-Prot database using the Sequest HT along with the Percolator algorithm on the Proteome Discoverer platform (Thermo). The tolerance of precursor and fragment ions was set at 10 ppm and 0.02 Da, respectively, and no specific enzyme was selected for the search. Concatenated target-decoy selection was validated based on q-values, and a false discovery rate (FDR) of 0.05 was used in the Percolator node as a peptide detection threshold. Only the 8-11 mer (K^b) and 8-12 mer (D^b) peptides with IC50 (NetMHC-4.0) < 5,000 were counted as natural MHC ligands. Ligandome analysis were performed twice in each condition and whole peptides in the identified in both experiments were used for analysis. Complete list used in analysis are shown in **Supplementary Tables 1**–**4**. Peptide analysis was performed by R venn-diagram package (ver. 3.5.2).

Construction of TCR-Expressing Vector

To generate a TCR α and β co-expression plasmid, the C-region of TCRα and β chain were first amplified from cDNA from wild type splenocytes and ligated into the pMX-IP vector (Cell Biolabs). Pd-reactive T cells were collected, RNA extracted using the RNeasy mini kit (QIAGEN), and then cDNA synthesized using Superscript III (ThermoFisher Scientific). The cDNA was then used to generate TCRα and β libraries as described previously (21). Each TCR library was mixed with a forward primer consisting of the annealing site of the adapter DNA (5'- AGCTAGTTAATTAAGGATCCTGATCACCG GACAGGAATTCC -3') and 20 bps overlapping the pMX-IP vector and a reverse primer specific for the C-region of the TCR α and β (for TCRα 5'- TGGTACACAGCAGGTTCTGGGTTC-3', for TCRβ 5'- CAAGGAGACCTTGGGTGGAGTCAC-3'). Next, TCR fragments were amplified by PCR. PCR fragments were ligated into the pMX-IP vector digested with BamHI and XhoI (TakaraBio) by mix with NEBuilder HiFi DNA Assembly Master Mix (New England Bio. Lab.) and incubation at 50°C for 15 min. The resulting vectors were transformed into NEB5α competent cells. Transformed cells were spread on LB agar plates and incubated for 16 hours at 37°C. Colonies were then collected, and mixed plasmids were purified using a QIAGEN miniprep kit.

Establishment of TCRα and β-Expressing TG40 Cell

Plat E cells (1 $x10^6$ cells) were seeded on 6-well plates, then 1.25 μg of each TCRα and β/pMX-IP plasmid was transfected using polyethylene imine (Polysciences). Two days after transfection, supernatant was collected, and 4 μg/ml of polybrene was added to the supernatant. Then, TG40 cells ($2x10^5$ cells) were mixed with supernatant and centrifuged at 1,800 g at 32°C for 60 min

and seeded in 24 well plates. Two days after transduction, cells were selected by 1 μg/ml puromycin (Wako). After 6 days of selection, TCRβ-expressing cells were sorted by FACS Aria III (BD Biosciences).

Activation of TCR-Expressing TG40 in Response to Pd

DC2.4 cells (1x10^4 cells) in 10% FBS/RPMI1640 (Wako) were seeded in 96-well flat bottom plates (FALCON). Six hours after cell seeding, cells were treated with 100 μM $PdCl_2$ and 25 U/ml recombinant mouse IFN-γ (Peprotech) for 18 hours. Then cells were washed with PBS, and co-cultured with TCR- transduced TG40 (2 x10^4 cells) for 24 hours. Expression of CD69 on TCRβ positive cells was analyzed by flow cytometry to examine activation of TG40 cells in response to Pd. In some experiments, prior to co-culture with TG40 cells, peptides on MHC class I were stripped as described previously (26).

Statistical Analyses

All data are presented as mean ± S.D. Significance of difference between two groups was determined using unpaired two-sided Student's t-test (**Figures 4B–E** and **Supplementary Figure 3C**) and one-way ANOVA with Tukey's multiple comparison (**Figures 1A, B**, **2**, **3D**, **4A** and **Supplementary Figure 1**, **2**, **4**, **5**). * and ** denote p<0.05 and p<0.01 compared to the control. N.S., not significant. All analyses were performed using Graphpad Prism 8 (GraphPad).

RESULTS

$PdCl_2$ Treatment Affects Antigenicity by MHC Class I

First, we asked whether Pd-treatment affects MHC class I/peptide complexes. To examine this, mice were injected with ovalbumin (OVA) protein and 12 hours after injection, $PdCl_2$ was injected intraperitoneally. After 12 hours, splenocytes were then analyzed by using antibody clone 25D1.16, which recognizes MHC class I H-2K^b-loading SIINFEKL, an OVA-derived 8-mer peptide. Splenocytes from mice injected with OVA alone exhibited increased 25D1.16 binding as compared with non-treated mice. Interestingly, splenocytes from mice treated with OVA and $PdCl_2$ exhibited reduced binding of 25D1.16 (**Figure 1A**, left panel). In contrast, the total H-2K^b level was comparable regardless of $PdCl_2$ treatment (**Figure 1A**, right panel) with H-2K^b equally upregulated after OVA treatment in the presence and absence of $PdCl_2$. It has been reported that commercial OVA protein contains LPS (27) and thus, this H-2K^b upregulation is thought to be the result of LPS contamination. Therefore, we performed *in vivo* experiment using SIINFEKL peptide (**Supplementary Figure 1**). When we used SIINFEKL peptide, we found that splenocytes from mice treated with SIINFEKL and $PdCl_2$ exhibited reduced binding of 25D1.16 as compared with group of SIINFEKL alone (**Supplementary Figure 1A**, left panel). In contrast, the total H-2K^b level was comparable regardless of $PdCl_2$ treatment

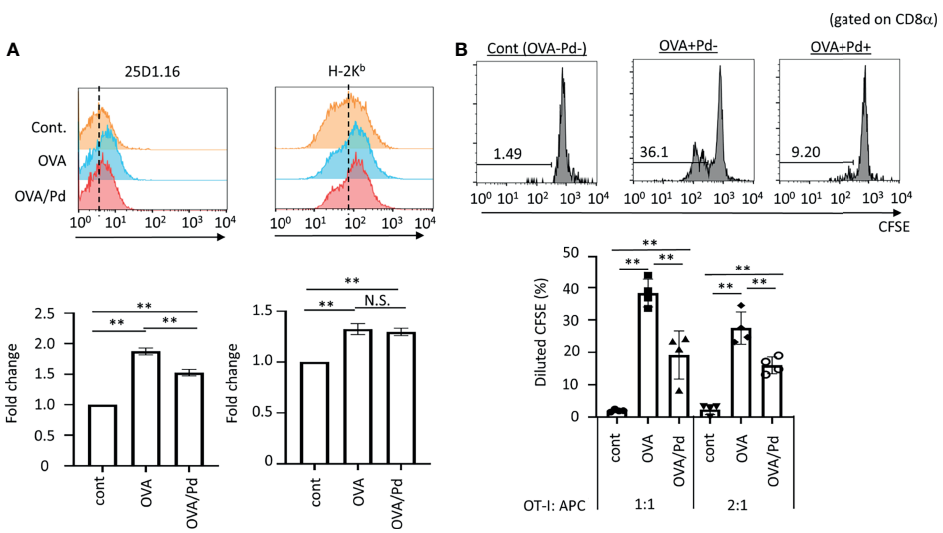

FIGURE 1 | Effect of $PdCl_2$ on antigenicity of splenocyte of mice treated with OVA. **(A)** Effect of 25D1.16 antibody binding in splenocyte of mice treated with $PdCl_2$. Mice were injected with OVA protein and 12 hours after injection, $PdCl_2$ was injected intraperitoneally. After 12 hours, splenocytes were then analyzed by using antibody clone 25D1.16. Orange histograms represent non-treated cells. Blue histograms represent splenocytes from mice treated with OVA protein. Red histograms represent splenocytes from mice treated with OVA proteins and $PdCl_2$. Bottom graphs show fold change of MFI of indicated antibodies to control. Error bars indicate ± S.D., of three independent experiments. **(B)** Antigenicity of Pd-modulated OVA-loading splenocytes. Antigen-presenting cells (APC) were prepared from mice treated with OVA protein and $PdCl_2$ described as **(A)**. After splenocytes were irradiated, these cells were cocultured with CFSE-labeled OT-I cells. (top) Histograms indicate representative results of CFSE dilution gated on CD8α. (bottom) The graphs show the mean % diluted CFSE. Error bars indicate ± S.D. (n=3). Data are representative of three independent experiments. One-way ANOVA with Tukey's multiple comparison. ** denote p<0.05 and p<0.01 compared to the control. N.S., not significant.

(**Supplementary Figure 1A**, right panel). Next, we examined whether reduction of 25D1.16 binding was resulted in attenuation of CD8 T cell recognition. To test this, we used OT-I mice, which are $OVA_{257-264}$-specific TCR transgenic mice (28). Antigen-presenting cells (APC) were prepared from mice treated with OVA protein and $PdCl_2$ as described above. These irradiated APCs were then cocultured with CFSE-labeled OT-I cells. APCs obtained from mice treated with OVA protein alone induced robust OT-I proliferation (**Figure 1B**), while cells obtained from OVA and $PdCl_2$-treated mice exhibited reduced OT-I proliferation (**Figure 1B**). We also found that reduction of OT-I proliferation by splenocyte of SIINFEKL/$PdCl_2$-treated mice as compared with that of SIINFEKL alone treated mice (**Supplementary Figure 1**). These results suggested three possibilities as follows; (1) $PdCl_2$ treatment reduced OVA peptide presentation on H-$2K^b$, (2) there is less of SIINFEKL-H-$2K^b$ available for recognition by antibody/OT-I cells or (3) $PdCl_2$ changed SIINFEKL-H-$2K^b$ (directly or indirectly) whilst SIINFEKL presentation is maintained.

Next, we also performed *in vitro* analysis using DC2.4 cells, a C57BL/6 (H-$2K^b$, H-$2D^b$) mouse-derived dendritic cell line (**Figure 2**). DC2.4 cells were treated with SIINFEKL peptide, and then cultured in the presence of $PdCl_2$ for 1 hour or 2 hours. These cells were stained with 25D1.16 and antibody for H-$2K^b$. Consistent with **Figure 1A**, SIINFEKL-treated DC2.4 cells exhibited increased binding of 25D1.16 antibody, and this effect was reduced by $PdCl_2$ treatment for 1 hour or 2 hours (**Figure 2A, B**). However, in contrast with **Figure 1A**, total H-$2K^b$ expression was also reduced after $PdCl_2$ treatment (**Figures 2A, B**). In addition, H-$2D^b$ expression, which was not relevant to SIINFEKL loading, also reduced as well as H-$2K^b$ after $PdCl_2$ treatment (**Figures 2A, B**). To examine the effect on antibody recognition by $PdCl_2$ treatment, DC2.4 cells were treated with $PdCl_2$ before SIINFEKL treatment, and then cells were stained with antibodies. As shown in **Figure 2C**, pretreatment with $PdCl_2$ did not affect 25D1.16 binding. This data suggested that $PdCl_2$ treatment did not affect recognition site of these antibodies in our experimental condition. To examine whether the reduction of 25D1.16 binding was the result due to MHC class I down-regulation, Pd-treated DC2.4 cells were cultured in the absence of $PdCl_2$ for an additional 60 min to aim to recover MHC class I expression. In this condition, we found that 25D1.16 binding was reduced whereas H-$2K^b$ level was comparable regardless cells were pre-cultured with $PdCl_2$ or not (**Figure 2D**). These data collectively suggested that $PdCl_2$ treatment alters MHC class I/peptide complexes. Thus, to further analyze the mechanism through which Pd treatment alters peptide presentation by $PdCl_2$, we used DC2.4 cells.

$PdCl_2$ Treatment Induces Alternative Peptide Presentation on MHC Class I

Next, to examine the mechanism underlying the reduction of 25D1.16 antibody binding in DC2.4 cells as shown in **Figure 2**, we focused on loading peptide on MHC class I molecules, H-$2K^b$ and H-$2D^b$ after $PdCl_2$ treatment. For these experiments we performed MHC class I ligandome analysis (25). As described in the Materials and Methods, DC2.4 cells were treated with $PdCl_2$ prior to immunoprecipitation of MHC class I (H-$2K^b$ and H-$2D^b$) and identification of the presented peptides by LC-MS/MS (**Figure 3** and **Supplementary Tables 1–4**). Then, we compared peptide list on H-$2K^b$ and H-$2D^b$ between the presence or absence of $PdCl_2$, respectively (Comparison of "Sequence" column in **Supplementary Tables**). When cells were treated with $PdCl_2$, 501 and 512 peptides were differentially loaded on H-$2K^b$ and H-$2D^b$ as compared with the absence of $PdCl_2$, respectively (**Figures 3A, B** purple area), indicating that $PdCl_2$ treatment affected alternative peptide loading on H-$2K^b$ and H-$2D^b$.

Furthermore, we analyzed source proteins from which the $PdCl_2$ treatment-induced peptides were derived (purple area in **Figures 3A, B**). The analysis steps show as follow: (1) Protein name was referenced from peptide sequence by Swissprot. (2) We extracted proteins which was designated by above 501/512 peptides induced by $PdCl_2$. (3) We examined whether these proteins were found in the list without $PdCl_2$. We found that 379 and 346 source proteins in H-$2K^b$ and H-$2D^b$, respectively, were not listed on the absence of $PdCl_2$, these results indicate that these peptides were derived from unique source protein (**Figure 3C**, yellow bar). On the other hand, 109 and 164 proteins bound to H-$2K^b$ and H-$2D^b$, respectively, were shared between presence and absence of $PdCl_2$ (**Figure 3C**, red bar).

To demonstrate the importance of differential peptide loading with T cell stimulation, we performed a peptide stripping experiment as described previously, with some modifications (26). First, the effect of peptide stripping was examined using antibody 25D1.16 and OVA_{257}-pulsed DC2.4 cells (**Supplementary Figure 2**). Binding of antibody 25D1.16 to SIINFEKL-pulsed DC2.4 cells was reduced by peptide stripping (**Supplementary Figure 2A**). Furthermore, CD69 expression on OT-I TCR-expressing TG40 cells was also reduced by coculture with peptide-stripped cells (**Supplementary Figure 2B**).

To examine whether the differential peptide presentation caused by $PdCl_2$ induces activation of Pd-responsive T cells, Pd-responsive T cells were established using LNs from mice sensitized and challenged with $PdCl_2$ as reported previously, with some modifications (24). After continuous and low dose Pd treatment, oligoclonal T cells were successfully established (**Supplementary Figures 3A, B**). In these cells, we found that highest frequent of TCR repertoire was TRAV16D/DV11-3-CAMRAYANKMIF-TRAJ47-03 and TRBV13-3-01-CASSDRTTNSDYTF-TRBJ1-2-01. Then RNA obtained from these cells was used to construct a TCR expression vector. These expression plasmids were then retrovirally transduced into TG40 cells (T cell hybridoma cell line lacking TCRα and TCRβ) and after selection with puromycin, TCRβ-expressing TG40 cells were sorted. Following co-culture with $PdCl_2$-pretreated DC2.4 for 24 hours, CD69 expression was analyzed as a marker of TG40 activation. We found that TG40 cells expressing the TCR library obtained from Pd-sensitized mice upregulated CD69 expression in response to $PdCl_2$-treated DC2.4 cells (**Figure 3D**). However, TG40 cells which express

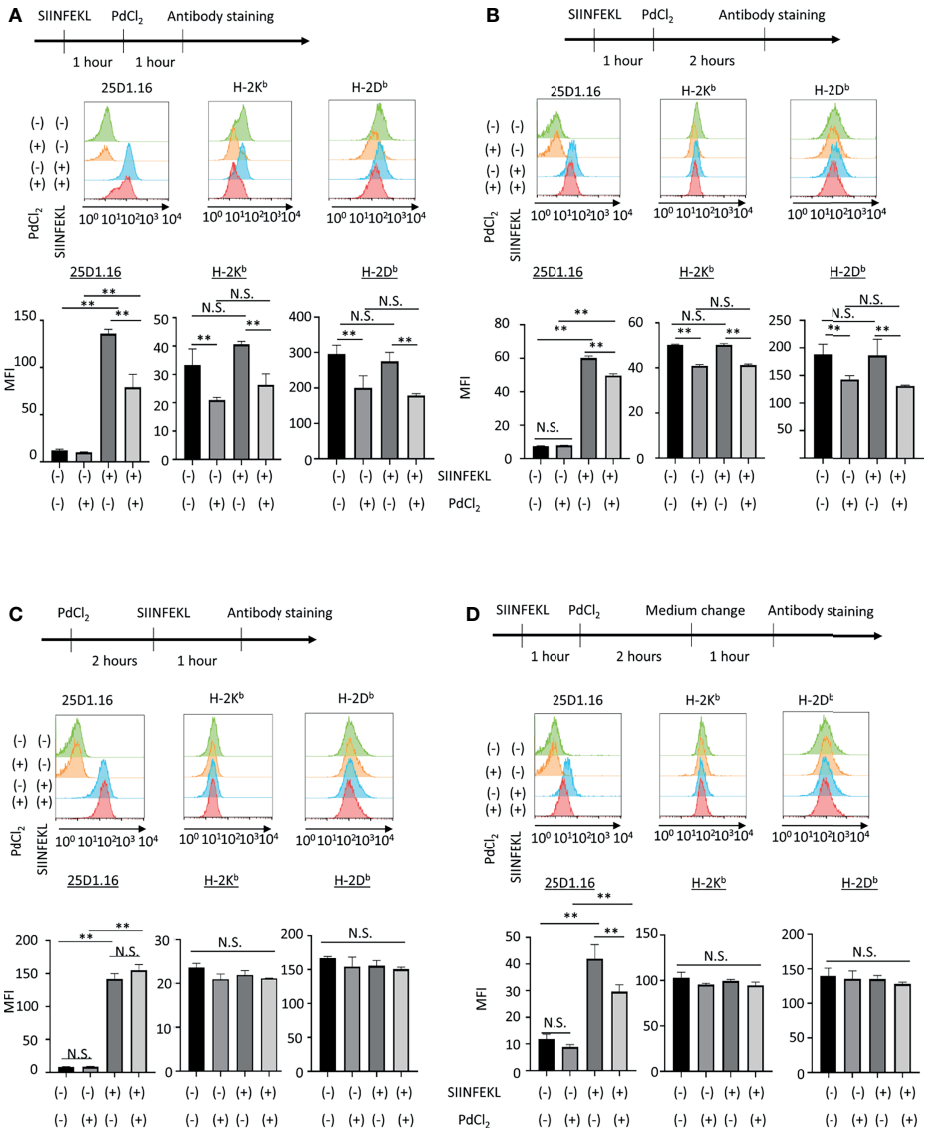

FIGURE 2 | *In vitro* analysis of the effect of $PdCl_2$ treatment on OVA peptide presentation by MHC class I. Alternative peptide presentation study in DC2.4 cells. DC2.4 cells were pulsed with SIINFEKL for 1 hour and then cells were treated with $PdCl_2$ for **(A)** 1 hour and **(B)** 2 hours. **(A, B)** Antibody staining was preformed just after Pd treatment. **(C)** Effect of $PdCl_2$ in antibody binding. DC2.4 cells were treated with $PdCl_2$ for 2 hours and cells were pulsed with SIINFEKL peptide for 1 hour and binding of antibody for SIINFEKL on H-2K^b (25D1.16), H-2K^b and H-2D^b. **(D)** SIINFEKL-treated DC2.4 cells were treated with $PdCl_2$ for 2 hours and cultured in $PdCl_2$-free media for 1 hour. Then, cells were stained with antibodies. Histograms shows (top) 25D1.16 antibody binding and (bottom) H-2K^b expression. The graph shows MFI of antibody binding. Error bars indicate ± S.D. (triplicated wells). Data are representative of three independent experiments. Statistical difference was determined One-way ANOVA with Tukey's multiple comparison. ** denote $p<0.05$ compared to the control. N.S., not significant.

TCR library from lymph node of naïve mice did not respond to $PdCl_2$-treated DC2.4 cells (**Supplementary Figure 3C**).

Thus, we examined the effect of peptide stripping after $PdCl_2$ treatment and co-culture with Pd-responsive T cells. We confirmed that CD69 expression on Pd-responsive TG40 cells was reduced following co-culture with peptide stripped $PdCl_2$-treated DC2.4 cells (**Figure 3D**, right 2 columns). These results suggest that the reason for the reduction in 25D1.16 binding following $PdCl_2$ treatment is due to alternative peptide loading on MHC class I.

MHC Class I Is Internalized Following $PdCl_2$ Treatment, Resulting in Alteration in Antigenicity

As shown in **Figure 2A**, Pd-treatment temporally reduces cell-surface expression of H-2K^b. To explore the behavior of MHC class I in response to $PdCl_2$ treatment, we analyzed MHC class I expression on the cell surface in response to $PdCl_2$ treatment. DC2.4 cells were treated with $PdCl_2$ and cultured for the indicated times (0, 15, 30, 60, and 120 min), and subsequent staining for surface MHC class I. $PdCl_2$ treatment resulted in a

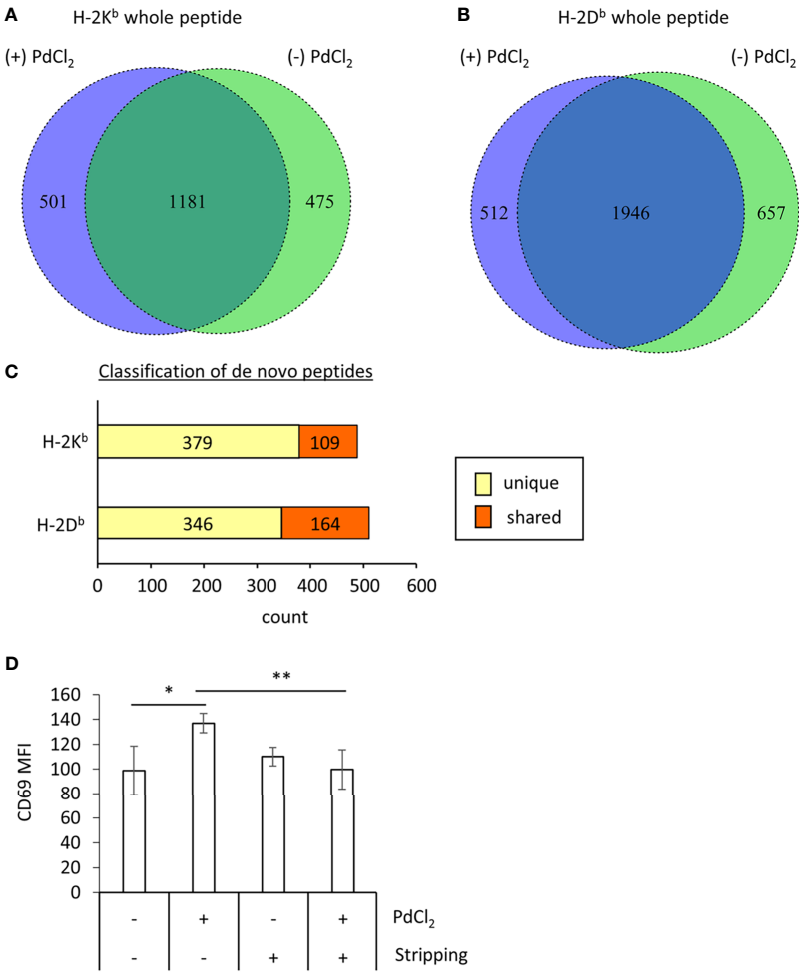

FIGURE 3 | MHC class I ligandome analysis of $PdCl_2$-treated cells. DC2.4 cells were treated with $PdCl_2$ and LPS (depicted as (+) $PdCl_2$) or LPS alone (depicted as (-) $PdCl_2$) for 18 hours before cells were lysed and H-2K^b and anti-H-2D^b immunoprecipitated, followed by analysis of presented peptides by LC-MS/MS. Ligandome analysis were performed twice for each condition and whole peptides in the identified in both experiments were used for analysis. Peptide lists were depicted in **Supplementary Tables 1–4**. **(A, B)** Comparison of peptide sequence between the presence and absence of $PdCl_2$ (**Supplementary Tables 1–4** "sequence" column). Differential presentation of peptides by **(A)** H-2K^b and **(B)** H-2D^b in cells treated with (purple area) and without (green area) $PdCl_2$. **(C)** Comparison of source proteins of peptides presented by H-2K^b and H-2D^b following $PdCl_2$ treatment of cells. Designated proteins of purple area in **(A, B)** were compared with the protein list in the absence of $PdCl_2$. "Unique" means proteins which were not listed in the absence of $PdCl_2$ whereas "Shared" means proteins which also listed in the without culture of $PdCl_2$. **(D)** CD69 expression on Pd-TCR/TG40 cells co-cultured with $PdCl_2$-treated DC2.4 cells. DC2.4 cells were cultured with $PdCl_2$ in the presence of recombinant mouse IFN-γ for 18 hours. After washing, DC2.4 cells were cocultured with Pd-TCR/TG40 cells and CD69 expression on TG40 was examined. The graph shows the MFI of CD69 expression on TCRβ-expressing cells. Error bars denote ± S.D. (quadruplicated samples, three independent experiments). Statistical differences were determined by one-way ANOVA with Tukey's multiple comparison. ** and * denote $p<0.05$ and $p<0.01$compared to the control, respectively.

reduction of surface MHC class I (H-2K^{b}D^b) within 15 min after which surface expression gradually recovered, albeit only partially, until 120 min (**Figure 4A**). Next, we assessed whether the reduction in MHC was due to degradation or internalization. To examine the level of MHC class I in $PdCl_2$-treated cells under permeabilizing conditions, DC2.4 cells were treated with $PdCl_2$ for 30 min, then cells were permeabilized and stained with antibodies for MHC class I. While surface MHC class I was reduced in the presence of $PdCl_2$ under non-permeabilizing conditions, total MHC expression in cells treated with $PdCl_2$ was comparable with that of non-treated cells (**Figure 4B**). In addition, western blot analysis confirmed that MHC class I levels of $PdCl_2$-treated cells are comparable with that of non-treated cells (**Figure 4C**). These data suggest that $PdCl_2$ treatment induces MHC class I internalization, and not degradation. Next, we followed the movement of MHC class I after $PdCl_2$ treatment. To this end, we used the 25D1.16 antibody to stain cells treated with SIINFEKL peptide prior to fixation and permeabilization. As shown in **Figure 4D**, surface staining of 25D1.16 was observed regardless of $PdCl_2$ treatment,

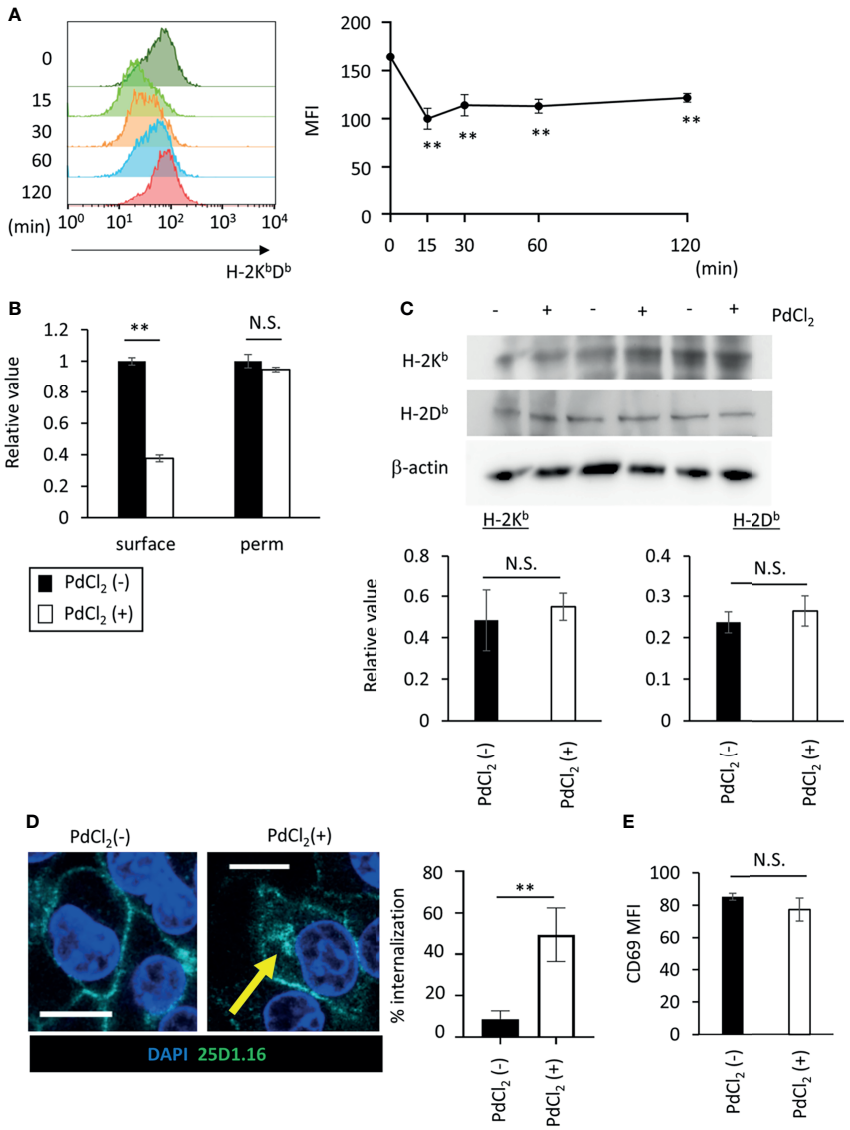

FIGURE 4 | $PdCl_2$ treatment induces temporal internalization of MHC molecules. **(A)** Surface MHC class I expression after $PdCl_2$ treatment. DC2.4 cells were treated with $PdCl_2$ and cultured for the indicated times (0, 15, 30, 60, and 120 min) and cells were stained for surface MHC class I. Representative histograms of MHC class I from four independent experiment (left panels). The graphs show MFI of MHC molecules (right panels). Error bars denote ± S.D. (triplicated samples, four independent experiments). Statistical difference was determined One-way ANOVA with Tukey's multiple comparison. ** denote $p<0.05$ compared to the control. **(B)** Flow cytometric analysis of total MHC class I ($H\text{-}2K^bD^b$) in permeabilized cells. Thirty minutes after Pd treatment, DC2.4 cells were fixed and permeabilized and subsequent staining with MHC class I. The graph shows relative value of MFI. MFI of untreated cells was set at 1. **(C)** Western blot analysis of MHC class I in DC2.4 cells treated with 25 U/ml rmIFNγ for 48 hours, and then treated with $PdCl_2$ for 30 min. Graphs show the relative value of $H\text{-}2K^b$ and $H\text{-}2D^b$ to β-actin. (triplicated samples, representative data from 2 independent experiments) **(B, C)** Statistical difference was determined unpaired two-sided Student's t-test. N.S. means not significantly difference. **(D)** Confocal microscopic analysis of internalization of MHC class I in response to $PdCl_2$. DC2.4 cells were cultured with 1 μg/ml SIINFEKL peptide and cells were treated with $PdCl_2$ for 30 min. Cells were then fixed, permeabilized, and stained with DAPI (blue) and 25D1.16 antibody (green). Arrow indicates the intracellular SIINFEKL-loading $H\text{-}2K^b$. Graph shows % of the mean internalization in the four fields. **(E)** DC2.4 cells were treated with $PdCl_2$ in the presence or absence of 0.25% NaN_3, and then these cells were co-cultured with Pd-TCR/TG40 cells for 24 hours followed by evaluation of CD69 expression on TCRβ–expressing cells as described in **Figure 3D**. The graph shows the MFI of CD69 expression on TCRβ-expressing cells. Error bars denote ± S.D. (quadruplicated samples, three independent experiments). Statistical differences were determined using unpaired two-sided Student's t-test. N.S. means not significantly difference.

but only following $PdCl_2$ treatment was staining also observed around the perinuclear area (**Figure 4D**), which has been reported as the recycling center (29). These results indicated that $PdCl_2$ treatment induced temporal internalization of MHC class I.

Finally, to examine the significance of MHC class I internalization on alternative peptide loading, DC2.4 cells were treated with $PdCl_2$ and LPS in the presence of sodium azide (NaN_3), which inhibits internalization of surface molecules. We

found that NaN_3 treatment partially suppresses MHC class I internalization in response to $PdCl_2$ treatment (**Supplementary Figure 4**). As a control experiment, we examined whether NaN_3 treatment affect antigenicity of exogenously added antigen. To this end, NaN_3-treated DC2.4 cells were pulsed with SIINFEKL, and then cells were co-cultured with OT-I TCR/TG40 and CD69 on TG40 cells was analyzed. As shown in **Supplementary Figure 5**, activation of OT-1/TG40 by NaN_3-treated DC2.4 that had been exogenously added with SIINFEKL was comparable with non-NaN_3 treated SIINFEKL-loading DC2.4 cells. The result suggested that NaN_3 treatment affected inhibition of membrane movement rather than cell metabolism. Then, to examine the antigenicity of $PdCl_2$-treated DC2.4 cells in inhibition of membrane movement, DC2.4 cells were treated with or without $PdCl_2$ in the presence NaN_3, and then these cells were co-cultured with Pd-responsive TG40 cells. We found that upregulation of CD69 expression on Pd-responsive TG40 cells, as shown in **Figure 3D**, is suppressed by NaN_3-treated DC2.4 cells (**Figure 4E**). Thus, MHC class I internalization by $PdCl_2$ is crucial for alternative peptide loading on MHC class I.

DISCUSSION

In this study, we show that Pd treatment affects MHC class I/peptide complexes by altering MHC class I peptide loading. The mechanism underlying this is the Pd-induced temporal internalization of MHC class I. Under normal conditions, cell surface MHC class I is spontaneously internalized and re-expressed (30), and this intracellular trafficking contributes to stable surface expression of MHC class I and presentation of self-antigens for monitoring of self (31). Here, we show for the first time that a metal, Pd, induces MHC class I internalization in the process of generating antigenicity.

$PdCl_2$ treatment induced alternative peptide loading on both H-2K^b and H-2D^b (**Figures 3A, B**) and $PdCl_2$-treated DC2.4 cells can activate Pd-responsive TCR-expressing TG40 cells (**Figure 3D**). The data suggested that alternative peptide loading induced by $PdCl_2$ treatment exert T cell-mediated antigenicity. In this study, we found that highest frequent TCR from *in vitro* low dose $PdCl_2$ stimulation was TRAV16D/DV11-3-CAMRAYANKMIF-TRAJ47-03 and TRBV13-3-01-CASSDRTTNSDYTF-TRBJ1-2-01 (**Supplementary Figure 3**). Although we detected TRAV7-TRAJ22 as the previous *in vivo* experiments (21), this TCR is not major repertoire in this study. There was a possibility that differential peptides might be presented by splenocyte in mice as compared with lymph node cells. Further analysis of the source proteins of these alternatively loaded peptides revealed that majority of source proteins were derived from proteins that differed from those of non-treated cells (**Figure 3C**). Abacavir is known to bind the F-pocket of the peptide-binding groove of HLA-B*57:01 resulting in alteration of the MHC-presented self-peptide repertoire (32, 33). Therefore, it is possible that $PdCl_2$ also affects the receiving groove of MHC class I, resulting in alternative peptide binding. In addition, 109 and 164 protein antigens that bound H-2K^b and H-2D^b, respectively, were shared between the presence and absence of $PdCl_2$ (**Figure 3C**). A previous study reported that Au (III) causes alteration of a model antigen to cryptic peptides (34). Thus, our results suggested that $PdCl_2$ treatment also affected alternative peptide loading through processing of antigenic proteins. To discern between these possibilities, a novel Pd indicator similar to Newport green which is an indicator of Ni, will be needed (35). Studies to further determine the intracellular localization of Pd will help reveal whether Pd binds to MHC class I and/or peptides during processing. In addition, as many metals exert cellular toxicity, it has a possibility that $PdCl_2$ treatment constitutes stress for the cells even if low dose $PdCl_2$. Thus, the relationship among temporal internalization of MHC class I, alternative peptide loading, and cellular stress by $PdCl_2$ will be interesting target for detailed understanding of antigenicity generation during Pd allergy.

As shown in **Figure 4A**, $PdCl_2$ treatment reduces surface expression of MHC class I, but does not affect the total cellular level of MHC class I (**Figures 4B, C**). This indicates that surface MHC class I is internalized in response to Pd treatment. Interestingly, $PdCl_2$-induced antigenicity was suppressed by inhibition of membrane movement (**Figure 4E**). While these results indicate that $PdCl_2$ treatment induces MHC class I internalization and alternative peptide loading, it should be noted that 0.25% NaN_3 treatment did not completely suppress this effect (**Supplementary Figure 4**). Overdose treatment of NaN_3 is highly cytotoxic and thus, this is an experimental limitation in this study. Therefore, additional approaches, such as use of molecules known to interfere with trafficking of MHC class I, will be needed in the future. It has been reported that during MHC class I recycling, Rab proteins induce membrane trafficking by cycling between an active GTP-bound state and inactive GDP-bound state (36). Moreover, intracellular trafficking of MHC I by Rab22a contributes to antigen cross-presentation (29). We found that MHC I internalization following $PdCl_2$ treatment occurred within a short time frame (within 15 min, **Figure 4A**). Therefore, we hypothesize that $PdCl_2$ treatment induces rapid Rab family activation/inactivation, resulting in MHC class I internalization. Further studies will be needed to confirm if this is the underlying mechanism controlling this process.

We show that Pd induces temporal MHC class I internalization and partially recovering. At steady state, spontaneous MHC recycling contributes to the stable expression of self-antigens required for tolerance (31, 37). We found that Pd responsive TCR-expressing TG40 cells are activated by incubation with $PdCl_2$-treated DC2.4 cells and this activation is inhibited by co-culture with DC2.4 cells, which suppress membrane movement (**Figures 3D**, **4E**). This suggests that Pd-induced MHC class I internalization is involved in the generation of antigenicity through alternative peptide loading and pathogenic T cell activation, which together are responsible for Pd allergy. This is a novel mechanism of tolerance breakdown in which Pd induces antigenicity of self-proteins through temporal MHC class I internalization. Furthermore, these

alternatively selected peptides may be candidate target molecules for therapeutic approaches to treat Pd allergy. However, further investigation will be required to determine the precise mechanism underlying this process in the development of Pd allergy.

DATA AVAILABILITY STATEMENT

The datasets presented in this study can be found in online repositories. The names of the repository/repositories and accession number(s) can be found below: ProteomeXchange, accession no: PXD028795.

ETHICS STATEMENT

The animal study was reviewed and approved by Institutional Committee for Use and Care of Laboratory Animals of Tohoku University.

AUTHOR CONTRIBUTIONS

Conducting experiments: KI, TK and ST. Acquiring data: KI, TK, and ST. Analyze data: KI, TK, and ST. Writing manuscript: KI, TK, and KO. Conceptualization: KI, TT, NH, and KO. Funding acquisition: TK, TT, NH, and KO. Supervision: TT and KO. All authors contributed to the article and approved the submitted version.

FUNDING

This work was supported by Grant-in-Aid for Scientific Research from the Japan Society for the Promotion of Science (JSPS) KAKENHI to KO (16H06497, 19H03835) and TK (JP19094976 and JP20240606) and the Japan Agency for Medical Research and Development (AMED) Grant to TK (JP19cm0106352) and partly supported by the Cooperative Research Project Program Joint Usage/Research Center at the Institute of Development, Aging and Cancer, Tohoku University to NH.

ACKNOWLEDGMENTS

The authors are grateful to Dr. Y. Nishimura (Kumamoto University), Dr. Emi Furusawa-Nishii (Juntendo University) and Dr. Y. Takeda (Tohoku University) for comment and suggestions. We thank M Kosuge, M. Itabashi, Y Suto, R. Tashiro, M. Ishikawa, S. Saito, D. Doi, K. Shibui, G. Ohuchi, K. Hasegawa, S. Tsuno, and S. Kosaka (Tohoku University) for supporting preparation of mice and performing experiments. We also thank the Biomedical Research Unit of Institute of Development, Aging and Cancer, Tohoku University for their technical support.

SUPPLEMENTARY MATERIAL

The Supplementary Material for this article can be found online at: https://www.frontiersin.org/articles/10.3389/fimmu.2021.736936/full#supplementary-material

Supplementary Figure 1 | Supplementary Figure 1 Effect of PdCl2 on antigenicity of splenocytes of mice treated with SIINFEKL peptide (A) Mice were injected with SIINFEKL and 12 hours after injection, PdCl2 was injected intraperitoneally. After 12 hours, splenocytes were then analyzed by using antibody clone 25D1.16. Orange histograms represent non-treated cells. Blue histograms represent splenocytes from mice treated with SIINFEKL. Red histograms represent splenocytes from mice treated with SIINFEKL and PdCl2. Bottom graph shows MFI of indicated antibodies. Error bars indicate ± S.D., three mice per group. The data are representative of three independent experiments. (B) Antigenicity of Pd-modulated SIINFEKL-loading splenocytes. Antigen-presenting cells (APC) were prepared from mice treated with SIINFEKL and PdCl2 described as supplementary Fig. 1A. After splenocytes were irradiated, these cells were cocultured with CFSE-labeled OT-I cells. (top) Histograms indicate representative results of CFSE dilution gated on CD8α. (bottom) The graphs show the mean % diluted CFSE. Error bars indicate ± S.D. (n=3). Data are representative of three independent experiments.

Supplementary Figure 2 | OVA peptide stripping effect on 25D1.16 binding and OT-I TCR recognitionDC2.4 cells were pulsed with OVA257-264 (SIINFEKL) for 1 hour. After washing, peptide was stripping. (A) 25D1.16 binding to peptide-stripped DC2.4 cells was examined by flow cytometry. The graph shows mean of MFI of 25D1.16. Error bars denote S.D. (triplicated samples, two independent experiments). (B) Peptide-stripped DC2.4 cells were co-cultured with OT-I TCR expressing TG40 cells. Twenty-four hours later, CD69 expression on TG40 cells were evaluated. Graph shows MFI of CD69 expression. Error bars denote S.D. (quadruplicated samples, three independent experiments).

Supplementary Figure 3 | TCR repertoire analysis of Pd responsive T cells and naïve lymph node cells The TCR repertoire of naïve LN cells and Pd-responsive T cells was analyzed by next generation sequencing. (A) 3-D graph of TRAV-TRAJ distribution. (B) Pie-chart of CDR3 frequency on TCRα chain. (C) CD69 expression on TCR, which obtained from naïve LN cells, -expressing TG40 cells co-cultured with PdCl2-treated DC2.4 cells as described in Fig 3D. The graph shows the MFI of CD69 expression on TCRβ-expressing cells. Error bars denote ±S.D. (quadruplicated samples, three independent experiments). Statistical differences were determined by unpaired two-sided Student's t-test

Supplementary Figure 4 | Inhibition of MHC class I internalization by NaN3Flow cytometric analysis following inhibition of membrane movement by NaN3 treatment. DC2.4 cells were treated with PdCl2 in the absence (left) or presence (right) of 0.25% NaN3 for 30 min and surface MHC class I was stained. The graph shows the relative value of MHC I expression compared to the control without PdCl2 treatment. Error bars denote ±S.D. (triplicated samples) One-way ANOVA with Tukey's multiple comparison. * and ** denote $p<0.05$ 0.01 compared to the control.

Supplementary Figure 5 | Figure 5 The effect of OT-I TCR/TG40 activation on NaN3-treated and exogenously SIINFEKL added-DC2.4.DC2.4 cells were treated with indicated dose of NaN3 for 30 min. After washing, cells were cocultured with OT-I TCR/TG40 cells in the presence of SIINFEKL peptide. Twenty-hours after coculture, CD69 expression was examined by flow cytometry. The graph shows MFI of CD69 expression. Error bars indicate ±S.D. (triplicated wells, three independent experiments). Statistical difference was determined One-way ANOVA with Tukey's multiple comparison. N.S., not significant.

Supplementary Tables 1–4 | Results of MHC ligandome analysis.

REFERENCES

1. Kashiwa K, Nishimura T, Saito A, Kubo H, Fukaya A, Tamai H, et al. Left Heart Bypass Support With the Rotaflow Centrifugal Pump(R) as a Bridge to Decision and Recovery in an Adult. *J Artif Organs Off J Japanese Soc Artif Organs* (2012) 15(2):207–10. doi: 10.1007/s10047-012-0632-x
2. Ueda T, Ueda K, Ito K, Ogasawara K, Kanetaka H, Mokudai T, et al. Visible-Light-Responsive Antibacterial Activity of Au-Incorporated TiO2 Layers Formed on Ti-(0-10)at%Au Alloys by Air Oxidation. *J Biomed Mater Res Part A* (2019) 107(5):991–1000. doi: 10.1002/jbm.a.36624
3. Okada M, Taketa H, Torii Y, Irie M, Matsumoto T. Optimal Sandblasting Conditions for Conventional-Type Yttria-Stabilized Tetragonal Zirconia Polycrystals. *Dental Mater Off Publ Acad Dental Mater* (2019) 35(1):169–75. doi: 10.1016/j.dental.2018.11.009
4. Yoshihisa Y, Shimizu T. Metal Allergy and Systemic Contact Dermatitis: An Overview. *Dermatol Res Pract* (2012) 2012:749561. doi: 10.1155/2012/749561
5. Garau V, Masala MG, Cortis MC, Pittau R. Contact Stomatitis Due to Palladium in Dental Alloys: A Clinical Report. *J Prosthet Dent* (2005) 93 (4):318–20. doi: 10.1016/j.prosdent.2005.01.002
6. Saito M, Arakaki R, Yamada A, Tsunematsu T, Kudo Y, Ishimaru N. Molecular Mechanisms of Nickel Allergy. *Int J Mol Sci* (2016) 17(2):E202–9. doi: 10.3390/ijms17020202
7. Lohr J, Knoechel B, Nagabhushanam V. Abbas AK. T-Cell Tolerance and Autoimmunity to Systemic and Tissue-Restricted Self-Antigens. *Immunol Rev* (2005) 204:116–27. doi: 10.1111/j.0105-2896.2005.00241.x
8. Schnuch A, Brasch J, Uter W. Polysensitization and Increased Susceptibility in Contact Allergy: A Review. *Allergy* (2008) 63(2):156–67. doi: 10.1111/j.1398-9995.2007.01590.x
9. Redwood AJ, Pavlos RK, White KD, Phillips EJ. HLAs: Key Regulators of T-Cell-Mediated Drug Hypersensitivity. *Hla* (2018) 91(1):3–16. doi: 10.1111/tan.13183
10. Schmidt M, Goebeler M. Immunology of Metal Allergies. *J der Deutschen Dermatol Gesellschaft = J German Soc Dermatol JDDG* (2015) 13(7):653–60. doi: 10.1111/ddg.12673
11. Yin L, Dai S, Clayton G, Gao W, Wang Y, Kappler J, et al. Recognition of Self and Altered Self by T Cells in Autoimmunity and Allergy. *Protein Cell* (2013) 4(1):8–16. doi: 10.1007/s13238-012-2077-7
12. Kalish RS. Antigen Processing: The Gateway to the Immune Response. *J Am Acad Dermatol* (1995) 32(4):640–52. doi: 10.1016/0190-9622(95)90351-8
13. Thierse HJ, Moulon C, Allespach Y, Zimmermann B, Doetze A, Kuppig S, et al. Metal-Protein Complex-Mediated Transport and Delivery of Ni2+ to TCR/MHC Contact Sites in Nickel-Specific Human T Cell Activation. *J Immunol* (2004) 172(3):1926–34. doi: 10.4049/jimmunol.172.3.1926
14. Bill JR, Mack DG, Falta MT, Maier LA, Sullivan AK, Joslin FG, et al. Beryllium Presentation to CD4+ T Cells Is Dependent on a Single Amino Acid Residue of the MHC Class II Beta-Chain. *J Immunol* (2005) 175(10):7029–37. doi: 10.4049/jimmunol.175.10.7029
15. Amicosante M, Fontenot AP. T Cell Recognition in Chronic Beryllium Disease. *Clin Immunol* (2006) 121(2):134–43. doi: 10.1016/j.clim.2006.03.012
16. Lu L, Vollmer J, Moulon C, Weltzien HU, Marrack P, Kappler J. Components of the Ligand for a Ni++ Reactive Human T Cell Clone. *J Exp Med* (2003) 197 (5):567–74. doi: 10.1084/jem.20021762
17. Potolicchio I, Festucci A, Hausler P, Sorrentino R. HLA-DP Molecules Bind Cobalt: A Possible Explanation for the Genetic Association With Hard Metal Disease. *Eur J Immunol* (1999) 29(7):2140–7. doi: 10.1002/(SICI)1521-4141(199907)29:07<2140::AID-IMMU2140>3.0.CO;2-Q
18. Minang JT, Arestrom I, Troye-Blomberg M, Lundeberg L, Ahlborg N. Nickel, Cobalt, Chromium, Palladium and Gold Induce a Mixed Th1- and Th2-Type Cytokine Response *In Vitro* in Subjects With Contact Allergy to the Respective Metals. *Clin Exp Immunol* (2006) 146(3):417–26. doi: 10.1111/j.1365-2249.2006.03226.x
19. Muris J, Feilzer AJ, Kleverlaan CJ, Rustemeyer T, van Hoogstraten IM, Scheper RJ, et al. Palladium-Induced Th2 Cytokine Responses Reflect Skin Test Reactivity. *Allergy* (2012) 67(12):1605–8. doi: 10.1111/all.12046
20. Kobayashi H, Kumagai K, Eguchi T, Shigematsu H, Kitaura K, Kawano M, et al. Characterization of T Cell Receptors of Th1 Cells Infiltrating Inflamed Skin of a Novel Murine Model of Palladium-Induced Metal Allergy. *PloS One* (2013) 8(10):e76385. doi: 10.1371/journal.pone.0076385
21. Takeda Y, Suto Y, Ito K, Hashimoto W, Nishiya T, Ueda K, et al. TRAV7-2*02 Expressing CD8(+) T Cells Are Responsible for Palladium Allergy. *Int J Mol Sci* (2017) 18(6):E1162–73. doi: 10.3390/ijms18061162
22. Kawano M, Nakayama M, Aoshima Y, Nakamura K, Ono M, Nishiya T, et al. NKG2D(+) IFN-Gamma(+) CD8(+) T Cells Are Responsible for Palladium Allergy. *PloS One* (2014) 9(2):e86810. doi: 10.1371/journal.pone.0086810
23. Iguchi N, Takeda Y, Sato N, Ukichi K, Katakura A, Ueda K, et al. The Antihistamine Olopatadine Regulates T Cell Activation in Palladium Allergy. *Int Immunopharmacol* (2016) 35:70–6. doi: 10.1016/j.intimp.2016.03.021
24. Pistoor FH, Kapsenberg ML, Bos JD, Meinardi MM, von Blomberg ME, Scheper RJ. Cross-Reactivity of Human Nickel-Reactive T-Lymphocyte Clones With Copper and Palladium. *J Invest Dermatol* (1995) 105(1):92–5. doi: 10.1111/1523-1747.ep12313366
25. Hongo A, Kanaseki T, Tokita S, Kochin V, Miyamoto S, Hashino Y, et al. Upstream Position of Proline Defines Peptide-HLA Class I Repertoire Formation and CD8(+) T Cell Responses. *J Immunol* (2019) 202(10):2849–55. doi: 10.4049/jimmunol.1900029
26. Langlade-Demoyen P, Levraud JP, Kourilsky P, Abastado JP. Primary Cytotoxic T Lymphocyte Induction Using Peptide-Stripped Autologous Cells. *Int Immunol* (1994) 6(11):1759–66. doi: 10.1093/intimm/6.11.1759
27. Tsuchiya K, Siddiqui S, Risse PA, Hirota N, Martin JG. The Presence of LPS in OVA Inhalations Affects Airway Inflammation and AHR But Not Remodeling in a Rodent Model of Asthma. *Am J Physiol Lung Cell Mol Physiol* (2012) 303(1):L54–63. doi: 10.1152/ajplung.00208.2011
28. Hogquist KA, Jameson SC, Heath WR, Howard JL, Bevan MJ, Carbone FR. T Cell Receptor Antagonist Peptides Induce Positive Selection. *Cell* (1994) 76 (1):17–27. doi: 10.1016/0092-8674(94)90169-4
29. Cebrian I, Croce C, Guerrero NA, Blanchard N, Mayorga LS. Rab22a Controls MHC-I Intracellular Trafficking and Antigen Cross-Presentation by Dendritic Cells. *EMBO Rep* (2016) 17(12):1753–65. doi: 10.15252/embr.201642358
30. van Endert P. Intracellular Recycling and Cross-Presentation by MHC Class I Molecules. *Immunol Rev* (2016) 272(1):80–96. doi: 10.1111/imr.12424
31. Jensen PE, Weber DA, Thayer WP, Westerman LE, Dao CT. Peptide Exchange in MHC Molecules. *Immunol Rev* (1999) 172:229–38. doi: 10.1111/j.1600-065x.1999.tb01368.x
32. Ostrov DA, Grant BJ, Pompeu YA, Sidney J, Harndahl M, Southwood S, et al. Drug Hypersensitivity Caused by Alteration of the MHC-Presented Self-Peptide Repertoire. *Proc Natl Acad Sci USA* (2012) 109(25):9959–64. doi: 10.1073/pnas.1207934109
33. Illing PT, Vivian JP, Dudek NL, Kostenko L, Chen Z, Bharadwaj M, et al. Immune Self-Reactivity Triggered by Drug-Modified HLA-Peptide Repertoire. *Nature* (2012) 486(7404):554–8. doi: 10.1038/nature11147
34. Griem P, Panthel K, Kalbacher H, Gleichmann E. Alteration of a Model Antigen by Au(III) Leads to T Cell Sensitization to Cryptic Peptides. *Eur J Immunol* (1996) 26(2):279–87. doi: 10.1002/eji.1830260202
35. Chervona Y, Arita A, Costa M. Carcinogenic Metals and the Epigenome: Understanding the Effect of Nickel, Arsenic, and Chromium. *Metallomics Integr Biometal Sci* (2012) 4(7):619–27. doi: 10.1039/c2mt20033c
36. Mayorga LS, Cebrian I. Rab22a: A Novel Regulator of Immune Functions. *Mol Immunol* (2019) 113:87–92. doi: 10.1016/j.molimm.2018.03.028
37. Thomas C, Tampe R. MHC I Chaperone Complexes Shaping Immunity. *Curr Opin Immunol* (2019) 58:9–15. doi: 10.1016/j.coi.2019.01.001

Conflict of Interest: The authors declare that the research was conducted in the absence of any commercial or financial relationships that could be construed as a potential conflict of interest.

The reviewer N.S has declared a shared affiliation with some of the authors KI, NH, KO to the handling editor at the time of review.

this article, or claim that may be made by its manufacturer, is not guaranteed or endorsed by the publisher.

frontiers in Immunology

ORIGINAL RESEARCH
published: 10 January 2022
doi: 10.3389/fimmu.2021.795053

Differences in Cellular Clearing Mechanisms of Aggregates of Two Subtypes of HLA-B27

Amit Kumar Thakur and Manni Luthra-Guptasarma *

Department of Immunopathology, Postgraduate Institute of Medical Education and Research (PGIMER), Chandigarh, India

Ankylosing spondylitis (AS) belongs to a group of diseases, called spondyloarthropathies (SpA), that are strongly associated with the genetic marker HLA-B27. AS is characterized by inflammation of joints and primarily affects the spine. Over 160 subtypes of HLA-B27 are known, owing to high polymorphism. Some are strongly associated with disease (e.g., B*2704), whereas others are not (e.g., B*2709). Misfolding of HLA-B27 molecules [as dimers, or as high-molecular-weight (HMW) oligomers] is one of several hypotheses proposed to explain the link between HLA-B27 and AS. Our group has previously established the existence of HMW species of HLA-B27 in AS patients. Still, very little is known about the mechanisms underlying differences in pathogenic outcomes of different HLA-B27 subtypes. We conducted a proteomics-based evaluation of the differential disease association of HLA B*2704 and B*2709, using stable transfectants of genes encoding the two proteins. A clear difference was observed in protein clearance mechanisms: whereas unfolded protein response (UPR), autophagy, and aggresomes were involved in the degradation of B*2704, the endosome–lysosome machinery was primarily involved in B*2709 degradation. These differences offer insights into the differential disease association of B*2704 and B*2709.

Keywords: HLA-B27 alleles, high molecular weight (HMW), aggregates, clearance, proteomics

OPEN ACCESS

Edited by:
Iñaki Alvarez, Universitat Autònoma de Barcelona, Spain

Reviewed by:
Cristina Corina Clement, Weill Cornell Medicine, United States
Fatemeh Navid, National Institute of Arthritis and Musculoskeletal and Skin Diseases (NIAMS), United States

***Correspondence:**
Manni Luthra-Guptasarma
guptasarma.manni@pgimer.edu.in; mguptasarma@yahoo.com

Specialty section:
This article was submitted to Antigen Presenting Cell Biology, a section of the journal Frontiers in Immunology

Received: *14 October 2021*
Accepted: *10 December 2021*
Published: *10 January 2022*

Citation:
Thakur AK and Luthra-Guptasarma M (2022) Differences in Cellular Clearing Mechanisms of Aggregates of Two Subtypes of HLA-B27. Front. Immunol. 12:795053. doi: 10.3389/fimmu.2021.795053

INTRODUCTION

Studies over the last two decades have helped to understand the link between the strong association of HLA-B27 and ankylosing spondylitis (AS). It has been established that the heavy chain of HLA-B27 has a tendency to misfold through the formation of either disulfide-linked dimers or oligomers/high-molecular-weight (HMW) species (1–3). Such misfolding events can occur in the endoplasmic reticulum (ER) prior to the assembly of the HLA trimer [consisting of the HLA heavy chain, the β2 microglobulin (β2m) chain, and bound nonameric peptide] to generate ER stress, together with activation of the unfolded protein response (UPR) and the subsequent activation of macrophages to produce cytokines causing inflammation (4). Misfolded forms of HLA-B27 have been observed on cell surfaces, in the form of β2m-free homodimers. These are believed to cause pathology through binding with killer immunoglobulin-like receptors (KIRs) and leucocyte immunoglobulin-like receptors (LILRs), or through deposition within synovial tissues, resulting in activation and regulation of the immune system (5).

Previously, we have proposed that β2m-free heavy chains of HLA-B27 can undergo a facile conformational change to allow a region of its own chain to bind to either the peptide-binding cleft of the same polypeptide chain (self-display) or the cleft of another polypeptide chain (cross-display). The latter was proposed to lead to the formation of large, soluble, HMW, degradation-resistant, long-surviving aggregates of the HLA-B27 heavy chain (6). We and others have also shown the existence of these HMW aggregates or oligomers of HLA chains in cells transfected with HLA-B27, as well as in AS patients (7, 8).

Although the above work provided clues explaining the link between the misfolding of HLA-B27 and AS, there are scanty data to explain the differential association of HLA-B27 subtypes with AS. Interestingly, despite the level of oligomerization in the disease-associated and non-disease-associated HLA-B27 subtypes being similar (3), the former differs from the latter by an increased tendency to accumulate in intracellular ER-derived vesicles, leading to ER-associated degradation (ERAD) of the heavy chains and the UPR, thereby causing upregulation of the proinflammatory cytokines (8).

Differential stabilities and half-lives of HMW species associated with the disease-associated HLA B*2704 and non-disease-associated HLA B*2709 subtypes have been noted by us (unpublished data). These HMW species might be anticipated to pose a problem for cellular machinery, in terms of mechanisms (especially quality control (QC) mechanisms) for their disposal. Therefore, we considered it necessary to evaluate whether cells transfected with disease-associated and non-disease-associated subtypes of HLA-B27 recruit different cellular machineries (QC processes) for their degradation and turnover.

Here, we provide evidence-based on proteomics and other molecular and cellular correlates to indicate that the disease-associated subtype, HLA B*2704, is mainly disposed off through activation of the UPR and activation of autophagy and the involvement of aggresomes. In contrast, the non-disease-associated subtype B*2709 is mainly disposed off through the endosome–lysosome machinery.

MATERIALS AND METHODS

Generation of Stable Transfectants of Full-Length Subtypes

One lakh cells (H1299) were cultured in complete growth media (Dulbecco's modified Eagle medium (DMEM) high glucose with 10% fetal bovine serum (FBS)), and following confluency of ~70%, cells were plated in serum-free growth media without antibiotics overnight. Cells were then individually transfected with full-length cDNA constructs of each of the two subtypes (B*2704 and B*2709, cloned in pEGFP plasmid, with green fluorescent protein (GFP) in fusion in the C-terminus of the HLA gene), using Lipofectamine™2000 (Invitrogen; Cat No. 11668019). After 6 h of transfection, complete media were added, i.e., DMEM (high glucose) supplemented with 10% FBS, and cells were grown further for 24 h. Stable transfectants were generated by plating cells with serial dilution onto a 96-well plate in DMEM (high glucose) + 10% FBS containing different concentrations of geneticin (200–800 μg/ml). Single-cell clones were selected and then were further grown in complete media.

Sample Preparation for Liquid Chromatography–Mass Spectrometry

Cells were detached using trypsin (cell culture, Gibco®) and centrifuged at 2,000 rpm for 5 min. The supernatant was discarded, and the pellet was washed using 1× TBS (50 mM of Tris-Cl, pH 7.5; 50 mM of NaCl), followed by the addition of protease inhibitors (Sigma; Cat No. P8340). Complete cell lysis was performed using 6MGnHCl (guanidine hydrochloride), followed by sonication and heating at 90°C for 5 min; lysate was centrifuged at 15,000 rpm for 20 min, and the supernatant was used for protein estimation by the bicinchoninic acid (BCA) protein assay kit (Sigma Aldrich, Inc.). Samples were reduced and alkylated with 10 mM of dithiothreitol (DTT; Sigma-Aldrich) and 50 mM of iodoacetamide (IAA; Sigma-Aldrich), respectively, for 1 h in the dark. The pH of diluted samples (10 times) was adjusted to 8–8.5 and trypsinized (Trypsin, Sigma-Aldrich) at 1:20 enzyme to protein ratio for 16 h at 37°C. Before sample clean-up using C18 clean-up columns, pH of each sample was adjusted to around 2 using 10% trifluoroacetic acid (TFA), followed by vacuum drying of samples and reconstitution using 0.1% formic acid. The protein concentration of each sample was determined using NanoDrop (Thermo Fisher Scientific) spectrophotometer, and equal amounts were loaded for liquid chromatography–mass spectrometry (LC-MS) analysis.

Mass Spectrometric Analysis of Peptide Mixtures

Tryptic peptides measuring 1 μg of each sample were analyzed using Orbitrap Fusion™ Tribrid™ Mass Spectrometer (Thermo Scientific, USA) coupled to EASY-nLC 1200 system equipped with nanoelectrospray ion source. Peptides were resolved on nano-LC reverse phase column (75 μm ID × 25 cm, packed with PepMap 2-μm C18 particles) for 95 min with a gradient of 5%–45% acetonitrile in 0.1% formic acid at a flow rate of 300 nl/min. MS1 survey scans were performed with a resolution of 120,000 and a mass range of 375–1,600 m/z, on the Orbitrap. Peptides with charge states 2–5 were sampled for MS2. Following higher-energy C-trap dissociation (HCD) activation, tandem MS (MS/MS) data were acquired using the ion trap analyzer in centroid mode. MS was operated in data-dependent acquisition mode using 30% HCD collision energy and automatic gain control (AGC) target of 5.0e5. Lock mass option was enabled for polydimethylcyclosiloxane (PCM) ions (m/z = 445.120025) for internal recalibration during the run. The MS/MS data have been deposited to the ProteomeXchange Consortium *via* the PRIDE partner repository (9) with the dataset identifier PXD027999.

Data Processing

The raw files generated were used for protein identification using Proteome Discoverer 2.4 (Thermo Fisher Scientific Inc., Austria) by searching against a standard *Homo sapiens* database from UniProtKB

Homo sapiens database UP000005640 using Sequest HT search engine with 20289 sequences. Sequest HT search criteria included tryptic cleavage with two missed cleavages, a precursor mass tolerance of 10 ppm, and fragment mass tolerance of 0.6 Da. Minimum peptide length was set at 6, and maximum peptide length was 144. Search criteria also included carbamidomethylation of cysteines as static modification and oxidation of methionine as a dynamic modification. Default settings were used for other parameters. Protein identification and quantitative analysis used more than two unique peptides; false discovery rate (FDR) of less than 1% and p-values <0.05 were required for relative quantification.

Bioinformatics Analysis

For the purposes of relative quantification analysis, we included all the proteins above 1.5 fold change. Pathway analyses were done using Database for Annotation, Visualization and Integrated Discovery (DAVID) (https://david.ncifcrf.gov/) and Integrated Molecular Pathway Level Analysis (IMPaLA) software. Boxplot and heat map were generated using Proteome discoverer 2.4. A principal component analysis (PCA) plot was generated using R software version 3.4.1. Functional network construction of protein–protein interactions (PPIs) was performed by STRING version 11 network.

Western Blotting

Stable transfectant cells of B*2704 and B*2709 were seeded in 6-well plates containing complete DMEM with 10% FBS; post 70%–80% confluency, cells were serum starved for 6 h and then treated with 50 μM of chloroquine (CQ), 100 nM of bafilomycin (Baf), or combination (CQ+Baf) for 12 h. Similarly, cells were seeded, serum starved for 6 h, and then treated with proteasomal inhibitor MG132 (15 μM) for 4 h and with the UPR inducer thapsigargin (TG) measuring 1 μM for 24 h. After treatment, cells were washed with 1× phosphate-buffered saline (PBS) and then trypsinized. Cells were pelleted after centrifugation at 2,000 rpm for 5 min, washed with 1× PBS, followed by lysis using radioimmunoprecipitation assay (RIPA) buffer (50 mM of Tris HCl, 1% Triton, 0.5% sodium deoxycholate, 0.1% sodium dodecyl sulfate (SDS), 2 mM of EDTA, 150 mM of NaCl, and a cocktail of protease inhibitors). Following incubation on ice for 30 min, centrifugation was performed at 12,000 rpm for 20 min at 4°C. The supernatants were collected and mixed with Laemmli loading buffer; equal amounts of sample (approx. 40 μg) were loaded onto 10% or 12% SDS–polyacrylamide gel electrophoresis (PAGE) gels for analysis of heavy chains and p62 or LC3, respectively. Gels (10%) were also run for cells treated or untreated with CQ, under non-reducing conditions (with SDS in the running buffer), to evaluate the presence of oligomeric species by Western blotting using the HC10 antibody. Blocking was done in 5% skim milk for 2 h at room temperature, before developing the blots using the following primary antibodies, incubated overnight at 4°C: heavy chain-specific HC10 antibody for detection of heavy chains and anti-LC3 (Novus Biologicals; Cat No. NB600-1384) and anti-p62 (Novus Biologicals; Cat No. NBP1-48320) antibodies for detection of autophagy markers. Mouse anti-horseradish peroxidase (anti-HRP) antibody (Invitrogen; Cat No-A0168-1ML) was used as secondary antibody for HC10 staining, and rabbit anti-HRP antibody (Invitrogen; A0545-1ML) was used for probing LC3 as well as p62. Blots were developed using Clarity Western ECL substrate (Bio-Rad; Cat No. 170-5061). Quantitation of signal intensities was performed using the ImageJ software and normalized against the house-keeping β-actin (Sigma; Cat No. A1978).

Confocal Microscopy

H1299 cells and stable transfectant cells of B*2704 and B*2709 were seeded on 24-well plates over coverslips. After approximately 50% confluency, cells were left untreated or treated with CQ (50 μM) or Baf (100 nM). After treatment, cells were fixed with 4% paraformaldehyde, permeabilized with 0.3% Triton-X 100, and blocked with 1% bovine serum albumin (BSA) for 30 min. Cells were incubated overnight at 4°C with primary antibodies against LC3, p62, and vimentin (Sigma; Cat No. V6389); anti-rabbit Alexa Fluor 568 (Invitrogen; Cat No A11011) was used as secondary antibody for visualizing LC3 and p62; and anti-mouse Alexa Fluor 594 (Invitrogen; Cat No. A11032) was used for imaging vimentin. Nuclear staining was done with DAPI. Images were acquired using an Olympus microscope. Images were analyzed using Fiji software. Colocalization was determined using ImageJ software by taking Pearson's coefficient value.

Real-Time PCR

H1299 and stable transfectant cells of B*2704 and B*2709 were seeded in 24-well plates, in the presence and absence of CQ. RNA was isolated using RNeasy mini kit (Qiagen), and cDNA was prepared using verso cDNA synthesis kit (Qiagen). One microliter of cDNA was added to each PCR master mix (Promega) (20 μl), containing 0.25 μM of each primer and 10 μl of 2× iTaq SYBR Green supermix (Bio-Rad Laboratories, Hercules, CA). The following protocol was used: 35 cycles of denaturation step at 95°C for 30 s, annealing at 60°C for 1 min, followed by extension at 72°C for 30 s, with a final standard dissociation protocol to obtain the melting profiles. The gene expression of various genes was evaluated using quantitative real-time PCR (Roche 480). Expression levels in non-transfected cells were used as the baseline. Relative quantification of the targets in each sample was carried out using the signal of GAPDH as a control. Relative gene expression levels were calculated according to the $2^{-\Delta\Delta Ct}$ method.

RESULTS

Identification of the Differentially Expressed Proteins in Cells Stably Transfected With Disease-Associated (B*2704) and Non-Disease-Associated (B*2709) Subtypes of HLA-B27

The NCI-H1299 (human non-small cell lung carcinoma cell line) cells (HLAA*2402, 3201; HLAB*4002, 4002) were used for the transfection of the two subtypes of HLA-B27, with the GFP fused to the C-terminus of each subtype. Previously, other cancer cell lines (such as HeLa cells) transfected with HLA-B27 alleles

(carrying fluorescent molecules at their C-terminal) have been similarly used as experimental cell models to study their intracellular trafficking (3). Label-free quantitation of stable transfectants of H1299 cells carrying disease associated, HLA B*2704, and non-disease associated, HLA B*2709, was carried out. This was done to examine protein QC mechanisms operating in respect of the two subtypes towards clearance of protein aggregates and maintenance of cellular homeostasis. A boxplot of protein abundances in 12 samples, composed of 6 samples each for the transfection-based expression of B*2704 and B*2709, is depicted in **Figure S1A**. The PCA data are presented in **Figure S1B**, illustrating the sample distribution of six B*2704 (red) and six B*2709 (green) samples, showing a clear separation of the two types of samples, based on 1,672 proteins (**Table S1**).

Further, hierarchical clustering analysis (**Figure 1**), with the relative abundance of each protein being color-coded and based on the z-score of the protein's normalized peak area), shows that of the 1,672 proteins detected and quantified in the cell extracts of the two subtypes, 261 proteins were upregulated in B*2704 samples compared with B*2709 samples, and 174 proteins were upregulated in the B*2709 samples compared with B*2704 samples (**Tables S2, S3**, respectively). The fold change was calculated from normalized abundances of proteins in both subtypes, and the UniProt accession numbers of proteins that are differentially upregulated (>1.5 fold) in the two subtypes (**Tables S2, S3**) were independently uploaded on DAVID (version 6.8) and IMPaLA (version 12) software, to examine enriched pathways contributed by the differentially expressed proteins in each subtype. In addition to unique pathways in the two subtypes of HLA-B27, the pathway analysis (**Figure 2** and **Tables S4, S5**) reveals some pathways related to protein clearance that are common to these subtypes, including protein processing in the ER and the proteasome. The list of proteins involved in these 2 pathways is presented in **Tables 1**, **2** for both B*2704 and B*2709, respectively.

Interestingly, in the case of B*2704, in addition to the above pathways, "autophagy" appeared among the top 25 annotation clusters (using the DAVID software) with a group enrichment score greater than 0.6 ($p = 0.08$). Further, using the IMPaLA software too, autophagy was one of the Kyoto Encyclopedia of Genes and Genomes (KEGG) pathways suggested for B*2704 ($p = 0.06$). The list of proteins implicated in the process of autophagy as indicated by these two software is presented in **Table 3**. The possibility of involvement of autophagy in B*2704 approached the borderline of significance, as suggested by both software independently. We decided, therefore, to investigate whether autophagy is indeed involved in the clearance of HMW

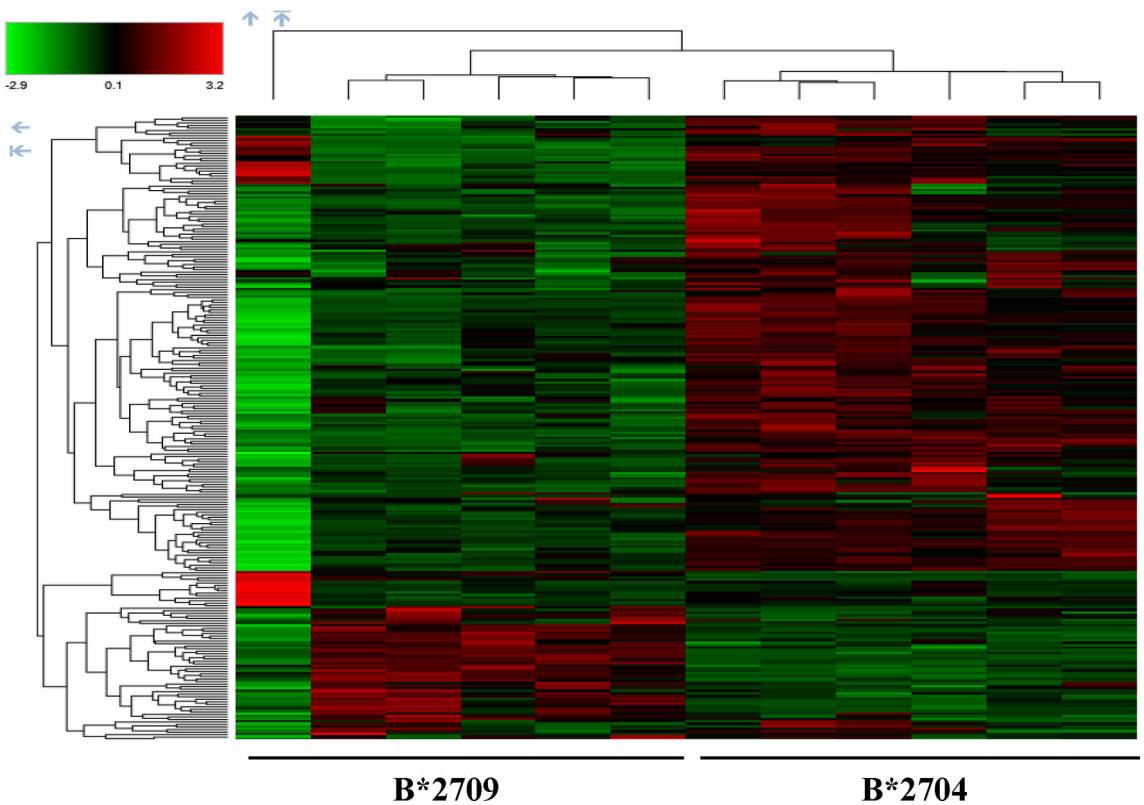

FIGURE 1 | Hierarchical clustering and heat map based on label-free proteome quantification, representing color-coded expression levels of differentially expressed proteins in cells transfected with the two subtypes of HLA-B27. Red color represents the upregulated proteins, while green shows the downregulated proteins in the two cell types, with 6 biological replicates in each case.

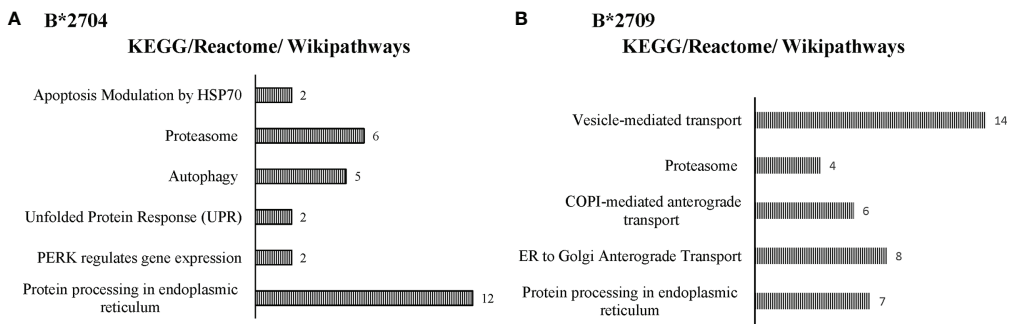

FIGURE 2 | Enriched biological pathways, along with respective protein counts (shown as numbers at the bar-edges) for proteins seen to be differentially upregulated in cells expressing B*2704 **(A)** and B*2709 **(B)**.

aggregates in this subtype, by carrying out separate confirmatory experiments, described later.

To examine potential interactions between differentially expressed proteins in each of the two subtypes, the STRING tool was employed. **Figures S2**, **S3** (left panels) show only the physical network, in an effort to minimize the network cluster; the edges indicate that the proteins are part of a physical complex (without signifying functional association). The panel on the right of **Figure S2** (B*2704) shows that some of the proteins upregulated in B*2704 are engaged in PPIs in the processes of UPR and autophagy. The differentially expressed proteins in B*2709, on the other hand, belong to the trans-Golgi network, or the endosomal–lysosomal pathway (**Figure S3**; right panel).

The differentially expressed proteins belonging to the pathway, "protein processing in ER" (obtained from DAVID software, in both subtypes), were also uploaded in the STRING software to determine the PPIs, as well as to deduce the contribution of the individual (upregulated) proteins present in the ER lumen, which facilitates three types of protein processing: a) protein folding with the help of lumenal chaperones and packaging into transport vesicles, to transport them to the Golgi complex; b) binding of BiP to the terminally misfolded proteins, to direct them towards degradation through the proteasome (ERAD); or c) accumulation of misfolded proteins in the ER, causing ER stress and activation of the UPR signalling pathway. **Tables S6, S7** list the biological processes as well as cellular components involved in "protein processing in ER" as determined using the STRING analysis in B*2704 and B*2709, respectively. Notably, the biological processes associated with the differentially expressed proteins in the case of B*2704-transfected cells included the UPR, response to ER stress, cellular response to oxidative stress, and regulation of the intrinsic apoptotic pathway (**Table S6**), whereas in the case of B*2709-transfected cells, the processes included ER to Golgi vesicle-mediated transport including COPII-coated vesicle cargo loading and receptor-

TABLE 1 | Statistically significant differentially expressed proteins classified under the KEGG pathway, protein processing in ER.

Protein name	UniProt ID	Mol. mass (kDa)	Unique peptides	Coverage (%)	Fold change
Proteins upregulated in B*2704 relative to B*2709					
B-cell receptor-associated protein 31 (BCAP31)	P51572	28	2	13	2.26
BCL2 associated athanogene 2 (BAG2)	O95816	23.8	6	48	2.03
DnaJ heat shock protein family (Hsp40) member B1 (DNAJB1)	P25685	38	3	22	1.61
DnaJ heat shock protein family (Hsp40) member B11 (DNAJB11)	Q9UBS4	40.5	3	11	1.52
Endoplasmic reticulum oxidoreductase 1 alpha	Q96HE7	54.4	3	112	1.59
Eukaryotic translation initiation factor 2 subunit alpha	P05198	36.1	10	36	1.68
Heat shock protein family A (Hsp 70) member 1A (HSPA1A)	P0DMV9		23		1.59
Heat shock protein family A (Hsp 70) member 5 (HSPA5)	P11021	72.3	30	44	1.67
Heat shock protein family A (HSPHA 110) member 5 (HSPH1)	Q92598	96.8	23	41	1.80
Ubiquilin-1 (UBQLN1)	Q9UMXO	62.5	2	9	1.62
Ubiquilin-2 (UBQLN2)	Q9UHD9	65.7	3	8	1.50
Proteins upregulated in B*2709 relative to B*2704					
Sec 13 homolog, nuclear pore and COPII coat complex component (Sec 13)	P55735	35.5	2	11	2.73
Sec 31 homolog A, COPII coat complex component (Sec 31A)	O94979	132.9	3	4	2.08
Calnexin (CANX)	P27824	67.5	9	24	1.54
Heat shock protein family A (Hsp70) member 4 like (HSPA4L)	O95757	94.5	7	17	1.72
Hypoxia upregulated (Hyou1)	Q9Y4L1	111.3	11	21	1.64
Protein disulfide isomerase family A (PDIA4)	P13667	72.9	13	26	1.78
Ribophorin II (RPN2)	P04844	69.2	8	25	1.63

KEGG, Kyoto Encyclopedia of Genes and Genomes; ER, endoplasmic reticulum.

TABLE 2 | Statistically significant, differentially expressed proteins classified under the KEGG pathway, "Proteasome".

Protein name	UniProt ID	Mol. mass (kDa)	Unique peptides	Coverage (%)	Fold change
Proteins upregulated in B*2704					
Proteasome 26S subunit, ATPase 1 (PSMC1)	P62191	49.2	8	24	1.62
Proteasome 26S subunit, ATPase 3 (PSMC3)	P17980	49.2	8	30	1.55
Proteasome 26S subunit, ATPase 6 (PSMC6)	P62333	44.1	8	31	1.61
Proteasome 26S subunit, non-ATPase 2 (PSMD2)	Q13200	29.5	5	25	1.64
Proteasome activator subunit 1 (PSME1)	Q06323	28.7	3	15	1.55
Proteasome subunit alpha 1 (PSMA1)	P25786	29.5	5	25	1.56
Proteins upregulated in B*2709					
Proteasome 26s subunit, non-ATPase 1 (PSMD1)	Q99460	105.8	5	11	1.63
Proteasome subunit beta 4 (PSMB4)	P28070	29.2	6	44	1.54
Proteasome subunit beta 7 (PSMB7)	Q99436	29.9	3	32	2.08

KEGG, Kyoto Encyclopedia of Genes and Genomes.

mediated endocytosis (**Table S7**), suggestive of the endosomal–lysosomal pathway (10, 11).

When the autophagy-related proteins (derived from DAVID software analysis, in the case of B*2704) were uploaded into the STRING software, it was seen that the processes included macroautophagy and selective autophagy, with the cellular components including the autophagosome, phagophore assembly site, and autophagosome membrane (**Table S8**).

In addition, use of the Gene Ontology software (http://geneontology.org/) led us to another possible pathway, i.e., aggresomal pathway, operating in the case of B*2704, with upregulation of proteins involved in retrograde transport and proteins characteristic of aggresomes, including proteins belonging to the BAG family (such as molecular chaperone regulator 3 or BAG3), sequestosome-1 (SQSTM1) and ubiquilin-1 (listed in **Table 3**) (12–14).

The overall picture that emerged from the above data is that unique pathways operate in respect of the processing of misfolded HLA chains of the two subtypes, in cells expressing them due to transfection. Proteomics-based analyses suggest clearance of aggregates through UPR, autophagy, and aggresomes in the case of B*2704 and the endosomal–lysosomal pathway in the case of B*2709.

Confirmation of Macroautophagy in B*2704-Transfected Cells

To confirm the involvement of macroautophagy in cells expressing B*2704 through transfection (as compared with cells expressing B*2709), we used the autophagy inhibitor CQ (50 μM). The presence of aggregates was checked by using the HLA heavy chain-specific mAb, HC10, and Western blotting. The presence of autophagy markers LC3 and p62 was also examined by Western blotting. In the HLA-B27-transfected, CQ-untreated (−CQ) cells, the expression of HC10 was significantly more in B*2704-transfected cells as compared with cells overexpressing B*2709 (**Figure 3A**), suggestive of increased expression of misfolded forms of HLA-B27 in B*2704-transfected cells.

Treatment with CQ caused significantly decreased HC10 binding ($p = 0.03$) in B*2704-expressing cells, unlike cells transfected with B*2709, which correlates with a corresponding decline and rise in oligomeric species, as seen under non-reducing SDS-PAGE conditions (**Figure S4**). However, surprisingly, significantly increased expression of autophagy markers LC3 and p62 was evident in B*2704-expressing cells, as compared with B*2709-expressing cells (**Figures 3C, D**). It would be expected that inhibition of autophagy (through CQ treatment) would result in a corresponding accumulation of heavy chains in B*2704-transfected cells, but on the contrary, we observed a decrease in HC10 binding. Considering the possibility that the aggregates in B*2704-expressing cells can possibly relieve the stress through other alternative pathways such as UPR, we examined the levels of UPR-related genes such as ATF4, BiP, and CHOP, consequent to CQ treatment; as expected, the levels of all three genes were significantly

TABLE 3 | List of proteins associated with autophagy and retrograde transport, identified to be upregulated in B*2704-transfected cells.

Protein name	Gene symbol	UniProt ID	Mol. mass (kDa)	Unique peptides	Coverage (%)	Fold change	Software
RAB7A, member RAS oncogene family (RAB 7A)	RAB7	P51149	23.5	5	31	1.54	DAVID/IMPaLA
Sequestosome-1	SQSTM1	Q13501	47.7	13/54	54	1.50	DAVID
Synaptosomal-associated protein 29 (SNAP29)	SNAP29	O95721	29	2	14	3.41	DAVID/IMPaLA
Ubiquilin-1 (UBQLN1)	UBQLN1	Q9UMXO	62.5	2	9	1.62	DAVID
Ubiquilin-2 (UBQLN2)	UBQLN2	Q9UHD9	65.7	3	8	1.50	DAVID
Microtubule-associated protein 1B		P46821	270.5	5	5	2.04	DAVID
Early endosome antigen 1	EEA1	Q15075	162.4	4	5	1.63	DAVID
Dynein light chain roadblock-type 1 DYNLRB1	DYNLRB1	Q9NP97	10.9	3	34	1.54	DAVID
Dynamin-binding protein DNMBP	DNMBP	Q6XZF7	177.2	4	5	1.54	DAVID

DAVID, Database for Annotation, Visualization and Integrated Discovery; IMPaLA, Integrated Molecular Pathway Level Analysis.

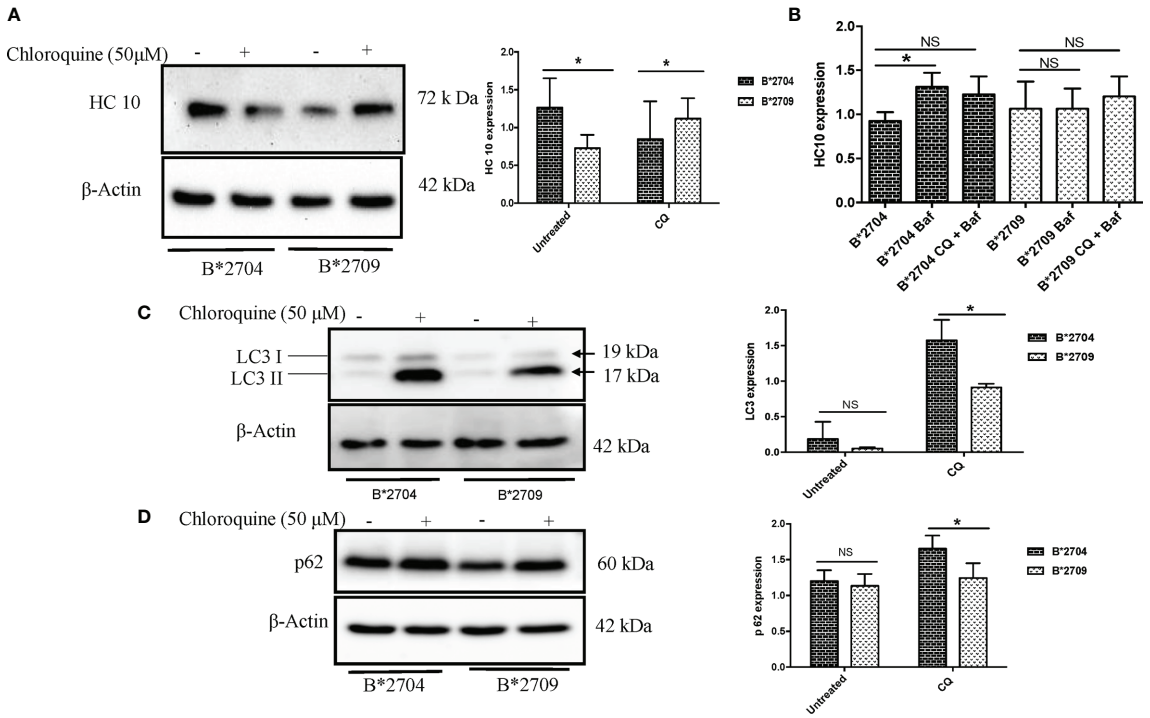

FIGURE 3 | Stable transfectants of pEGFP-HLA-B27 subtypes (B*2704 and B*2709), in the absence (untreated) or presence of CQ, were probed with HC10 antibody **(A)** and also treated with Baf and Baf+CQ **(B)** for detection of heavy chains. Expression levels of autophagy markers LC3 **(C)** and p62 **(D)** were evaluated. Western blotting was done, and actin levels were probed to serve as loading control for all samples to allow normalization of the signals. In each panel, histograms show densitometry data (mean ± SD) from 3 experiments corresponding to the Western blotting, using ImageJ software. Baf, bafilomycin; CQ, chloroquine. NS, non significant ($p > 0.05$); *$p < 0.05$.

increased for B*2704-transfected cells upon treatment with CQ for 12 h (**Figure S5**). Therefore, we propose that the UPR pathway is responsible for the clearance of proteins following autophagic inhibition, leading to reduced accumulation of HC10 reactive species.

Further, we wished to use another autophagy inhibitor, Baf, which is a potent inhibitor of the Vacuolar H+ATPase (15), which controls lysosomal pH, as well as a combination of CQ and Baf to observe the convergent effects on the accumulation of heavy chains as well as autophagy markers. Clearly, a 12-h treatment of B*2704-expressing cells with Baf alone led to a significant increase ($p = 0.02$) in the expression of HC10 reactive species, and a combination of the two inhibitors also showed an increase, although the increase was not significant ($p = 0.07$) (**Figure 3B**).

Interestingly, when the cells were treated with CQ, significantly increased binding of HC10 was observed ($p = 0.04$) in the case of B*2709-expressing cells (unlike that seen in cells transfected with B*2704), as shown in **Figure 3A**. The increased HC10 reactivity following CQ treatment in B*2709 is intriguing, given that the autophagy markers were significantly more in cells expressing B*2704 and not in B*2709-transfected cells (as also expected from the proteomics-based data) (**Figures 3C, D**). This was rationalized as follows: the drug CQ is generally used as an autophagy inhibitor, but recently, it has been found that it can also inhibit the endosomal–lysosomal pathway (16). Therefore, we hypothesize that in the case of cells expressing B*2709, the increased signal of HC10 upon CQ treatment could have arisen as a consequence of CQ-induced inhibition of the endosomal–lysosomal pathway (16). This was in line with the proteomics data (above) with confirmation of the involvement of this pathway in B*2709 cells, which if inhibited by CQ would be expected to lead to decreased clearance of aggregated species of B*2709 with a consequent increase in HC10 reactivity. Confocal microscopy was also carried out to analyze the autophagy markers LC3 and p62 (**Figures 4**, **5**, respectively; **Figure S6**) using both inhibitors CQ and Baf.

In B*2704-expressing cells, CQ (**Figure 4A**) and Baf (**Figure 4B**) treatments led to increased expression of LC3 puncta, with colocalization of GFP and LC3 signals. Statistically increased colocalization of signals of GFP and LC3 was observed in B*2704-transfected cells vs. B*2709-transfected cells upon treatment with CQ ($p = 0.03$) as well as with Baf ($p = 0.02$).

Since, both CQ and Baf increase the pH within the lysosomes, the autophagic degradation is compromised (15, 17), with the resulting accumulation of autophagic vacuoles. Such LC3-positive autophagic vacuoles are more evident in B*2704-expressing cells than in the case of B*2709-expressing cells, suggesting impairment of an ongoing autophagic process in the former (**Figure 4**).

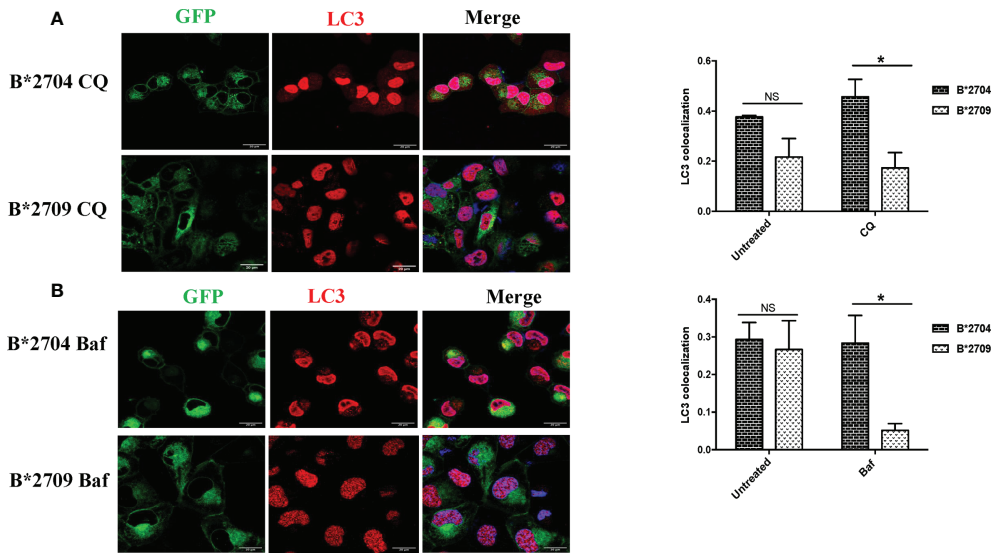

FIGURE 4 | Cells transfected with GFP fusion constructs of the disease-associated, B*2704, and non-disease-associated, B*2709, subtypes were treated with chloroquine (CQ) **(A)** and bafilomycin (Baf) **(B)**. Immunofluorescence staining was performed by confocal microscopy using anti-LC3 antibody (probed with anti-rabbit Alexa Fluor 568) (red). Nuclear staining was done using DAPI (blue). Colocalization was determined using ImageJ software through Pearson's coefficient value. Scale bar, 20 μm. GFP, green fluorescent protein. NS, non significant ($p > 0.05$); *$p < 0.05$.

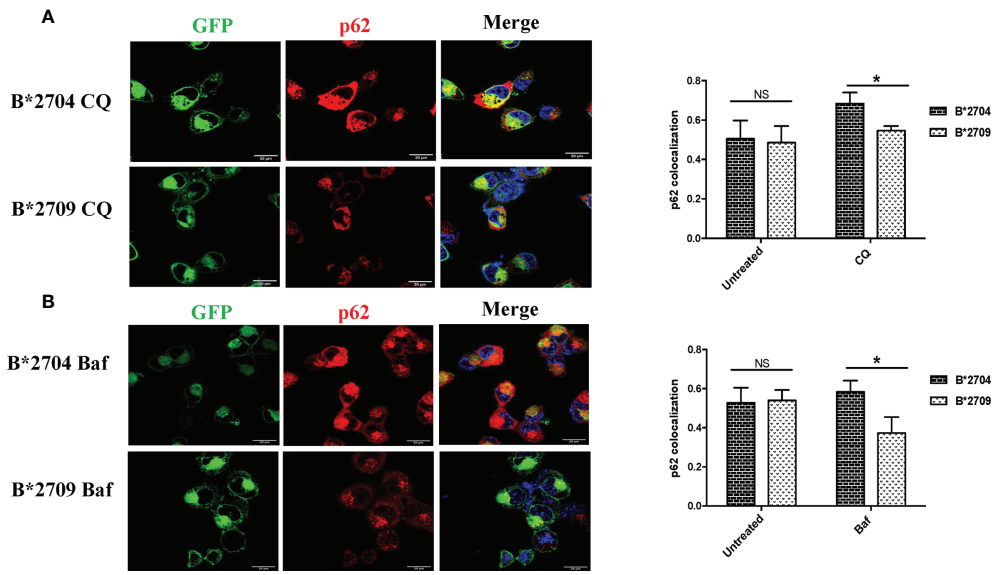

FIGURE 5 | Cells transfected with GFP fusion constructs of the disease-associated, B*2704, and non-disease-associated, B*2709, subtypes were treated with chloroquine (CQ) **(A)** and bafilomycin (Baf) **(B)**. Immunofluorescence staining was performed under confocal microscopy using anti-p62 antibody (probed with anti-rabbit Alexa Fluor 568) (red). Nuclear staining was done using DAPI (blue). Scale bar, 20 μm. GFP, green fluorescent protein. NS, non significant ($p > 0.05$); *$p < 0.05$.

We also evaluated the effects of these inhibitors on the expression of p62, which is degraded by autophagy (**Figure 5**; **Figure S6**). Treatment with CQ and Baf results in increased colocalization of GFP (originating from HLA-B27 heavy chains) and p62 in B*2704-expressing cells as compared with B*2709-transfected cells ($p = 0.03$ and $p = 0.02$, respectively).

Aggresomal Pathway in B*2704

To understand the role of the aggresomal pathway in B*2704 (as suggested by Gene Ontology software analyses), we checked the expression of the intermediate filament protein, vimentin, which is known to form a cage-like structure surrounding aggresomes (18, 19). An observation of the GFP signal together with DAPI staining

(for nuclei) showed that HLA B*2704-transfected cells formed perinuclear aggresome-like structures, which were absent in B*2709-transfected cells (**Figure 6**). Colocalization studies showed that, unlike the B*2709-transfected cells, the GFP signal colocalized with vimentin in the perinuclear region in the B*2704-expressing cells, indicative of aggresome formation (**Figure 6**).

Unfolded Protein Response Involvement in B*2704-Transfected Cells and Proteasomal Pathway Involvement in B*2709-Transfected Cells

To assess the role of proteasome-mediated degradation and UPR in degradation of HLA-B27 aggregates, we used, respectively, the proteasomal inhibitor (MG132) and an inducer of UPR, TG (inhibitor of the Ca^{2+} pump in ER), individually, i.e., in separate experiments on the respective transfected cells. The formation of aggregates was assessed by HC10 staining on Western blotting. Treatment with MG132 resulted in significantly increased binding of HC10 in B*2709-transfected cells (unlike that observed with B*2704-transfected cells), suggesting that the aggregates in the case of the B*2709-transfected cells are actively degraded by the proteasome (**Figure 7A**). Following the treatment with the UPR inducer, TG (inhibitor of the Ca^{2+} pump in ER), significantly decreased binding of HC10 was observed in samples of both the subtypes; however, the reduction was observed to be greater with the disease-associated subtype (B*2704) than with the non-disease-associated subtype (B*2709) (**Figure 7B**), implying a better UPR response by the former than the latter. One of the three UPR programs employed by cells to regulate cellular homeostasis is the attenuation of *de novo* protein synthesis through phosphorylation of the protein translation initiation factor 2 (eIF2α) (20). An examination of the proteomics data revealed that this was the case for B*2704, wherein eukaryotic translation initiation factor 2 subunits 1 and 2, and eukaryotic translation initiation factor 2A were increased, as compared with cells expressing B*2709 after transfection, by 1.68-fold, 1.59-fold, and 1.65-fold, respectively (**Table S2**).

In order to confirm and compare the UPR response in the two subtypes, the two types of transfected cells were treated with MG132, and phosphorylation of eiF2α was assessed by Western blotting. It was observed that the expression of phospho-eIF2α was more in the case of B*2704 as compared with B*2709 (**Figure S7**), confirming once again that UPR plays an important role in the former.

Additionally, real-time PCR was carried out for the two types of transfected cells, for validation of some of the important proteins identified through the proteomics study. The expression of BiP and ubiquilin-1 was significantly increased in B*2704, as compared with B*2709 (**Figure 7C**), implying the role of UPR and autophagy in the former subtype. A significant increase in expression was observed for SEC13, PDI, and Hyou1 in B*2709-transfected cells (**Figure 7C**), confirming the importance of vesicle transport or endosomal pathway in these cells. **Table 4** lists the comparative fold-changes of proteins, as determined by proteomics and real-time expression studies.

DISCUSSION

Out of the >160 known subtypes of HLA-B27 (21), some are disease associated, such as B*2704 and B*2705, while others are non-disease associated, e.g., B*2709 and B*2706. Among these well-known subtypes, B*2704 is strictly associated with the disease,

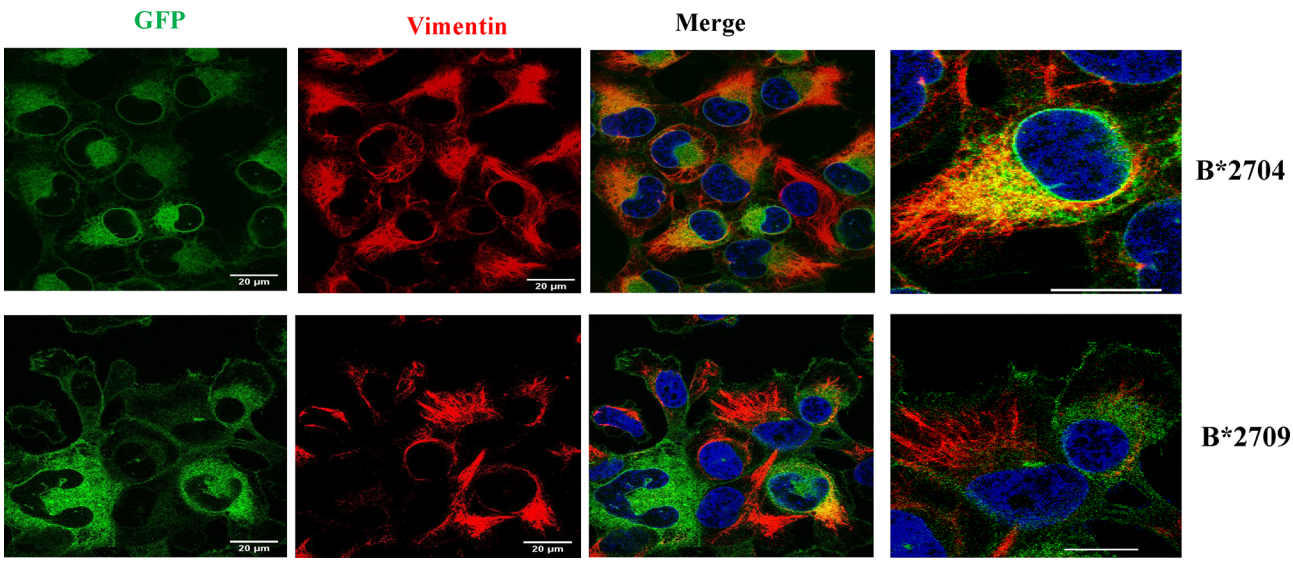

FIGURE 6 | Representative confocal microscopy images of cells transfected with GFP-fusion (green) constructs of B*2704 and B*2709 subtypes, using anti-vimentin antibody (probed with anti-mouse Alexa Fluor 594; red). Nuclei were stained with DAPI (blue). Merged images of GFP with vimentin, as well as vimentin with DAPI, are also shown. Scale bar, 20 µm. Images shown on the right are enlarged views of a section of the merged image. GFP, green fluorescent protein.

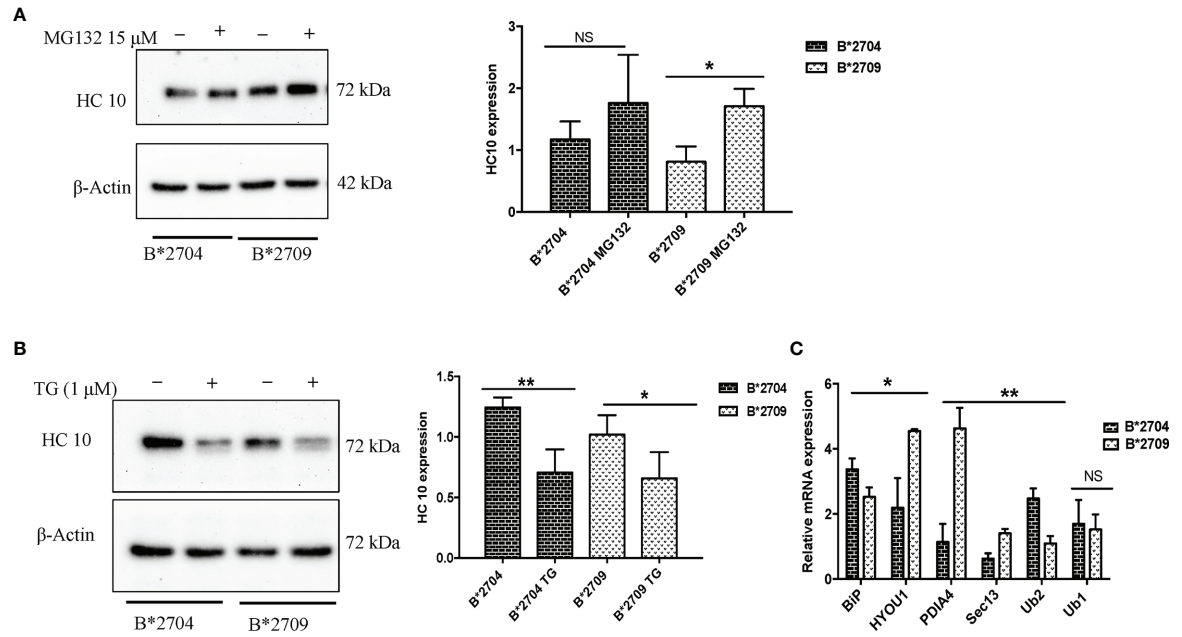

FIGURE 7 | Stable transfectants of pEGFP-HLA-B27 subtypes (B*2704 and B*2709), untreated (– or UT), or treated with MG132 (+) **(A)** or thapsigargin **(B)**. The blots were probed with HC10. Actin levels were probed to serve as loading control for all samples and allow normalization of the signals. In each panel, histograms show densitometry data (mean ± SD) from 3 experiments corresponding to the Western blotting, using ImageJ software. Real-time PCR was carried out for expression of UPR markers, BiP, ubiquilin-1 and ubiquilin-2, and vesicle transport markers HYOU, PDI, and SEC13 **(C)**. Histogram shows data (mean ± SD) from 3 experiments for each marker. NS, non significant ($p > 0.05$); *$p < 0.05$; **$p < 0.01$.

while B*2705 is sometimes not associated with the disease (22), and the disease-association status of B*2706 has been controversial, mainly because it is a rare subtype, and therefore, there are only a few studies reported for HLA-B*2706. This has made it difficult to ascribe the association status of B*2706 with certainty (23). These observations dictated our choice of the two reliable representatives of the disease-associated and non-disease-associated subtypes, and accordingly, we decided to focus on B*2704 as a definite representation of the disease-associated subtype and B*2709 as a non-associated subtype.

It has been previously well documented that fusion of fluorescent proteins to various HLA-B27 subtypes does not interfere with their interaction with β2m, or export to the plasma membrane in a fully folded conformation; such fusion proteins of different subtypes of HLA-B27 display comparable levels of ME1- and HC10-reactive HLA-B (3). Therefore, we performed a comparative and unbiased analysis of the proteomes of cells expressing GFP fusion constructs of the disease-associated HLA chains (B*2704) and non-disease-associated HLA chains (B*2709), which allowed us to decipher the operating QC mechanisms in both subtypes.

Misfolded proteins in the ER trigger a stress response, called the UPR, which tries to restore normal cellular homeostasis through the activation of one or more of the three sensors: IRE1α, PERK, and ATF6 (24). Cellular homeostasis by UPR occurs through i) decrease in *de novo* protein synthesis, or ii) by increasing the folding efficiency of proteins by inducing the expression of chaperones, or iii) by increased degradation of the misfolded proteins *via* the ERAD pathway through ubiquitination and processing in the proteasomal system. ERAD in turn can regulate other QC systems such as UPR and autophagy (and *vice versa*) (25). It is pertinent to note that UPR signalling does not necessarily invoke all three arms of the UPR pathway (26). For example, prolonged ER stress in

TABLE 4 | Comparison of fold change of protein expression for selected proteins, determined by proteomics-based evaluation as well as by real-time PCR analysis.

Protein	Fold change in proteomics	Fold change in real-time PCR	HLA B-27 subtype
BiP	1.67	3.37	B*2704
Ubiquilin-1 (UBQLN1)	1.62	1.69	B*2704
Ubiqilin-2 (UBQLN2)	1.5	2.47	B*2704
Sec 13	2.73	1.4	B*2709
Hypoxia upregulated (Hyou1)	1.64	4.63	B*2709
Protein disulfide isomerase family A (PDIA4)	1.78	4.5	B*2709

neurodegenerative diseases leads to activation of UPR signalling, triggering a set of pro-death programs (27); however, it has been seen that XBP1 generation through splicing (involved in IRE1 signalling) is dispensable in the process and does not contribute to the neurodegeneration associated with prion protein misfolding (28). In our study too, we did not observe any splicing of XBP1 in B*2704 or B*2709-transfected cells. Further, there was no difference in the level of splicing observed between the two types of cells upon treatment with MG132, implying that in this case too, XBP-1 is dispensable in the UPR pathway (data not shown).

Label-free quantitation data comparing upregulated proteins in B*2704-transfected cells (with respect to B*2709-transfected cells) showed upregulation of the following six proteins related to UPR: i) BiP, ii) phospho-eIF2, iii) ubiquilin-1, iv) ubiquilin-2, v) sequestosome, and vi) Rab7. BiP or HSPA5 is a master regulator for ER stress, which controls the activation of UPR signalling. It is required for ER integrity and ER stress-induced autophagy (29). Phosphorylated eIF2 represses the translational machinery in response to stress through the UPR process. Thus, the overexpression of BiP and phospho-eIF2α in B*2704 indicates activation of UPR. It may be noted that the phosphorylation of eIF2α has also been shown to be a central event for the stimulation of autophagy (30). Accordingly, upregulation of ubiquilin-1 (UBQLN1) and ubiquilin-2 (UBQLN2) in B*2704-transfected cells was observed. The ubiquilins are thought to play a role in regulating the maturation of autophagy and expanding the involvement of ubiquitin-related proteins in autophagy; *UBQLN2* is implicated in macroautophagy through its indirect interaction with LC3 (14). These proteins are also important components of the protein QC process, regulating different protein degradation mechanisms and pathways, including the ubiquitin–proteasome system (UPS) and the ERAD pathway. UBQLN2 plays a role in ERAD, by its binding to ubiquinated substrates to drive degradation by the 26S proteasome (31). UBQLN1 has been reported to be associated with Alzheimer's disease (32), while UBQLN 2 has gained importance because of its association with amyotrophic lateral sclerosis and frontotemporal dementia (ALS/FTD) pathogenesis (33). Sequestosome or ubiquitin-binding protein p62 is an autophagy adapter protein that binds to the target (cargo) and undergoes LC3-mediated delivery to the autophagosomes for lysosomal proteolysis (34). Finally, RAB7 is a member of the family of GTPases present on the late endosomes, which is crucial for complete autophagic flux (35, 36). Therefore, increased expression of all six proteins clearly points towards UPR and autophagy playing a predominant role in the clearance of aggregates in B*2704-transfected cells.

During the initiation of autophagy, LC3-I is cleaved and lipidated to form LC3-II; p62 is another autophagy marker, which is sequestered within autophagosomes, followed by degradation by lysosomes (37). Treatment with CQ induces the formation of autophagosomes, with inhibition of autophagosome degradation in the later stage of autophagy (38). The decrease in HC10-specific forms of B*2704 observed in the presence of CQ may be justified on the basis of the fact that although CQ treatment inhibits autophagy, it can induce ER stress as well as UPR through the PERK-eIF2α-ATF4 pathway (39), so that the clearance of aggregated forms of the protein may be UPR-driven. This was indeed found to be so, as exemplified by the increase in activation of UPR genes (by real-time PCR) and phosphorylation of eIF2α. Using a potent inhibitor like Baf led to significantly increased accumulation of heavy chains of B*2704-expressing cells, clearly indicative of autophagic pathway. The difference in levels of accumulation of HC10 reactive species upon treatment with CQ and Baf may result from the fact that although both CQ and Baf cause changes in intra-lysosomal pH change, the mechanisms of inhibition for the two inhibitors are not the same (16).

Interestingly, however, in the case of B*2709-transfected cells, treatment with CQ led to increased aggregate formation (HC10 reactivity). Since CQ has been shown to induce an autophagy-independent severe disorganization of Golgi and endo-lysosomal networks (16), we propose that the increase in the HC10 signal, following treatment with CQ, occurs because of impairment of vesicle fusion, or due to disruption of the endosomal lysosomal pathway (11) in which proteins are received from ER in the form of vesicles, and internalized with help of receptors present on the membranes of vesicles (which fuse with late endosome and finally with lysosomes where aggregates are degraded by the acidic pH).

A comparison of LC3 levels in transfected cells in the absence and presence of CQ showed that LC3 levels increased in both B*2704 and B*2709-transfected cells upon CQ treatment. This was expected in the former (because of the autophagy pathway operating in these cells as discussed above) but not in the latter and was somewhat puzzling. This is rationalized on the basis of the new concept that has emerged over the last few years, referred to as "non-canonical autophagy" involving CQ-induced parallel induction of single-membrane endolysosomal LC3 lipidation, which is proposed to regulate the fusion of vesicles with lysosomes (40, 41). We believe that in the case of B*2709-transfected cells, where removal of aggregates of misfolded HLA chains occurs through the endosomal–lysosomal pathway, such an increase in LC3 would be entirely expected.

The observation of aggresome formation in B*2704-expressing cells was expected since clearance of misfolded proteins accumulated in the aggresomes also occurs through the macroautophagy pathway (42), already determined to be operating in these cells. Another result to support the formation of aggresomes was the proteomics study-based observation of increased expression of proteins associated with the dynein–dynactin system (upregulation by 1.54-fold of dynein light chain roadblock-type 1 or DYNLRB1) in B*2704-transfected cells, which plays a critical role in the retrograde transport of cargo of misfolded proteins, along microtubules, for processing at perinuclear aggresomes (43). Also, SQSTM1 (or p62) and the Hsp70 co-chaperone, BAG3, are proteins known to be associated with dynein–dynactin (12, 13); p62 scaffolding protein is required for dynein function in trafficking cargo to the perinuclear region of the cell along the degradative pathways (13), and BAG3 is involved in chaperone-based aggresome

targeting, which is independent of substrate ubiquitination (12). p62 and BAG3 were enriched in B*2704-transfected cells by 1.5-fold and 1.73-fold, respectively (as listed in **Table 3**). Some of the other proteins involved in retrograde transport were also upregulated in B*2704; these include synaptosomal-associated protein 29 (44) ubiquilin-1 (45), early endosome antigen 1 (46), and the dynamin-binding protein (43, 47) (**Table 3**), supporting the retrograde transport of cargo to aggresomes.

From all of the above, it is clear that in B*2704-transfected cells, besides UPR, macroautophagy (involving the generation of a double-membrane autophagosome, which forms non-selectively around bulk cytoplasm) may cause carriage of the misfolded B*2704 protein molecules through a series of vesicular fusion events into the lysosomes for subsequent pH-dependent degradation by lysosomal hydrolases (48).

There could be several reasons for the failure of UPR and autophagy to clear the B*2704 aggregates. Degradation pathways adopted by aggregates can vary, depending on whether the protein is in soluble or fibrillar form and whether it bears any post-translational modifications. It is possible that the aggregates formed by B*2704 are more stable and resistant to degradation; indeed, our previous studies have hinted at this possibility (6) since the α1 and α2 domains of B*2709 are less stable to chemical and thermal denaturation than the corresponding domains of B*2705 (49). Such long-lived proteins would be expected to follow the autophagic pathway rather than the proteasomal machinery, which is more suited for short-lived proteins (50). In any case, such aggregates would not be able to pass through the proteasome. It is also possible that such aggregated proteins would resist being dissociated easily from the components of the autophagic pathway before being delivered to the lysosome. Although autophagy appears to operate to clear the B*2704 aggregates, the kinetics of the clearance mechanism may not be suited to the number of aggregates and the rate of autophagic clearance. It is also possible that the aggregates are resistant to the low pH of lysosomes, resulting in a buildup of protein in lysosomes (akin to the lysosomal storage disorders) (51). This possibility will need further examination.

Accumulation of misfolded forms of B*2704, including dimers and oligomers or HMW aggregates, is expected to cause increased ER stress and UPR. In the case of dimers, several studies have proposed that interaction of such dimers with natural killer (NK) cells, myelomonocytes, and lymphocytes, can result in stimulation and proliferation of KIR3DL2+ CD4+ T lymphocytes, with consequent production of proinflammatory cytokines such as IL-23 and IL-17; these cytokines can further collaborate with TNF-α or IFN-γ, thereby causing sustained immune activation with effects on bone construction and contributing to the disease pathogenesis (4, 5, 52, 53). We propose that HMW species of B*2704 may behave in a similar manner.

In the case of B*2709-transfected cells, proteomic data analyses using available software packages suggested that the proteomes of B*2709-transfected cells are enriched in proteins facilitating vesicle-mediated transport from the ER to Golgi, COPII vesicle coating, vesicle transport, receptor-mediated endocytosis, and the proteasomal pathway (**Tables S4, S5**). These processes are facilitated by proteins such as SEC13, SEC31, heat shock protein 70 (Hsp70), and PDIA4 found to be upregulated in B*2709 cells (**Table S3**). The SEC13/SEC31 proteins are required for the generation of COPII vesicles, which direct the budding of vesicles from the ER and play an important role in the anterograde transport of proteins to Golgi (54). Hypoxia upregulated protein 1 (or Hyou1) belongs to the Hsp 70 family and was found to be upregulated by 1.64-fold in B*2709; it plays an important role in protein folding and secretion in the ER (55). PDIA4 belongs to the protein disulfide isomerase (PDI) family of ER proteins that catalyze protein folding and thiol–disulfide interchange reactions (56).

Previous studies have demonstrated evidence of HLA-B27 misfolding in the gut of AS patients and activation of autophagy (but not UPR) regulating intestinal modulation of IL-23 (57). Autophagy in combination with ERAD has also been suggested to play a role in the clearance of excess HLA class I heavy chains expressed in transgenic rats (58). Further, there are other studies implicating the importance of UPR as an intracellular stress response pathway (induced by misfolded forms of HLA-B27 in B27/hβ2m transgenic rats) (59, 60), responsible for causing an innate immune activation (61), cytokine dysregulation, and increased production of proinflammatory cytokine axis (62, 63).

The novelty of this study is that this is the first proteomics-based study seeking to explain the differential disease association of the HLA-B27 subtypes with respect to differences in the mechanism of disposal of HMW aggregates of HLA-B27 molecules. The ER QC processes (such as ERAD and UPR), as well as autophagy, have been previously shown to bring about the elimination of HLA-B27 misfolded proteins, and our data also show that these pathways are important, but only as far as B*2704 is concerned. Here too, we additionally provide data to show the importance of aggresomes in garbage disposal, which are degraded by autophagy upon transport to an autophagosome. On the other hand, it is noteworthy that the disposal of misfolded species in the non-disease-associated B*2709 subtype occurs mainly through the endosomal–lysosomal pathway, which has not been talked about as yet in the field of spondyloarthropathies.

This observation of a stark difference in disposal mechanisms involving B*2704 and B*2709 not only will aid in better understanding of AS disease pathogenesis but could also provide insights into the better design of therapeutics, e.g., along the lines of diseases such as multiple myeloma, where a combinatorial approach of using proteasome, autophagy, and aggresome inhibitors was used to induce a cellular stress response of apoptosis (64, 65).

DATA AVAILABILITY STATEMENT

The original contributions presented in the study are publicly available and have been deposited to the ProteomeXchange Consortium via the PRIDE partner repository with the dataset identifier PXD027999.

AUTHOR CONTRIBUTIONS

Study design: ML-G. Acquisition of data: AT. Analysis and interpretation: AT and ML-G. Manuscript preparation: AT and ML-G. Statistical analysis: AT and ML-G.

FUNDING

This work was supported by a grant from the Department of Biotechnology, Government of India (BT/PR28516/MED/30/2022/2018).

ACKNOWLEDGMENTS

Dr. Rajendra Kumar is thanked for his help with the preparation of confocal images. Dr. Manish Kumar Rana is thanked for generation of stable cell lines for the HLA-B27 subtypes (to be discussed in a separate publication).

SUPPLEMENTARY MATERIAL

The Supplementary Material for this article can be found online at: https://www.frontiersin.org/articles/10.3389/fimmu.2021.795053/full#supplementary-material

Supplementary Figure 1 | Boxplots representing abundance distribution of proteins in cells expressing B*2704 (blue colour) and B*2709 (orange colour) **(A)**, made using Proteome Discoverer (version 2.4). Principal Component Analysis (PCA) carried out using R software (version 3.4.1) **(B)**.

Supplementary Figure 2 | Protein–protein interaction analysis (conducted by the String database, version 11.0) of 261 proteins found to be upregulated in cells expressing B*2704 **(A)**. The proteins related to Unfolded Protein Response **(B)** and autophagy pathway **(C)** are also shown.

Supplementary Figure 3 | Protein–protein interaction analysis (conducted by the String database, version11.0) of 174 proteins found to be upregulated in cells expressing B*2709 **(A)**. The proteins related to vesicle transport from ER to Golgi are also shown **(B)**.

Supplementary Figure 4 | Western blot corresponding to non-reducing SDS-PAGE gel electrophoresis of lysates derived from cells transfected with B*2704 and B*2709 under conditions of absence and presence of CQ. Blots were probed with HC 10 antibody to analyze the oligomeric species. Images were taken under short and long exposures to better highlight the presence of differently oligomerized species in each case.

Supplementary Figure 5 | Real Time PCR was carried out to evaluate the expression of UPR markers for non-transfected cells (H1299) and transfected cells expressing B*2704 and B*2709, following treatment with CQ (50μM) for 12h.

Supplementary Figure 6 | Immunofluorescence staining was performed for H1299 cells **(A)**, cells transfected with B*2704 **(B)** and B*2709 (**(C)** subtypes by confocal microscopy using anti-LC3 and anti-p62 antibody (probed with anti-rabbit Alexa Fluor 568) (red). Nuclear staining was done using DAPI (Blue).

Supplementary Figure 7 | Stable transfectants of pEGFP-HLA-B27 subtypes (B*2704 and B*2709), treated with (+) or without (-) the proteasomal inhibitor, MG132, and probed with anti-phospho-eIF2α antibody.

REFERENCES

1. McMichael A, Bowness P. HLA-B27: Natural Function and Pathogenic Role in Spondyloarthritis. *Arthritis Res Ther* (2002) 4:1–6. doi: 10.1186/ar571
2. Kollnberger S, Bird LA, Roddis M, Hacquard-Bouder C, Kubagawa H, Bodmer HC, et al. HLA-B27 Heavy Chain Homodimers Are Expressed in HLA-B27 Transgenic Rodent Models of Spondyloarthritis and Are Ligands for Paired Ig-Like Receptors. *J Immunol* (2004) 173:1699–710. doi: 10.4049/jimmunol.173.3.1699
3. Giquel B, Carmouse S, Denais C, Cherfa A, Chimenti M, Fert I, et al. Two HLA–B27 Alleles Differently Associated With Spondylarthritis, B* 2709 and B* 2705, Display Similar Intracellular Trafficking and Oligomer Formation. *Arthritis Rheum: Off J Am Coll Rheumatol* (2007) 56:2232–43. doi: 10.1002/art.22725
4. DeLay ML, Turner MJ, Klenk EI, Smith JA, Sowders DP, Colbert RA. HLA–B27 Misfolding and the Unfolded Protein Response Augment Interleukin-23 Production and Are Associated With Th17 Activation in Transgenic Rats. *Arthritis Rheum* (2009) 60:2633–43. doi: 10.1002/art.24763
5. Cauli A, Piga M, Dessole G, Porru G, Floris A, Vacca A, et al. Killer-Cell Immunoglobulin-Like Receptors (KIR) and HLA-Class I Heavy Chains in Ankylosing Spondylitis. *Drug Dev Res* (2014) 75:S15–9. doi: 10.1002/ddr.21187
6. Luthra-Guptasarma M, Singh B. HLA-B27 Lacking Associated Beta2-Microglobulin Rearranges to Auto-Display or Cross-Display Residues 169-181: A Novel Molecular Mechanism for Spondyloarthropathies. *FEBS Lett* (2004) 575:1–8. doi: 10.1016/j.febslet.2004.08.037
7. Sharma R, Vasishta RK, Sen RK, Luthra-Guptasarma M. Refolding of HLA-B27 Heavy Chains in the Absence of β2m Yields Stable High Molecular Weight (HMW) Protein Forms Displaying Native-Like as Well as Non-Native-Like Conformational Features: Implications for Autoimmune Disease. *Biochim Biophys Acta (BBA)-Mol Basis Dis* (2007) 1772:1258–69. doi: 10.1016/j.bbadis.2007.10.005
8. Jeanty C, Sourisce A, Noteuil A, Jah N, Wielgosik A, Fert I, et al. HLA-B27 Subtype Oligomerization and Intracellular Accumulation Patterns Correlate With Predisposition to Spondyloarthritis. *Arthritis Rheumatol* (2014) 66:2113–23. doi: 10.1002/art.38644
9. Vizcaino JA, Cote RG, Csordas A, Dianes JA, Fabregat A, Foster JM, et al. The Proteomics Identifications (PRIDE) Database and Associated Tools: Status in 2013. *Nucleic Acids Res* (2013) 41(Database issue):D1063–9. doi: 10.1093/nar/gks1262
10. Hu Y-B, Dammer EB, Ren R-J, Wang G. The Endosomal-Lysosomal System: From Acidification and Cargo Sorting to Neurodegeneration. *Trans Neurodegeneration* (2015) 4:1–10. doi: 10.1186/s40035-015-0041-1
11. Sun Z, Brodsky JL. Protein Quality Control in the Secretory Pathway. *J Cell Biol* (2019) 218:3171–87. doi: 10.1083/jcb.201906047
12. Gamerdinger M, Kaya AM, Wolfrum U, Clement AM, Behl C. BAG3 Mediates Chaperone-Based Aggresome-Targeting and Selective Autophagy of Misfolded Proteins. *EMBO Rep* (2011) 12:149–56. doi: 10.1038/embor.2010.203
13. Calderilla-Barbosa L, Seibenhener ML, Du Y, Diaz-Meco M-T, Moscat J, Yan J, et al. Interaction of SQSTM1 With the Motor Protein Dynein–SQSTM1 Is Required for Normal Dynein Function and Trafficking. *J Cell Sci* (2014) 127:4052–63. doi: 10.1242/jcs.152363
14. N'Diaye E, Kajihara KK, Hsieh I, Morisaki H, Debnath J, Brown EJ. PLIC Proteins or Ubiquilins Regulate Autophagy-Dependent Cell Survival During Nutrient Starvation. *EMBO Rep* (2009) 10:173–9. doi: 10.1038/embor.2008.238
15. Bowman EJ, Siebers A, Altendorf K. Bafilomycins: A Class of Inhibitors of Membrane ATPases From Microorganisms, Animal Cells, and Plant Cells. *Proc Natl Acad Sci U.S.A.* (1988) 85:7972–6. doi: 10.1073/pnas.85.21.7972
16. Mauthe M, Orhon I, Rocchi C, Zhou X, Luhr M, Hijlkema K-J, et al. Chloroquine Inhibits Autophagic Flux by Decreasing Autophagosome-Lysosome Fusion. *Autophagy* (2018) 14:1435–55. doi: 10.1080/15548627.2018.1474314

17. Poole B, Ohkuma S. Effect of Weak Bases on the Intralysosomal pH in Mouse Peritoneal Macrophages. *J Cell Biol* (1981) 90:665–9. doi: 10.1083/jcb.90.3.665
18. Kopito RR. Aggresomes, Inclusion Bodies and Protein Aggregation. *Trends Cell Biol* (2000) 10:524–30. doi: 10.1016/S0962-8924(00)01852-3
19. Johnston JA, Ward CL, Kopito RR. Aggresomes: A Cellular Response to Misfolded Proteins. *J Cell Biol* (1998) 143:1883–98. doi: 10.1083/jcb.143.7.1883
20. Lee J-H, Jeong J, Jeong EM, Cho S-Y, Kang JW, Lim J, et al. Endoplasmic Reticulum Stress Activates Transglutaminase 2 Leading to Protein Aggregation. *Int J Mol Med* (2014) 33:849–55. doi: 10.3892/ijmm.2014.1640
21. Khan MA. An Update on the Genetic Polymorphism of HLA-B*27 With 213 Alleles Encompassing 160 Subtypes (and Still Counting). *Curr Rheumatol Rep* (2017) 19:9. doi: 10.1007/s11926-017-0640-1
22. Yang T, Duan Z, Wu S, Liu S, Zeng Z, Li G, et al. Association of HLA-B27 Genetic Polymorphisms With Ankylosing Spondylitis Susceptibility Worldwide: A Meta-Analysis. *Mod Rheumatol* (2014) 24:150–61. doi: 10.3109/14397595.2013.852856
23. Van Gaalen FA. Does HLA-B*2706 Protect Against Ankylosing Spondylitis? A Meta-Analysis. *Int J Rheum Dis* (2012) 15:8–12. doi: 10.1111/j.1756-185X.2011.01676.x
24. Ma Y, Hendershot LM. The Mammalian Endoplasmic Reticulum as a Sensor for Cellular Stress. *Cell Stress Chaperones* (2002) 7:22224. doi: 10.1379/1466-1268(2002)007<0222:TMERAA>2.0.CO;2
25. Qi L, Tsai B, Arvan P. New Insights Into the Physiological Role of Endoplasmic Reticulum-Associated Degradation. *Trends Cell Biol* (2017) 27:430–40. doi: 10.1016/j.tcb.2016.12.002
26. Hiramatsu N, Chiang W-C, Kurt TD, Sigurdson CJ, Lin JH. Multiple Mechanisms of Unfolded Protein Response-Induced Cell Death. *Am J Pathol* (2015) 185:1800–8. doi: 10.1016/j.ajpath.2015.03.009
27. Remondelli P, Renna M. The Endoplasmic Reticulum Unfolded Protein Response in Neurodegenerative Disorders and Its Potential Therapeutic Significance. *Front Mol Neurosci* (2017) 10:187. doi: 10.3389/fnmol.2017.00187
28. Hetz C, Lee A-H, Gonzalez-Romero D, Thielen P, Castilla J, Soto C, et al. Unfolded Protein Response Transcription Factor XBP-1 Does Not Influence Prion Replication or Pathogenesis. *Proc Natl Acad Sci U.S.A.* (2008) 105:757–62. doi: 10.1073/pnas.0711094105
29. Wang M, Wey S, Zhang Y, Ye R, Lee AS. Role of the Unfolded Protein Response Regulator GRP78/BiP in Development, Cancer, and Neurological Disorders. *Antioxid Redox Signaling* (2009) 11:2307–16. doi: 10.1089/ars.2009.2485
30. Humeau J, Leduc M, Cerrato G, Loos F, Kepp O, Kroemer G. Phosphorylation of Eukaryotic Initiation Factor-2α (Eif2α) in Autophagy. *Cell Death Dis* (2020) 11:1–12. doi: 10.1038/s41419-020-2642-6
31. Xia Y, Yan LH, Huang B, Liu M, Liu X, Huang C. Pathogenic Mutation of UBQLN2 Impairs Its Interaction With UBXD8 and Disrupts Endoplasmic Reticulum-Associated Protein Degradation. *J Neurochem* (2014) 129:99–106. doi: 10.1111/jnc.12606
32. El Ayadi A, Stieren ES, Barral JM, Boehning D. Ubiquilin-1 and Protein Quality Control in Alzheimer Disease. *Prion* (2013) 7:164–9. doi: 10.4161/pri.23711
33. Renaud L, Picher-Martel V, Codron P, Julien J-P. Key Role of UBQLN2 in Pathogenesis of Amyotrophic Lateral Sclerosis and Frontotemporal Dementia. *Acta Neuropathol Commun* (2019) 7:1–11. doi: 10.1186/s40478-019-0758-7
34. Shaid S, Brandts CH, Serve H, Dikic I. Ubiquitination and Selective Autophagy. *Cell Death Differ* (2013) 20:21–30. doi: 10.1038/cdd.2012.72
35. Kuchitsu Y, Fukuda M. Revisiting Rab7 Functions in Mammalian Autophagy: Rab7 Knockout Studies. *Cells* (2018) 7:215. doi: 10.3390/cells7110215
36. Zhan L, Chen S, Li K, Liang D, Zhu X, Liu L, et al. Autophagosome Maturation Mediated by Rab7 Contributes to Neuroprotection of Hypoxic Preconditioning Against Global Cerebral Ischemia in Rats. *Cell Death Dis* (2017) 8:e2949–9. doi: 10.1038/cddis.2017.330
37. Runwal G, Stamatakou E, Siddiqi F, Puri C, Zhu Y, Rubinsztein DC. LC3-Positive Structures Are Prominent in Autophagy-Deficient Cells. *Sci Rep* (2019) 9:10147. doi: 10.1038/s41598-019-46657-z
38. Cai Y, Cai J, Ma Q, Xu Y, Zou J, Xu L, et al. Chloroquine Affects Autophagy to Achieve an Anticancer Effect in EC109 Esophageal Carcinoma Cells *In Vitro*. *Oncol Lett* (2018) 15:1143–8. doi: 10.3892/ol.2017.7415
39. Nakano K, Masui T, Yogo A, Uchida Y, Sato A, Kasai Y, et al. Chloroquine Induces Apoptosis in Pancreatic Neuroendocrine Neoplasms *via* Endoplasmic Reticulum Stress. *Endocrine-related Cancer* (2020) 27:431–9. doi: 10.1530/ERC-20-0028
40. Florey O, Gammoh N, Kim SE, Jiang X. Overholtzer M. V-ATPase and Osmotic Imbalances Activate Endolysosomal LC3 Lipidation. *Autophagy* (2015) 11:88–99. doi: 10.4161/15548627.2014.984277
41. Jacquin E, Leclerc-Mercier S, Judon C, Blanchard E, Fraitag S, Florey O. Pharmacological Modulators of Autophagy Activate a Parallel Noncanonical Pathway Driving Unconventional LC3 Lipidation. *Autophagy* (2017) 13:854–67. doi: 10.1080/15548627.2017.1287653
42. Simms-Waldrip T, Rodriguez-Gonzalez A, Lin T, Ikeda AK, Fu C, Sakamoto KM. The Aggresome Pathway as a Target for Therapy in Hematologic Malignancies. *Mol Genet Metab* (2008) 94:283–6. doi: 10.1016/j.ymgme.2008.03.012
43. Bonifacino JS, Rojas R. Retrograde Transport From Endosomes to the Trans-Golgi Network. *Nat Rev Mol Cell Biol* (2006) 7:568–79. doi: 10.1038/nrm1985
44. Cheng XT, Zhou B, Lin MY, Cai Q, Sheng ZH. Axonal Autophagosomes Recruit Dynein for Retrograde Transport Through Fusion With Late Endosomes. *J Cell Biol* (2015) 209:377–86. doi: 10.1083/jcb.201412046
45. Regan-Klapisz E, Sorokina I, Voortman J, de Keizer P, Roovers RC, Verheesen P, et al. Ubiquilin Recruits Eps15 Into Ubiquitin-Rich Cytoplasmic Aggregates *via* a UIM-UBL Interaction. *J Cell Sci* (2005) 118:4437–50. doi: 10.1242/jcs.02571
46. Sivan G, Weisberg AS, Americo JL, Moss B. Retrograde Transport From Early Endosomes to the Trans-Golgi Network Enables Membrane Wrapping and Egress of Vaccinia Virus Virions. *J Virol* (2016) 90:8891–905. doi: 10.1128/JVI.01114-16
47. Terenzio M, Di Pizio A, Rishal I, Marvaldi L, Di Matteo P, Kawaguchi R, et al. DYNLRB1 Is Essential for Dynein Mediated Transport and Neuronal Survival. *Neurobiol Dis* (2020) 140:104816. doi: 10.1016/j.nbd.2020.104816
48. Shacka JJ, Roth KA, Zhang J. The Autophagy-Lysosomal Degradation Pathway: Role in Neurodegenerative Disease and Therapy. *Front Biosci* (2008) 13:718–36. doi: 10.2741/2714
49. Rana MK, Luthra-Guptasarma M. Differences in Conformational Stability of the Two Alpha Domains of the Disease-Associated and Non-Disease-Associated Subtypes of HLA-B27. *Int J Biol Macromol* (2017) 94:233–45. doi: 10.1016/j.ijbiomac.2016.08.066
50. Ji CH, Kwon YT. Crosstalk and Interplay Between the Ubiquitin-Proteasome System and Autophagy. *Mol Cells* (2017) 40:441–9. doi: 10.14348/molcells.2017.0115
51. Settembre C, Fraldi A, Rubinsztein DC, Ballabio A. Lysosomal Storage Diseases as Disorders of Autophagy. *Autophagy* (2008) 4:113–4. doi: 10.4161/auto.5227
52. Zhu W, He X, Cheng K, Zhang L, Chen D, Wang X, et al. Ankylosing Spondylitis: Etiology, Pathogenesis, and Treatments. *Bone Res* (2019) 7:22. doi: 10.1038/s41413-019-0057-8
53. Smith JA. Regulation of Cytokine Production by the Unfolded Protein Response; Implications for Infection and Autoimmunity. *Front Immunol* (2018) 9:422. doi: 10.3389/fimmu.2018.00422
54. Hu H, Gourguechon S, Wang CC, Li Z. The G1 Cyclin-Dependent Kinase CRK1 in Trypanosoma Brucei Regulates Anterograde Protein Transport by Phosphorylating the COPII Subunit Sec31. *J Biol Chem* (2016) 22:15527–39. doi: 10.1074/jbc.M116.715185
55. Rao S, Oyang L, Liang J, Yi P, Han Y, Luo X, et al. Biological Function of HYOU1 in Tumors and Other Diseases. *OncoTargets Ther* (2021) 14:1727–35. doi: 10.2147/OTT.S297332
56. Anelli T, Sitia R. Protein Quality Control in the Early Secretory Pathway. *EMBO J* (2008) 23:315–27. doi: 10.1038/sj.emboj.7601974
57. Ciccia F, Accardo-Palumbo A, Rizzo A, Guggino G, Raimondo S, Giardina A, et al. Evidence That Autophagy, But Not the Unfolded Protein Response, Regulates the Expression of IL-23 in the Gut of Patients With Ankylosing Spondylitis and Subclinical Gut Inflammation. *Ann Rheum Dis* (2014) 73:1566–74. doi: 10.1136/annrheumdis-2012-202925
58. Navid F, Layh-Schmitt G, Sikora KA, Cougnoux A, Colbert RA. The Role of Autophagy in the Degradation of Misfolded HLA–B27 Heavy Chains. *Arthritis Rheumatol* (2018) 70:746–55. doi: 10.1002/art.40414
59. Turner MJ, Sowders DP, DeLay ML, Mohapatra R, Bai S, Smith JA, et al. HLA-B27 Misfolding in Transgenic Rats Is Associated With Activation of the

Unfolded Protein Response. *J Immunol* (2005) 175:2438–48. doi: 10.4049/jimmunol.175.4.2438
60. Turner MJ, DeLay ML, Bai S, Klenk E, Colbert RA. HLA–B27 Up-Regulation Causes Accumulation of Misfolded Heavy Chains and Correlates With the Magnitude of the Unfolded Protein Response in Transgenic Rats: Implications for the Pathogenesis of Spondylarthritis-Like Disease. *Arthritis Rheum* (2007) 56:215–23. doi: 10.1002/art.22295
61. Colbert RA, DeLay ML, Layh-Schmitt G, Sowders DP. HLA–B27 Misfolding and Spondyloarthropathies. *Prion* (2009) 3:15–26. doi: 10.4161/pri.3.1.8072
62. Colbert RA, Tran TM, Layh-Schmitt G. HLA-B27 Misfolding and Ankylosing Spondylitis. *Mol Immunol* (2014) 57:44–51. doi: 10.1016/j.molimm.2013.07.013
63. Feng Y, Ding J, Fan CM, Zhu P. Interferon-γ Contributes to HLA-B27-Associated Unfolded Protein Response in Spondyloarthropathies. *J Rheumatol* (2012) 39:574–82. doi: 10.3899/jrheum.101257
64. Chhabra S. Novel Proteasome Inhibitors and Histone Deacetylase Inhibitors: Progress in Myeloma Therapeutics. *Pharmaceuticals* (2017) 10:40. doi: 10.3390/ph10020040
65. Moriya S, Komatsu S, Yamasaki K, Kawai Y, Kokuba H, Hirota A, et al. Targeting the Integrated Networks of Aggresome Formation, Proteasome, and Autophagy Potentiates ER Stress–Mediated Cell Death in Multiple Myeloma Cells. *Int J Oncol* (2015) 46:474–86. doi: 10.3892/ijo.2014.2773

Conflict of Interest: The authors declare that the research was conducted in the absence of any commercial or financial relationships that could be construed as a potential conflict of interest.

Publisher's Note: All claims expressed in this article are solely those of the authors and do not necessarily represent those of their affiliated organizations, or those of the publisher, the editors and the reviewers. Any product that may be evaluated in this article, or claim that may be made by its manufacturer, is not guaranteed or endorsed by the publisher.

frontiers in Immunology

ORIGINAL RESEARCH
published: 10 February 2022
doi: 10.3389/fimmu.2022.802690

Intravenous Immunoglobulin Therapy Restores the Quantity and Phenotype of Circulating Dendritic Cells and CD4$^+$ T Cells in Children With Acute Kawasaki Disease

Nana Wang[1†], Zhongyue Chen[1†], Fan Zhang[1], Qianwen Zhang[1], Ling Sun[1], Haitao Lv[1], Bo Wang[1], Jie Shen[1], Xufang Zhou[1], Feiyan Chen[1], Binwei Zhang[1], Lijun Meng[2], Huiting Zhou[3], ZhenJiang Bai[4] and Jie Huang[1]*

[1] Department of Cardiology, Children's Hospital of Soochow University, Suzhou, China, [2] Department of Hematology, Children's Hospital of Soochow University, Suzhou, China, [3] Pediatric Research Institute of Soochow University, Suzhou, China, [4] Department of Pediatric Intensive Care Unit, Children Hospital of Soochow University, Suzhou, China

Background: Intravenous immunoglobulin (IVIG) showed its therapeutic efficacy on Kawasaki disease (KD). However, the mechanisms by which it reduces systemic inflammation are not completely understood. Dendritic cells (DCs) and T cells play critical roles in the pathogenic processes of immune disorders. Assessing the quantity of DC subsets and T cells and identifying functional molecules present on these cells, which provide information about KD, in the peripheral blood may provide new insights into the mechanisms of immunoglobulin therapy.

Methods: In total, 54 patients with KD and 27 age-matched healthy controls (HCs) were included in this study. The number, percentage, and phenotype of DC subsets and CD4$^+$ T cells in peripheral blood were analyzed through flow cytometry.

Results: Patients with KD exhibited fewer peripheral DC subsets and CD4$^+$ T cells than HCs. Human leucocyte antigen-DR (HLA-DR) expression was reduced on CD1c$^+$ myeloid DCs (CD1c$^+$ mDCs), whereas that on plasmacytoid DCs (pDCs) did not change significantly. Both pDCs and CD1c$^+$ mDCs displayed significantly reduced expression of co-stimulatory molecules, including CD40, CD86. pDCs and CD1c$^+$ mDCs presented an immature or tolerant phenotype in acute stages of KD. Number of circulating pDC and CD1c$^+$ mDC significantly inversely correlated with plasma interleukin-6 (IL-6) levels in KD patients pre-IVIG treatment. No significant differences were found concerning the DC subsets and CD4$^+$ T cells in patients with KD with and without coronary artery lesions. Importantly, these altered quantity and phenotypes on DC subsets and CD4$^+$ T cells were restored to a great extent post-IVIG treatment. T helper (Th) subsets including Th1 and Th2 among CD4$^+$ T cells did not show alteration pre- and post-IVIG treatment, although the Th1-related cytokine IFN-γ level in plasma increased dramatically in patients with KD pre-IVIG treatment.

OPEN ACCESS

Edited by:
Luis C. Anton, Spanish National Research Council (CSIC), Spain

Reviewed by:
Hiroyuki Wakiguchi, Yamaguchi University, Japan
Marco Antonio Yamazaki-Nakashimada, National Institute of Pediatrics (Mexico), Mexico
Janusz Ksiazyk, Children's Memorial Health Institute (IPCZD), Poland

***Correspondence:**
Jie Huang
j.shuang@163.com

†These authors have contributed equally to this work and share first authorship

Specialty section:
This article was submitted to Antigen Presenting Cell Biology, a section of the journal Frontiers in Immunology

Received: *27 October 2021*
Accepted: *13 January 2022*
Published: *10 February 2022*

Citation:
Wang N, Chen Z, Zhang F, Zhang Q, Sun L, Lv H, Wang B, Shen J, Zhou X, Chen F, Zhang B, Meng L, Zhou H, Bai Z and Huang J (2022) Intravenous Immunoglobulin Therapy Restores the Quantity and Phenotype of Circulating Dendritic Cells and CD4$^+$ T Cells in Children With Acute Kawasaki Disease. Front. Immunol. 13:802690. doi: 10.3389/fimmu.2022.802690

Conclusions: pDCs and CD1c$^+$ mDCs presented an immature or tolerant phenotype in acute stages of KD, IVIG treatment restored the quantity and functional molecules of DCs and CD4$^+$ T cells to distinct levels *in vivo*, indicating the involvement of DCs and CD4$^+$ T cells in the inflammation in KD. The findings provide insights into the immunomodulatory actions of IVIG in KD.

Keywords: Kawasaki disease, intravenous immunoglobulin, dendritic cells, CD4$^+$ T cells, immune disorders

INTRODUCTION

Kawasaki disease (KD) is a febrile systemic vasculitis that predominately affects children less than 5 years of age and is the leading cause of acquired cardiac disorders in children (1). Increasing evidence supports that immune-mediated inflammation plays an essential role in the pathophysiology of KD. However, to date, the mechanisms involved in the etiology of KD have not been completely elucidated. It has been thought to be triggered by different antigens that causes a series of aberrant innate and adaptive immune responses (2). Dendritic cells (DCs) are professional antigen presenting cells playing a key role in inducing the activation of naive T cells and bridging innate and adaptive immunity (3–7). DCs recognize the presence of pathogens through pattern recognition receptors, including TLRs, and further migrate from the periphery to the lymph nodes to present pathogen-derived antigens to T cells. Studies have indicated that DCs and T cells could play a key role in KD pathogenesis because mature and activated DCs and T cells expressing the HLA-DR antigen have been reported to infiltrate the coronary artery and skin lesions in patients with KD (8, 9) and in the LCCWE-induced coronary artery lesion mouse model (10). The previous experiments clearly demonstrate that KD leads to a decline in DC numbers (11); however, the maturation status of the surviving DCs remain unclear. Altered activation and effector subsets (Th1 and Th2) have been reported but no consistent conclusion has been drawn yet.

Intravenous immunoglobulin (IVIG) treatment remains the most effective therapy currently for KD. Although the underlying mechanisms are not fully elucidated, it is well-accepted that IVIG cures patients by down-regulating inflammatory responses, which further protects the vascular system and myocardium from immune-mediated damage. Diverse mechanisms have been suggested to explain the anti-inflammatory activity of IVIG, including the neutralization of microbial toxins or cytokines (12), suppression of T- and B- cell activation (13), promotion of apoptosis of peripheral blood lymphocytes (14), regulation of Th17/Treg cell balance (15), and reduction in cytokine release (16, 17). However, only a few studies have investigated the action of IVIG on DCs and CD4$^+$ T cells in KD. Systemic studies on DCs and T cells are warranted to gain insights into the role of these immune cells in the KD pathogenesis and IVIG treatment.

In this study, we determined the frequency, number, phenotype of peripheral pDC and CD1c$^+$ mDC, expression of the inhibitory receptors on CD4$^+$ T cells and helper T cell subsets in patients suffering from KD and the changes of these parameters over the course of IVIG treatment.

Abbreviations: CBA, Cytometric bead array; DCs, Dendritic cells; HCs, Healthy controls; FBS, fetal bovine serum HLA-DR, Human leucocyte antigen-DR; IVIG, intravenous immunoglobulin; IL, Interleukin; IFN-γ, Interferon-γ; KD, Kawasaki disease; mDCs, myeloid dendritic cells; pDCs, plasmacytoid dendritic cells; MFI, Mean fluorescence intensity; NLR, neutrophil to lymphocyte ratio; PD-1, Programmed cell death 1; PMA, phorbol myristate acetate; TIM-3, T-cell immunoglobulin and mucin domain 3; Th, T helper; TIGIT, T-cell immunoglobulin and ITIM domain; TNF-α, Tumor necrosis factor-α; 7-AAD, 7-aminoactinomycin D.

MATERIALS AND METHODS

Participants

A total of 54 with KD admitted to the Department of Cardiology, Children's Hospital of Soochow University, from June 2020 to June 2021 participated in this study. All the participants conformed to the diagnostic criteria revised by AHA Kawasaki Disease Guideline (18). All patients received intravenous immunoglobulin (IVIG,2 g/kg) in addition to oral aspirin (30-50 mg/kg/day) as an initial treatment. Patients who fulfilled at least one of the following criteria were excluded: 1) having received corticosteroids and immunosuppressive drugs, 2) having received their initial IVIG infusion in other hospitals, 3) refused IVIG infusion, and 4) IVIG resistance, 5) recurrent KD. Echocardiography was performed in all the patients before the IVIG treatment. Measurements of the diameter of the left main coronary artery (LCA), the anterior descending branch (LAD), the circumflex artery (CX), and the right coronary artery (RCA)were normalized based on the body surface area and expressed as a Z score (standard deviation units from the mean). A Z score ≥ 2 was to indicate coronary artery lesion (19). In total, 27 age-matched healthy subjects were enrolled as controls who had received routine regular physical examinations were enrolled as healthy controls (HCs). Clinical parameters such as the white blood cells (WBC), neutrophil count, lymphocyte count, C reactive protein (CRP) level, and Prealbumin were recorded from both patients and healthy controls. The parents of all the study participants were informed about the study, and they provided informed consent.

Flow Cytometry Analysis

Peripheral blood (2 mL) was collected from both healthy controls (HCs) and patients at two time points: before IVIG treatment (pre-IVIG) and 3 days after completing initial IVIG treatment (post-IVIG). Peripheral blood leukocytes were isolated from

EDTA-blood through red blood cell lysis within 4 h. Briefly, red blood cells (RBCs) were lysed using human erythrocyte lysing solution (BioLegend), and samples were washed twice with phosphate-buffered saline (PBS) without $Ca2^+$ and $Mg2^+$. After the samples were washed, peripheral blood leukocytes were resuspended in PBS containing 2.5% fetal bovine serum (FBS) and incubated at 4°C for 30 min in the dark with the following fluorochrome-conjugated monoclonal antibodies including surface CD3-FITC (SK7), CD14-FITC (HCD14), CD15-FITC (HI98), CD16-FITC (3G8), CD19-FITC (HIB19), CD20-FITC (2H7), CD56-FITC (MEM-188), HLA-DR-PE/CY7 (L243), CD123-APC(6H6), CD1c-PE(L161), CD86-PE/CY7(IT2.2), CD40-BV421(5C3), CD4-BV421 (RPA-T4), Tim3-APC (F38-2F2), TIGIT-PE (A15153G), and PD-1-BV510 (NAT105).All the samples were washed and analyzed using the Attune NxTflow cytometer (LifeTechnology). Approximately 3×10^6 and 1×10^6 of peripheral blood leukocytes were used to analyze DCs and $CD4^+$ T cells by flow cytometry, respectively. All antibodies were purchased from BioLegend (San Diego, CA, USA) or BD Biosciences (San Diego, CA, USA). Staining was performed as previously described (20). Total DCs (Pan-DCs) were characterised as negative for lineage markers (CD3, CD14, CD15, CD16, CD19, CD20, and CD56) and positive for HLA-DR. The myeloid DCs and plasmacytoid DCs subsets were characterised as $CD1c^+$ and $CD123^+$, respectively. Dead cells were excluded through 7-aminoactinomycin D (7-AAD; BioLegend) viability staining. The absolute number of $CD1c^+$ mDCs and pDCs was calculated from the peripheral blood leukocytes count multiplied by the proportion of each subset within peripheral blood leukocytes per milliliter, as determined by flow cytometric analysis.

Intracellular Cytokine Determination of $CD4^+$ T Cells

For the detection of intracellular cytokines by flow cytometry, peripheral blood leukocytes were cultured in 10% fetal calf serum in RPMI-1640 and incubated for 5 h at 37°C under 5% CO_2 in the presence of 5 ng/mL phorbol myristate acetate (PMA), 0.5 μg/mL ionomycin, and Golgiplug (containing monensin, 1/1000 final concentration). Cells were washed and stained with anti-CD4 at 4°C for 30 min in the dark. After washed twice, cells were fixed with lysing buffer (BD Biosciences), permeabilized with permeabilization solution (BD Biosciences), and were then incubated with antibodies against IFN-γ and IL-4 (BD Biosciences) for intracellular staining, according to the manufacturer's instructions. Th1 and Th2 cells were identified as $CD4^+$IFN-γ^+ and $CD4^+$IL-4^+, respectively. Dead cells were excluded using a fixable live/dead dye (Invitrogen). The data were analyzed using FlowJo v10.4 software (FlowJo, OR, USA).

Plasma Cytokine Measurement

The Human Th1/Th2/Th17 Kit (BD Biosciences) was used to measure plasma cytokine levels. IL-2, IL-4, IL-6, IFN-γ, TNF-α, IL-17A, and IL-10 levels were assessed. Data were analyzed using CBA software. The individual cytokine concentrations were indicated by their fluorescence intensities. The concentrations of all the cytokines were reported in picogram per milliliter.

Statistical Analysis

Statistical analysis was performed using IBM SPSS Statistics 26.0. All data are expressed as median (interquartile range). For comparison between patients with KD and HCs, Mann-Whitney U-test was used. The Wilcoxon signed-rank test for paired samples was used for comparing the patients before and after IVIG treatment. The significance of difference in sex distribution in patients and controls was analyzed using the chi-square test. Correlations were analyzed using the Spearman correlation test. A P value of < 0.05 was considered significant.

RESULTS

Baseline Characteristics

A total of 54 patients with KD and 27 healthy controls were recruited based on our inclusion and exclusion criteria. Their characteristics are shown in **Table 1**. No significant differences in age and sex were observed between the groups. The WBC and neutrophil count and prealbumin and CRP levels were significantly higher in patients with KD before IVIG treatment than in HCs, whereas no significant difference was observed in the absolute lymphocyte count. After IVIG treatment, WBC and neutrophil counts and the CRP level decreased rapidly to an almost normal level, whereas the prealbumin level remained lower. According to echocardiography parameters, 52 patients with KD were divided into two groups: KD without coronary artery lesion (CALs; KD-NCAL) group (n = 40) and KD with CAL (KD-CAL) group (n = 14) (**Table 2**). No significant differences were observed in terms of WBC, neutrophil, and lymphocyte counts; neutrophil to lymphocyte ratio (NLR); and CRP and prealbumin levels between the KD-CAL and KD-NCAL groups.

IVIG Treatment Restored the Distribution of DC Subsets

To identify DC subsets, the gating strategy of total DCs and their subsets was shown in **Figure 1A**. Quantitative flow cytometric analysis revealed that the frequency and absolute number of pDCs and $CD1c^+$ mDCs among pan-DCs was significantly decreased in patients with KD pre-IVIG compared with those in healthy controls ($P < 0.0001$, **Figure 1B**; $P < 0.0001$, **Figure 1B**; $P < 0.0001$, **Figure 1C**; $P < 0.0001$, **Figure 1C**; respectively). This means that the distribution of DC subsets was different from that of HCs, with reduced frequency and number of pDCs and $CD1c^+$ mDCs. Importantly, we found significantly recovered frequency and absolute number of pDCs and $CD1c^+$ mDCs in patients post IVIG therapy ($P = 0.0812$, **Figure 1B**; $P = 0.0006$, **Figure 1B**; $P < 0.0001$, **Figure 1C**; $P < 0.0001$, **Figure 1C**; respectively). Although the percentage of both DC subsets in patients with KD did not recover to their levels observed in HCs ($P < 0.0001$, **Figure 1B**; $P < 0.0001$, **Figure 1C**; respectively), the absolute number of both DC subsets was same as that found in HCs ($P = 0.2255$, **Figure 1B**; $P = 0.1730$, **Figure 1C**; respectively).

TABLE 1 | Characteristics of the study population.

Parameters	Kawasaki disease		Healthy controls
	Pre-IVIG	Post-IVIG	
Number	54	54	27
Age, months	35.5 (18.75-56.25)	35.5 (18.75-56.25)	45 (36-56)
Sex, male/female	29/25	29/25	16/11
Fever duration before diagnosis	5 (4.0-6.25)	5 (4.0-6.25)	–
WBC, 10^9/L	13.67 (10.59-15.95)†,‡	7.54 (5.41-10.47)	7.38 (6.16-8.33)
Neutrophil, 10^9/L	8.21 (6.09-11.36)†,‡	2.59 (1.6-3.9)	2.58 (2.23-3.35)
Lymphocytes,10^9/L	3.21 (2.52-4.12)	3.38 (2.66-4.88)	3.68 (2.89-4.08)
CRP, mg/L	49.04 (34.42-85.57)†,‡	5.9 (3.12-11.86)†	0.16 (0.11-0.42)
NLR	2.52 (1.79-3.88)†,‡	0.78 (0.52-1.02)	0.77 (0.63-1.09)
Prealbumin, mg/L	75.5 (58.0-87.25)†,‡	166 (137.75-200)†	207 (190-225)

Baseline characteristics of the participants. Data shown are median (quartile spacing) or the number of cases. -, this data was not detected; CRP, C-reactive protein; NLR, neutrophil to lymphocyte ratio; WBC, white blood cell counts.
$^{\dagger}P < 0.05$ vs. the healthy controls. $^{\ddagger}P < 0.05$ vs. the post-IVIG treatment

TABLE 2 | Characteristics of patients with KD classified according to coronary artery lesions or not.

Parameters	Kawasaki disease		*P* value
	NCAL	CAL	
Number	40	14	
Age, months	33.5 (20.0-50.0)	45.4 (14.5-66.75)	0.4125
Sex, male/female	22/18	7/7	0.7468
Fever duration before diagnosis	6 (4-6.75)	4.5 (4-6.25)	0.2937
WBC, 10^9/L	13.67 (10.14-15.97)	13.96 (11.43-15.77)	0.5737
Neutrophil, 10^9/L	8.16 (6.09-11.95)	8.37(6.09-11.10)	0.8979
Lymphocytes,10^9/L	3.17 (2.53-4.11)	3.32 (2.19-4.30)	0.6427
CRP, mg/L	45.72 (29.14-79.61)	67.24 (38.95-105.28)	0.2690
NLR	2.52 (1.82-3.78)	2.36 (1.61-4.30)	0.7596
Prealbumin, mg/L	76 (59.5-88)	71.5 (52.25-80.25)	0.2645

Baseline characteristics of the participants. Data shown are median (quartile spacing) or the number of cases. CAL, coronary artery lesion; CRP, C-reactive protein; NCAL, without coronary artery lesion; NLR, neutrophil to lymphocyte ratio; WBC, white blood cell counts.

IVIG Induced Phenotypic Changes of Circulating DCs in KD Patients

Next, we compared the expressions of the antigen presenting molecule HLA-DR and co-stimulatory molecules (CD40 and CD86) in the two DC subsets in the peripheral circulation of patients with KD and HCs. These molecules are critical for DCs to elicit adaptive immune responses.

Although no significant significance was observed between pre-and post-IVIG treatment in patients with KD and HCs in terms of pDCs, the MFI of the antigen presenting molecule HLA-DR exhibited a decreasing trend (P = 0.1822, **Figure 2B**; P = 0.3130, **Figure 2B**; respectively). CD40 percentage on pDCs in patients pre-IVIG treatment and MFI considerably decreased ($P < 0.0001$, **Figure 2C**; $P < 0.0001$, **Figure 2C**; respectively). IVIG treatment significantly elevated the percentage and MFI of CD40 expression on pDCs; however, they were not at normal levels as observed in HCs (P = 0.0010, **Figure 2C**; P = 0.0170, **Figure 2C**; respectively). Similarly, we found that the percentage and MFI of CD86 expression on pDCs were significantly lower in patients with KD pre-IVIG treatment than those in HCs (P = 0.0006, **Figure 2E**; P = 0.0091, **Figure 2E**; respectively). The percentage and MFI of CD86 in pDC was increased in patients after IVIG treatment, with no difference between patients post-IVIG treatment and HCs (P = 0.5288, **Figure 2E**; P = 0.5158, **Figure 2E**; respectively).

For $CD1c^+$ mDCs, we observed significantly decreased MFI of HLA-DR in patients with KD pre-IVIG treatment compared with that in HC, with no difference between post treatment and HCs ($P < 0.0001$, **Figure 2B**; P = 0.1368, **Figure 2B**; respectively). Differing from pDCs, drastic change of co-stimulatory molecule on $CD1c^+$ mDCs in patients was CD86 instead of CD40. A drastic decrease in the MFI and of CD86 percentage was observed on $CD1c^+$ mDCs in the patients before treatment ($P < 0.0001$, **Figure 2F**; $P < 0.0001$, **Figure 2F**; respectively). IVIG treatment significantly elevated the percentage and MFI of CD86 expression on $CD1c^+$ mDCs in patients with KD; however, these parameters were significantly lower than those in HCs ($P < 0.0001$, **Figure 2F**; $P < 0.0001$, **Figure 2F**; respectively). We did not observe obvious changes in terms of the percentage and MFI of CD40 on $CD1c^+$ mDCs between patients with KD and HCs (P = 0.6815, **Figure 2D**; P = 0.1609, **Figure 2D**; respectively).

Collectively, data presented in **Figures 1** and **2** indicated that the quantity of DCs and functional molecules on DCs were impaired in patients pre-IVIG treatment. IVIG treatment restored the quantity of DCs and functional molecules on DCs to distinct levels, indicating a possible role of DCs in the recovery of patients after IVIG treatment.

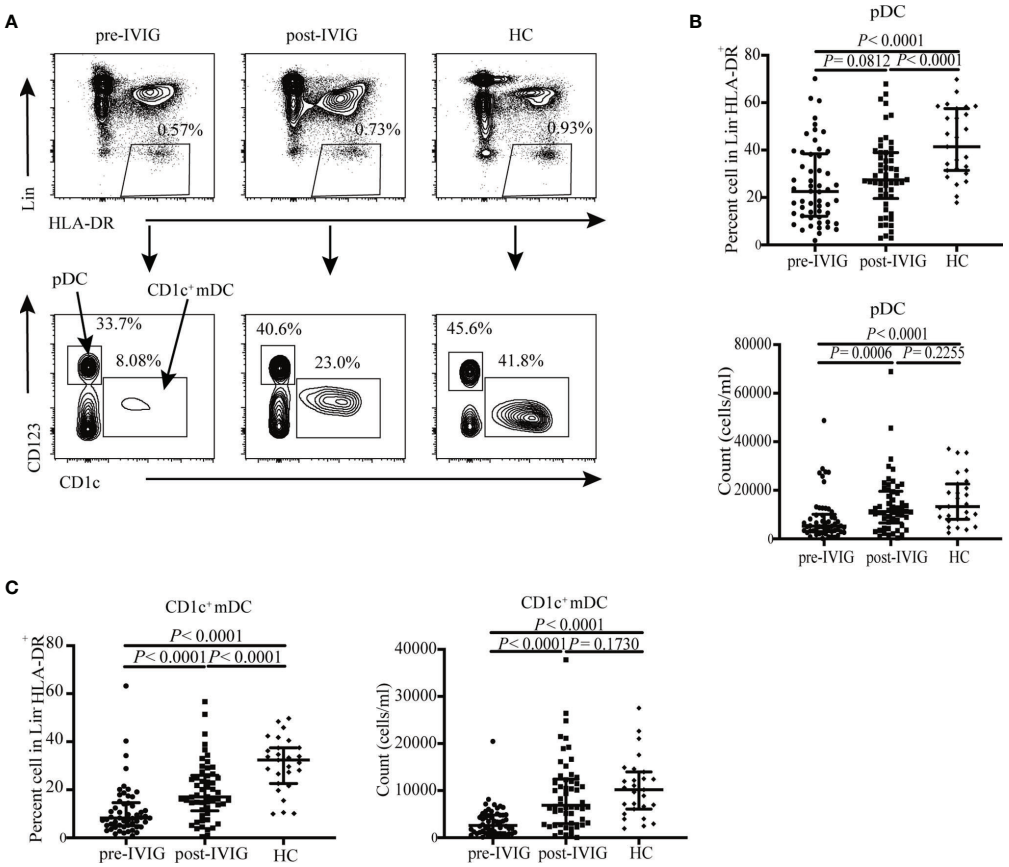

FIGURE 1 | DC subsets distribution in HCs (n = 27) and KD patients pre- and post-IVIG treatment (n = 54). **(A)** Identification of circulating DC subsets in blood using flow cytometry, Pan-DCs were gated as Lin^- $HLA\text{-}DR^+$, pDCs and $CD1c^+$ mDCs were defined as Lin^- $HLA\text{-}DR^+$ $CD123^+$ and Lin^- $HLA\text{-}DR^+$ $CD1c^+$ cells, respectively. Representative profiles of the circulating DCs subsets are shown. **(B)** Plots show percentage and number of circulating pDCs in patients with KD and controls. **(C)** Plots show percentage and number of circulating $CD1c^+$ mDCs in patients with KD and HCs. Horizontal bars represent median values, and error bars represent the interquartile range.

TIM-3$^+$ CD4$^+$ T Cells Are Reduced Post-IVIG Treatment

Considering the impaired quantity and functional molecules on DCs in patients with acute KD patients, we further assessed $CD4^+$ T cells because DCs are the critical regulators of $CD4^+$ T cells. The percentage and absolute number of $CD4^+$ T cells were decreased in the peripheral blood of patients pre-IVIG treatment compared with those in HCs ($P < 0.0001$, **Figure 3A**; $P = 0.0034$, **Figure 3B**; respectively). Inhibitory receptors such as programmed cell death 1 (PD-1), T cell immunoglobulin and ITIM domain (TIGIT), and T cell immunoglobulin and mucin domain 3 (TIM-3) are important molecules controlling T cell effector responses (21). Inhibitory receptors have been involved in the pathophysiology of various human diseases, including autoimmune diseases (21, 22), sepsis (23), and cancer (24). However, the expression of these inhibitory receptors on $CD4^+$ T cells has not been reported previously in KD. To determine whether these inhibitory receptors are involved in the pathogenesis of KD, we used flow cytometry to assess the expressions of PD-1, TIGIT, and TIM-3 on peripheral $CD4^+$ T cells. Representative flow cytometric analyses are shown in **Figure 3C**, patients with KD were found to exhibit a significantly higher expression of TIM-3 on $CD4^+$ T cells pre-IVIG treatment than HCs, whereas no changes in PD-1 or TIGIT were observed between them ($P < 0.0001$, **Figure 3F**; $P = 0.2990$, **Figure 3D**; $P = 0.0812$, **Figure 3E**; respectively). IVIG treatment significantly reduced percentage TIM-3 expression on $CD4^+$ T cells but not to a normal level as seen in HCs ($P = 0.0034$, **Figure 3F**). The percentage of $CD4^+$ T cells expressing the TIGIT was increased post IVIG treatment ($P = 0.0012$, **Figure 3E**).

Unaltered Th1/Th2 Polarization of CD4$^+$ T Cells in KD Patients

Although many studies have focused on T helper cytokines, most of them have determined the cytokines in plasma instead of $CD4^+$ T cells. To understand the biology of $CD4^+$ T cells, frequencies of different $CD4^+$ T-cell subsets were analyzed based on cytokine patterns after *in vitro* stimulation of the T-cell receptor (TCR) signal. Production of intracellular IFN-γ and IL-4, which are the representative factors of Th1 and Th2, respectively, in $CD4^+$ T cells, was analyzed in the peripheral blood of patients with KD and HCs.

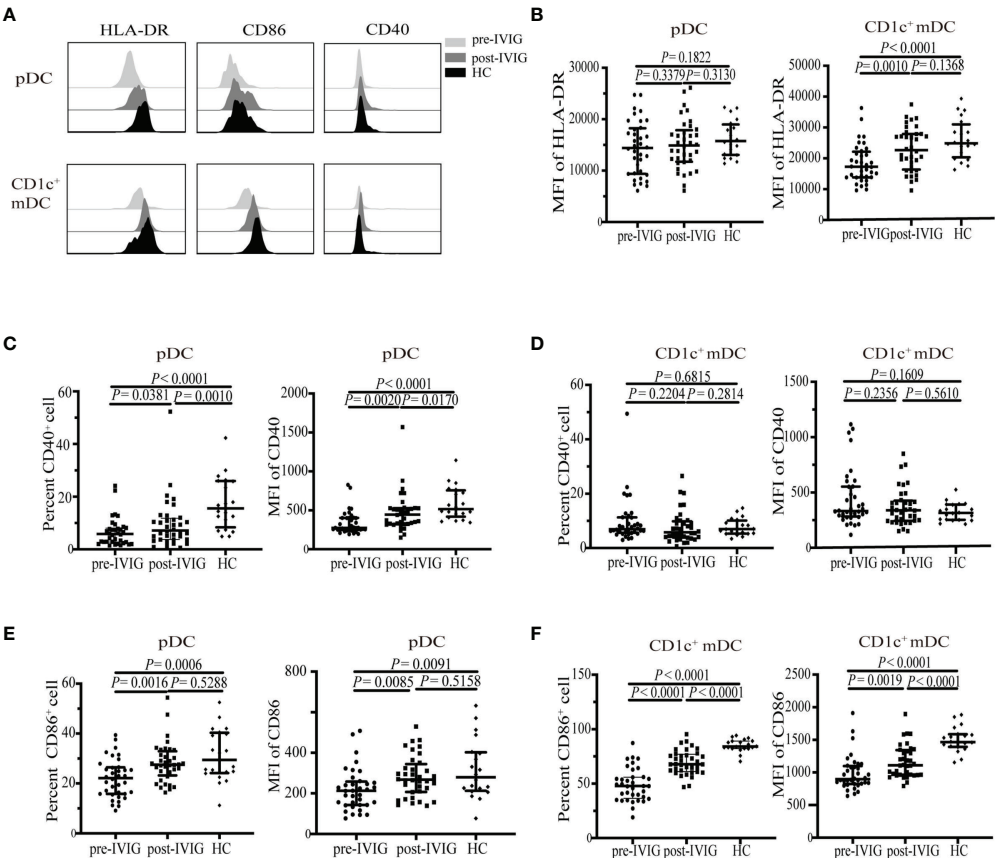

FIGURE 2 | Expression of HLA-DR, CD86 and CD40 on circulating DC subsets from healthy control (HC) (n = 20) and KD patients pre-and post-IVIG treatment (n = 36). **(A)** Representative histograms of HLA-DR, CD86, CD40 in DC subsets from a healthy control and KD patients pre-and post-IVIG treatment. **(B)** HLA-DR MFI on pDCs and CD1c$^+$ mDCs in KD patients and HCs. **(C, D)** Percentage and MFI of CD40$^+$ on pDCs and CD1c$^+$ mDCs in patients with KD and HCs. **(E, F)** Percentage and MFI of CD86$^+$ on pDCs and CD1c$^+$ mDCs in patients with KD and HCs. Horizontal bars represent median values, and error bars represent the interquartile range. MFI, mean fluorescent intensity.

The gating strategy for determining Th1 and Th2 cells is shown in **Figure 4A**. Neither the onset of KD nor IVIG treatment altered the percentages of Th1 and Th2 in CD4$^+$ T cells ($P = 0.9851$, **Figure 4B**; $P = 0.7776$, **Figure 4B**; $P = 0.3980$, **Figure 4C**; $P = 0.5509$, **Figure 4C**; respectively).

We further measured the level of a panel of Th subset–related cytokines in the plasma of patients with KD and HCs. Of these, the plasma level of IL-4 was very low or undetectable in either study population (date not shown). IL-17A, IFN-γ, TNF-α, IL-6, IL-10, and IL-2 levels were higher in patients with KD pre-IVIG than in HCs ($P = 0.0464$, **Figure 4D**; $P = 0.0020$, **Figure 4E**; $P = 0.0084$, **Figure 4F**; $P < 0.0001$, **Figure 4G**; $P < 0.0001$, **Figure 4H**; $P = 0.0138$, **Figure 4I**; respectively). These results are consistent with those previously reported (15, 25). After IVIG treatment, plasma levels of IL-17A and IL-2 returned to normal ($P = 0.2258$, **Figure 4D**; $P = 0.1145$, **Figure 2I**; respectively), the levels of other cytokines including IFN-γ, TNF-α, IL-6, and IL-10 did not decrease markedly but slightly deviated from normal levels ($P = 0.0122$, **Figure 4E**; $P = 0.0108$, **Figure 2F**; $P < 0.0001$, **Figure 4G**; $P = 0.0056$, **Figure 4H**; respectively).

Increased Level of IL-6 in Plasma Correlated With Decreased Number of pDC and CD1c$^+$ mDC in KD Patients Pre-IVIG Treatment

In order to analyze the correlation between cytokines and immunocytes, we performed the Spearman correlation analysis. In our study, only plasma IL-6 level significantly inversely correlated with circulating pDC count (r = -0.5491, $P = 0.0183$) (**Figure 5A**) and CD1c$^+$ mDC count (r = -0.6618, $P = 0.0028$) (**Figure 5B**), while no correlations were found between IL-6 level and CD4$^+$ T cell count in KD patients pre-IVIG treatment (**Supplementary Table 1**). There were no significant correlations between the number of pDC, CD1c$^+$ mDC and CD4$^+$ T cell and cytokines (IL-17A, IFN-γ, TNF-α, IL-10 and IL-2) (**Supplementary Table 1**). After IVIG treatment, neither the number of pDC, CD1c$^+$ mDC, nor CD4$^+$ T cell correlated significantly with the cytokines (**Supplementary Table 2**). We next analyzed the correlation between cytokines and the percentage of circulating Th subsets. Plasma levels of IFN-γ positively correlated with the percentage of circulating Th1 in

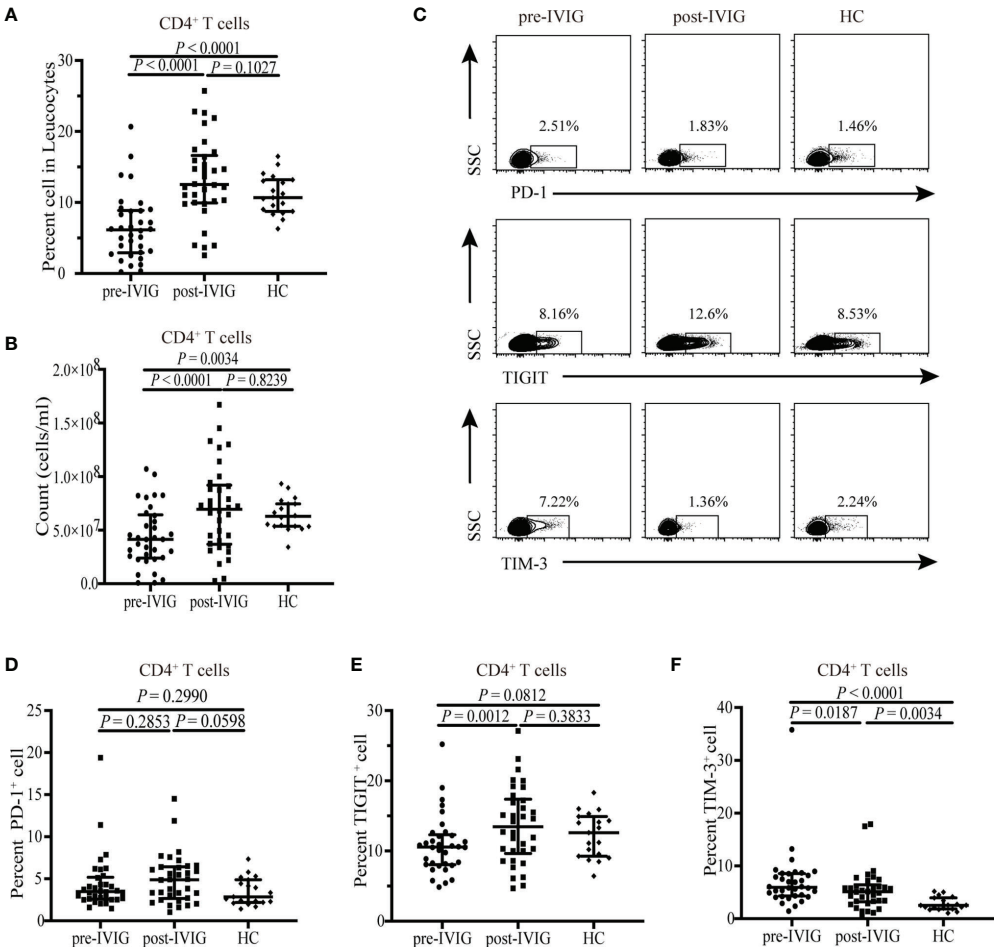

FIGURE 3 | Flow cytometry detection of the expression of PD-1, TIGIT, and TIM-3 on $CD4^+$ T cells from healthy control (HC) (n = 19) and KD patients pre- and post-IVIG treatment (n = 34). Graphs show **(A, B)** Percentage and number of $CD4^+$ T cells among peripheral blood leucocytes in KD patients and HCs. **(C)** Representative dot plots of PD-1, TIGIT, and TIM-3 are shown on gated $CD4^+$ T cells. **(D)** Expression of PD-1 on $CD4^+$ T cells in patients with KD and HCs. **(E)** Expression of TIGIT on $CD4^+$ T cells in patients with KD and HCs. **(F)** Expression of TIM-3 expression on $CD4^+$ T cells in patients with KD and HCs. Horizontal bars represent median values, and error bars represent the interquartile range. MFI, mean fluorescent intensity.

KD patients pre-IVIG treatment (r = 0.6132, P = 0.0197) (**Figure 5C**), while no correlations were found between the percentage of Th1 and other cytokines (IL-17A, TNF-α, IL-10, IL-6 and IL-2). There were no significant correlations between the percentage of circulating Th2 and cytokines (**Supplementary Table 3**). Following treatment, neither the percentage of Th1, nor Th2 correlated significantly with the cytokines (**Supplementary Table 4**).

Numbers and Phenotypic Properties on DC Subsets and $CD4^+$ T Cells in Patients With CAL and Without CAL Pre-IVIG Treatment

To investigate the correlation among DC subsets, $CD4^+$ T cells, and CAL, we performed a subgroup analysis comparing patients with and without CAL (KD-CAL and KD-NCAL groups). The number and proportion of circulating pDCs and $CD1c^+$ mDCs were not significantly different in KD-CAL and KD-NCAL groups (**Table 3**). The expressions of HLA-DR, CD86, and CD40 on pDCs and $CD1c^+$ mDCs did not differ significantly between KD-CAL and KD-NCAL groups (**Table 4**). Furthermore, no difference was observed in the number, proportion, and TIM-3 receptor expression of $CD4^+$ T cells between the two groups (**Table 5**).

DISCUSSION

In this study, we reported that the frequency and number of pDCs and $CD1c^+$ mDCs and the expression of the antigen presenting molecule HLA-DR and co-stimulatory molecules, CD86 and/or CD40, on DCs decrease in acute stages of KD. IVIG treatment restored the quantity of DCs and functional molecules on DCs to distinct levels. In addition, our data indicated that the frequency and number of $CD4^+$ T cells

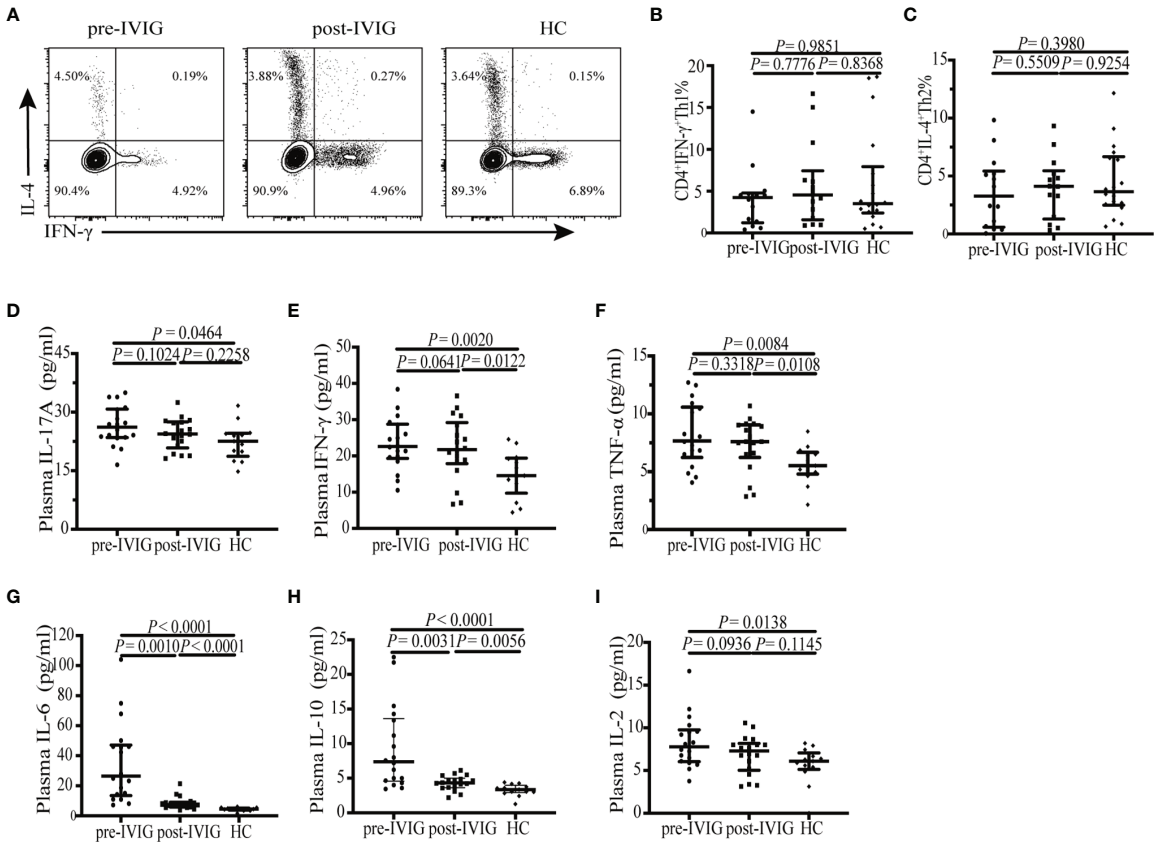

FIGURE 4 | Flow cytometry analysis of the intracellular cytokine and plasma cytokine levels. **(A)** The gating strategy for determining $CD4^+$ IFN-γ^+ Th1 and $CD4^+$ IL-4^+ Th2 cells is shown. **(B)** Percentage of circulating $CD4^+$ IFN-γ^+ Th1 cells in patients with KD (n = 14) and HCs (n = 18). **(C)** Percentage of circulating $CD4^+$ IL-4^+ Th2 cells in patients with KD (n = 14) and HCs (n = 18). **(D–I)** Plasma levels of the cytokines IL-17A, IFN-γ, TNF-α, IL-6, IL-10, IL-2 were detected in patients with KD (n = 19) and HCs (n = 13) using cytometric bead array. Horizontal bars represent median values, and error bars represent the interquartile range.

decreased in peripheral blood leukocytes in patients pre-IVIG treatment and were restored to a normal level post-IVIG treatment. The expression of the inhibitory receptor TIM-3 on peripheral $CD4^+$ T cells increased in patients pre-IVIG treatment and decreased post- IVIG treatment but not to a normal level (**Figure 6**). Although the levels of characteristic inflammatory cytokines including IL-2, IL-6, IFN-γ, TNF-α, IL-17A, and IL-10 in patients with acute KD increased significantly compared with those in HCs, which is consistent with previous reports, we did not observe any changes in Th subsets when gated on peripheral $CD4^+$ T cells. No significant differences were observed concerning the quantity and phenotype of DC subsets and $CD4^+$ T cells in patients with KD with and without CALs. Moreover, we also found circulating numbers of pDC and $CD1c^+$ mDC significantly inversely correlated with plasma IL-6 levels, and plasma IFN-γ levels were positively associated with the percentage of circulating Th1 in KD patients pre-IVIG treatment.

For DC subsets, contradictory results have been reported in humans regarding numerical abnormalities of peripheral blood DC subtypes in KD (11, 26). Suda et al. reported a decreased number of circulating mDCs but not of pDCs (11). Burns et al. reported an increase in circulating mDCs but not in pDCs in the acute phase of KD (26). Such contradictory results may be related to the different markers used for DC classification because DCs were identified through Lin^- (CD3, CD14, CD15, CD16, CD19, CD20, CD56) and HLA-DR staining, the makers of DC staining in our study are consistent with those of previous report (19). However, Suda et al. (11) identified DCs as Lin^- (CD3, CD14, CD16, CD19, CD20, CD56) and HLA-DR. Burns et al. (26) relied upon CD11b and CD11c markers to identify DCs. Reduction in the number of DCs may be because of alterations in DC viability, impaired differentiation with progenitor cells, or altered tissue distribution under inflammation, although the precise mechanism remains to be further validated. Studies have suggested that DCs migrate from the periphery to the site of coronary artery injury, given that mature and activated DCs infiltrate and accumulate around the coronary arteries. In conjunction with alterations in the percentage and absolute number of DC subsets, markers expressed on the surface of DCs that reflect their function are also significantly altered in KD. Expression of HLA-DR, a professional antigen presenting molecule, decreased significantly on both pDCs and $CD1c^+$ mDCs in KD. We observed down-regulated expressions of CD40 and CD86 on pDCs in patients with KD compared with

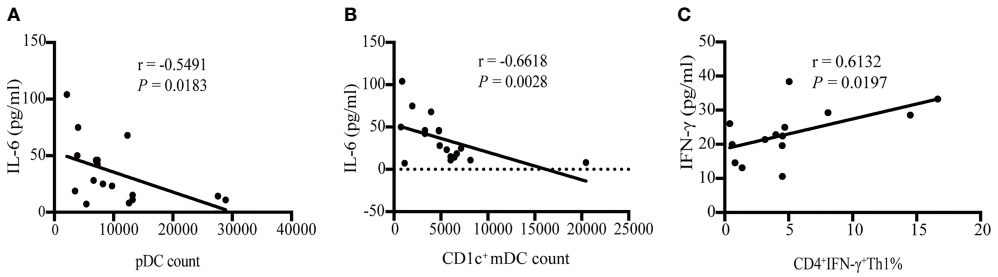

FIGURE 5 | Spearman correlation between cytokines and immunocytes. **(A)** Correlation analysis of IL-6 level and pDC count in KD patients pre-IVIG treatment (n = 18). **(B)** Correlation analysis of IL-6 level and CD1c$^+$ mDC count in KD patients pre-IVIG treatment (n = 18). **(C)** Correlation analysis of IFN-γ level and the percentage of circulating CD4$^+$ IFN-γ$^+$ Th1 in KD patients pre-IVIG treatment (n = 14).

TABLE 3 | Percentage and number of DC subsets between KD patients with and without CAL.

Parameters	Kawasaki disease		*P* value
	NCAL (n = 40)	CAL (n = 14)	
pDCs%	18.45 (11.82-32.28)	31.15 (14.24-41.48)	0.1671
pDCs (/ml)	4964 (2979-7212)	10425 (4024-24450)	0.0725
CD1c$^+$ mDCs%	7.84 (4.72-14.93)	8.44 (5.69-15.28)	0.8668
CD1c$^+$ mDCs (/ml)	2440 (900-4846)	3146 (1688-4937)	0.6498

Data shown are median (quartile spacing) or the number of cases. CAL, coronary artery lesion; NCAL, without coronary artery lesion.

those in HCs. Similarly, CD1c$^+$ mDCs also exhibited significantly lower levels of CD86; however, the expression of CD40 did not differ compared with that in HCs. Studies have established that mature DCs display a phenotype characterised by high surface expression of antigen presenting molecules and co-stimulatory molecules such as CD86 and CD40 (27, 28). Immature DCs are known to have a lower potential to activate T cells (29). Our results indicated that the circulating pDCs and CD1c$^+$ mDCs in patients with KD might reflect a tolerant or less mature phenotype in this condition. Importantly, studies on humans and animal models have indicated the presence of mature and activated DCs in CALs (8), which is probably due to an increased efflux of more mature DCs into the affected coronary artery and/or an increased influx of less mature DCs from the bone marrow. However, the assumption requires further validation.

The patients in our study exhibited a profoundly decreased percentage and number of CD4$^+$ T cells, consistent with a previous report by Lee et al. (30). Numerous immunological studies on peripheral blood lymphocytes have been conducted, however, the role of T cells and the functional state of Th1 and Th2 cells remains controversial. Matsubara et al. reported a decrease in the number of Th1 type CD3$^+$ T cell in the peripheral blood of patients with acute stage of KD and suggested the presence of a Th1/Th2 imbalance, particularly Th2 dominance (31). Lee et al. reported that both Th1 and Th2 cells may be activated simultaneously during the acute stage of KD (25), whereas Kimura et al. suggested that the production of Th1 and Th2 cytokines is suppressed at the level of transcriptional regulation in KD (32). Interestingly, we did not observe any change in Th subsets among CD4$^+$ T cells between patients with KD and HCs. Lee et al. (25) determined the cytokines in plasma instead of CD4$^+$ T cells. Kimura et al. (32) analyzed mRNA levels of T-bet and GATA-3, along with those of IFN-γ and IL-4, in peripheral blood mononuclear cells but not in CD4$^+$ T cells. Th1 (IFN-γ-producing CD4$^+$ T cells) and Th2 (IL-4-producing CD4$^+$ T cells) cells were identified by intracellular cytokine staining in our study. These experimental differences, as well as other methodological differences may account for the discrepancy. The function of T cells is regulated by inhibitory receptors such as PD-1, TIGIT, and TIM-3 (21). In this regard, none of the studies have reported the expression of PD-1, TIGIT, and TIM-3 expression in human CD4$^+$ T cells. Augmented TIM-3 expression was observed on CD4$^+$ T cells, whereas no changes in PD-1 and TIGIT expressions were observed in patients with KD prior to treatment with those in HCs. Given that TIM-3 is a negative regulatory molecule on CD4$^+$ T cells, patients with KD might exhibit CD4$^+$ T cells in a more suppressed state than HCs.

However, no significant differences were found concerning the quantity and phenotype of DC subsets and CD4$^+$ T cells in patients with and without CAL in the acute phase of KD. Studies have reported the associations of CALs with several clinical variables, particularly CRP and NLR. In our clinical data, patients with CAL exhibited no significant elevation in CRP and NLR. The reason for these discrepant results is unclear; however, it may be related to various factors including different genetic backgrounds (33), pathogen species (34), and epigenetic effects (35).

Overall, these results strongly implicated that pDCs, CD1c$^+$ mDCs and CD4$^+$ T cells are in a suppressed state in the acute phase of KD. Our results are not consistent with the findings of

TABLE 4 | HLA-DR, CD86 and CD40 expression on DC subsets between KD patients with and without CAL.

Parameters	Kawasaki disease		*P* value
	NCAL (n = 29)	CAL (n = 13)	
MFI of HLA-DR on pDCs	11826 (8605-15739)	16625 (13268-18988)	0.0586
MFI of HLA-DR on $CD1c^+$ mDCs	16360 (13777-21717)	18561 (14376-22444)	0.5586
$CD86^+$ expression on pDCs%	22.6 (15.8-27.2)	20.5 (15.25-28.0)	0.7543
$CD86^+$ expression on $CD1c^+$ mDCs%	47.8 (38.56-56.2)	47.7 (34.4-60.15)	0.6534
MFI of CD86 on pDCs	224 (142-294)	204 (149-242)	0.6147
MFI of CD86 on $CD1c^+$ mDCs	915 (850-1145)	967 (738-1102)	0.3914
$CD40^+$ expression on pDCs%	4.20 (2.05-7.61)	6.07 (3.41-11.65)	0.0866
$CD40^+$ expression on $CD1c^+$ mDCs%	8.29 (6.21-17.65)	6.45 (5.21-12.1)	0.1310
MFI of CD40 on pDCs	274 (239-404)	341 (274-430)	0.0997
MFI of CD40 on $CD1c^+$ mDCs	430 (318-1007)	304 (265-577)	0.0643

Data shown are median (quartile spacing) or the number of cases. CAL, coronary artery lesion; NCAL, without coronary artery lesion.

TABLE 5 | $CD4^+$ T cells and $TIM3^+$ $CD4^+$ T cells between KD patients with and without CAL.

Parameters	Kawasaki disease		*P* value
	NCAL (n = 25)	CAL (n = 9)	
$CD4^+$ T cells %	6.47 (4.68-9.71)	3.83 (2.30-7.29)	0.0859
$CD4^+$ T cells (/ml)	42034115 (24620739-62163389)	41448706 (24919683-74148861)	0.9842
$TIM\text{-}3^+$ expression on $CD4^+$ T cells %	5.58 (4.20-7.81)	6.93 (4.92-8.73)	0.2717

Data shown are median (quartile spacing) or the number of cases. CAL, coronary artery lesion; NCAL, without coronary artery lesion.

Burns et al. (26), who reported an increased number of mDCs expressing CD86 in the acute KD phase. This difference might be because of the inclusion of CD14-positive cells, since monocytes have CD14 on their cell surface, whereas mDCs generally lack CD14. It remains uncertain whether peripheral blood T cells are activated in acute KD phases. The increased expression of TIM-3 on $CD4^+$ T cells as observed in patients with KD may be associated with the suppression of the immune response. Our results are consistent with those of a study by Kuijpers et al. (36), who reported that a dysregulated TcR/CD3-dependent T cell unresponsiveness in acute KD. Additionally, Matsubara et al. (37) suggested that T cells in the peripheral blood of patients with KD were not activated because of the low expression levels of intracellular CTLA-4. Ikeda et al. (38) performed the microarray analysis of peripheral blood mononuclear cells and reported that the expressions of genes involved in antigen processing and presentation, the TCR signalling pathway, and the B-cell receptor signalling pathway were downregulated in acute phase KD. Thus, the decline in the number of pDCs and $CD1c^+$ mDCs in patients with KD and their immature phenotype and the increase in TIM-3 expression on $CD4^+$ T cells suggested a deficiency in the defensive system of patients with KD and may account for a high infection rate in these patients.

The mechanisms of action of IVIG in KD have been studied extensively; however, the role of DCs and $CD4^+$ T cells in the resolution of inflammation in response to IVIG treatment has rarely been investigated. A study demonstrated the stimulation of normal donor tolerogenic mDCs *in vitro*, with Fc-induced IL-10 secretion, which influenced the differentiation of T cells to regulatory T cells; this finding indicated that the protective effects of IVIG treatment were, at least, partly mediated by Fc (26). In this study, the number of circulating pDCs and $CD1c^+$ mDCs increased to the normal levels after IVIG treatment. Moreover, IVIG treatment restored the expression of HLA-DR, CD86, and CD40 on DC subsets to different degrees. In addition, the $CD4^+$ T cells were affected by IVIG treatment. The percentage of $CD4^+$ T cells expressing the inhibitory receptor TIM-3 was decreased after IVIG treatment. A previous study reported that TIM-3 expression on Treg has been associated with increased suppressive Treg activity (39). IVIG can both modulate Treg cell function and increase Treg cell expansion (15). The reason for this inconsistency may be that the TIM-3 expression is not limited to Treg cells, and it has been shown to be expressed on Th1 cells and $CD8^+$ T cytotoxic type 1 cells (21, 40). Nonetheless, the expression of TIM-3, which is considered an important immuno-inhibitory receptor, in any cell subgroup is correlated with the induction of the immunosuppressive function (41). According to our study, however, the total level of TIM-3 expression on $CD4^+$ T cells was significantly decreased (although to a small extent) post-IVIG therapy; and according to the data on the plasma cytokines, the level of immunosuppressive molecule IL-10 was significantly decreased post-IVIG therapy. Thus, we speculate that the restoration of the cell number and phenotype of $CD4^+$ T cells is involved in the recovery of the immune system of the patients post- IVIG therapy to a certain degree. To the best of our knowledge, this study is the first to describe the variation in inhibitory receptor expression on $CD4^+$ T cells in KD. These results demonstrated that IVIG induced multiple phenotypic and functional changes in DC subsets and $CD4^+$ T cells, mainly by promoting the resolution of inflammation, in patients with KD. The specific mechanisms leading to these effects should be further investigated.

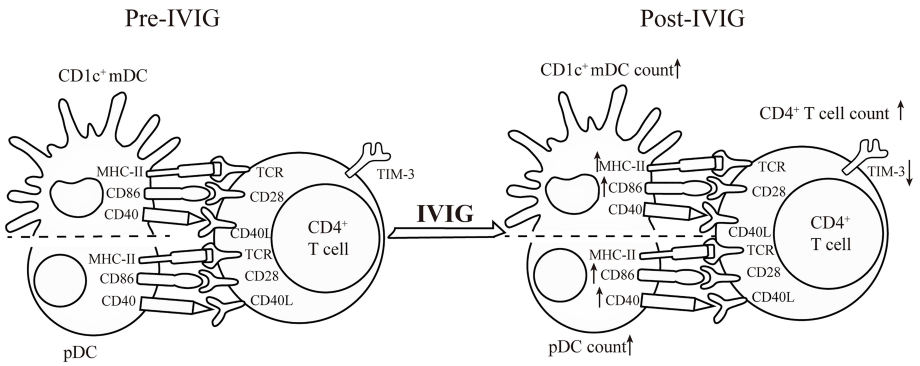

FIGURE 6 | Cartoon chart shows the effects of IVIG on the quantity and functional molecules of DC subsets and $CD4^+$ T cells in KD patients.

In this study, we found that elevation of plasma IL-6 was associated with decreased number of pDC and $CD1c^+$ mDC in patients with KD pre-IVIG treatment. A previous study by Dawicki et al. demonstrated that IL-6 act to selectively promote the accumulation of DC subsets into an inflamed lymph node in mouse model in response to bacterial peptidoglycan (42). Alternatively, Lin et al. showed that IL-6 plays an important role in the apoptosis of cDC1 in mouse model of pancreatic cancer (43). We speculate that IL-6 elevation in KD may be associated with increased recruitment of DC subsets from blood to the affected tissues or increased DCs apoptosis, which awaits further verification. Additionally, there was a significant positive correlation between Th1 and IFN-γ. IFN-γ is one of the major functional cytokines produced by Th1, of note, IFN-γ is also important for Th1 maintenance and production (44, 45). This is in accordance with our findings that peripheral Th1 and plasma IFN-γ were positively correlated.

Our study has some limitations. First, this preliminary study included a relatively small cohort of patients. Large-scale, multi-centre prospective studies are needed to confirm our findings. Second, this study involved short-term IVIG treatment; therefore, additional studies are required to elucidate the effects of IVIG on DC subsets and T cells throughout the entire inflammatory phase. Third, a further analysis of the function of these circulating DCs in patients with KD was hampered by a small number of DCs in the peripheral circulation. Hence, to confirm the functional characteristics of DCs and $CD4^+$ T cells, further *in vitro* and animal studies are needed. Fourth, we could not analyse the relationship between IVIG-nonresponsive and DC subsets and $CD4^+$ T cells because our study did not incorporate this study group. These issues will be addressed in our subsequent studies.

Collectively, our data indicated that IVIG could restore the percentage, number, and expression of effector molecules in DC subsets. Similarly, the frequencies and absolute numbers of abnormally reduced $CD4^+$ T cells increased. Moreover, the expression of TIM-3 on $CD4^+$ T decreased after IVIG treatment, suggesting that IVIG played a role in inhibiting TIM-3 expression, which might be one of the mechanisms of action of IVIG in KD treatment. Changes in DC subsets and $CD4^+$ T cells contributed to the restoration of the immune balance, which can be used as an indicator of clinical monitoring of the immune status in patients with KD. This study offers us an insight into KD pathogenesis and provides a new perspective for understanding the mechanisms of action of IVIG.

DATA AVAILABILITY STATEMENT

The original contributions presented in the study are included in the article/**Supplementary Material**. Further inquiries can be directed to the corresponding author.

ETHICS STATEMENT

The experimental protocols were established following the Declaration of Helsinki and approved by the Ethics Committee of Children's Hospital of Soochow University. Written informed consent to participate in this study was provided by the participants' legal guardian/next of kin.

AUTHOR CONTRIBUTIONS

JH and LM designed and supervised the study and revised the manuscript. FZ, QZ, XZ, FC, and BZ collected clinical information and samples. LM and NW wrote the manuscript. NW and ZC carried out the experiments, and analyzed, and interpreted the data. LM, ZB, HZ, LS, HL, BW, and JS interpreted the data and discussed the results, which are vital for the formation of conception. All authors participated in the manuscript review. The authors read and approved the final manuscript.

FUNDING

This work is supported by the National Natural Science Foundation of China (31670853), the Natural Science Foundation of Jiangsu Province (BK20190053), the Medical Science Program of Jiangsu Province (H2019002), the Talent Engineering Project of Jiangsu Province (BRA2018393), the

Science and Technology Project of Jiangsu Province (BE2019672), the Suzhou Clinical Medicine Expert Project (GSWS2019015), the Science and Technology Program of Suzhou (SYS2018067), and the Postgraduate Research &Practice Innovation Program of Jiangsu Province (KYCX20_2725).

SUPPLEMENTARY MATERIAL

The Supplementary Material for this article can be found online at: https://www.frontiersin.org/articles/10.3389/fimmu.2022.802690/full#supplementary-material

REFERENCES

1. Singh S, Vignesh P, Burgner D. The Epidemiology of Kawasaki Disease: A Global Update. *Arch Dis Child* (2015) 100(11):1084–8. doi: 10.1136/archdischild-2014-307536
2. Burns J, Hsieh L, Kumar J, Behnamfar N, Shimizu C, Sivilay N, et al. Characterization of Circulating Immune Cells in Acute Kawasaki Disease Suggests Exposure to Different Antigens. *Clin Exp Immunol* (2020) 202 (3):263–72. doi: 10.1111/cei.13506
3. Steinman R. Decisions About Dendritic Cells: Past, Present, and Future. *Annu Rev Immunol* (2012) 30:1–22. doi: 10.1146/annurev-immunol-100311-102839
4. O'Keeffe M, Mok W, Radford K. Human Dendritic Cell Subsets and Function in Health and Disease. *Cell Mol Life Sci* (2015) 72(22):4309–25. doi: 10.1007/s00018-015-2005-0
5. Rossi M, Young J. Human Dendritic Cells: Potent Antigen-Presenting Cells at the Crossroads of Innate and Adaptive Immunity. *J Immunol* (2005) 175 (3):1373–81. doi: 10.4049/jimmunol.175.3.1373
6. Balan S, Saxena M, Bhardwaj N. Dendritic Cell Subsets and Locations. *Int Rev Cell Mol Biol* (2019) 348:1–68. doi: 10.1016/bs.ircmb.2019.07.004
7. Merad M, Sathe P, Helft J, Miller J, Mortha A. The Dendritic Cell Lineage: Ontogeny and Function of Dendritic Cells and Their Subsets in the Steady State and the Inflamed Setting. *Annu Rev Immunol* (2013) 31:563–604. doi: 10.1146/annurev-immunol-020711-074950
8. Yilmaz A, Rowley A, Schulte D, Doherty T, Schröder N, Fishbein M, et al. Activated Myeloid Dendritic Cells Accumulate and Co-Localize With CD3+ T Cells in Coronary Artery Lesions in Patients With Kawasaki Disease. *Exp Mol Pathol* (2007) 83(1):93–103. doi: 10.1016/j.yexmp.2007.01.007
9. Sato N, Sagawa K, Sasaguri Y, Inoue O, Kato H. Immunopathology and Cytokine Detection in the Skin Lesions of Patients With Kawasaki Disease. *J Pediatr* (1993) 122(2):198–203. doi: 10.1016/s0022-3476(06)80113-7
10. Schulte D, Yilmaz A, Shimada K, Fishbein M, Lowe E, Chen S, et al. Involvement of Innate and Adaptive Immunity in a Murine Model of Coronary Arteritis Mimicking Kawasaki Disease. *J Immunol* (2009) 183 (8):5311–8. doi: 10.4049/jimmunol.0901395
11. Suda K, Kishimoto S, Takahashi T, Nishino H, Okamura H, Teramachi Y, et al. Circulating Myeloid Dendritic Cells Is Decreased in the Acute Phase of Kawasaki Disease. *Exp Clin Cardiol* (2013) 04(10):272. doi: 10.4172/2155-9880.1000272
12. Shimozato T, Iwata M, Tamura N. Suppression of Tumor Necrosis Factor Alpha Production by a Human Immunoglobulin Preparation for Intravenous Use. *Infect Immun* (1990) 58(5):1384–90. doi: 10.1128/iai.58.5.1384-1390.1990
13. Leung D, Burns J, Newburger J, Geha R. Reversal of Lymphocyte Activation *In Vivo* in the Kawasaki Syndrome by Intravenous Gammaglobulin. *J Clin Invest* (1987) 79(2):468–72. doi: 10.1172/jci112835
14. Yi Q, Li C, Yang X. Effect of Intravenous Immunoglobulin on Inhibiting Peripheral Blood Lymphocyte Apoptosis in Acute Kawasaki Disease. *Acta Paediatr* (2001) 90(6):623–7. doi: 10.1080/080352501750258667
15. Guo M, Tseng W, Ko C, Pan H, Hsieh K, Kuo H. Th17- and Treg-Related Cytokine and mRNA Expression Are Associated With Acute and Resolving Kawasaki Disease. *Allergy* (2015) 70(3):310–8. doi: 10.1111/all.12558
16. Ephrem A, Chamat S, Miquel C, Fisson S, Mouthon L, Caligiuri G, et al. Expansion of CD4+CD25+ Regulatory T Cells by Intravenous Immunoglobulin: A Critical Factor in Controlling Experimental Autoimmune Encephalomyelitis. *Blood* (2008) 111(2):715–22. doi: 10.1182/blood-2007-03-079947
17. Altara R, Mallat Z, Booz G, Zouein F. The CXCL10/CXCR3 Axis and Cardiac Inflammation: Implications for Immunotherapy to Treat Infectious and Noninfectious Diseases of the Heart. *J Immunol Res* (2016) 2016:4396368. doi: 10.1155/2016/4396368
18. McCrindle B, Rowley A, Newburger J, Burns J, Bolger A, Gewitz M, et al. Diagnosis, Treatment, and Long-Term Management of Kawasaki Disease: A Scientific Statement for Health Professionals From the American Heart Association. *Circulation* (2017) 135(17):e927–99. doi: 10.1161/cir.0000000000000484
19. Dallaire F, Dahdah N. New Equations and a Critical Appraisal of Coronary Artery Z Scores in Healthy Children. *J Am Soc Echocardiogr* (2011) 24(1):60–74. doi: 10.1016/j.echo.2010.10.004
20. Meng L, Bai Z, He S, Mochizuki K, Liu Y, Purushe J, et al. The Notch Ligand DLL4 Defines a Capability of Human Dendritic Cells in Regulating Th1 and Th17 Differentiation. *J Immunol* (2016) 196(3):1070–80. doi: 10.4049/jimmunol.1501310
21. Anderson A, Joller N, Kuchroo V. Lag-3, Tim-3, and TIGIT: Co-Inhibitory Receptors With Specialized Functions in Immune Regulation. *Immunity* (2016) 44(5):989–1004. doi: 10.1016/j.immuni.2016.05.001
22. Wang S, Zhang X, Leng S, Xu Q, Sheng Z, Zhang Y, et al. Immune Checkpoint-Related Gene Polymorphisms Are Associated With Primary Immune Thrombocytopenia. *Front Immunol* (2020) 11:615941. doi: 10.3389/fimmu.2020.615941
23. McBride M, Patil T, Bohannon J, Hernandez A, Sherwood E, Patil N. Immune Checkpoints: Novel Therapeutic Targets to Attenuate Sepsis-Induced Immunosuppression. *Front Immunol* (2020) 11:624272. doi: 10.3389/fimmu.2020.624272
24. von Witzleben A, Fehn A, Grages A, Ezić J, Jeske S, Puntigam L, et al. Prospective Longitudinal Study of Immune Checkpoint Molecule (Icm) Expression in Immune Cell Subsets During Curative Conventional Therapy of Head and Neck Squamous Cell Carcinoma (Hnscc). *Int J Cancer* (2021) 148 (8):2023–35. doi: 10.1002/ijc.33446
25. Lee S, Kim Y, Hyun M, Kim Y, Kim H, Lee Y. T-Helper Cytokine Profiles in Patients With Kawasaki Disease. *Korean Circ J* (2015) 45(6):516–21. doi: 10.4070/kcj.2015.45.6.516
26. Burns J, Song Y, Bujold M, Shimizu C, Kanegaye J, Tremoulet A, et al. Immune-Monitoring in Kawasaki Disease Patients Treated With Infliximab and Intravenous Immunoglobulin. *Clin Exp Immunol* (2013) 174(3):337–44. doi: 10.1111/cei.12182
27. Reis e Sousa C. Dendritic Cells in a Mature Age. *Nat Rev Immunol* (2006) 6 (6):476–83. doi: 10.1038/nri1845
28. Tan J, O'Neill H. Maturation Requirements for Dendritic Cells in T Cell Stimulation Leading to Tolerance Versus Immunity. *J Leukoc Biol* (2005) 78 (2):319–24. doi: 10.1189/jlb.1104664
29. Ganguly D, Haak S, Sisirak V, Reizis B. The Role of Dendritic Cells in Autoimmunity. *Nat Rev Immunol* (2013) 13(8):566–77. doi: 10.1038/nri3477
30. Lee H, Kim D, Noh G, Lee K. Effects of Intravenous Immune Globulin on the Peripheral Lymphocyte Phenotypes in Kawasaki Disease. *Yonsei Med J* (1996) 37(5):357–63. doi: 10.3349/ymj.1996.37.5.357
31. Matsubara T, Katayama K, Matsuoka T, Fujiwara M, Koga M, Furukawa S. Decreased Interferon-Gamma (IFN-Gamma)-Producing T Cells in Patients With Acute Kawasaki Disease. *Clin Exp Immunol* (1999) 116(3):554–7. doi: 10.1046/j.1365-2249.1999.00899.x
32. Kimura J, Takada H, Nomura A, Ohno T, Mizuno Y, Saito M, et al. Th1 and Th2 Cytokine Production Is Suppressed at the Level of Transcriptional Regulation in Kawasaki Disease. *Clin Exp Immunol* (2004) 137(2):444–9. doi: 10.1111/j.1365-2249.2004.02506.x
33. Kuo H, Li S, Guo M, Huang Y, Yu H, Huang F, et al. Genome-Wide Association Study Identifies Novel Susceptibility Genes Associated With Coronary Artery Aneurysm Formation in Kawasaki Disease. *PLoS One* (2016) 11(5):e0154943. doi: 10.1371/journal.pone.0154943

34. Tahara M, Baba K, Waki K, Arakaki Y. Analysis of Kawasaki Disease Showing Elevated Antibody Titres of Yersinia Pseudotuberculosis. *Acta Paediatr* (2006) 95(12):1661–4. doi: 10.1080/08035250600750080
35. Kuo H, Li S, Huang L, Huang Y. Epigenetic Hypomethylation and Upregulation of Matrix Metalloproteinase 9 in Kawasaki Disease. *Oncotarget* (2017) 8(37):60875–91. doi: 10.18632/oncotarget.19650
36. Kuijpers T, Wiegman A, van Lier R, Roos M, Wertheim-van Dillen P, Pinedo S, et al. Kawasaki Disease: A Maturational Defect in Immune Responsiveness. *J Infect Dis* (1999) 180(6):1869–77. doi: 10.1086/315111
37. Matsubara T, Anwar R, Fujiwara M, Ichiyama T, Furukawa S. CTLA-4 (CD152) Expression in Peripheral Blood T Cells in Kawasaki Disease. *Clin Exp Immunol* (2003) 132(1):169–73. doi: 10.1046/j.1365-2249.2003.02109.x
38. Ikeda K, Yamaguchi K, Tanaka T, Mizuno Y, Hijikata A, Ohara O, et al. Unique Activation Status of Peripheral Blood Mononuclear Cells at Acute Phase of Kawasaki Disease. *Clin Exp Immunol* (2010) 160(2):246–55. doi: 10.1111/j.1365-2249.2009.04073.x
39. Gupta S, Thornley T, Gao W, Larocca R, Turka L, Kuchroo V, et al. Allograft Rejection Is Restrained by Short-Lived TIM-3+PD-1+Foxp3+ Tregs. *J Clin Invest* (2012) 122(7):2395–404. doi: 10.1172/jci45138
40. Veenstra R, Taylor P, Zhou Q, Panoskaltsis-Mortari A, Hirashima M, Flynn R, et al. Contrasting Acute Graft-Versus-Host Disease Effects of Tim-3/Galectin-9 Pathway Blockade Dependent Upon the Presence of Donor Regulatory T Cells. *Blood* (2012) 120(3):682–90. doi: 10.1182/blood-2011-10-387977
41. Tang R, Rangachari M, Kuchroo V. Tim-3: A Co-Receptor With Diverse Roles in T Cell Exhaustion and Tolerance. *Semin Immunol* (2019) 42:101302. doi: 10.1016/j.smim.2019.101302
42. Dawicki W, Jawdat D, Xu N, Marshall J. Mast Cells, Histamine, and IL-6 Regulate the Selective Influx of Dendritic Cell Subsets Into an Inflamed Lymph Node. *J Immunol* (2010) 184(4):2116–23. doi: 10.4049/jimmunol.0803894
43. Lin J, Huffman A, Wattenberg M, Walter D, Carpenter E, Feldser D, et al. Type 1 Conventional Dendritic Cells Are Systemically Dysregulated Early in Pancreatic Carcinogenesis. *J Exp Med* (2020) 217(8):e20190673. doi: 10.1084/jem.20190673
44. Sheng W, Yang F, Zhou Y, Yang H, Low P, Kemeny D, et al. STAT5 Programs a Distinct Subset of Gm-Csf-Producing T Helper Cells That Is Essential for Autoimmune Neuroinflammation. *Cell Res* (2014) 24(12):1387–402. doi: 10.1038/cr.2014.154
45. Noubade R, Krementsov D, Del Rio R, Thornton T, Nagaleekar V, Saligrama N, et al. Activation of P38 MAPK in CD4 T Cells Controls IL-17 Production and Autoimmune Encephalomyelitis. *Blood* (2011) 118(12):3290–300. doi: 10.1182/blood-2011-02-336552

Conflict of Interest: The authors declare that the research was conducted in the absence of any commercial or financial relationships that could be construed as a potential conflict of interest.

Publisher's Note: All claims expressed in this article are solely those of the authors and do not necessarily represent those of their affiliated organizations, or those of the publisher, the editors and the reviewers. Any product that may be evaluated in this article, or claim that may be made by its manufacturer, is not guaranteed or endorsed by the publisher.

frontiers in Immunology

ORIGINAL RESEARCH
published: 02 March 2022
doi: 10.3389/fimmu.2022.833515

Celastrol Downmodulates Alpha-Synuclein-Specific T Cell Responses by Mediating Antigen Trafficking in Dendritic Cells

Lam Ng[1], Xiaohui Wang[1], Chuanbin Yang[2,3], Chengfu Su[2,4], Min Li[2†] and Allen Ka Loon Cheung[1*†]*

[1] Department of Biology, Faculty of Science, Hong Kong Baptist University, Kowloon Tong, Hong Kong SAR, China, [2] Mr. & Mrs. Ko Chi Ming Center for Parkinson Disease Research, School of Chinese Medicine, Hong Kong Baptist University, Kowloon Tong, Hong Kong SAR, China, [3] Department of Geriatrics, Shenzhen People's Hospital (The Second Clinical Medical College, Jinan University; The First Affiliated Hospital, Southern University of Science and Technology), Shenzhen, China, [4] College of Pharmacy, Henan University of Chinese Medicine, Zhengzhou, China

OPEN ACCESS

Edited by:
Luis C. Anton, Spanish National Research Council (CSIC), Spain

Reviewed by:
Cristina Corina Clement, Cornell University, United States
Srinivasa Reddy Bonam, Institut National de la Santé et de la Recherche Médicale (INSERM), France

***Correspondence:**
Allen Ka Loon Cheung
akcheung@hkbu.edu.hk
Min Li
limin@hkbu.edu.hk

[†]These authors have contributed equally to this work and share last authorship

Specialty section:
This article was submitted to Antigen Presenting Cell Biology, a section of the journal Frontiers in Immunology

Received: 11 December 2021
Accepted: 07 February 2022
Published: 02 March 2022

Citation:
Ng L, Wang X, Yang C, Su C, Li M and Cheung AKL (2022) Celastrol Downmodulates Alpha-Synuclein-Specific T Cell Responses by Mediating Antigen Trafficking in Dendritic Cells. Front. Immunol. 13:833515. doi: 10.3389/fimmu.2022.833515

Parkinson's Disease (PD) is a neurodegenerative disease that affects the elderly. It is associated with motor dysfunction due to the accumulation of misfolded or aggregated fibrillar alpha-synuclein (α-syn) in the mid-brain. Current treatments are mainly focused on relieving the symptoms but are accompanied by side effects and are limited in halting disease progression. Increasing evidence points to peripheral immune cells underlying disease development, especially T cells contributing to α-syn-related neuroinflammation in PD. The onset of these cells is likely mediated by dendritic cells (DCs), whose role in α-syn-specific responses remain less studied. Moreover, Traditional Chinese medicine (TCM)-derived compounds that are candidates to treat PD may alleviate DC-T cell-mediated immune responses. Therefore, our study focused on the role of DC in response to fibrillar α-syn and subsequent induction of antigen-specific T cell responses, and the effect of TCM Curcumin-analog C1 and *Tripterygium wilfordii* Hook F-derived Celastrol. We found that although fibrillar α-syn did not induce significant inflammatory or T cell-mediating cytokines, robust pro-inflammatory T cell responses were found by co-culturing fibrillar α-syn-pulsed DCs with α-syn-specific $CD4^+$ T cells. Celastrol, but not C1, reduced the onset of pro-inflammatory T cell differentiation, through promoting interaction of endosomal, amphisomal, and autophagic vesicles with fibrillar α-syn, which likely lead to its degradation and less antigen peptides available for presentation and T cell recognition. In conclusion, regulating the intracellular trafficking/processing of α-syn by DCs can be a potential approach to control the progression of PD, in which Celastrol is a potential candidate to accomplish this.

Keywords: Celastrol, Parkinson's Disease, α-synuclein, dendritic cell, $CD4^+$ T cell subsets, endo-lysosomal pathway, autophagy

INTRODUCTION

Parkinson's Disease (PD) is the second most common neurodegenerative disease in the world, affecting approximately 10 million people worldwide who are aged over 60 (1). PD is characterized by impaired motor symptoms due to the progressive loss of functions or cell death of dopaminergic neurons in the par compacta of substantia nigra (SNpc) or caudate putamen (CPu) of the brain (2). α-Synuclein (α-syn) is a presynaptic protein that is expressed abundantly in the mammalian brain and peripheral tissues (3). Under normal physiological conditions, it exists in its intrinsic unfolded monomeric conformation allowing its interactions with other proteins, such as SNARE complex proteins, to perform normal cell trafficking functions (4). One pathological hallmark of PD is the accumulation of misfolded α-syn protein inclusions forming Lewy bodies inside the neuronal cells that are caused by either familial inherited gene mutations or idiopathic factors (5–7). The abnormal α-syn in the shape of the β-sheet structure serve as nucleation sites, which further recruit endogenous monomeric α-syn, convert into soluble oligomeric form that at a later stage, aggregate into insoluble fibrillar form (8, 9). It is proposed that accumulation of oligomeric or fibrillar α-syn leads to dopaminergic neuronal cell death and activates the brain resident microglia causing neuroinflammation (10, 11). Dysregulated and prolonged neuroinflammation will lead to more neuronal cell death and compromise the integrity of the blood–brain barrier (BBB), favor the recruitment and infiltration of peripheral immune cells which could worsen the disease (12–14).

In PD patients, T cells were found in the brain parenchyma and the relative abundance of T cells in peripheral blood was decreased compared to healthy control (12, 15). Despite this, the frequency of Th1, Th17 but not Treg subsets were elevated in PD patients and associated with the increased serum levels of IL-6 and IL-17 and decreased IL-10 and TGF-β (16, 17). The polarization of these subsets is governed by cytokines. Th1 differentiation is dependent on IL-12, IL-18, and IFN-γ that trigger T-box transcription factor TBX21 (T-bet) transcription factor; Th17 uses retinoic acid receptor-related orphan receptor gamma t (RORγt) transcription factor induced by IL-1β, IL-6, IL-23, and TGF-β; Treg differentiation depends on forkhead box P3 (FoxP3) stimulated by IL-10, IL-2, and TGF-β (18–21). In PD patients, these T cells can recognize α-syn peptides even before the onset of motor symptoms (22, 23). Moreover, brain neurons that express IL-17 receptors are prone to neuronal cell death driven by IL-17 and NFκB activation (24).

DCs provide the three signals for $CD4^+$ T cell activation and differentiation, through major histocompatibility complex class II (MHC-II) antigen presentation (signal 1), co-stimulatory molecules (signal 2), and cytokines (signal 3) (25, 26). Normally, absence or low abundance of peripheral DCs are found in the central nervous system (CNS). In PD, peripheral DCs could migrate across the BBB and uptake the α-syn aggregates in the brain, then proceed to the cervical lymph nodes, where they increase the expression of MHC-II and present the α-syn antigenic peptides to activate antigen-specific T cells (13, 27, 28). Previous studies have demonstrated that the frequency of DCs in the blood of PD patients declined but increased in the CNS, where they could respond to α-syn aggregates and trigger neuroinflammation (29, 30). However, it remains controversial whether DCs mature in response to α-syn. DCs treated with α-syn resulted in an upregulation in the expression of co-stimulatory molecules CD80 and CD86 and also MHC-II (31), while others found no differences in the activation markers for DCs between PD patients and healthy control (32).

Endo-lysosomal degradation of foreign antigens internalized by antigen presenting cells (APCs) has long been reported for antigen presentation and mediating T cell immunity (33–35). Also, autophagy was shown to play a vital role in degrading protein aggregates for antigen presentation, which is inhibited by α-syn fibrils (36, 37). There is evidence on the linkage between autophagy gene mutations and the accumulation of α-syn (38). Moreover, mutation of autophagy-related Leucine-rich repeat kinase 2 (LRRK2) could promote DC antigen presentation to $CD4^+$ T cells (39). Furthermore, α-syn can escape from lysosomal degradation by rupturing endosomal and lysosomal vesicles and resulting in increased reactive oxygen species (ROS) and inflammasome activation (40). It is reported that the limited proteolytic reaction also favors MHC class II-peptide loading and presentation to $CD4^+$ T cells (41). Ras-related protein in brain (Rab) proteins are important in mediating vesicular trafficking for endocytosis, autophagy, and lysosomal degradation. They are characterized with respect to their intracellular localizations and trafficking functions. Usually, Rab5 and Rab14 (early endosome markers), Rab7 (late endosome marker), Rab11 (recycling endosome marker), and Rab9 and Lamp1 (lysosome markers), form the different stages of the endo-lysosomal pathway (42). In addition, Rab proteins play a role in autophagy by interacting with Beclin1 and LC3 (43, 44), which may be related to the trafficking of α-syn for antigen processing and presentation in DCs. To assist in defining the importance of these pathways, we used two traditional Chinese medicine (TCM)-derived compounds which are previously shown as potential autophagy inducers: C1—a novel Curcumin analog (45), and Celastrol—a natural bioactive compound derived from *Tripterygium wilfordii* Hook F (TWHF) (46, 47), where the latter also displayed anti-inflammatory effect in different diseases (48, 49). Though, whether these drugs have any effects against α-syn-specific T cell immune response have not been investigated. Therefore, we hypothesized that Celastrol and C1 could decrease DC-mediated α-syn-specific pro-inflammatory T cell responses by modulating the trafficking pathways that could possibly favor the processing of α-syn leading to reduced T cell activation.

In this study, we addressed three main issues: 1) Monocyte-derived DCs (MoDCs) response toward α-syn stimulation; 2) $CD4^+$ T cell subsets abundance in response to α-syn-pulsed MoDCs; and, 3) the interactions of endo-lysosomal and autophagic pathway components with α-syn in MoDCs. Interestingly, our data showed that α-syn treatment did not induce higher expression of antigen presentation molecules nor cytokines gene transcription in MoDCs, but still stimulated

robust inflammatory α-syn specific $CD4^+$ T cell responses. Both endo-lysosomal and autophagic pathways are associated with α-syn, where colocalizations of Rab and autophagosomal proteins with α-syn were found. Treatment of MoDCs with α-syn appeared to downregulate the expression of Rab and autophagosomal proteins, indicating the possibility that α-syn regulated its interaction with antigen processing components which limited its degradation and allowed the activation of T cells. Lastly, Celastrol (but not C1) could inhibit α-syn-specific T cell responses, likely through the induction of higher colocalization of α-syn with $Rab5^+$ and $Rab7^+$ vesicles and autophagosomes, which suggest a more effective degradation that may assist in minimizing antigen presentation to $CD4^+$ T cells.

MATERIALS AND METHODS

$CD14^+$ Monocytes Isolation and Differentiation Into MoDCs

Peripheral blood mononuclear cells (PBMCs) were freshly isolated from the whole blood of anonymous healthy human blood donors using Lymphoprep (Cat. No. 07851, Stemcell Technologies). Usage of healthy human blood received approval from the HKBU Research Ethics Committee (#REC/19-20/0110). $CD14^+$ monocytes were isolated from the freshly prepared PBMCs using CD14 microbeads, human (Cat. No. 130-050-201, Miltenyi Biotec) according to manufacturer protocol. To generate MoDCs, $CD14^+$ cells were cultured at a density of 1×10^6 cells/ml in RPMI 1640 medium (Cat. No. 11875-085, Gibco) supplemented with 10% Fetal Bovine Serum (FBS) (Cat. No. 10270-106, Gibco), 1% Penicillin–Streptomycin (10,000 U/ml) (Cat. No. 15140-122, Gibco), 25 μg/ml rhIL-4 (Cat. No. 200-04, PeproTech), and 25 μg/ml rhGM-CSF (Cat. No. 300-03, PeproTech) for 5–7 days, with 50% medium change every 3 days. Cells were incubated at 37°C, 5% CO_2.

Reverse Transcription Quantitative Real-Time PCR (qRT-PCR)

MoDCs were seeded at a density of 1×10^6 cells/ml in RPMI 1640 medium 1% FBS in 24-well cell culture plate overnight at 37°C, 5% CO_2. C1 (1 μM) and Celastrol (0.25 μM) were added to pre-treat MoDCs for 1 h and recombinant Human Alpha-synuclein protein aggregate (Active) (fibrillar α-syn) (Cat. No. ab218819, Abcam) (1 μg/ml) was used to treat MoDCs for another 4 h. Cells were harvested, and total RNA was extracted using RNAiso Plus followed by cDNA generation by PrimeScript™ RT Master Mix (Cat. No. RR047A, Takara). Quantitative real-time PCR was carried out with the TB Green Premix Ex Taq II (Tli RNase H Plus) (Cat. No. RR820A, Takara) using StepOnePlus™ Real Time System (Cat. No. 4376600, Invitrogen). The following primer pairs were used: GAPDH, 5′-ACAGTCCATGCCATCACTGCC-3′, 5′-GCCTGCTTCACCACCTTCTTG-3′; IL-1β, 5′-ATGATGGCTTATTACAGTGGCAA-3′, 5′-GTCGGAGATTCGTAGCTGGA-3′; IL-6, 5′-AGACAGCCACTCACCTCTTC-3′, 5′-AGTGCCTCTTTGCTGCTTTC-3′; IL-23, 5′-TTTTCACAGGGGAGCCTTCT-3′, 5′-ACTGAGGCTTGGAATCTGCT-3′; TNF-α, 5′-GTCAACCTCCTCTCTGCCAT-3′, 5′-CCAAAGTAGACCTGCCCAGA-3′; TGF-β, 5′-CACGTGGAGCTGTACCAGAA-3′, 5′-GAACCCGTTGATGTCCACTT-3′; IL-10, 5′-GACTTTAAGGGTTACCTGGGTTG-3′. 5′-TCACATGCGCCTTGATGTCTG-3′. Relative expression was calculated by normalizing to GAPDH and by ΔΔCT method. The ΔΔCT method was used to calculate the relative expression of each gene with reference to GAPDH, which were then normalized to α-syn only treatment.

BV2 Culturing and Treatment

Mouse BV2 microglia cell line was purchased from Elabscience (Cat. No. EP-CL-0493) and cultured in DMEM, high glucose (Cat. No. 11965-126, Gibco) supplemented with 10% FBS. Cells were incubated at 37 °C, 5% CO_2 and subcultured when cell confluency reached 80–90%. Before treatment, BV2 were seeded in DMEM medium with 10% FBS in 24-well cell culture plate overnight at 37 °C, 5% CO_2. The next day, lipopolysaccharide (LPS) (100 ng/ml) was used to prime the cells for 3 h in DMEM medium with 10% FBS and washed 3 times with PBS and replaced with fresh DMEM medium. Then, fibrillar α-syn in a concentration of 1 μg/ml was used to treat the BV2 cells for 3 h. Cells were harvested and subjected to qRT-PCR using similar methods as above.

Flow Cytometry for MoDC Surface Markers

MoDCs were seeded at a density of 1×10^5 cells/ml in RPMI 1640 medium 1% FBS in 24-well cell culture plate overnight at 37°C, 5% CO_2. C1 (1 μM) and Celastrol (0.25 μM) were added to pre-treat MoDCs for 1 h followed by the addition of fibrillar α-syn (1 μg/ml) for 24 h. In some cases, TNF-α (50 ng/ml) was added together with fibrillar α-syn. LPS (100 ng/ml) was used as the positive control. Afterward, MoDCs were collected and washed with fluorescence-activated cell sorter (FACS) buffer (PBS + 1% FBS) and incubated for 30 min at 4°C in 100 μl FACS Buffer with BV421 Mouse anti-Human HLA-ABC (Cat. No. 565332, BD Pharmingen), APC Mouse anti-Human HLA-DR (Cat. No. 560896, BD Pharmingen), PE-Cy7 Mouse anti-Human CD86 (Cat. No. 561128, BD Pharmingen) and FITC Mouse anti-Human CD80 (Cat. No. 555683, BD Pharmingen) antibodies. Flow cytometry was performed following standard protocols on a BD FACSCanto™ II cytometer.

MoDC Stimulation of Antigen-Specific $CD4^+$ T Cells

α-Syn peptide-specific $CD4^+$ T cells were generated according to the previous protocol (50) with some modifications. Briefly, freshly isolated PBMCs (5×10^6 cells/ml) were first cultured in RPMI + 10% FBS + 1% GlutaMAX (Cat. No. 35050-061, Gibco) and stimulated with α-syn peptide EQVTNVGGAVVTGVT (5 μg/ml) (ChinaPeptides) with reference to previous studies (22). One day after stimulation, rhIL-2 (100 IU/ml) (Cat. No. 200-02, Preprotech) was added to the cell culture for 7 days, with 50% media change and replenishment of rhIL-2 every 3 days. Frozen

autologous PBMCs were stimulated with the same α-syn peptide (5 μg/ml) overnight and were added into the original PBMCs culture in a ratio of 1:10 for re-stimulation for another 7 days, with 50% media change and replenishment of rhIL-2 every 3 days. Simultaneously, MoDCs were generated as mentioned above and cultured for 6 days. Prior to the co-culture experiment, MoDCs were pre-treated with either C1 (1 μM) or Celastrol (0.25 μM) for 1 h followed by treating with fibrillar α-syn (1 μg/ml) overnight in RPMI + 10% FBS + 1% GlutaMAX. Also, rhIL-2 concentration of the PBMCs culture was reduced to 20 IU/ml to minimize its effect on T cells but to maintain survival. On the day of the co-culturing experiment, total $CD4^+$ T cells were isolated from the PBMCs culture using $CD4^+$ T Cell Isolation Kit, human (Cat. No. 130-096-533, Miltenyi Biotec) and added into the MoDCs culture in a ratio of MoDCs:T cell = 1:5 and cultured for 1 day or 3 days. α-Syn-specific $CD4^+$ T cell only was served as the negative control. One day after the co-culture experiment, half of the suspension cells were harvested for flow cytometry analysis of surface CD3, CD4, CD25, and intracellular IFN-γ and T-bet expression using FITC Mouse anti-Human CD3 (Cat. No. 555339, BD Pharmingen), V500 Mouse anti-Human CD4 (Cat. No. 560768, BD Pharmingen), APC-Cy7 Mouse anti-Human CD25 (Cat. No. 557753, BD Pharmingen), PE-Cy7 Mouse anti-Human IFN-γ (Cat. No. 557643, BD Pharmingen) and PerCP-Cy5.5 Mouse anti-Human T-bet (Cat. No. 561316, BD Pharmingen) antibodies. While on day 3 of the co-culturing experiment, the remaining suspension cells were harvested for flow cytometry analysis of surface CD3, CD4, CD25, and intracellular IL-17A, RORγt and FoxP3 expression using FITC Mouse anti-Human CD3 (Cat. No. 555339, BD Pharmingen), V500 Mouse anti-Human CD4 (Cat. No. 560768, BD Pharmingen), APC-Cy7 Mouse anti-Human CD25 (Cat. No. 557753, BD Pharmingen), Alexa Fluor 647 Mouse anti-Human RORγt (Cat. No. 563620, BD Pharmingen), PerCp-Cy5.5 Mouse anti-Human IL-17A (Cat. No. 560799, BD Pharmingen) and PE Mouse anti-Human FoxP3 (Cat. No. 560046, BD Pharmingen) antibodies. Flow cytometry was performed following standard protocols on a BD FACSCanto™ II cytometer.

Immunofluorescence Analysis of Rab and Autophagy-Related Proteins Using Confocal Microscopy

MoDCs (1×10^5 cells/200 μl) were seeded on Nunc™ Lab-Tek™ II 8-well Chambered Coverglass w/non-removable wells (1.5 Borosilicate Glass) (Cat. No. 155409, Invitrogen) in RPMI with 1% FBS overnight at 37 °C, 5% CO_2. For studying endo-lysosomal pathway, C1 (1 μM) and Celastrol (0.25 μM) were added to pre-treat MoDCs for 1 h followed by the addition of 1 μg/ml fibrillar α-syn for 15, 30, and 60 min. Cells were then fixed with 2% paraformaldehyde (PFA) for 20 min at room temperature, permeabilized using the blocking and permeabilizing buffer composed of PBS with 5% Normal Goat Serum (Cat. No. 31873, Invitrogen), 3% Bovine Serum Albumin (BSA) (Cat. No. 9048-46-8, Sigma) and 0.5% Triton X-100 for 20 min, 4 °C. Following washing, primary antibodies were used for overnight incubation in the staining buffer of PBS with 3% BSA and 0.1% Triton X-100 overnight at 4°C: for early endosome markers, Mouse anti-Rab5 (1:200) (Cat. No. ab66746, Abcam) and Rabbit anti-Rab14 (1:200) (Cat. No. ab40938, Abcam) were incubated with 15 min samples; late endosome marker, Mouse anti-Rab7 (1:500) (Cat. No. ab50533, Abcam) and recycling endosome maker Rabbit anti-Rab11 (1:500) (Cat. No. ab36112, Abcam) were incubated with 30 min samples; lysosome markers, Mouse anti-Rab9 (1:500) (Cat. No. MA3-067, Invitrogen) and Rabbit anti-Lamp1 (1:300) (Cat. No. ab24170, Abcam) were incubated with 60 min samples. All samples were also probed with Chicken anti-α-syn (1:1,000) (Cat. No. ARG10689, Arigobio) in the staining buffer of PBS with 3% BSA and 0.1% Triton X-100 overnight at 4 °C.

For studying autophagic pathways, after C1 or Celastrol pre-treatment, MoDCs were treated with 1 μg/ml fibrillar α-syn for 4, 6 or 16 h. Cells were then fixed and permeabilized as mentioned above. Primary antibodies of early autophagosome marker, Rabbit anti-Beclin1 (1:200) (Cat. No. ab62557, Abcam) and early endosome marker, Mouse anti-Rab5 (1:500) were incubated with 4 h samples; autophagosome cargo protein p62 (SQSTM1), Mouse anti-SQSTM1/p62 (1:200) (Cat. No. ab56416, Abcam) was incubated with 6 h samples; autophagosome marker, Rabbit anti-LC3B (1:300) (Cat. No. NB100-2220, Novus Biologicals) and late endosome marker, Mouse anti-Rab7 (1:500) were incubated with 16 h samples. All samples were also probed with Chicken anti-α-syn (1:1,000) in the staining buffer of PBS with 3% BSA and 0.1% Triton X-100 overnight at 4°C.

Following primary antibody staining, cells were washed 3 times with PBS + 0.01% Triton X-100. Secondary antibodies Alexa Fluor 488 Goat anti-Rabbit (1:1,000) (Cat. No. A27034, Invitrogen), Alexa Fluor 647 Goat anti-Mouse (1:1,000) (Cat. No. A28181, Invitrogen) and DyLight anti-Chicken IgY H&L (1:500) (Cat. No. ab96948, Abcam) were used for fluorescence staining at room temperature for 1 h in darkness. Cells were washed 3 times again with PBS with 0.01% Triton X-100. Cell nuclei were stained with Hoechst 33258 (1:800) (Cat. No. ab228550, Abcam) for 20 min at 4 °C in darkness. Lastly, cells were mounted using ibidi mounting medium (Cat. No. 50001, ibidi) and signals were acquired using Leica TCS SP5 confocal microscopy and images were analyzed using the LAS AF software (Leica). The number of Rab5, Rab7, Rab9, Rab11, Rab14, Beclin1, LC3 positive puncta and their colocalizations with α-syn were counted and colocalization intensity values were analyzed using ImageJ software (http://imagej.nih.gov/ij/) (51).

Western Blot

Cells were collected and washed with PBS, followed by lysing with lysis buffer (10 mM Tris–HCl (pH 7.5), 200 mM NaCl, 1 mM EDTA, 1 mM DTT, 0.5% NP-40, 10 μg/ml aprotinin, 10 μg/ml leupeptin, 1.25 μg/ml pepstatin A, 1 mM PMSF) on ice for 45 min. Lysates were then centrifuged at 13,000×*g*, 4°C for 30–45 min. Supernatants were collected and protein concentration was measured using Pierce™ BCA Protein Assay Kit (Cat. No. 23225, Thermo Scientific) according to the manufacturer's instructions. Protein samples were mixed with 5× loading buffer (250 mM Tris–HCl (pH 6.8), 10% SDS, 30% glycerol, 5% β-mercaptoethanol, 0.02% bromophenol blue) and were boiled at 98°C for 5 min before being loaded into 10–12% SDS-PAGE gel

for electrophoresis and transferred to Immobilon®-P polyvinylidene difluoride (PVDF) (Cat. No. P2938, Sigma) membrane using a Mini Trans-Blot Electrophoretic Transfer Cell (Bio-Rad). Membranes were blocked with 0.5% BSA and 5% blotting-grade blocker (Biorad) in PBS-T or TBS-T for 1 h at room temperature and blotted with aforementioned primary antibodies Rabbit anti-Rab5, Mouse anti-Rab7, Rabbit anti-Beclin1, Mouse anti-SQSTM1/p62, Rabbit anti-LC3B and anti-beta-Actin, clone RM112 monoclonal antibody (Cat. No. MABT523, Merck Millipore) (1:500–1:1,000) overnight at 4°C, followed by incubating with secondary antibodies HRP conjugate Donkey Anti-Rabbit antibody (Cat. No. AP182P, Merck Millipore) or HRP conjugated Goat Anti-Mouse antibody (Cat. No. AP130P, Merck Millipore) (1:10,000) for 1 h at room temperature. Membrane blots were developed using SuperSignal™ West Pico PLUS Chemiluminescent Substrate (Cat. No. 34580, Thermo Scientific) or SuperSignal™ West Femto Maximum Sensitivity Substrate (Cat. No. 34094, Thermo Scientific). Signals were detected by ChemiDoc (Bio-Rad) and band intensities were quantified using ImageJ software.

Immunoprecipitation

Immunoprecipitation of Rab5-GTP or Rab7-GTP from MoDCs using (Cat. No. 83701, NewEast Biosciences) and Anti-Active Rab7 Mouse Monoclonal Antibody (Cat. No. 26923, NewEast Biosciences) according to the manufacturer protocol with some modifications. Briefly, cells were lysed using 1× Assay/Lysis Buffer with 10 μg/ml aprotinin, 10 μg/ml leupeptin, 1.25 μg/ml pepstatin A, 1 mM PMSF for 30–45 min on ice. Lysates were centrifuged at 13,000×*g*, 4°C for 30–45 min. Supernatants were collected and protein concentration was measured using Pierce™ BCA Protein Assay Kit according to manufacturer's instructions. Afterward, lysates were incubated with either Mouse anti-Rab5-GTP or Mouse anti-Rab7-GTP primary antibody (1 μg) pre-conjugated with protein A/G agarose slurry (20 μl) in 500 μl of 1× Assay/Lysis Buffer with protease inhibitors for a maximum of 2 h, 4°C, with gentle rotation for immunoprecipitation. Afterward, 5× loading buffer was used to elute the targeted proteins by boiling at 98°C for 5 min and the protein lysates were subjected to SDS-PAGE as described above. Membranes were blocked with TBS-T + 3% BSA and incubated with either Rabbit anti-Rab5 or Mouse anti-Rab7 primary antibody (1:1,000) in TBS-T + 3% BSA overnight at 4°C, followed by incubating with Recombinant Protein G (HRP) Cat. No. (ab7460, Abcam) (1:1,000) in TBS-T + 3% BSA for 1 h at room temperature. Membrane blots were developed using SuperSignal™ West Pico PLUS Chemiluminescent Substrate or SuperSignal™ West Femto Maximum Sensitivity Substrate. Signals were detected by ChemiDoc (Bio-Rad) and quantified using ImageJ software. A total of 25 μg of total cell lysates were used as input control.

Analysis of C1 and Celastrol Potential Targets in α-Syn Antigen Trafficking and Presentation Using Online Tools

The putative protein targets associated with C1 and Celastrol were predicted using SwissTargetPrediction tool (http://www.swisstargetprediction.ch). The protein–protein interaction networks of the predicted targets were generated using the STRING database (http://www.string-db.org/) (52). Potential proteins and pathways that are related to antigen processing and presentation were identified and grouped. Details of the analysis can be found in **Supplementary Figures 10–12** and **Tables S1, S2**.

Statistical Analysis

Data generated were from at least three independent experiments. Results were presented as the mean ± standard deviation (SD), unless specified. Statistical significance was calculated by the One-way ANOVA and Tukey's multiple comparisons test were used to analyze differences among treatment groups, unless specified. A probability value of $P < 0.05$ was considered statistically significant.

RESULTS

MoDCs Activation and Inflammatory Responses Towards Fibrillar α-Syn

To understand the role of DC in stimulating α-syn-specific T cell responses, we first treated MoDCs with fibrillar α-syn, and evaluated the effect of C1 and Celastrol by pre-treatment. The expression of antigen presenting MHC-I (or HLA-A,B,C) and MHC-II (or HLA-DR), co-stimulatory CD80 and CD86, and also the inflammatory cytokine gene expression were assessed. MoDCs were pre-treated with C1 or Celastrol for 1 h before being treated with fibrillar α-syn for another 4 h. Gene expression of pro-inflammatory cytokines IL-1β, IL-6, IL-23, TNF-α, and anti-inflammatory IL-10 and TGF-β were assessed by qRT-PCR. When compared to the untreated cells, α-syn had no significant induction of cytokine gene expression (**Figure 1**). However, treatment using the same α-syn on mouse microglia BV2 cells resulted in the upregulation of these cytokines (**Supplementary Figure 1**). Interestingly, a significant reduction of IL-1β, IL-6, and TNF-α gene expression and a slight upregulation of anti-inflammatory IL-10 gene expression were observed with Celastrol pre-treatment while C1 had no effects (**Figures 1A, B, D, E**). Our results suggested that α-syn had minimal effects on inflammatory cytokine gene expression in MoDCs, but this can still be modulated by Celastrol.

We next determined the surface expression of MHC-I, MHC-II, CD80, and CD86 on fibrillar α-syn-treated MoDCs. After 24 h of treatment, we found that fibrillar α-syn had no significant effect on the expression of these molecules in both cell frequencies (%) or mean fluorescence intensities (MFI) when compared to the negative control (**Figure 2** and **Supplementary Figure 2**). TNF-α treated DCs can complement antigen uptake and DC maturation (53–55). In our experiments, however, though TNF-α led to upregulation of MHC-I, MHC-II, and CD86 in all treatments, the effect of subsequent α-syn stimulation appears to be negligible (**Supplementary Figure 3**). C1 and Celastrol had no effects in this experiment. Therefore, α-syn did not result in MoDCs upregulation of

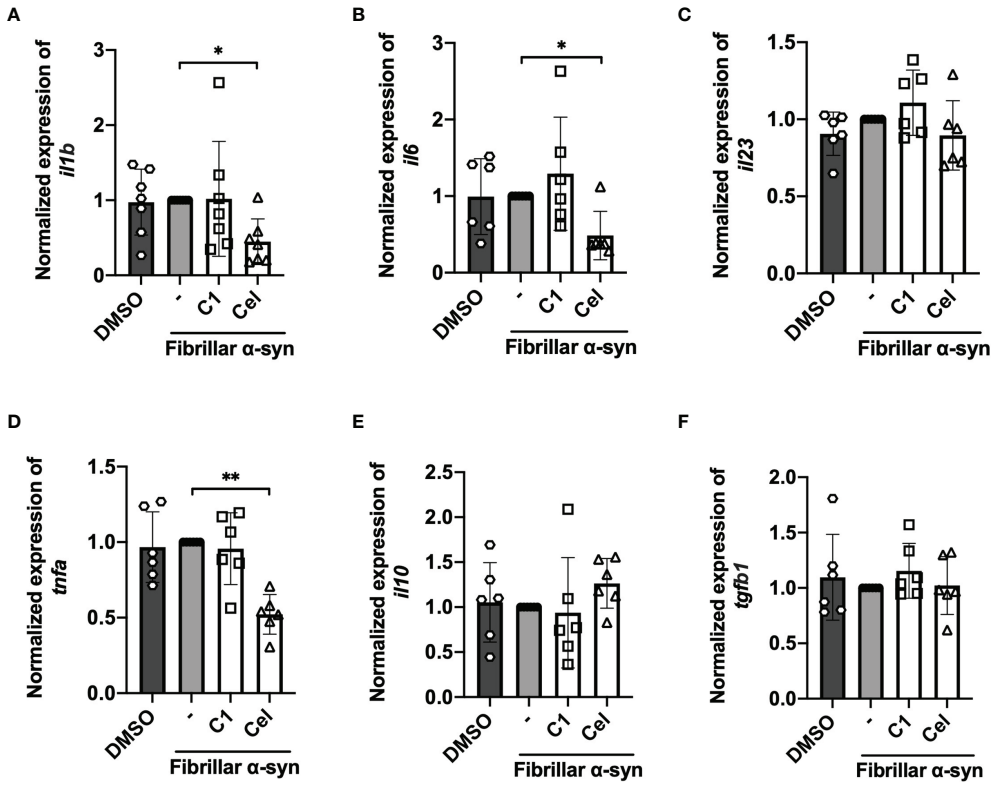

FIGURE 1 | Inflammatory cytokine gene expression of fibrillar α-syn-treated MoDCs. MoDCs were pre-treated with C1 (1 μM) or Celastrol (0.25 μM) for 1 h followed by treating with fibrillar α-syn (1 μg/ml) for 4 h. Relative qRT-PCR measured gene expression compared to GAPDH were calculated and were then normalized to α-syn only treatment. **(A)** *il1b*, **(B)** *il6*, **(C)** *il23*, **(D)** *tnfa*, **(E)** *il10*, and **(F)** *tgfb1*. Column graph data represents mean ± SD from 5 individual experiments. Statistical significance was calculated by one-way ANOVA and Tukey's multiple comparisons test, $^{*}P < 0.05$, $^{**}P < 0.01$.

antigen presentation molecules, co-stimulatory molecules, or cytokines.

α-Syn-Treated MoDC Elicited Pro-Inflammatory CD4$^+$ T Cells That is Counteracted by Celastrol

Even though α-syn-treated MoDCs had minimal responses, we next sought to examine whether these cells are capable to induce T cell responses using a co-culture model. α-syn-specific CD4$^+$ T cells were generated using a similar protocol (50, 56), then co-cultured (in a ratio of 5:1) with autologous α-syn-pulsed MoDCs with or without C1 or Celastrol pre-treatment. Flow cytometric analysis was performed to measure the abundance of T-bet$^+$IFN-γ$^+$ (Th1) on day 1, and RORγt$^+$IL-17A$^+$ (Th17) and CD25$^+$FoxP3$^+$ (Treg) cells on day 3, among CD3$^+$CD4$^+$ T cells after co-culture (**Supplementary Figure 4**). Data showed ~30% Th1 cells, ~40% Th17 cells, and ~20% Treg cells were stimulated by α-syn-pulsed MoDCs (**Figures 3A–D**). Of interest, within the Treg population stimulated by α-syn-pulsed MoDCs, ~20% of the cells co-expressed RORγt (**Figure 3F**). Celastrol pre-treatment of α-syn-pulsed MoDCs significantly reduced the frequencies of these T cell subsets, with 4-fold and 3.5-fold reduction in Th1 and Th17 cell frequencies, respectively (**Figures 3B, C**). It also improved the Th17/Treg ratio as there was a 2-fold decrease in Treg abundance (**Figures 3D, E**). In contrast, C1 pre-treatment resulted in a modest decrease in Th17 cells. We further found that Celastrol, but not C1, resulted in decreased FoxP3$^-$RORγt$^+$ and FoxP3$^+$RORγt$^+$ subpopulations while increased FoxP3$^+$RORγt$^-$ cells among CD3$^+$CD4$^+$CD25$^+$ cells (**Supplementary Figure 4B**). Therefore, although α-syn treatment of MoDCs did not trigger the upregulation of antigen presentation molecules, α-syn-specific Th1, Th17, and Treg cells were still induced. Moreover, Celastrol appears to counteract this likely through a mechanism that does not involve the classic surface expressed MHC-II and co-stimulatory molecules.

The Colocalization of α-Syn With Endo-Lysosomal Compartments is Modulated by Celastrol in MoDCs

To understand how α-syn is trafficked in MoDCs leading to CD4$^+$ T cell activation, and how Celastrol inhibited this, we next sought to examine the association of endo-lysosomal pathway proteins with α-syn in MoDCs. To this end, we tracked the colocalization of fibrillar α-syn with intracellular Rab5, Rab7, Rab9, Rab11, Rab14 proteins and lysosome marker Lamp1 at various timepoints using confocal microscopy. At 15 min, α-syn was colocalized with early endosomal marker Rab5, which implies that α-syn was likely uptaken through endocytosis by

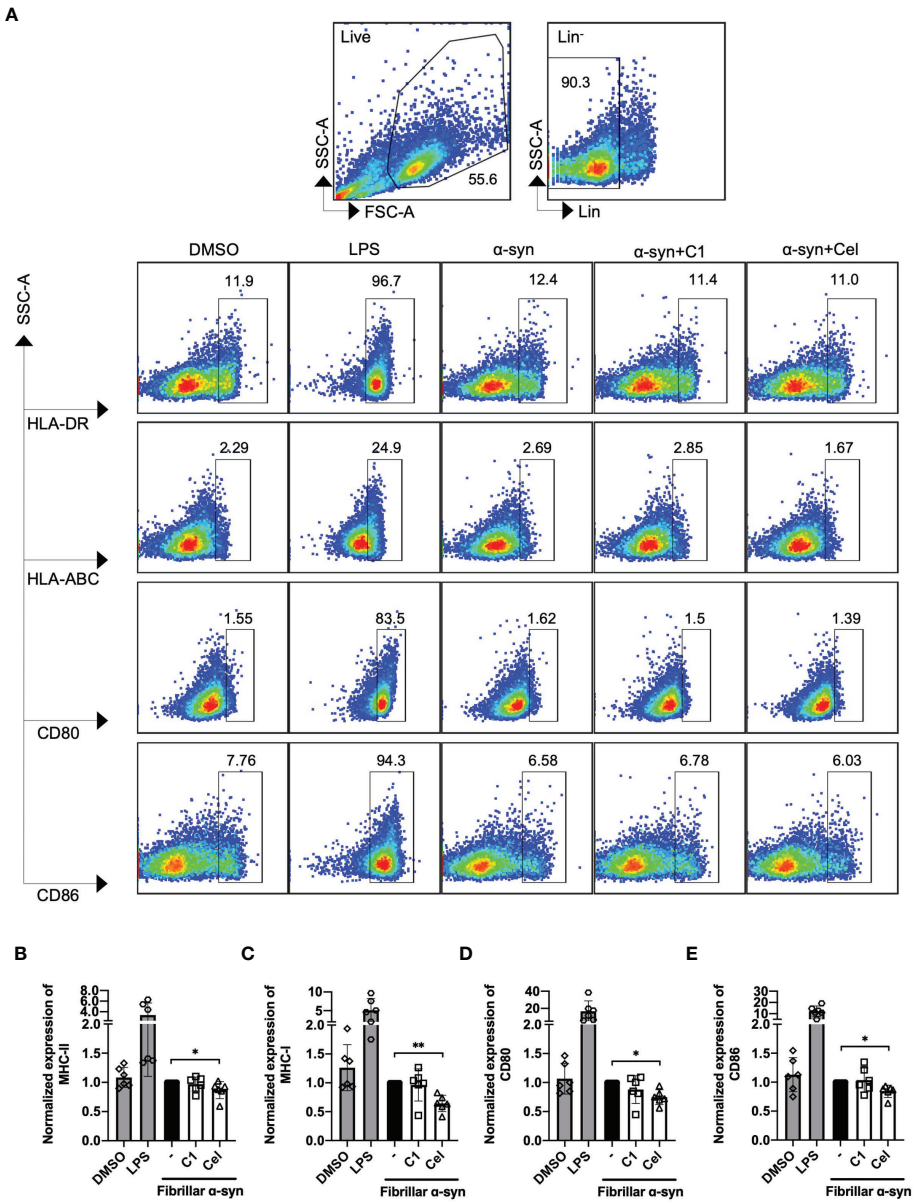

FIGURE 2 | Analysis of surface expression of MHC-I/II and co-stimulatory molecules of fibrillar α-syn-treated MoDCs. MoDCs were pre-treated with C1 (1 μM) or Celastrol (0.25 μM) for 1 h followed by treatment with fibrillar α-syn (1 μg/ml) for 24 h. Surface expression of HLA-ABC, HLA-DR, CD80, and CD86 were assessed by flow cytometry. **(A)** Gating strategy and representative dot plots of HLA-DR (MHC-II), HLA-ABC (MHC-I), and CD80, CD86 expression from 6 individual experiments are shown. Live cells were first identified followed by gating lineage$^-$ cells representing MoDCs. Cells were further gated as HLA-DR$^+$, HLA-ABC$^+$, CD80$^+$, and CD86$^+$ cells. DMSO as the negative control and LPS as the positive control. **(B–E)** Column graphs showing frequencies of positive cells normalized to α-syn only treatment. Column graph data represents mean ± SD from 6 individual experiments. Statistical significance was calculated by one-way ANOVA and Tukey's multiple comparisons test, $^*P < 0.05$, $^{**}P < 0.01$.

MoDCs (**Figure 4A**). At 30 min, trafficking to late endosomes occurred as α-syn was shown to colocalize with Rab7$^+$ vesicles (**Figure 4C**). Another 30 min later, it appeared that α-syn containing vesicles were fused with lysosomes as they were colocalized with Lamp1 or Rab9, where the latter may mediate late endosome and lysosome fusion (**Figures 4E, G**). Interestingly, Celastrol increased the colocalization of α-syn with Rab5$^+$ and Rab7$^+$ vesicles (**Figures 4B, D**), but not with Rab9$^+$ and Lamp1$^+$ vesicles (**Figures 4F, H**). Besides, we also observed increased colocalization of α-syn with Rab14$^+$ and Rab11$^+$ vesicles under Celastrol treatment (**Supplementary Figure 5**), which are mainly found on early endosomes and recycling endosomes, respectively. However, this was unlikely a consequence of increased endosome formation as Celastrol had no significant upregulation on the number of Rab5$^+$, Rab7$^+$, Rab9$^+$, Rab14$^+$, Rab11$^+$ and Lamp1$^+$ vesicles in MoDCs

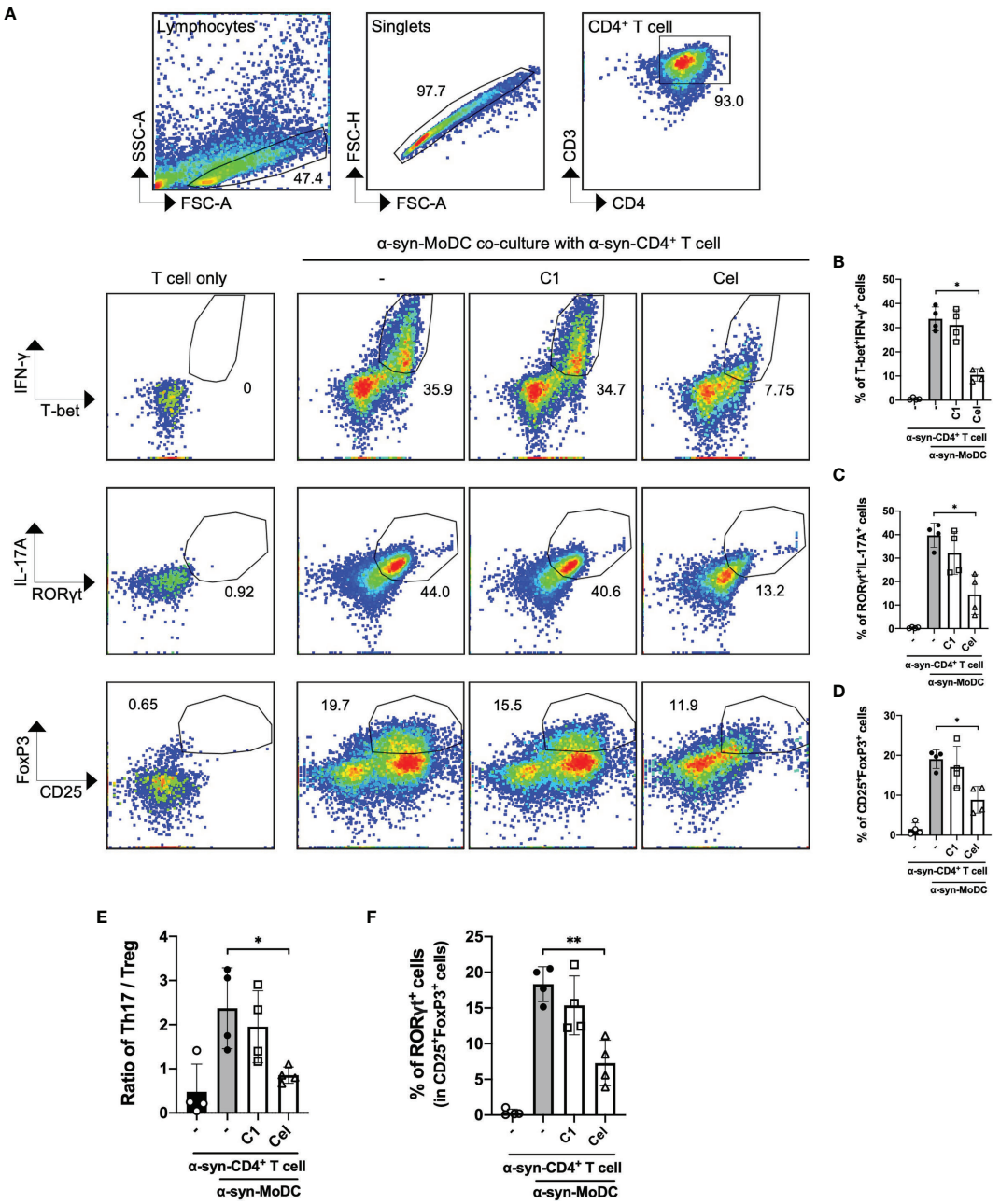

FIGURE 3 | α-Syn-specific CD4$^+$ T cell subsets stimulated by α-syn-pulsed MoDCs. α-syn specific CD4$^+$ T cells (α-syn-CD4$^+$ T cell) were co-cultured with MoDCs pre-treated with C1 (1 μM) or Celastrol (0.25 μM) for 1 h followed by α-syn treatment (α-syn-MoDC) and examined by flow cytometry. **(A)** Representative dot plots of 4 individual experiments showing frequencies of T-bet$^+$IFN-γ$^+$ (Th1), RORγt$^+$IL-17A$^+$ cells (Th17), and CD25$^+$FoxP3$^+$ (Treg) CD4$^+$ T cells. α-syn-specific CD4$^+$ T cells only served as the negative control. **(B–D)** Column graphs of flow cytometry results for the different subsets. **(E)** Ratio of Th17 to Treg in the co-culture conditions from 4 individual experiments. **(F)** Column graph showing percentage of RORγt expression in CD25$^+$FoxP3$^+$ (Treg) cells under different treatment conditions in 4 individual experiments. Column graph data represents mean ± SD from 4 individual experiments. Statistical significance was calculated by one-way ANOVA and Tukey's multiple comparisons test, $^*P < 0.05$, $^{**}P < 0.01$.

(**Supplementary Figure 6**). On the other hand, C1 had no significant effect except decreased the number of Rab9 and α-syn colocalization (**Figure 4F**). These results suggest that α-syn could enter the endo-lysosomal pathway that may then be processed and generate α-syn peptides for antigen presentation.

α-Syn is Found in Amphisomes in MoDCs

The endo-lysosomal pathway can converge with the autophagic pathway through fusion of autophagosomes with late endosomes to form amphisomes, which the engulfed proteins can be directed for degradation when fused with lysosomes (57, 58).

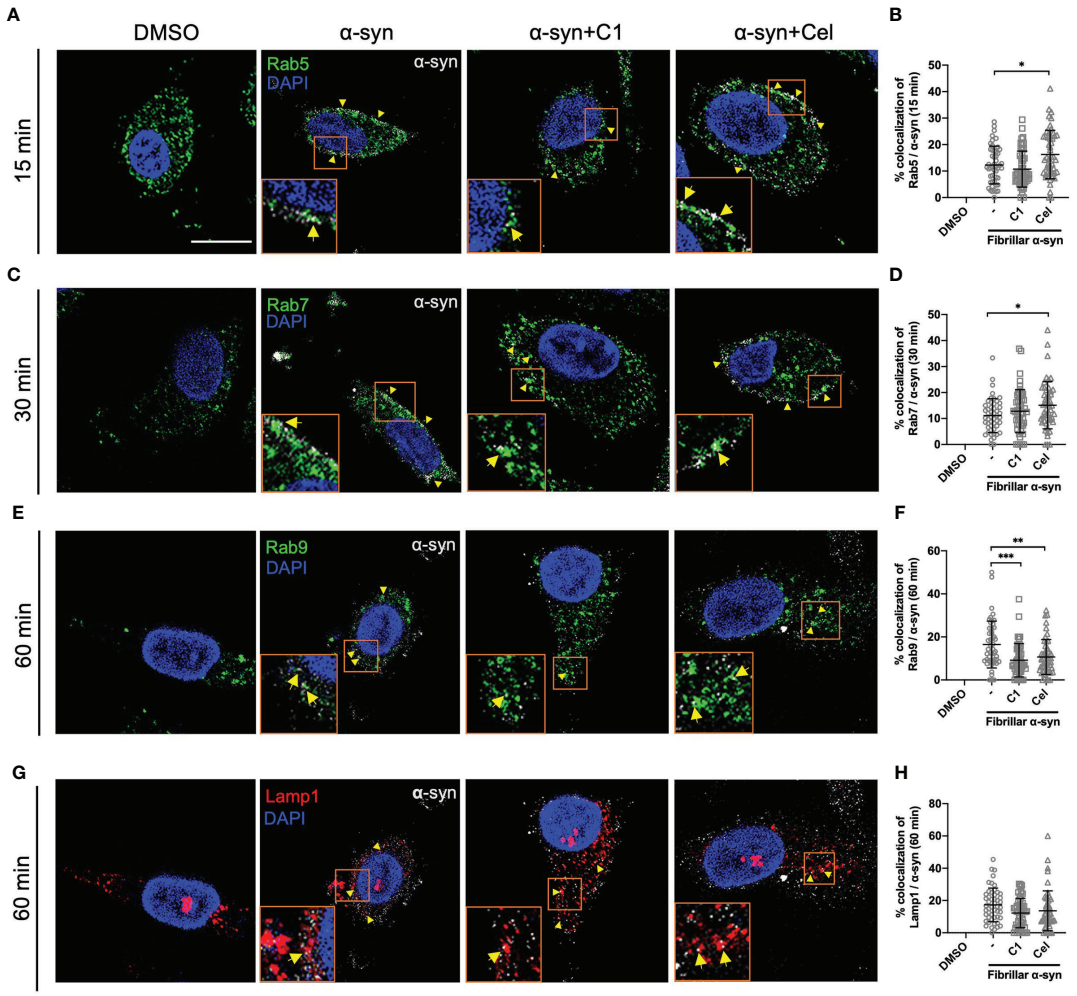

FIGURE 4 | Intracellular Rab proteins colocalization with fibrillar α-syn in MoDCs. MoDCs were pre-treated with C1 (1 μM) or Celastrol (0.25 μM) for 1 h followed by treatment with fibrillar α-syn (1 μg/ml) for 15, 30 or 60 min. Rab5, Rab7, or Rab9 (green), Lamp1 (red) and α-syn (white) were immunostained for the corresponding timepoint with DAPI (blue) and observed under the confocal microscope. Representative images showing colocalization (yellow arrows) of Rab proteins with α-syn under different treatments and dot plots showing the percentage of colocalization. **(A, B)** Colocalization of Rab5 and α-syn at 15 min post α-syn treatment, **(C, D)** colocalization of Rab7 and α-syn at 30 min post α-syn treatment, **(E, F)** colocalization of Rab9 and α-syn at 60 min post α-syn treatment, and **(G, H)** colocalization of Lamp1 and α-syn at 60 min post α-syn treatment. Images are representative of 50 individual cells. Scale bar: 10 μm. Each dot in the dot plots represents data of a cell and the mean ± SD of 50 individual cells is indicated. Statistical significance was calculated by one-way ANOVA and Tukey's multiple comparisons test, $^{*}P < 0.05$, $^{**}P < 0.01$, $^{***}P < 0.001$.

Rab5 can be involved in autophagosome formation and, conversely, Beclin1 is also associated with Rab5-mediated endosomal trafficking (59, 60). Thus, we next tested whether fibrillar α-syn is also trafficked to autophagic and amphisomal components in MoDCs. MoDCs were treated with fibrillar α-syn for 4 h or 16 h and assessed for colocalization of autophagy-related Beclin1 and LC3 with α-syn, and their association with Rab5 and Rab7 proteins, respectively. Expectedly, Beclin1 or LC3 were found colocalized with α-syn (**Figures 5A, C, E, G**). Rab5 or Rab7 were also found colocalized in these puncta, indicating the formation of amphisomes (**Figures 5A, D, E, H** and **Supplementary Figure 7**). These data suggest that apart from the endo-lysosomal pathway, autophagic pathway is also associated with the trafficking of α-syn in MoDCs, where the formation of $LC3^{+}Rab7^{+}$ amphisomes occurred, indicating the convergence of the two pathways. Moreover, Celastrol, but not C1, markedly increased the number of Rab5/Beclin1/α-syn and Rab7/LC3/α-syn puncta (**Figures 5D, H**), and also the autophagic $Beclin1^{+}$ and $LC3^{+}$ puncta (**Supplementary Figures 8B, E**). Also, Rab7/LC3 amphisomes were increased by 2.2-fold under Celastrol treatment, suggesting that Celastrol can induce both the autophagic and amphisomal vesicles interaction with α-syn (**Supplementary Figure 8F**). To confirm the confocal microscopy data, western blot analysis was performed on MoDCs at 4 and 16 h post α-syn treatment. Beclin1 protein level was found to be downregulated following α-syn treatment compared to control but appears to be rescued by Celastrol treatment (**Figures 6A, B**). Similarly, while the protein level of

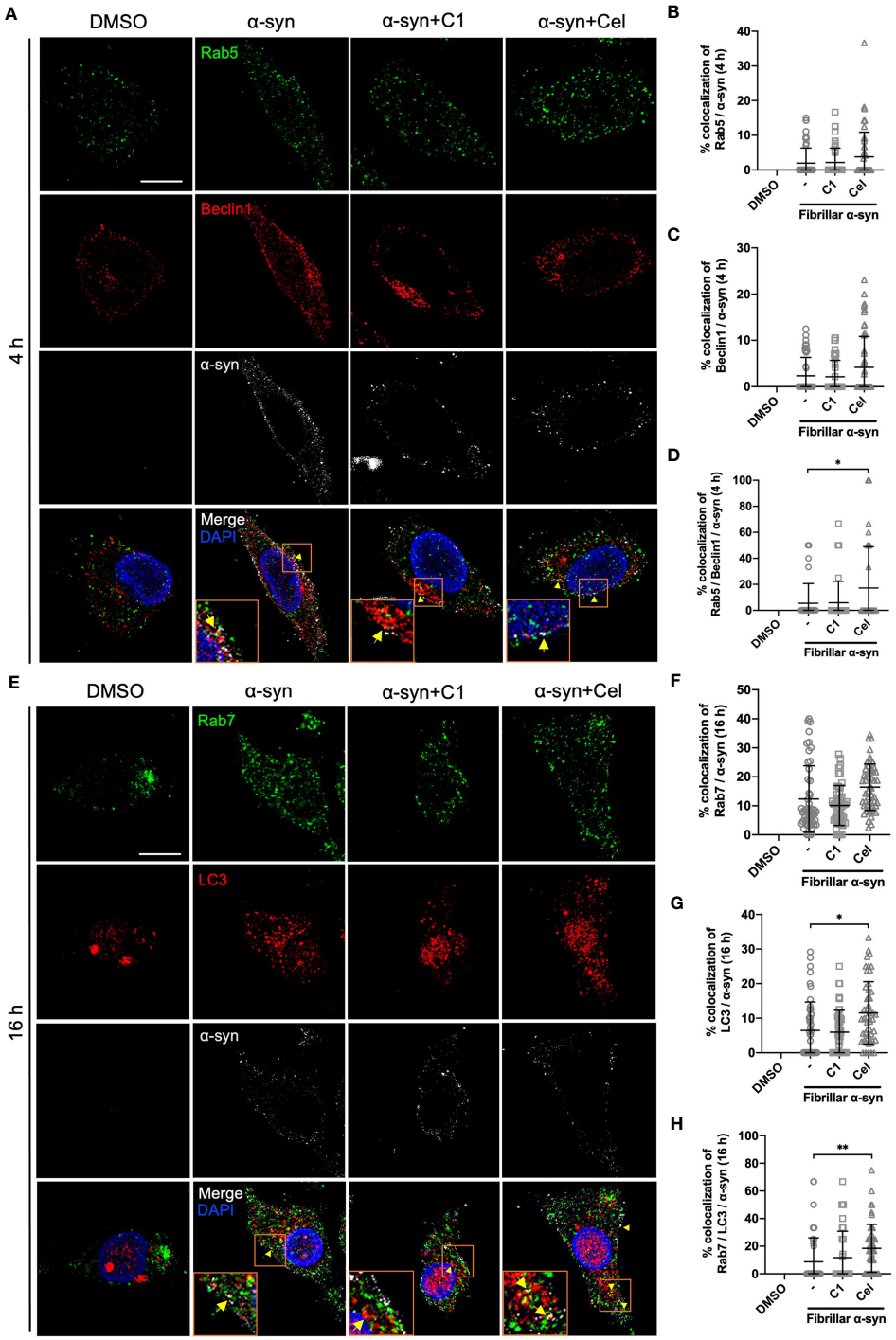

FIGURE 5 | Colocalization of Rab proteins and autophagosome markers with fibrillar α-syn in MoDCs. MoDCs were pre-treated with C1 (1 μM) or Celastrol (0.25 μM) for 1 h followed by treatment with fibrillar α-syn (1 μg/ml) for 4 h or 16 h. Different Rab proteins (green) and autophagosome proteins (red) were immunostained for the corresponding timepoint along with α-syn (white) and DAPI (blue) and observed under the confocal microscope. **(A)** Representative images showing individual staining and merged images showing colocalization (yellow arrows) of Rab5 (green) and Beclin1 (red) with α-syn at 4 h post α-syn treatment. Scale bar: 10 μm. Dot plots showing the percentage of colocalization between **(B)** Rab5 and α-syn, **(C)** Beclin1 and α-syn and **(D)** Rab5, Beclin1 and α-syn. **(E)** Representative images showing individual staining and merged images showing colocalization (yellow arrows) of Rab7 (green) and LC3 (red) with α-syn at 16 h post α-syn treatment. Scale bar: 10 μm. Dot plots showing the percentage of colocalization between **(F)** Rab7 and α-syn, **(G)** LC3 and α-syn and **(H)** Rab7, LC3 and α-syn. Images are representative of 50 individual cells. Each dot in the dot plots represents data of a cell and the mean ± SD of 50 individual cells is indicated. Statistical significance was calculated by one-way ANOVA and Tukey's multiple comparisons test, $^{*}P < 0.05$, $^{**}P < 0.01$.

LC3-I or LC3-II had no significant change after α-syn treatment, Celastrol increased the LC3-II : LC3-I conversion ratio (**Figures 6E, F**). Furthermore, we tested the expression of p62 in α-syn treated MoDCs, where its decreased expression indicates autophagy flux. We found that α-syn treatment upregulated p62 expression which was counteracted by Celastrol (**Supplementary Figures 9C, D**). Moreover, an increased p62 colocalization with α-syn in Celastrol pre-treated MoDCs was observed (**Supplementary Figures 9A, B**). These data largely supported the notion that fibrillar α-syn can be encapsulated in autophagic components which likely allowed the processing of α-syn through autophagy. However, this happens to a lesser extent in MoDCs but can be alleviated by Celastrol. Lastly, the level of active GTP forms of Rab5 and Rab7 were upregulated by Celastrol pre-treatment (**Figures 6G–J**), in corroboration with the above data. Together, Celastrol not only induced autophagy by upregulating Beclin1 expression, reducing p62 expression and increasing LC3 conversion, but it can also trigger the amphisomal pathway with increased functional Rab5 and Rab7 proteins to interact with autophagic components for trafficking of α-syn towards the lysosomal-mediated processing.

DISCUSSION

Neuroinflammation aroused by peripheral immune cells in response to abnormal α-syn has been highlighted in the progression of PD (30, 61). In particular, the involvement of DCs in mediating α-syn-specific T cells that causes detrimental effects to dopaminergic neurons has been reported with elevated pro-inflammatory Th1 and Th17 subsets in PD patients (12, 16, 62). However, the underlying mechanism that triggers these DC-T responses remains poorly understood. Herein, we demonstrated that fibrillar α-syn were trafficked to both endo-lysosomal and autophagic pathways in MoDCs, suggesting the use of these pathways for lysosomal processing of α-syn. However, these processes were altered by the fibrillar α-syn protein aggregate itself such as the suppression of autophagic pathways, but the endo-lysosomal pathway still resulted in α-syn peptides that may be used for antigen presentation for the activation of Th1 and Th17 cells. In parallel, we also tested the effectiveness of two TCM compounds (C1 and Celastrol) that may modulate this mechanism. While C1 and Celastrol can promote autophagy (45–47), and the latter can suppress inflammatory response (48), nevertheless, we found that only Celastrol promoted the colocalization of fibrillar α-syn with endo-lysosomal, amphisomal and autophagic markers in MoDCs. The likelihood of these events lies in Celastrol being able to promote the complete degradation of α-syn, which leads to decreased antigenic peptides available for antigen presentation, and thereby reduced the T cell responses. Overall, this study provided insights into an antigen trafficking-related immune mechanism in regulating pro-inflammatory α-syn-specific T cells for potential therapeutic intervention against PD.

While most studies of T cell polarization in the brain focused on the roles of microglia and astrocytes (63, 64), here, we demonstrated the ability of peripheral MoDCs in triggering pro-inflammatory α-syn-specific $CD4^+$ T cell differentiation in the co-culture experiments. A significant proportion of Th1 and Th17 cells was found compared to Treg cells (**Figure 3**). A shift of pro-inflammatory Th1 and Th17 cell subsets in PD patients had also been reported (16, 65), which likely contributed to the development of neuroinflammation through secreting pro-inflammatory cytokines IFN-γ and IL-17A that are elevated in the serum of PD patients (17). These cytokines could lead to neuronal cell death (24, 66), activate neurotoxic M1-like microglia and astrocytes (67), promote macrophages and B cells infiltration into the brain (68), and also inhibit Treg function in neuronal repair and suppression of pro-inflammatory T cells cytotoxicity towards dopaminergic neurons (69–71). Therefore, the balance of the pro-inflammatory and regulatory T cell subsets is important to prevent the progression of PD, where intervention on DC response to α-syn may shed light.

To date, whether fibrillar α-syn could induce APC activation remains controversial. Some studies reported an upregulation of MHC and co-stimulatory molecules in α-syn treated DCs, while others found no differences (or even a decrease) in α-syn processing and presentation in patient-derived DCs compared to healthy control (31, 32, 72, 73). In our results, fibrillar α-syn did not upregulate MHC-II and co-stimulatory molecules expression on MoDCs or cytokine production (**Figures 1**, **2**). Indeed, oligomeric β-amyloid in Alzheimer's Disease (AD) was also reported to have no effect on MHC-II expression on brain-derived or bone marrow-derived DCs (74), or even a reduction in the abundance of $MHC\text{-}II^{hi}$ DCs in mice (75). Taken together with our data, brain self-proteins appear to have a minimal upregulation effect on DC antigen presenting capacity, which may allow the escape of immune surveillance of α-syn and β-amyloid associated with T cells leading to detrimental protein aggregation (74, 76). In our experiments, however, α-syn-pulsed MoDCs could still trigger α-syn-specific T cell responses that may drive neuroinflammation in PD. Whether they have any effects on α-syn-expressing neurons remains to be investigated. Moreover, the presentation to and induction of the α-syn-specific T cells could be attributed to mechanisms besides DC-T immunological synapse formation. One possibility could be related to exosomes derived from APC. The role of exosomes in initiating inflammatory T cells has been reported with α-syn-activated microglia (77), and exosomes derived from MoDCs express surface MHC-I/II and co-stimulatory molecules that can activate antigen-specific $CD4^+$ T cells (78–80). One report demonstrated DC-derived exosomes could stimulate antigen-specific $CD4^+$ T cells in the presence of MHC-II-deficient DCs in mice (81), which may be one possible scenario in our experimental co-culture of α-syn-pulsed MoDCs and the α-syn-specific $CD4^+$ T cell responses. Although we did not address the involvement of exosomes directly, we did observe the interaction between the recycling endosomal marker Rab11 and α-syn, where Rab11 has been reported to facilitate

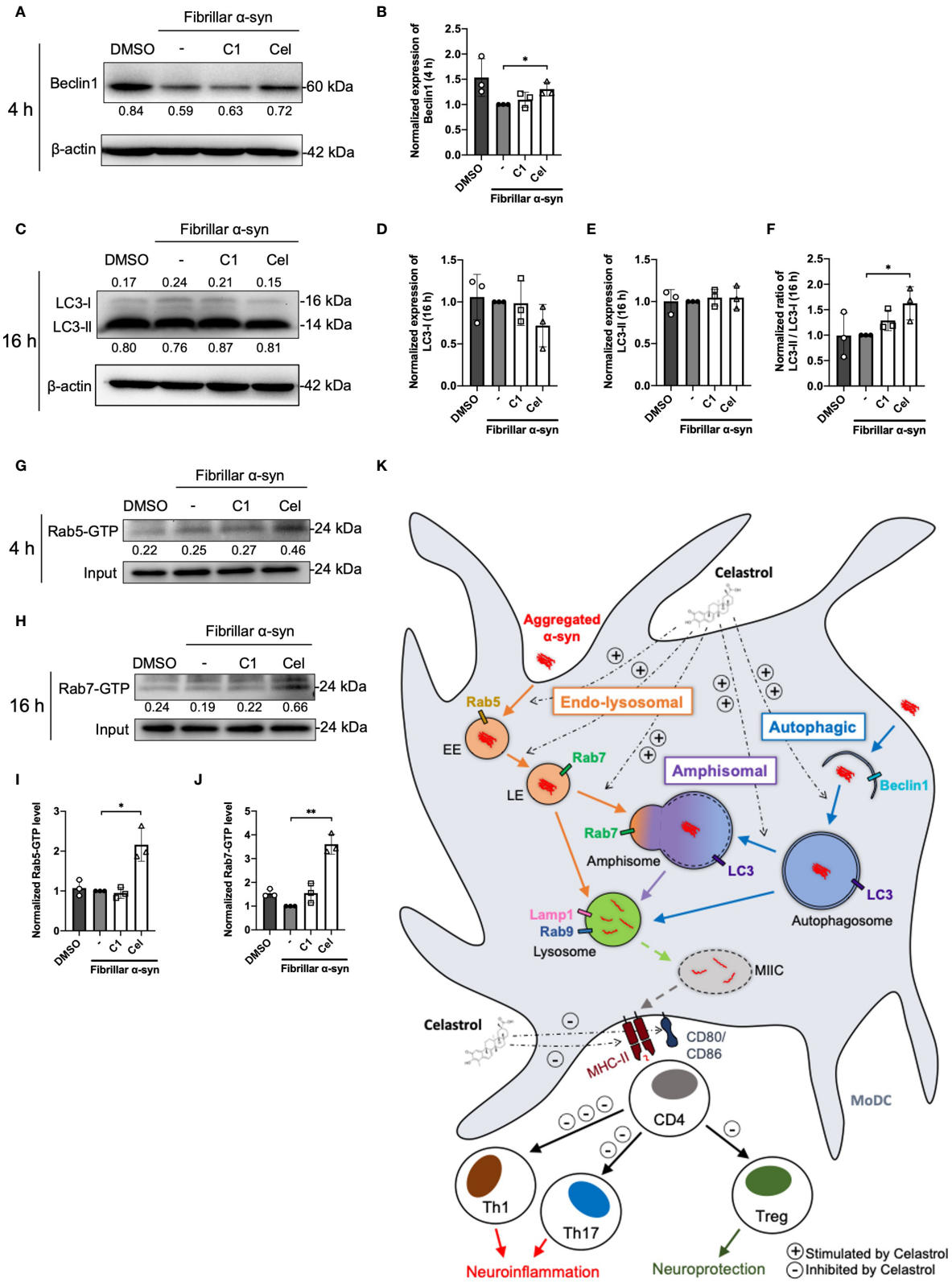

FIGURE 6 | Continued

FIGURE 6 | Autophagosome markers and Rab-GTP protein expression level in α-syn treated MoDCs. **(A)** The expression of Beclin1 in drug pre-treated MoDCs was determined by Western Blot at 4 h post α-syn treatment. Relative expressions of Beclin1 to β-actin were quantified by ImageJ and indicated on the blots, which were further normalized to α-syn only treatment shown in **(B)**. Column graph data represents mean ± SD from 3 individual experiments. **(C)** The expressions of LC3-I and LC3-II in drug pre-treated MoDCs were determined by Western Blot at 16 h post α-syn treatment. Relative expressions of LC3-I or LC3-II to β-actin were quantified using ImageJ and indicated on the blots, which were further normalized to α-syn only treatment shown in **(D, E)**. **(F)** The ratio of LC3-II to LC3-I in each treatment was calculated and further normalized to α-syn only treatment. Column graph data represents mean ± SD from 3 individual experiments. **(G)** Active Rab5-GTP **(H)** and Rab7-GTP were immunoprecipitated and their relative expressions towards whole cell lysate input control were quantified by ImageJ and indicated on blots, which were further normalized to α-syn only treatment shown in **(I, J)**. Column graph data represents mean ± SD from 3 individual experiments. Statistical significance was calculated by one-way ANOVA and Tukey's multiple comparisons test, $^{*}P < 0.05$, $^{**}P < 0.01$. **(K)** Schematic diagram of α-syn aggregates trafficking in MoDCs underlying antigen presentation and $CD4^+$ T cell activation. Following uptake, α-syn interacts with components of three antigen trafficking and processing pathways: 1) Endo-lysosomal pathway (orange) beginning from $Rab5^+$ early endosome (EE) to $Rab7^+$ late endosome (LE) and to $Rab9^+$/$Lamp1^+$ lysosome degradation; 2) autophagic pathway (blue) starting from autophagosome formation ($Beclin1^+$) enclosing aggregated α-syn, matured with LC3 and then to $Rab9^+$/$Lamp1^+$ lysosome degradation; 3) amphisomal pathway (purple) involves the fusion of $Rab7^+$ LE from the endo-lysosomal pathway with $LC3^+$ autophagosome from the autophagic pathway, which may also be regulated by the formation of $Rab5^+$/$Beclin1^+$ vesicles, and consequently fuse with $Rab9^+$/$Lamp1^+$ lysosomes. These three pathways could possibly allow the processing of the encapsulated α-syn by lysosomes and provide α-syn antigen peptides at different extent for MHC-II presentation to $CD4^+$ T cells and trigger differentiation into Th1, Th17 and Treg subsets that may contribute to either neuroinflammation or neuroprotection. Celastrol promotes the colocalization of α-syn with $Rab5^+$ EE and $Rab7^+$ LE in the endo-lysosomal pathway, with autophagosome in the autophagic pathway, and the formation of amphisome containing α-syn in the amphisomal pathway. The increased α-syn interaction with components from degradation pathways likely favored the processing of α-syn and reduced α-syn peptides presentation to $CD4^+$ T cell and decreased the frequencies of Th1, Th17 and Treg subsets.

exosome formation (82). Further investigation on exosomes derived from α-syn-pulsed MoDCs may explain how they trigger α-syn-specific T cell activation and differentiation during PD.

Endo-lysosomal or autophagic pathway for degradation of antigen and loading onto MHC-II are important in regulating efficient antigen presentation to $CD4^+$ T cells (41, 83, 84). It remains poorly understood how α-syn peptides are generated for MHC-II antigen presentation, especially in DCs. Our data showed that both endo-lysosomal and autophagic components are associated with fibrillar α-syn in MoDCs (**Figures 4**, **5**), indicating the intracellular trafficking of α-syn into these pathways. α-syn were initially found enclosed in early $Rab5^+$ endosomes, which were then trafficked to late $Rab7^+$ endosomes (**Figures 4A–D**), in which Rab5 to Rab7 conversion was reported to be important for effective antigen degradation and presentation (85). Lastly, fusion of α-syn containing vesicles with $Lamp1^+$ lysosomes occurred which could be an indication of lysosomal degradation of α-syn (**Figures 4G, H**), and is regulated by Rab9 (**Figures 4E–H**). This likely generated α-syn peptides that may be transported to the MHC-II compartment (MIIC) where loading of α-syn peptides onto the MHC-II for presentation to $CD4^+$ T cells takes place (86–88). On the other hand, trafficking of fibrillar α-syn into autophagic pathway was also observed. α-Syn were found colocalized with Beclin1 and later with LC3 in MoDCs (**Figure 5**). Moreover, these two pathways can also converge to initiate the formation of amphisome, which is the fusion of early/late endosome with autophagosome where the content will be degraded by lysosomes (89, 90). Indeed, besides autophagy, this alternative pathway has been reported for cargo degradation and MHC-II presentation in processing bacterial and tumor antigens in B cells and DCs (87, 88, 91, 92). We observed the presence of Rab5/Beclin1/α-syn and Rab7/LC3/α-syn puncta which indicates that fibrillar α-syn can also be found in amphisomes in MoDCs (**Figure 5** and **Supplementary Figure 7**). In short, our data provide evidence that intracellular trafficking of α-syn can be associated with three pathways in MoDCs: endo-lysosomal pathway, autophagic pathway and amphisomal pathway for lysosomal-mediated degradation. However, the efficiency of these pathways in degrading α-syn appeared to be modulated by α-syn. Previous studies reported that limited antigen degradation capacity favors the generation of MHC-II peptides which can be counteracted by increased autophagy (41, 93, 94). The pathway and the association of the fibrillar α-syn processing that is the most important for MoDCs in antigen presentation to stimulate pro-inflammatory or regulatory α-syn-specific $CD4^+$ T cell responses in PD remains to be investigated.

In the attempt to uncover potential TCM against PD and the effect on the underlying immune mechanisms, we investigated whether *Curcumin* analog C1 or TWHF-derived Celastrol can modulate α-syn interaction with Rab and autophagy-related proteins that may underly the activation of α-syn-specific T cells by MoDCs. C1 is an activator of TFEB, which is an important inducer of autophagy (45); but it failed to promote the interaction of endosomes, amphisomes and autophagosomes with fibrillar α-syn in MoDCs (**Figures 4**, **5**), and only resulted in a slight reduction of Th1 and Th17 frequencies (**Figure 3**). In contrast, Celastrol demonstrated immune-modulating effects throughout our experiments. First, it limited T cell activation by reducing cytokine gene transcription capacity of MoDCs and decreasing MHC-II and co-stimulatory molecules expression (**Figures 1**, **2**). Second, it enhanced fibrillar α-syn colocalization with Rab5 early endosomes and Rab7 late endosomes (**Figure 4**). Third, it promoted autophagic pathways with increased Beclin1 protein level, and enhanced LC3-I to LC3-II conversion which indicate autophagosome maturation and possibly promoted autophagosome degradation indicated from the decreased p62 expression. It also increased colocalization between α-syn and $p62^+$ vesicles or $LC3^+$ autophagosomes, enhanced Rab protein activities and their colocalizations with autophagosomes and α-syn for amphisomes (**Figures 5**, **6** and **Supplementary Figures 7–9**). Taken together, these events possibly aided the trafficking of α-syn for degradation by lysosomes and likely resulted in excessive α-syn processing (or complete degradation) that led to the unavailability

of antigenic peptides to be loaded onto MHC-II (95). Thereby, brought about a significant reduction of pro-inflammatory T cell subsets and Th17/Treg ratio (**Figure 3**). Therefore, apart from being an autophagy inducer for the degradation of aggregated α-syn, Celastrol showed its anti-inflammatory function in regulating MoDC-T cell responses in PD. Besides PD, studies have shown the anti-inflammatory role of Celastrol in other autoimmune diseases. For instance, it can regulate NF-κB and provides neuroprotection by suppressing pro-inflammatory cytokines TNF-α and IL-1β in AD brain, downregulate IL-6 and IL-17 expression in rheumatoid arthritis mice model, or suppress microgliosis and inflammatory cytokine production in the optic nerve of experimental autoimmune encephalomyelitis model (48, 96–98). However, whether Celastrol can dampen autoreactive inflammatory DC-T cell inflammatory responses in these diseases remain to be investigated. Altogether, Celastrol can downmodulate α-syn-specific T cell responses due to the enhancement of autophagic and amphisomal pathways.

The specific targets for Celastrol to mediate these pathways remain elusive. Thus, we used the SwissTargetPrediction tool and the STRING database to identify putative targets (**Supplementary Figures 11, 12**). Some possibilities for Celastrol include proteins involved in arachidonic acid (AA) inflammatory pathways (e.g., PLA2G4A), where AA is elevated in PD mice model and also associated with Rab5 endocytosis and antigen presentation (99–102). The function of PLA2G4A is to catalyze the release of AA and it is found expressed in DCs, where induced expression can lead to inflammatory T cell responses (103, 104). Others also found its role in autophagy flux and neuronal loss post brain trauma (105). Another potential target, PTPN11, is involved in the MAPK-signaling pathway, and this protein was reported to be crucial for the induction of DC-mediated Th17 activities in anti-fungal responses (106). Androgen receptor (AR) is a known target of Celastrol to induce autophagy in cancers (107), but its role in PD is not understood. However, AR can be destabilized by Celastrol and result in the regulation of peripheral T cell proliferation and Th1 differentiation to inhibit autoimmune diseases (108, 109). On the other hand, the targets of Celastrol are not associated with C1, where the potential protein targets appear to be more diverse in functions (**Supplementary Figure 12**). Only cathepsin (CTS) is involved in α-syn degradation (110) (**Supplementary Figures 10, 12**). Altogether, the putative targets of Celastrol are more specific in regulating inflammatory T cell responses, where an explanation of its effect in our DC-T cell co-culture experiments lies within. Overall, this study provided additional understanding of Celastrol to be used as a treatment for PD in the reduction of DC-mediated pro-inflammatory T cells against α-syn.

DATA AVAILABILITY STATEMENT

The raw data supporting the conclusions of this article will be made available by the authors, without undue reservation.

ETHICS STATEMENT

The studies involving human participants were reviewed and approved by the Hong Kong Baptist University Research Ethics Committee (#REC/19-20/0110). Written informed consent for participation was not required for this study in accordance with the national legislation and the institutional requirements.

AUTHOR CONTRIBUTIONS

LN and AC designed and performed the experiments, analyzed the data, and wrote the manuscript. XW conducted the BV2 experiments. CY, CS and ML provided reagents and critical comments. CY, ML and AC supervised the study. All authors listed have made a substantial, direct, and intellectual contribution to the work and approved it for publication.

FUNDING

This study was supported by the Health and Medical Research Fund (HMRF) (18170032), the Interdisciplinary Research Matching Scheme (RC-IRCs-1718-03), the Faculty Research Grant (FRG2/17–18/066), the Faculty Start-up Fund (SCI-17-18-01), the Tier 2 Start-up Grant (RC-SGT2/18–19/SCI/007), and the Research Council Start-up Grant of Hong Kong Baptist University (to AC). This study was also partly supported by HMRF17182541, HMRF17182551, GRF/HKBU12100618 from the Hong Kong Government, the National Natural Science Foundation of China (81703487, and 81773926), and the Shenzhen Science and Technology Innovation Commission (JCYJ20180302174028790, JCYJ20180507184656626) (to ML).

SUPPLEMENTARY MATERIAL

The Supplementary Material for this article can be found online at: https://www.frontiersin.org/articles/10.3389/fimmu.2022.833515/full#supplementary-material

REFERENCES

1. Hirsch L, Jette N, Frolkis A, Steeves T, Pringsheim T. The Incidence of Parkinson's Disease: A Systematic Review and Meta-Analysis. *Neuroepidemiology* (2016) 46(4):292–300. doi: 10.1159/000445751
2. Michel PP, Hirsch EC, Hunot S. Understanding Dopaminergic Cell Death Pathways in Parkinson Disease. *Neuron* (2016) 90(4):675–91. doi: 10.1016/j.neuron.2016.03.038
3. Kahle PJ, Neumann M, Ozmen L, Haass C. Physiology and Pathophysiology of Alpha-Synuclein. Cell Culture and Transgenic Animal Models Based on a Parkinson's Disease-Associated Protein. *Ann N Y Acad Sci* (2000) 920:33–41. doi: 10.1111/j.1749-6632.2000.tb06902.x
4. Burré J, Sharma M, Tsetsenis T, Buchman V, Etherton MR, Südhof TC. Alpha-Synuclein Promotes SNARE-Complex Assembly In Vivo and *In Vitro*. *Science* (2010) 329(5999):1663–7. doi: 10.1126/science.1195227

5. Ball N, Teo WP, Chandra S, Chapman J. Parkinson's Disease and the Environment. *Front Neurol* (2019) 10:218. doi: 10.3389/fneur.2019.00218
6. Maries E, Dass B, Collier TJ, Kordower JH, Steece-Collier K. The Role of Alpha-Synuclein in Parkinson's Disease: Insights From Animal Models. *Nat Rev Neurosci* (2003) 4(9):727–38. doi: 10.1038/nrn1199
7. Petrucelli L, O'Farrell C, Lockhart PJ, Baptista M, Kehoe K, Vink L, et al. Parkin Protects Against the Toxicity Associated With Mutant Alpha-Synuclein: Proteasome Dysfunction Selectively Affects Catecholaminergic Neurons. *Neuron* (2002) 36(6):1007–19. doi: 10.1016/s0896-6273(02)01125-x
8. Bousset L, Pieri L, Ruiz-Arlandis G, Gath J, Jensen PH, Habenstein B, et al. Structural and Functional Characterization of Two Alpha-Synuclein Strains. *Nat Commun* (2013) 4:2575. doi: 10.1038/ncomms3575
9. Yacoubian TA, Standaert DG. Reaping What You Sow: Cross-Seeding Between Aggregation-Prone Proteins in Neurodegeneration. *Mov Disord* (2014) 29(3):306. doi: 10.1002/mds.25766
10. Cebrián C, Loike JD, Sulzer D. Neuroinflammation in Parkinson's Disease Animal Models: A Cell Stress Response or a Step in Neurodegeneration? *Curr Top Behav Neurosci* (2015) 22:237–70. doi: 10.1007/7854_2014_356
11. Li Q, Barres BA. Microglia and Macrophages in Brain Homeostasis and Disease. *Nat Rev Immunol* (2018) 18(4):225–42. doi: 10.1038/nri.2017.125
12. Brochard V, Combadière B, Prigent A, Laouar Y, Perrin A, Beray-Berthat V, et al. Infiltration of CD4+ Lymphocytes Into the Brain Contributes to Neurodegeneration in a Mouse Model of Parkinson Disease. *J Clin Invest* (2009) 119(1):182–92. doi: 10.1172/jci36470
13. Hatterer E, Touret M, Belin M-F, Honnorat J, Nataf S. Cerebrospinal Fluid Dendritic Cells Infiltrate the Brain Parenchyma and Target the Cervical Lymph Nodes Under Neuroinflammatory Conditions. *PloS One* (2008) 3 (10):e3321. doi: 10.1371/journal.pone.0003321
14. Louveau A, Harris TH, Kipnis J. Revisiting the Mechanisms of CNS Immune Privilege. *Trends Immunol* (2015) 36(10):569–77. doi: 10.1016/j.it.2015.08.006
15. Stevens CH, Rowe D, Morel-Kopp MC, Orr C, Russell T, Ranola M, et al. Reduced T Helper and B Lymphocytes in Parkinson's Disease. *J Neuroimmunol* (2012) 252(1-2):95–9. doi: 10.1016/j.jneuroim.2012.07.015
16. Kustrimovic N, Comi C, Magistrelli L, Rasini E, Legnaro M, Bombelli R, et al. Parkinson's Disease Patients Have a Complex Phenotypic and Functional Th1 Bias: Cross-Sectional Studies of CD4+ Th1/Th2/T17 and Treg in Drug-Naïve and Drug-Treated Patients. *J Neuroinflamm* (2018) 15 (1):205. doi: 10.1186/s12974-018-1248-8
17. Yang F, Li B, Li L, Zhang H. The Clinical Significance of the Imbalance of Th 17 and Treg Cells and Their Related Cytokines in Peripheral Blood of Parkinson's Disease Patients. *Int J Clin Exp Med* (2016) 9(9):17946–51.
18. Huang Y, Liu Z, Cao B-B, Qiu Y-H, Peng Y-P. Treg Cells Attenuate Neuroinflammation and Protect Neurons in a Mouse Model of Parkinson's Disease. *J Neuroimmune Pharmacol* (2020) 15(2):224–37. doi: 10.1007/s11481-019-09888-5
19. Revu S, Wu J, Henkel M, Rittenhouse N, Menk A, Delgoffe GM, et al. IL-23 and IL-1β Drive Human Th17 Cell Differentiation and Metabolic Reprogramming in Absence of CD28 Costimulation. *Cell Rep* (2018) 22 (10):2642–53. doi: 10.1016/j.celrep.2018.02.044
20. Storelli E, Cassina N, Rasini E, Marino F, Cosentino M. Do Th17 Lymphocytes and IL-17 Contribute to Parkinson's Disease? A Systematic Review of Available Evidence. *Front Neurol* (2019) 10:13(13). doi: 10.3389/fneur.2019.00013
21. Zúñiga LA, Jain R, Haines C, Cua DJ. Th17 Cell Development: From the Cradle to the Grave. *Immunol Rev* (2013) 252(1):78–88. doi: 10.1111/imr.12036
22. Lindestam Arlehamn CS, Dhanwani R, Pham J, Kuan R, Frazier A, Rezende Dutra J, et al. α-Synuclein-Specific T Cell Reactivity Is Associated With Preclinical and Early Parkinson's Disease. *Nat Commun* (2020) 11(1):1875. doi: 10.1038/s41467-020-15626-w
23. Sulzer D, Alcalay RN, Garretti F, Cote L, Kanter E, Agin-Liebes J, et al. T Cells From Patients With Parkinson's Disease Recognize α-Synuclein Peptides. *Nature* (2017) 546(7660):656–61. doi: 10.1038/nature22815
24. Sommer A, Marxreiter F, Krach F, Fadler T, Grosch J, Maroni M, et al. Th17 Lymphocytes Induce Neuronal Cell Death in a Human iPSC-Based Model of Parkinson's Disease. *Cell Stem Cell* (2018) 23(1):123–31.e126. doi: 10.1016/j.stem.2018.06.015
25. Kapsenberg ML. Dendritic-Cell Control of Pathogen-Driven T-Cell Polarization. *Nat Rev Immunol* (2003) 3(12):984–93. doi: 10.1038/nri1246
26. Sprent J. Antigen-Presenting Cells. Professionals and Amateurs. *Curr Biol* (1995) 5(10):1095–7. doi: 10.1016/s0960-9822(95)00219-3
27. Benkler M, Agmon-Levin N, Shoenfeld Y. Parkinson's Disease, Autoimmunity, and Olfaction. *Int J Neurosci* (2009) 119(12):2133–43. doi: 10.3109/00207450903178786
28. Ludewig P, Gallizioli M, Urra X, Behr S, Brait VH, Gelderblom M, et al. Dendritic Cells in Brain Diseases. *Biochim Biophys Acta* (2016) 1862(3):352–67. doi: 10.1016/j.bbadis.2015.11.003
29. Ciaramella A, Salani F, Bizzoni F, Pontieri FE, Stefani A, Pierantozzi M, et al. Blood Dendritic Cell Frequency Declines in Idiopathic Parkinson's Disease and is Associated With Motor Symptom Severity. *PloS One* (2013) 8(6): e65352. doi: 10.1371/journal.pone.0065352
30. Harms AS, Thome AD, Yan Z, Schonhoff AM, Williams GP, Li X, et al. Peripheral Monocyte Entry is Required for Alpha-Synuclein Induced Inflammation and Neurodegeneration in a Model of Parkinson Disease. *Exp Neurol* (2018) 300:179–87. doi: 10.1016/j.expneurol.2017.11.010
31. Alam MM, Yang D, Trivett AL, Li X-Q, Oppenheim JJ. Alpha-Synuclein (αs) Acts as an Alarmin to Promote Dendritic Cell Activation and Proinflammatory Immune Response. *J Immunol* (2019) 202(1 Supplement):68.17–7.
32. Álvarez-Luquín DD, Arce-Sillas A, Leyva-Hernández J, Sevilla-Reyes E, Boll MC, Montes-Moratilla E, et al. Regulatory Impairment in Untreated Parkinson's Disease Is Not Restricted to Tregs: Other Regulatory Populations Are Also Involved. *J Neuroinflamm* (2019) 16(1):212. doi: 10.1186/s12974-019-1606-1
33. Burgdorf S, Kurts C. Endocytosis Mechanisms and the Cell Biology of Antigen Presentation. *Curr Opin Immunol* (2008) 20(1):89–95. doi: 10.1016/j.coi.2007.12.002
34. Iwasaki A, Medzhitov R. Control of Adaptive Immunity by the Innate Immune System. *Nat Immunol* (2015) 16(4):343–53. doi: 10.1038/ni.3123
35. Prashar A, Schnettger L, Bernard EM, Gutierrez MG. Rab GTPases in Immunity and Inflammation. *Front Cell Infect Microbiol* (2017) 7:435. doi: 10.3389/fcimb.2017.00435
36. Brundin P, Dave KD, Kordower JH. Therapeutic Approaches to Target Alpha-Synuclein Pathology. *Exp Neurol* (2017) 298(Pt B):225–35. doi: 10.1016/j.expneurol.2017.10.003
37. Decressac M, Mattsson B, Weikop P, Lundblad M, Jakobsson J, Björklund A. TFEB-Mediated Autophagy Rescues Midbrain Dopamine Neurons From α-Synuclein Toxicity. *Proc Natl Acad Sci USA* (2013) 110(19):E1817–26. doi: 10.1073/pnas.1305623110
38. Bonam SR, Tranchant C, Muller S. Autophagy-Lysosomal Pathway as Potential Therapeutic Target in Parkinson's Disease. *Cells* (2021) 10 (12):3547. doi: 10.3390/cells10123547
39. Kubo M, Nagashima R, Kurihara M, Kawakami F, Maekawa T, Eshima K, et al. Leucine-Rich Repeat Kinase 2 Controls Inflammatory Cytokines Production Through NF-κb Phosphorylation and Antigen Presentation in Bone Marrow-Derived Dendritic Cells. *Int J Mol Sci* (2020) 21(5):1890. doi: 10.3390/ijms21051890
40. Freeman D, Cedillos R, Choyke S, Lukic Z, McGuire K, Marvin S, et al. Alpha-Synuclein Induces Lysosomal Rupture and Cathepsin Dependent Reactive Oxygen Species Following Endocytosis. *PloS One* (2013) 8(4): e62143. doi: 10.1371/journal.pone.0062143
41. Manoury B. Proteases: Essential Actors in Processing Antigens and Intracellular Toll-Like Receptors. *Front Immunol* (2013) 4:299. doi: 10.3389/fimmu.2013.00299
42. Junutula JR, De Maziére AM, Peden AA, Ervin KE, Advani RJ, van Dijk SM, et al. Rab14 Is Involved in Membrane Trafficking Between the Golgi Complex and Endosomes. *Mol Biol Cell* (2004) 15(5):2218–29. doi: 10.1091/mbc.e03-10-0777
43. Barth S, Glick D, Macleod KF. Autophagy: Assays and Artifacts. *J Pathol* (2010) 221(2):117–24. doi: 10.1002/path.2694
44. Szatmári Z, Sass M. The Autophagic Roles of Rab Small GTPases and Their Upstream Regulators: A Review. *Autophagy* (2014) 10(7):1154–66. doi: 10.4161/auto.29395
45. Song JX, Sun YR, Peluso I, Zeng Y, Yu X, Lu JH, et al. A Novel Curcumin Analog Binds to and Activates TFEB In Vitro and In Vivo Independent of

MTOR Inhibition. *Autophagy* (2016) 12(8):1372–89. doi: 10.1080/15548627.2016.1179404
46. Liu X, Zhao P, Wang X, Wang L, Zhu Y, Song Y, et al. Celastrol Mediates Autophagy and Apoptosis via the ROS/JNK and Akt/mTOR Signaling Pathways in Glioma Cells. *J Exp Clin Cancer Res* (2019) 38(1):184. doi: 10.1186/s13046-019-1173-4
47. Shi J, Li J, Xu Z, Chen L, Luo R, Zhang C, et al. Celastrol: A Review of Useful Strategies Overcoming its Limitation in Anticancer Application. *Front Pharmacol* (2020) 11:558741. doi: 10.3389/fphar.2020.558741
48. Allison AC, Cacabelos R, Lombardi VR, Alvarez XA, Vigo C. Celastrol, a Potent Antioxidant and Anti-Inflammatory Drug, as a Possible Treatment for Alzheimer's Disease. *Prog Neuropsychopharmacol Biol Psychiatry* (2001) 25(7):1341–57. doi: 10.1016/s0278-5846(01)00192-0
49. Liu J, Lee J, Salazar Hernandez MA, Mazitschek R, Ozcan U. Treatment of Obesity With Celastrol. *Cell* (2015) 161(5):999–1011. doi: 10.1016/j.cell.2015.05.011
50. Mo Y, Cheung AKL, Liu Y, Liu L, Chen Z. Imaging and Analysis on the Interaction Between Human Antigen-Pulsed Vδ2 T Cells and Antigen-Specific CD4 T Cells. *STAR Protoc* (2021) 2(2):100453. doi: 10.1016/j.xpro.2021.100453
51. Schneider CA, Rasband WS, Eliceiri KW. NIH Image to ImageJ: 25 Years of Image Analysis. *Nat Methods* (2012) 9(7):671–5. doi: 10.1038/nmeth.2089
52. Szklarczyk D, Gable AL, Nastou KC, Lyon D, Kirsch R, Pyysalo S, et al. The STRING Database in 2021: Customizable Protein-Protein Networks, and Functional Characterization of User-Uploaded Gene/Measurement Sets. *Nucleic Acids Res* (2021) 49(D1):D605–12. doi: 10.1093/nar/gkaa1074
53. Lu YC, Yeh WC, Ohashi PS. LPS/TLR4 Signal Transduction Pathway. *Cytokine* (2008) 42(2):145–51. doi: 10.1016/j.cyto.2008.01.006
54. Mbongue JC, Nieves HA, Torrez TW, Langridge WH. The Role of Dendritic Cell Maturation in the Induction of Insulin-Dependent Diabetes Mellitus. *Front Immunol* (2017) 8:327. doi: 10.3389/fimmu.2017.00327
55. Trevejo JM, Marino MW, Philpott N, Josien R, Richards EC, Elkon KB, et al. TNF-Alpha -Dependent Maturation of Local Dendritic Cells Is Critical for Activating the Adaptive Immune Response to Virus Infection. *Proc Natl Acad Sci U.S.A.* (2001) 98(21):12162–7. doi: 10.1073/pnas.211423598
56. Mo Y, Cheung AKL, Liu Y, Liu L, Chen Z. Delta42PD1-TLR4 Augments Gammadelta-T Cell Activation of the Transitional Memory Subset of CD4 (+) T Cells. *iScience* (2020) 23(10):101620. doi: 10.1016/j.isci.2020.101620
57. Baixauli F, López-Otín C, Mittelbrunn M. Exosomes and Autophagy: Coordinated Mechanisms for the Maintenance of Cellular Fitness. *Front Immunol* (2014) 5:403. doi: 10.3389/fimmu.2014.00403
58. Hansen TE, Johansen T. Following Autophagy Step by Step. *BMC Biol* (2011) 9(1):39. doi: 10.1186/1741-7007-9-39
59. Ao X, Zou L, Wu Y. Regulation of Autophagy by the Rab GTPase Network. *Cell Death Differ* (2014) 21(3):348–58. doi: 10.1038/cdd.2013.187
60. Hammerling BC, Najor RH, Cortez MQ, Shires SE, Leon LJ, Gonzalez ER, et al. A Rab5 Endosomal Pathway Mediates Parkin-Dependent Mitochondrial Clearance. *Nat Commun* (2017) 8(1):14050. doi: 10.1038/ncomms14050
61. Martin HL, Santoro M, Mustafa S, Riedel G, Forrester JV, Teismann P. Evidence for a Role of Adaptive Immune Response in the Disease Pathogenesis of the MPTP Mouse Model of Parkinson's Disease. *Glia* (2016) 64(3):386–95. doi: 10.1002/glia.22935
62. Jiang S, Gao H, Luo Q, Wang P, Yang X. The Correlation of Lymphocyte Subsets, Natural Killer Cell, and Parkinson's Disease: A Meta-Analysis. *Neurol Sci* (2017) 38(8):1373–80. doi: 10.1007/s10072-017-2988-4
63. Codolo G, Plotegher N, Pozzobon T, Brucale M, Tessari I, Bubacco L, et al. Triggering of Inflammasome by Aggregated α-Synuclein, an Inflammatory Response in Synucleinopathies. *PloS One* (2013) 8(1):e55375. doi: 10.1371/journal.pone.0055375
64. Nagatsu T, Sawada M. Inflammatory Process in Parkinson's Disease: Role for Cytokines. *Curr Pharm Des* (2005) 11(8):999–1016. doi: 10.2174/1381612053381620
65. Ettle B, Kuhbandner K, Jörg S, Hoffmann A, Winkler J, Linker RA. α-Synuclein Deficiency Promotes Neuroinflammation by Increasing Th1 Cell-Mediated Immune Responses. *J Neuroinflamm* (2016) 13(1):201. doi: 10.1186/s12974-016-0694-4
66. Giuliani F, Goodyer CG, Antel JP, Yong VW. Vulnerability of Human Neurons to T Cell-Mediated Cytotoxicity. *J Immunol* (2003) 171(1):368–79. doi: 10.4049/jimmunol.171.1.368
67. Prajeeth CK, Dittrich-Breiholz O, Talbot SR, Robert PA, Huehn J, Stangel M. IFN-γ Producing Th1 Cells Induce Different Transcriptional Profiles in Microglia and Astrocytes. *Front Cell Neurosci* (2018) 12:352. doi: 10.3389/fncel.2018.00352
68. Appel SH. CD4+ T Cells Mediate Cytotoxicity in Neurodegenerative Diseases. *J Clin Invest* (2009) 119(1):13–5. doi: 10.1172/jci38096
69. Dombrowski Y, O'Hagan T, Dittmer M, Penalva R, Mayoral SR, Bankhead P, et al. Regulatory T Cells Promote Myelin Regeneration in the Central Nervous System. *Nat Neurosci* (2017) 20(5):674–80. doi: 10.1038/nn.4528
70. Lee GR. The Balance of Th17 Versus Treg Cells in Autoimmunity. *Int J Mol Sci* (2018) 19(3):730. doi: 10.3390/ijms19030730
71. Reynolds AD, Stone DK, Hutter JA, Benner EJ, Mosley RL, Gendelman HE. Regulatory T Cells Attenuate Th17 Cell-Mediated Nigrostriatal Dopaminergic Neurodegeneration in a Model of Parkinson's Disease. *J Immunol* (2010) 184(5):2261–71. doi: 10.4049/jimmunol.0901852
72. Harms AS, Cao S, Rowse AL, Thome AD, Li X, Mangieri LR, et al. MHCII Is Required for α-Synuclein-Induced Activation of Microglia, CD4 T Cell Proliferation, and Dopaminergic Neurodegeneration. *J Neurosci* (2013) 33(23):9592–600. doi: 10.1523/jneurosci.5610-12.2013
73. Rostami J, Fotaki G, Sirois J, Mzezewa R, Bergström J, Essand M, et al. Astrocytes Have the Capacity to Act as Antigen-Presenting Cells in the Parkinson's Disease Brain. *J Neuroinflamm* (2020) 17(1):119. doi: 10.1186/s12974-020-01776-7
74. Gericke C, Mallone A, Engelhardt B, Nitsch RM, Ferretti MT. Oligomeric Forms of Human Amyloid-Beta(1-42) Inhibit Antigen Presentation. *Front Immunol* (2020) 11:1029. doi: 10.3389/fimmu.2020.01029
75. Ferretti MT, Merlini M, Späni C, Gericke C, Schweizer N, Enzmann G, et al. T-Cell Brain Infiltration and Immature Antigen-Presenting Cells in Transgenic Models of Alzheimer's Disease-Like Cerebral Amyloidosis. *Brain Behav Immun* (2016) 54:211–25. doi: 10.1016/j.bbi.2016.02.009
76. Benner EJ, Banerjee R, Reynolds AD, Sherman S, Pisarev VM, Tsiperson V, et al. Nitrated Alpha-Synuclein Immunity Accelerates Degeneration of Nigral Dopaminergic Neurons. *PloS One* (2008) 3(1):e1376. doi: 10.1371/journal.pone.0001376
77. Thome AD, Atassi F, Wang J, Faridar A, Zhao W, Thonhoff JR, et al. Ex Vivo Expansion of Dysfunctional Regulatory T Lymphocytes Restores Suppressive Function in Parkinson's Disease. *NPJ Parkinson's Dis* (2021) 7(1):41. doi: 10.1038/s41531-021-00188-5
78. Admyre C, Grunewald J, Thyberg J, Gripenbäck S, Tornling G, Eklund A, et al. Exosomes With Major Histocompatibility Complex Class II and Co-Stimulatory Molecules Are Present in Human BAL Fluid. *Eur Respir J* (2003) 22(4):578–83. doi: 10.1183/09031936.03.00041703
79. Johansson SM, Admyre C, Scheynius A, Gabrielsson S. Different Types of In Vitro Generated Human Monocyte-Derived Dendritic Cells Release Exosomes With Distinct Phenotypes. *Immunology* (2008) 123(4):491–9. doi: 10.1111/j.1365-2567.2007.02714.x
80. Pinnell JR, Cui M, Tieu K. Exosomes in Parkinson Disease. *J Neurochem* (2021) 157(3):413–28. doi: 10.1111/jnc.15288
81. Théry C, Duban L, Segura E, Véron P, Lantz O, Amigorena S. Indirect Activation of Naïve CD4+ T Cells by Dendritic Cell-Derived Exosomes. *Nat Immunol* (2002) 3(12):1156–62. doi: 10.1038/ni854
82. Chutna O, Gonçalves S, Villar-Piqué A, Guerreiro P, Marijanovic Z, Mendes T, et al. The Small GTPase Rab11 Co-Localizes With α-Synuclein in Intracellular Inclusions and Modulates its Aggregation, Secretion and Toxicity. *Hum Mol Genet* (2014) 23(25):6732–45. doi: 10.1093/hmg/ddu391
83. Gutiérrez-Martínez E, Planès R, Anselmi G, Reynolds M, Menezes S, Adiko AC, et al. Cross-Presentation of Cell-Associated Antigens by MHC Class I in Dendritic Cell Subsets. *Front Immunol* (2015) 6:363. doi: 10.3389/fimmu.2015.00363
84. Joffre OP, Segura E, Savina A, Amigorena S. Cross-Presentation by Dendritic Cells. *Nat Rev Immunol* (2012) 12(8):557–69. doi: 10.1038/nri3254
85. Scott CC, Vacca F, Gruenberg J. Endosome Maturation, Transport and Functions. *Semin Cell Dev Biol* (2014) 31:2–10. doi: 10.1016/j.semcdb.2014.03.034
86. Kleijmeer M, Ramm G, Schuurhuis D, Griffith J, Rescigno M, Ricciardi-Castagnoli P, et al. Reorganization of Multivesicular Bodies Regulates MHC

Class II Antigen Presentation by Dendritic Cells. *J Cell Biol* (2001) 155 (1):53–63. doi: 10.1083/jcb.200103071
87. Münz C. Antigen Processing for MHC Class II Presentation via Autophagy. *Front Immunol* (2012) 3:9. doi: 10.3389/fimmu.2012.00009
88. You L, Mao L, Wei J, Jin S, Yang C, Liu H, et al. The Crosstalk Between Autophagic and Endo-/Exosomal Pathways in Antigen Processing for MHC Presentation in Anticancer T Cell Immune Responses. *J Hematol Oncol* (2017) 10(1):165. doi: 10.1186/s13045-017-0534-8
89. Ganesan D, Cai Q. Understanding Amphisomes. *Biochem J* (2021) 478 (10):1959–76. doi: 10.1042/bcj20200917
90. Ojha CR, Lapierre J, Rodriguez M, Dever SM, Zadeh MA, DeMarino C, et al. Interplay Between Autophagy, Exosomes and HIV-1 Associated Neurological Disorders: New Insights for Diagnosis and Therapeutic Applications. *Viruses* (2017) 9(7):176. doi: 10.3390/v9070176
91. Birmingham CL, Smith AC, Bakowski MA, Yoshimori T, Brumell JH. Autophagy Controls Salmonella Infection in Response to Damage to the Salmonella-Containing Vacuole. *J Biol Chem* (2006) 281(16):11374–83. doi: 10.1074/jbc.M509157200
92. Schmid D, Pypaert M, Münz C. Antigen-Loading Compartments for Major Histocompatibility Complex Class II Molecules Continuously Receive Input From Autophagosomes. *Immunity* (2007) 26(1):79–92. doi: 10.1016/j.immuni.2006.10.018
93. Delamarre L, Pack M, Chang H, Mellman I, Trombetta ES. Differential Lysosomal Proteolysis in Antigen-Presenting Cells Determines Antigen Fate. *Science* (2005) 307(5715):1630–4. doi: 10.1126/science.1108003
94. Dengjel J, Schoor O, Fischer R, Reich M, Kraus M, Müller M, et al. Autophagy Promotes MHC Class II Presentation of Peptides From Intracellular Source Proteins. *Proc Natl Acad Sci USA* (2005) 102 (22):7922–7. doi: 10.1073/pnas.0501190102
95. Brazil MI, Weiss S, Stockinger B. Excessive Degradation of Intracellular Protein in Macrophages Prevents Presentation in the Context of Major Histocompatibility Complex Class II Molecules. *Eur J Immunol* (1997) 27 (6):1506–14. doi: 10.1002/eji.1830270629
96. Lanzillotta A, Porrini V, Bellucci A, Benarese M, Branca C, Parrella E, et al. NF-κb in Innate Neuroprotection and Age-Related Neurodegenerative Diseases. *Front Neurol* (2015) 6:98. doi: 10.3389/fneur.2015.00098
97. Venkatesha SH, Yu H, Rajaiah R, Tong L, Moudgil KD. Celastrus-Derived Celastrol Suppresses Autoimmune Arthritis by Modulating Antigen-Induced Cellular and Humoral Effector Responses. *J Biol Chem* (2011) 286 (17):15138–46. doi: 10.1074/jbc.M111.226365
98. Yang H, Liu C, Jiang J, Wang Y, Zhang X. Celastrol Attenuates Multiple Sclerosis and Optic Neuritis in an Experimental Autoimmune Encephalomyelitis Model. *Front Pharmacol* (2017) 8:44. doi: 10.3389/fphar.2017.00044
99. Harizi H, Gualde N. The Impact of Eicosanoids on the Crosstalk Between Innate and Adaptive Immunity: The Key Roles of Dendritic Cells. *Tissue Antigens* (2005) 65(6):507–14. doi: 10.1111/j.1399-0039.2005.00394.x
100. Lee HJ, Bazinet RP, Rapoport SI, Bhattacharjee AK. Brain Arachidonic Acid Cascade Enzymes Are Upregulated in a Rat Model of Unilateral Parkinson Disease. *Neurochem Res* (2010) 35(4):613–9. doi: 10.1007/s11064-009-0106-6
101. Mayorga LS, Colombo MI, Lennartz M, Brown EJ, Rahman KH, Weiss R, et al. Inhibition of Endosome Fusion by Phospholipase A2 (PLA2) Inhibitors Points to a Role for PLA2 in Endocytosis. *Proc Natl Acad Sci USA* (1993) 90 (21):10255–9. doi: 10.1073/pnas.90.21.10255
102. Zhang C, Li A, Gao S, Zhang X, Xiao H. The TIP30 Protein Complex, Arachidonic Acid and Coenzyme A Are Required for Vesicle Membrane Fusion. *PloS One* (2011) 6(6):e21233. doi: 10.1371/journal.pone.0021233
103. Chock SP, Schmauder-Chock EA, Cordella-Miele E, Miele L, Mukherjee AB. The Localization of Phospholipase A2 in the Secretory Granule. *Biochem J* (1994) 300(Pt 3):619–22. doi: 10.1042/bj3000619
104. Hardman CS, Chen YL, Salimi M, Jarrett R, Johnson D, Järvinen VJ, et al. CD1a Presentation of Endogenous Antigens by Group 2 Innate Lymphoid Cells. *Sci Immunol* (2017) 2(18):5918. doi: 10.1126/sciimmunol.aan5918
105. Sarkar C, Jones JW, Hegdekar N, Thayer JA, Kumar A, Faden AI, et al. PLA2G4A/cPLA2-Mediated Lysosomal Membrane Damage Leads to Inhibition of Autophagy and Neurodegeneration After Brain Trauma. *Autophagy* (2020) 16(3):466–85. doi: 10.1080/15548627.2019.1628538
106. Deng Z, Ma S, Zhou H, Zang A, Fang Y, Li T, et al. Tyrosine Phosphatase SHP-2 Mediates C-Type Lectin Receptor-Induced Activation of the Kinase Syk and Anti-Fungal TH17 Responses. *Nat Immunol* (2015) 16(6):642–52. doi: 10.1038/ni.3155
107. Guo J, Huang X, Wang H, Yang H, e0140745. Celastrol Induces Autophagy by Targeting AR/miR-101 in Prostate Cancer Cells. *PloS One* (2015) 10(10): e0140745. doi: 10.1371/journal.pone.0140745
108. Kissick HT, Sanda MG, Dunn LK, Pellegrini KL, On ST, Noel JK, et al. Androgens Alter T-Cell Immunity by Inhibiting T-Helper 1 Differentiation. *Proc Natl Acad Sci USA* (2014) 111(27):9887–92. doi: 10.1073/pnas.1402468111
109. Lai JJ, Lai KP, Zeng W, Chuang KH, Altuwaijri S, Chang C. Androgen Receptor Influences on Body Defense System via Modulation of Innate and Adaptive Immune Systems: Lessons From Conditional AR Knockout Mice. *Am J Pathol* (2012) 181(5):1504–12. doi: 10.1016/j.ajpath.2012.07.008
110. McGlinchey RP, Lee JC. Cysteine Cathepsins Are Essential in Lysosomal Degradation of α-Synuclein. *Proc Natl Acad Sci USA* (2015) 112(30):9322–7. doi: 10.1073/pnas.1500937112

Conflict of Interest: The authors declare that the research was conducted in the absence of any commercial or financial relationships that could be construed as a potential conflict of interest.

Publisher's Note: All claims expressed in this article are solely those of the authors and do not necessarily represent those of their affiliated organizations, or those of the publisher, the editors and the reviewers. Any product that may be evaluated in this article, or claim that may be made by its manufacturer, is not guaranteed or endorsed by the publisher.

frontiers | Frontiers in Immunology

CORRECTION
published: 20 May 2022
doi: 10.3389/fimmu.2022.907993

Corrigendum: Celastrol Downmodulates Alpha-Synuclein-Specific T Cell Responses by Mediating Antigen Trafficking in Dendritic Cells

Lam Ng[1], Xiaohui Wang[1], Chuanbin Yang[2,3], Chengfu Su[2,4], Min Li[2†] and Allen Ka Loon Cheung[1*†]*

[1] Department of Biology, Faculty of Science, Hong Kong Baptist University, Kowloon Tong, Hong Kong SAR, China, [2] Mr. & Mrs. Ko Chi Ming Center for Parkinson Disease Research, School of Chinese Medicine, Hong Kong Baptist University, Kowloon Tong, Hong Kong SAR, China, [3] Department of Geriatrics, Shenzhen People's Hospital (The Second Clinical Medical College, Jinan University; The First Affiliated Hospital, Southern University of Science and Technology), Shenzhen, China, [4] College of Pharmacy, Henan University of Chinese Medicine, Zhengzhou, China

OPEN ACCESS

Approved by:
Frontiers in Editorial Office, Frontiers Media SA, Switzerland

***Correspondence:**
Allen Ka Loon Cheung
akcheung@hkbu.edu.hk
Min Li
limin@hkbu.edu.hk

†These authors have contributed equally to this work and share last authorship

Specialty section:
This article was submitted to Antigen Presenting Cell Biology, a section of the journal Frontiers in Immunology

Received: *30 March 2022*
Accepted: *10 May 2022*
Published: *20 May 2022*

Citation:
Ng L, Wang X, Yang C, Su C, Li M and Cheung AKL (2022) Corrigendum: Celastrol Downmodulates Alpha-Synuclein-Specific T Cell Responses by Mediating Antigen Trafficking in Dendritic Cells. Front. Immunol. 13:907993. doi: 10.3389/fimmu.2022.907993

Keywords: Celastrol, Parkinson's Disease, a-synuclein, dendritic cell, CD4+ T cell subsets, endo-lysosomal pathway, autophagy

A Corrigendum on:

Celastrol Downmodulates Alpha-Synuclein-Specific T Cell Responses by Mediating Antigen Trafficking in Dendritic Cells

By Ng L, Wang X, Yang C, Su C, Li M and Cheung AKL (2022) Front. Immunol. 13:833515. doi: 10.3389/fimmu.2022.833515

In the published article, there was an error regarding the affiliation for Min Li. Instead of having affiliations 2,3, the author should only be affiliated to 2.

The authors apologize for this error and state that this does not change the scientific conclusions of the article in any way. The original article has been updated.

frontiers in Immunology

ORIGINAL RESEARCH
published: 04 March 2022
doi: 10.3389/fimmu.2022.810824

A Spontaneous H2-Aa Point Mutation Impairs MHC II Synthesis and CD4$^+$ T-Cell Development in Mice

Yun Zhao[1], Juan Xiong[1,2], Hai-Xia Chen[1], Min Zhang[1], Li-Na Zhou[3], Yin-Fang Wu[1], Wei-Jie Li[1], Xia Fei[1], Fei Li[1], Chen Zhu[1], Wen Li[1], Song-Min Ying[1,4], Lie Wang[3], Zhi-Hua Chen[1]* and Hua-Hao Shen[1,5]**

[1] Key Laboratory of Respiratory Disease of Zhejiang Province, Department of Respiratory and Critical Care Medicine, Second Affiliated Hospital of Zhejiang University School of Medicine, Hangzhou, China, [2] Department of Drug Candidate, Qihan Bio Inc., Hangzhou, China, [3] Institute of Immunology, Zhejiang University School of Medicine, Hangzhou, China, [4] International Institutes of Medicine, the Fourth Affiliated Hospital of Zhejiang University School of Medicine, Yiwu, China, [5] State Key Lab of Respiratory Disease, National Clinical Research Center for Respiratory Disease, Guangzhou, China

OPEN ACCESS

Edited by:
Eddie A. James,
Benaroya Research Institute,
United States

Reviewed by:
Dipankar Nandi,
Indian Institute of Science (IISc), India
Masaaki Miyazawa,
Kindai University, Japan

***Correspondence:**
Hua-Hao Shen
huahaoshen@zju.edu.cn
Zhi-Hua Chen
zhihuachen@zju.edu.cn
Lie Wang
wanglie@zju.edu.cn

Specialty section:
This article was submitted to Antigen Presenting Cell Biology, a section of the journal Frontiers in Immunology

Received: 08 November 2021
Accepted: 10 February 2022
Published: 04 March 2022

Citation:
Zhao Y, Xiong J, Chen H-X, Zhang M, Zhou L-N, Wu Y-F, Li W-J, Fei X, Li F, Zhu C, Li W, Ying S-M, Wang L, Chen Z-H and Shen H-H (2022) A Spontaneous H2-Aa Point Mutation Impairs MHC II Synthesis and CD4$^+$ T-Cell Development in Mice. Front. Immunol. 13:810824. doi: 10.3389/fimmu.2022.810824

Major histocompatibility complex class II (MHC II) is an essential immune regulatory molecule that plays an important role in antigen presentation and T-cell development. Abnormal MHC II expression can lead to immunodeficiency, clinically termed as type II bare lymphocyte syndrome (BLS), which usually results from mutations in the MHC II transactivator (CIITA) and other coactivators. Here, we present a new paradigm for MHC II deficiency in mice that involves a spontaneous point mutation on H2-Aa. A significantly reduced population of CD4$^+$ T cells was observed in mice obtained from the long-term homozygous breeding of *autophagy-related gene microtubule-associated protein 1 light chain 3 β* (Map1*lc3b*, *Lc3b*) knockout mice; this phenotype was not attributed to the original knocked-out gene. MHC II expression was generally reduced, together with a marked deficiency of H2-Aa in the immune cells of these mice. Using cDNA and DNA sequencing, a spontaneous H2-Aa point mutation that led to false pre-mRNA splicing, deletion of eight bases in the mRNA, and protein frameshift was identified in these mice. These findings led to the discovery of a new type of spontaneous MHC II deficiency and provided a new paradigm to explain type II BLS in mice.

Keywords: MHC II, CD4$^+$ T cells, immunodeficiency, H2-Aa, point mutation

INTRODUCTION

As an important immune regulator, major histocompatibility complex class II (MHC II), which is a heterodimer consisting of an α chain and a β chain, plays a key role in the immune response (1). MHC II genes are constitutively expressed in immune cells such as B cells, dendritic cells, and thymus epithelial cells (2). The expression of MHC II in B and dendritic cells is essential for antigen presentation (3), while MHC II expression in thymus epithelial cells contributes to CD4$^+$ T-cell development (4). In addition, macrophages can express a higher level of MHC II following stimulation with interferon-γ (IFN-γ) (5). The aberrant expression of class II proteins has been implicated in immune dysfunction, and a lack of MHC II causes an immunodeficiency called type II BLS (6). CD4$^+$ T cells are an important T-cell subtype. Hematopoietic stem cells differentiate into

common lymphoid progenitor cells and migrate to the thymus which is the main site for lymphocyte development. Upon undergoing T-cell receptor (TCR) rearrangement, positive selection, and negative selection, mature T cells are generated and finally delivered to peripheral immune organs to execute immune function (7). MHC II plays an important role in T-cell selection, and only T cells with moderate affinity to MHC II but low affinity to MHC II self-antigen can ultimately develop into mature $CD4^+$ T cells (8). Therefore, patients with type II BLS exhibit severely hampered T-cell activation and greatly reduced $CD4^+$ T-cell counts.

MHC II transactivator (CIITA) is a non-DNA-binding protein factor that is recruited to the enhancer complex of MHC II genes and predominantly regulates MHC II expression. CIITA expression acts as a master switch in immune responses (9). CIITA interacts with DNA-binding proteins, such as RFX factors, including RFXANK/RFXB, RFX5, RFXAP, and CREB, to form an anchor in the large transcriptosome complex. Therefore, the abnormal expression of these proteins can result in MHC II deficiency, namely, type II BLS which has a very low incidence clinically. In previous reports, patients displayed some genetic defects in factors such as CIITA, RFXANK, RFX5, and RFXAP; nearly every patient had a specific defect in the transcription factor that is essential for MHC II expression. However, some atypical cases still exist wherein the genetic defect is undefined and the mutations in MHC II genes are not clear (10).

In the present study, we observed an immunodeficient phenotype in mice that were obtained from the homozygous breeding of *lc3b* knockout mice. The obtained mice showed impaired MHC II synthesis and diminished $CD4^+$ T-cell development, which is unlikely to be due to impairment of the original gene. We also confirmed that the immunodeficiency in this mouse strain was not related to the CIITA transcriptosome complex, but resulted from a spontaneous *H2-Aa* point mutation, which led to the errant splicing of pre-mRNA and frameshift of protein.

RESULTS

We accidentally observed $CD4^+$ T-cell deficiency in mice that were obtained from long-term homozygous breeding of *lc3b* knockout mice. The population of $CD4^+$ T cells was significantly decreased in the thymus (**Figures 1A, B**) and spleen (**Figures 1C, D**) of these mice. However, this phenotype was not observed in the original mice, which were not products of long-term homozygous breeding (**Figures S1A–D**). This indicated that the impairment of $CD4^+$ T cells in these mice was independent of the original gene knockout. The development of $CD4^+$ T cells involves two critical processes: differentiation from progenitor cells in the bone marrow and TCR- and MHC II-mediated T-cell maturation in the thymus. To determine the stage at which $CD4^+$ T-cell development was impaired, we performed bone marrow transfer experiments. Wild-type mice that received the bone marrow of knockout mice had a $CD4^+$ T-cell population similar to those receiving the bone marrow of wild-type mice (**Figures 1E, F**). However, receiving the bone marrow of wild-type mice failed to rescue the $CD4^+$ T-cell defect in knockout mice (**Figures 1G, H**). These data suggest that $CD4^+$ T-cell deficiency in knockout mice likely occurs in the thymus.

After common lymphocyte progenitors migrate from the bone marrow to thymus, positive selection and negative selection are required for normal T-cell development. MHC II plays an important role in T-cell selection, especially in $CD4^+$ T cells. Interestingly, we found that MHC II expression in the thymus epithelial cells of knockout mice was significantly lower than that in wild-type mice (**Figures 2A–C**). In addition, the number of thymus epithelial cells was significantly lower than that in wild-type mice (**Figure 2D**). We also performed immunofluorescence staining of CD326 in the frozen section of the thymus tissue (**Figure 2E**). The results were consistent with flow cytometry which indicated that the absolute number of thymic epithelial cells was decreased in the knockout mice. Moreover, overexpressing $CD4^+$ TCR by crossing with OT-II mice failed to rescue their phenotype (**Figures S2A, B**), which revealed that the extraordinary $CD4^+$ T-cell population was not dependent on specific TCR rearrangement. We also checked MHC II expression in the bone marrow, thymus, and spleen (**Figures 2F–H**), and the data demonstrated that the decline of MHC II expression in these mice was generally observed in different immune cell types. Macrophages express a low level of MHC II in the normal state but display high MHC II expression upon IFN-γ treatment. Interestingly, IFN-γ failed to induce the expression of MHC II in macrophages from knockout mice (**Figure 2I**). These data suggest that $CD4^+$ T-cell deficiency in these mice resulted from the loss of MHC II expression.

To further investigate the cause of MHC II defects in this mouse strain, we performed RNA-seq with dendritic cells and IFN-γ-treated macrophages from knockout and wild-type mice. Only the expression of *H2-Aa* was significantly reduced in the knockout mice, while H2-Ab1 displayed a similar expression level (**Figures 3A, B**). We confirmed this phenomenon in isolated dendritic cells, B cells, and IFN-γ-treated macrophages. The results showed that the H2-Aa protein was almost completely absent in knockout mice (**Figures 3E, H, K**). However, the mRNA was still notably retained, although it was significantly decreased compared with the wild-type controls (**Figures 3C, F, I**). In contrast, the H2-Ab1 mRNA remained the same in knockout mice (**Figures 3D, G, J**), but the protein was decreased significantly (**Figures 3E, H, K**). However, IFN-γ could induce the expression of H2-Ab1, not H2-Aa, in macrophages of knockout mice. These data suggest that the knockout mice lacked H2-Aa, mainly at the post-transcriptional level. As a subunit of MHC II, the loss of H2-Aa could result in MHC II deficiency and subsequently lead to an abnormal $CD4^+$ T-cell population.

Furthermore, we explored the mechanisms of the loss of H2-Aa protein expression. We treated the B cells of knockout mice with MG132, a proteasome inhibitor, and Lys05, a lysosome inhibitor, and both failed to rescue MHC II deficiency and H2-Aa deletion. Moreover, MG132 alone induced a slight reduction in H2-Aa expression (**Figures 4A–D**). This indicated that the loss of H2-Aa

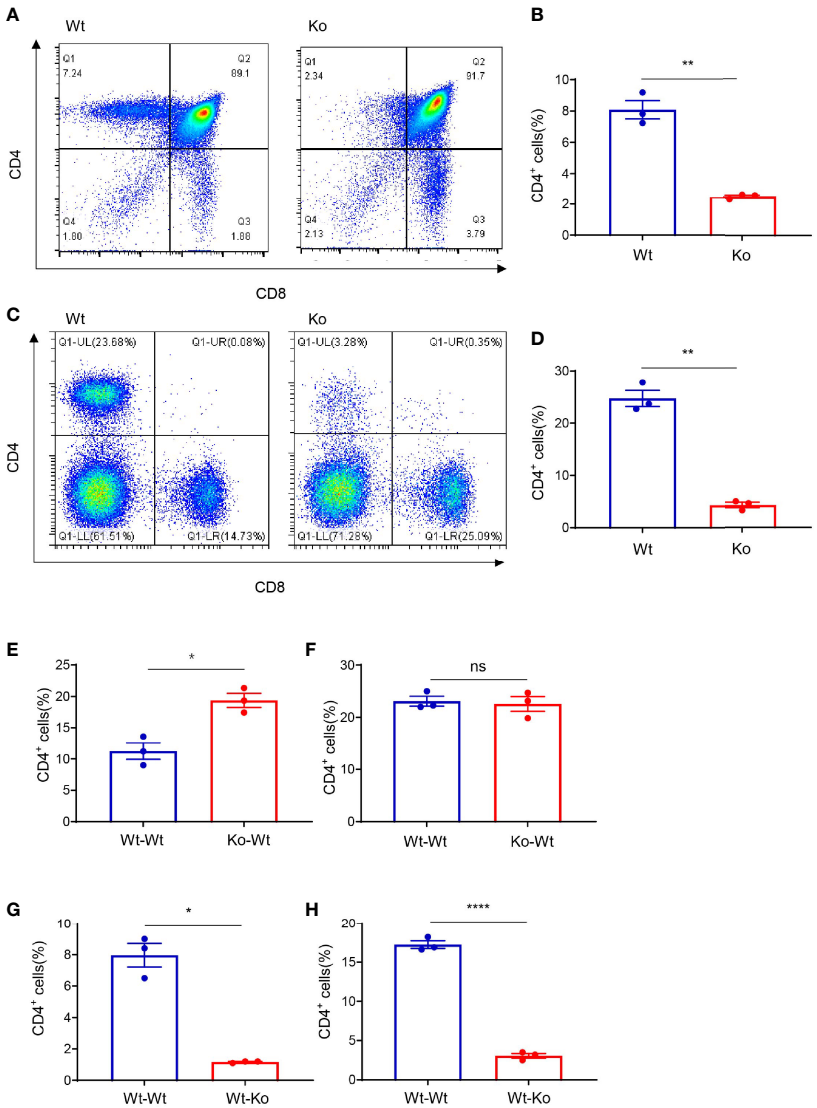

FIGURE 1 | Thymus-dependent CD4$^+$ T-cell deficiency was accidentally observed during long-term homozygous breeding of *lc3b* knockout mouse strain. **(A, C)** Representative images of flow cytometry of the thymus **(A)** and spleen **(C)** of wild-type and knockout mice. **(B, D)** Proportion of CD4$^+$ T cells in the thymus **(B)** and spleen **(D)** of wild-type and knockout mice. **(E, F)** Proportion of CD4$^+$ T cells in the thymus **(E)** and spleen **(F)** of wild-type mice (respectively receiving bone marrow from wild-type mice and knockout mice). **(G, H)** Proportion of CD4$^+$ T cells in the thymus **(G)** and spleen **(H)** of wild-type mice and knockout mice both (receiving bone marrow from wild-type mice). Data **(A–H)** are representative of three to four mice for each group. Error bars, mean ± SEM. $P > 0.05$ (ns), $P \leq 0.05$ (*), $P \leq 0.01$ (**), $P \leq 0.0001$ (****).

was not a result of increased protein degradation. Translocation from the nucleus to the cytoplasm and movement of the ribosome are required for mRNA translation to proteins. To determine whether the nuclear plasma transport process of H2-Aa was normal, we performed nuclear mass separation, which was successful in detecting the mRNA levels of metastasis-associated lung adenocarcinoma transcript 1 (malat1) and the levels of Histone H3 and Calregulin proteins (**Figures S3A, B**). We detected the H2-Aa mRNA levels in the nucleus and cytoplasm, and the data showed that there was no difference between the knockout and wild-type mice (**Figure 4E**), which indicated that the mRNA of H2-Aa could be smoothly transported to the cytoplasm after transcription in the nucleus. In the following study, we analyzed the ribosome profile of B cells in knockout and wild-type mice and isolated ribosomes at different stages to detect the *H2-Aa* mRNA level. The data demonstrated that B cells in knockout mice had a ribosome profile similar to that of wild-type mice (**Figure S3C**). *H2-Aa* mRNA was present at each stage of the ribosome, which was the same as that in the wild-type mice (**Figure 4F**). This indicated that the movement of *H2-Aa* mRNA on ribosomes was normal. Therefore, the defects did not arise during transport from the nucleus to the cytoplasm or during movement of ribosomes, nor did the defects occur due to protein degradation. Hence, we hypothesized that the H2-Aa protein loss might result from false

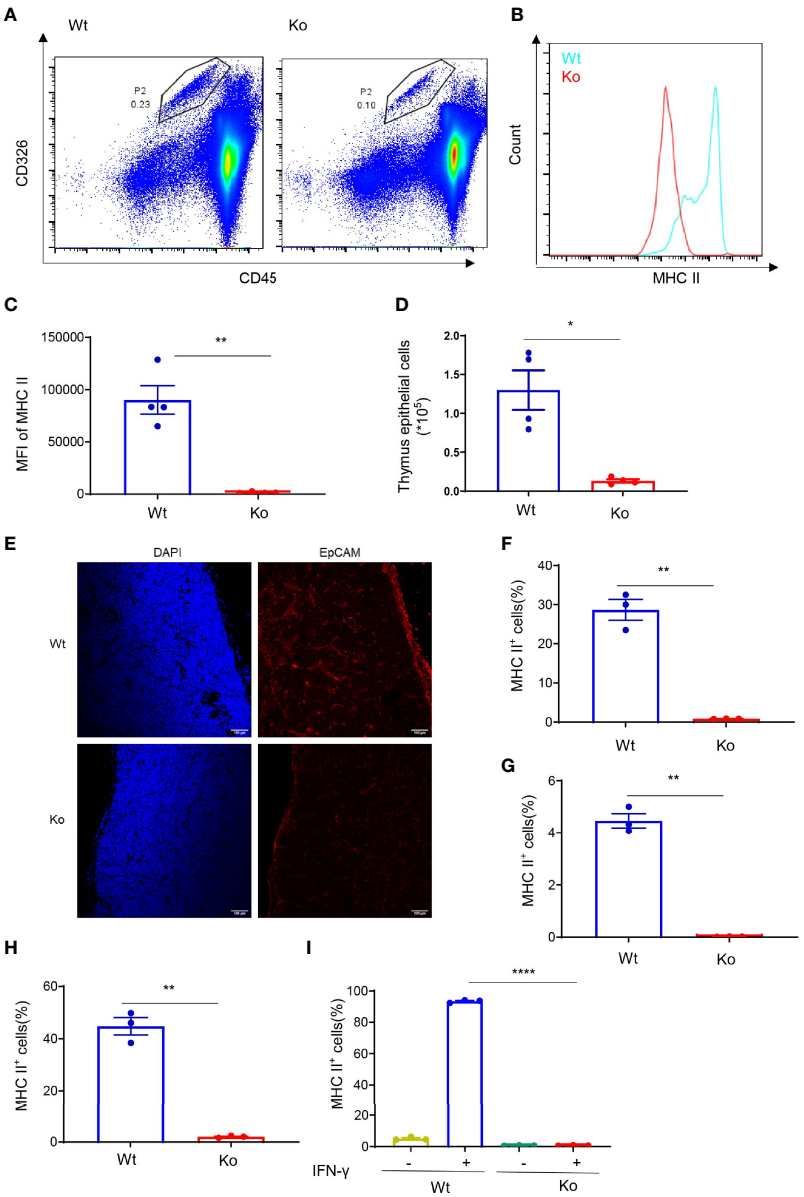

FIGURE 2 | Decreased MHC II expression in the specific mouse strain. **(A)** Representative images of flow cytometry of thymus epithelial cells in wild-type and knockout mice. **(B, C)** Expression of MHC II in thymus epithelial cells of wild-type and knockout mice. **(B)** Overlaid histogram of flow cytometry. **(C)** MFI of MHC II. **(D)** Number of thymus epithelial cells in wild-type and knockout mice. **(E)** Immunofluorescence staining of CD326 in the frozen section of thymus tissue from wild-type and knockout mice. **(F–H)** Expression of MHC II in bone marrow **(F)**, thymus **(G)**, and spleen **(H)** of wild-type and knockout mice. **(I)** Expression of MHC II in bone marrow-derived macrophages of wild-type and knockout mice treated with 20 ng/ml IFN-γ for 24 h. Data **(C, D, F–I)** are representative of three to four mice for each group. Error bars, mean ± SEM. $P \leq 0.05$ (*), $P \leq 0.01$ (**), $P \leq 0.0001$ (****).

mRNA. We then performed sequencing analysis and surprisingly found a deletion of eight bases of *H2-Aa* mRNA (**Figure 4G**). We treated 293T cells with full-length or eight-base deletion Flag-H2-Aa plasmid, and then detected the H2-Aa or Flag expression by Western blotting. Although there was no difference in Flag expression, H2-Aa was not observed in the eight-base deletion group (**Figure 4H**). These results indicated that eight-base deletion in the mRNA could lead to frameshift of the protein. To further understand the presence of false mRNA of *H2-Aa*, we sequenced the DNA of knockout mice and found a spontaneous point mutation in *H2-Aa*. The key to recognition of pre-RNA splicing is to determine the splicing site, which complies with the GT-AG rule. The mutation from A to G caused the splicing recognition to malfunction until the next AG position (**Figure 4I**). Therefore, in knockout mice, wrong pre-mRNA splicing, deletion of eight bases in mRNA, and frameshift of H2-Aa protein eventually resulted in the loss of this protein and subsequent immunodeficiency. Based on all these results, we delineated a

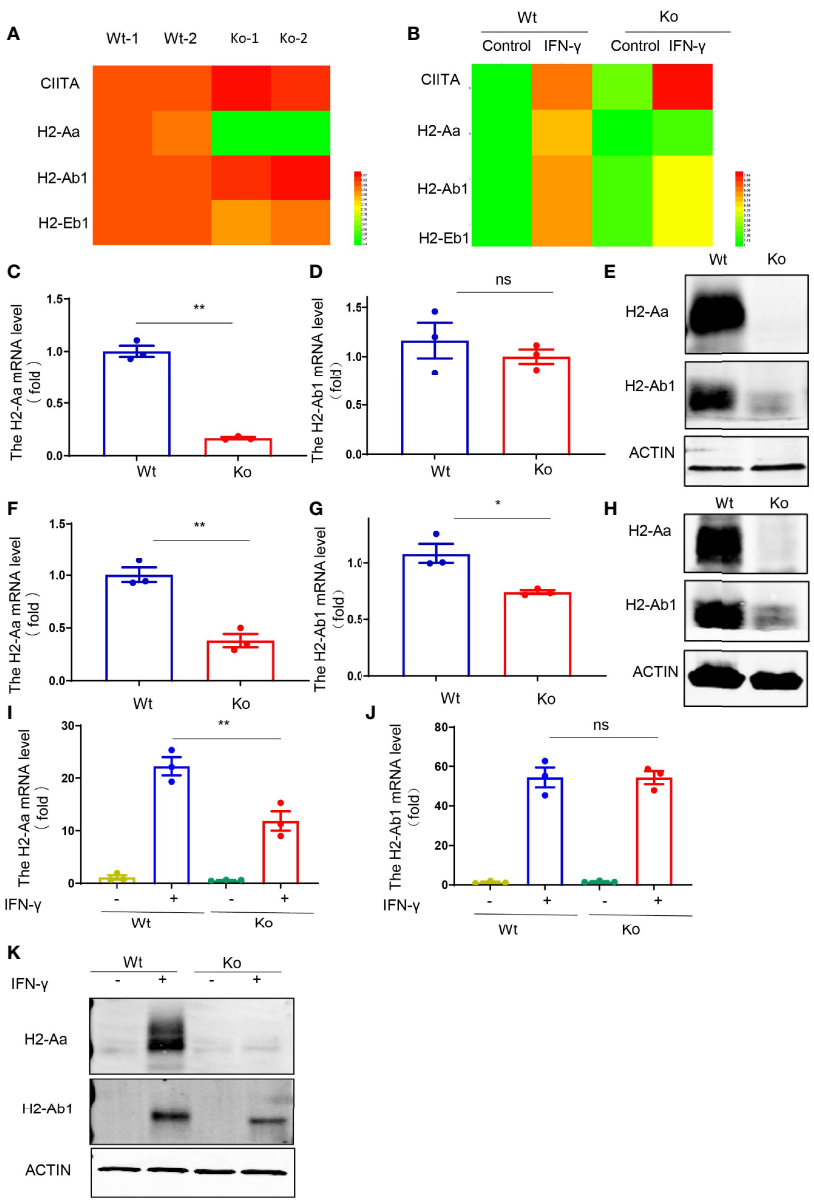

FIGURE 3 | Reduced H2-Aa protein expression in specific mouse strain. **(A, B)** Heatmap of MHC II-associated gene expression obtained using RNA sequencing of bone marrow dendritic cells **(A)** and IFN-γ treated bone marrow-derived macrophages **(B)** in wild-type and knockout mice. **(C–E)** Expression levels of mRNA and protein **(E)** of H2-Aa **(C)** and H2-Ab1 **(D)** in bone marrow dendritic cells of wild-type and knockout mice. **(F–H)** Expression levels of mRNA and protein **(H)** of H2-Aa **(F)** and H2-Ab1 **(G)** in spleen B cells of wild-type and knockout mice. **(I–K)** Expression levels of mRNA and protein **(K)** of H2-Aa **(I)** and H2-Ab1 **(J)** in bone marrow-derived macrophages treated with IFN-γ for 24 h in wild-type and knockout mice. Data **(C, D, F, G, I, J)** were representative of three independent experiments. Error bars, mean ± SEM. $P > 0.05$ (ns), $P \leq 0.05$ (*), $P \leq 0.01$ (**).

model to clarify the consequences of the mutation leading to low expression of MHC class II and type II BLS phenotype (**Figure 4J**).

DISCUSSION

In this study, we observed impaired MHC II synthesis and $CD4^+$ T-cell development when *lc3b* knockout mice underwent long-term homozygous breeding. Although autophagy was shown to play an essential role in T-cell proliferation, survival, and activation (11), knockout of autophagy-related protein ATG5 displayed no influence on T-cell development in the thymus (12). In addition, autophagy contributes significantly to MHC II antigen presentation, but not to MHC II expression (13–16). However, in the process of long-term homozygous breeding, $lc3b^{-/-}$ mice exhibited an *H2-Aa* spontaneous point mutation and consequent MHC II loss and $CD4^+$ T-cell deficiency.

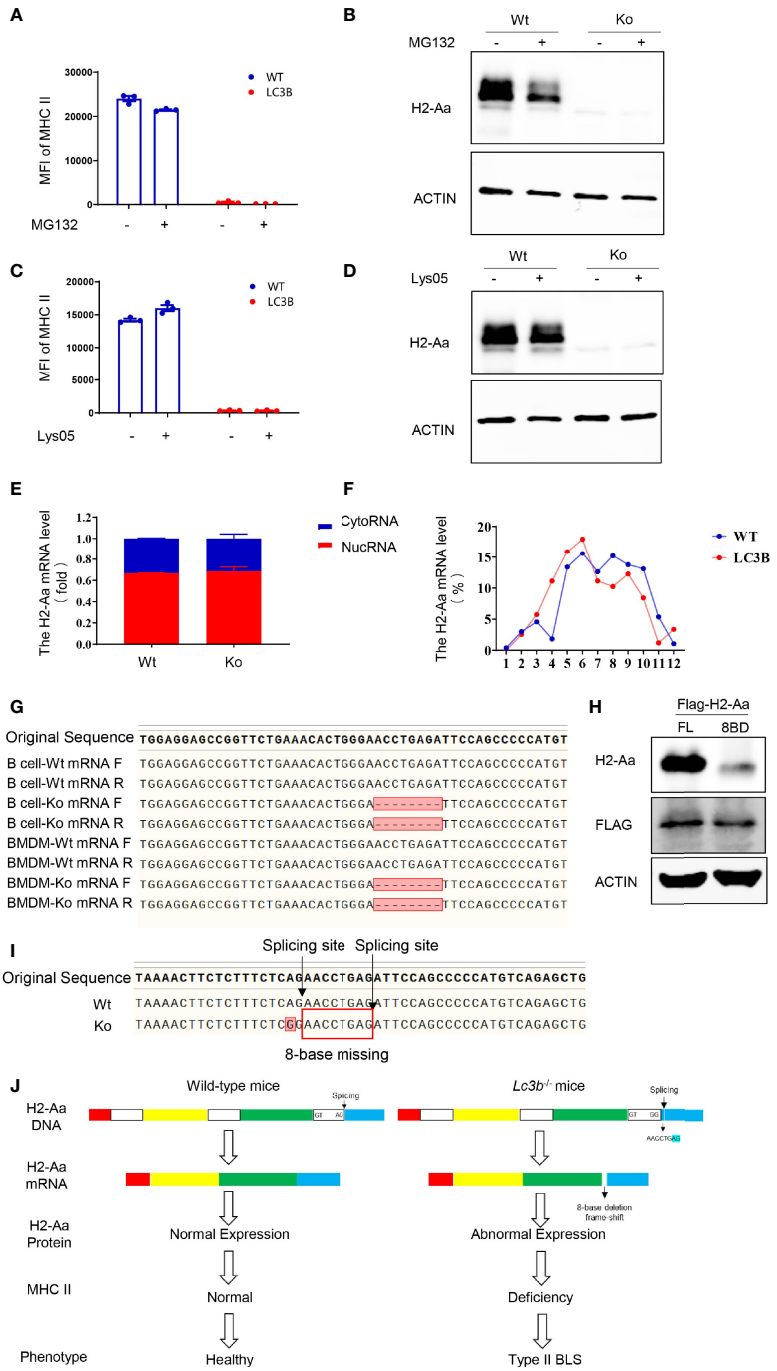

FIGURE 4 | A point mutation on H2-Aa results in pre-mRNA false splicing and protein frameshift in this specific mouse strain. **(A, B)** MHC II **(A)** and H2-Aa **(B)** expression of B cells treated with MG132 in wild-type and knockout mice. **(C, D)** MHC II **(C)** and H2-Aa **(D)** expression of B cells treated with Lys05 in wild-type and knockout mice. **(E)** Respective H2-Aa expression in the nucleus and cytoplasm in B cells of wild-type and knockout mice. **(F)** Analysis of ribosome profiles of B cells in wild-type mice and knockout mice and H2-Aa expression was detected at each stage of ribosome using quantitation real-time PCR. **(G)** Forward and reverse sequences of B cells and bone marrow-derived macrophage cDNA in wild-type and knockout mice were obtained and aligned. **(H)** 293T cells were transfected with full-length or eight-base deletion Flag-H2-Aa plasmid and the expressions of Flag and H2-Aa were detected by Western blot. **(I)** DNA of bone marrow-derived macrophages in wild-type and knockout mice was isolated and sequences were aligned. A point mutation was observed and it could induce wrong pre-mRNA splicing and deletion of eight bases in mRNA. **(J)** The molecular biology model of type II BLS phenotype in *lc3b*$^{-/-}$ mice. A mutation from A to G caused the splicing recognition to malfunction until the next AG position Therefore, in *lc3b*$^{-/-}$ mice, wrong pre-mRNA splicing, deletion of eight bases in mRNA, and frameshift of H2-Aa protein eventually resulted in the loss of H2-Aa protein and subsequent immunodeficiency. Data **(A, C)** are replicated in three independent experiments. Error bars, mean ± SEM.

However, why this mutation occurs in these knockout mice and whether the mutated gene and mutation site are specific remain to be clarified. A previous study revealed a relationship between autophagy and DNA damage. Autophagy plays an important role in DNA damage response (DRR) and autophagy is induced during DDR. Autophagy is crucial to genome stability and inhibiting autophagy may induce genomic instability and DNA damage response (17, 18). Thus, it is plausible that the mutation observed in *lc3b*$^{-/-}$ mice might have resulted from genomic instability; however, this requires further investigation.

We observe that CD4^{+} T-cell deficiency in this knockout mouse strain resulted from a reduction in MHC II expression. In addition, there were fewer thymus epithelial cells in the knockout mice than in the wild-type controls. However, we could not conclude that the reduced number of TECs resulted from the lack of MHC class II. Saldana et al. found that sonic hedgehog can regulate the differentiation of thymus epithelial cells. Conditional deletion of sonic hedgehog from TECs in the adult thymus results in alterations in TEC differentiation and consequent changes in T-cell development. Although TEC numbers are reduced, the cell surface expression of MHC II on medullary TECs was increased (19). This suggests that there is no direct relationship between thymus epithelial cell differentiation and MHC II expression. Therefore, in this study, the reduction of TEC number in this knockout mouse strain may be at least partially independent of MHC II deficiency induced by the *H2-Aa* point mutation. Theoretically, both MHC II deficiency and loss of TEC can impair CD4^{+} T-cell development. In the current study, we focused on the mechanistic study of MHC II deficiency, but paid little attention to the mechanisms of TEC loss. Liang et al. demonstrated that mTOR is essential for TEC development and maturation by regulating proliferation and Wnt signaling activity through autophagy (20). Thus, LC3B or autophagy could contribute to the reduction of thymus epithelial cells.

In this study, H2-Aa loss led to MHC II deficiency in *lc3b*$^{-/-}$ mice. In B cells and BMDC, the mRNA levels of H2-Ab1 were slightly but not significantly decreased in the knockout mice; however, the protein levels were significantly decreased compared with the wild-type controls. Interestingly, IFN-γ could induce the expression of H2-Ab1, for both mRNA and protein, in BMDM derived from *lc3b*$^{-/-}$ mice. Besides, there were no mutations in H2-Ab1 (data not shown). It is not clear why the H2-Ab1 protein was decreased. One plausible explanation is that H2-Aa deficiency might lead to the function loss of H2-Ab1, and thus, the translated H2-Ab1 protein was degraded.

In this study, MG132 and Lys05 failed to rescue MHC II and H2-Aa deficiencies. This suggested that protein degradation is not the cause of H2-Aa reduction in knockout mice. In addition, we found that MG132 alone reduced the expression of H2-Aa. Tewari et al. demonstrated a cytosolic pathway for MHC class II-restricted antigen processing, which was dependent on the proteasome and TAP (21). Bhat et al. further pointed out that Sug1, a 19S proteasome ATPase, played a critical role in the transcription of MHC class II, and the absence of the ATPase-binding domain increased the half-life of CIITA, but blocked MHC class II surface expression (22). These studies demonstrated the intimate connection between MHC II expression and the proteasome. These results are consistent with those of previous studies and provide a useful complement. The molecular mechanisms underlying the proteasome-dependent regulation of H2-Aa expression need to be clarified further.

MHC II is a crucial immune regulator, whose abnormal expression can lead to immune deficiency. Type II BLS is a rare, autosomal recessive immunodeficiency disease. Cells from typical type II BLS patients lack constitutive and inducible expression of all MHC II genes, similar to the phenotype observed in *lc3b*$^{-/-}$ mice used in this study. Therefore, these patients exhibited severely impaired T-cell activation and significantly reduced CD4^{+} cell number. The MHC II genes have two loci in mice: I-A and I-E. Mice of the H2b haplotype lack the expression of MHC II Ea molecule due to a loss-of-function deletion of about 600 bp in the promoter and first exon of the Ea gene, which results in the deficiency of I-E (23). However, our RNA-seq results showed that the mice used in this study exhibited a rather lower H2-Ea expression compared with H2-Aa (data not shown), indicating that the MHC II expression in these cells and mice was principally based on H2-IA. Therefore, this study focused on H2-IA, but not on H2-IE. To date, due to the lack of I-A, each type II BLS patient has a specific defect in a transcription factor that is necessary for MHC class II expression. Wiszniewski et al. described a family with an L469 mutation in *CIITA* that presented as an attenuated case, accompanied by residual MHC II expression in their report (24). Apart from *CIITA*, genes such as *RFXANK*, *RFX5*, and *RFXAP* were also affected in patients with type II BLS. The proteins encoded by these genes formed a complex that regulated the expression of MHC II. Some atypical cases still exist where the genetic defect is undefined. In this study, we observed a new paradigm of type II BLS in *lc3b*$^{-/-}$ mice, demonstrating a mechanism that is different from those reported in previous studies. Although these findings were observed in mice, this study provides a new potential mechanism of type II BLS.

Pre-mRNA splicing is required for the maturation of mRNA. The key to recognition of pre-RNA splicing is to determine the splicing site, which complies with the GT-AG rule. The composition of the 5′ splice site, or donor splice site, includes a nearly invariant "GT" dinucleotide sequence along with less conserved residues downstream. In rare cases, a "GC" dinucleotide also can be documented to serve as the 5′ splice site, while an "AG" at the 3′ end is required in the 3′ splice site or in the acceptor splice site (25). In this study, a point mutation from A to G at the 3′ end of H2-Aa caused the splicing recognition to malfunction until the next AG position, which induced the deletion of eight bases in mRNA and the eventual loss of this protein. The eight-base deletion appeared in the origination of exon 5 and led to a change in the amino acid sequences of this exon. We noted that the transmembrane domain and intracellular domain of H2-Aa were both located in this exon, and abnormal transmembrane domain could greatly influence the expression of the H2-Aa protein, likely resulting in the almost complete absence of H2-Aa in knockout mice.

In summary, we observed a spontaneous *H2-Aa* point mutation in mice obtained from the homozygous breeding of *lc3b*$^{-/-}$ mice. This mutation induced the errant splicing of pre-mRNA, eight-base deletion of mRNA, frameshift of protein, and consequent deficiency of MHC II. However, whether LC3B or autophagy specifically contributed to this point mutation requires further investigation.

MATERIALS AND METHODS

Mice

Lc3b$^{-/-}$ and OT-II mice (C57BL/6) were originally obtained from the Jackson Laboratory and housed at Zhejiang University Laboratory Animal Center. *Lc3b*$^{-/-}$ mice were bred homozygously for approximately 10 generations. More detailed information on the animal experiments is provided below. All experimental protocols were approved by the Ethical Committee for Animal Studies at Zhejiang University in 2021. The animal ethics approval number was ZJU20210302 and the period of validity was 4 years.

Antibodies and Primers

Antibodies used for flow cytometry were purchased from eBioscience (San Diego, U.S.A.): CD4 (GK1.5), CD8 (53-6.7), CD45 (30-F11), CD326 (G8.8), MHC II (M5/114.15.2), and B220 (RA3-6B2). The antibodies used for Western blot were as follows: Calregulin and Histone H3 were obtained from Santa Cruz Biotechnology (Dallas, U.S.A.), Flag (D190828) was purchased from Sangon Biotech (Shanghai, China), and H2-Aa (A18325) and H2-Ab1 (A18658) were custom-made from ABclonal Technology (Wuhan, China). The antibody CD326 for IF was obtained from Santa Cruz Biotechnology. The primers used for quantitative real-time PCR were as follows: *Actb* forward: 5′-AGAGGGAAATCGTGCGTGAC-3′, reverse: 5′-CAATAGTGATGACCTGGCCGT-3′; *H2-Aa* forward: 5′-CTGACCACCATGCTCAGCCTCT-3′, reverse: 5′-TACTGGCCAATGTCTCCAGGAG-3′; *H2-Ab1* forward: 5′-ACCCAGCCAAGATCAAAGTGC-3′, reverse: 5′-TGCTCCACGTGACAGGTGTAGA-3′; *Malat1* forward: 5′-CACTTGTGGGGAGACCTTGT-3′, reverse: 5′-GTTACCAGCCCAAACCTCAA-3′; *U6* forward: 5′-CGCTTCGGCAGCACATATACTAAAATTGGAAC-3′, reverse: 5′-GCTTCACGAATTTGCGTGTCATCCTTGC-3′. The primers used for sequencing were as follows: DNA sequencing: 5′-GTGTGTATGAGCTCTGTCATCTTCTGCACTT-3′, reverse: 5′-TCATAAAGGCCCTGGGTGTCT-3′; cDNA sequencing: forward: 5′-CTGACCACCATGCTCAGCCTCT-3′, reverse: 5′-TCATAAAGGCCCTGGGTGTCT-3′.

Preparation of B Cells, Dendritic Cells, and Bone Marrow-Derived Macrophages

B cells were isolated from mouse spleens using magnetic bead separation. Dendritic cells and macrophages were derived through bone marrow-induced differentiation. GM-CSF (20 ng/ml) was used for dendritic cell differentiation, while M-CSF (10 ng/ml) was used for macrophage differentiation. In addition, macrophages were subjected to IFN-γ (20 ng/ml) treatment to induce MHC II expression.

Bone Marrow Transfer

Bone marrow transfer (BMT) was performed by transplanting the total BMCs (5×10^6) from 8-week-old male mice (donor) into lethally irradiated (X-ray radiation at a dose of 8 Gy) 8-week-old male mice (recipient) through the tail vein. Phenotype analysis was conducted 2 months after BMT.

Nuclear and Cytoplasm Separation

The cell pellet was collected and suspended in 5× volume-cell-weight CE buffer (10 mM HEPES, pH 7.9, 1.5 mM MgCl2, 10 mM KCl, proteinase inhibitor cocktail, and fresh 0.075% NP-40). The cells were incubated on ice for 10 min and centrifuged at 1500rpm for 10 min at 4°C. The supernatant and pellet contained the cytoplasm and nuclei, respectively. The nuclei were with CE buffer without NP-40 to avoid cytoplasmic contamination. Moderate AG RNAex Pro Reagent was added for RNA extraction.

Ribosome Profile

Before collection, purified B cells were incubated with 100 μg/ml cycloheximide (CHX) for 5 min at 37°C. The cells were then washed twice with PBS containing 100 μg/ml CHX, 1× protease inhibitor cocktail, and 100 U RNase inhibitor and pelleted using centrifugation. Cell pellets were lysed in 500 μl lysis buffer (200 mM KCl, 15 mM $MgCl_2$, 20 mM HEPES pH 7.5, 0.5% Triton X-100, 100 μg/ml CHX, 100 U RNase inhibitor, 1× protease inhibitor cocktail, 1 mM DTT) and incubated for 15 min on ice and centrifuged at 14,000 rpm for 5 min at 4°C. The supernatants were layered over a 10%–50% sucrose gradient plus 100 μg/ml CHX, 1× protease inhibitor cocktail, and 1 mM DTT and centrifuged at 38,000 rpm for 2 h at 4°C using Beckmann Coulter SW41 Ti rotors. Gradients were fractionated using a BioComp Piston Gradient Fractionator with continuous A260 measurements. Twelve fractions were manually collected from each gradient.

Plasmid Transfection

Plasmid transfection was performed with polyethylenimine, linear MW 25,000 (Polysciences) following the manufacturer's protocol. Cells were seeded to each well of six-well plates for 24 h before transfection. The infection medium was replaced with fresh growth medium after being incubated with 293T cells for 36 h. Cells were collected for Western blot assay.

RNA Isolation and Quantitative Real-Time PCR Analysis

Total RNA was extracted from the total cellular, nuclei, cytoplasmic, and ribosomal fractions using AG RNAex Pro Reagent (AG21102). RNA was reverse-transcribed using Evo M-MLV RT Premix for qPCR (AG11706), and cDNA was used for quantitative real-time PCR with SYBR Green Premix Pro Taq HS qPCR Kit (AG11701) on a StepOne Real-Time PCR System (Applied Biosystems, Foster City, CA, USA) to determine the expression levels of mouse *H2-Aa*, *Malat1*, and *U6*. The products used above were purchased from Accurate Biotechnology (Hunan) Co., Ltd. (Changsha, China) and all procedures were

performed according to the manufacturer's protocol. The data were normalized to *Actb* expression levels. The primers used are listed above.

Western Blot Assay

Cells were prepared with RIPA lysis buffer (Beyotime, Shanghai, China, P0013B) in the presence of protease inhibitor cocktail (Roche Diagnostics GmbH, 04-693-116-001). Lysates were loaded to SDS–PAGE and immunoblotted with relevant antibodies using standard methods.

Flow Cytometry

Cytoflex (Beckman Coulter) was used to identify cell surface markers. Cell sorting was performed by Moflo Astrios EQ (Beckman Coulter). All the results were analyzed by CytExpert or FlowJo X software. Fluorescence-conjugated antibodies are listed above.

Immunofluorescence Staining

Thymus tissues were embedded in the optimal cutting temperature (OCT) and cut into 6 μm pieces at −20°C for immunofluorescence staining. The frozen sections were stained with anti-CD326 according to the manufacturer's protocol. Fluorescent images were captured with an Olympic FV3000 laser scanning confocal microscope.

Statistical Analyses

Statistical tests were performed using GraphPad Prism software (version 9.0; San Diego, CA, USA). Data were assessed using a parametric statistical test (*t*-test for differences between two groups, one-way ANOVA for those between multiple groups) and presented as mean ± SEM. Differences were considered significant if $P \leq 0.05$ (*), $P \leq 0.01$ (**), $P \leq 0.001$ (***), and $P \leq 0.0001$ (****).

DATA AVAILABILITY STATEMENT

The original contributions presented in the study are included in the article/**Supplementary Material**. Further inquiries can be directed to the corresponding authors.

ETHICS STATEMENT

The animal study was reviewed and approved by the Ethical Committee for Animal Studies at Zhejiang University. Written informed consent was obtained from the owners for the participation of their animals in this study.

AUTHOR CONTRIBUTIONS

H-HS, Z-HC, and LW designed and supervised the study. YZ, JX, H-XC, MZ, L-NZ, Y-FW, W-JL, XF, FL, and CZ performed the experiments. WL and S-MY supervised the experiments. YZ and JX prepared the figures. YZ, H-HS, Z-HC, and LW drafted the manuscript. All authors contributed to the article and approved the submitted version.

FUNDING

This work was supported by the Major Project (82090012 to H-HS), General Projects (31970826 to Z-HC), and Key Project (81930003 to H-HS) from the National Natural Science Foundation of China, and the Major Project from the Natural Science Foundation of Zhejiang Province (LD21H010001 to Z-HC).

SUPPLEMENTARY MATERIAL

The Supplementary Material for this article can be found online at: https://www.frontiersin.org/articles/10.3389/fimmu.2022.810824/full#supplementary-material

Supplementary Figure 1 | The $CD4^+$ T cell deficiency of the mice is independent of the original gene knockout. **(A, C)** Representative images of flow cytometry of thymus **(A)** and spleen**(C)** in wild-type and original knockout mice. **(B, D)** Proportion of $CD4^+$ T cells in thymus **(B)** and spleen **(D)** in wild-type and original knockout mice. Data **(B, D)** are representative of 3–4 mice for each group. Error bars, mean ± SEM.

Supplementary Figure 2 | $CD4^+$ TCR overexpression fails to rescue $CD4^+$ T cell deficiency in the specific mouse strain. **(A, B)** Knockout mice were crossbred with OT-II mice to get four genotypes: Wt mice, Ko mice, OT-II mice, and OT-II- Ko mice. T cell population detecting using flow cytometry of thymus **(A)** and spleen**(B)** in these four genotypes.

Supplementary Figure 3 | Quality control of cytoplasmic separation and ribosome profile. **(A)** The respective nuclear and cytoplasmic *Malat1* expression of in B cells of wild-type and knockout mice. **(B)** Calregulin and Histone H3 expression in nuclear and cytoplasm extracts for quality control of cytoplasmic separation. **(C)** Ribosome profile of B cells in wild-type and knockout mice. **(D)** *U6* expression in each stage of ribosome for quality control of ribosome profile.

REFERENCES

1. Dixon AM, Roy S. Role of Membrane Environment and Membrane-Spanning Protein Regions in Assembly and Function of the Class II Major Histocompatibility Complex. *Hum Immunol* (2019) 80:5–14. doi: 10.1016/j.humimm.2018.07.004
2. Roche PA, Furuta K. The Ins and Outs of MHC Class II-Mediated Antigen Processing and Presentation. *Nat Rev Immunol* (2015) 15:203–16. doi: 10.1038/nri3818
3. Neefjes J, Jongsma ML, Paul P, Bakke O. Towards a Systems Understanding of MHC Class I and MHC Class II Antigen Presentation. *Nat Rev Immunol* (2011) 11:823–36. doi: 10.1038/nri3084
4. Li W, Kim MG, Gourley TS, McCarthy BP, Sant'Angelo DB, Chang CH. An Alternate Pathway for CD4 T Cell Development: Thymocyte-Expressed MHC Class II Selects a Distinct T Cell Population. *Immunity* (2005) 23:375–86. doi: 10.1016/j.immuni.2005.09.002
5. Reith W, LeibundGut-Landmann S, Waldburger JM. Regulation of MHC Class II Gene Expression by the Class II Transactivator. *Nat Rev Immunol* (2005) 5:793–806. doi: 10.1038/nri1708
6. Reith W, Mach B. The Bare Lymphocyte Syndrome and the Regulation of MHC Expression. *Annu Rev Immunol* (2001) 19:331–73. doi: 10.1146/annurev.immunol.19.1.331

7. Zuniga-Pflucker JC. T-Cell Development Made Simple. *Nat Rev Immunol* (2004) 4:67–72. doi: 10.1038/nri1257
8. Takaba H, Takayanagi H. The Mechanisms of T Cell Selection in the Thymus. *Trends Immunol* (2017) 38:805–16. doi: 10.1016/j.it.2017.07.010
9. Wright KL, Ting JP. Epigenetic Regulation of MHC-II and CIITA Genes. *Trends Immunol* (2006) 27:405–12. doi: 10.1016/j.it.2006.07.007
10. Ting JP, Trowsdale J. Genetic Control of MHC Class II Expression. *Cell* (2002) 109 Suppl:S21–33. doi: 10.1016/S0092-8674(02)00696-7
11. Bronietzki AW, Schuster M, Schmitz I. Autophagy in T-Cell Development, Activation and Differentiation. *Immunol Cell Biol* (2015) 93:25–34. doi: 10.1038/icb.2014.81
12. Pua HH, Dzhagalov I, Chuck M, Mizushima N, He YW. A Critical Role for the Autophagy Gene Atg5 in T Cell Survival and Proliferation. *J Exp Med* (2007) 204:25–31. doi: 10.1084/jem.20061303
13. Dengjel J, Schoor O, Fischer R, Reich M, Kraus M, Muller M, et al. Autophagy Promotes MHC Class II Presentation of Peptides From Intracellular Source Proteins. *Proc Natl Acad Sci USA* (2005) 102:7922–7. doi: 10.1073/pnas.0501190102
14. Schmid D, Pypaert M, Munz C. Antigen-Loading Compartments for Major Histocompatibility Complex Class II Molecules Continuously Receive Input From Autophagosomes. *Immunity* (2007) 26:79–92. doi: 10.1016/j.immuni.2006.10.018
15. Paludan C, Schmid D, Landthaler M, Vockerodt M, Kube D, Tuschl T, et al. Endogenous MHC Class II Processing of a Viral Nuclear Antigen After Autophagy. *Science* (2005) 307:593–6. doi: 10.1126/science.1104904
16. Ireland JM, Unanue ER. Autophagy in Antigen-Presenting Cells Results in Presentation of Citrullinated Peptides to CD4 T Cells. *J Exp Med* (2011) 208:2625–32. doi: 10.1084/jem.20110640
17. Chao T, Shih HT, Hsu SC, Chen PJ, Fan YS, Jeng YM, et al. Autophagy Restricts Mitochondrial DNA Damage-Induced Release of ENDOG (Endonuclease G) to Regulate Genome Stability. *Autophagy* (2021) 17 (11):3444–60. doi: 10.1080/15548627.2021.1874209
18. Galati S, Boni C, Gerra MC, Lazzaretti M, Buschini A. Autophagy: A Player in Response to Oxidative Stress and DNA Damage. *Oxid Med Cell Longev* (2019) 2019:5692958. doi: 10.1155/2019/5692958
19. Saldana JI, Solanki A, Lau CI, Sahni H, Ross S, Furmanski AL, et al. Sonic Hedgehog Regulates Thymic Epithelial Cell Differentiation. *J Autoimmun* (2016) 68:86–97. doi: 10.1016/j.jaut.2015.12.004
20. Liang Z, Zhang L, Su H, Luan R, Na N, Sun L, et al. MTOR Signaling is Essential for the Development of Thymic Epithelial Cells and the Induction of Central Immune Tolerance. *Autophagy* (2018) 14:505–17. doi: 10.1080/15548627.2017.1376161
21. Tewari MK, Sinnathamby G, Rajagopal D, Eisenlohr LC. A Cytosolic Pathway for MHC Class II-Restricted Antigen Processing That is Proteasome and TAP Dependent. *Nat Immunol* (2005) 6:287–94. doi: 10.1038/ni1171
22. Bhat KP, Truax AD, Brooks JK, Greer SF. Association of the 19S Proteasomal ATPases With the ATPase-Binding Domain of CIITA Is Essential for CIITA Stability and MHC Class II Expression. *Immunol Cell Biol* (2010) 88:807–16. doi: 10.1038/icb.2010.45
23. Hannestad K, Scott H. The MHC Haplotype H2b Converts Two Pure Nonlupus Mouse Strains to Producers of Antinuclear Antibodies. *J Immunol* (2009) 183:3542–50. doi: 10.4049/jimmunol.0900579
24. Wiszniewski W, Fondaneche MC, Le Deist F, Kanariou M, Selz F, Brousse N, et al. Mutation in the Class II Trans-Activator Leading to a Mild Immunodeficiency. *J Immunol* (2001) 167:1787–94. doi: 10.4049/jimmunol.167.3.1787
25. Montes M, Sanford BL, Comiskey DF, Chandler DS, Splicing RNA. And Disease: Animal Models to Therapies. *Trends Genet* (2019) 35:68–87. doi: 10.1016/j.tig.2018.10.002

Conflict of Interest: JX was employed by Qihan Bio Inc.

The remaining authors declare that the research was conducted in the absence of any commercial or financial relationships that could be construed as a potential conflict of interest.

Publisher's Note: All claims expressed in this article are solely those of the authors and do not necessarily represent those of their affiliated organizations, or those of the publisher, the editors and the reviewers. Any product that may be evaluated in this article, or claim that may be made by its manufacturer, is not guaranteed or endorsed by the publisher.

frontiers in Immunology

ORIGINAL RESEARCH
published: 30 March 2022
doi: 10.3389/fimmu.2022.847617

Computer-Based Immunoinformatic Analysis to Predict Candidate T-Cell Epitopes for SARS-CoV-2 Vaccine Design

Xueyin Mei[1†], *Pan Gu*[2†], *Chuanlai Shen*[3], *Xue Lin*[4*] *and Jian Li*[1*]

[1] Key Laboratory of Developmental Genes and Human Disease, Ministry of Education, School of Life Science and Technology, Southeast University, Nanjing, China, [2] Department of Math and Computer Sciences, College of Letters and Science, University of Wisconsin–Madison, Madison, WI, United States, [3] Department of Microbiology and Immunology, Medical School of Southeast University, Nanjing, China, [4] Department of Bioinformatics, School of Biomedical Engineering and Informatics, Nanjing Medical University, Nanjing, China

OPEN ACCESS

Edited by:
Iñaki Alvarez,
Universitat Autònoma de Barcelona, Spain

Reviewed by:
Hadida Yasmin,
Cooch Behar Panchanan Barma University, India
Masanori Matsui,
Saitama Medical University, Japan

***Correspondence:**
Xue Lin
xue.lin@njmu.edu.cn
Jian Li
jianli2014@seu.edu.cn

[†]These authors have contributed equally to this work

Specialty section:
This article was submitted to Antigen Presenting Cell Biology, a section of the journal Frontiers in Immunology

Received: 03 January 2022
Accepted: 28 February 2022
Published: 30 March 2022

Citation:
Mei X, Gu P, Shen C, Lin X and Li J (2022) Computer-Based Immunoinformatic Analysis to Predict Candidate T-Cell Epitopes for SARS-CoV-2 Vaccine Design. Front. Immunol. 13:847617. doi: 10.3389/fimmu.2022.847617

Since the first outbreak of coronavirus disease 2019 (COVID-19), caused by severe acute respiratory syndrome coronavirus 2 (SARS-CoV-2) in 2019, its high infectivity led to its prevalence around the world in an exceptionally short time. Efforts have been made to control the ongoing outbreak, and among them, vaccine developments are going on high priority. New clinical trials add to growing evidence that vaccines from many countries were highly effective at preventing SARS-CoV-2 virus infection. One of them is B cell-based vaccines, which were common during a pandemic. However, neutralizing antibody therapy becomes less effective when viruses mutate. In order to tackle the problem, we focused on T-cell immune mechanism. In this study, the mutated strains of the virus were selected globally from India (B.1.617.1 and B.1.617.2), United Kingdom (B.1.1.7), South Africa (B.1.351), and Brazil (P.1), and the overlapping peptides were collected based on mutation sites of S-protein. After that, residue scanning was used to predict the affinity between overlapping peptide and HLA-A*11:01, the most frequent human leukocyte antigen (HLA) allele among the Chinese population. Then, the binding free energy was evaluated with molecular docking to further verify the affinity changes after the mutations happen in the virus genomes. The affinity test results of three epitopes on spike protein from experimental validation were consistent with our predicted results, thereby supporting the inclusion of the epitope $_{374}$FSTFKCYGL$_{382}$ in future vaccine design and providing a useful reference route to improve vaccine development.

Keywords: SARS-CoV-2, S protein, T-cell epitopes, molecular docking, vaccine

INTRODUCTION

Coronavirus disease 2019 (COVID-19) caused by severe acute respiratory syndrome coronavirus 2 (SARS-CoV-2) has been and is still a large threat to human health. Its name comes from its crown-like spike protein structures. Although SARS-CoV-2 is found to share similar structures with other coronaviruses like SARS-CoV, its higher binding affinity to host cells makes it more transmissible

than others and more difficult to control. Its influence has spread to over 200 countries, and more than two billion people have suffered under its infection (1). Vaccines are proven to be one of the most effective ways to prevent the disease and help the world to recover. Around the world, more than 200 vaccine candidates are proposed (2). Besides traditional inactivated virus vaccines, forms of viral vector and subunit vaccine are emerging to increase protectiveness against the virus (1). Although some laudable effects have been achieved, other challenges, including the decreasing effectiveness of circulating vaccines against certain mutated strains of the virus and failure of long-term strong immunity, remain controversial (1). SARS-CoV-2 virus is composed of RNAs, and during its infection of cells, copying errors occur, which are called mutations (3). A group of viruses that possesses similar inherited traits is named as a variant. Due to their differences from the original virus, both prevention and treatment become challenging.

Four structural proteins, spike, membrane, envelope, and nucleocapsid, together form the SARS-CoV-2. Although studies have shown that T-cell epitopes on other proteins can also activate immune response and they can also be useful in vaccine development, compared to spike proteins, they are not as promising as spike proteins in many ways (4). SARS-CoV-2 binds with angiotensin-converting enzyme 2 (ACE2), and its spike (S) protein on the surface of virion mediates virus entry to host cells that is achieved by fusing viral and cellular membrane (1). S protein can be cleaved into S1 part and S2 part. S1 domain is responsible for receptor binding, and S2 protein participates in protein fusion (5). Part of S1 domain functioned as a receptor-binding domain (RBD) so when SARS-CoV-2 virus attacks target cells, such subdomain will bind to ACE2. Then, S2 domain can further process the binding (6). Therefore, mutations on S protein may change binding abilities of the virus and ACE2 and make people more vulnerable to infection. Moreover, study results revealed that over 1,800 mutations occurred on S protein of the virus, and some of the main mutations are a result of S protein mutations. Fortunately, by analyzing every mutation on the S protein, potential epitopes can be discovered and the importance of S protein in virus interaction with human cells makes it attractive to be used as a vaccine target (7).

T cells are found to have high correlations with providing immunity against SARS-CoV-2 virus. By targeting T cells, vaccines can trigger both acquired and innate immunity in human bodies (8). Human leukocyte antigen (HLA), as an integral part of viral antigen presentation pathway, plays a crucial role in the occurrence and development of infectious diseases. Virus-specific CD8+ T cells recognize HLA class I peptide complexes and induce apoptosis of infected cells to control viral infection. Recent studies have shown that individual HLA genotypes may differ in inducing T cell-mediated antiviral responses, with HLA-A*11:01 having a relatively high ability to present SARS-CoV-2 antigen. And individuals with HLA-1*11:01 genotype may trigger a more potent T cell-mediated antiviral response to SARS-CoV-2 (9). Therefore, our study aims to discover epitopes with potential to interact with HLA-A*11:01 commonly found in the Chinese population for vaccines to induce long-term immunity. In order to activate CD8+ T cells, potential T-cell epitopes, part of proteins that is in charge of such activation of human immune systems to fight against pathogens is needed to be discovered to be used in epitope-based vaccine designs (10). Traditionally, biology and chemistry experiments were used to find out the epitopes, but due to the high cost of experiments and advancement of technology, mass deployment of bioinformatic tools to provide reliable results and before using experiment as verification greatly lowers the cost and saves time of prediction (1). We started by comparing the S protein amino acid sequence of the original strain with that of variants, and with the help of proto-peptide overlapping peptide library, overlapping peptides covering the mutation site are generated for the next step. We filtered out the peptides with immunogenicity by using NetMHCpan 4.1 (https://www.cbs.dtu.dk/services/NetMHCpan/) to evaluate the affinity between these overlapping peptide and major histocompatibility complex (MHC) molecules and picked HLA peptides with matching amino acids and overlapping peptides with immunogenicity. Binding affinity after mutation between them is predicted by molecular mechanics-generalized Born surface area (MM-GBSA) residue scanning functionality of BioLuminate (version 1.0, Schrödinger, LLC, NY, USA, 2020-1), and pairs with a higher possibility to bind will be recorded. Additionally, molecular docking and dynamics simulation were used to verify the interaction result between protein and peptide. Finally, immunogenic peptide fragments were obtained by qualitative affinity test and physical and chemical properties of the vaccine (**Figure 1**). In this study, the prediction and screening of T-cell epitopes based on computer methods have opened up new doors for the design of effective vaccines.

MATERIALS AND METHODS

Extracting Data

Mutated strains with a high prevalence in the world are picked from India (B.1.617.1 and B.1.617.2), United Kingdom (B.1.1.7), South Africa (B.1.351), and Brazil (P.1). S protein genome sequences of these strains (Accession no. YP_0097243901.1) are downloaded from NCBI database (www.ncbi.nlm.nih.gov) since S protein is responsible for helping the virus enter host cells by their interactions with ACE2 (11). With help from GISAID (www.gisaid.org) and outbreak.info (https://outbreak.info/), we collected a total of 36 mutation sites in the S region of these epidemic variants.

Filtering Data

The receptor-binding domain (RBD) of SARS-CoV-2 spike protein plays a crucial role in binding to human ACE2, so our focus was on mutations in RBD regain (319-541AA). Side chains of amino acids can be classified as polar or non-polar and hydrophobic or hydrophilic, and because non-polar or weakly polar chains have difficulty interacting with water, they are

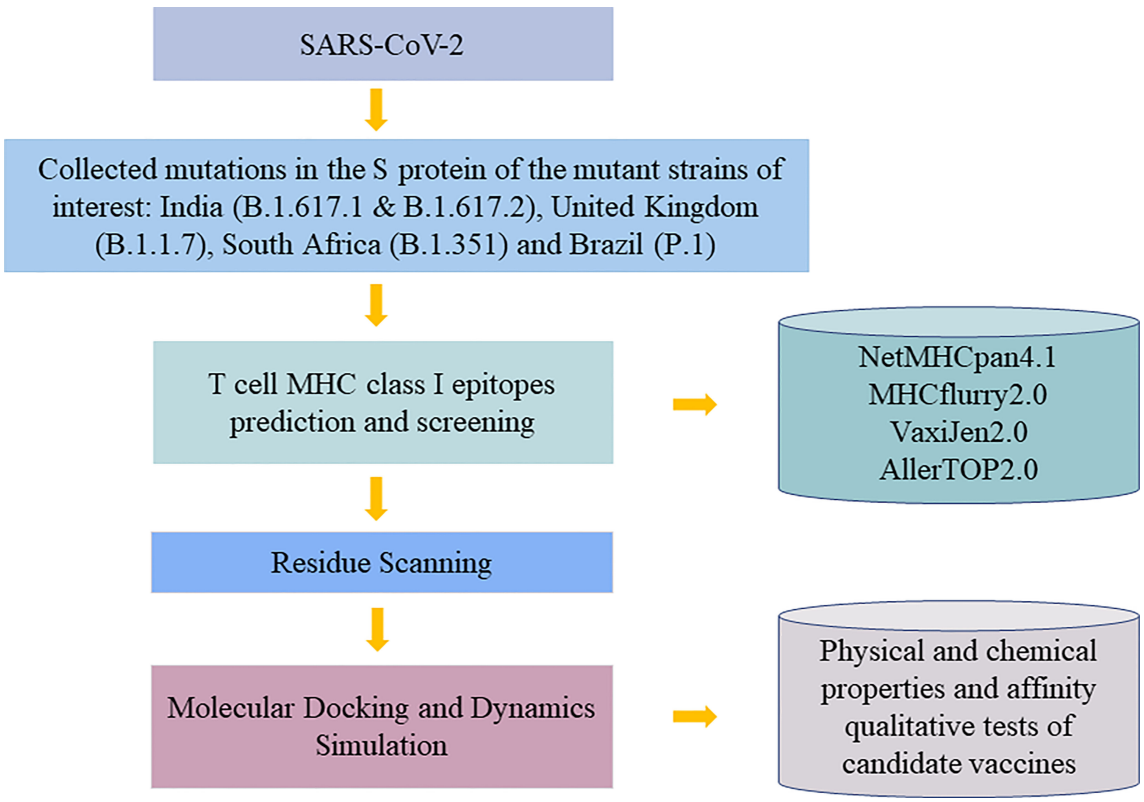

FIGURE 1 | Flowchart in the vaccine design study.

hydrophobic. Studies have shown that there are many hydrophobic amino acids on the site of antigen and antibody binding (12), so we also took the sites that are mutated into hydrophobic amino acids in the S protein as the research objects of interest. We hypothesized that epitopes generated based on these mutated sites as well as the mutated sites in the most immunogenic region of the S protein named RBD (13) might be more likely to be presented to the cell surface by MHC molecules and recognized by T cells. In addition, the high-frequency D614G mutation that appeared in these five variants was also considered to be interesting, since several studies emphasized the impact of D614G variant on transmission effectiveness (14). Therefore, a total of 18 mutations based on 16 sites were used for proto-peptide, resulting in a 19-length overlapping peptide containing the mutated site.

T-Cell Major Histocompatibility Complex Class I Epitope Prediction and Screening

In this study, HLA-A*11:01, the most common allele of HLA-I in the Chinese population, was selected for epitope prediction (15). MHC Class I restrictive CD8+ T cell-binding epitopes were identified by using NetMHCpan4.1 (https://services.healthtech.dtu.dk/). The peptide length was 8–14 mer, and the default thresholds of 0.5% strong binding agent and 2% weak binding agent were used to filter out peptide allele with binding affinity. To verify the result and increase accuracy, we also made use of MHCflurry2.0 tool (16) to predict the most possible MHC–peptide binding pairs. Thereafter, VaxiJen2.0 server (http://www.ddg-pharmfac.net/vaxijen/VaxiJen/VaxiJen.html) and AllerTOP v. 2.0 server (https://www.ddg-pharmfac.net/AllerTOP/) were used to screen candidate peptide epitopes with antigenicity and non-allergenicity.

Residue Scanning With Prime Molecular Mechanics-Generalized Born Surface Area

Human MHC-I molecules are highly polymorphic and have a specific peptide motif preference (17). In order to determine the HLA structure to which the immunogenic peptide is attached, we used residue scanning module with MM-GBSA method in Schrödinger software (LLC, NY, USA, 2020-1) to select structure with the strongest affinity as the subsequent docking receptor. The HLA 3D structure of this research was downloaded from Protein Data Bank (RCSB PDB) (https://www.rcsb.org/). According to binding properties of HLA polypeptides where the second position and the end position are significant binding sites, the HLA structure with high consistency with the amino acids in the binding pocket of the predicted epitope peptide was preferentially chosen to get mutation.

Binding affinity after mutation between immunogenic peptides and HLA-derived peptides is calculated by MM-GBSA Residue Scanning functionality of BioLuminate (version1.0, Schrödinger, LLC, NY, USA, 2020-1). Concurrent

mutations of all amino acids are allowed, and side-chain prediction with backbone sampling refinement is chosen. Although according to Schrödinger's official guide, the affinity calculated from the tool may not be consistent with the experimental result, the ranking of affinity result agrees with the experimental result. Therefore, a lower binding affinity represents stronger binding. Some studies used 3 kcal/mol to define places where mutations may have a strong influence on affinity (18). Here, we use 5 kcal/mol to define the boundary. Thus, after calculating affinity before and after mutations, mutations with an increase in affinity and value not greater than 5 kcal/mol are selected for the next step.

Molecular Docking

Glide (Schrödinger 2020-1 release) uses a series of hierarchical filters to search for possible favorable peptide interactions at receptor-binding sites (19). In molecular docking study, preprocessed HLA3D structure was used as the starting structure in Peptide Docking of Glide module, and the peptide poses were generated by inputting the sequence of epitopes. In the docking process, the binding sites of HLA peptides need to be defined, and the network box was generated to define the docking location. Using the Superposition workbench, the pose with the highest backbone similarity [lowest root mean square deviation (RMSD) value] with the original skeleton will be used for the next step.

Molecular Dynamics Simulation

For molecular dynamics (MD) simulation, maestro's Desmond module (Schrödinger 2020-1 release) was used. A system builder panel with the OPLS3e force field was used to set up a biological system before MD simulation. The SPC model of water considered for solvating the system and an orthorhombic box with a 10Å buffer distance was generated. In this work, a total of 100-ns MD simulation was running on a GPU at 300K temperature and 1.01325 bar pressure. Simulation Interaction Diagram shows the interaction of peptide–protein such as RMSD images that determine the stability of the complex. The simulated complex was visualized by Pymol software (version 2.0, Schrödinger, LLC) to observe the polar contacts between ligand and receptor.

Experimental Validation of Affinity Between Candidate Peptides and HLA-A*11:01

The Octet® system is based on Bio-Layer Interferometry (BLI) to screen and characterize molecular interactions (20). The binding affinities of HLA-A*11:01 protein and candidate epitopes were performed on the Octet R8 system (Sartorius, German). Biotinylated protein was immobilized on SSA sensors for 20 min, and the signal approached a height of about 4 nm. PBST buffer solution [phosphate buffered saline (PBS)+0.02%Tween20 +1% dimethyl sulfoxide (DMSO)] was utilized to dilute the peptides to 100, 50, 25, 12.5, 6.25, 3.125 μM, respectively. The whole polypeptide–protein interaction system was balanced, bound, and dissociated for 60 s, and the binding curve was drawn using Octet® analysis studio 12.2 software. The final epitopes were concluded from analyzing the physicochemical properties of the candidate epitopes obtained by ProtParam online tool of ExPASy server (https://web.expasy.org/protparam/) and the experimental results of affinity.

RESULTS

Amino Acid Mutation in S Region of Five Mutants

In this study, details about 16 mutation sites of interest on S protein obtained from five SARS-COV-2 variants are shown in **Figure 2**.

T-Cell Epitope Prediction and Analysis of Antigenicity and Hypersensitivity

A total of 38 potential T-cell epitopes were predicted by the NetMHCpan4.0 server and MHCflurry, which docked on the HLA-A*11:01 allele in an energy-favorable manner. Antigenicity was predicted using the VaxiJen tool, with a threshold of 0.4 for possible antigens (21). **Table 1** shows the antigenic and non-allergenic epitopes paired with HLA-A*11:01 after screening, and their VaxiJen scores resulted in the optimal 13 epitopes based on the 7 mutation sites.

Residue Scanning of Predicted CD8 T-Cell Epitopes With HLA-A*11:01

The anchor position of HLA self-binding peptides is mainly the second and terminal amino acids. Considering the properties and lengths of amino acids of the candidate epitopes, we selected the structure with the most similar peptide docking pattern from HLA-A*11:01 for amino acid mutation prediction. In this study, 57 affinity values that were obtained from these 13 epitopes are shown in **Table S1**. Here, we show the performance of each candidate epitope with HLA-A*11:01 receptor after initial screening (**Table 2**). Since a smaller affinity represents greater binding abilities of mutant bond than its parent protein, we filtered candidate epitopes with a threshold of △affinity of 5 kcal/mol (22) for further kinetic studies. During the analysis, $_{13}$SQCVNFTTR$_{21}$, which exhibited strong affinity with a change value of -10.06 kcal/mol, and peptide $_{378}$KCYGLSPTK$_{386}$, with △affinity value of 4.46 kcal/mol, were both included in the subsequent study. Inherent in this approach is the problem that some HLA structures like 5GRD cannot be directly mutated because two cysteines will form disulfide bonds, and candidate peptides are inconsistent with HLA self-binding peptides in number. To circumvent this, we directly performed molecular docking in Glide module of Schrödinger software (LLC, NY, USA, 2020-1) on these structures.

Molecular Dynamics Simulation of the Post-Docking Structure

Peptide Docking in the Biologics module of Schrödinger software was used to study the interaction between HLA molecules and

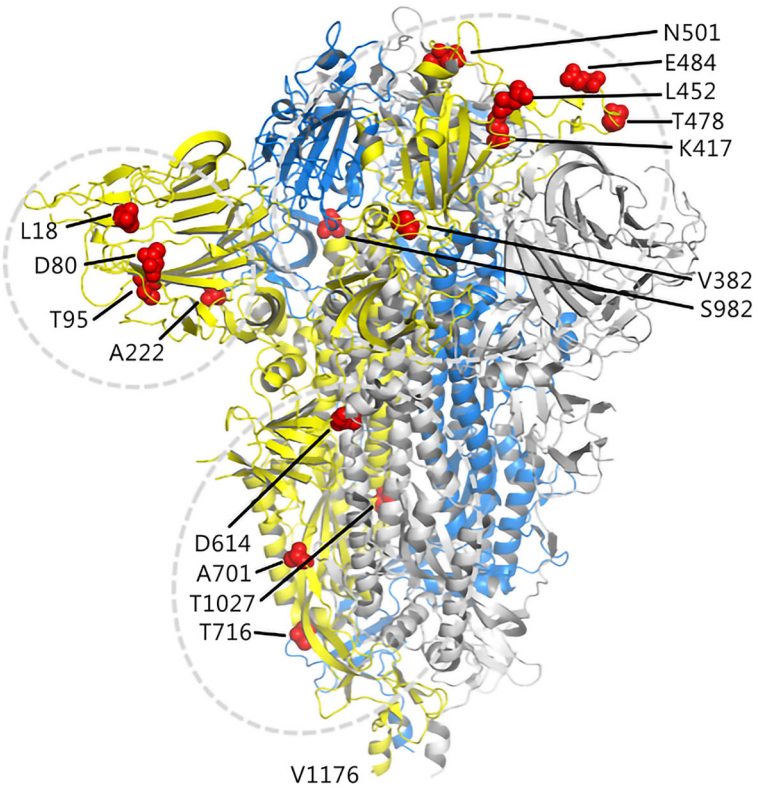

FIGURE 2 | Illustration of candidate sites on the S protein. The three chains of the trimer structure of S protein (PDB 7DF3) are shown in cartoon and represented as yellow, marine, and gray. The mutation sites of interest are shown as red spheres.

epitope peptides. The Docking result was reflected by the RMSD value of carbon skeleton. A smaller RMSD value indicates higher similarity in the structure of the docking peptide is with the conformation of the original HLA peptide (23), which allows for optimal matching of shapes and interactions between epitopes and HLA molecules. Following the screening after residue scanning calculation, seven epitopes and their wild-type peptides were docked with the corresponding HLA receptor, and the docked model was used as the initial structure of dynamics simulation.

In this work, Desmond module (Schrödinger 2020-1 release) was used to conduct 100-ns simulation, and RMSD values of the system provided a good estimate of whether the docking complex was in a stable state (24). Our study found that the RMSD values of the complexes of HLA-A*11:01 and the epitopes based on different mutation sites were different from those of the wild-type complexes. These complexes reach their own stable conformation at different times, and their stability might fluctuate slightly over time.

It was observed from **Figures 3A, B** that the stable conformation of $_{13}$SQCVNFTTTR$_{21}$-HLA-A*11:01(1Q94) complex was achieved at RMSD 1.7 Å. However, in the dynamic system before this epitope mutation, there is still a downward fluctuation until the last 50 ns. In the case of the RMSD of peptide $_{12}$SSQCVNFTTTR$_{21}$ compound with HLA-A*11:01 (5GRD), the interaction was observed to become stable and at ~1.25 Å in the end. Differently, the results of RMSD of $_{12}$SSQCVNLTTTR$_{21}$ complex displayed a substantial fluctuation between 0 and 100 ns. As for another HLA-A*11:01 crystal structure 2HN7 docking with $_{12}$SSQCVNFTTTR$_{21}$ epitope, the RMSD value of the complex showed a slight upward trend. We can also find it was unstable before the mutation (**Figures 3C–F**). In addition, **Figures 3G, H** represents that $_{444}$KVGGNYNYR$_{452}$-HLA-A*11:01(1QVO) complex has a large fluctuation. While assessing the RMSD of wild compound $_{444}$KVGGNYNYL$_{452}$-HLA-A*11:01(1QVO), the results of RMSD displayed a clear upward trend between 0 and 60 ns, but subsequently, the compound got stable.

As shown in **Figures 4A–F**, Compound HLA-A*11:01 (5GRD) and $_{381}$GLSPTKLNDL$_{390}$ attained 1.25Å RMSD at the beginning of simulation and remained stable between 1.25 and 1.5Å after 60 ns, while its wild system fluctuates slightly in the last 50 ns. In the case of $_{374}$FSTFKCYGL$_{382}$-HLA-A*11:01 (5GRD) complex, it was observed to have a steady increase from 0 to 50 ns in its RMSD result but subsequently stabilized between 1.25 and 2.0 Å after 50 ns, and its wild system is relatively balanced. Notably, the RMSD trajectories of complex consisting of $_{378}$KCYGLSPTK$_{386}$ exhibited a significant fluctuation in binding to the receptor of HLA-A*11:01(1X7Q). The complex reached ~2.4 Å from 0 to 35 ns; however, this value

TABLE 1 | T cell-predicted epitopes of selected mutation sites based on antigenicity and allergenicity.

MHC I Allele	Mutation Sites	Epitopes	VaxiJen Score	Antigenicity	Allergenicity
HLA-A*11:01	L18F	SQCVNFTTR	1.7440	Probable antigen	Non-allergen
		SSQCVNFTTR	1.7772	Probable antigen	Non-allergen
	T95I	GVYFASIEK	0.4008	Probable antigen	Non-allergen
	V382L	KCYGLSPTK	1.6366	Probable antigen	Non-allergen
		GLSPTKLNDL	1.7584	Probable antigen	Non-allergen
		FSTFKCYGL	0.5941	Probable antigen	Non-allergen
	K417T	GTIADYNYK	1.8607	Probable antigen	Non-allergen
		TGTIADYNYK	1.7029	Probable antigen	Non-allergen
	L452R	KVGGNYNYR	1.5212	Probable antigen	Non-allergen
	T1027I	ASANLAAIK	0.5724	Probable antigen	Non-allergen
	V1176F	GINASFVNIQK	0.9624	Probable antigen	Non-allergen
		INASFVNIQK	1.1168	Probable antigen	Non-allergen
		NASFVNIQK	1.2242	Probable antigen	Non-allergen

These red fonts represent mutated amino acids and are presented as single-letter abbreviations.

TABLE 2 | The performance of selected epitopes and HLA structures screened according to the minimum △affinity.

Mutation Sites	Epitopes	HLA-A*11:01 PDB ID	△ Affinity kcal/mol	△ Stability kcal/mol	△ Hydropathy	△ Prime Energy kcal/mol
L18F	SQCVNFTTR	1Q94	-10.06	15.78	1.59	-59.45
	SSQCVNFTTR	5GRD			Docking	
		2HN7	-1.46	40.9	2.46	-108.71
T95I	GVYFASIEK	1Q94	12.28	-4.83	1.31	28.19
V382L	KCYGLSPTK	1X7Q	4.46	6.74	1.98	-34.89
	GLSPTKLNDL	5GRD			Docking	
		2HN7	46.13	21.03	-0.10	-18.60
	FSTFKCYGL	5GRD			Docking	
		1Q94	48.44	28.29	0.82	105.10
K417T	GTIADYNYK	1Q94	24.29	16.60	-0.02	-9.39
	TGTIADYNYK	1QVO	45.73	4.00	-0.53	-32.80
L452R	KVGGNYNYR	1QVO			Docking	
		1X7Q	8.70	8.65	-0.74	-159.55
T1027I	ASANLAAIK	6JOZ	37.35	-0.85	0.19	14.91
V1176F	GINASFVNIQK	4MJ5	51.90	45.37	-1.86	7.21
	INASFVNIQK	1QVO	31.29	2.31	0.74	-53.95
	NASFVNIQK	6JOZ	27.27	5.48	1.55	-68.51

These red fonts represent mutated amino acids and are presented as single-letter abbreviations.

remarkably decreased after 35 ns and remained stable at 40~70 ns and finally stabilized around 1.6 Å after an upward fluctuation. Differently, the RMSD of its wild peptide $_{378}$KCYGVSPTK$_{386}$ compound with HLA-A*11:01(1X7Q) remained stable in the early stage, but fluctuated in the latter 20 ns.

MM-GBSA Calculates the Binding Free Energy

In order to determine the binding interaction between candidate epitopes and MHC-I molecules, we quantitatively evaluated the binding free energy of the peptide–HLA complex using MM-GBSA method (25). We obtained the MM-GBSA results of 1,000 frames of complex with 125 frames interval and selected the corresponding frame interval to calculate the average value according to the stable region of RMSD value of the optimized conformation by MD. As predicted in **Table 3**, our results demonstrate the changes in binding free energy of site-based epitopes before and after mutation. Except for epitopes $_{12}$SSQCVNFTTR$_{21}$ and $_{444}$KVGGNYNYR$_{452}$, the remaining mutation-based epitopes showed more favorable binding free energy than wild-type peptide, that is, more negative numerically. It is noteworthy that three candidate epitopes obtained by mutation V382L all showed favorable binding to HLA-A*11:01 after mutation. Among them, $_{374}$FSTFKCYGL$_{382}$ achieved the strongest binding free energy (-91.949 kcal/mol) after mutation among all candidate epitopes. In other words, these four peptides ($_{13}$SQCVNFTTR$_{21}$/$_{378}$KCYGLSPTK$_{386}$/$_{381}$GLSPTKLNDL$_{390}$/$_{374}$FSTFKCYGL$_{382}$) are more likely to bind to T cells.

Interaction Analysis of Candidate Epitopes

In the study, epitopes based on mutation L18F and V382L showed potential binding against HLA-A*11:01. In the case of L18F, epitope $_{13}$SQCVNFTTR$_{21}$ established six polar contacts with TYR9, GLU63, ASN66, GLN70, GLN155, and TYR159 of HLA-A*11:01(1Q94), while the wild one possessed one less interaction with residues ASP74, ASP77, ASP116, LYS146, and TRP147. From the perspective of the configuration of peptide binding to HLA, the candidate epitopes are more consistent with the conformation of peptide docking with HLA, which is convex in the middle and flat at both ends (**Figures 5A, B**).

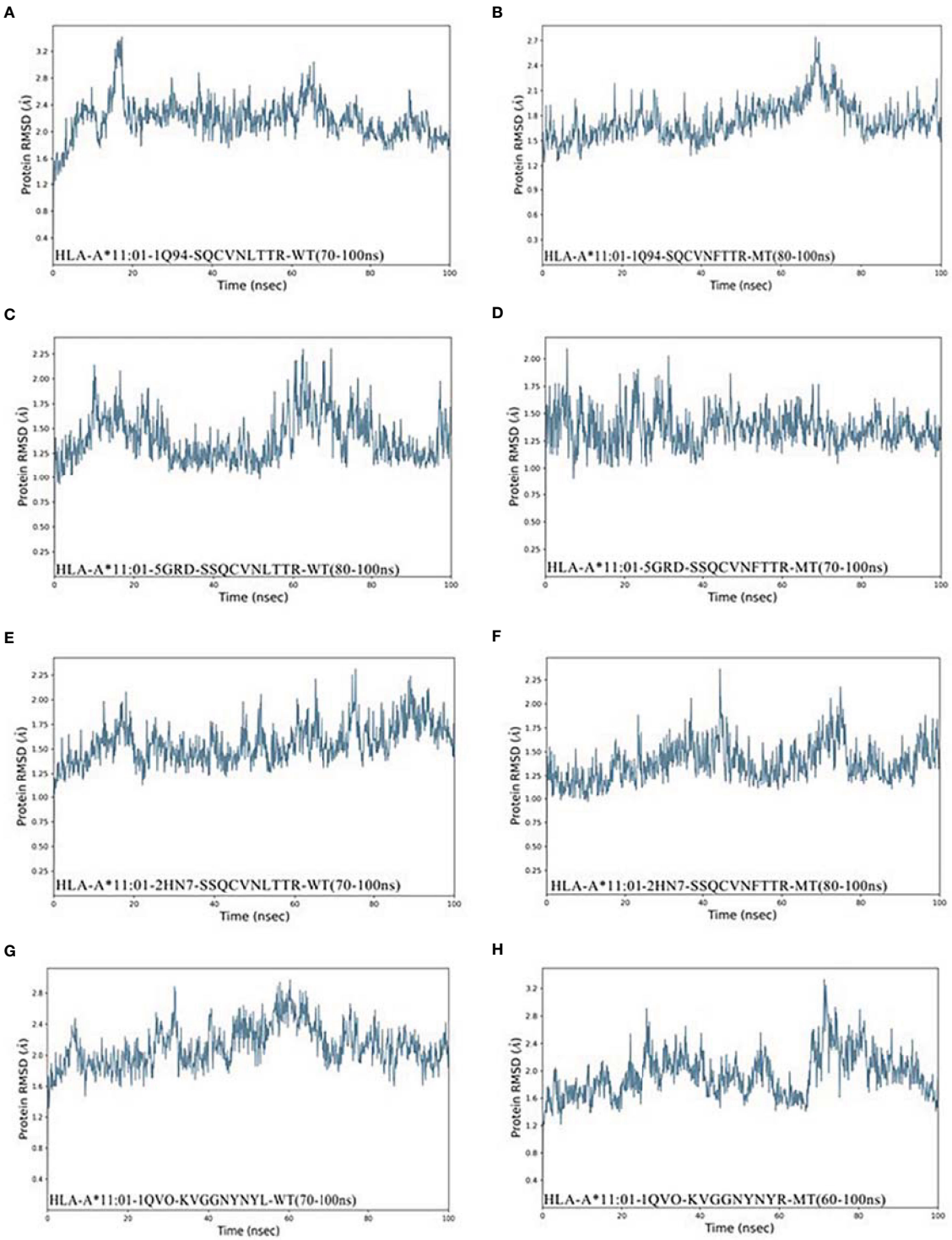

FIGURE 3 | RMSD plot of the HLA-A*11:01-epitopes, indicating stability. **(A)** HLA-A*11:01(1Q94)-SQCVNLTTR (WT). **(B)** HLA-A*11:01(1Q94)-SQCVNFTTR (MT). **(C)** HLA-A*11:01(5GRD)-SQCVNLTTR (WT). **(D)** HLA-A*11:01(5GRD)-SQCVNFTTR (MT). **(E)** HLA-A*11:01(2HN7)-SSQCVNLTTR (WT). **(F)** HLA-A*11:01(2HN7)-SSQCVNFTTR (MT). **(G)** HLA-A*11:01(1QVO)-KVGGNYNYL (WT). **(H)** HLA-A*11:01(1QVO)-KVGGNYNYR (MT). RMSD, root mean square deviation; MT, mutation type; WT, wild type.

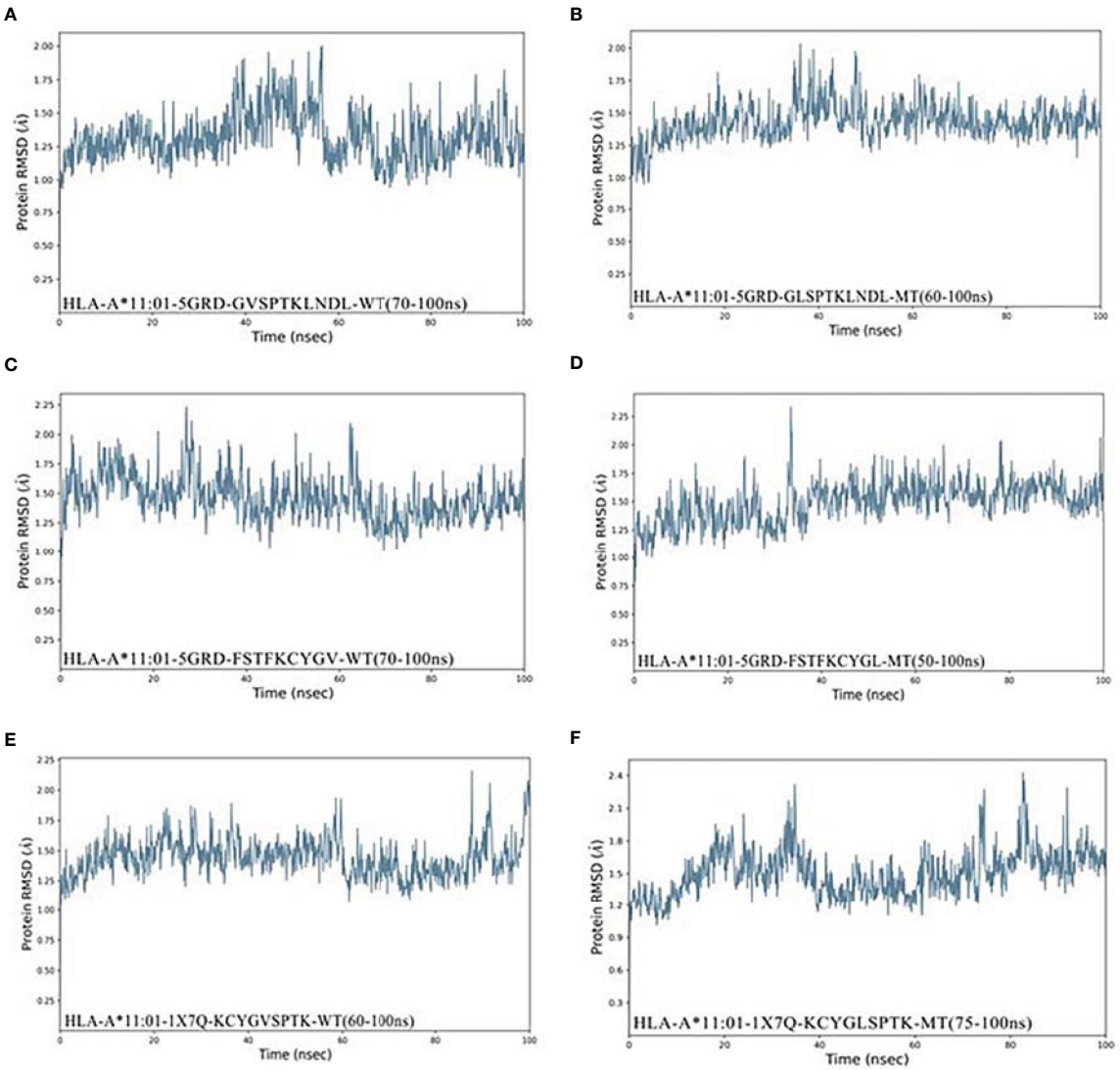

FIGURE 4 | RMSD plot of the HLA-A*11:01-epitopes based on V382L. **(A)** HLA-A*11:01(5GRD)-GVSPTKLNDL (WT). **(B)** HLA-A*11:01(5GRD)-GLSPTKLNDL (MT). **(C)** HLA-A*11:01(5GRD)-FSTFKCYGV (WT). **(D)** HLA-A*11:01(5GRD)-FSTFKCYGL (MT). **(E)** HLA-A*11:01(1X7Q)-KCYGVSPTK (WT). **(F)** HLA-A*11:01(1X7Q)-KCYGLSPTK (MT). RMSD, root mean square deviation; MT, mutation type; WT, wild type.

TABLE 3 | Results of binding free energy after MD simulation with HLA-A*11:01 and selected epitopes.

Mutation Sites	Epitopes	HLA-A*11:01 PDB ID	Binding Free Energy (WT) kcal/mol	Binding Free Energy (MT) kcal/mol
L18F	SQCVNFTTR	1Q94	-40.506	-78.177
	SSQCVNFTTR	5GRD	-88.204	-51.707
	SSQCVNFTTR	2HN7	-68.863	-57.243
	KCYGLSPTK	1X7Q	-60.699	-77.538
V382L	GLSPTKLNDL	5GRD	-54.390	-85.368
	FSTFKCYGL	5GRD	-36.461	-91.949
L452R	KVGGNYNYR	1QVO	-93.064	-49.170

These red fonts represent mutated amino acids and are presented as single-letter abbreviations.

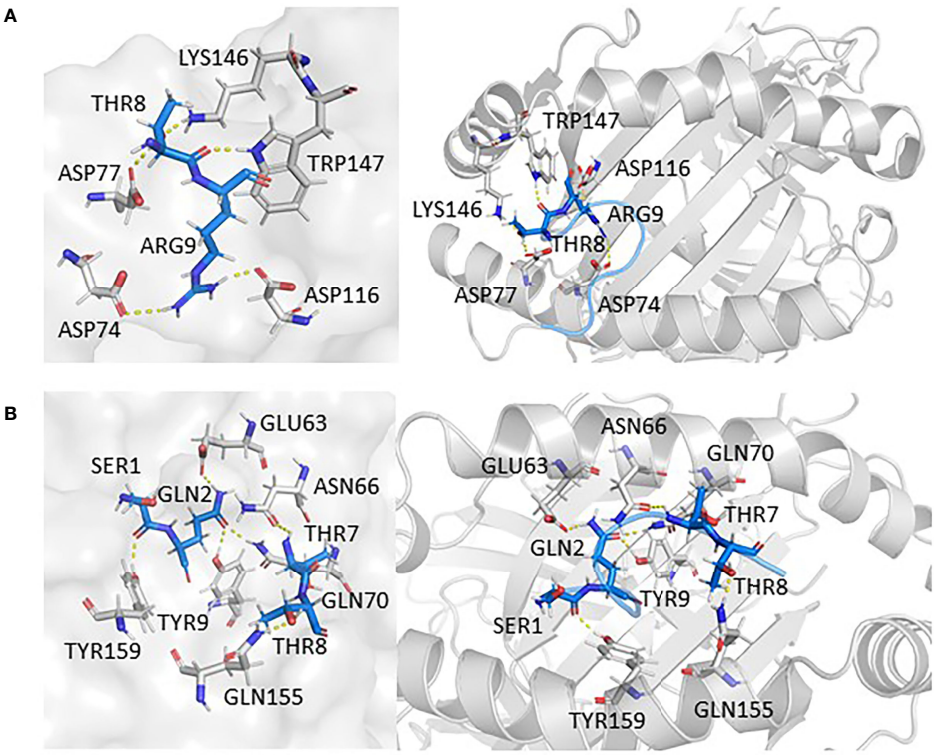

FIGURE 5 | The interaction between epitopes obtained from L18F and HLA-A*11:01. Here, epitopes are shown in marine, HLA structure is shown in gray. **(A)** HLA-A*11:01(1Q94)-SQCVNLTTR (WT). **(B)** HLA-A*11:01(1Q94)-SQCVNFTTR (MT). RMSD, root mean square deviation; MT, mutation type; WT, wild type.

In addition, findings within **Figures 6A–F** presented the interaction information of other epitopes from V382L. $_{381}$GLSPTKLNDL$_{390}$–HLA-A*11:01(5GRD) complex was stabilized by six polar contacts with amino acid residues GLN70, ASP77, TYR99, ASP116, and LYS146, while the wild one formed four bond interactions with residues ARG65 and ARG163 (**Figures 6A, B**). As for $_{374}$FSTFKCYGL$_{382}$, it possessed six polar contacts with residues ASN66, GLN70, GLN72, ASP77, ARG114, and GLN155 of HLA-A*11:01(5GRD), whereas its wild-type $_{374}$FSTFKCYGV$_{382}$ only had one interaction with residue GLN156 (**Figures 6C, D**). Another epitope peptide $_{378}$KCYGLSPTK$_{386}$ was also obtained based on V382L; it expressed six interactions with residues TYR9, GLU63, ASN66, TYR99, and GLN155 of HLA-A*11:01(1X7Q). By contrast, its wild type formed only four interactions (**Figures 6E, F**).

Physicochemical Properties and Affinity Experiments of Candidate Epitopes

Based on previous computer predictions, higher binding affinities to HLA-A*11:01 that may ultimately affect T-cell clearance were observed in four epitopes, and the results were further confirmed by BLI for assay analysis. After the biotinylated synthetic peptides were immobilized on the super streptavidin (SSA) sensor, the binding and dissociation curves were monitored in real time. As shown in **Figure 7**, dynamic fitting results indicate that the experiment is a typical process of fast combination and fast dissociation. Here we reported the affinities between the epitope $_{13}$SQCVNFTTR$_{21}$ and HLA molecule; its wild-type peptide and HLA molecule were not detected. However, the epitope peptides obtained based on V382L mutation showed relatively ideal affinity values, and the data exhibited a stronger binding between the mutant epitope and HLA molecule. It is worth noting that the epitope $_{374}$FSTFKCYGL$_{382}$ provides a relatively small dissociation constant (KD = 5.947E-06M) through sufficient interaction (**Table 4**). In order to obtain a more comprehensive prediction, we further used ProtParam to calculate multiple physical and chemical parameters of the peptide candidate epitopes and finally screened the epitope $_{374}$FSTFKCYGL$_{382}$. This particular epitope exhibits a theoretical isoelectric point (PI) of 8.20, and the aliphatic index was 43.33 and the instability index was -3.53. The results of physicochemical properties of candidate epitopes are listed in **Table 5**.

DISCUSSION

At present, different vaccine strategies are being used in vaccine research for COVID-19, such as RNA, non-replicating viral vectors, peptides, and DNA (26). Among them, peptide vaccines have attracted wide attention due to their antiviral, antitumor, and other infective functions, as well as the advantages of cheapness, safety, and strong specificity. As with natural infections, SARS-CoV-2 vaccination stimulates a strong

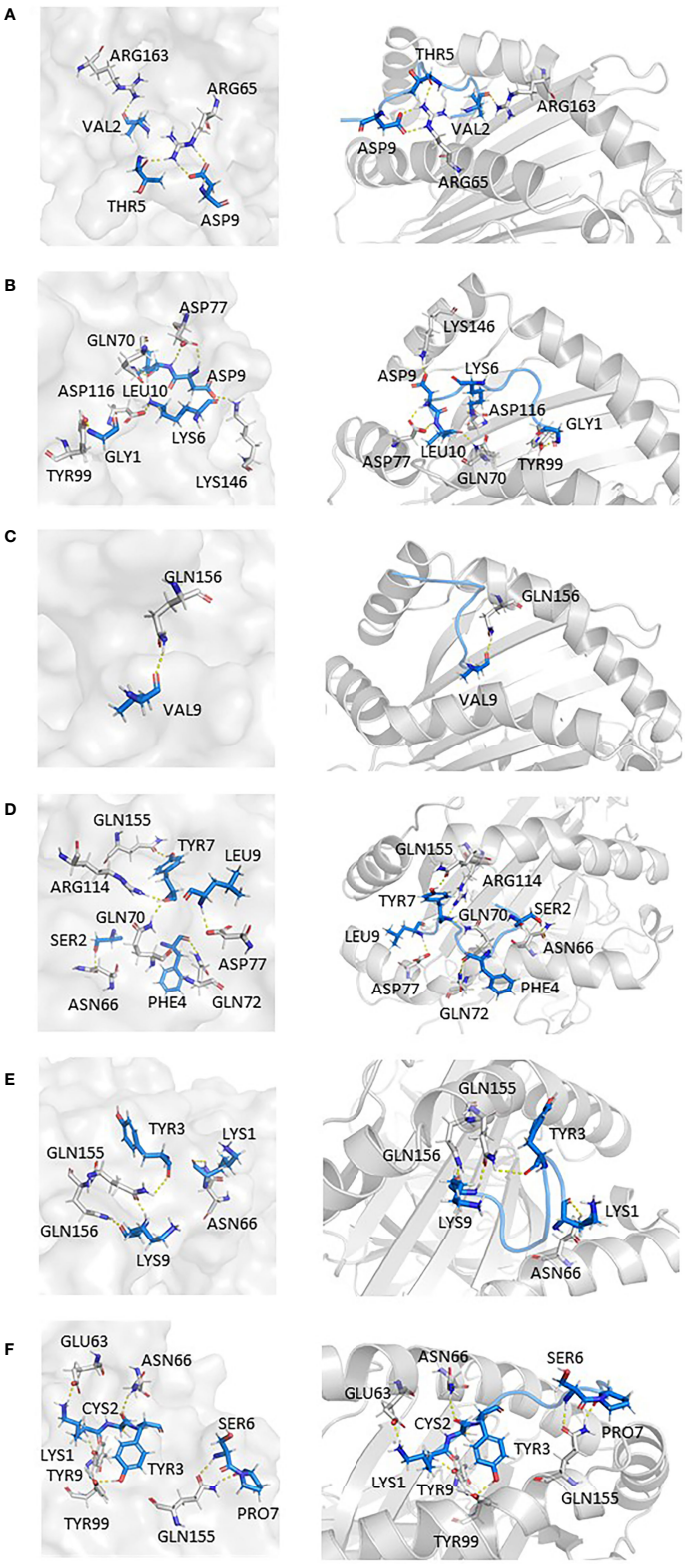

FIGURE 6 | Epitopes obtained from V382L interaction with HLA-A*11:01; epitopes are shown in marine, HLA structure is shown in gray. **(A)** HLA-A*11:01(5GRD)-GVSPTKLNDL (WT). **(B)** HLA-A*11:01(5GRD)-GLSPTKLNDL (MT). **(C)** HLA-A*11:01(5GRD)-FSTFKCYGV (WT). **(D)** HLA-A*11:01(5GRD)-FSTFKCYGL (MT). **(E)** HLA-A*11:01(1X7Q)-KCYGVSPTK (WT) **(F)** HLA-A*11:01(1X7Q)-KCYGLSPTK (MT).

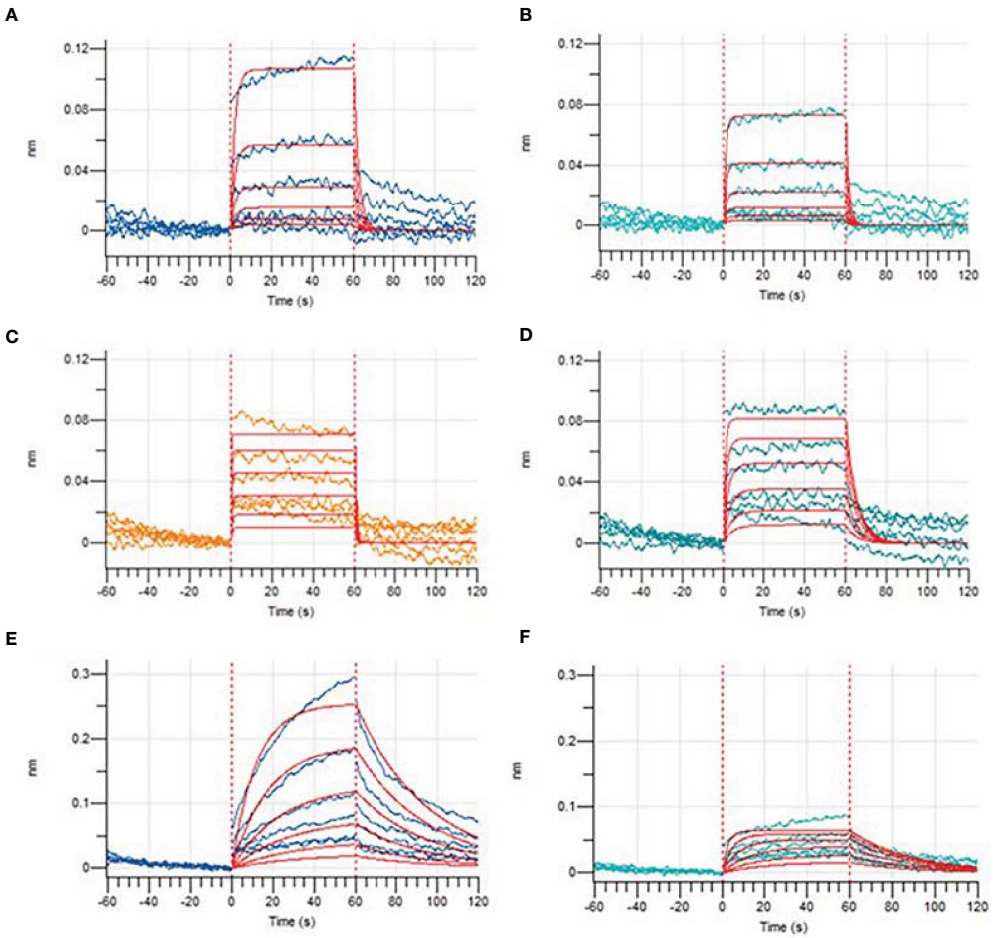

FIGURE 7 | Binding affinities of epitopes before and after mutations obtained by Bio-Layer Interferometry (BLI). Binding dissociation curve between wild-type peptide GVSPTKLNDL **(A)**, KCYGVSPTK **(C)**, FSTFKCYGV **(E)**, mutated epitope GLSPTKLNDL **(B)**, KCYGLSPTK **(D)**, and FSTFKCYGL **(F)** and HLA-A*11:01.

TABLE 4 | Kinetic analysis by BLI of the binding studies of epitopes to HLA molecular.

Wild Peptide	K_D (M)	Epitopes (MT)	K_D (M)
SQCVNLTTR	Non-binding	SQCVNFTTR	Non-binding
KCYGVSPTK	2.347E-05	KCYGLSPTK	2.302E-05
GVSPTKLNDL	6.557E-04	GLSPTKLNDL	3.190E-04
FSTFKCYGV	2.911E-05	FSTFKCYGL	5.947E-06

MT, mutation type.

TABLE 5 | Physicochemical properties of candidate epitopes.

Candidate Epitopes	Theoretical PI	Instability Index (Indication)	Aliphatic Index	Half-Life (Mammalian reticulocytes)
SQCVNFTTR	7.96	-3.17 (stable)	32.22	1.9 h
KCYGLSPTK	9.20	48.28 (unstable)	43.33	1.3 h
GLSPTKLNDL	5.84	44.45 (unstable)	117.00	30 h
FSTFKCYGL	8.20	-3.53 (stable)	43.33	1.1 h

Theoretical PI, theoretical isoelectric point.

cellular and humoral immune response that plays a vital protective role in the body (27). Safavi et al. (28) pointed out that T-cell immunity may be more durable than humoral immunity in controlling the novel coronavirus infection. Some other studies have also demonstrated that CD8+ T cells can generally target a variety of SARS-CoV-2 antigens and recognize epitopes from various viral antigens through a series of combinations of T-cell receptors (TCRs), which are crucial for

mediating viral clearance and are key to long-term immunity, and protection memory CD8+ T cells can provide against secondary infection (29). Spike protein of SARS-CoV-2 has been included in the focus of vaccine design because of its high specificity and ability to induce a strong immune response. In particular, the RBD region is widely considered as a key protein target for vaccine design and development of neutralizing antibodies as therapeutic agents (30).

In this study, we used immunoinformatics methods to analyze the S protein of SARS-CoV-2 variants prevalent in the world and various advanced tools to identify potential T-cell epitopes of SARS-CoV-2. Here, we conducted further screening of epitopes through residue scanning calculation to obtain antigenicity and non-allergenicity candidate epitopes for molecular docking and dynamics simulation. Our MD simulations revealed that four epitopes ($_{13}$SQCVNFTTR$_{21}$, $_{378}$KCYGLSPTK$_{386}$, $_{381}$GLSPTKLNDL$_{390}$, and $_{374}$FSTFKCYGL$_{382}$) were involved in the interaction with HLA-A*11:01 in a more active way than prior to the mutation. Evidenced by ProtParam's (31) analysis on physicochemical properties of these selected epitopes, epitopes $_{378}$KCYGLSPTK$_{386}$ and $_{381}$GLSPTKLNDL$_{390}$ with instability index >40 are not considered. To verify results from these four epitopes, we performed wet experiments, in which the affinity between $_{13}$SQCVNFTTR$_{21}$ and HLA-A*11:01 was not detected as expected. Due to satisfactory results in both qualitative affinity experiments and physicochemical analysis, we finally proposed $_{374}$FSTFKCYGL$_{382}$ epitope for the design of vaccine against SARS-CoV-2.

Now, the Omicron variant, which originated in South Africa, has been declared a variant of concern (VOC) by the World Health Organization. Studies have shown that Omicron carries a large number of mutations that may be associated with immune evasion. With the rapid spread of Omicron variants around the world, we also extended our research to Omicron (32). According to the complete study procedure presented in this study, we analyzed the effect of mutations in the S protein of Omicron strain on binding affinity of HLA-A*11:01-restricted CD8+ T-cell epitopes. Seventy epitopes containing mutated sites predicted by NetMHCpan 4.1 and MHCflurry2.0 were obtained. After screening for antigenicity and allergenicity, as well as affinity predicted by residue scanning module, 13 epitopes were finally used for MD simulation. After filtering out the unstable epitopes, we obtained four epitopes worthy of subsequent experimental verification. Our data showed that epitopes $_{366}$SVLYNLAPFFAFK$_{378}$ containing S371L, S373P, S375F, and T376A (binding free energy: -75.434 kcal/mol), $_{539}$VNFNFNGLK$_{547}$ containing T547K (binding free energy: -113.461 kcal/mol), $_{672}$ASYQTQTK$_{679}$ containing N679K mutation sites (binding free energy: -66.8471 kcal/mol), and $_{672}$ASYQTQTKSHR$_{682}$ containing N679K and P681H mutation sites (binding free energy: -106.701 kcal/mol) showed stronger affinity with HLA-A* 11:01 than their wild peptide.

In recent years, computer-based prediction methods have been widely favored in biological research because of their abilities to generate analytical value in a fast and cost-effective manner and thus have also been used in the early stages of vaccine development. Our study provides a very important and reasonable antigen prediction strategy, including analysis of hotspot mutations, prediction of mutant peptides, screening of immunogenic peptides, and structure-based docking simulation, to help us predict potential T-cell epitopes. However, this study is not flawless and it does have limitations. First of all, relatively few HLA types were covered, and they were mainly targeted at the Chinese population. Therefore, the study of T-cell immunity in a variety of HLA types should be considered in the direction of future studies. Secondly, due to the limitations of computer research, inaccuracy of software algorithms may have an impact on the experimental results. Therefore, the comprehensive evaluation of various analytical methods and the verification of wet experiment can better assist vaccine design.

In conclusion, the application of immunoinformatics enabled us to identify four unique immunogenic non-allergic T-cell epitopes from the S protein of the mutant of interest, promising to be associated with HLA-A*11:01 immune response. In the experiment, the epitope $_{374}$FSTFKCYGL$_{382}$ has a stronger affinity. Our results suggest that site-based immunoinformatics analysis procedures may be useful for the development and detection of specific T-cell epitopes for multiple SARS-CoV-2 variants.

DATA AVAILABILITY STATEMENT

The original contributions presented in the study are included in the article/**Supplementary Material**. Further inquiries can be directed to the corresponding authors.

AUTHOR CONTRIBUTIONS

XM and PG collected and analyzed the data and wrote the article. CS designed this study. XL supervised this study and revised the article. JL designed and organized the whole research. All authors contributed to the article and approved the submitted version.

FUNDING

This work was supported by the National Natural Science Foundation of China (31871322, 31900473, 82041006), the COVID-19 Emergency Research Fund of Zhejiang University of China (2020XGZX021), and the Fundamental Research Funds for the Central Universities (2242021k10004). The funding bodies were not involved in the study design, data collection, data analysis, and data interpretation.

SUPPLEMENTARY MATERIAL

The Supplementary Material for this article can be found online at: https://www.frontiersin.org/articles/10.3389/fimmu.2022.847617/full#supplementary-material

REFERENCES

1. Chung JY, Thone MN, Kwon YJ. COVID-19 Vaccines: The Status and Perspectives in Delivery Points of View. *Adv Drug Deliv Rev* (2021) 170:1–25. doi: 10.1016/j.addr.2020.12.011
2. Wang R, Hozumi Y, Yin C, Wei GW. Mutations on COVID-19 Diagnostic Targets. *Genomics* (2020) 112(6):5204–13. doi: 10.1016/j.ygeno.2020.09.028
3. Sharma K, Koirala A, Nicolopoulos K, Chiu C, Wood N, Britton PN. Vaccines for COVID-19: Where Do We Stand in 2021? *Paediatr Respir Rev* (2021) 39:22–31. doi: 10.1016/j.prrv.2021.07.001
4. Fehr AR, Perlman S. Coronaviruses: An Overview of Their Replication and Pathogenesis. *Methods Mol Biol* (2015) 1282:1–23. doi: 10.1007/978-1-4939-2438-7_1
5. Vishwakarma P, Yadav N, Rizvi ZA, Khan NA, Chiranjivi AK, Mani S, et al. Severe Acute Respiratory Syndrome Coronavirus 2 Spike Protein Based Novel Epitopes Induce Potent Immune Responses *In Vivo* and Inhibit Viral Replication *In Vitro*. *Front Immunol* (2021) 12:613045. doi: 10.3389/fimmu.2021.613045
6. Lin HT, Chen CC, Chiao DJ, Chang TY, Chen XA, Young JJ, et al. Nanoparticular CpG-Adjuvanted SARS-CoV-2 S1 Protein Elicits Broadly Neutralizing and Th1-Biased Immunoreactivity in Mice. *Int J Biol Macromol* (2021) 193(Pt B):1885–97. doi: 10.1016/j.ijbiomac.2021.11.020
7. Abd Albagi SO, Al-Nour MY, Elhag M, Tageldein Idris Abdelihalim A, Musa Haroun E, Adam Essa ME, et al. A Multiple Peptides Vaccine Against COVID-19 Designed From the Nucleocapsid Phosphoprotein (N) and Spike Glycoprotein (S) *via* the Immunoinformatics Approach. *Inform Med Unlocked* (2020) 21:100476. doi: 10.1016/j.imu.2020.100476
8. Singh H, Jakhar R, Sehrawat N. Designing Spike Protein (S-Protein) Based Multi-Epitope Peptide Vaccine Against SARS COVID-19 by Immunoinformatics. *Heliyon* (2020) 6(11):e05528. doi: 10.1016/j.heliyon.2020.e05528
9. Tomita Y, Ikeda T, Sato R, Sakagami T. Association Between HLA Gene Polymorphisms and Mortality of COVID-19: An in Silico Analysis. *Immun Inflamm Dis* (2020) 8(4):684–94. doi: 10.1002/iid3.358
10. Wang YD, Sin WY, Xu GB, Yang HH, Wong TY, Pang XW, et al. T-Cell Epitopes in Severe Acute Respiratory Syndrome (SARS) Coronavirus Spike Protein Elicit a Specific T-Cell Immune Response in Patients Who Recover From SARS. *J Virol* (2004) 78(11):5612–8. doi: 10.1128/jvi.78.11.5612-5618.2004
11. Mamedov T, Yuksel D, Ilgın M, Gurbuzaslan I, Gulec B, Yetiskin H, et al. Plant-Produced Glycosylated and *In Vivo* Deglycosylated Receptor Binding Domain Proteins of SARS-CoV-2 Induce Potent Neutralizing Responses in Mice. *Viruses* (2021) 13(8):1595. doi: 10.3390/v13081595
12. Culpepper DJ, Maddox MK, Caldwell AB, McFarland BJ. Systematic Mutation and Thermodynamic Analysis of Central Tyrosine Pairs in Polyspecific NKG2D Receptor Interactions. *Mol Immunol* (2011) 48(4):516–23. doi: 10.1016/j.molimm.2010.10.007
13. Lu L, Chu AW, Zhang RR, Chan WM, Ip JD, Tsoi HW, et al. The Impact of Spike N501Y Mutation on Neutralizing Activity and RBD Binding of SARS-CoV-2 Convalescent Serum. *EBioMedicine* (2021) 71:103544. doi: 10.1016/j.ebiom.2021.103544
14. Cheng YW, Chao TL, Li CL, Wang SH, Kao HC, Tsai YM, et al. D614G Substitution of SARS-CoV-2 Spike Protein Increases Syncytium Formation and Virus Titer *via* Enhanced Furin-Mediated Spike Cleavage. *mBio* (2021) 12(4):e0058721. doi: 10.1128/mBio.00587-21
15. Lu H, Tang B, He Y, Zhou W, Qiu J, Li Y. Identification of HLA–A*1101–restricted Cytotoxic T Lymphocyte Epitopes Derived From Epidermal Growth Factor Pathway Substrate Number 8. *Mol Med Rep* (2016) 14(6):4999–5006. doi: 10.3892/mmr.2016.5888
16. O'Donnell TJ, Rubinsteyn A, Laserson U. MHCflurry 2.0: Improved Pan-Allele Prediction of MHC Class I-Presented Peptides by Incorporating Antigen Processing. *Cell Syst* (2020) 11(4):418–9. doi: 10.1016/j.cels.2020.09.001
17. Zaitoua AJ, Kaur A, Raghavan M. Variations in MHC Class I Antigen Presentation and Immunopeptidome Selection Pathways. *F1000Res* (2020) 9:1177. doi: 10.12688/f1000research.26935.1
18. Duan J, Lupyan D, Wang L. Improving the Accuracy of Protein Thermostability Predictions for Single Point Mutations. *Biophys J* (2020) 119(1):115–27. doi: 10.1016/j.bpj.2020.05.020
19. Fadaka AO, Aruleba RT, Sibuyi NRS, Klein A, Madiehe AM, Meyer M. Inhibitory Potential of Repurposed Drugs Against the SARS-CoV-2 Main Protease: A Computational-Aided Approach. *J Biomol Struct Dyn* (2020) 12:1–13. doi: 10.1080/07391102.2020.1847197
20. Petersen RL. Strategies Using Bio-Layer Interferometry Biosensor Technology for Vaccine Research and Development. *Biosensors (Basel)* (2017) 7(4):49. doi: 10.3390/bios7040049
21. Doytchinova IA, Flower DR. VaxiJen: A Server for Prediction of Protective Antigens, Tumour Antigens and Subunit Vaccines. *BMC Bioinf* (2007) 8:4. doi: 10.1186/1471-2105-8-4
22. Beard H, Cholleti A, Pearlman D, Sherman W, Loving KA. Applying Physics-Based Scoring to Calculate Free Energies of Binding for Single Amino Acid Mutations in Protein-Protein Complexes. *PloS One* (2013) 8(12):e82849. doi: 10.1371/journal.pone.0082849
23. Shanthirabalan S, Chomilier J, Carpentier M. Structural Effects of Point Mutations in Proteins. *Proteins* (2018) 86(8):853–67. doi: 10.1002/prot.25499
24. Sawant S, Patil R, Khawate M, Zambre V, Shilimkar V, Jagtap S. Computational Assessment of Select Antiviral Phytochemicals as Potential SARS-Cov-2 Main Protease Inhibitors: Molecular Dynamics Guided Ensemble Docking and Extended Molecular Dynamics. *Silico Pharmacol* (2021) 9(1):44. doi: 10.1007/s40203-021-00107-9
25. Khater S, Kumar P, Dasgupta N, Das G, Ray S, Prakash A. Combining SARS-CoV-2 Proofreading Exonuclease and RNA-Dependent RNA Polymerase Inhibitors as a Strategy to Combat COVID-19: A High-Throughput in Silico Screening. *Front Microbiol* (2021) 12:647693. doi: 10.3389/fmicb.2021.647693
26. Cuspoca AF, Díaz LL, Acosta AF, Peñaloza MK, Méndez YR, Clavijo DC, et al. An Immunoinformatics Approach for SARS-CoV-2 in Latam Populations and Multi-Epitope Vaccine Candidate Directed Towards the World's Population. *Vaccines (Basel)* (2021) 9(6):581. doi: 10.3390/vaccines9060581
27. Goletti D, Petrone L, Manissero D, Bertoletti A, Rao S, Ndunda N, et al. The Potential Clinical Utility of Measuring Severe Acute Respiratory Syndrome Coronavirus 2-Specific T-Cell Responses. *Clin Microbiol Infect* (2021) 27(12):1784–9. doi: 10.1016/j.cmi.2021.07.005
28. Safavi A, Kefayat A, Mahdevar E, Abiri A, Ghahremani F. Exploring the Out of Sight Antigens of SARS-CoV-2 to Design a Candidate Multi-Epitope Vaccine by Utilizing Immunoinformatics Approaches. *Vaccine* (2020) 38(48):7612–28. doi: 10.1016/j.vaccine.2020.10.016
29. Jung JH, Rha MS, Sa M, Choi HK, Jeon JH, Seok H, et al. SARS-CoV-2-Specific T Cell Memory is Sustained in COVID-19 Convalescent Patients for 10 Months With Successful Development of Stem Cell-Like Memory T Cells. *Nat Commun* (2021) 12(1):4043. doi: 10.1038/s41467-021-24377-1
30. Hu W, He M, Wang X, Sun Q, Kuang M. Specific CD8(+) TCR Repertoire Recognizing Conserved Antigens of SARS-CoV-2 in Unexposed Population: A Prerequisite for Broad-Spectrum CD8(+) T Cell Immunity. *Vaccines (Basel)* (2021) 9(10):1093. doi: 10.3390/vaccines9101093
31. Wilkins MR, Gasteiger E, Bairoch A, Sanchez JC, Williams KL, Appel RD, et al. Protein Identification and Analysis Tools in the ExPASy Server. *Methods Mol Biol* (1999) 112:531–52. doi: 10.1385/1-59259-584-7:531
32. Mazzoni A, Vanni A, Spinicci M, Capone M, Lamacchia G, Salvati L, et al. SARS-CoV-2 Spike-Specific CD4+ T Cell Response Is Conserved Against Variants of Concern, Including Omicron. *Front Immunol* (2022) 13:801431. doi: 10.3389/fimmu.2022.801431

Conflict of Interest: The authors declare that the research was conducted in the absence of any commercial or financial relationships that could be construed as a potential conflict of interest.

Advantages of publishing in Frontiers

OPEN ACCESS
Articles are free to read for greatest visibility and readership

FAST PUBLICATION
Around 90 days from submission to decision

HIGH QUALITY PEER-REVIEW
Rigorous, collaborative, and constructive peer-review

TRANSPARENT PEER-REVIEW
Editors and reviewers acknowledged by name on published articles

Frontiers
Avenue du Tribunal-Fédéral 34
1005 Lausanne | Switzerland

Visit us: www.frontiersin.org
Contact us: frontiersin.org/about/contact

REPRODUCIBILITY OF RESEARCH
Support open data and methods to enhance research reproducibility

DIGITAL PUBLISHING
Articles designed for optimal readership across devices

FOLLOW US
@frontiersin

IMPACT METRICS
Advanced article metrics track visibility across digital media

EXTENSIVE PROMOTION
Marketing and promotion of impactful research

LOOP RESEARCH NETWORK
Our network increases your article's readership